To avoid issues relating to nomenclatural acts, minor sections of this article which reported on the naming of a new species, and which did not make it into the final publication, have been redacted.

A specimen-based phylogenetic analysis of Diplodocidae (Dinosauria, Sauropoda) with the description of a new genus and species from the Upper Jurassic Morrison Formation of Wyoming, USA

PeerJ Reviewing Manuscript

Diplodocidae are among the best known sauropod dinosaurs. Several species were described in the late 1800s or early 1900s. Since then, numerous additional specimens were recovered in the USA, Tanzania, Portugal, as well as possibly Spain, England, and Asia. To date, the clade includes about 12 to 15 different species, some of them with questionable taxonomic status (e.g. '*Diplodocus*' *hayi* or *Dyslocosaurus polyonychius*). However, intrageneric relationships of the multi-species, iconic genera *Apatosaurus* and *Diplodocus* are still poorly known. The way to resolve this issue is a specimen-based phylogenetic analysis, which was done for *Apatosaurus*, but is here performed for the first time for the entire clade of Diplodocidae.

Any type specimen previously proposed to belong to Diplodocidae was included in the study, as are relatively complete referred specimens, in order to increase the degree of overlapping material. For specimens subsequently suggested to be non-diplodocid sauropods, their hypothesized sister taxa were included as outgroups. Additionally, a new specimen from the Upper Jurassic Morrison Formation of northern Wyoming (USA) is described herein (SMA 0011). The specimen is recovered as a new diplodocine species. It preserves material from nearly all parts of the skeleton, including a skull, anterior, middle, and posterior cervical vertebrae, a complete dorsal vertebral column, sacral elements, and fore- and hindlimb material with fairly complete manus and pedes. Thereby, SMA 0011 considerably increases anatomical overlap between the sometimes fragmentary holotype specimens of the earlier described diplodocid species, allowing for more significant results in the specimen-based phylogenetic analysis.

The current phylogenetic analysis includes 76 operational taxonomic units, 45 of which belong to Diplodocidae. The specimens were scored for 477 morphological characters,

representing one of the most extensive phylogenetic analyses done within sauropod dinosaurs. The resulting cladogram recovers the classical arrangement of diplodocid relationships. Basing on a newly developed numerical approach to reduce subjectivity in the decision of specific or generic separation, species that have historically been included into well-known genera like *Apatosaurus* or *Diplodocus*, were detected to be actually generically different. According to this approach, the famous genus *Brontosaurus* is considered valid, and evidence further suggests that also *Elosaurus parvus* (previously referred to *Apatosaurus*) or '*Diplodocus*' *hayi* represent unique genera. The study increases our knowledge about individual variation, and helps to decide how to score multi-species genera. Such a specimen-based phylogenetic analysis thus proves a valuable tool to validate historic species in sauropods, and in paleontology as a whole.

PeerJ Reviewing Manuscript

Emanuel Tschopp (1, 2, 3) and Octávio Mateus (1, 2)

1) GeoBioTec, Faculdade de Ciências e Tecnologia, Universidade Nova de Lisboa, Monte de Caparica, Portugal

2) Museu da Lourinhã, Rua João Luis de Moura, 95, 2530-158 Lourinhã, Portugal

3) Dipartimento di Scienze della Terra, Università di Torino, Italy

Corresponding author: Emanuel Tschopp, Museu da Lourinhã, Rua João Luis de Moura, 95, 2530-158 Lourinhã, Portugal; +393426314421, tschopp.e@gmail.com

PeerJ Reviewing Manuscript

Introduction

Overview of diplodocid sauropods

The sauropod dinosaur clade Diplodocidae includes some of the most iconic sauropods. With their greatly elongated necks and tails, diplodocids constitute one of the typical popular images of sauropod dinosaurs. The clade is historically important, having provided the first published reconstruction of an entire sauropod skeleton ('*Brontosaurus*' *excelsus*; Marsh, 1883), the first complete sauropod skull to be described (*Diplodocus*; Marsh, 1884), and the first mounted sauropod specimen (*Apatosaurus* AMNH 460; Matthew, 1905). Diplodocids range from relatively small to gigantic sauropod species (*Kaatedocus siberi* Tschopp and Mateus, 2012, to *Supersaurus vivianae* Jensen, 1985, respectively), and include the well-known genera *Apatosaurus* Marsh, 1877a, *Diplodocus* Marsh, 1878, and *Barosaurus* Marsh, 1890. Their possible first occurrence dates to the Middle Jurassic of England (*Cetiosauriscus stewarti* Charig, 1980; but see Heathcote and Upchurch, 2003, or Rauhut et al., 2005, for a differential identification of *Cetiosauriscus*). Diplodocidae reaches a peak in diversity in the Late Jurassic, with finds from North America, Tanzania, Zimbabwe, Portugal, Spain, as well as possibly England, Georgia, and China (Upchurch and Mannion, 2009; Mannion et al., 2012). To date, no convincing evidence exists for their presence in the Cretaceous (Whitlock et al., 2011), but their probable extinction at the Jurassic-Cretaceous boundary still remains a mystery (Taylor et al., 2011).

In recent phylogenetic trees, Diplodocidae consistently forms the sister group to the clade Dicraeosauridae, with which they form Flagellicaudata, which in turn is included, together with the Rebbachisauridae, in Diplodocoidea (e.g. Upchurch, 1998; Wilson, 2002, 2005; Harris and Dodson, 2004; Upchurch et al., 2004a; Rauhut et al., 2005; Harris, 2006c; Sereno et al., 2007; Whitlock, 2011a; Carballido et al., 2012b; Mannion et al., 2012; Tschopp and Mateus, 2013b). The taxonomy of the clade was historically somewhat confused, with “Diplodocidae” being used in the same way as Diplodocoidea today (see e.g. McIntosh, 1990a, b). In the following, we use the taxonomy and definitions as clarified by Taylor and Naish (2005).

Whereas the vast majority of diplodocid species were described in the late 1800s and early 1900s, additional taxa still continue to be discovered (see Tab. 1). The high rate of early descriptions, particularly during the so-called bone wars in the late 1800s, resulted also in a high amount of species that are now considered invalid, questionable, or synonymous (Taylor, 2010). Species recognition is furthermore hampered by the fact that many of the holotype specimens are

PeerJ Reviewing Manuscript

PeerJ Reviewing Manuscript

incomplete and fragmentary (e.g. *Diplodocus longus* YPM 1920), or appear to include bones of more than one individual (e.g. *Apatosaurus ajax* YPM 1860). Due to the absence of field notes or quarry maps in many of these cases, it remains difficult or even impossible to confidently assign the individual bones to particular animals. Given that the majority of the sites in the Upper Jurassic Morrison Formation, which yielded about three quarters of the reported diplodocid genera, are multi-taxon assemblages, it is possible that some of these holotype specimens include material from different species. This renders meaningful diagnoses for the species and thus the identification of new material highly difficult. However, the detailed studies of original material and their corresponding field notes by McIntosh and Berman (1975), Berman and McIntosh (1978), McIntosh (1981, 1990a, 1995, 2005), and McIntosh and Carpenter (1998), provided a wealth of important information concerning the composition of diplodocid holotype specimens and species recognition. Nonetheless, only one study that tested the validity of single species by means of phylogenetic methods has been published to date, focusing on the genus *Apatosaurus* only (Upchurch et al., 2004b). By using individual specimens as operational taxonomic units (OTUs), Upchurch et al. (2004b) succeeded in obtaining a significant result, which generally supported the traditional view of *Apatosaurus* intrarelationships.

The specimen-based phylogenetic analysis is herein extended to the entire clade of Diplodocidae, and combined with the most recent analyses of diplodocoid interrelationships (Whitlock, 2011a; Mannion et al., 2012; Tschopp and Mateus, 2013b). It includes all holotype specimens of every single putative diplodocid species ever described (see Tab. 2). The phylogenetic analysis is furthermore expanded by adding reasonably complete and articulated referred specimens from various sites in the Morrison Formation (e.g. *Diplodocus* sp. AMNH 223, Osborn, 1899; or *Barosaurus* sp. AMNH 6341, McIntosh, 2005). Among the additional OTUs are also eight specimens from the Howe Ranch in the vicinity of Shell (Bighorn Basin, Wyoming), one of which is herein described for the first time and identified as previously unknown species.

Howe Ranch: a rediscovered diplodocid Eldorado

The Howe Ranch sites have produced a high number of partially to almost completely articulated dinosaur skeletons, sometimes even with soft tissue preservation (see Brinkmann and Siber, 1992; Ayer, 2000; Schwarz et al., 2007c; Tschopp, 2008; Siber and Möckli, 2009; Christiansen and Tschopp, 2010; Tschopp and Mateus, 2013b). Three sites proved particularly productive: the Howe Quarry, the Howe-Stephens Quarry, and the Howe-Scott Quarry (Fig. 1). The Howe Quarry was first worked by Barnum Brown for the American Museum of Natural History (New

PeerJ Reviewing Manuscript

York, USA) in 1934, and was later relocated and completely excavated by a team from the Sauriermuseum Aathal (Switzerland), led by Hans-Jakob 'Kirby' Siber (Brown, 1935; Ayer, 2000; Michelis, 2004; Tschopp and Mateus, 2013b). The other two sites, as well as several smaller, less productive spots at various stratigraphy levels within the Morrison Formation, have since been discovered nearby and excavated by the SMA (Ayer, 2000; Siber and Möckli, 2009; Christiansen and Tschopp, 2010; Fig. 2). All three major sites yielded well-preserved and at least partially articulated diplodocid specimens, both apatosaurine and diplodocine, of varying ontogenetic stages (Fig. 3; Tab. 3). Only one of these specimens has yet been formally described (even including the AMNH material from 1934), and now constitutes the holotype of *Kaatedocus siberi* (Tschopp and Mateus, 2013b).

Due to the good preservation of the SMA material, the addition of these specimens to a specimen-based phylogenetic analysis as attempted herein is of great importance. By doing so, the anatomical overlap among different OTUs is greatly increased – a very welcome fact, when many of the holotypes are fragmentary and only include few bones, as is the case in Diplodocidae. In particular two specimens with articulated and almost complete skulls (SMA 0004 and 0011) yield important new data. Although the clade Diplodocidae has produced the most skulls within sauropods (Whitlock et al., 2010), only two diplodocine (CM 3452, HMNS 175) and three apatosaurine specimens (CM 3018/11162, CMC 7180, YPM 1860) with possibly articulated skull material were reported to date (Holland, 1906, 1924; McIntosh and Berman, 1975; Berman and McIntosh, 1978; Barrett et al., 2011). Other than CM 11162, which is probably the skull of CM 3018 (Berman and McIntosh, 1978), none of them has yet been described in detail. This renders the identification of disarticulated skull material extremely difficult, and impedes specimen-based phylogenetic analyses. The new specimens described herein thus finally allow detailed reassessments of fragmentary material, including type skeletons and disarticulated skulls.

Institutional abbreviations

AC, Beneski Museum of Natural History, Amherst College, Amherst, Massachusetts, USA; **AMNH**, American Museum of Natural History, New York City, New York, USA; **ANS**, Academy of Natural Sciences, Philadelphia, Pennsylvania, USA; **BYU**, Brigham Young University, Museum of Paleontology, Provo, Utah, USA; **CCG**, Chengdu College of Geology, Sichuan, China; **CM**, Carnegie Museum of Natural History, Pittsburgh, Pennsylvania, USA; **CMC**, Cincinnati Museum Center, Cincinnati, Ohio, USA; **CMNH**, Cleveland Museum of Natural History, Cleveland, Ohio, USA; **CPT**, Conjunto Paleontológico de Teruel, Dinópolis, Teruel, Spain; **DMNS**, Denver Museum of Nature and Science, Denver, Colorado, USA; **DNM**,

Dinosaur National Monument, Jensen, Utah, USA; **FMNH**, Field Museum of Natural History, Chicago, Illinois, USA; **GCP**, Grupo Cultural Paleontológico de Elche, Museo Paleontológico de Elche, Elche, Spain; **GMNH**, Gunma Museum of Natural History, Gunma, Japan; **HMNS**, Houston Museum of Nature and Science, Houston, TX, USA; **ISIR**, Paleontological Collection, Geology Museum, Indian Statistical Institute, Calcutta, India; **IVPP**, Institute of Vertebrate Paleontology and Paleoanthropology, Chinese Academy of Sciences, Beijing, China; **KUVP**, Kansas University Natural History Museum, Lawrence, Kansas, USA; **LACM**, Los Angeles County Museum of Natural History, Los Angeles, USA; **MACN**, Museo Argentino de Ciencias Naturales, Neuquén, Argentina; **MB.R.**, Museum für Naturkunde, Berlin, Germany; **MCF**, Museo Carmen Funes, Plaza Huincul, Neuquén, Argentina; **MCNV**, Museo de Ciencias Naturales, Valencia, Spain; **MDS**, Museo de Dinosaurios de Salas de los Infantes, Salas de los Infantes, Burgos, Spain; **MIGM**, Museu Geológico do Instituto Geológico e Mineiro de Portugal, Lisboa, Portugal; **ML**, Museu da Lourinhã, Lourinhã, Portugal; **MNN**, Musée National du Niger, Niamey, Republic of Niger; **MOZ**, Museo Provincial de Ciencias Naturales 'Prof. Dr. Juan A. Olsacher', Zapala, Neuquén, Argentina; **MPCA**, Museo Provincial Carlos Ameghino, Cipolletti, Río Negro, Argentina; **MPEF**, Museo Paleontológico Egidio Feruglio, Trelew, Argentina; **MUCPv**, Museum of the University of Comahue-Patagonia, Argentina; **NHMUK**, Natural History Museum, London, United Kingdom; **NMB**, Staatliches Naturhistorisches Museum Braunschweig, Germany; **NMMNH**, New Mexico Museum of Natural History and Science, Albuquerque, New Mexico, USA; **NSMT**, National Museum if Nature and Science, Tokyo, Japan; **OMNH**, Sam Noble Oklahoma Museum of Natural History, Norman, Oklahoma, USA; **PMU**, Evolutionsmuseet Paleontologi, University of Uppsala, Uppsala, Sweden; **SMA**, Sauriermuseum Aathal, Aathal, Switzerland; **SMNS**, Staatliches Museum für Naturkunde, Stuttgart, Germany; **Tate**, Tate Geological Museum, Casper College, Casper, Wyoming, USA; **UMNH**, Utah Museum of Natural History, Salt Lake City, Utah, USA; **USNM**, United States National Museum, Smithsonian Institution, Washington DC, USA; **UUVP**, University of Utah, Salt Lake City, Utah, USA; **UW**, University of Wyoming Geological Museum, Laramie, Wyoming, USA; **WDC**, Wyoming Dinosaur Center, Thermopolis, Wyoming, USA; **YPM**, Yale Peabody Museum, New Haven, Connecticut, USA; **ZDM**, Zigong Dinosaur Museum of Sichuan Province, China.

Anatomical abbreviations

a, articular; **aal**, acetabular articulation surface length; **ac**, acetabular surface; **aCd,** anterior caudal vertebrae; **acdl**, anterior centrodiapophyseal lamina; **acf**, anterior condyle fossa; **acl**,

PeerJ Reviewing Manuscript

acromion length; **acm**, acromion; **acpl**, anterior centroparapophyseal lamina; **acr**, acromial ridge; **aCV**, anterior cervical vertebrae; **adt**, anterodorsal tuberosity; **aDV,** anterior dorsal vertebrae; **af**, astragalus foramen; **al**, accessory lamina; **amb**, ambiens process; **amc**, amphicoelous; **amCd**, anterior-most caudal vertebrae; **amp**, amphiplatyan; **an**, angular; **anp**, antotic process; **aof**, antorbital fenestra; **ap**, anterior process; **apd**, anteroposterior depth; **apf**, anterior pneumatic fossa; **apl**, anteroposterior length; **aprl**, anterior process length; **apw**, anteroposterior width; **ar**, anterior ramus; **as**, astragalus; **asl**, accessory spinal lamina; **asp**, ascending process; **at**, atlas; **ato**, anterior tooth; **avl**, anteroventral lip; **aW**, anterior width; **ax**, axis; **axr**, axial rib; **Bc,** braincase; **bic**, biconvex; **bns**, bifid neural spine; **bo**, basioccipital; **bph**, basipterygoid hook; **bpr**, basipterygoid process; **bs**, basisphenoid; **bt**, basal tuber; **c**, carpal; **ca**, coracoid articulation; **cal**, calcaneum; **can**, crista antotica; **cap**, capitulum; **cc**, cnemial crest; **Cd**, caudal vertebra; **cdf**, centrodiapophyseal fossa; **CF**, coracoid foramen; **Ch**, chevrons; **chf**, chevron facet; **cl**, centrum length; **cl-cd**, centrum length without condyle; **cmw**, centrum minimum width; **co**, coracoid; **comp**, compressed; **cph**, centrum posterior height; **cpol**, centropostzygapophyseal lamina; **cpr**, crista prootica; **cprf**, centroprezygapophyseal fossa; **cprl**, centroprezygapophyseal lamina; **CR**, cervical ribs; **CV**, cervical vertebra; **cw**, centrum width; **d**, dentary; **dapd**, distal anteroposterior depth; **das**, anterior spur on diapophysis; **db**, distal blade; **dCd**, distal caudal vertebrae; **dds**, dorsal spur on diapophysis; **de**, dentin; **def**, deformed; **dg**, distal groove; **dH**, distal dorsoventral height; **di**, diapophysis; **dip**, distal process; **dlr**, dorsolateral ridge; **dp**, diapophysis posterior process; **dpc**, deltopectoral crest; **dpcl**, length deltopectoral crest; **DR**, dorsal ribs; **dro**, distal roller; **dsf**, dorsal spinal fossa; **dt**, denticles; **dtw**, distal transverse width; **DV**, dorsal vertebra; **dw**, dorsal width; **ec**, epicondyle; **EFS**, external fundamental system; **emf,** external mandibular fenestra; **en**, enamel; **ep**, ectopterygoid; **epi**, epipophysis; **er**, ectopterygoid ramus; **est**, estimated; **ex**, exoccipital; **f**, frontal; **fe**, femur; **fh**, femoral head; **fi**, fibula; **fic**, fibular condyle; **fif**, fibular facet; **Fl**, forelimb; **fm**, foramen magnum; **FS**, facial skull; **ft**, fourth trochanter; **gh**, greatest height; **GL**, glenoid; **h**, humerus; **Hap**, dorsoventral height anterior process; **hc**, haemal canal; **hcd**, height condyle; **hct**, height cotyle; **Hdlp**, dorsoventral height dorsolateral process; **Hdmp**, dorsoventral height dorsomedial process; **hh**, humeral head; **Hl**, hindlimb; **hna**, height neural arch; **hns**, height neural spine; **Hvr**, dorsoventral length ventral ramus; **hya**, hypantrum; **hys**, hyposphene; **ic**, interclavicle; **icg**, intercondylar groove; **il**, ilium; **inc**, incomplete; **int sprl**, interrupted spinoprezygapophyseal lamina; **ip**, iliac peduncle; **is**, ischium; **isa**, ischial articular surface; **isal**, ischial articular surface length; **j**, jugal; **la**, lacrimal; **L aop**, length antotic process; **Lap**, length anterior process; **lco**, lateral condyle; **L cpr**, length crista prootica; **LJ**, lower jaw;

PeerJ Reviewing Manuscript

Ll-oc, lateral length contributing to orbit; **lprl**, lateral process length; **Lpp**, length posterior process; **lprzc**, lateral prezygapophyseal cavity; **lr**, lateral ridge; **ls**, laterosphenoid; **lsc**, lateral spine cavity; **lsp**, lateral spur; **lspol**, lateral spinopostzygapophyseal lamina; **Ltb**, length tooth-bearing portion; **ltf**, laterotemporal fenestra; **Lv**, length ventral edge **m**, maxilla; **Ma**, manus; **maxH**, maximum dorsoventral height; **maxW**, maximum transverse width; **MB**, morphotype B element; **mc**, metacarpal; **mCd**, mid-caudal vertebrae; **mco**, medial condyle; **mCV**, mid-cervical vertebrae; **mDV**, mid-dorsal vertebrae; **minH**, minimum dorsoventral height; **minW**, minimum transverse width; **mp**, medial process; **mr**, medial ridge; **mspol**, medial spinopostzygapophyseal lamina; **msw**, midshaft width; **mt**, median tubercle; **mts**, metatarsal; **n**, external nares; **na**, nasal; **naf**, neural arch foramen; **nc**, neural canal; **ncs**, neurocentral synostosis; **nf**, nutrient foramen; **ns**, neural spine; **o**, orbit; **oc**, occipital condyle; **of**, obturator foramen; **olf**, olfactory foramen; **opc**, opisthocoelous; **opf**, optic foramen; **os**, orbitosphenoid; **p**, parietal; **pa**, palate; **pabh**, preacetabular blade height; **pap**, parapophysis; **papd**, proximal anteroposterior depth; **paof**, preantorbital fossa; **par bns**, parallel bifurcated neural spine; **pas**, proximal articular surface; **pCd**, posterior caudal vertebrae; **pcdl**, posterior centrodiapophyseal lamina; **PcG**, pectoral girdle; **pcpl**, posterior centroparapophyseal lamina; **pCV**, posterior cervical vertebrae; **pd**, proximal depth; **pdd**, proximodistal depth; **pDV**, posterior dorsal vertebrae; **Pe**, Pes; **pf**, prefrontal; **phm**, manual phalanx; **php**, pedal phalanx; **pl**, pleurocoel; **plc**, posterolateral crest; **plp**, posterolateral process; **pm**, premaxilla; **pnf**, pneumatic foramina; **po**, postorbital; **pocdf**, postzygapophyseal centrodiapophyseal fossa; **podl**, postzygodiapophyseal lamina; **popr**, paroccipital process; **posl**, postspinal lamina; **poz**, postzygapophysis; **pp**, posterior process; **pp-fp**, distance posterior process to frontoparietal suture; **ppapd**, pubic peduncle anteroposterior depth; **ppf**, posterior pneumatic fossa; **ppfo**, postparietal foramen; **pph**, pneumatopore height; **ppl**, pneumatopore length; **ppw**, pubic peduncle transverse width; **pra**, proatlas; **prap**, preacetabular process; **prapl**, preacetabular process length; **prc**, procoelous; **prcdf**, prezygapophyseal centrodiapophyseal fossa; **prdl**, prezygodiapophyseal lamina; **pre**, pre-epipophysis; **pro**, prootic; **prpl**, prezygoparapophyseal lamina; **prsl**, prespinal lamina; **prz**, prezygapophysis; **ps**, proximal spur; **psr**, parasphenoid rostrum; **pt**, pterygoid; **ptc**, platycoelous; **ptf**, posttemporal fenestra; **pto**, posterior tooth; **ptr**, vertical distance from proximal articular surface to trochanter; **pts**, prezygapophysis transverse sulcus; **ptw**, proximal transverse width; **pu**, pubis; **pua**, pubic articular surface; **pual**, pubic articular surface length; **pup**, pubic peduncle; **pupl**, pubic peduncle length; **pvf**, posteroventral flanges; **pvfo**, posteroventral fossa; **PvG**, pelvic girdle; **pvl**, posteroventral lip; **pvlp**, posterior ventrolateral process; **pw,** posterior width; **q**, quadrate; **qj**,

PeerJ Reviewing Manuscript

quadratojugal; **qr**, quadrate ramus; **r**, radius; **rt**, tubercle for articulation with radius; **sa**, surangular; **saf**, surangular foramen; **sc**, scapula; **sdf**, spinodiapophyseal fossa; **sh**, shaft height; **snc**, sagittal nuchal crest; **so**, supraoccipital; **SP**, sternal plates; **spdl**, spinodiapophyseal lamina; **spof**, spinopostzygapophyseal fossa; **spol**, spinopostzygapophyseal lamina; **sprl**, spinoprezygapophyseal lamina; **sprl ab**, spinoprezygapophyseal lamina anterior bulge; **sq**, squamosal; **sqr**, squamosal ramus; **SR**, sternal ribs; **stf**, supratemporal fenestra; **SV**, sacral vertebrae; **sw**, shaft width; **sy**, sacricostal yoke; **sym**, symphysis; **T**, teeth; **tb**, tibia; **tc**, tooth crown; **tic**, tibial condyle; **tif**, tibial facet; **tp**, transverse process; **tpol**, interpostzygapophyseal lamina; **tprl**, interprezygapophyseal lamina; **tr**, tooth root; **tub**, tuberculum; **u**, ulna; **ucp**, ulnar condylar processes; **ung**, ungual; **ut**, tubercle for articulation with ulna; **v**, vomer; **vk**, ventral keel; **vlh**, ventral longitudinal hollow; **vlr**, ventrolateral ridge; **vmc**, ventral median constriction; **vsf**, ventral spinal fossa; **wcd**, width condyle; **wct**, width cotyle; **wf**, wear facet; **wpo**, width across postzygapophyses; **wpr**, width across prezygapophyses; **Wn**, width notch.

Other abbreviations

AmAl, *Amphicoelias altus*; **AtIm**, *Atlantosaurus immanis*; **AuBo**, *Australodocus bohetii*; **C23-1**, state 1 of character 23; **CeSt**, *Cetiosauriscus stewarti*; **EI**, elongation index; **ew**, equal weighting **HaPr**, *Haplocanthosaurus priscus*; **HOS**, histological ontogenetic stage; **HQ**, Howe Quarry; **HScQ**, Howe-Scott Quarry; **HStQ**, Howe-Stephens Quarry; **iw**, implied weighting; **mdA**, more derived Apatosaurines; **mdD**, more derived Diplodocoidea; **mdE**, more derived Eusauropoda; **MOS**, morphological ontogenetic stage **OTU**, operational taxonomic unit; **PMI**, premaxilla-maxilla index; **RI**, robustness index; **SI**, slenderness index; **SHQ**, Spring Hill Quarry; **SuVi**, *Supersaurus vivianae*; **ToAf**, *Tornieria africana*.

Description of a new diplodocine species

Locality

The new specimen described in the following (SMA 0011) was found at the Howe-Scott quarry, one of three major sites on the Howe Ranch, north of Shell, Wyoming. The Howe-Scott quarry is located between the better known Howe Quarry (Brown, 1935; Ayer, 2000; Michelis, 2004; Tschopp and Mateus, 2013b) and the Howe-Stephens quarry (Ayer, 2000; Schwarz et al., 2007c; Christiansen and Tschopp, 2010; Fig. 1). The site was found in 1995 by a team from the Sauriermuseum Aathal, Switzerland, and excavated in three periods (1995, 2000, 2002-2003). Stratigraphically, it lies just slightly above the Howe-Stephens quarry, 30 meters above the J-5, and 30 meters below the K-1 unconformities, which define the lower and upper limits of the

PeerJ Reviewing Manuscript

Morrison Formation, respectively (Michelis, 2004; Fig. 2). In addition to SMA 0011, five partial diplodocid specimens (mostly appendicular material), a possible brachiosaur hindlimb, two partly-to-almost complete *Hesperosaurus* (Ornithischia, Stegosauria), some *Othnielosaurus* bones (Ornithischia, Neornithischia), numerous shed theropod teeth, carbonized wood, and various freshwater shells were recovered at the Howe-Scott quarry (Michelis, 2004; ET, pers. obs., 2003). However, none of these specimens has yet been formerly described or identified.

Material

SMA 0011. The specimen SMA 0011 consists of an almost complete, disarticulated skull, eleven cervical vertebrae (probably CV 1-6, 8, 9, 11, 12, and 15, see below), the complete dorsal column, including several dorsal and sternal ribs, a partial sacrum, the right scapula and coracoid, both humeri, the left ulna, radius and manus, the right ilium and pubis, a left ischium, femur, tibia, fibula and nearly complete pes. The specimen was found in two parts: 1) skull and vertebral column from the atlas to DV 3, and 2) dorsal vertebrae 4 to 10, sacrum, and appendicular elements (Fig. 4). It is interpreted to belong to a single individual due to matching size, no overlap of elements, and an extremely similar pattern of neurocentral closure in cervical and dorsal vertebrae (see below). The specimen SMA 0011 was excavated in 1995 and 2000.

Systematic Paleontology

Dinosauria Owen, 1842

Sauropoda Marsh, 1878

Eusauropoda Upchurch, 1995

Neosauropoda Bonaparte, 1986

Diplodocoidea Marsh, 1884 (see Upchurch, 1995)

Flagellicaudata Harris and Dodson, 2004

Diplodocidae Marsh, 1884

Diplodocinae Marsh, 1884

Galeamopus gen. nov.

Type species. *Galeamopus hayi* (Holland, 1924)

Diagnosis. *Galeamopus* is diagnosed by the following autapomorphies: portion of the parietal contributing to the skull roof is practically inexistent (unique among Flagellicaudata), a foramen in the notch that separates the two basal tubera (unique among Diplodocinae), well-developed anteromedial processes on the atlantal neurapophyses, which are distinct from the posterior wing (unique among Diplodocoidea), the posterior wing of atlantal neurapophyses remains of subequal

PeerJ Reviewing Manuscript

width along most of its length (unambiguous), and the axial prespinal lamina develops a transversely expanded, knob-like tuberosity at its anterior end (unambiguous).

Etymology. 'Galeam' means helmet, and 'opus' need, necessity in Latin, remembering and honoring the two 'Williams' intimately connected with the genoholotype specimen HMNS 175: William H. Utterback and William J. Holland. The English name 'William' derives from the German name 'Wilhelm', meaning “want helmet, protection”. Utterback found HMNS 175 in 1902 and Holland described its braincase in 1906, and named the holotype species *G. hayi* as *Diplodocus hayi* in 1924 – although already stating that the morphological differences between *G. hayi* and *Diplodocus* might prove to allow the erection of a new genus in future. *Galeamopus* is also an allusion to the fact that the fragile braincase is the only described part of the holotype skeleton to date. Last but not least, the referred specimen SMA 0011 was informally called “Max”, after the kid's story 'Max and Moritz' from the German writer Wilhelm Busch.



PeerJ Reviewing Manuscript

[redacted]

Comments. The holotype specimen SMA 0011 is housed at Sauriermuseum Aathal, Switzerland. This museum is open to the public, and director, vice-director, and staff, are allowing and even actively offering their specimens for various research purposes (see Schwarz et al., 2007; Klein and Sander, 2008; Christiansen and Tschopp 2010; Carballido et al. 2012a; Klein et al., 2012; Tschopp and Mateus, 2013a, 2013b). The excavations are very well documented, and the preparation of the material follows the latest scientific standards. For all his scientific and educational effort with the Sauriermuseum, its founder and present director Hans-Jakob Siber received the honorary doctor title of the University of Zurich (Switzerland) as well as the Amanz-Gressly Award of the Swiss Society of Paleontology in 2010. The museum recognizes the scientific importance of holotype specimens, and takes all efforts to preserve them and provide permanent public access. The policy is publicly stated on their homepage (http://www.sauriermuseum.ch/de/museum/wissenschaft/wissenschaft.html).
The specimen itself is currently being further prepared in order to mount it. In the display mount, particular attention will be payed to easy access for researchers.

Description of SMA 0011

Terminology. Anatomical terms are used following the traditional use of anterior and posterior instead of cranial and caudal. Vertebral laminae and fossae are described following the nomenclature of Wilson (1999) and Wilson et al. (2011), respectively, with the changes proposed by Tschopp and Mateus (2013b).

Skull (Figs 5-14; Tab. 4)

The skull of *Galeamopus* [redacted] SMA 0011 has a typically diplodocid shape. It is elongate, with the external nares retracted and dorsally facing, and slender, peg-like teeth (Figs 5-7). Given the completeness of the skull, a reconstruction was created in cooperation with the Portuguese illustrator Simão Mateus (ML; Fig. 8). When comparing with recent reconstructions of the skull of *Diplodocus* (Wilson and Sereno, 1998; Whitlock, 2011b), it can be seen that *Galeamopus* has a more triangular skull outline in lateral view, and more sinuous ventral maxillary edges in dorsal

PeerJ Reviewing Manuscript

view (Fig. 8).

Premaxilla. The premaxillae are completely preserved. They are anteroposteriorly long and transversely narrow elements that contact each other medially and the maxillae laterally. The posterior end of the premaxillae delimits the nasal opening anteriorly. In dorsal view, the elements are narrow in their central part and widen anteriorly and posteriorly. The anterior edge is straight to slightly convex, whereas the posterior margin is deeply concave, such that the two premaxillae together form a triangular process that enters the nasal opening. The medial margin is straight, and the lateral one concave due to the central narrowing of the element. Some nutrient foramina are present on the anterior-most portion of the dorsal surface, as is a groove originating at the premaxillary-maxillary contact, and extending obliquely anteromedially. The groove is faint and relatively short, not reaching either the anterior or the medial margin. Such a groove was usually interpreted as typical for dicraeosaurids (Remes, 2009; Whitlock, 2011a), but is also present in other diplodocids (ET, pers. obs., 2011). However, a fading out is uncommon in dicraeosaurids, where the groove is distinct (Janensch, 1935; Remes, 2009). Ventrally, the anterior portion of the premaxillae thickens slightly dorsoventrally in order to bear the replacement teeth, but not to the extent seen in USNM 2673 (ET, pers. obs., 2011). Five teeth are mounted, but only four alveoli are present in the left element, whereas the right premaxilla appears to show five. The alveoli of the articulated premaxillae do not contact each other medially, such that there would be space for two more teeth in between, or a gap. At the border with the maxilla, where the premaxilla narrows from the broader anterior part to the narrow central part, the two bones form an elongated fossa which bears the subnarial and the anterior maxillary foramen. Both foramina lie on the medial edge of the maxilla, very close together.

Maxilla. Only the right maxilla is preserved, and complete. The broad anterior portion bears a posterior process, which contacts the jugal and quadratojugal, and a posterodorsal process, which contacts the lacrimal, nasal, and possibly the prefrontal. The maxilla forms the dorsal, anterior, and anteroventral margins of the antorbital fenestra, and completely encloses the preantorbital fossa and fenestra. Unlike *Kaatedocus* and *Dicraeosaurus*, the preantorbital fossa is pierced by a large fenestra. The fenestra is dorsally capped by a distinct ridge similar to *Diplodocus*, but unlike *Apatosaurus*. This distinct dorsal edge was previously thought to represent an autapomorphy of *Diplodocus*, but was shown to be present in other taxa as well (Tschopp and Mateus, 2013b). The preantorbital fenestra does not fill the entire preantorbital fossa: the anterior-most area remains closed by a thin bony wall. The fossa is anterodorsally accompanied by a short, narrow groove more or less following the curvature of the anterior end of the dorsal

PeerJ Reviewing Manuscript

rim of the fossa. The posterior end of the fossa is interconnected with the central portion of the antorbital fenestra by a distinct groove that extends posterodorsally to the dorsal corner of the posterior process, which is regarded as an autapomorphy herein (Fig. 9). Remaining parts of the dorsal surface of the maxilla do not bear other distinctive morphological features, with the exception of the anterior-most portion, where a few nutrient foramina can be seen, similar to those present on the premaxilla.

Prefrontal. Both prefrontals are present and complete. They contact the frontals posteriorly, the nasals medially, the lacrimal laterally, and the maxilla anterolaterally. The prefrontals are short, anteroposteriorly convex elements. Their lateral margin is straight, the medial one with an anterior and a posterior concavity for the attachment of the nasal and the frontal, respectively. A sharply pointed, medially projecting process separates the two concavities. The posterior edge is anterolaterally-posteromedially oriented, forming a hook-like posteromedial process as is typical for Diplodocidae (Wilson, 2002; Whitlock, 2011a). The process almost reaches the frontal midlength, as is the case in diplodocine skulls CM 3452 and 11161 (ET, pers. obs., 2011). Anteriorly, the prefrontal tapers to a narrow tip, which is slightly dorsoventrally expanded. The left element bears a small nutrient foramen on the dorsal surface of the anterior part. The ventromedial edge is very distinct.

Frontal. Both frontals are completely preserved. They contact the prefrontal anterolaterally, the nasal anteromedially, the other frontal medially, the parietal posteromedially, and the postorbital posterolaterally. Ventrally, the frontal makes contact with the braincase, articulating with the orbitosphenoid. The frontals have a smooth dorsal surface, which is slightly convex posterolaterally-anteromedially. Their medial border is generally straight, but curves laterally at its posterior and anterior ends. Both a pineal fenestra (as in dicraeosaurids; width 14mm) and an anterior notch are thus present (as in *Kaatedocus*; length 18mm). The anterior notch is rather V-shaped than U-shaped as in *Kaatedocus*, and wider than in *Spinophorosaurus* (Knoll et al., 2012; Tschopp and Mateus, 2013b). The anterior margin of the frontal is strongly convex in order to accommodate the posterior, hook-like process of the prefrontal anterolaterally. From the posterior-most point of the posterior process of the prefrontal, the frontal has a straight edge extending obliquely anterolaterally, before it reaches the lateral edge, with which it includes a very acute angle. The lateral border is distinctly concave in dorsal view, smooth in its anterior part, but becoming highly rugose posteriorly, close to where it articulates with the postorbital. Posteriorly, the lateral and posterior edges form an acute angle. The lateral portion of the posterior margin is slightly displaced anteriorly, compared to the medial portion, resulting in a

PeerJ Reviewing Manuscript

somewhat sinuous posterior edge. Ventrally, the frontals are marked by a distinct ridge, extending obliquely from the anterolateral corner, below the posterior process of the prefrontal, to an elevated, broad area for the attachment of the braincase.

Postorbital. Both elements are complete. The postorbital is a triradiate bone with an anterior process articulating with the jugal, a posterior process overlapping the squamosal laterally, and a dorsomedial process covering the frontal posteriorly and connecting to the anterolateral process of the parietal posteromedially, thereby excluding the frontal from the margin of the supratemporal fenestra. Anteromedially, the dorsomedial process abuts the antotic process of the braincase. The anterior process has a subtriangular cross section, long dorsally and ventrally, with a narrow lateral and an even thinner medial margin. The anterior process is dorsally slightly concave. Towards anterior, it tapers to a point. The posterior process is short and triangular. At its base, one (on the right postorbital) or two (on the left element) nutrient foramina can be seen. The process is compressed transversely. The dorsomedial process is dorsoventrally concave anteriorly and convex posteriorly. It is relatively high dorsoventrally, but narrow anteroposteriorly. It is anteroposteriorly broader laterally than medially. The anterior face of the dorsomedial process is marked by a horizontal ridge at its base. The ridge supports the posterior edge of the frontal.

Jugal. Both jugals are preserved and complete. The jugal is a flat, relatively large bone with a posterior process contacting the postorbital, and a dorsal process articulating with the lacrimal. The main portion connects to the quadratojugal ventrally and the maxilla anteriorly. The jugal forms the anteroventral rim of the orbit, the posteroventral border of the antorbital fenestra, as well as the anterodorsal edge of the laterotemporal fenestra. The bases of the dorsal and posterior processes are relatively broad, before they taper dorsally and posteriorly, respectively. The anterior edge of the jugal is slightly concave, as is the anteroventral margin. Therefore, these two edges include an acute angle.

Quadratojugal. The quadratojugals are both complete. They are transversely thin bones with a posterior dorsal process overlying the quadrate laterally, and a long anterior ramus contacting the jugal dorsally and the maxilla anteriorly. The quadratojugals form the anteroventral margins of the laterotemporal fenestra, and the ventral border of the skull. The anterior ramus of the quadratojugal is narrow at its base but extends dorsoventrally towards its anterior end. The ventral edge is almost straight; it is thus the concave dorsal margin of the anterior ramus that accounts mostly for this dorsoventral expansion. The shape of the anterior margin is not discernible in the mounted skull. The dorsal process is less than half the length of the anterior process. It is inclined posterodorsally, as in all diplodocids (Upchurch, 1998; Wilson, 2002;

PeerJ Reviewing Manuscript

Whitlock, 2011a). It is anteroposteriorly convex externally, relatively broad at its base, and tapers to a point dorsally, reaching about midlength of the quadrate shaft.

Lacrimal. Only the dorsal half of the left lacrimal is present. It is a narrow element expanding towards its dorsal end, where it contacts the posterodorsal process of the maxilla anteriorly, the prefrontal dorsally, and possibly the nasal medially. Ventrally, the lacrimal would contact the jugal, if preserved. The lacrimal is the element separating the orbit from the antorbital fenestra. It is anteroposteriorly narrow in its ventral half, with a triangular cross section, being flat externally but bearing a distinct dorsoventral ridge internally. The anterior edge develops a short, but dorsoventrally high, anterior process at its dorsal end. The posterior margin is generally straight, with only a weak bulge on its dorsal portion. The dorsal-most end curves backwards, below the prefrontal. The internal ridge becomes slightly higher dorsally, posteriorly enclosing the lacrimal foramen, which is small and shallow in SMA 0011.

Quadrate. Only the right quadrate is preserved, but it is complete. It has a complex anatomy, with a quadrate shaft articulating with the squamosal and the paroccipital process posterodorsally and posteroventrally, respectively; a pterygoid flange interconnecting the outer skull with the pterygoid medially; and a ventral ramus being overlapped by the quadratojugal externally and bearing the articulating surface with the lower jaw ventrally. The quadrate shaft is elongate posteriorly, and has concave dorsal and lateroventral surfaces. The lateral edge is a thin crest, where it is not capped by the squamosal or the quadratojugal. The posterior surface of the quadrate shaft and the ventral ramus is shallowly concave, forming the quadrate fossa. The pterygoid flange originates on the medial half of the quadrate shaft. It is very thin mediolaterally, but anteroposteriorly long, and curves medially at its dorsal tip. The dorsal edge of the flange is straight and more or less horizontally oriented. The medial side of the pterygoid flange is concave, but does not form such a distinct fossa like that which is present autapomorphically in *Kaatedocus* (Tschopp and Mateus, 2013b). The ventral ramus is subtriangular in cross-section, with concave anterior and posterolateral surfaces. It has a thinner lateral than medial margin. The articular surface is subtriangular, with a concave anterior border, and a pointed posterior corner. The entire ventral ramus of the quadrate of SMA 0011 is posterodorsally inclined, as in all diplodocids (Upchurch, 1998; Wilson, 2002; Whitlock, 2011a).

Squamosal. Both squamosals are preserved, but lack a part of their anterior process (the right one more so than the left). The squamosals form the posteroventral corner of the skull. They have a complicated morphology, having to accommodate a variety of elements from the braincase and outer skull. The anterior process overlies the posterior end of the quadrate. Dorsally, the

PeerJ Reviewing Manuscript

squamosal is laterally covered by the posterior process of the postorbital, and forms the external margin of the supratemporal fenestra. Posteriorly it contacts the paroccipital processes, and dorsoposteriorly the posterolateral process of the parietal. The squamosal is strongly curved posterolaterally. The anterior process appears to be the longest of all squamosal processes, even though it is not preserved in its entire length. The ventral edge of the squamosal develops a short ventral projection at its posterior end, similar to, but much less distinct than the ventral prong as present in advanced dicraeosaurids (Salgado and Calvo, 1992; Whitlock, 2011a). A concave area appears to be present on the laterodorsal surface, in order to accommodate the posterior process of the postorbital. Other morphological features are difficult to observe in the articulated and reconstructed skull of SMA 0011.

Parietal. Both parietals are complete but slightly distorted. They are tightly sutured with the frontals anteriorly, and develop a short anterolateral process to contact the dorsomedial process of the postorbital, with which they form the anterior margin of the supratemporal fenestra. The posterior face of the parietal contacts the exoccipital and the supraoccipital medioventrally. The posterolateral process of the parietal forms the posterior margin of the supratemporal fenestra and reaches the squamosal laterally. The dorsal portion of the parietal in SMA 0011 is very narrow. The two elements do not touch each other medially, but this appears to be due to postmortem breakage of the extremely thin bone behind the parietal fenestra, which the parietals form together with the frontals. The dorsal portion is flat, and not well separated from the posterior surface by a ridge like that present in *Kaatedocus*. It widens anteroposteriorly at its lateral end, where it develops a short anterolateral and a long and dorsoventrally deep posteroventral process. The parietal thus contributes most to the margin of the supratemporal fenestra. The posterior surface has an oblique ventromedial border, which has a very sinuous suture together with the supraoccipital. The dorsal margin of the posterolateral process is straight as well, and does not cover the anterior border of the supratemporal fenestra in posterior view. Their ventral edges are excluded from the posttemporal fenestra by the squamosal and a laterally projecting spur of the exoccipital.

Supraoccipital. The supraoccipital is complete, and fused with the parietals and the exoccipital-opisthotic complex. It is a somewhat hexagonal bone, that contacts the parietals dorsolaterally, the exoccipital-opisthotic complex ventrolaterally, and borders the foramen magnum ventrally. The supraoccipital is fused with the exoccipital-opisthotic, and the suture is barely visible. The dorsolateral edges of the supraoccipital are slightly concave. The ventrolateral edges are only laterally indicated. More medially, the suture is not traceable up to the foramen magnum, but

PeerJ Reviewing Manuscript

probably extended below the two distinct tubercles located dorsolaterally to the foramen magnum. These tubercles served for the attachment of the proatlases. The tubercles are ellipsoid, and oriented with their long axes extending dorsomedially-ventrolaterally. The elevation is much more distinct ventrally than dorsally. The dorsal portion of the supraoccipital bears a complex arrangement of ridges and concavities, as if it would lack an additional element topping this structure. No distinct sagittal ridge is present, but if an element is lacking, it could be this element that forms the crest (Fig. 10). However, it has never been reported that the sagittal nuchal crest derives from an additional skull element. This would thus be highly unusual and possibly autapomorphic. The supraoccipital is widest slightly more ventrally than dorsally. No distinct foramina are present close to the border with the parietal, unlike in *Kaatedocus* (Tschopp and Mateus, 2013b). The dorsolateral edges of the supraoccipital are straight, not concave as in *Apatosaurus* CM 11162, or MB.R.2388, where it forms a distinct dorsal elevation (Berman and McIntosh, 1978; Remes, 2009).

Exoccipital-opisthotic complex. This outer portion of the braincase is completely preserved. No sutures can be seen between the exoccipital and the opisthotic. They bear two elongate paroccipital processes that extend lateroventrally to articulate with the squamosal and the posterior end of the quadrate. Ventrally, the exoccipital-opisthotic borders almost the entire the foramen magnum except for a small dorsal contribution of the supraoccipital. The exoccipital contributes the dorsolateral corners to the occipital condyle. As in *Suuwassea* and *Diplodocus* CM 11161, the exoccipital almost excludes the basioccipital from the participation in the dorsal surface of the occipital condyle (Harris, 2006a). The paroccipital processes have slightly convex external surfaces, but do not bear a ridge as in *Kaatedocus* (Tschopp and Mateus, 2013b). The ventral edge is straight, only the dorsal corner of the distal end is expanded dorsally, resulting in a distinctly concave dorsal edge. The lateral margin of the paroccipital process is subtriangular, with a longer, vertically oriented dorsal portion, and a shorter, laterally inclined ventral part. In lateral view, it is straight, unlike the curved ends of *Suuwassea* (Harris, 2006a; ANS 21122, ET, pers. obs., 2011).

Basioccipital and basisphenoid. The basioccipital forms the main portion of the occipital condyle. It is relatively short and connects the articular surface of the occipital condyle with the basal tubera, which are of about the same width. The articular surface is offset from the condylar neck. Narrow ridges connect the central part of the condylar neck with the posteromedial corner of the basal tubera, and the lateral face with the posterolateral corner. The posterior surface of the basal tubera is therefore concave, as are the lateral surfaces of the basioccipital. The basal tubera

PeerJ Reviewing Manuscript

PeerJ Reviewing Manuscript

are box-like, and separated by a distinct, but relatively narrow notch. The ventral edges of the tubera form a nearly straight line in posterior view, whereas the anterior edges are angled in a wide V-shaped manner in ventral view. Anteriorly, the basipterygoid processes attach to the tubera. In the reconstructed skull, they are mounted slightly dorsal to their actual location, above the anteroventral end of the crista prootica. When articulated properly, they would be elongate (5.3 times longer than wide) and straight, and would also include a narrower angle than as mounted. This is important as shorter and more widely diverging basipterygoid processes are typical for *Apatosaurus*, whereas narrower angles are present in *Diplodocus* (Berman and McIntosh, 1978). The processes are not as well connected at their base as is the case in *Kaatedocus* (Tschopp and Mateus, 2013b). The distal ends of the basipterygoid processes are expanded.

Orbitosphenoid. The orbitosphenoids delimit the endocranial cavity anteriorly, and attach to the frontals and parietals dorsally, themselves medially, and the laterosphenoids lateroventrally. Each orbitosphenoid is relatively wide dorsally and develops an anteroventral process, which is expanded at its end and separates the two openings for cranial nerves II medially (the optic foramen) and III laterally (the trigeminal foramen; Janensch, 1935; Harris, 2006a; Balanoff et al., 2010). Other than in *Suuwassea* (Harris, 2006a), the optic foramen is bridged over by bone medially. Anterodorsally, the two orbitosphenoids form the olfactory fenestra together with the frontals (Janensch, 1935; Balanoff et al., 2010), and posterolaterally, at the junction with the laterosphenoid, the foramen for cranial nerve IV (the trochlear foramen; Balanoff et al., 2010) defines the outline of the orbitosphenoid.

Laterosphenoid. The laterosphenoid mainly consists of a crest that develops the antotic process posterodorsally and extends anteroventrally to join the crista prootica. It connects to the parietal posteriorly, the orbitosphenoid anterodorsally, and the prootic posteroventrally. As the orbitosphenoid, also the laterosphenoid outline is defined by various openings: the cranial nerves III and IV anterodorsally at the junction with the orbitosphenoid, the facial foramen posterodorsally (cranial nerve V; Balanoff et al., 2010), as well as the oculomotor foramen and the abducens foramen anteroventrally (Balanoff et al., 2010).

Prootic. The prootic lies between the laterosphenoid anterodorsally, the parietal and paroccipital processes posterodorsally, and the basisphenoid anteroventrally. It bears the well-developed crista prootica, which extends relatively far laterally, but is very thin dorsoventrally. It does not end in an additional transverse expansion anteriorly, as is typical for dicraeosaurids (Janensch, 1935). Posteriorly, the crista prootica extends to the base of the paroccipital processes, where it separates

foramina IX to XI from XII (Janensch, 1935; Harris, 2006a).

Pterygoid. The left pterygoid is preserved, but is only partly prepared (Fig. 11). The pterygoid connects the quadrate posterolaterally with the basipterygoid processes posteromedially, the ectopterygoid and palatine anterolaterally, and the vomer anteromedially. The two elements would join along the midline of the skull. The pterygoid of SMA 0011 resembles the same bone in CM 3452 in its dorsoventrally deeper shape compared to *Camarasaurus* and *Giraffatitan* (McIntosh and Berman, 1975). It bears a shallow articulation facet for the basipterygoid processes, without a hook-like process as present in dicraeosaurids and *Camarasaurus* (Wilson, 2002; Whitlock, 2011a).

Hyoid. Only the right hyoid is preserved, but appears to be almost complete (Fig. 12). It is a narrow bone, with a distinct upward curve at midlength. The anterior ramus becomes transversely flattened towards its anterior end, which bears a shallow longitudinal groove on the medial side. The hyoid slightly widens dorsoventrally where it curves upwards and towards the squamosal, as was shown in *Tapuiasaurus* (Zaher et al., 2011). The posterodorsal end is rounded and offset from the shaft by a distinct rim.

Mandible

Dentary. Both dentaries are preserved. The dentary is the anterior-most bone of the lower jaw and the only one bearing teeth. Posteriorly, it is followed by the surangular dorsally and the angular ventrally. Internally, it is overlain by the splenial ventrally. The dentary is a thin bone with a dorsoventrally high dentigerous portion, developing the typical 'chin' of flagellicaudatans (Upchurch, 1998; Whitlock, 2011a). Posterior to the tooth bearing portion, the dentary tapers dorsoventrally, the right one much more so than the left. The symphysis is oblong and strongly anteriorly inclined.

Surangular. Both surangulars are present. This bone is very flat transversely, curves ventrally at its posterior end and bears a foramen at its highest point, which is also the highest point of the entire lower jaw. The jaw thus does not develop a coronoid eminence.

Angular. Both angulars are preserved but incomplete anteriorly. They are concave externally, due to the laterally curving ventral edge. They taper relatively continuously anteriorly, but abruptly at their posterior ends, where they expand transversely in order to accommodate the articular, which is not preserved.

?Prearticular. Both prearticulars appear to be present, but are partly hidden in the mount or only partially prepared (Fig. 13). They are very thin, elongate bones that taper posteriorly. A very shallow groove marks the probable lingual surface, extending anteroposteriorly, following the

PeerJ Reviewing Manuscript

somewhat sinuous curve of the dorsal edge of the bone. In its anterior half, the bone becomes slightly thicker and curves outwards.

Teeth. The teeth have the typical diplodocoid, peg-like shape (Fig. 14). They are slightly wrinkled but do not have denticles. Worn teeth usually have one single wear facet at a low angle to the long axis of the tooth, but some teeth also show two facets that are conjoined medially. In these teeth, the lingual facet is more steeply inclined than the labial one. The crown tips are slightly wider than deep, which is especially well visible in replacement and/or unworn teeth, which have a very weakly spatulate upper-most crown. The enamel is distributed evenly on all sides, and no grooves mark the lingual face. In the jaws, the teeth are inclined anteriorly compared to the long axis of the jaw, and set side-by-side without overlapping each other. There are at least eleven, possibly twelve, dentary teeth.

Cervical vertebrae (Figs 15-22; Tab. 5)

Proatlas. The right proatlas is preserved and complete (Fig. 15). It is strongly curved and tapers distally. The proximal articular surface is ovoid, with the largest width located in the dorsal half. The medial surface is concave, the lateral one convex. The proatlas of SMA 0011 is different from the element in *Kaatedocus* due to its much narrower distal tip.

Atlas. The atlantal centrum is not fused to the neurapophyses (Fig. 16). It has a well-developed anteroventral process as is typical for diplodocids, but convergently present in several other sauropods (Mannion, 2011; Whitlock, 2011a). A large foramen lies between the posterior knobs of the intercentrum. The lateral surface of the centrum is concave and bears a foramen as well. The neurapophyses have a relatively wide base, and turn upwards and backwards to articulate with the prezygapophyses of the axis. A wide medial process develops anteriorly, as in AMNH 969 (Holland, 1906). This process articulates with the proatlas, and is much better developed than in *Diplodocus carnegii* CM 84 or *Kaatedocus* (Hatcher, 1901; Tschopp and Mateus, 2013b). A small but distinct subtriangular process is present on the opposite side of the medial process, projecting laterally.

Axis. The axis of SMA 0011 (Fig. 16A) has a closed but still slightly visible neurocentral synostosis, and separate cervical ribs. The centrum is opisthocoelous. The pleurocoel extends over almost the entire centrum, with short horizontal ridges at its anterior and posterior end. No vertical subdivision of the pleurocoel is present. Anteriorly, the pleurocoel extends onto the parapophysis. The ventral surface of the centrum bears a distinct longitudinal keel in its posterior portion. The parapophysis is rounded, and faces anterolaterally and slightly ventrally. The neural arch is high and weakly posteriorly inclined. The prezygapophyses are not preserved. The only

PeerJ Reviewing Manuscript

well-defined lamina is the podl. The prsl is slightly expanded transversely at its anterior end, similar to, but not as distinct as in AMNH 969 (ET, pers. obs., 2011). The diapophysis projects somewhat posteriorly, but does not bear a distinct posterior process. In lateral view, the anterior edge of the neural spine is slightly concave at its base, and straight in the upper part. The spine top is rugose, slightly expanded transversely, and entirely restricted anterior to the postzygapophyseal facets. This anterior restriction is unusual for sauropods, but present in *Diplodocus carnegii* CM 84 (Hatcher, 1901), and could thus represent a diplodocine synapomorphy. Other than in CM 84, however, the neural spine summit of SMA 0011 develops a posterior projection, similar to *Giraffatitan* (Janensch, 1950). The spol is strongly concave, becoming vertical on the upper part. Small epipophyses are present laterally above the postzygapophyses, which do not project backwards. A large rugose area is present on the lateral side of spine, slightly above mid-height. It is of subtriangular shape, broader towards the spol, and with a pointed, elongate tip towards the center of the sdf. This rugosity could be homologous to the distal lateral expansion in the axis of *Camarasaurus* or *Suuwassea* (Madsen et al., 1995; Harris, 2006b), just that the neural spine top is much more elevated in SMA 0011. Such a rugosity appears to be absent in the element of *Diplodocus carnegii* (Hatcher, 1901). The postzygapophyses of the axis of SMA 0011 slightly overhang the centrum posteriorly, and bear subtriangular facets with a straight border anteriorly.

Postaxial cervical vertebrae. Eleven cervical vertebrae are present. They were found in four blocks, with CV 1-6 constituting the first one (Figs 16, 17), CV 8 and 9 the second (Fig. 18), CV 11 and 12 the third set (Fig. 19), and CV 15 (Fig. 20) was recovered articulated with the first three dorsal vertebrae. The interpretation of the gaps is mainly based on the position of the bones in the quarry, and on the fact that diplodocid cervical series are generally considered to comprise 15 vertebrae (Hatcher, 1901; Gilmore, 1936; Upchurch, 1998; Wilson, 2002; Whitlock, 2011a). However, since only two nearly complete, and largely articulated diplodocid necks have been reported to date (*Diplodocus carnegii* CM 84, lacking the atlas, Hatcher, 1901; *Apatosaurus louisae* CM 3018, Gilmore, 1936), this count may also have been different in diplodocid genera other than *Apatosaurus* or *Diplodocus*. A more detailed study of the morphological changes within the cervical column will be needed to show if the present assignment is correct, but is out of the scope of this description. For a phylogenetic assessment of the specimen, it is sufficient to order the single vertebrae in anterior, mid-, and posterior cervical vertebrae, which is perfectly possible in the present case.

The cervical centra are all opisthocoelous and relatively elongate. As is typical for nearly all

PeerJ Reviewing Manuscript

sauropods, the most elongated elements are the mid-cervical vertebrae. All cervical centra have well-developed pleurocoels extending over the entire length of the centrum, and also invading the dorsal surfaces of the parapophyses. The internal structure of the pleurocoel varies along the column: the anterior and posterior horizontal ridges described in the axis disappear by CV 4, and a vertical subdivision in anterior and posterior pneumatic fossae becomes visible in CV 3, and is pronounced from CV 5 backwards. The subdividing ridge is oriented anterodorsally-posteroventrally, as in *Kaatedocus* (Tschopp and Mateus, 2013b). The posterior pneumatic fossae of CV 5 and 6 bear a large, slightly ellipsoid foramen at their anterior end, and become pointed posteriorly, due to the development of a shallow posteroventral fossa, which diagnoses most Diplodocinae (except *Kaatedocus*; Tschopp and Mateus, 2013b). From CV 6 backwards, the anterior pneumatic fossa becomes subdivided by a horizontal ridge at about mid-height. The ventral portion of the anterior fossa becomes vertically divided in CV 11. The latter is also the first element in the series to show a separation of the posterior-most portion of the posterior pneumatic fossa. In addition, CV 12 also has a horizontally subdivided posteroventral fossa. In CV 15, the pleurocoel becomes less complex again.

In CV 15, the anterior condyle is damaged, so that it reveals the internal structure. The condyle is composed of large internal cavities, surrounded by 2-4 mm thick, relatively dense bony struts. The arrangement appears symmetric, with a subtriangular cavity dorsomedially, and two subcircular cavities following both medially and laterally.

The parapophyses become slightly anteroposteriorly elongate in CV 3 and 4. They project ventrolaterally in all elements, and are interconnected with the anterior condyle through a transversely wide, somewhat rugose area. The fossa on its dorsal surface is subdivided by a short, oblique ridge from CV 6 backwards. In CV 11 and 12, the parapophysis is subtriangular, being long anteroposteriorly, and wider posteriorly than anteriorly.

The ventral surface is hourglass-shaped and relatively narrow in anterior and mid-cervical vertebrae, but becomes relatively wide posteriorly. In anterior cervical vertebrae, it bears a distinct longitudinal keel on its anterior half, with well visible pneumatic foramina lateral to it in CV3, but less so in more posterior elements. In CV 3, a shallow ventral ridge is also present on the posterior end, but already in CV 4 this ridge cannot be seen anymore. The ventral surfaces of CV 5 and more posterior vertebrae are concave without any traces of ridges or pneumatic foramina. Posteriorly, they are bordered by distinct posteroventral flanges, which is a synapomorphy of Diplodocinae, according to Tschopp and Mateus (2013b). These flanges become rugose ventrally in CV 15.

PeerJ Reviewing Manuscript

None of the centra are fused with the corresponding cervical ribs. The neurocentral synostosis is closed but visible in the anterior and posterior cervical vertebrae, whereas in posterior mid-cervical vertebrae it is completely open. Where it is closed, the zigzagging neurocentral synostosis is better visible anteriorly than posteriorly (Fig. 21). In the most anterior and posterior elements, the synostosis becomes extremely faint to completely obliterated posteriorly. It lies on top of the centrum, such that the entire pedicels of the neural arches are detached in the unfused elements. The synostosis line is highest in the anterior half and descends anteriorly and posteriorly.

The neural arch is high in anterior cervical vertebrae, but becomes lower posteriorly. In all elements, it appears very fragile and slender, with very thin but distinct lamination. In posterior cervical vertebrae, the neural arch is somewhat displaced anteriorly, reaching close to the anterior condyle, but being well distant from the posterior edge of the centrum. The displacement reaches its maximum in CV 15.

The prezygapophyses project anteriorly and slightly dorsally in most elements. Close to the cervico-dorsal transition, they become more elevated. They bear suboval facets in CV 3, with the long axis extending anteroposteriorly. From CV 4 onwards, the facets become subtriangular, with the tip located medially. The facets are convex as in all diplodocines (McIntosh, 1990b; Wilson, 2002; Whitlock, 2011a). Only in CV 5 are they concave, but this appears to be due to taphonomic distortion. In CV 8 and 9, the articular facets are elevated on pedestals, but no transverse sulcus is present posteriorly, unlike in *Kaatedocus* (Tschopp and Mateus, 2013b). The prezygapophyses cap the prcdf dorsally, which in CV 5 and 6 is subdivided by a vertical accessory lamina connecting acdl and prdl right at the diapophysis. Anteriorly, the prezygapophyses are ventrally supported by the cprl, which is single in anterior cervical vertebrae. From CV 8 backwards, the cprl is divided, with one distinct and few short, weak accessory lamina in the prcdf. The accessory laminae subdividing the prcdf become stronger in more posterior elements. Weak pre-epipophyses mark the lateral surface anteriorly in CV 4 and more posterior elements. Only in CV 10 do they extend anterior to the prezygapophyseal facet. This is in contrast to *Kaatedocus*, where the majority of mid- and posterior cervical vertebrae bear anteriorly projecting pre-epipophyses (Tschopp and Mateus, 2013b). Posteriorly on the prezygapophyseal process, the anterior portion of the sdf develops a deep, but not well defined fossa in CV 3.

The sprl is distinct on the prezygapophyseal process, disappears around midlength of the dorsal portion, and becomes visible again on the spine top in anterior cervical vertebrae. In mid-cervical vertebrae, the sprl is weak to almost absent on the prezygapophyseal process, as is typical for

PeerJ Reviewing Manuscript

Diplodocinae (Tschopp and Mateus, 2013b). In posterior cervical vertebrae, the sprl is again better developed. Due to a backwards curve of the spine top in anterior cervical vertebrae, the sprl has a somewhat sinuous appearance in lateral view in these elements. Below the backwards curve, the sprl extends almost vertically in CV 3 to 5, but becomes posteriorly inclined in more posterior vertebrae. A prsl is present at the base of neural arch in unbifurcated spines, which reach back to CV 8, as in *Barosaurus* (McIntosh, 2005).

The diapophysis is entirely located in the anterior half of the vertebra. It is supported by distinct acdl, prdl, podl, and pcdl. The acdl and prdl are separated along their entire length, a feature typical for *Apatosaurus*, and usually absent in diplodocines. The pcdl is almost horizontal, and the podl steeply inclined in CV 3, but in CV 4 and more posterior elements, they approach each other, forming a more acute angle anteriorly. In anterior elements, the podl and pcdl unite before curving laterally, but more posteriorly they remain separate as the acdl and prdl, and the pocdf is therefore extended onto the posterior surface of the diapophysis. They do not form such distinct posterior processes such as those present in *Kaatedocus* (Tschopp and Mateus, 2013b). The pcdl bifurcates anteriorly in the mid-cervical vertebrae, whereas in more posterior elements two parallel pcdl are present. This sheds new light on serial variation of these characters, as they are used to distinguish different species in some cases (e.g. *Apatosaurus parvus* or *Australodocus bohetii*; Upchurch et al., 2004b; Remes, 2007). However, since in the majority of cases (*Apatosaurus parvus* UW 15556, or *Barosaurus lentus* AMNH 6341 and YPM 429; Gilmore, 1936; Upchurch et al., 2004b; ET, pers. obs., 2011) only one of these states is present, they are still considered as taxonomically informative. The cdf lies directly ventral to the diapophyseal process. In CV 15 of SMA 0011, a short but stout accessory lamina is present in the posterior portion of the fossa. In mid- and posterior vertebrae of SMA 0011, an accessory lamina is present between the pcdl and podl, facing posteriorly. In CV 12, there is even a second vertical accessory lamina subdividing the pocdf. Dorsomedial to the accessory lamina, the pocdf is pierced by a large foramen, such that the pocdf is interconnected with the spof. A similar state appears to be present in the anterior cervical vertebrae of *Dicraeosaurus* MB.R.4886 (ET, pers. obs., 2011), a partial mid-cervical vertebra of *Suuwassea* ANS 21122 (Harris, 2006b: fig. 8B), and *Eobrontosaurus* Tate-001, but in these taxa, the borders of the opening seem to be broken (ET, pers. obs.). Fossae at the same location are present in many taxa, including *Diplodocus* or *Supersaurus* (Hatcher, 1901; ET, pers. obs., 2013), but none of them opens up into a large foramen as in SMA 0011 (Fig. 22).

The sdf is of generally simple morphology. In CV 5 and 6, a shallow but dorsally well offset

PeerJ Reviewing Manuscript

fossa is located close to the spine summit. In CV 6 and 8, the sdf bears a distinct, dorsoventrally elongate fossa posterolateral to the sprl, at about mid-height of the metapophysis. From CV 8 backwards, a vertical accessory lamina follows the sprl posteriorly, as in *Diplodocus carnegii* CM 84 (Hatcher, 1901). No subfossae are present in the sdf of posterior cervical vertebrae, but in CV 15, the sdf becomes clearly delimited dorsally, just below the anteroposterior narrowing of the spine top.

The neural spine undergoes distinct changes in development and orientation from anterior to posterior. In anterior cervical vertebrae, it is vertical, and dorsoventrally elongate, reaching well above the postzygapophyses. The axis, as well as CV 3 and 4 have a distinctly posteriorly turning spine summit, as can also be seen in the corresponding elements of *Eobrontosaurus*. There is an abrupt change in height from CV 5 to 6, resulting in a smaller total height of CV 6 compared to CV 5. Such a development has only been described in *Dicraeosaurus* (Janensch, 1929a), but neural spines are often incomplete, where anterior cervical vertebrae have been found (e.g. *Diplodocus carnegii* CM 84, *Apatosaurus louisae* CM 3018; Hatcher, 1901; Gilmore, 1936), which makes a thorough assessment of this character difficult. However, SMA 0011 is clearly different from the state in *Kaatedocus siberi* SMA 0004, as well as the indeterminate diplodocines AMNH 7530, 7535, and CM 3452, where the anterior cervical neural spines are low, and total vertebral height continuously increases throughout the vertebral column (Tschopp and Mateus, 2013b; ET, pers. obs., 2011). From CV 6 backwards, the cervical neural spines of SMA 0011 decrease in relative length, compared to pedicel height, but remain vertical. Towards the cervico-dorsal transition, neural spine height increases again, such that CV 15 has a highly elevated spine summit. In this vertebra, the spine summit is also strongly anteriorly inclined. The distal-most part of the neural spine of CV 15 is anteroposteriorly short but elongated dorsoventrally. Bifurcation of the spine is present, but only from CV 9 backwards, as is the case in *Barosaurus* AMNH 6341 (McIntosh, 2005). Unbifurcated neural spines slightly expand transversely towards their distal end, similar to the state in *Suuwassea emilieae* (Harris, 2006b). Posteriorly, the spol are thin but project far posterodorsally, and connect to each other across the spine summit. Therefore, they enclose a distinct and deep spof. Elements with bifid neural spines have a median tubercle. The lateral surface of the neural spine summits becomes rugose in posterior vertebrae.

Following the changing orientation and elevation of the spine, the spol also has a quite variable morphology from anterior to posterior cervical vertebrae: it is strongly concave in CV 3, and less so in CV 4, due to the more expressed backwards leaning of the spine top in CV 3. The spol is

PeerJ Reviewing Manuscript

gently curved in CV 5, but forms a 90° angle in CV 6. Due to the low spine top, the spol is almost horizontal in CV 8 to 12. In CV 15, it becomes concave again, but remains almost horizontal posteriorly, where it unites with the epipophysis. The latter is well developed in all cervical vertebrae, often overhanging the postzygapophyses. It constitutes the posterior end of the spol, and is often pointed. The postzygapophyseal facets are suboval to subcircular in the anterior cervical vertebrae, but become subtriangular more posteriorly, with the tip pointing medially. They are concave and thus face both downwards and outwards. They are ventrally supported by a vertical, single cpol.

Dorsal vertebrae (Figs 23-28; Tab. 6)

Dorsal vertebrae 1 and 2. The first two dorsal vertebrae are still embedded in matrix, and only the right sides are prepared (Figs 23, 24). The diapophysis is not preserved in either vertebra, and DV 2 also lacks the right metapophysis and postzygapophysis. The anterodorsal part of the right lateral surface of the centrum of DV 2 is reconstructed, including the neurocentral synostosis. The dorsal vertebrae 1 and 2 more closely resemble the cervical vertebrae than more posterior elements of the dorsal sequence. Compared to the last cervical vertebra, DV 1 and 2 have a considerably deeper diapophysis, and less distinct epipophyses. Their centra are opisthocoelous, and have an intermediate elongation compared to the last cervical and DV 3. The lateral surface is marked by elongate pleurocoels that occupy the central and anterior portion of the centrum. In DV 2, the pleurocoel is more restricted towards the anterior than in DV 1, being almost entirely situated above the parapophysis. The parapophysis lies anteroventral to the pleurocoels, which extend onto its dorsal face. Posteroventral flanges are present, but become less distinct in DV 2. The ventral surface is concave and broad, with a shallow longitudinal ridge located anteriorly. The neural arch height is more or less equal to centrum length, not counting the condyle. As in anterior and posterior cervical vertebrae, the neurocentral synostosis is closed, but still visible in its anterior half. The neural spine is divided. The prezygapophysis is broad, and projects slightly anterior to the condyle in both vertebrae, although it is more vertically oriented in DV 2. A weak pre-epipophysis is present, but does not extend beyond the prezygapophyseal facet. The sprl is strongly concave, due to the strong anterior inclination of the spine top. The prdl does not contact the acdl directly, but they are interconnected by a vertical lamina below the diapophysis. The latter is thus slightly elevated above the centrum, and dorsoventrally high. The broken diapophysis of DV 2 reveals large open spaces that are surrounded by narrow laminae of relatively dense bone tissue. Both the acdl and the pcdl are only slightly inclined. The pocdf is subdivided by a strong, laterally facing, almost vertical accessory lamina, forming a

PeerJ Reviewing Manuscript

PeerJ Reviewing Manuscript

posteroventral branch of the podl. This differs from the posterior cervical vertebrae, where the accessory lamina in the pocdf faces posteriorly. Unlike the mid- and posterior cervical vertebrae, DV 1 and 2 do not have any fenestra connecting the pocdf with the spof. The spine summit is anteroposteriorly narrow, and inclined anteriorly, but the inclination decreases in DV 2 and more posterior elements. The lateral surface of the spine is marked by the sdf, which is well delimited dorsally, similar to the state in CV 15. From the top of the sdf, the spine of DV 1 and 2 forms a narrow anterodorsal projection. The medial surface of the spine (visible in DV 2) is slightly convex and smooth, unlike the subtriangular shape present in most apatosaurs (e.g. NSMT-PV 20375; Upchurch et al., 2004b).

Dorsal vertebrae 3 and 4. Both elements are broken and deformed such that it is difficult to understand their morphology in detail (Figs 25, 26). Dorsal vertebra 3 lacks the right diapophysis and neural spine, such that the internal surface of the left spine is visible in the mount. The dorsal portion of the centrum and ventral half of the neural arch are crushed, and various pieces of each became intermingled. Dorsal vertebra 4 preserves a very deformed centrum, mounted in anteroventral view, which is not fused with the neural arch. A part of the neural arch is preserved intermingled with the fractured pieces of DV 3.

The dorsal vertebrae from DV 3 towards the sacrum are considerably shorter than DV 1 and 2, but remain of about the same length (not considering the condyle). DV 3 has a strongly opisthocoelous centrum, whereas DV 4 is only slightly opisthocoelous. A distinct pleurocoel is present on the anterodorsal corner of the lateral side. It is shorter than in DV 1 or 2. The position of the parapophysis is difficult to see, but appears to be still on the centrum, above the pleurocoel in DV 3, whereas the centrum of DV 4 does not show any traces of a parapophysis. The ventral side of DV 3 is well delimited by posterior ridges between the lateral and ventral surfaces. A broad, but relatively distinct midline ridge marks the anterior half of the ventral side of the centrum of DV 3. The articulation surface of the centrum of DV 4 for the neurocentral synchondrosis is broad and curved. The neural canal is narrowest at midlength of the centrum. The neural arch of DV 3 is higher, but more anteroposteriorly compressed, than in DV 2. The prezygapophysis is relatively short. The sprl is oriented almost vertically, and no strong anterior inclination of the neural spine is present anymore. The medial side of the neural spine of DV 3 is gently convex, and slightly wider anteroposteriorly than in DV 2. Postzygapophyses are not preserved.

Mid- to posterior dorsal vertebrae (DV 5 to 10). Dorsal vertebra 5 is lacking its right neural arch, diapophysis, and spine, as well as the distal tip of the left diapophysis (Fig. 27). Dorsal

vertebra 6 lacks the anterior part of the centrum, the right diapophysis, parapophysis, and prezygapophysis, and the spine top. In dorsal vertebra 7, the right diapophysis, parapophysis, and the spine top are missing. Dorsal vertebrae 8 and 9 lack the right diapophysis and parapophysis. The last dorsal vertebra lacks the neural spine process, whereas the arch below the postzygapophysis, the diapophysis, and the prezygapophyses are preserved (Fig. 28).

The mid- and posterior dorsal centra are short, and generally amphiplatyan to amphicoelous. Only DV 5 shows a weak anterior condyle. The pleurocoel is largest in DV 6 to 8, occupies the dorsal half of the centrum, and extends slightly onto the pedicels, below the neurocentral synchondrosis. The ventral surface is convex, and not well separated from the lateral side. The centrum is slightly shorter ventrally than at mid-height. In DV 6 and 7, a zigzagged line marks the neurocentral synostosis at the dorsal edge of the centrum. Dorsal vertebrae 8 to 10 have unfused neurocentral synchondroses. The neural arch is high, with highly elevated postzygapophyses, resulting in longer pedicels than neural spines in at least DV 5 to 8. Pre- and postzygapophyses are on more or less a horizontal line. The pedicels below do not show a strong lamination, but the acpl, pcdl, and cpol can be well distinguished. Dorsal vertebrae 6 to 9 furthermore show a weakly developed pcpl. An accessory lamina can be found in DV 7, connecting the pcdl with the podl, and in DV 8 between the prpl and the prdl. The presence and development of the hyposphene-hypantrum articulation cannot be distinguished due to the articulated state of the vertebrae. The parapophysis lies at mid-height on the pedicels in DV 6, at two thirds in DV 7 and at three fourths in DV 8. More posteriorly, the parapophysis seems to have been attached to the prezygapophysis. The spine is relatively low in DV 5 to 8, and only in DV 9 and probably 10 does it exceed the pedicel height. The spines are situated above the posterior-most portion of the centrum, and are vertically oriented. This differs from the strongly anteriorly inclined posterior dorsal neural spines of *Diplodocus* (Hatcher, 1901; Gilmore, 1932). The sprl is vertical in DV 6, strongly dorsoventrally convex in DV 7 and 8, and slightly convex in DV 9. The spdl is short and only expressed at its ventral end. Dorsally it merges with the spol, which extends onto the lateral surface of the spine. The posl, or possibly medial spol, is straight and vertical. Due to the preservation and mounting, it cannot be distinguished at this point how far back the bifurcation proceeds. The last definitively bifid neural spines are present in DV 5.

Ribs

Cervical ribs. The cervical ribs are thin, fragile elements. The axial cervical rib has almost no tuberculum, and is thus a straight, elongate, and transversely compressed sheet of bone (Fig. 16). Anterior to mid-cervical ribs are longer than their corresponding centra, but they only overlap a

PeerJ Reviewing Manuscript

small portion of the following vertebra (Figs 16, 17). The anterior process is distinct, but very short in CR 3, and pointed in anterior and mid-cervical ribs. It becomes very broad and rounded anteriorly in posterior cervical ribs, with a central longitudinal lamina connecting to the capitulum. The tuberculum is posteriorly inclined in anterior cervical ribs, and subtriangular in cross-section at midlength. The rib itself is concave internally, with a lamina connecting the tuberculum with the capitulum internally, producing two separate fossae anteriorly and posteriorly. Cervical rib 6 bears a pneumatic foramen internally on the capitulum.

Dorsal ribs. Several ribs have been recovered associated with the dorsal series, but the correct position of the single elements cannot be confidently determined at this point. There is some information from the quarry maps that the rib associated with DV 1 (as interpreted herein) looks much like a cervical rib. It is short, with a straight shaft, and has the typical anterior process of cervical ribs. However, the rib is detached from the centrum, as in all presacral vertebrae of SMA 0011. Also, if the vertebra herein described as DV 1 would actually be the last cervical vertebra, the second dorsal vertebra would be considerably shorter than the first. Such an early length decrease in the dorsal column would be unusual, and different from *Diplodocus* or *Barosaurus*, where this happens between DV 2 and 3 (CM 84, or AMNH 6341; Hatcher, 1901; McIntosh, 2005). The cervical-like rib shape of DR 1 is thus interpreted to be due to cervicalization, which appears to be an important evolutionary trend within diplodocids (McIntosh, 2005).

More posterior ribs are transversely compressed to slightly subtriangular at midshaft. Some of the elements have anteroposteriorly expanded distal ends (probably the anterior ribs, see Schwarz et al., 2007a), whereas others taper to a point. The capitulum is generally elongate, and the tuberculum low, but distinct. Between them, a relatively thin sheet of bone forms a triangular bony plate, which in at least some of the elements bears a ridge externally, but remains flat internally (contrary to the state in most other diplodocines). None of the ribs bear pneumatic foramina. The longest preserved rib has a length of 1400 mm (measured along the curve).

Sternal ribs. Several morphotype C elements (sensu Tschopp and Mateus, 2013a) were recovered associated with SMA 0011, but remain unprepared. They are elongate, narrow bones. No additional information can be gleaned to date that would help to confirm or discard the interpretation of Claessens (2004) and Tschopp and Mateus (2013a) that these elements are sternal ribs.

Forelimb (Figs 29-32; Tab. 7)

Scapula R, external view. The right scapula lacks the dorsal part of the acromion and of the distal end of the blade (Fig. 29). The acromion and the blade form an acute angle, but the

PeerJ Reviewing Manuscript

acromial ridge is only very slightly developed. The area anterior to the acromial ridge is concave. The posteroventral edge is mostly straight, and does not bear a triangular process as present in some *Camarasaurus* specimens, or *Dystrophaeus* (Osborn and Mook, 1921; McIntosh, 1997). The distal end of the blade is slightly curving ventrally as in *Apatosaurus excelsus* YPM 1980 (Upchurch et al., 2004b). The anterodorsal, or acromial edge of the scapula is much more concave, due to the stronger extensions of both the dorsal portion of the acromion, as well as the indicated widening of the distal shaft, which starts more anteriorly on this edge than on the posteroventral one. No oval rugose tubercle is present on the base of the shaft, unlike in *Apatosaurus excelsus* YPM 1980 (Upchurch et al., 2004b; ET, pers. obs., 2011).

Coracoid R, external view. The coracoid is somewhat tear-drop shaped (Fig. 29), with a concave anterodorsal edge, and a strongly, continuously convex, narrow dorsal margin, unlike the squared coracoids of apatosaurs (Riggs, 1903; Bakker, 1998). The coracoid foramen is completely enclosed, but the coracoid is not fused with the scapula. The bone is gently convex dorsoventrally. It curves slightly medially at its anterior margin. No distinct notch is present anterior to the glenoid surface. The glenoid is strongly transversely expanded at its center, and tapers dorsally and ventrally. The glenoid surface and the articulation surface with the scapula enclose an angle of about 155°.

Humerus R, anterior view. The right humerus is complete but slightly compressed anteroposteriorly (Fig. 30A). It is widely expanded at its proximal end, both laterally and medially. The distal end is expanded as well, but less so. The proximal portion is concave transversely, and does not bear a central rugose tubercle as present in the apatosaur AMNH 6114 (ET, pers. obs., 2011). The deltopectoral crest does not extend to midshaft. Its distal end is distinct and follows the lateral margin. It is not transversely expanded as would be typical for titanosaurids (Wilson, 2002; Curry Rogers, 2005). The crest is concave laterally, but this depression is probably exaggerated taphonomically. Two ridges mark the distal end anteriorly, indicating the extensions of the medial and lateral condyles. The ridges are relatively well visible and extend proximally. The medial condyle is much more prominent than the lateral one.

Ulna L, anterior view. The ulna lacks the proximal-most portion of the anterior arm of the condylar processes. The bone is strongly transversely compressed in its proximal half (Fig. 30B). It is generally slender, with a triradiate proximal end. The anterior arm is considerably longer than the lateral one, even though this is enhanced due to compression. The ulna has relatively strongly concave anterolateral and posterolateral surfaces. The lateral arm is somewhat wider than the anterior one. The distal part of the anteromedial surface bears two strong and elevated,

PeerJ Reviewing Manuscript

longitudinal ridges. They proceed both distally and proximally, but narrower and with a smooth surface. Proximally, the more lateral of the two ridges extends above midlength. Distally, the more medial ridge is more pronounced, reaching the distal articular surface. The distal end is expanded medially and somewhat transversely. The articular surface is subtriangular in outline.

Radius L, anterior view. The radius is complete, but its proximal end is compressed (Fig. 30B). It has thus a narrow, ellipsoid outline, but would probably be subcircular if undeformed. The shaft appears subrectangular in cross-section. As in the ulna, also the distal end of the radius is slightly expanded. The posterolateral surface bears at least one longitudinal ridge on its distal portion for the articulation with the ulna (more is obscured due to the mounting in matrix).

Carpal L. The carpal is a block-like element (Fig. 30B). Only one has been found in the otherwise articulated manus. The entire bone is relatively rugose and articulates with the radius. Comparison with the carpal elements found in other diplodocids (Hatcher, 1902; Gilmore, 1936; Bedell and Trexler, 2005) would suggest that it has been mounted upside down, although it was mounted as found, according to the quarry maps. If the mount is correct, it has a flat proximal, and an irregular, but transversely convex distal surface, contrary to the case in other diplodocids (Hatcher, 1902; Gilmore, 1936; Bedell and Trexler, 2005). It is anteroposteriorly wider at its medial end than laterally. There are no distinct articulation surfaces for the metacarpals, unlike the state in *Camarasaurus* (Tschopp, 2008). The carpal of SMA 0011 is longer proximodistally than the element known from the apatosaurs CM 3018 or UW 15556 (Hatcher, 1902; Gilmore, 1936). The anterior surface is concave transversely. Other than in apatosaurs, where the carpal articulated with both the ulna and the radius, and capped the median three metacarpals proximally (Hatcher, 1902; Gilmore, 1936), the carpal of SMA 0011 appears to overlie metacarpals I, II, and possibly III. This is the same arrangement as found in the articulated manus of WDC-FS001A (Bedell and Trexler, 2005).

Metacarpals L, anterior view. All metacarpals are complete and articulated (Fig. 30B). They are relatively elongate bones, but less than in *Camarasaurus* (Tschopp, 2008). Metacarpal III is the longest, followed by mc II, IV, I, and V (Tab. 7). Metacarpal I and II have subrectangular proximal articulation surfaces, mc III and IV triangular ones. Metacarpal I is relatively stout, with distinct anterior, lateral, and medial surfaces. The lateral condyle is much longer proximodistally than the medial one. This results in a strongly inclined distal surface, such that the phalanges project posteromedially in the articulated manus. Metacarpal II has very distinct, straight anteromedial and anterolateral edges. The proximal and distal ends are slightly expanded in all directions. The distal surface slightly curves into the anterior surface. Its lateral and medial

PeerJ Reviewing Manuscript

condyles are only visible in distal and posterior view. The proximal portions of both the medial and lateral surfaces are concave, laterally more than medially. Metacarpal III has a very distinct posterior corner of the proximal surface, probably connecting to a median ridge on the posterior surface, as is typical for Sauropoda (Upchurch et al., 2004a). Whereas no distinct transition from the anterior onto the medial surface occurs on mc III, the lateral face is clearly separated. The proximally and distal articular surfaces are slightly twisted. The distal surface is ellipsoid, and does not extend considerably onto the anterior face. Metacarpal IV has a triangular proximal articulation surface, with a concave medial edge. As in mc III the shaft of mc IV is twisted, and a distinction of the anterior face is not possible. The distal articular surface is subtriangular as well, with the apex anteriorly, and inclined medial and lateral edges. Two condyles are visible posteriorly. The apex of the distal articular surface curves onto the anterior face. Metacarpal V is short and widely expanded transversely at its proximal end. The distal end is lacking, but the preserved parts indicate that it is transversely expanded. This expansion occurs perpendicular to the proximal one.

Manual non-ungual phalanges L, anterior view. The manual non-ungual phalanges are relatively short and stocky (Fig. 30B). They are wider than long, as is typical for the eusauropod manus (Bonnan, 2003). The manual phalanx I-1 is mounted in posterior view. The proximal surface is concave anteroposteriorly. The phalanx I-1 has a concave posterior surface, with a proximally projecting ventral lip. Its medial surface is shorter than the lateral one, enhancing the outwards twist of the ungual phalanx even more. Well-developed medial and lateral condyles are present distally. The lateral extension of the posterolateral edge forms a thin, short crest (Fig. 31). Nothing similar is present in the manus of *Camarasaurus* (Osborn, 1904; Tschopp, 2008), but too few articulated proximal manual phalanges are known in diplodocids in order to decide if this might be autapomorphic in SMA 0011 or is instead more widespread within the clade. A phalanx figured by Jensen (1985: fig. 1E) appears to show a similar development of the posterolateral edge, but has not been identified below Sauropod indet. (Jensen, 1985). The manual phalanx II-1 has a concave proximal surface, which is probably ovoid in outline (only the dorsal portion can be seen as it is currently mounted). It is only minimally wider than the shaft. The medial surface is broader, but shorter than the lateral one. The anterior surface is convex transversely. The distal articular surface is expanded transversely, and the well-developed condyles extend onto the lateral surfaces. The manual phalanx II-2 is a vestigial, suboval bony nubbin. A distinct ridge separates the proximal and distal surfaces. The manual phalanges III-1 and IV-1 are very similar, with III-1 being slightly larger. They have concave proximal articular surfaces, transversely more

PeerJ Reviewing Manuscript

so than anteroposteriorly. The surfaces are suboval in outline, and their anterior margins are pronounced medially. The anterior surfaces are concave proximodistally, but slightly convex transversely. The distal surfaces are without condyles. They have a continuous, rounded surface, which curves proximally at its medial and lateral end, almost reaching the proximal articular surface. The medial and lateral surfaces are thus practically nonexistent. The lack of medial and lateral condyles implies that there were no vestigial terminal phalanges in these digits, unlike in *Camarasaurus* (Tschopp, 2008). The unusual shape of phm III-1 and IV-1 (as mounted) resembles phm V-1 in the camarasaur SMA 0002 (Tschopp, 2008). Given that no additional phalanx was found to mount with digit V, the elements mounted on the third and fourth digit might actually represent phm IV-1 and V-1. Both of these bones were not found articulated with their corresponding metacarpals, which makes a definitive assignment difficult. However, given that the manus would otherwise be complete, the mount is herein interpreted to be right, and no, or only a vestigial phalanx would have been present in digit V. Comparing with the manus of the camarasaur SMA 0002, this would indicate that the peculiar shape without distal condyles of phm III-1, and IV-1 of SMA 0011, or phm V-1 of SMA 0002 represent an intermediate stadium of phalangeal reduction, between the usual phalangeal shape and the nubbin-like vestigial elements found with digits two of both SMA 0011 and SMA 0002 (Tschopp, 2008).

Manual ungual L, anterior view. One ungual is present, and situated on the first digit (Fig. 30B). It is a long, high, and transversely compressed element. The proximal surface is tear-drop shaped, with a laterally curving anterior tip, and a widened posterior portion, where the articular surface lies. Anterior to the articular surface, the proximal surface projects somewhat proximally, and is rugose. This rugosity extends as a short ridge posteriorly, into the articular surface. The medial surface is convex anteroposteriorly. A short groove marks the distal-most portion, which is slightly elevated (about 1 mm) above the more proximal portion of the claw, and shows a different surface texture (Fig. 32). The latter might represent fossilized remnants of the keratinous sheet covering the claw. The lateral surface is almost plane, with a long, proximodistally extending, straight groove covering the distal half of the surface.

Hindlimb (Figs 33-35; Tab. 8)

Ilium R, external view. The ilium lacks a large part of its posterior upper portion. The preacetabular process has a very pointed apex, which is pointing anterolaterally. The anterior portion is strongly concave, with the ventral margin facing laterally. The ventral preacetabular border and the pubic process form an angle of 90°, which is uncommon in *Diplodocus*, but present in the holotype of *Galeamopus hayi* (Hatcher, 1901; HMNS 175, ET, pers. obs., 2010). A

PeerJ Reviewing Manuscript

triangular depression is located laterally at the base of the pubic process, with horizontal and medio- and lateroventrally inclined sides. This is similar to the putative diplodocid ilium from Spain (CPT-1074; Royo-Torres and Cobos, 2004; ET, pers. obs., 2012). The pubic peduncle is distinctly concave transversely at its posterior end, but fractures indicate that the concavity is exaggerated and that the transverse width of the pubic peduncle would be slightly larger. The ischial tubercle is facing slightly laterally. The acetabular margin is thinnest just posterior to the pubic peduncle, and extends transversely both posteriorly and anteroventrally, reaching the articulation surfaces of the ischium and pubis.

Pubis R, internal view. The right pubis is almost complete. Its anterodorsal corner is slightly eroded, and the middle portion of the ischial articulation is missing. The entire bone is relatively slender (Fig. 33A). The pubic foramen is closed, and located in the proximal third of the ischial articulation. Even though eroded, the anterodorsal corner does not seem to bear a very pronounced ambiens process, as seen in *Diplodocus* or *Supersaurus* (Hatcher, 1901; Lovelace et al., 2007). This corner is laterally expanded, and from here, the pubis slightly tapers along the acetabular surface. The medial surface of the proximal half of the bone is proximodistally concave and transversely slightly convex. The latter convexity becomes more pronounced towards midlength, where the ventral margin curves back from the expanded ischial articulation to the narrow midshaft. The dorsal edge of the pubis is gently concave. Its anterior end is expanded both transversely and anteroposteriorly. The narrowest portion of the shaft lies at about two thirds of the entire length of the pubis.

Ischium L, internal view. The ischium lacks the posterior half of the shaft (Fig. 33B). Its proximal portion is wide and concave. The acetabular surface is inclined, such that the medial border forms a thin crest. This crest is relatively straight in medial view, but concave and curved in proximal view. Unlike the state in rebbachisaurids, the acetabular surface does not expand towards the articulation surfaces for the ilium and the pubis (Calvo and Salgado, 1995; Whitlock, 2011a). The iliac process has thus no distinct neck, and is relatively narrow. The pubic articulation is much longer, and straight in medial view. It curves slightly medially towards its ventral end. The shaft is weakly convex at its base, separating the concave acetabular portion from the again shallowly concave posterior shaft. The dorsal and ventral margins are parallel, only the posterior-most preserved portion of the dorsal edge indicates a slight dorsal expansion towards the end, as is typical for diplodocids (McIntosh, 1990a, b; Upchurch, 1998; Wilson, 2002). No distinct ridges or scars can be seen on the internal surface. Oblique, minuscule elongated cavities indicate the presence of a now eroded shallow ridge extending from about

PeerJ Reviewing Manuscript

midlength of the ventral edge of the shaft proximodorsally onto the convex base of the shaft and ending on the dorsal margin where it curves into the acetabular portion.

Femur L, posterior view. The greater trochanter and the intercondylar groove are missing in the femur of SMA 0011 (Fig. 34A). The medial edge is gently curved below the femoral head, not as distinct as in *Dyslocosaurus* (McIntosh et al., 1992). The head is not well separated from the shaft ventrally. The fourth trochanter terminates slightly above midlength. It is entirely located on the posterior surface of the shaft, but close to the medial border proximally. The distal end of the fourth trochanter curves distinctly laterally. The distal condyles of the femur project far posteriorly. The lateral condyle bears an epicondyle. Both condyles expand slightly outwards, and the medial one projects further distally than the lateral one. In posterior view, the two condyles are slightly inclined medially.

Tibia L, anterior view. The tibia is complete (Fig. 34B). It is slightly expanded at both ends. A small convexity marks the distal end of the medial edge, similar, but broader and less distinct than in *Dyslocosaurus* (AC 663, ET, pers. obs., 2011). The cnemial crest is somewhat displaced distally, and distally thicker than proximally. The proximal end appears longer transversely than anteroposteriorly, but not the entire surface is visible. This also precludes the assessment of the outline of the proximal articular surface, which is subrectangular in apatosaurines, whereas it is subtriangular in diplodocines (Lovelace et al., 2007), and would thus yield further information on the correct taxonomic assignment of SMA 0011.

Fibula L, anterior view. The fibula is a slender bone, with a strongly expanded proximal end, and less so distally (Fig. 34B). The proximal end is transversely compressed. The attachment site for the iliofibularis muscle is situated slightly above midheight, as in *Diplodocus* (Whitlock, 2011a).

Astragalus L, anterior view. The astragalus is wedge-shaped in both anterior and proximal views (Fig. 35A). The anteromedial corner is reduced. Proximally, the astragalus is marked by a high ridge connecting to the ascending process, which extends backwards to the posterior end. The high, broad ridge separates the two fossae for the articulation with the tibia medially and the fibula laterally. The tibial fossa is larger, and subdivided by a more shallow, anteroposteriorly oriented ridge in a medial and a lateral portion. The fibular fossa is relatively uniform, with the anterior edge more developed than the posterior one. It is thus visible in posterior view, a diplodocoid synapomorphy, convergently acquired by *Jobaria* (Whitlock, 2011a).

Metatarsals L, anterior view. All left metatarsals were recovered complete (Fig. 35B). The metatarsals III and IV are the longest, mt I and II the stoutest elements (Tab. 8). Metatarsal I is

PeerJ Reviewing Manuscript

very stocky, and has a D-shaped proximal surface. The anterior surface is considerably shorter medially than laterally, resulting in angled proximal and distal surfaces, compared to the long axis of the shaft. The anterior surface bears few nutrient foramina, as is the case in *Cetiosauriscus* and *Suuwassea*, but not in camarasaurs (Harris, 2007; Tschopp, 2008; NHMUK R3078, ET, pers. obs., 2011). Distally, the lateral condyle projects much further than the medial, and develops a distinct posterolateral process, as is typical for diplodocids (McIntosh, 1990a, b). The medial surface is slightly convex, the lateral one concave for the reception of mt II. The distal articular surface bears a distinct intercondylar groove visible in anterior view. Metatarsal II has a more squared proximal surface, and also the anterior surface is less trapezoidal than in mt I. However, the proximal and distal articular surfaces are still angled to the long-axis of the shaft. As mt I, also mt II has a strong posterolateral process. The distal portion of the anterolateral edge bears a distinct rugosity, which does not extend onto the anterior surface, unlike in *Dyslocosaurus* AC 663 or *Cetiosauriscus* NHMUK R3078 (McIntosh et al., 1992; ET, pers. obs., 2011). Metatarsal II of SMA 0011 has a very distinct anteromedial edge, but a less developed anterolateral one. No intercondylar groove can be seen between the distal condyles in anterior view. Metatarsal III is elongate, with a narrow shaft and greatly expanded proximal and distal ends. The proximal and distal articular surfaces stand perpendicular to the shaft axis. The proximal articular surface is subrectangular to subtriangular, with the posterior margin being shorter than the anterior one. It is relatively flat, and does not show distally curving edges as in mt I and II. A weak, narrow rugosity marks the distal end of the anterolateral edge. Metatarsal IV is similarly elongate as mt III, but the proximal expansion reaches further down the shaft. The proximal end seems slightly twisted in respect to the long axis. It is subtriangular in outline, with a concave posterior margin, resembling the shape of mt IV of the camarasaur SMA 0002, but with a less well-developed concavity (Tschopp, 2008). The surface is flat, as in mt III. The shaft is smooth, without any distinct rugosities. The distal end does only have incipient condyles, which are hardly recognizable in both anterior and distal views. The metatarsal V has the typical paddle-shaped outline known from almost all sauropods (Bonnan, 2005). The proximal articulation surface is subtriangular, with the apex pointing anteriorly. From there, a ridge extends distally, separating the proximal portion of the anterior surface from the medial one. The ridge disappears in the distal half. The shaft is smooth, unlike in mt V of the camarasaur SMA 0002 (Tschopp, 2008). The distal surface is a single, convex facet.

Pedal non-ungual phalanges L, anterior view. The left pes of SMA 0011 preserves four proximal non-ungual phalanges (Fig. 35C). They are relatively short bones with a flat proximal

PeerJ Reviewing Manuscript

articular surface, and subsequently less well-developed distal condyles, from php I-1 to php IV-1. The pedal phalanx I-1 is slightly wedge-shaped, with a considerably shorter lateral than medial surface. Therefore, the distal condyles face laterodistally, resulting in the typical lateral deflection of the pedal unguals of eusauropods (Bonnan, 2005). The anterior surface is transversely narrower than the posterior surface. Due to the semi-emerged mounting method, which covers the posterior half of the phalanx, the angle between the posterior and the proximal surface cannot be determined. Pedal phalanges II-1 and III-1 are similar in general shape. The former is slightly broader than php III-1, which has subequal widths and lengths (Tab. 8). The medial condyle of both phalanges is transversely compressed, but projects further distally than the lateral one. The phalanx mounted as php IV-1 has a similar outline as php II-1, but is about half its size. The surfaces are relatively undefined, and distal condyles are barely distinguishable. This implies that if a second phalanx was present in the same digit, it was most probably vestigial. The indistinct shape of this element suggests that it might actually also represent php III-2 or php V-1. In *Apatosaurus* and *Camarasaurus*, php IV-1 has a distinct shape in being the only element with a longer lateral than medial surface (Gilmore, 1936; Tschopp, 2008). It usually also shows distinct medial and lateral condyles, at least in distal view (Hatcher, 1901; Gilmore, 1936; Janensch, 1961; Bonnan, 2005; Tschopp, 2008), unlike the element mounted as php IV-1 in the pes of SMA 0011.

Pedal unguals L, anterior view. Three unguals are present in the left pes of SMA 0011 (Fig. 35C). As mounted, this amounts to a pedal phalangeal formula of 2-2-2-1-0. This, however, is most probably underestimated, as comparisons with other diplodocid feet, and the questionable assignment of php IV-1 indicate (Hatcher, 1901; Gilmore, 1936; Janensch, 1961; Bonnan, 2005). The pedal unguals are sickle-shaped, and decreasing in length from the first to the third. They are strongly transversely compressed, but this is possibly slightly exaggerated due to taphonomy. The anterior edge is strongly curved and narrow. The medial surfaces are convex, the lateral sides concavoconvex anteroposteriorly. The pedal unguals are wider transversely in their plantar half, especially at the proximal end, where the wider area bears the proximal articular surface. The ungual III is the most stout element, as the proximal width remains more or less the same from ungual I to III, whereas the length decreases.

Ontogeny

The specimen SMA 0011 shows a variety of features that were previously reported to indicate a juvenile age of the animal. Cranial ontogeny in diplodocids was extensively discussed by Whitlock et al. (2010), who proposed the following juvenile features in *Diplodocus*: a relatively

PeerJ Reviewing Manuscript

rounded snout, with tooth rows that reach further back, and a large orbit. Whereas the latter is typical for most amniotes (Varricchio, 1997; Whitlock et al., 2010), the first two characteristics also occur in subadults to adults of other diplodocines, showing that at least in *Diplodocus*, ontogeny is recapitulating phylogeny (Tschopp and Mateus, 2013b). The skull of SMA 0011 has an orbit of about the same relative size as CM 11161, and thus relatively smaller than the juvenile CM 11255 (Whitlock et al., 2010). However, the snout is more rounded, reaching only 72% in the PMI, compared to more than 80% in CM 11161 (Whitlock, 2011b). Taken together, this indicates a more basal phylogenetic position of SMA 0011 compared to *Diplodocus* CM 11161. Another feature in the skull of SMA 0011 deserves special notion: the canal connecting the preantorbital fossa with the antorbital fenestra. This canal could indicate that the posterior and dorsal processes of the maxilla start growing out of the main body of the maxilla independently, and that only late in ontogeny, they fuse posteriorly.

Osteological characteristics of young age in the postcranial skeleton of SMA 0011 include unfused vertebral centra and neural arches, unfused cervical ribs, the ilium, which is detached from the sacrum, and a separate scapula and coracoid (Gilmore, 1925; Janensch, 1961; McIntosh, 1990b; Wedel and Taylor, 2013). Other characteristics often proposed to be an indicator for a young age, but absent in SMA 0011, are open coracoid and pubic foramina, or relatively smooth articular surfaces of the long bones (Hatcher, 1903; McIntosh, 1990b; Bonnan, 2003; Schwarz et al., 2007c). Furthermore, the lacking fusion of sacral vertebrae was shown to reflect ontogeny (Riggs, 1903; Mook, 1917; Wedel and Taylor, 2013), and the sternal plates are thought to adopt their definitive shape in adult animals only (Wilhite, 2003, 2005), but neither the sacrum nor any sternal plate are preserved in SMA 0011. Carpenter and McIntosh (1994) furthermore proposed that the longitudinal ridges on the distal shafts of radius and ulna develop during ontogeny, but this could also be a taxonomically valid character, given that *Dyslocosaurus* or *Diplodocus* appear to have them much less developed than *Apatosaurus* (ET, pers. obs., 2011). Wilson (1999), Bonnan (2007), Schwarz et al. (2007c), and Carballido and Sander (2013) showed that vertebral lamination and pneumaticity increases during ontogeny, but only the smallest neosauropod specimens show largely reduced pleurocoels and laminae (equivalent to the MOS 1; Schwarz et al., 2007c; Carballido and Sander, 2013; CM 566, SMA 0009, ET, pers. obs., 2011). Wedel et al. (2000) reported an increase in cervical centra elongation of 35-65% in *Apatosaurus*. However, their calculation was based on juvenile vertebrae from Oklahoma, identified as *Apatosaurus* by Carpenter and McIntosh (1994), but some of them might actually belong to *Camarasaurus* (Upchurch et al., 2004b). Increase in centrum elongation was also shown to

PeerJ Reviewing Manuscript

happen during ontogeny of *Europasaurus* (Carballido and Sander, 2013). Recently, it has furthermore been suggested that the bifurcation of the neural spine is ontogenetically controlled (Woodruff and Fowler, 2012).

Given the presence of both open neurocentral synchondroses as well as closed synostoses in some cervical and dorsal vertebrae of SMA 0011, the present specimen qualifies for MOS 3 and 4 of Carballido and Sander (2013), which in *Europasaurus* already show all phylogenetically significant characters of the species (Carballido and Sander, 2013). The same was hypothesized for *Suuwassea emilieae* ANS 21122 (Hedrick et al., 2012) and *Bonitasaura salgadoi* (Gallina, 2011, 2012) and is thus here regarded to be valid as well for SMA 0011. Contrary to Woodruff and Fowler (2012), the immature state of some vertebrae of SMA 0011 does thus not appear to be correlated with the posterior onset of neural bifurcation, which is herein regarded as phylogenetically significant. Furthermore, Woodruff and Fowler (2012) based their assessment on material that has not yet been identified to genus or species level, and given that this feature changes among different genera (McIntosh, 2005), their results remain doubtful.

Histology. The histology of the scapula, humerus, and femur of SMA 0011 has been studied by Klein and Sander (2008). This allows for an accurate comparison of morphological and histological ontogenetic markers. Both the humerus as well as the femur of SMA 0011 were classified within HOS stage 9, whereas the scapula showed a varying degree of remodeling from medial to lateral (Klein and Sander, 2008). This is the same age as suggested for *Suuwassea* (Hedrick et al., 2012) and *Bonitasaura* (Gallina, 2012), and is probably the stage, where sexual maturity is reached (Klein and Sander, 2008), although the timing of sexual maturity is still a matter of debate (Hedrick et al., 2012).

Timing of neurocentral closure. The pattern of neurocentral closure is variable among archosaurs (Brochu, 1996; Irmis, 2007; Birkemeier, 2011; Ikejiri, 2012). Even within Sauropoda, varying patterns have been reported (Harris, 2006b; Irmis, 2007; Gallina, 2011; Carballido and Sander, 2013). The incomplete nature and rare finds of immature specimens result in additional difficulties, and only very little information is available from articulated or associated vertebral columns (Gilmore, 1925; Harris, 2006b; Schwarz et al., 2007c; Gallina, 2011; Carballido et al., 2012a). The current specimen is thus of special importance for the study of neurocentral closure in sauropods.

SMA 0011 has closed, but visible neurocentral synostoses in anterior and posterior cervical vertebrae, and in anterior and mid-dorsal vertebrae. Mid-cervical, one mid-dorsal, and all posterior dorsal vertebrae of SMA 0011 have open neurocentral synchondroses. No cervical rib is

PeerJ Reviewing Manuscript

fused to its corresponding centrum. Given that long bone histology revealed that SMA 0011 already reached sexual maturity (Klein and Sander, 2008), it seems that open synchondroses still occurred in sexually mature sauropods. In *Suuwassea*, the same is the case for caudal vertebrae, but all preserved presacral vertebrae are fused (Harris, 2006b). However, only fragmentary mid- and posterior cervical, and no mid- and posterior dorsal vertebrae are preserved in ANS 21122, which are the only elements still showing unfused centra and neural arches in SMA 0011. As SMA 0011, also ANS 21122 has unfused cervical ribs, a separate scapula and coracoid, but a closed coracoid foramen and relatively rugose articular surfaces of the longbones (Harris, 2006b, 2007; Hedrick et al., 2012). The two specimens therefore seem to be of about the same individual age. The titanosaur *Bonitasaura* MPCA-460 appears to show a slightly different pattern of neurocentral closure, with a completely fused axis, but open anterior cervical and dorsal vertebrae, and closed posterior elements (Gallina, 2011). However, also MPCA-460 was shown to fit into HOS 9 (Gallina, 2012). These three specimens therefore indicate that neurocentral closure was delayed and only completed after sexual maturity in sauropods. They also show that the pattern of closure is not as simple as previously thought: based on comparisons with crocodiles, and on partial finds of specimens with open synchondroses and closed neurocentral synostoses, a posterior-to-anterior sequence was postulated (Brochu, 1996; Irmis, 2007; Birkemeier, 2011; Ikejiri, 2012; Tschopp and Mateus, 2013b). However, SMA 0011 shows that - at least in diplodocids - in both the cervical and the dorsal column, the middle elements fuse last, and that within one single vertebra, the fusion starts posteriorly and progresses anteriorly (Fig. 21). Adding the information from *Suuwassea* ANS 21122, anterior cervical vertebrae appear to fuse first (also in SMA 0011, these are the ones where the synchondroses are the least visible), followed by anterior dorsal and posterior cervical vertebrae, posterior dorsal vertebrae, whereas mid-cervical, mid-dorsal, and anterior to mid-caudal vertebrae fuse last. This varies from *Bonitasaura*, where a posterior-to-anterior pattern was proposed both within the postaxial cervical and in the dorsal columns (Gallina, 2011). A general posterior-to-anterior fusion pattern also appears to be present in at least one *Camarasaurus* (Trujillo et al., 2011), and the small juvenile, probably basal titanosauriform SMA 0009, which already have closed, but still visible synchondroses in anterior caudal vertebrae (Schwarz et al., 2007c; Carballido et al., 2012a). Different fusion patterns might thus prove to be a taxonomically valid character, with Macronaria showing a faster neurocentral closure than Diplodocoidea, and following a more strict posterior-to-anterior pattern, at least in the single vertebral regions. However, too few specimens are known to date, where neurocentral closure can be directly compared with histology, in order to

PeerJ Reviewing Manuscript

evaluate this character statistically. Nonetheless, these finds have further implications for the individual age of the holotype specimen of *Kaatedocus siberi*, SMA 0004 (Tschopp and Mateus, 2013b). The latter does not show any traces of neurocentral synostoses in any cervical vertebra, and also has completely fused cervical ribs (Tschopp and Mateus, 2013b). Being a diplodocine, this implies that Tschopp and Mateus (2013b) were right in identifying SMA 0004 as at least subadult specimen, which retained a relatively small size. Moreover, as Carballido and Sander (2013) showed for *Europasaurus*, sauropod vertebrae already show the majority of the phylogenetically informative characters of their respective species before the completion of the neurocentral closure.

Specimen-based phylogenetic analysis of Diplodocidae

Methods

The phylogenetic analysis is based on Whitlock (2011a), with changes introduced by Mannion et al. (2012) and Tschopp and Mateus (2013b), and combined with the specimen-based analysis of *Apatosaurus* by Upchurch et al. (2004b). The taxon list was extended in order to include all holotypes of putative diplodocid taxa, as well as reasonably complete specimens previously assigned to any diplodocid taxon (Tab. 1). The OTU slots for the diplodocid genera and species used in the previously published analyses were substituted by single specimens. Based on earlier publications or personal observations of the specimens, 243 characters were added to the version published in Tschopp and Mateus (2013b). Changes and character deletions proposed by Tschopp et al. (2013) were applied. Operational taxonomic units were scored based on personal observations where possible, on published descriptions where existing, or on photos from fellow researchers (Tab. S1).

Phylogenetic analysis

The phylogenetic analysis was performed with the software TNT (Goloboff et al., 2008), using the New Technology Search tool and enabling all options (Sect. Search, Ratchet, Drift, and Tree Fusing). Of the 53 multi-state characters, 23 were treated as ordered (explained in the character descriptions below). The consensus tree was stabilized five times with factor 75.

Main analyses. Several preliminary analyses were run in order to test previous hypotheses that unified several specimens into one individual (see below). By doing so, the data set was reduced from 81 operational taxonomic units to 76, which decreased the percentage of highly incomplete taxa and increased taxon overlap, which would otherwise have been very low (Tab. S2). The final reduced data set was again analyzed with the above stated settings. Additionally, in order to find

PeerJ Reviewing Manuscript

all possible shortest trees, the TNT script 'bbreak' was used with tree bisection and reconnection (command: bbreak=tbr safe). A reduced consensus tree was produced by using the heuristic method (Trees > Comparison > Agreement subtrees). Specimens not represented in the reduced consensus were added one by one to check their possible phylogenetic positions. Subsequently, pruned trees were generated (Trees > Comparison > Pruned Trees), with the parameters different from the default set as follows: up to 4 taxa, list as text. Since the three taxon combinations proposed by the 'pruned tree analysis' include only six specimens in total, a strict consensus tree was generated excluding all of these six OTUs a posteriori.

Given the low consistency index (CI) and thus high number of homoplasies in the dataset, an additional analysis with the same settings, but under implied weighting was conducted. Implied weighting calculates and adapts the weight of the characters during the analysis, based on the consistency index of the single characters (Goloboff, 1993). As characters with a high number of homoplasies in a specimen-based analysis are possibly coding for individual variation, and thus not phylogenetically significant, downweighting of these characters would be expected to yield more accurate results. Furthermore, as ontogenetic changes generally occur in a similar way in closely related taxa, and given that the dataset includes several putative juvenile to subadult specimens (YPM 1901, SMA 0009, CM 566, and possibly ANS 21122, SMA 0004, CM 3452, SMA 0011, AMNH 7530, AMNH 7535, SMA O25-8, SMA D16-3), characters describing them are probably more homoplastic than others and thus downweighted as well. Downweighting of the homoplastic characters was preferred over deleting, because certain characters were only homoplastic in one part of the tree. Traits variable within one clade can thus still be diagnostic for another group.

Support values. For both analyses, symmetric resampling was preferred over bootstrapping or jackknifing for quantifying node support (Analyze > Resample; using the default settings). Symmetric resampling is not affected by differential weighting of the characters, and thus a more meaningful value for the analysis with implied weights (Goloboff et al., 2003). For better comparison between the trees of the two methods, the same method was used for both analyses.

In order to quantify overlap within the single clades recovered, an overlap index was created together with F. Tschopp (Jona, Switzerland), indicating how many characters of the total 477 are available for analysis between the ingroup species. Overlaps were defined as the number of specimens for which a character was scorable, minus one, because if only one specimen of the group preserves a certain bone, no anatomical overlap is present in order to compare with other specimens of the same group. The index increases when more characters are scored in at least

PeerJ Reviewing Manuscript

two specimens, or when the number of specimens scorable for the same character is enlarged. It thus combines a measure for the completeness of the matrix with the comparability of single characters within specimens of a single group. Thereby, it gives an idea of the strength of the matrix to recover certain clades. However, it does not provide a measure for the significance of the result, as incomplete specimens might still bear taxonomically highly significant characters, which allow to identify it even to genus or species level. The overlap index is thus especially useful to evaluate taxa changing their positions between different trees. By calculating the overlap index for the sister group arrangements including the questionable taxon, researchers get an idea of how well the arrangement is supported based on overlapping skeletal material.

Positional terms for vertebrae

Serial variation within the vertebral column is highly developed in sauropods, and of taxonomical importance (Wilson, 2002, 2012). The high variability requires detailed character descriptions restricted not only to cervical, dorsal or caudal vertebrae, but even to areas within the respective portions of the column. It is thus general use in phylogenetic analyses that characters are restricted to anterior cervical vertebrae, or mid- and posterior caudal vertebrae, for example (Wilson, 2002; Upchurch et al., 2004a, b; Whitlock, 2011a; Mannion et al., 2012; Tschopp and Mateus, 2013b). However, a majority of the papers using phylogenetic analyses do not state how they define these subdivisions. The definitions used in the present analysis mostly follow the ones proposed by Mannion et al. (2013), and are summarized in table 10.

Material

Ingroup specimens phylogenetic analysis

The following individual, presumed diplodocid, specimens were included in the ingroup of the phylogenetic analysis. All of these are reasonably complete specimens of reputed diplodocid species, or constitute the holotypes of taxa, irrespective of completeness, which have been either referred or associated to Diplodocidae. Previous classifications and assignments, as well as comments on the likelihood that they represent singular individuals, are given below, alphabetically ordered. Outgroups comprise species-, or genus-level taxa from non-neosauropod Eusauropoda, Macronaria, as well as closely related Diplodocoidea. They are not further discussed here.

***Amphicoelias altus*, AMNH 5764 and AMNH 5764 ext.** The holotype of *Amphicoelias altus* originally included a tooth, two dorsal vertebrae, a pubis, and a femur (Cope, 1877a). A scapula, coracoid, and an ulna were later provisionally referred to the specimen (Osborn and Mook, 1921).

PeerJ Reviewing Manuscript

PeerJ Reviewing Manuscript

However, the strongly expanded distal end of the scapula, and the relatively deep notch anterior to the glenoid on the coracoid actually resemble more *Camarasaurus* than any diplodocid (ET, pers. obs., 2011). The same accounts for the single tooth stored at AMNH (Osborn and Mook, 1921). The tooth has already been excluded from scores of *A. altus* in recent phylogenetic analyses (Whitlock, 2011a; Mannion et al., 2012), which is followed here. Two different preliminary phylogenetic analyses were performed with a reduced (excluding the scapula and coracoid) and the extended holotype material (including all referred elements). As both analyses yielded the same position for the specimens, the reduced holotype was preferred in the final analysis. The risk of adding dubious information from potentially wrongly referred material was thus circumvented. More detailed analysis is needed in order to refine these assignments.

'*Amphicoelias*' *latus*, AMNH 5765. This is a fragmentary specimen comprising four caudal vertebrae and a right femur from the same site as the holotypes of *Camarasaurus supremus* and *Amphicoelias altus* (Cope, 1877a; Osborn and Mook, 1921; Carpenter, 2006). Both the vertebrae and the femur show greater resemblance with *Camarasaurus* than to *Amphicoelias*, which led Osborn and Mook (1921) to synonymize *A. latus* with *C. supremus*.

***Apatosaurus ajax*, YPM 1860.** The holotype of *Apatosaurus ajax* also constitutes the genoholotype of *Apatosaurus*. During collection and shipping it became intermingled with YPM 1840, the holotype of *Atlantosaurus immanis* (McIntosh, 1995). As a result, it is currently difficult to distinguish the two individuals, even though they come from different quarries. I follow the suggestions of Berman and McIntosh (1978) and McIntosh (1995), in deciding which elements of the mingled taxa presently comprise the holotype of *Apatosaurus ajax*. The only material not confidently referable to either specimen is a braincase currently labeled 'YPM 1860'. In order to investigate the taxonomic implications of the attribution of this braincase to the types of *Apatosaurus ajax* or *Atlantosaurus immanis*, two supplementary analyses were performed with scores of the braincase added to YPM 1840 and 1860, respectively. Adding the information from the braincase to YPM 1840, tree length increases but positions of the two specimens remain the same. An assignment of the braincase to the holotype of *Apatosaurus ajax* appears thus more parsimonious, indicating that it was labeled right.

***Apatosaurus ajax*, AMNH 460.** This specimen was recovered as *Apatosaurus ajax* in the specimen-based phylogenetic analysis of Upchurch et al. (2004b). Because AMNH 460 is mounted with reconstructed contribution of other specimens, caution has to be used, in order to not code characters based on reconstructed bones or elements actually belonging to other specimens (for a list of bones belonging to AMNH 460, see table S1).

***Apatosaurus ajax*, NSMT-PV 20375.** Described by Upchurch et al. (2004b), this specimen is the only fully described skeleton previously referred to *A. ajax*. It is relatively complete, although abnormal length ratios of the humerus, radius and metacarpal III suggest that NSMT-PV 20375 might be composed of more than one individual, possibly including bones of the *Camarasaurus* specimens found intermingled in the quarry (Upchurch et al., 2004b). These forelimb elements were thus excluded from scores of the OTU in the present analysis.

'*Apatosaurus*' *grandis*, YPM 1901. Marsh (1877a) initially assigned this species to *Apatosaurus*, but subsequently referred it to *Morosaurus* (Marsh, 1878; later synonymized with *Camarasaurus*: Mook, 1914). There is some confusion about the correct assignment of several bones to either the holotype YPM 1901 or the referred specimens YPM 1902 or YPM 1905 from the same quarry (see Ostrom and McIntosh, 1966). Herein, scores are included from all elements potentially belonging to YPM 1901 (according to Ostrom and McIntosh, 1966). As all three specimens were referred to *Camarasaurus*, this should have no influence on the ingroup relationships of the current phylogenetic analysis.

***Apatosaurus laticollis*, YPM 1861.** *Apatosaurus laticollis* is based on a single, fragmentary cervical vertebra (Marsh, 1879). Subsequent studies proposed that this vertebra actually belongs to the same individual as the holotype material of *Atlantosaurus immanis* (YPM 1840), which were both found in the Lakes Quarry 1 (McIntosh, 1995). Here, the specimens were kept apart in order to evaluate this hypothesis.

***Apatosaurus louisae*, CM 3018 (holotype) and CM 11162.** The most complete specimen of *Apatosaurus* is CM 3018, a postcranial skeleton that was preliminarily described as new species by Holland (1915a) and followed by a detailed monographic treatment by Gilmore (1936). An obvious diplodocid skull (CM 11162) was found near it, but the historical referral of the latter specimen remained confused for a time (Holland, 1915b, 1924; Berman and McIntosh, 1978). Because *Apatosaurus* was thought to have a more *Camarasaurus*-like skull at the time, Holland's proposal that CM 11162 was the actual skull of CM 3018 (Holland, 1915b, 1924) was largely unaccepted by others (e.g. Gilmore, 1936). Only with the detailed description and study of the specimen by Berman and McIntosh (1978) did CM 11162 become the now widely accepted skull-form of *Apatosaurus.* Given the small distance between skull and postcrania in the quarry, as well as the perfectly fitting size of the cranial occipital condyle and postcranial atlas, the probability that the two belong to the same individual is very high (Holland, 1915b; Berman and McIntosh, 1978). Accordingly, the OTU representing the holotype of *Apatosaurus louisae* in the present analysis comprises scoring from both CM 3018 and 11162.

PeerJ Reviewing Manuscript

***Apatosaurus louisae*, CM 3378.** The specimen was identified as *Apatosaurus louisae* in the analysis of Upchurch et al. (2004b). Although never described in detail, CM 3378 yields important information on the number of vertebrae in *Apatosaurus*, as this specimen is the only known with an articulated, uninterrupted vertebral column from the mid-cervical region to the last caudal vertebra (Holland, 1915b; McIntosh, 1981). CM 3378 was found at the Dinosaur National Monument, associated with a diplodocid skull (CM 11161; interpreted as *Diplodocus*), as well as appendicular elements. However, according to McIntosh (1981), these materials cannot be attributed to the same individual as CM 3378 with certainty, and no scores from them were thus included in this OTU.

***'Apatosaurus' minimus*, AMNH 675.** Initially described as new species of *Apatosaurus* (Mook, 1917), AMNH 675 is now generally considered an indeterminate sauropod, with affinities to Titanosauriformes, based on the shape of the ilia and the six sacral vertebrae (McIntosh, 1990a). In order to test this, *Isisaurus colberti* was added to the analysis. *Isisaurus* has the typical titanosaurian sacrum with six vertebrae and the preacetabular lobe oriented perpendicular to the vertebral axis (Jain and Bandyopadhyay, 1997), as is the case in AMNH 675. At AMNH, a diplodocid chevron is also accessioned in AMNH 675. However, because AMNH record indicate it was 'found loose with other Bone Cabin Quarry material', we excluded scoring it as part of *A. minimus*.

***Apatosaurus parvus*, UW 15556.** This specimen was found by the Carnegie Museum, intermingled with the holotype specimen of *Elosaurus parvus*, CM 566 (Hatcher, 1902; Peterson and Gilmore, 1902). It first bore the specimen number CM 563, but was later transferred to the University of Wyoming (McIntosh, 1981). Usually identified as *A. excelsus* (Gilmore, 1936), a specimen-based phylogenetic analysis supported the retention of the species *parvus* for CM 566 and UW 15556 (Upchurch et al., 2004b).

***Apatosaurus* sp., FMNH P25112.** Riggs (1903) described this specimen (formerly FMNH 7163) as *A. excelsus*, which led him to two important conclusions: 1) *Brontosaurus* is a junior synonym of *Apatosaurus*, and 2) during ontogeny, additional vertebrae are added from the dorsal and caudal series to the sacrum. Later, the specimen-based phylogenetic analysis of Upchurch et al. (2004b) recovered it on a disparate branch within *Apatosaurus*, suggesting that FMNH P25112 represents a novel species. The specimen is mounted at FMNH together with the neck and forelimbs of FMNH P27021 (W. Simpson, pers. comm., 2013).

***Apatosaurus* sp., ML 418.** This specimen is very badly preserved. One dorsal vertebra has been prepared and was identified as a possible *Apatosaurus* or *Dinheirosaurus* (Antunes and Mateus,

PeerJ Reviewing Manuscript

2003; Mateus, 2005; Mannion et al., 2012). Additional unprepared material includes dorsal rib fragments, and a partial tibia. A mid- or posterior cervical vertebra of the same individual was lost due to the friable preservation, and scores concerning the cervical vertebrae therefore base on photographs.

***Atlantosaurus immanis*, YPM 1840.** This is possibly the same individual as YPM 1861 (*Apatosaurus laticollis*), and it was mingled with YPM 1860 (*Apatosaurus ajax*) during shipping (see above). McIntosh (1995) tried to separate them based on their color, and on the sparse field notes. In the YPM collections, the specimens remain tagged as they have been before McIntosh's study, therefore it is difficult to reproduce his results. Scores for an ischium of YPM 1840 are based on personal observation, whereas cervical and dorsal vertebral characters are derived from the literature (Marsh, 1896; Ostrom and McIntosh, 1966; Upchurch et al., 2004b).

***Australodocus bohetii*, holotype and paratype.** The holotype and paratype are two successive mid-cervical vertebrae from the same individual (Remes, 2007). Mannion et al. (2013) suggested *Australodocus* to be a non-lithostrotian titanosaur. Accordingly, *Ligabuesaurus leanzai* was added to the taxon list in order to include a possible closely related derived titanosauriform that has anatomical overlap with *A. bohetii*.

***Barosaurus affinis*, YPM 419.** The holotype of *B. affinis* consists only of pedal material, and has no overlap with the holotype of *B. lentus* (Marsh, 1890, 1899). Because they come from the same quarry, the two species were usually regarded as synonyms (Lull, 1919; McIntosh, 2005). McIntosh (2005) identified the elements as mt I and partial mt II, but the latter is herein interpreted to represent the proximal portion of mt V instead. The bone is widely expanded, and has the typical 'paddle'-shape of the metatarsal V in sauropods (ET, pers. obs., 2011).

***Barosaurus lentus*, YPM 429.** Although this specimen is the genoholotype of *Barosaurus* (Marsh, 1890; Lull, 1919), most characterization of *Barosaurus* is based on another, more complete, and articulated specimen (AMNH 6341, see below). YPM 429 as presently available has a high degree of reconstruction, especially in some cervical vertebrae.

***Barosaurus* sp., AMNH 6341.** This specimen is the most complete probable *Barosaurus* (McIntosh, 2005). It was collected in three parts and subsequently separated by different institutions (USNM, CM, and UUVP), but later brought together by B. Brown for the AMNH (Bird, 1985). Some doubts exist concerning the correct attribution of a tibia-fibula pair, which might also belong to a *Diplodocus* specimen found in the vicinity of AMNH 6341 (McIntosh, 2005).

***Barosaurus* sp., AMNH 7530.** Both the holotype specimen of *Kaatedocus siberi* (SMA 0004)

PeerJ Reviewing Manuscript

and AMNH 7530 were found at Howe Quarry (Michelis, 2004; Tschopp and Mateus, 2013b). AMNH 7530 is tagged as *Barosaurus* on display at AMNH, probably based on a tentative identification made by Brown (1935), but without detailed study. AMNH 7530 is an important specimen for diplodocid taxonomy because it includes articulated anterior and mid-cervical vertebrae and a partial skull.

***Barosaurus* sp., AMNH 7535.** This specimen was recovered with *Kaatedocus siberi* SMA 0004 and AMNH 7530 at Howe Quarry (Michelis, 2004; Tschopp and Mateus, 2013b), and has been simply cataloged as *Barosaurus* in the collections of the AMNH (likely by B. Brown; Brown, 1935). AMNH 7535 largely preserves the same elements as SMA 0004 and AMNH 7530, and appears to be of about the same size. A partial tail is also accessioned under AMNH 7535, but given the chaotic distribution of specimens in the quarry (Tschopp and Mateus, 2013a: fig. 1), it is impossible to confidently attribute disparate and disarticulated portions to any single common individual. A diplodocid quadrate that was initially cataloged under AMNH 7535 now bears the number AMNH 30070. Since the original attribution of this quadrate to AMNH 7535 was probably based on their vicinity in the quarry, two analyses were performed with and without the information of this bone, yielding the same phylogenetic position in both iterations. On both instances, information from the caudal series were omitted from scores of AMNH 7535. Scores on the quadrate were retained in the final analysis because AMNH 30070 shows some differences with the quadrates known from *Kaatedocus* (e.g. lack of the small fossa dorsomedially on the quadrate shaft, ET, pers. obs., 2011), as do also the cervical vertebrae.

***Barosaurus* sp., CM 11984.** Together with YPM 429 and AMNH 6341, CM 11984 represents a third, relatively complete, likely *Barosaurus* specimen (McIntosh, 2005). Some of the material of CM 11984 is still unprepared, and further crucial information on *Barosaurus* can be expected once these are freed from matrix. In addition to the vertebral column, a pes is accessioned under CM 11984, which McIntosh (2005) considered to have a dubious association with the remaining material, given the chaotic quarry situation at Dinosaur National Monument. Therefore, this pes is not considered as part of the scoring of CM 11984.

***Brachiosaurus* sp., SMA 0009.** Initially described as a diplodocid (Schwarz et al., 2007c), a reassessment of the systematic position of SMA 0009 after further preparation of the mid-cervical vertebrae revealed probable titanosauriform affinities (Carballido et al., 2012a). Because Carballido et al. (2012a) suggested that SMA 0009 represents an immature *Brachiosaurus*, *B. altithorax* (Riggs, 1904; Taylor, 2009) was included in the dataset.

***Brontosaurus amplus*, YPM 1981.** The type of *B. amplus* (Marsh, 1881) is generally accepted as

PeerJ Reviewing Manuscript

synonym to *Apatosaurus excelsus* (Gilmore, 1936; McIntosh, 1990a, 1995; Upchurch et al., 2004b), but has never been described in detail.

***Brontosaurus excelsus*, YPM 1980.** The holotype of *Brontosaurus excelsus* (now commonly synonymized with *Apatosaurus*) was the first to be published with a reconstruction of the entire skeleton (Marsh, 1883), and is still one of the best preserved diplodocid specimens worldwide. For the mount at YPM it was extensively reconstructed, such that special care has to be taken when scoring its characters from the original specimen.

***Cetiosauriscus stewarti*, NHMUK R3078.** The holotype specimen was first described in the early 1900s (Woodward, 1905) as *Cetiosaurus leedsi*. However, Huene (1927) identified '*Cetiosaurus*' *leedsi* as a separate genus, *Cetiosauriscus*, and highlighted the then referred specimen NHMUK R3078 as exemplifying the new genus. NHMUK R3078 was made the holotype of *Cetiosauriscus stewarti* (Charig, 1980), which later was instated as the type species of *Cetiosauriscus* (Charig, 1993). It was included in Diplodocidae by McIntosh (1990b), based on pedal morphology, but subsequent analyses proposed a closer relationship with the non-neosauropod eusauropods *Mamenchisaurus* or *Omeisaurus*, as well as with *Tehuelchesaurus* (Heathcote and Upchurch, 2003). *Mamenchisaurus* and *Omeisaurus* were thus included in the present analysis in order to test these competing hypotheses. A detailed restudy of the material is in preparation by P. Mannion and P. Upchurch (pers. comm., 2011, 2012), and will doubtlessly reveal more valid characters. Since personal observation of the caudal vertebrae of *Spinophorosaurus nigerensis* revealed high similarity with *Cetiosauriscus*, *S. nigerensis* was added to the matrix, in order to appraise the phylogenetic role of their morphological similarities.

***Dinheirosaurus lourinhanensis*, ML 414.** The holotype of *Dinheirosaurus lourinhanensis* was originally referred to *Lourinhasaurus alenquerensis* by Dantas et al. (1998), but Bonaparte and Mateus (1999) realized that ML 414 represents a different genus. Contrary to the phylogenetic assignment of *L. alenquerensis*, which is now thought to be a basal macronarian (see below), the diplodocid affinities of *D. lourinhanensis* are well supported by four phylogenetic analyses (Rauhut et al., 2005; Whitlock, 2011a; Mannion et al., 2012; Tschopp and Mateus, 2013b).

***Diplodocus carnegii*, CM 84.** The holotype of *D. carnegii* is one of few specimens of *Diplodocus* that includes cervical vertebrae. It is mounted at CM, and completed with bones from various other specimens: CM 94, 307, 21775, 33985, HMNS 175, USNM 2673, and AMNH 965 (McIntosh, 1981; Curtice, 1996). Scores of the holotype of *D. carnegii* are based on this mounted specimen, with effort taken to ensure that only material from CM 84 was included. *D. carnegii* was erected based on comparisons to AMNH 223, which showed some differences in caudal

PeerJ Reviewing Manuscript

neural spine orientation. If compared with the original type material, the differences are not as clear, and were in fact disputed by Gilmore (1932).

***Diplodocus carnegii*, CM 94.** This specimen was described as a paratype of *D. carnegii* (Hatcher, 1901). Both holotype and paratype specimens were found in the same quarry, from where also material of other genera was recovered (Hatcher, 1901). Oddly, CM 94 includes two pairs of ischia, which casts some doubt on the true attribution of bones to individual specimens (McIntosh, 1981; ET, pers. obs., 2011). As both pairs of ischia show the same characteristics, we included the entire material excluding one pair of ischia from the OTU representing CM 94 (including some bones mounted with the holotype of *Galeamopus hayi* HMNS 175, see below). However, further studies are needed in order to definitively assign the various bones among the at-least two individuals present.

***Diplodocus* cf. *carnegii*, WDC-FS001A.** This specimen has not been described entirely, but is the most complete referral to *Diplodocus* that has a manus with associated hindlimb and axial material (Bedell and Trexler, 2005). The specimen was found in two spatial clusters in the quarry, but the lack of duplicated bones, the two similarly sized humeri, and osteological indications of a single ontogenetic stage led Bedell and Trexler (2005) to identify the materials as belonging to a single individual with affinities to *D. carnegii*.

***Diplodocus lacustris*, YPM 1922.** The original type material of *D. lacustris* comprises teeth, a premaxilla, and a maxilla (Marsh, 1884). However, personal observations at YPM reveal that the cranial bones clearly belong to Camarasaurus or a morphologically similar taxon, and that there is no relationship between them and the teeth. Mossbrucker and Bakker (2013) describe a newly found putative apatosaur maxilla and two premaxillae from the same quarry, proposing that they might belong to the same individual as the teeth of YPM 1922. However, given the lacking field notes from the first excavations, such a referral will be difficult to prove. Therefore, in the present analysis, only the teeth were scored for *D. lacustris*.

***Diplodocus longus*, YPM 1920.** YPM 1920 constitutes the genoholotype of *Diplodocus* (Marsh, 1878), and has thus special taxonomic importance. Unfortunately, it is highly incomplete, with only two nearly complete caudal vertebrae, and few additional fragmentary anterior to mid-caudal vertebrae identifiable in the YPM collections. A chevron was reported as belonging to the same individual (Marsh, 1878; McIntosh and Carpenter, 1998), but it could not have been located at YPM in 2011. Other articulated vertebrae were found in the field but discarded due to their friable preservation (McIntosh and Carpenter, 1998). Extraneous materials were once assigned to the same specimen, including a skull, femur, tibia, fibula, astragalus, and five metatarsals (still

PeerJ Reviewing Manuscript

accessioned under YPM 1920), as well as an ulna, radius, and partial manus assigned YPM 1906 (McIntosh and Carpenter, 1998). However, only the caudal series and the chevron can be surely identified as belonging to the holotypic individual (McIntosh and Carpenter, 1998), as scored in the present analysis.

***Diplodocus* sp., AMNH 223.** The specimen was first described as *Diplodocus longus* (Osborn, 1899). It was the first reasonably articulated specimen of *Diplodocus* and thus became one of the important specimens to base comparisons to (see Hatcher, 1901). Three partial cervical neural arches, described and figured by Osborn (1899), could not be located at AMNH (ET, pers. obs., 2010, 2011). Coding of these elements is thus based entirely on Osborn (1899).

***Diplodocus* sp., AMNH 969.** This skull and associated atlas and axis were identified as *D. longus*, based on an earlier report of a skull allegedly belonging to the holotype specimen of *D. longus*, YPM 1920 (Marsh, 1884; Holland, 1906). However, the only reported *Diplodocus* specimen with an articulated skull and anterior cervical vertebrae is CM 3452, of which only the skull has been described (Holland, 1924). Since no anterior cervical vertebrae are definitely attributable to *D. longus*, the only comparison that can be made is with the *D. carnegii* type specimens, of which only CM 84 preserves the axis. As the two differ in morphology (e.g. of the prespinal lamina), AMNH 969 was herein regarded *Diplodocus* sp., before the analysis (see below).

***Diplodocus* sp., CM 3452.** On display at CM, this specimen is the only possible *Diplodocus* with articulated skull and anterior cervical vertebrae (McIntosh and Berman, 1975). However, the cervical vertebrae have not been described, and no detailed study has been done in order to identify the species CM 3452 belongs to. Comparison with other specimens referred to *Diplodocus* is hampered due to very little anatomical overlap.

***Diplodocus* sp., CM 11161.** This specimen is only a skull. It was described as *Diplodocus longus* by Holland (1924) and McIntosh and Berman (1975), based on comparisons with the earlier reported putative *Diplodocus* skulls AMNH 969, USNM 2672, and 2673. However, because all of them were disarticulated and found in quarries that also produced other diplodocid genera, care must be taken concerning these identifications. Our knowledge of diplodocid skulls to date suggests that they are extremely similar to each other, and very few distinguishing characters have yet been proposed (Berman and McIntosh, 1978; McIntosh, 2005; Harris, 2006a; Remes, 2006; Whitlock et al., 2010; Whitlock, 2011b; Tschopp and Mateus, 2013b; Whitlock and Lamanna, 2012). Thus, it is refrained here from referring CM 11161 to any species of *Diplodocus* until postcranial diagnostic traits are robustly linked to cranial morphologies.

PeerJ Reviewing Manuscript

***Diplodocus* sp., DMNS 1494.** This specimen is a relatively complete, articulated find from the Dinosaur National Monument. The only disarticulated elements are the right scapulacoracoid and the left hindlimb. These elements were not included in the present analysis because DMNS 1494 was found intermingled with other skeletons (V. Tidwell, pers. comm., 2010). DMNS 1494 was collected by the Carnegie Museum, and later transferred to DMNS for exhibit. A right fibula and astragalus of the same specimen remained at CM (presently CM 21763; McIntosh, 1981). The specimen has never been formally described, but is ascribed to *D. longus* (e.g. Gillette, 1991). Together with CM 84, DMNS 1494 is the only *Diplodocus* specimen included here with articulated, and complete cervical vertebrae.

***Diplodocus* sp., USNM 2672.** Like AMNH 969, USNM 2672 preserves a partial skull and atlas. It was the first diplodocid skull to be reported, and was initially included among the holotype of *D. longus*, YPM 1920 (Marsh, 1884). However, the skull and holotypic caudal vertebrae were not found in articulation or even close association, therefore this attribution has to be regarded as questionable (McIntosh and Carpenter, 1998), and the two specimens were treated as distinct OTUs.

***Diplodocus* sp., USNM 10865.** Although USNM 10865 is one of the most complete *Diplodocus* specimens, it has only been preliminarily described and was tentatively referred to *D. longus* by Gilmore (1932). USNM 10865 was found close to the articulated *Barosaurus* AMNH 6341 ('#340' in Gilmore, 1932; McIntosh, 2005). According to McIntosh (2005), two sets of left lower legs of different lengths were found associated with USNM 10865. The shorter set was mounted by Gilmore (1932), but McIntosh (2005) suggests that this assignment might have been wrong. For the character relating to the tibia/femur length, the higher ratio was therefore used, following McIntosh (2005).

***Dyslocosaurus polyonychius*, AC 663.** The only specimen of this putative diplodocid sauropod consists of solely appendicular elements of dubious origin and association (McIntosh et al., 1992). No field notes exist, but personal observations of differing color and preservation led to the conclusion that at least the supposed php III-1 was probably not collected at the same place as the rest of the holotype specimen. It is therefore excluded from scores of *Dyslocosaurus* in this phylogenetic analysis. A more detailed reassessment of this specimen is in progress (Tschopp and Nair, in prep.), and might reveal additional information on its taxonomic affinities. The phylogenetic position yielded in the present analysis is regarded as preliminary.

***Dystrophaeus viaemalae*, USNM 2364.** This specimen is highly fragmentary, but was identified as possibly diplodocoid by McIntosh (1990b; his 'Diplodocidae' conforms to the current use of

PeerJ Reviewing Manuscript

the Diplodocoidea). The type material is only partly prepared, which largely impedes identifying crucial character states. The type locality was relocated in the mid-1990s, and more material of the probable holotypic individual was excavated, of which only a phalanx has been identifiable (Gillette, 1996a, b). However, Gillette (1996a, b) states that more material is probably present, such that additional information on *Dystrophaeus* might be forthcoming. Both in the initial description (Cope, 1877b) and a reassessment (Huene, 1904), several of the bones were misidentified: metacarpal V (according to Huene, 1904) is most probably a metacarpal I, based on the angled distal articular surface (McIntosh, 1997; ET, pers. obs., 2011). Cope (1877b) correctly identified a partial scapula (contra Huene, 1904, who thought it was a pubis), but misidentified a complete ulna and a partial radius as humerus and ulna, respectively, as already recognized by Huene (1904).

***Dystylosaurus edwini*, BYU 4503.** The holotype of *Dystylosaurus edwini* is an anterior dorsal vertebra (Jensen, 1985). There is some doubt concerning its taxonomic affinities: it has been identified as either brachiosaurid (Paul, 1988; McIntosh, 1990b; Upchurch et al., 2004a; Chure et al., 2006) or diplodocid, possibly even from the same individual as the *Supersaurus vivianae* holotype scapulacoracoid (Curtice and Stadtman, 2001; Lovelace et al., 2007). It was included in a preliminary analysis as an OTU independent from *Supersaurus vivianae* BYU and WDC DMJ-021 in order to clarify its taxonomic status. The results yielded 102 most parsimonious trees, where *Dystylosaurus* always grouped with the two *Supersaurus* OTUs, which sometimes include *Dinheirosaurus* ML 414, *Diplodocus hayi* HMNS 175, *Barosaurus affinis* YPM 419, or *Diplodocus lacustris* YPM 1922 within the same branch. In 31 out of 102 most parsimonious trees *Dystylosaurus* and the two *Supersaurus* OTUs formed sister taxa. This result corroborates the hypothesis of Curtice and Stadtman (2001) and Lovelace et al. (2007) that the *Dystylosaurus* holotypic vertebra is *Supersaurus*, and most probably from the same individual as the *Supersaurus* holotype. In the definitive analysis BYU 4503 was thus included as part of the combined OTU representing the BYU specimens of *Supersaurus vivianae*.

***Elosaurus parvus*, CM 566.** CM 566 is a small juvenile that is generally referred to *Apatosaurus excelsus* (McIntosh, 1995), or constitutes the independent species *Apatosaurus parvus* together with an adult specimen (UW 15556; Upchurch et al., 2004b), with which it was found associated (Peterson and Gilmore, 1902). However, it was initially described as a unique genus (Peterson and Gilmore, 1902).

***Eobrontosaurus yahnahpin*, Tate-001.** Initially described as *Apatosaurus yahnahpin* (Filla and Redman, 1994), a separate genus was erected for the specimen (Bakker, 1998), partly based on

PeerJ Reviewing Manuscript

differences in coracoid morphology to *Apatosaurus*. The specimen has been considered a camarasaurid (Upchurch et al., 2004a), but more recently, Mannion (2010) suggested diplodocid affinities. The taxon has never been included in any phylogenetic analysis, but a detailed description of the entire material appears to be in preparation (R. Bakker, pers. comm., cited in Mannion, 2010).

***Galeamopus hayi*, HMNS 175.** The holotype specimen was initially housed at CM (as CM 662), prior to residing in Cleveland for a time (formerly CMNH 10670). Holland (1924) described it as a novel species of *Diplodocus*, based solely on cranial characters. At that time, *Apatosaurus* was thought to bear a *Camarasaurus*-like skull (see Berman and McIntosh, 1978), which probably influenced researchers to identify any elongate, diplodocid skull as *Diplodocus*. McIntosh (1990a), amongst others, later suggested that '*D.*' *hayi* might actually not be a *Diplodocus*, but a unique genus, based on various similarities with *Apatosaurus* in the cranium, forelimb, and tail. Because the specimen is mounted at HMNS (together with reconstructions and original bones from CM 94; McIntosh, 1981), it is only of limited accessibility. Based on the results of the present phylogenetic analysis (see below), '*Diplodocus*' *hayi* HMNS 175 is herein referred to its own genus *Galeamopus*, of which it constitutes the genoholotype specimen (see above).

***Galeamopus* [redacted] SMA 0011.** This specimen is described here for the first time, and found to form its own species (see above). It has been mentioned by Klein and Sander (2008) as Diplodocinae indet.

***Kaatedocus siberi*, SMA 0004.** Before its detailed examination, the holotype of *Kaatedocus siberi* was generally reported as *Diplodocus* (Ayer, 2000) or *Barosaurus* (Michelis, 2004). Subsequently, a description and phylogenetic reappraisal of SMA 0004 revealed its generic separation from *Diplodocus* and *Barosaurus* (Tschopp and Mateus, 2013b).

***Losillasaurus giganteus*, MCNV Lo-1 to 26.** The OTU represents an individual containing the holotypic caudal vertebra, Lo-5, the paratypes Lo-10 and Lo-23, and several additional elements. All the bones of MCNV Lo-1 to 26 were found associated and no duplication of bones occurred (Casanovas et al., 2001). *Turiasaurus* was added as recent phylogenetic studies proposed them to be sister taxa (Royo-Torres et al., 2006, 2009; Royo-Torres and Upchurch, 2012).

***Lourinhasaurus alenquerensis*, lectotype.** The species was first described by Lapparent and Zbyszewski (1957) as referable to *Apatosaurus*, but later included into *Camarasaurus* (McIntosh, 1990a). Subsequently, Dantas et al. (1998) erected a new genus for the species, but only Antunes and Mateus (2003) clearly assigned a specific type specimen to the species. The genus was usually recovered as basal macronarian in phylogenetic analyses (Upchurch et al., 2004a; Royo-

PeerJ Reviewing Manuscript

Torres and Upchurch, 2012; Mocho et al., 2014).

***Seismosaurus hallorum*, NMMNH 3690.** The holotype of *S. hallorum* was initially described as *S. halli*, and as one of the largest sauropods ever (Gillette, 1991). However, this was mainly based on an incorrect assignment of the position of some mid-caudal vertebrae (Curtice, 1996; Herne and Lucas, 2006). Subsequent reanalysis of the specimen revealed that it is indistinguishable from *Diplodocus*, and that it probably belongs to the same species as AMNH 223 and USNM 10865 (Lucas et al., 2006; Lovelace et al., 2007). Gillette himself (1994) corrected the species name from *halli* to *hallorum*, as he did not apply the right latin ending for the plural in the initial description (Gillette, 1991, 1994). Because the corrected name has since been used more widely than the original proposal, it is followed here. Herne and Lucas (2006) added a femur (NMMNH 25079) from the same quarry to the holotype individual, which is also used to score the taxon in the analysis herein.

***Supersaurus vivianae* BYU (various specimen numbers).** *Supersaurus vivianae* is based on a scapulacoracoid (Jensen, 1985; Curtice et al., 1996; Curtice and Stadtman, 2001; Lovelace et al., 2007). It was found at the Dry Mesa Quarry, intermingled with other large bones of diplodocid, brachiosaurid, and camarasaurid affinities (Jensen, 1985, 1987, 1988; Curtice and Stadtman, 2001). Jensen (1985) described three new taxa based on this material: *Supersaurus vivianae*, *Dystylosaurus edwini*, and *Ultrasauros macintoshi*. Subsequent study of the Dry Mesa specimens indicates that the holotypic dorsal vertebra of *Dystylosaurus*, as well as a dorsal vertebra referred to *Ultrasauros* by (Jensen, 1985, 1987) probably belonged to the same individual as the holotypic scapulacoracoid of *Supersaurus vivianae* (Curtice and Stadtman, 2001). Lovelace et al. (2007) revised this referral based on a new find from Wyoming, agreeing in large parts with Curtice and Stadtman (2001). Since a preliminary analysis of the phylogenetic affinities of *Dystylosaurus* (see above) further corroborated this referral, a combined OTU was used for the final analysis.

***Supersaurus vivianae* WDC DMJ-021.** WDC DMJ-021 is a reasonably articulated skeleton and represents the most complete specimen of *S. vivianae* (Lovelace et al., 2007). It is not directly comparable with the holotype, because no scapulacoracoid was found. Nevertheless, based on the overlap with additional material attributed to the holotypic individual (see above; Lovelace et al., 2007), the identification of WDC DMJ-021 as *S. vivianae* has been widely accepted.

***Suuwassea emilieae*, ANS 21122.** *Suuwassea* was initially identified as flagellicaudatan with uncertain affinities to Diplodocidae or Dicraeosauridae (Harris and Dodson, 2004). Further analyses pointed to a closer relationship with the Dicraeosauridae (Whitlock and Harris, 2010; Whitlock, 2011a), which would mean that *Suuwassea* is the only North American representative

PeerJ Reviewing Manuscript

of this taxon.

***Tornieria africana*, holotype.** The holotype specimen was found at the locality A at Tendaguru, Tanzania (Fraas, 1908; Remes, 2006). *Tornieria* was initially described as *Gigantosaurus africanus* Fraas, 1908, but Sternfeld (1911) noted that this generic name was preoccupied, proposing the combination *Tornieria africana* as replacement. Janensch (1922) suggested synonymy of *Tornieria* and *Barosaurus*, resulting in the combination *Barosaurus africanus*, and later referred much more material from various quarries to the same genus (Janensch, 1935, 1961). However, in a reassessment of the entire material, which also resurrected the name *Tornieria africana*, only two or three individuals were positively identified as belonging to *Tornieria* (Remes, 2006). Remes (2006) identified additional material from the same quarry, and most probably from the same individual as the holotype. I therefore follow Remes (2006) by including all the *Tornieria* material found at locality A in the holotypic OTU.

***Tornieria africana*, skeleton k.** A second specimen of *T. africana* comes from the k-quarry at Tendaguru and was the only individual found at that site (Heinrich, 1999; Remes, 2006). Initially relatively complete with semi-articulated vertebral column and numerous appendicular elements, much of it has been lost or was destroyed during World War II (Remes, 2006). For these elements, descriptions and figures in Janensch (1929b) were used to complement the scoring.

Character list

Skull

C1: Premaxillary anterior margin, shape: without step (0); with marked but short step (1); with marked and long step (2) (Upchurch, 1998; Wilson and Sereno, 1998; modified by Carballido et al., 2012b; Fig. 36).

Comments. The character describes the presence and development of a horizontal portion of the premaxilla, which lies anterior to the nasal process. The step, when present, is best visible in lateral view. It was initially proposed by Upchurch (1998), who scored the Diplodocoidea as unknown or inapplicable, due to a supposed absence of the ascending process. However, some diplodocoids, (e.g. *Suuwassea*) clearly show a distinction between the anterior main body and the posterior ascending process in dorsal view, where they show an abrupt narrowing (Harris, 2006a; ANS 21122, ET, pers. obs., 2011). Diplodocoidea should therefore be scored as '0'. A third state was added in order to distinguish Brachiosauridae from other macronarian sauropods (Carballido et al., 2012b). The character is treated as ordered, due to the gradual change in morphology.

C2: Premaxilla, external surface: without anteroventrally orientated vascular grooves originating

PeerJ Reviewing Manuscript

from an opening in the maxillary contact (0); vascular grooves present (1) (Wilson, 2002; Sereno et al., 2007; Fig. 37).

Comments. The presence of these grooves was previously found as a synapomorphy of Dicraeosauridae (Whitlock, 2011a; Mannion et al., 2012). However, faint grooves originating at the premaxillary-maxillary contact are also visible in *Nigersaurus* (Sereno et al., 2007) and in some diplodocid specimens. In the latter, they fade anteriorly, shortly after the suture (e.g. in CM 11161, 11162, SMA 0011, USNM 2672). In the present analysis, all of these specimens are scored as apomorphic.

C3: Premaxilla, shape in dorsal view: main body massive, with proportionally short ascending process distinct (0); single elongate unit, distinction between body and process nearly absent (1) (Upchurch, 1998; wording modified; Fig. 37).

Comments. Upchurch (1998) formulated this character differently, based on his interpretation that the ascending process of the premaxilla was absent in Diplodocoidea. As stated above, this is not the case. The wording of the derived state was thus changed accordingly.

C4: Premaxilla, angle between lateral and medial margins of premaxilla as seen in dorsal view: > 40° (0); 17°-40° (1); < 17° (2) (Upchurch, 1999; modified; Tab. S3).

Comments. Upchurch (1999) was the first to note significant differences in these angles between diplodocoids (around 10°), nemegtosaurids (18°), and remaining taxa (e.g. *Giraffatitan*, 30°; Upchurch, 1999: fig. 7). He used this character (with two states) as one of several that supported the inclusion of Nemegtosauridae within Diplodocoidea (Upchurch, 1999), a view now falsified by nearly complete finds of new nemegtosaurids that show them to be deeply nested titanosaurians, but with convergences with Diplodocoidea (Wilson, 2002; Curry Rogers, 2005; Zaher et al., 2011). The OTUs included in this dataset were rescored for this character based on figures or on original material. Because the lateral margin is concave to sinuous in most taxa, a straight line was drawn from the anterior-most point of the premaxillary-maxillary contact to the point where the lateral edge curves medially, at the base of the ascending process. The results (Tab. S3) indicate that the distribution of the character scores is not as straightforward as previously thought: *Shunosaurus*, as well as some specimens of *Camarasaurus* appear to show similarly narrow angles as *Dicraeosaurus* and *Suuwassea*. A third state was thus added, such that diplodocid and rebbachisaurid OTUs now score in the narrow-most range, and *Mamenchisaurus* and *Jobaria* are classed as significantly wide-angled taxa. Because the plesiomorphic state is state one, the character was left unordered.

C5: Premaxilla, posteroventral edge of ascending process in lateral view: concave (0); straight

PeerJ Reviewing Manuscript

and dorsally oriented (1); straight, and directed posterodorsally (2) (Whitlock, 2011a; wording modified; Fig. 36).

Comments. Whitlock (2011a: p.35) described the character as follows: 'Ascending process of the premaxilla, shape in lateral view: convex (0); concave, with a large dorsal projection (0); sub-rectilinear and directed posterodorsally (1)'. This formulation is misleading and the states overlap with those of character 1, which describes the premaxillary 'step'. Varying morphologies of the ascending process, following the states of Whitlock (2011a), were observed among the included taxa regarding the posteroventral edge of the ascending process – the margin that delimits the nasal opening anteriorly. The description of the character was adapted, reducing the character to only encompass the orientation of the posteroventral edge, thereby avoiding overlap with character 1. The directional terms in the states are meant in relation to a horizontally oriented ventral edge of the maxilla. Since no state is obviously intermediate relative to the other two, the character is left unordered.

C6: Premaxilla, posterolateral process and the lateral process of the maxillary, shape: without midline contact (0); with midline contact forming a marked narial depression, subnarial foramen not visible laterally (1) (Wilson, 2002; Fig. 38).

Comments. Whitlock (2011a) reversed the polarity of this character, due to a more limited outgroup sampling. With the inclusion of *Shunosaurus* (Mannion et al., 2012), the most basal OTU again lacks the midline contact, as is the case in Diplodocoidea. The original phrasing of Wilson (2002) is therefore preferred.

C7: Premaxilla, dorsoventral depth of anterior portion: remains the same as posteriorly, or widens gradually (0); widens considerably, and abruptly (1) (Harris, 2006a; Fig. 39).

Comments. Harris (2006a) stated this difference as useful to distinguish *Suuwassea* (which retains the same depth) from *Diplodocus* (which widens). A similar, narrow premaxilla is furthermore present in *Kaatedocus* (Tschopp and Mateus, 2013b). The character is difficult to observe in articulated skulls, but single elements do show a significant difference.

C8: Subnarial foramen and anterior maxillary foramen, position: well distanced from one another (0); separated by narrow bony isthmus (1) (Wilson, 2002; Fig. 40).

C9: Maxilla, large foramen anterior to the preantorbital fossa, separated by a narrow bony bridge: absent (0); present (1) (Zaher et al., 2011; wording modified; Fig. 38).

Comments. Generally, sauropod maxillae are pierced by a number of small foramina anteriorly, probably for innervation or blood supply of the replacement teeth. The foramen described by Zaher et al. (2011) in *Tapuiasaurus*, however, is relatively large, and closely attached to the

PeerJ Reviewing Manuscript

preantorbital fossa. The same is the case in *Dicraeosaurus hansemanni* MB.R.2336 (Janensch, 1935), but not in diplodocids.

C10: Maxilla, large foramen posterior to anterior maxillary foramen, dorsal to preantorbital fossa: absent (0); present (1) (New; Fig. 38).

Comments. Few diplodocid specimens show a large foramen posterior to the anterior maxillary foramen (e.g. *Kaatedocus* SMA 0004). This foramen cannot be the same as the one described in character 9, given that both are present in *Dicraeosaurus*.

C11: Anterior maxillary foramen, location: detached from maxillary-premaxillary boundary, facing dorsally (0); lies on medial edge of maxilla, opening medially into the premaxillary-maxillary boundary (1) (New; Fig. 38).

Comments. Usually, diplodocids have the subnarial and the anterior maxillary foramina enclosed within a single, elongated fossa at the maxillary-premaxillary boundary (Wilson and Sereno, 1998; Whitlock, 2011b). However, in *Kaatedocus*, the anterior maxillary foramen is detached and laterally positioned, within a unique, small fossa. It thus resembles the plesiomorphic state present in *Jobaria* or *Camarasaurus* (Wilson and Sereno, 1998; Sereno et al., 1999), although it is still much closer to the subnarial foramen. Primitive outgroup taxa (those normally basal to *Jobaria*) were coded as unknown, as it is unclear if the intermaxillary foramen that is present in these taxa (e.g. He et al., 1988; Ouyang and Ye, 2002) is homologous to the anterior maxillary foramen or the subnarial foramen.

C12: Maxilla, canal connecting the antorbital fenestra and the preantorbital fossa: absent (0); present (1) (New; Fig. 38).

Comments. Such a canal is only present in SMA 0011, and is thus interpreted as autapomorphy of *Galeamopus* [redacted] Taxa without a preantorbital fossa were scored as unknown in order to avoid absence coding.

C13: Maxilla, dorsal process, posterior extent: anterior to or even with posterior process (0); extending posterior to posterior process (1) (Whitlock, 2011a; Fig. 36).

Comments. The character is applied to skulls in lateral view, with the ventral edge of the maxillary oriented horizontally.

C14: Maxilla-quadratojugal contact: absent or small (0); broad (1) (Yu, 1993; Fig. 36).

Comments. Upchurch (1998) reported some difficulties in scoring some taxa to his version of this character, which was defined as a simple absence-presence feature. Reduced, small contacts are present in *Camarasaurus*, but only diplodocids are known to have developed a broad area where the maxilla contacts the quadratojugal (Upchurch, 1998; Wilson and Sereno, 1998).

PeerJ Reviewing Manuscript

Therefore, Whitlock (2011a) redefined the states, such that the apomorphic state now describes a synapomorphy of at least Diplodocidae (it is unknown in Dicraeosauridae and Rebbachisauridae). The derived state appears to be a convergence in some nemegtosaurids (Upchurch, 1998; Wilson, 2005).

C15: Preantorbital fossa: absent (0); present (1) (Tschopp and Mateus, 2013b; Fig. 36).

Comments. Although some flagellicaudatan taxa have reduced to entirely closed preantorbital fenestrae, all show a distinct fossa, which is otherwise only present in some nemegtosaurids (Wilson, 2005).

C16: Preantorbital fossa, if present: with relatively indistinct borders (0); dorsally capped by a thin, distinct crest (1) (Wilson, 2002; modified; Fig. 38).

Comments. Wilson (2002) originally proposed the presence of a dorsally capped preantorbital fenestra as autapomorphy of *Diplodocus*. A broader survey of this character shows that within Flagellicaudata, the absence of this dorsal crest is instead only known from a single apatosaur skull (CM 11162), and thus might represent an autapomorphy of *Apatosaurus louisae*.

C17: Preantorbital fenestra: reduced to absent (0); present, occupying at least 50% of the preantorbital fossa (1) (Berman and McIntosh, 1978; Fig. 39).

Comments. Upchurch (1995) was the first to use this feature in a phylogenetic analysis. Tschopp and Mateus (2013b) modified the character, and included the dorsal crest as well. However, since these two features are not correlated (*Kaatedocus* has a dorsal crest but a reduced to absent fenestra), the states were adjusted, and a ratio is given to distinguish the small opening in *Dicraeosaurus* from the large ones in *Galeamopus*, for example. Large preantorbital fenestrae are convergently present in nemegtosaurids (Wilson, 2005; Zaher et al., 2011).

C18: Antorbital fenestra, maximum diameter: much shorter than orbital maximum diameter, less than 90% of orbit (0); subequal to orbital maximum diameter, greater than 90% orbit (1) (Yu, 1993; modified; Tab. S4).

Comments. Wilson (2002) proposed the character without any clear state boundaries, which were later added by Whitlock (2011a), and changed herein from 85% to 90% in order to have *Mamenchisaurus* within the plesiomorphic state.

C19: Antorbital fenestra, anterior extension: is restricted posterior to preantorbital fossa (0); reaches above preantorbital fossa (1) (New; Fig. 36).

Comments. The character has to be scored with the ventral border of the maxilla oriented horizontally. Within flagellicaudatans, the derived state is most developed in *Kaatedocus* SMA 0004, but nemegtosaurids like *Rapetosaurus* have extremely elongated antorbital fenestrae that

PeerJ Reviewing Manuscript

even reach anterior to the entire preantorbital fossa (Curry Rogers and Forster, 2004).

C20: Antorbital fenestra, shape of dorsal margin: straight or convex (0); concave (1) (Whitlock, 2011a; Fig. 36).

Comments. The diplodocine skull AMNH 969 appears to have a convex dorsal margin at first glance. However, the presence of a lateral projection in the upper half of this edge indicates that the convex shape might be due to deformation. The lateral projection in AMNH 969 is at the same location, and has the same shape as the osteological feature producing the concave dorsal edge of the antorbital fenestra in CM 11161. AMNH 969 is thus interpreted to be derived and thus share the flagellicaudatan synapomorphy.

C21: External nares, position: retracted to level of orbit, facing laterally (0); retracted to position between orbits, facing dorsally or dorsolaterally (1) (McIntosh, 1989; Upchurch, 1995; modified by Whitlock, 2011a; Fig. 36).

Comments. Upchurch (1995) was the first to include this character in a phylogenetic analysis, based on observations made by McIntosh (1989). Whitlock (2011a) adjusted the state description, since the reduced taxon sampling made a third state redundant (anterior to orbit, the plesiomorphic state in Sauropoda; Upchurch, 1995).

C22: External nares, maximum diameter: shorter than orbital maximum diameter (0); longer than orbital maximum diameter (1) (Upchurch, 1995; modified by Wilson and Sereno, 1998).

Comments. Upchurch (1995) initially defined the character states in relation to skull length, but later, Wilson and Sereno (1998) changed them to relate with orbital diameter. The latter has since been widely used and is thus retained here.

C23: Prefrontal, medial margin, shape: without distinct anteromedial projection (0); curving distinctly medially anteriorly to embrace the anterolateral corner of the frontal (1) (New; Fig. 41).

Comments. In some basal sauropods, the prefrontal is located entirely anterior to the frontal. These cases are scored as plesiomorphic.

C24: Prefrontal, posterior process size: small, not projecting far posterior of frontal-nasal suture (0); elongate, approaching parietal (1) (Wilson, 2002; Fig. 42).

Comments. This character is not as straight-forward as it seems. Care has to be taken that one observes the frontal and prefrontal in exactly perpendicular view. In some reconstructed dorsal views of the skull of *Diplodocus* (Wilson and Sereno, 1998; Whitlock, 2011b), the posterior extension of the prefrontal is remarkable, but this is due to the view, in which the reconstruction is drawn. The frontal slants posteriorly, and more posterior distances therefore appear shorter. In direct dorsal view, differences in distance between taxa diminish. However, the character remains

PeerJ Reviewing Manuscript

PeerJ Reviewing Manuscript

informative: in diplodocids like *Apatosaurus* or *Diplodocus*, the posterior process of the prefrontal almost reaches or surpasses the midlength of the frontal, whereas in Rebbachisauridae or in *Kaatedocus* and *Tornieria*, it remains restricted to about the anterior third (Fig. 42).

C25: Prefrontal, posterior process shape: straight (0); hooked (1) (Wilson, 2002; modified; Fig. 42).

Comments. As the posterior elongation of the prefrontal, also this character was initially defined in a somewhat ambiguous way (flat/hooked). *Nigersaurus* does have a posteriorly facing, pointed prefrontal. The description 'flat' therefore does not fit very well, and it is replaced by 'straight'. Hooked is herein interpreted to describe a medially curving posterior process, such that its posterior end forms the medial-most extension of the prefrontal.

C26: Frontals, midline contact (symphysis): patent suture (0); fused in adult individuals (1) (Salgado and Calvo, 1992; Yu, 1993; Fig. 40).

Comments. Fusion of skull bones is usually considered an ontogenetic feature (Varricchio, 1997; Whitlock et al., 2010). However, the ontogenetic stages, when fusion begins, might still be different between taxa and thus phylogenetically significant. This appears to be the case here, where the braincases of *Dicraeosaurus* and *Amargasaurus* have completely obliterated sutures between the frontals, whereas large-sized diplodocid skulls do not (e.g. CM 11161). Nonetheless, it remains possible that non-dicraeosaurid sauropods fuse their frontals at an old age. In future, it might be helpful to constrict the character to a specific age-range (possibly subadult or early adult), but to date, the exact individual age of the specimens showing the fused frontals remains unknown.

C27: Frontal, anteroposterior length: long, > 1.4 times minimum transverse width (0); short, 1.4 or less times minimum transverse width (1) (Gauthier, 1986; modified; Tab. S5).

Comments. This character was widely used in phylogenetic analyses of sauropod dinosaurs (Upchurch, 1998; Wilson, 2002; Whitlock, 2011a; Mannion et al., 2012; Tschopp and Mateus, 2013b), with varying definitions of the state boundaries. In addition, it was often unclear if minimum or maximum transverse width was intended (e.g. Whitlock, 2011a; Tschopp and Mateus, 2013b). As shown in table S5, there are significant differences in the ratios, with more distinct changes when comparing frontal length and minimum transverse width. Therefore, state boundaries were herein defined numerically, which also led to some differential scorings compared to Tschopp and Mateus (2013b). *Kaatedocus*, for example, is now well within the ratios for the apomorphic state.

C28: Frontal-nasal suture, shape: flat or slightly bowed anteriorly (0); v-shaped, pointing

posteriorly (1) (Whitlock, 2011a; Fig. 41).

Comments. The frontals of *Galeamopus hayi* might have a posteriorly pointing nasal contact as well (Holland, 1906). However, the nasals are not preserved in this specimen, and it seems thus more appropriate to code HMNS 175 as unknown.

C29: Frontals, distinct anterior notch medially between the two elements: absent (0); present (1) (Tschopp and Mateus, 2013b; modified; Fig. 40).

Comments. The shape description of the notch was excluded from the character in order to include also *Spinophorosaurus*, and SMA 0011 in the apomorphic state. The frontal usually becomes extremely thin in this part, and it is thus easily broken. Since in these three taxa/specimens, the notch still appears genuine, the character was retained. Tschopp and Mateus (2013b) mentioned this feature as autapomorphy of *Kaatedocus*. Given that a similar notch is present in SMA 0011, this character might actually be more widespread within Diplodocidae. In fact, many specimens (e.g. *Apatosaurus* CM 11162) show broken anteromedial edges in the frontal, which makes it difficult to evaluate this character. Additional, new finds of diplodocid frontals might shed some more light on the distribution of this character.

C30: Frontals, dorsal surface: without paired grooves facing anterodorsally (0); grooves present, extend on to nasal (1) (Whitlock, 2011a; Fig. 40).

Comments. Grooves appear to be present on the frontals of the dicraeosaurid *Amargasaurus cazaui* (Salgado and Calvo, 1992: fig. 2B), but these extend onto the prefrontals and not the nasals, and do not extend as far posteriorly as in *Limaysaurus*. *Amargasaurus* is thus scored as plesiomorphic, following Whitlock (2011a).

C31: Frontal, lateral edge in dorsal view: relatively straight (0); deeply concave (1) (New; Fig. 42).

Comments. This character has a somewhat ambiguous distribution. There is some difference in the shapes taken together in the plesiomorphic state as well: Rebbachisauridae, in contrast with most other taxa, have a weakly convex lateral frontal edge. Diplodocids exhibit varying shapes: *Apatosaurus* and *Diplodocus* have concave edges, whereas *Kaatedocus* or *Tornieria* have straight margins.

C32: Frontal, contribution to dorsal margin of orbit: less than 1.5 times the contribution of prefrontal (0); at least 1.5 times the contribution of prefrontal (1) (Whitlock, 2011a; modified by Mannion et al., 2012; Tab. S6).

Comments. The lengths of the frontal and prefrontal are measured in a straight line in lateral view, from the mid-point of the frontal-prefrontal articulation to the anterior-most (prefrontal) or

PeerJ Reviewing Manuscript

posterior-most (frontal) point. Whitlock (2011a) proposed the character leaving a gap between plesiomorphic and apomorphic states (subequal, or twice), which was changed by Mannion et al. (2012). A comparative analysis of the included specimens confirms the utility of the boundary proposed by Mannion et al. (2012).

C33: Frontal, free lateral margin: rugose (0); smooth (1) (Tschopp and Mateus, 2013b; Fig. 42).

Comments. Rugosities are present around the dorsal margin of almost all sauropods, but in some cases, they are shifted onto the prefrontal or the postorbital. Tschopp and Mateus (2013b) hypothesized that the rugosities served for an attachment of a palpebral element.

C34: Frontal, contribution to margin of supratemporal fenestra/fossa: present (0); absent, frontal excluded from anterior margin of fenestra/fossa (1) (Wilson and Sereno, 1998; Fig. 40).

Comments. In the derived state, the frontal is excluded from a contribution to the margin of the supratemporal fenestra by a contact between the medial process of the postorbital and the anterolateral process of the parietal.

C35: Frontal-parietal suture, position of medial portion: closer to anterior extension of supratemporal fenestra (0); closer to posterior extension (1) (Tschopp and Mateus, 2013b; modified; Fig. 40).

Comments. Tschopp and Mateus (2013b) formulated the character inspired by Remes (2006), who mentioned the position of the fronto-parietal suture as a feature to distinguish *Tornieria* from *Diplodocus*. They used a three-partite character, with an intermediate state close the the central portion of the supratemporal fenestra (Tschopp and Mateus, 2013b). The position of the suture is difficult to assess in some diplodocid specimens, because it describes a strongly sinuous curve (e.g. CM 11161, Fig. 42). The character is thus restricted to the medial portion of the suture herein. By doing so, it becomes clear that the majority of *Diplodocus* skulls shifted the suture backwards, whereas all other specimens have it anteriorly located. The posterior dislocation might thus prove to be an autapomorphy of *Diplodocus.* The intermediate state becomes redundant.

C36: Pineal (parietal) foramen between frontals and parietals: present (0); absent (1) (Yu, 1993; modified; Fig. 40).

Comments. This character was proposed combined with the presence of a postparietal foramen (Yu, 1993). The two are herein separated in two characters, because *Kaatedocus* SMA 0004 has a postparietal but no pineal foramen (Tschopp and Mateus, 2013b). The presence of a pineal foramen is often difficult to assess due to breakage of the area around the fronto-parietal suture (McIntosh, 1990b; Upchurch et al., 2004a; Harris, 2006a). However, in some specimens, the

PeerJ Reviewing Manuscript

presence or absence of this feature is genuine, and it thus appears appropriate to include this character. Specimens, where the presence of the foramen has been doubted previously are scored as unknown. At the current state of knowledge, the presence seems to be a retained plesiomorphy characterizing the Dicraeosauridae, but in many diplodocid specimens its presence cannot be dismissed yet.

C37: Orbit, anterior-most point: anterior to the anterior extremity of lateral temporal fenestra (0); roughly even with or posterior to anterior extent of lateral temporal fenestra (1) (Gauthier, 1986; Upchurch, 1995; modified by Whitlock, 2011a; Fig. 36).

Comments. The original character was a multistate character (Upchurch, 1995). Given the limited taxon sampling of Whitlock (2011a) and the herein presented analysis, the third state becomes redundant (infratemporal fenestra restricted posterior to orbit).

C38: Orbital ventral margin, anteroposterior length: broad, with subcircular orbital margin (0); reduced, with acute orbital margin (1) (Wilson and Sereno, 1998; Fig. 36).

Comments. The derived state results in a teardrop-shape of the orbit. With the ventral margin of the maxilla held horizontally, the 'ventral margin' would be better described with 'anteroventral corner'.

C39: Postorbital, posterior process: present (0); absent (1) (Wilson, 2002; Fig. 36).

Comments. The postorbital is usually a triradiate bone, with a relatively short posterior process that overlaps the squamosal. The latter is absent in rebbachisaurids (Wilson, 2002; Whitlock, 2011a).

C40: Jugal, contribution to antorbital fenestra: very reduced or absent (0); large, bordering approximately one-third of its perimeter (1) (Berman and McIntosh, 1978; Upchurch, 1995; modified by Whitlock, 2011a; Fig. 43).

Comments. Recognized as distinctive feature of Diplodocoidea by Berman and McIntosh (1978), the contribution of the jugal to the antorbital fenestra was first used as phylogenetic character by Upchurch (1995). Whitlock (2011a) defined the state boundaries quantitatively.

C41: Jugal, contact with ectopterygoid: present (0); absent (1) (Upchurch, 1995; Fig. 44).

Comments. The development of this character is barely known in sauropods. If preserved, the osteology of the palatal complex is often left obscured by matrix due to stability reasons. At the current state of knowledge, the ectopterygoid becomes anteriorly dislocated in Neosauropoda, and contacts the maxilla instead of the jugal. Future CT scanning of additional skulls will yield more detailed results.

C42: Jugal, posteroventral process: short and broad (0); narrow and elongate (1) (New; Fig. 43).

PeerJ Reviewing Manuscript

Comments. This character shows varying shapes in the skulls traditionally identified as *Diplodocus* (CM 11161 has a short process, whereas in all other skulls they are elongated). However, too few diplodocid jugals are preserved entirely in order to evaluate the distribution of this character to date.

C43: Jugal, dorsal process: present (0); absent (1) (Yu, 1993; polarity inverted; Fig. 43).

Comments. Yu (1993) proposed the dorsal process as a synapomorphy for Diplodocidae. However, no jugal is known from dicraeosaurids, and such a process is also present in *Shunosaurus*, *Omeisaurus*, and *Mamenchisaurus* (Janensch, 1935; He et al., 1988; Salgado and Calvo, 1992; Chatterjee and Zheng, 2002; Ouyang and Ye, 2002). Since the latter basal taxa show dorsal processes of the jugal, the character polarity was inverted relative to the original version (Yu, 1993). Although they are scored the plesiomorphic state, Diplodocidae are still distinguishable from *Shunosaurus* and the other taxa by the strong development of the dorsal process, and its anterior displacement. In *Omeisaurus*, e.g., the dorsal process is short and located at midlength of the jugal-lacrimal suture (He et al., 1988).

C44: Jugal, anterior spur dorsally, which projects into antorbital fenestra: absent (0); present (1) (New; Fig. 43).

Comments. Such a spur is present in many diplodocid specimens, although in USNM 2672, it only occurs on the left side (ET, pers. obs., 2011). However, the possibility to develop such a spur still appears to be restricted to Diplodocidae, and the character is thus used in the analysis. USNM 2672 is scored as 'present'.

C45: Quadratojugal, position of anterior terminus: anterior margin of orbit or posteriorly restricted (0); beyond anterior margin of orbit (1) (Whitlock, 2011a; modified; Fig. 36).

Comments. The character is coded with the ventral margin of the maxilla held horizontally. State boundaries by Whitlock (2011a: posterior to middle of orbit, anterior margin or beyond) were adjusted because all diplodocoids show strongly elongated anterior processes that end significantly anterior to the orbit. On the other hand, in *Mamenchisaurus* or *Brachiosaurus*, they reach the anterior margin of the orbit (Janensch, 1935; Ouyang and Ye, 2002), which would request a coding as apomorphic when following the description of Whitlock (2011a).

C46: Quadratojugal, angle between anterior and dorsal processes: less than or equal to 90°, so that the quadrate shaft is directed dorsally (0); greater than 90°, approaching 130°, so that the quadrate shaft slants posterodorsally (1) (Gauthier, 1986; Upchurch, 1995; Fig. 36).

Comments. The angle between the quadratojugal processes reach their maximum in the large skulls CM 11161 and 11162. In smaller skulls (of both ontogenetically younger as well as

PeerJ Reviewing Manuscript

phylogenetically more basal specimens), the angle is of approximately 110° (e.g. *Kaatedocus* SMA 0004; Tschopp and Mateus, 2013b), but still clearly in the derived state.

C47: Lacrimal, anterior process: absent (0); present (1) (Wilson, 2002; polarity reversed by Mannion et al., 2013; Fig. 36).

Comments. Wilson (2002) initially proposed the character with inverted polarity. This was changed by Mannion et al. (2013), and herein in order to have the chosen outgroups showing the plesiomorphic state. An anterior process is usually interpreted to be absent in diplodocoids. However, *Galeamopus* [redacted] SMA 0011 and *Dicraeosaurus* do have one. On the other hand, it is possible that the feature is more widespread among Diplodocoidea, but that the anterior process is obscured by the posterodorsal process of the maxilla. The latter partly overlaps the anterior process of the lacrimal in SMA 0011. The presence of an anterior process of the lacrimal would otherwise be one of the distinguishing characteristics between diplodocoids and nemegtosaurids (Wilson, 2005).

C48: Lacrimal, dorsal portion of lateral edge: flat (0); bears dorsoventrally elongate, shallow ridge (1); bears a dorsoventrally short laterally projecting spur (2) (Tschopp and Mateus, 2013b; Fig. 38).

Comments. There is some evidence that this character is ontogenetically controlled (Tschopp and Mateus, 2013b): only small skulls show the laterally projecting spur. The character is retained here in order to test its validity. The character is treated as ordered due to intermediate morphologies.

C49: Quadrate, articular surface shape: quadrangular in ventral view, orientated transversely (0); roughly triangular in shape (1); thin, crescent-shaped surface with anteriorly directed medial process (2) (Whitlock, 2011a; Fig. 45).

Comments. The character is treated as ordered as state '1' is intermediate in morphology.

C50: Quadrate, short transverse ridge medially on posterior side of ventral ramus, close to the articular surface with the lower jaw: absent (0); present (1) (New; Fig. 46).

Comments. This ridge is a small detail which appears to be synapomorphic for Diplodocidae. Most of the diplodocid quadrates could not have been investigated in original for this character. Therefore a more detailed evaluation of this character has to be undertaken in order to corroborate the presence or absence of such a ridge, and its taxonomic utility.

C51: Quadrate fossa, depth: shallow (0); deeply invaginated (1) (Russell and Zheng, 1993; Fig. 46).

C52: Quadrate, shallow, second fossa medial to pterygoid flange on quadrate shaft (not the

PeerJ Reviewing Manuscript

quadrate fossa): absent (0); present, becoming deeper towards its anterior end (1) (Tschopp and Mateus, 2013b; wording modified; Fig. 47).

Comments. The medial surface of the pterygoid flange is nearly always concave, but concave dorsoventrally. In SMA 0004, as well as some other diplodocid specimens, the second fossa is transversely concave, lies anteriorly on the posterior shaft, medial to where the pterygoid flange originates. There is a chance that the character might be ontogenetic, given that no large-sized skull has yet been identified to bear this second fossa. The character was slightly reworded from its original version (Tschopp and Mateus, 2013b) in order to describe the location of the fossa better.

C53: Quadrate, dorsal margin: concave, such that pterygoid flange is distinct from quadrate shaft (0); straight, without clear distinction of posterior extension of pterygoid flange (1) (New; Fig. 47).

C54: Quadrate, posterior end (posterior to posterior-most extension of pterygoid ramus): short and stocky (0); elongate and slender (1) (New; Fig. 47).

C55: Squamosal, anterior extent: restricted to postorbital region (0); extends well past posterior margin of orbit (1); extends beyond anterior margin of orbit (2) (Whitlock, 2011a; Fig. 36).

Comments. The anterior extent of the squamosal is measured with the ventral border of the maxilla oriented horizontally. The character is treated as ordered.

C56: Squamosal-quadratojugal contact: present (0); absent (1) (Upchurch, 1995; Fig. 48).

Comments. In diplodocids, where no contact is present, the distance between the squamosal and the quadratojugal varies (Whitlock et al., 2010; Whitlock and Lamanna, 2012). However, most of the diplodocid specimens do not preserve the entire anterior ramus of the squamosal (ET, pers. obs., 2011) and it seems thus premature to include the distance as a phylogenetic character.

C57: Squamosal, posteroventral margin: smooth, or with short and blunt ventral projection (0); with prominent, ventrally directed 'prong' (1) (Whitlock, 2011a; modified; Fig. 48).

Comments. The original character description of Whitlock (2011a) was modified, and an additional binary character was added (see below) in order to describe better the state in *Kaatedocus*, where a short ventral projection of the squamosal is present.

C58: Squamosal, posteroventral margin: smooth, without ventral projection (0); ventral projection present (1) (Whitlock, 2011a; modified; Fig. 48).

Comments. A short projection is present in almost all preserved flagellicaudatan skulls. On the contrary, most non-flagellicaudatan sauropods do have smooth posteroventral margins of the squamosal.

PeerJ Reviewing Manuscript

C59: Parietal, contribution to posttemporal fenestra: present (0); absent (1) (Wilson, 2002; Fig. 49).

Comments. The absence of parietal contribution to the posttemporal fenestra is sometimes difficult to observe due to imperfectly preserved or distorted skulls. All diplodocid skulls have exoccipitals that bear a dorsolateral spur, which forms the dorsomedial end of the posttemporal fenestra (the 'posttemporal process' of Harris, 2006a). Additionally, most of them have dorsally extended distal ends of the paroccipital processes, which curve back towards the exoccipital spur. These two prominences are interconnected by the squamosal in complete diplodocid skulls (CM 11161, ET, pers. obs., 2011).

C60: Parietal, portion contributing to skull roof, anteroposterior length/transverse width: wide, > 50% (0); narrow, 7-50% (1); practically nonexistent, < 7% (2) (New; Tab. S7).

Comments. In some taxa, the posterior-most point of the fronto-parietal suture is located posterior to the supratemporal fenestra. The minimum values are compared in this ratio. The character was treated as ordered in the present analysis.

C61: Parietal, distance separating supratemporal fenestrae: less than 1.5 times the width of the long axis of the supratemporal fenestra (0); at least 1.5 times the length of the long axis of the supratemporal fenestra (1) (Wilson, 2002; modified by Mannion et al., 2012; Tab. S8).

Comments. The original character states of Wilson (2002) left a gap (subequal, or double). The distance between the supratemporal fenestrae in many diplodocid specimens does not reach two times the maximum diameter of the fenestra, which led Mannion et al. (2012) to adjust the state boundaries. Specimens were remeasured where possible (Tab. S8), for others scorings of Wilson (2002) or Mannion et al. (2012) were used. The new measurements show that the ratios are often overestimated, and that there seem to be three clusters of taxa (less than one: *Brachiosaurus*, and probably *Mamenchisaurus*, *Omeisaurus*, *Jobaria*, *Turiasaurus*; between one and 1.6 times: *Spinophorosaurus*, *Camarasaurus*, *Kaatedocus*, CM 11161 and 11162; more than 1.6 times, *Suuwassea*, *Galeamopus*, CM 3452, and probably Rebbachisauridae and Dicraeosauridae). However, a more inclusive study of this character should be performed in order to recognize the most useful state boundaries for phylogenetic analyses. At the moment it seems wisest to stay with the proposed version of Mannion et al. (2012).

C62: Parietal, posterolateral process, dorsal edge in posterior view: straight, and ventrolaterally oriented, so that the supratemporal fenestra is slightly facing posteriorly as well (0); convex, so that the postorbital and thus the supratemporal fenestra are not visible (1) (Tschopp and Mateus, 2013b; Fig. 49).

PeerJ Reviewing Manuscript

Comments. The posterior view of the skull corresponds to the view parallel to the long axis of the occipital condylar neck, which was found to be oriented parallel to the lateral semicircular canal, thus indicating the neutral head position (Schmitt, 2012).

C63: Parietal, occipital process, dorsoventral height: low, subequal to less than the diameter of the foramen magnum (0); high, nearly twice the diameter of the foramen magnum (1) (Wilson, 2002; modified; Tab. S9).

Comments. Measurements are taken in strict posterior view (see above). Height is measured vertically between the dorsal-most and ventral-most extension of the occipital process, and the foramen magnum. In case of the occipital process, the dorsal- and ventral-most points are usually transversely shifted against each other. The measurement are therefore taken between horizontal lines intersecting the extremes. The state boundaries are tentatively set at 1.5, but more inclusive analyses would have to be undertaken in order to score this character adequately.

C64: Parietal, occipital process, distal end: ventrolaterally oriented, such that dorsolateral edge is straight or convex (0); curving laterally, such that dorsolateral edge becomes concave distally (1) (New; Fig. 49).

Comments. The distal end of the posterolateral process of the parietal of non-diplodocine flagellicaudatans curves outwards to meet the squamosal. This is not the case in the diplodocine skulls examined for this analysis.

C65: Parietal, distinct horizontal ridge separating dorsal from posterior portion: absent, transition more or less confluent (0); present, creating a distinct nuchal fossae below the ridge (1) (Tschopp and Mateus, 2013b; wording modified; Fig. 50).

Comments. This character is best observable in oblique posterolateral view, if one does not have the specimens at hand. In the derived state, the transverse ridge caps the nuchal fossa dorsally, creating a distinct concavity below it. Given that small skulls appear to have this feature most expressed (AMNH 7530, CM 3452, SMA 0004), there is some possibility that the nuchal fossae become shallower during ontogeny.

C66: Postparietal foramen: absent (0); present (1) (Upchurch, 1995; Fig. 40).

Comments. Postparietal foramina have been interpreted to be a dicraeosaurid synapomorphy (Whitlock, 2011a), but were recently shown to be present as well in Diplodocidae (Tschopp and Mateus, 2013b). The opening is located at the posteromedial corner of the two parietals, where they meet the supraoccipital. It might be associated with a vertical groove internally on the supraoccipital (Remes, 2006; see below), but additional CT studies would have to be performed in order to check for the presence or absence of this groove in specimens without the postparietal

PeerJ Reviewing Manuscript

foramen. Many diplodocid specimens are damaged in this region of the skull, which makes it difficult to verify the presence of the foramen, and impedes an evaluation of its distribution among flagellicaudatans. The definitive presence in *Kaatedocus*, and the unknown state in the two apatosaur skulls CM 11162 and YPM 1860 (due to crushing; ET, pers. obs., 2011), indicates that it might be plesiomorphic for Flagellicaudata, subsequently lost in *Tornieria* and *Diplodocus*.

C67: Paroccipital process (popr), posterior face: smooth/flat (0); with longitudinal ridge along popr body extending from dorsomedial to ventrolateral corners (1) (Tschopp and Mateus, 2013b; Fig. 51).

Comments. Most of the specimens examined have a slightly convex posterior face of the paroccipital processes. However, few have such a distinct ridge as is present in *Kaatedocus*. In the latter, this ridge is accompanied by a rugose area at its dorsomedial origin. None of these structures are present in CM 11161, for example.

C68: Paroccipital process distal terminus: expanded vertically (0); not expanded (dorsal and ventral edges are subparallel) (1) (Upchurch, 1998; modified; Fig. 49).

Comments. Upchurch (1998) included two morphologies in one character: the dorsoventral expansion, and the rounded or straight distal edge. The shape of the distal edge is difficult to assess qualitatively, as many specimens have slightly convex, or somewhat triangular lateral ends of the paroccipital process (e.g. *Suuwassea* ANS 21122, or *Kaatedocus* SMA 0004, Fig. 49). Therefore, the character description was limited to the distal expansion.

C69: Paroccipital process, distal end in lateral view: straight (0); curved (1) (New; Fig. 52).

Comments. Due to the slight posterior orientation of the paroccipital processes in many sauropod taxa, a strict lateral view of the skull does often not allow for an accurate coding of this character. Also, on pictures of articulated skulls it is often difficult to see the distal end of the paroccipital process well enough, because it is partly obscured by the squamosal. In most cases, a posterolateral instead of lateral view would thus be more helpful.

C70: Supratemporal fenestra: present, relatively large (anteroposterior diameter is at least 5% of occiput width) (0); absent, or greatly reduced (so that anteroposterior diameter is less than 5% of occipital width) (1) (Wilson, 2002; modified by Mannion et al., 2012).

Comments. Wilson (2002) proposed this feature as present/absent character, but Mannion et al. (2012) showed that one of Wilson's (2002) derived taxa (*Limaysaurus*) actually has a supratemporal fenestra, although an extremely reduced one. Since this is a derived state of Rebbachisauridae, and all diplodocid skulls show large openings, no additional measuring was done for this analysis.

PeerJ Reviewing Manuscript

C71: Supratemporal fenestra, maximum diameter: more than 1.2 times greatest diameter of foramen magnum (0); less than 1.2 times the greatest length of foramen magnum (1) (Yu, 1993; modified by Mannion et al., 2012).

Comments. Mannion et al. (2012) introduced the quantitative state boundaries to the original description (Yu, 1993). Basically, this character is an extension of the previous one, with the exception that *Nigersaurus* is impossible to score due to the complete absence of the supratemporal fenestra in this taxon. In addition to *Limaysaurus*, the quantitative boundaries of Mannion et al. (2012) also include the dicraeosaurids *Dicraeosaurus* and *Amargasaurus*, which have reduced supratemporal fenestra as well, but not to the extent shown by Rebbachisauridae. As stated above, the difference in relative size of the supratemporal fenestrae between the mentioned taxa and Diplodocidae is large, and thus no additional measurements were taken in order to test the boundaries proposed by Mannion et al. (2012).

C72: Supraoccipital, anterodorsal margin: internally concave, associated with a channel extending ventrally on the internal face (0); straight (1) (Remes, 2006; Fig. 53).

Comments. The channel was proposed by Remes (2006) as a distinguishing character between *Tornieria* and Dicraeosauridae, where the presence of the canal is coupled with the presence of a postparietal fenestra. However, as shown in *Kaatedocus*, these two features are not necessarily correlated. A separate coding for the two characters is thus justifiable. This is the first analysis to include this character.

C73: Supraoccipital, dorsal extension: high and vaulted, such that the dorsolateral edges are strongly sinuous (0); low, with the dorsolateral edges straight (1) (Remes, 2006; Fig. 49).

Comments. Remes (2006) used this character in order to distinguish *Tornieria* from *Apatosaurus*, but did not include it in his phylogenetic analysis. The present analysis is thus the first one to do so.

C74: Supraoccipital: sagittal nuchal crest: broad, weakly developed (0); narrow, sharp, and distinct (1) (Whitlock, 2011a; Fig. 54).

Comments. The nuchal crest lies on the midline of the supraoccipital, extending dorsoventrally. A narrow, sharp crest was previously thought to be a synapomorphy for Dicraeosauridae, but Tschopp and Mateus (2013b) showed that it also occurs in certain diplodocids.

C75: Supraoccipital, foramen close to contact with parietal: absent (0); present (1) (Tschopp and Mateus, 2013b; Fig. 54).

Comments. This foramen is called external occipital foramen by Balanoff et al. (2010), and is sometimes located entirely on the supraoccipital (*Dicraeosaurus hansemanni* MB.R.2379,

PeerJ Reviewing Manuscript

Janensch, 1935), and in other cases on the suture with the parietal (*Kaatedocus siberi* SMA 0004, ET, pers. obs., 2010). Only taxa with well visible foramina are coded as apomorpic.

C76: Crista prootica, size: rudimentary (0); expanded laterally into dorsolateral process (1) (Salgado and Calvo, 1992; Upchurch, 1995; Fig. 55).

Comments. Although diplodocids have a laterally protruding crista prootica (e.g. SMA 0011), only dicraeosaurids develop distinct lateral processes at the anteroventral ends of the crista prootica.

C77: Occipital condyle, articular surface: well offset from condylar neck (0); continuously grading into condylar neck (1) (New; Fig. 56).

Comments. Whereas in more basal sauropods the articular surface of the occipital condyle is usually well delimited, and offset from the condylar neck by a distinct ridge, diplodocids generally do not have such a clear distinction. The character states are most easily distinguished in dorsal view.

C78: Basioccipital, contribution to dorsal side of occipital condylar neck: present and broad, around 1/3 of entire dorsal side (0); reduced to absent (1) (Harris and Dodson, 2004; Fig. 49).

Comments. Harris and Dodson (2004) proposed the narrow contribution of the basioccipital to the dorsal face of the occipital condyle as characteristic for *Suuwassea*. A wider survey of the distribution of this character showed that the contribution of the basioccipital to the dorsal side of the occipital condylar neck is reduced in some diplodocid specimens as well.

C79: Basioccipital, distance from base of occipital condyle to base of basal tubera (best visible in lateral view): short, such that area is gently U-shaped in lateral view (0); elongate, with a flat portion between occipital condyle and basal tubera (1) (Tschopp and Mateus, 2013b; wording modified; Fig. 52).

Comments. The distance is taken relative to the height of the basal tuber, creating a narrow U-shape or a shallow, wide concavity in lateral view (Fig. 52).

C80: Basioccipital depression between foramen magnum and basal tubera: absent (0); present (1) (Wilson, 2002; Fig. 57).

Comments. The depression is a concave area on the posterolateral sides of the basioccipital, which is different from the concavity on the posterior face of the basal tubera described in character 85.

C81: Basioccipital, pit between occipital condyle and basal tubera: absent (0); present (1) (New; Fig. 58).

Comments. Various pits can be present in the area around the basal tubera: YPM 1860 bears one

PeerJ Reviewing Manuscript

within the notch between the tubera (see below), and a second one on the basioccipital posterior to the tubera (which is the one described here). Also the basipterygoid recess is located close by, but anterior to the basal tubera on the basisphenoid, instead of the basioccipital.

C82: Basal tubera: globular (0); box-like (1) (Whitlock et al., 2010; Fig. 59).

Comments. Whitlock et al. (2010) used this character as one of the features distinguishing the juvenile diplodocid skull CM 11255 from *Apatosaurus*. It is herein used for the first time as a phylogenetic character.

C83: Basal tubera, breadth: <1.3 times (0); 1.3-1.85 times (1); >1.85 times occipital condyle width (2) (Wilson, 2002; modified; Tab. S10).

Comments. The character was initially defined without clear state borders, and only with two states (Wilson, 2002). Mannion (2011) suggested to further subdivide the character, based on a wider survey of this ratio among sauropods. Mannion's (2011) table was here extended and the character state boundaries were modified following higher-level taxonomy and gaps in the distribution of the values.

C84: Basal tubera: distinct from basipterygoid (0); reduced to slight swelling on ventral surface of basipterygoid (1) (Whitlock, 2011a; Fig. 60).

Comments. The use of this character and its coding overlaps with an additional character proposed by Wilson (2002): 'Basal tubera, anteroposterior depth: approximately 33%, or more, of dorsoventral height (0); sheetlike, less than 33% (normally around 20%) dorsoventral height (1)'. Whitlock's (2011a) character is herein preferred as the directional terms used in Wilson (2002) are sometimes confusing due to varying orientations of the basal tubera of Diplodocoidea and non-diplodocoid sauropods.

C85: Basal tubera, shape of posterior face: convex (0); flat (1); slightly concave (2) (Whitlock, 2011a; modified by Tschopp and Mateus, 2013b; Fig. 60).

Comments. The 'posterior face' of the basal tubera is herein intended to be the side facing the occipital condyle. The concavity described herein is different from the concavity sometimes present on the lateral side of the basioccipital (see above).

C86: Basal tubera, posteroventral face: continuous (0); marked by a distinct transverse ridge (1) (New; Fig. 60).

Comments. The surface of the basal tubera is usually regularly rugose, and without distinct structuring. SMA 0004, however, bears a distinct transverse ridge on the posteroventral face of its basal tubera.

C87: Basal tubera, longest axes: parallel (0); in an angle to each other, pointing towards the

PeerJ Reviewing Manuscript

occipital condyle (1) (New; Fig. 61).

Comments. The character is to be coded based on a view perpendicular to the orientation of the basipterygoid processes. It is inspired by the character of Tschopp and Mateus (2013b) describing the anterior margin of the tubera as V- or U-shaped, which included two differing morphologies in the same character (orientation of the tubera and shape of the anterior margin). The two morphologies are here treated as different characters (see below). In some cases (e.g. CM 11162), the outline of the tubera is subtriangular, with a more or less right angle pointing posterolaterally. These cases were treated as apomorphic, because the longest distance follows the obliquely oriented hypotenuse of the triangle.

C88: Basal tubera, anterior edge: straight or convex (0); concave (1) (Tschopp and Mateus, 2013b; Fig. 61).

Comments. The second of the two characters inspired by Tschopp and Mateus' (2013b) character about the anterior margin of the basal tubera. The anterior edge is the one facing towards the basipterygoid processes, which in non-diplodocoid sauropods is oriented rather anteroventrally. In specimens with angled basal tubera (see above), the anterior margin is oriented obliquely.

C89: Basal tubera in posterior view: facing ventrolaterally (0); facing straight ventrally, forming a horizontal line (1) (Tschopp and Mateus, 2013b; wording modified; Fig. 59).

Comments. Some specimens (in particular non-flagellicaudatans) have rounded basal tubera, which extend onto the lateral surface of the basioccipital. These are treated as plesiomorphic, because the line projecting through the medial- and lateral-most points of the tubera is oblique in these cases.

C90: Basal tubera, foramen in notch that separates the two tubera: absent (0); present (1) (Tschopp and Mateus, 2013b; Fig. 58).

Comments. This foramen is one of three openings that can be present in this area (see above and below). However, the pit described in this character cannot be homologous to the other ones because it is present together with the basipterygoid recess in HMNS 175 (Holland, 1906), and together with the basioccipital pit in YPM 1860 (ET, pers. obs., 2011).

C91: Basisphenoid/basipterygoid recess: absent (0); present (1) (Wilson, 2002; polarity reversed; Fig. 58)

Comments. The basipterygoid recess is a pit located anteriorly to the basal tubera, on the basisphenoid. Its absence was considered autapomorphic for *Apatosaurus*, representing a reversal to the plesiomorphic state in Sauropoda (Wilson, 2002). However, in the phylogenetic analysis, Wilson (2002) scored *Apatosaurus* as having a recess, sharing this state with basal sauropods like

PeerJ Reviewing Manuscript

Shunosaurus. The character was organized as a presence/absence character, with the presence being plesiomorphic (Wilson, 2002). Assuming that the discussion of the autapomorphies is right, polarity of the character states was inverted herein. The basipterygoid recess might be confused with the pits located in the notch between the tubera or the one posterior to them (see above), so it is important to state that it lies anterior to the tubera, between the bases of the basipterygoid processes.

C92: Basipterygoid processes: widely diverging (> 60°) (0); intermediate, 31°-60° (1); narrowly diverging (< 31°) (2) (Yu, 1993; modified; Fig. 55; Tab. S11).

Comments. There are several modes to measure the angle between the processes, and no previous analysis defines how this angle should be measured. Here, divergence is measured between lines drawn from the basisphenoid center, where the bases of the basipterygoid processes meet, to the anteromedial-most point of the processes. This is preferably done in posterior or posteroventral view, perpendicular to the longitudinal axis of the processes. The present measuring technique yields slightly different results compared to earlier studies, but general trends are similar.

C93: Basipterygoid processes, orientation: directed more than 75° to skull roof (normally perpendicular) (0); angled less than 75° to skull roof (normally approximately 45°) (1) (McIntosh, 1990b; modified; Tab. S12).

Comments. New numeric state boundaries were established, because a survey of diplodocoid braincases showed that there is more variety than previously recognized (Tab. S12). However, the difference was already recognized as taxonomically important by McIntosh (1990b). The angle is measured between the skull roof and a line through the center of the proximal and distal ends. This is important, as especially macronarian basipterygoid processes tend to curve backwards at their distal ends, thereby increasing the angle as measured here.

There is some possibility that this character is correlated with the large angle between the anterior and dorsal quadratojugal processes and the backwards inclination of the ventral ramus of the quadrate. This entire region is interconnected by the pterygoid, and the anterior shifting of the basisphenoid-pterygoid articulation due to the changed orientation of the basipterygoid processes might have been caused by, or the reason for the more anteriorly orientated ventral ramus of the quadrate, and therefore also the widening of the angle between the quadratojugal processes. However, since few to no skulls are known of basal diplodocoid taxa, which might show intermediate states, if they were present, the characters are retained separate here, lacking definitive evidence of correlation.

PeerJ Reviewing Manuscript

Furthermore, there is some indication that the character could be ontogenetically controlled: the two relatively small diplodocine skulls CM 3452 and SMA 0004 have both somewhat larger angles compared to larger specimens (Tab. S12), and lower angles in the quadratojugal. However, further studies are needed to decide if this is really ontogenetic, or if it could be taxonomically significant.

C94: Basipterygoid processes, ratio of length:basal transverse diameter: < 4 (0); = or > 4.0 (1) (Wilson, 2002; modified; Fig. 55; Tab. S13).

Comments. The character was initially defined as ratio of length to maximum basal diameter (Wilson, 2002). However, maximum basal diameter is often oriented dorsoventrally (at least in diplodocids), which means that one cannot take the measurements in a picture of the processes in ventral view only. Also, dorsoventral height changes considerably, and continuously towards the base of the processes in some specimens (e.g. *Dicraeosaurus hansemanni* MB.R.2379; Janensch, 1935; Fig. 55), and in lateral view, it is sometimes difficult to decide where exactly the base of the process is situated. Therefore, and because ventral views are obtainable more frequently than lateral views, the ratio length/basal transverse diameter is preferred herein. The dimensions should be measured perpendicular to each other. Wilson (2002) initially left a gap in the definition of the states (2 or less, 4 or more), which was corrected for by Mannion et al. (2012). However, as a more rigorous assessment of these ratios shows (Tab. S13), the state boundary should rather be set to four, the derived, elongate state resulting as a shared synapomorphy for Diplodocinae and Dicraeosauridae.

Measuring the basipterygoid processes in such a way leads to much higher elongation ratios for the holotype of *Kaatedocus siberi* (SMA 0004) than reported in its initial description (Tschopp and Mateus, 2013b). The low ratio also served as local autapomorphy for the genus (Tschopp and Mateus, 2013b). Following the results presented herein, this is most probably an artifact based on differing measurement protocols, as Tschopp and Mateus (2013b) compared length with dorsoventral height, which is the maximum basal diameter in SMA 0004 (Tschopp and Mateus, 2013b). The current measurements show that *Kaatedocus* is actually well in the range of Diplodocinae, which can easily be distinguished from *Apatosaurus louisae* CM 11162 (Tab. S13).

C95: Basipterygoid, area between the basipterygoid processes and parasphenoid rostrum: is a mildly concave subtriangular region (0); forms a deep slot-like cavity that passes posteriorly between the bases of the basipterygoid processes (1) (Upchurch, 1995, 1998; Fig. 55).

C96: Basipterygoid processes, orientation of proximal-most portions: same as central portion of shaft (0); parallel to each other, outwards curve of shaft happens only more anteriorly (1) (New;

PeerJ Reviewing Manuscript

Fig. 62).

Comments. The development of this character is best seen in ventral view. In the derived state, the parallel portion of the basipterygoid processes are often interconnected dorsomedially by a thin sheet of bone. On the other hand, a similar sheet can also be present if the processes are entirely straight.

C97: Basipterygoid processes, distal end: straight (0); curving outwards (1) (New; Fig. 57).

Comments. This character compares the distal end of the basipterygoid process with the central portion. It is thus different from the feature described in character 96.

C98: Basipterygoid processes, distal lateral expansion: absent (0); present (1) (New; Fig. 57).

Comments. Only abrupt distal expansions are coded as apomorphic. Gradually extending processes are treated as plesiomorphic.

C99: Parasphenoid rostrum, groove on dorsal edge: absent (0); present (1) (Upchurch, 1995, 1998; modified; Fig. 55).

Comments. Upchurch (1995, 1998) proposed the character combining the presence of a dorsal groove with the lateral shape of the rostrum, thereby implying that the dorsoventrally thin parasphenoid of diplodocoids would not bear dorsal grooves. However, a more detailed study of diplodocoids shows that the groove is actually present in most of them.

C100: Optic foramen: paired (0); unpaired (1) (Berman and McIntosh, 1978; Sander et al., 2006; Fig. 63).

Comments. The optic foramen is lying close to the midline, within the orbitosphenoid in most sauropod taxa. Generally, they are separated medially by a narrow bony bridge, which is absent in some diplodocoid specimens (e.g. *Suuwassea*, Harris, 2006a). Sander et al. (2006) were the first to include the character into a phylogenetic analysis.

C101: Palatobasal contact, shape: pterygoid with small facet (0); dorsomedially orientated hook (1) (Wilson, 2002; modified by Tschopp and Mateus, 2013b; Fig. 64).

Comments. Tschopp and Mateus (2013b) deleted a third state present in the original character, which describes the specific rocker-like morphology of this region in nemegtosaurid sauropods (Wilson, 2002). Since no taxon of this clade is included, the additional state is redundant.

C102: Pterygoid, transverse flange (i.e. ectopterygoid process) position: between orbit and antorbital fenestra (0); anterior to antorbital fenestra (1) (Upchurch, 1995; Fig. 44).

Comments. The transverse flange of the pterygoid connects to the maxilla through the ectopterygoid (Upchurch et al., 2004a).

C103: Vomer, anterior articulation: maxilla (0); premaxilla (1) (Wilson, 2002; polarity reversed;

PeerJ Reviewing Manuscript

Fig. 44).

Comments. Polarity was reversed compared to Wilson's (2002) character due to the limited taxon sampling.

C104: Dentary, anteroventral margin shape: gently rounded (0); sharply projecting triangular process or 'chin' (1) (Upchurch, 1998; Fig. 65).

Comments. Usually considered a flagellicaudatan synapomorphy, also some specimens of *Camarasaurus* show a weak ventral expansion at the anterior extreme of the lower jaw. However, this never reaches the chin-like state as present in *Diplodocus*, and *Camarasaurus* is thus included in the plesiomorphic state here.

C105: Dentary, cross-sectional shape of symphysis: oblong or rectangular (0); subtriangular, tapering sharply towards ventral extreme (1); subcircular (2) (Whitlock, 2011a; Fig. 65).

Comments. Diplodocids have ventrally tapering symphyses, but they do not taper to a point as in dicraeosaurids (Whitlock and Harris, 2010) and have thus still to be scored as plesiomorphic.

C106: Dentary, tuberosity on labial surface near symphysis: absent (0); present (1) (Whitlock and Harris, 2010; reworded by Whitlock, 2011a; Fig. 66).

Comments. This character was originally proposed by Whitlock and Harris (2010) to unite *Suuwassea* and *Dicraeosaurus*.

C107: Dentary, anterolateral corner: not expanded laterally beyond mandibular ramus (0); expanded beyond lateral mandibular ramus (1) (Whitlock, 2011a; Fig. 66).

Comments. The derived state of this character describes the extreme case of character 112. To date, it is only known in the rebbachisaurid *Nigersaurus* (Sereno et al., 2007).

C108: Mandible, coronoid eminence: strongly expressed, clearly rising above plane of dentigerous portion (0); absent (1) (Whitlock, 2011a; Fig. 65).

Comments. Some diplodocids have dorsally expanded coronoid areas, but they do not reach above the plane of the dentigerous portion.

C109: Surangular foramen: absent (0); present (1) (New; Fig. 67).

Comments. The location of the surangular foramen can vary in different taxa. Usually, it is situated in the anterior, horizontally oriented portion, but in some cases it is shifted posteriorly.

C110: External mandibular fenestra: present (0); absent (1) (McIntosh, 1990b; Russell and Zheng, 1993; Fig. 67).

Comments. The presence is a retained plesiomorphy, shared with early sauropodomorphs (Wilson, 2002).

C111: Snout shape in dorsal view: premaxilla-maxilla index (PMI; Whitlock et al., 2010) < 67%

PeerJ Reviewing Manuscript

(0); 67-85% (1); > 85% (2) (Upchurch, 1998; Whitlock, 2011a; modified; Tab. S14).

Comments. In order to avoid gaps, an intermediate state was added to Whitlock's (2011a) version. The state boundaries were chosen following high-level phylogenetic differences. Measurements taken on photos from slightly different angles of the skulls CM 3452, 11161, 11162, and SMA 0011 show that the orientation of the skull has a relatively high influence on the measured PMI (Tab. S14). In order to avoid this, the same measurements were taken in more than one picture of the same skulls, where possible. In future, one should check and remeasure this ratio in all diplodocid skulls, making sure that they are always taken in exactly the same orientation. Best results are to be expected with the ventral maxillary edge oriented horizontally. Whitlock et al. (2010) reported that the snout becomes more squared during ontogeny in diplodocids. It might thus be possible that more juvenile specimens become artificially grouped closer to more basal taxa when including this character. The character was treated as ordered.

Teeth

C112: Shape of tooth row in occlusal view: follows curvature of dentary (0); anterolateral corner of tooth row displaced labially (1) (Whitlock and Harris, 2010; Fig. 66).

Comments. In dicraeosaurids, it seems to be the tooth row, which is mostly responsible for the squared appearance of the lower jaw. The ventral portions of the dentary would be much more rounded (Whitlock and Harris, 2010). The diplodocid AMNH 969 has a similar development as *Suuwassea*.

C113: Tooth rows, length: restricted anterior to orbit (0); restricted anterior to antorbital fenestra (1); restricted anterior to subnarial foramen (2) (Gauthier, 1986; modified by Whitlock, 2011a; Fig. 36).

Comments. In order to score this character, the skull should be hold with the ventral margin of the maxilla oriented horizontally. The tooth row is usually more anteriorly restricted in the lower jaw than in the maxilla. Here, the maxillary tooth row is used as a reference. As the snout shape, also the anterior restriction of the tooth row was interpreted as juvenile feature (Whitlock et al., 2010). The character is treated as ordered.

C114: Dentary teeth, number: greater than 17 (0); 10-17 (1); 9 or fewer (2) (Wilson and Sereno, 1998; modified by Carballido et al., 2012b; Tab. S15).

Comments. Carballido et al. (2012b) added a third state to distinguish *Demandasaurus* and *Suuwassea* from other sauropod specimens. Since the reduction of the number of dentary teeth was accomplished and reversed several times, it is not entirely clear how evolution worked in this case. The character was therefore left unordered.

PeerJ Reviewing Manuscript

C115: Replacement teeth per alveolus, number: three or fewer (0); four or more (1) (Wilson, 2002).

Comments. The number of replacement teeth appears to change between the tooth-bearing bones of the same individual (D. Schwarz-Wings, pers. comm., 2012). However, maximum number of replacement teeth is still informative, and therefore the character was retained.

C116: Teeth, crown-to-crown occlusion: present (0); absent (1) (Wilson and Sereno, 1998; polarity reversed by Whitlock, 2011a).

C117: Teeth, wear facets shape: v-shaped (0); planar (1) (Wilson and Sereno, 1998; modified; Fig. 68).

Comments. The initial character (Wilson and Sereno, 1998) was first adapted by Sereno et al. (2007), in order to include the paired planar facets of *Nigersaurus*. Here, the shape and number of wear facets are considered independent characters (see character 118).

C118: Teeth, occlusal pattern: paired wear facets (0); single facet (1) (Wilson and Sereno, 1998; modified; Fig. 69).

Comments. See character 117.

C119: Teeth, SI values for tooth crowns: < 3.4 (0); 3.4 or greater (1) (McIntosh, 1989; Upchurch, 1998; modified; Tab. S16).

Comments. The SI value describes the slenderness of the teeth. It was defined as crown length/mesiodistal width (Upchurch, 1998). The state borders were changed, following large gaps apparently corresponding to higher-level taxonomy (Tab. S16).

C120: Tooth crowns, orientation: aligned slightly anterolingually, tooth crowns overlap (0); aligned along jaw axis, crowns do not overlap (1) (Wilson and Sereno, 1998; polarity reversed by Whitlock, 2011a; Fig. 67).

C121: Tooth crowns, cross-sectional shape at midcrown: D-shaped (0); cylindrical (1) (Russell and Zheng, 1993; modified by Wilson and Sereno, 1998; Fig. 70).

Comments. Unworn diplodocoid teeth often have ellipsoid cross-sections. However, this is different from the spatulate non-diplodocoid teeth as e.g. typical for *Camarasaurus*. Teeth of the latter genus have a slightly concave lingual face, unlike the convex surface of diplodocoids. In the absence of nemegtosaurid titanosaurs, which show similarly shaped teeth (Upchurch, 1999; Wilson, 2005), the derived state results as unambiguous synapomorphy of Diplodocoidea.

C122: Teeth, orientation relative to long axis of jaw: perpendicular (0); oriented anteriorly (procumbent) (1) (Upchurch, 1998; Fig. 67).

Comments. Tooth orientation is best recognized in the posterior-most teeth in the maxilla and

PeerJ Reviewing Manuscript

dentary.

C123: Teeth, longitudinal grooves on lingual aspect: absent (0); present (1) (Wilson, 2002; Fig. 68).

Comments. Wilson (2002) initially scored only rebbachisaurids with the derived state. However, several non-diplodocoid taxa with spatulate teeth actually have a midline ridge on the lingual face of their teeth, creating two grooves mesially and distally to it (e.g. Osborn and Mook, 1921; Ouyang and Ye, 2002). Consequently, these taxa are scored as derived here as well.

C124: Teeth, thickness of enamel asymmetric labiolingually: absent (0); present (1) (Whitlock, 2011a; Fig. 70).

Comments. This feature can be observed easily in wear facets or cross-sections.

C125: Teeth, marginal denticles: present (0); absent (1) (McIntosh, 1990b; Fig. 68).

Comments. There is some morphological variation in the location of the denticles (Carballido et al., 2012b), but as no diplodocid shows denticles, this simplified version of the character is used herein.

Cervical vertebrae

C126: Presacral neural spines, bifurcation: absent (0); present (1) (McIntosh, 1989; Wilson, 2002; modified; Tab. S17).

Comments. Wilson (2002) divided this character into the different regions, where the bifurcation can be present. However, like this, taxa with unbifurcated neural spines are coded several times for the same state. In the present analysis, presence of bifurcation and the first bifid element are treated as two different characters (see character 140).

C127: Number of cervical vertebrae: < 13 (0); 14-15 (1); 16 or more (2) (McIntosh, 1990b; modified; Tab. S18).

Comments. The character is used in various versions in different phylogenetic analyses (Upchurch, 1998; Wilson, 2002; Whitlock, 2011a), depending on their specific focus. Herein, the states are adjusted to fit the included taxa, excluding redundancy. Only one diplodocid specimen preserves a complete neck (*Apatosaurus louisae* CM 3018), and even here, the possibility of lacking elements cannot be ruled out entirely, due to gaps between certain cervical vertebrae as they were found (McIntosh, 2005). A second specimen (*Diplodocus carnegii* CM 84) lacks the atlas, and seems otherwise complete, although the same concerns account as in CM 3018 (McIntosh, 2005). However, as the more anterior and posterior elements in these cases fit well together, we followed McIntosh (2005) in assuming that no vertebra was lost at the position of these gaps in CM 84 and 3018. McIntosh (2005) suggested that *Barosaurus* had 16 cervical

PeerJ Reviewing Manuscript

vertebrae, instead of 15 as *Apatosaurus* and *Diplodocus*. The assumption was primarily based on the fact that AMNH 6341 only has nine dorsal vertebrae, and that the neosauropod presacral column generally consists of 25 elements (McIntosh, 2005). Since none of the *Barosaurus* specimens preserves an entire neck, none of the *Barosaurus* OTUs can be coded for this character. The inability to code incomplete specimens might be circumvented by using additive binary characters (Upchurch, 1998). However, this would imply that the corresponding multistate character is continuous (Wilson, 2002), which means that the number of cervical vertebrae could not increase directly by more than one element during speciation. Given that the contrary is shown to be possible in dorsal and sacral vertebrae of mice (Wellik and Capecchi, 2003), it seems reasonable to argue that the same accounts for sauropod cervical vertebrae. The character is thus treated as unordered herein. This also indicates that 'analysis 1' of Mannion et al. (2012), where these characters are treated as unordered, should be preferred over 'analysis 2'.

C128: Cervical vertebrae width to height ratio: less than 0.5 (0); 0.5-1.5 (1); more than 1.5 (2) (Upchurch et al., 2004b; modified; Tab. S19).

Comments. Upchurch et al. (2004b: p. 105) defined the ratio as follows: „Height is measured from the top of the neural spine to the ventral surface of the centrum. Width is defined as the distance between the distal tips of the diapophyses." A third state was added (less than 0.5) as derived dicraeosaurids have a distinctly lower ratio compared to other flagellicaudatans. Given that evolution appears to have worked in both directions, the character is left unordered.

C129: Cervical pneumatopores (pleurocoels): absent (0); present (1) (McIntosh, 1990b; Upchurch, 1995; Fig. 71).

Comments. McIntosh (1990b) already used this character to distinguish advanced sauropods from the most basal forms, but Upchurch (1995) was the first to include it into a phylogenetic analysis.

C130: Cervical centra, internal pneumaticity: absent (0); present with single and wide cavities (1); present, with several small and complex internal cavities (2) (Upchurch, 1998; Wilson and Sereno, 1998; modified by Carballido et al., 2012b; Fig. 72).

Comments. Introduced as character by Upchurch (1998) and Wilson and Sereno (1998), only Wedel et al. (2000) and Wedel (2003) analyzed the distribution of this feature in detail. Carballido et al. (2012b) divided the original character, which did not discriminate between cervical and dorsal vertebrae (Upchurch, 1998; Wilson and Sereno, 1998).

C131: Cervical vertebrae, small fossa on posteroventral corner: absent (0); shallow, anteroposteriorly elongate fossa present, posteroventral to pleurocoel (1) (Whitlock, 2011a; Fig.

PeerJ Reviewing Manuscript

71).

Comments. *Kaatedocus siberi* SMA 0004, AMNH 7530, and the apatosaurines YPM 1980 and AMNH 460 have shallow depressions at the same place, but they do not create distinct fossae as in *Barosaurus* or *Diplodocus* (see Hatcher, 1901; McIntosh, 2005), and are thus coded as plesiomorphic.

C132: Cervical centra, midline keels on ventral surface: prominent and plate-like (0); reduced to low ridges (1) (Upchurch, 1998; Upchurch et al., 2004a; modified; Fig. 73).

Comments. Since the presence or absence is already coded for in following characters, the complete absence is here excluded from the original character description (Upchurch, 1998; Upchurch et al., 2004a), and taxa without ventral ridges are scored as unknown.

C133: Cervical vertebrae, longitudinal sulcus on ventral surface: absent (0); present (1) (Upchurch, 1995, 1998; Fig. 73).

Comments. Due to the lateroventral projecting cervical parapophyses of *Apatosaurus*, cervical vertebrae of this genus have a concave anterior portion of the ventral surface. However, this is the case in almost all sauropod taxa, and therefore only specimens with transversely concave ventral surfaces throughout the entire length of the centrum are herein scored as apomorphic.

C134: Cervical vertebra, posterior projection on transverse processes: present (0); absent (1) (Remes et al., 2009; polarity reversed; Fig. 74).

Comments. A distinct, triangular posterior projection marks the transverse process of *Spinophorosaurus* and many diplodocines. Posteriorly convex transverse processes are not considered projections. Due to reduced taxon sampling, the character polarity of the original version (Remes et al., 2009) was inverted here.

C135: Cervical vertebrae, posterior extension of posterior centrodiapophyseal lamina: is anteriorly restricted (0); reaches below posterior end of neural canal (1) (New; Figs 71, 75).

Comments. *Apatosaurus* specimens appear to have a consistently more developed pcdl compared to Diplodocinae. The only apatosaur specimen with an anteriorly restricted pcdl is the juvenile holotype of *Elosaurus parvus*, CM 566. The development of vertebral laminae has previously been linked with ontogeny (Carballido and Sander, 2013; Schwarz et al., 2007b).

C136: Cervical vertebrae, short second posterior centrodiapophyseal lamina ventral to the one uniting with the dorsal shelf of the diapophysis: absent (0); present (1) (New; Fig. 76).

Comments. The presence of a short accessory pcdl appears to be linked with the bifurcation of the pcdl in more posterior elements in *Galeamopus* (see above). However, bifurcated pcdl also occur in some apatosaur specimens which do not have an additional pcdl in more anterior

PeerJ Reviewing Manuscript

elements (e.g. UW 15556; Gilmore, 1936), and therefore, these morphologies are treated as independent characters.

C137: Cervical vertebrae, foramen on dorsal side of postzygodiapophyseal lamina, just anterior to base of neural spine process: absent (0); present (1) (Remes, 2007; Fig. 76).

Comments. Distinct foramina in the sdf are usually considered typical for brachiosaurids, and their presence in *Australodocus* was therefore one of the reasons why Whitlock (2011c) reinterpreted *Australodocus bohetii* as a titanosauriform, instead of a diplodocine as initially proposed (Remes, 2007). However, also *Barosaurus* sometimes shows small foramina in similar positions (YPM 429, ET, pers. obs., 2011), but they are usually less prominent. The putative juvenile *Brachiosaurus* specimen SMA 0009 does not have such foramina, but since the development of pneumatic structures appears to be ontogenetically controlled (Carballido and Sander, 2013; Schwarz et al., 2007c), this might be explained like that.

C138: Cervical vertebrae, epipophysis: reduced to absent (0); pronounced, forming a distinct projection above the postzygapophysis (1) (Remes et al., 2009; modified; Fig. 76).

C139: Cervical vertebrae, pneumatized epipophyses: absent (0); present (1) (New; Fig. 77).

Comments. The pneumatic foramen can be situated anteriorly as in *Diplodocus carnegii* (CM 84, 94, ET, pers. obs., 2011), or posteriorly as in *Barosaurus lentus* YPM 429 (ET, pers. obs., 2011).

C140: Cervical neural spines, first bifid element, if present: CV 3 (0); first mCV (1); posterior mCV (2); restricted to pCV (3) (Wilson, 2002; modified; Tab. S17).

Comments. Taxa with unbifurcated neural spines are scored as unknown. The subdivision into anterior, mid-, and posterior cervical vertebrae depends on the number of elements in the column (Tab. 10). Absolute numbers other than CV 3, which is the first postaxial cervical element, would thus be misleading and are avoided here. The character is treated as ordered.

C141: Cervical vertebrae, unbifurcated neural spines in anterior/posterior view: with parallel lateral edges or converging (0); distal end expanded laterally (1) (New; Fig. 78).

Comments. The real distribution of this character within Diplodocidae is difficult to assess to date, as there are only few specimens reported that preserve complete neural spines of anterior, unbifurcated neural spines.

C142: Cervical vertebrae, summits of bifid neural spines: are laterally compressed (0); are rounded (1) (Upchurch et al., 2004b; Fig. 74).

Comments. The derived state of this character is shared by some apatosaur specimens and *Suuwassea*. The spine summits in most other taxa with bifurcated spines are generally anteroposteriorly elongate, and transversely compressed, resulting in narrow sheets of bone. In

PeerJ Reviewing Manuscript

Suuwassea as well as some apatosaur specimens, the lateral edge of the spine summit is distinctly convex, producing a semi-circular outline. Some other taxa (e.g. *Kaatedocus*; Tschopp and Mateus, 2013b) have medial ridges connecting the summit with the base, but these are always relatively shallow, and do not form rounded outlines.

C143: Proatlas, distal end: broadly rounded (0); narrow and elongate, almost pointed (1) (New; Fig. 79).

C144: Atlantal intercentrum, anteroventral lip: absent, anterior edge of intercentrum straight in lateral view (0); present, anterior edge of intercentrum concave (1) (Wilson, 2002; modified; Fig. 80).

Comments. Initially regarded as flagellicaudatan synapomorphy (Wilson, 2002), the presence of an anteroventral lip is now known to be present in *Mongolosaurus* as well (Mannion, 2011). Following the original description of the character states (Wilson, 2002: intercentrum shape in lateral view: rectangular or ventrally longer than dorsally), also *Camarasaurus* and other non-flagellicaudatan taxa would have to be scored as apomorphic. However, they do not show a distinct anteroventral lip, resulting in a strongly concave anterior edge of the intercentrum, when seen in lateral view.

C145: Atlantal intercentrum, foramen between posterior ventrolateral processes: absent (0); present (1) (New; Fig. 80).

C146: Atlantal neurapophyses, anteromedial process: weakly developed (0); well-developed and distinct from posterior wing (1) (New; Fig. 81).

Comments. The anteromedial process corresponds to the prezygapophyses of more posterior elements. It articulates with the posterior end of the proatlas. In *Kaatedocus*, this process is relatively short transversely, and curves gradually into the posterior process, whereas in SMA 0011 and AMNH 969, the anteromedial process is distinct and at least as wide transversely as long anteroposteriorly.

C147: Atlantal neural arch, small subtriangular, laterally projecting spur at base: absent (0); present (1) (New; Fig. 81).

Comments. When present, this spur is located at the base of the neurapophysis, opposite to the position of the anteromedial process, and much smaller. It is also present in some, but not all *Camarasaurus* specimens (Ikejiri, 2004).

C148: Atlantal neurapophyses, posterior wing: gradually tapering along its length (0); of subequal width along most of its length (1) (New; Fig. 81).

Comments. The posterior wing of the neurapophysis articulates with the prezygapophysis of the

PeerJ Reviewing Manuscript

axis.

C149: Atlantal neural arch: without foramen (0); with foramen (1) (Wilson, 2002; Whitlock, 2011a; Fig. 81).

Comments. Wilson (2002) proposed the presence of such a foramen as an autapomorphy of *Apatosaurus*, and it was included as character in the phylogenetic analysis of Whitlock (2011a). Due to the small number of preserved atlantal neurapophyses, only one specimen can currently be positively assigned to the apomorphic state (*Apatosaurus louisae* CM 3018). It could thus also represent a species autapomorphy, instead of being valid for the entire genus.

C150: Axial centrum, pneumatic fossae on ventrolateral edges, right posterior to parapophyses: absent (0); present (1) (New; Fig. 82).

Comments. Many specimens have a well-developed median keel on their ventral surfaces. In lateral view, this sometimes appears like a bifurcation of the ventrolateral edge, although this is not the case. The apomorphic state of the character proposed herein only includes fossae bordered by ridges that originate at the parapophysis anteriorly.

C151: Axis, prespinal lamina: of constant width (0); developing a transversely expanded, knob-like tuberosity at its anterior end (1) (New; Fig. 83).

C152: Axis, postspinal lamina: absent (0); present (1) (Harris and Dodson, 2004; Fig: 82).

C153: Axis neural spine: projects beyond posterior border of centrum (0); terminates in front of or at posterior border of centrum (1); is restricted anterior to postzygapophyseal facets (2) (New; Fig. 83).

Comments. Due to intermediate morphologies, this character is treated as ordered.

C154: Anterior cervical vertebrae, total height/centrum length ratio: < 0.9 (0); 0.9-1.2 (1); > 1.2 (usually around 1.5) (1) (Whitlock, 2011a; modified; Tab. S20).

Comments. Total height is herein measured between the ventral-most expansion of the centrum (usually the parapophysis or posterior cotyle). A third state was added in order to distinguish apatosaurs from *Diplodocus*. Given the high amount of changes in ratios during evolution, as indicated by the analysis, the character is left unordered.

C155: Cervical vertebrae 2 and 3, centrum length: moderate length increase, CV3 < 1.3 x CV 2 (0); length increases considerably CV 3 at least 1.3 x CV 2 (1) (Russell and Zheng, 1993; Tab. S21).

Comments. Even though this does not seem to follow higher-level taxonomy, there are two groups with ratios well separated from each other (Tab. S21). The state boundaries are therefore set in order to distinguish between these two groups.

PeerJ Reviewing Manuscript

C156: Anterior cervical vertebrae, posterior edge of anterior condyle: anteriorly inclined (0); posteriorly inclined (1) (New; Fig. 84).

Comments. This character is strictly applicable to anterior cervical vertebrae. In SMA 0011, which has apomorphic anterior vertebrae, CV 6 and more posterior elements show the usual anteriorly inclined edge.

C157: Anterior cervical centra, pleurocoels: single (0); subdivided (1) (New; Fig. 84).

Comments. The subdivision of the pleurocentral cavity is sometimes regarded as ontogenetically controlled (Carballido and Sander, 2013; Schwarz et al., 2007b). However, given that the completely mature anterior cervical vertebrae (sensu Carballido and Sander, 2013) of the *Kaatedocus siberi* holotype SMA 0004 have undivided pleurocoels, in contrast to the still immature vertebrae of other specimens like SMA 0011 (see above), at least some taxonomic differences appear to be present.

C158: Anterior cervical vertebrae, pleurocoel extending onto dorsal surface of parapophysis: absent (0); present (1) (Upchurch, 1998; modified by Whitlock, 2011a; polarity reversed; Fig. 84).

Comments. Upchurch (1998) distinguished between continuous extensions or fossae that are separated from the main anterior pneumatic fossa or pleurocoel by a transverse ridge. The latter distinction was abandoned by Whitlock (2011a), who instead divided the character into the different regions (anterior and mid- and posterior cervical vertebrae, see below). Character polarity was herein reversed as basal outgroups used in the present analysis do have expanded pleurocoels.

C159: Anterior cervical vertebrae, longitudinal ridge on ventral surface: present (0); absent (1) (Upchurch, 1998; modified).

Comments. The ventral ridge (if present) can have various morphologies in diplodocid specimens, which is accounted for in other characters of this analysis. In addition to the original version of Upchurch (1998; character 132 herein), a strict presence-absence character was included for both anterior and mid- and posterior cervical vertebrae in the present analysis. The subdivision is necessary as in some specimens, the presence of a ventral keel is restricted to anterior elements only (*Suuwassea* ANS 21122, *Eobrontosaurus* Tate-001, *Galeamopus* [redacted] SMA 0011). This indicates that incomplete necks without ventral keels on posterior cervical vertebrae might still bear midline ridges anteriorly. For the various developments of the keels see figure 73, which shows mid- and posterior cervical vertebrae, but the morphology is the same in anterior elements.

PeerJ Reviewing Manuscript

C160: Anterior cervical vertebrae, paired pneumatic fossae on ventral surface: absent (0); present (1) (Whitlock, 2011a).

Comments. Like the ventral keel, also the paired pneumatic foramina are sometimes restricted to the anterior cervical vertebrae (e.g. in SMA 0011, see above). Whereas the presence of paired pneumatic foramina imply the presence of a ventral keel as well, this does not apply the other way around, as shown by the anterior cervical vertebrae of *Kaatedocus* SMA 0004 (Tschopp and Mateus, 2013b). The characters are therefore retained as independent. The morphology of the foramina is equal in anterior and mid- and posterior cervical vertebrae, where present (see Fig. 73).

C161: Anterior cervical vertebrae, prespinal lamina: absent (0); present (1) (Carballido et al., 2012b; Figs 78, 84).

Comments. In some diplodocid specimens, it appears that the prespinal lamina in undivided vertebrae gives rise to the median tubercle in divided, more posterior elements. However, given the presence of a prespinal lamina in *Camarasaurus* (Madsen et al., 1995), which does not have a median tubercle between bifurcated neural spines, these two characters should be treated as independent.

C162: Anterior and mid-cervical centra, pleurocoel pierced by one or two large, rounded foramina around centrum midlength: absent (0); present (1) (New; Fig. 85).

Comments. Such a foramen is not present in the anterior-most elements, but very distinct in CV 5 or 6 of SMA 0011, whereas it disappears again by CV 8 or 9. In SMA 0011, these foramina are situated at the anterior end of the posterior pneumatic fossa. Taxa where CV 5 to 7 or 8 are not preserved, and other elements do not show such a development, are scored as unknown. Similarly distinct, rounded foramina are only present in *Supersaurus* (Lovelace et al., 2007), and *Australodocus* (Remes, 2007; Whitlock, 2011c).

C163: Anterior and mid-cervical vertebrae, spinoprezygapophyseal lamina: continuous as a lamina (0); reduced to ridge or totally interrupted in the middle (at base of prezygapophysis) (1) (Tschopp and Mateus, 2013b; Fig. 86).

C164: Anterior and mid-cervical neural spines height: high (project well above the level of postzygapophyses) (0); low (terminates level with postzygapophyses) (1) (Upchurch et al., 2004b; modified; Fig. 76).

Comments. This character is similar to character 168. It was added because it includes anterior cervical vertebrae, which are different in height among diplodocids and within Diplodocinae, and because it would have differing state boundaries, if it would be treated numerically.

PeerJ Reviewing Manuscript

C165: Anterior and mid-cervical neural spines, dorsoventrally elongate coel on lateral surface: absent (0); present (1) (Mannion et al., 2012; modified; Fig. 85).

Comments. The presence of a dorsoventrally elongate fossa in the spinodiapophyseal fossa is usually used as derived character for posterior cervical vertebrae only (Mannion et al., 2012). However, there are differences in anterior and mid-cervical neural arches as well, which appear to be phylogenetically significant.

C166: Mid-cervical centra, anteroposterior length/height of posterior face: 2.5-3.2 (0); 3.3-4.4 (1); 4.5+ (2) (Upchurch, 1995; modified; Tab. S22).

Comments. Elongation index as used herein is measured following the protocol of Wilson and Sereno (1998: total centrum length/height posterior cotyle). The mean elongation index is used for this metric. *Tornieria* specimen k is scored '2' as the centrum length to width ratio is very high (5.4; Remes, 2006), and thus a high EI as used herein can be expected with confidence.

C167: Mid-cervical pre-epipophyses anterior extreme: about the same as prezygapophyseal facet (0); projects considerably anterior to articular facet, forming a distinct spur (1) (Sereno et al., 1999; Fig. 86).

Comments. A distinct anterior extension of the pre-epipophysis was used as autapomorphy for *Australodocus bohetii* within Diplodocidae (Remes, 2007). However, it has been shown to be present in *Kaatedocus* as well, as also in some non-diplodocid sauropods (Sereno et al., 1999; Ksepka and Norell, 2006; Tschopp and Mateus, 2013b). Taxa without pre-epipophyses are scored as unknown.

C168: Mid-cervical neural spine height: considerably shorter than height of neural arch, <0.45 (0); subequal to height of neural arch, 0.45-1.6 (1); considerably higher than neural arch, >1.6 (2) (Rauhut et al., 2005; modified; Tab. S23).

Comments. Neural arch height is measured in a vertical line from the centrum to the dorsal edge of the postzygapophyses, neural spine height from dorsal edge of the postzygapophyses to the spine summit. The centrum is oriented such that the ventral floor of the neural canal is horizontal. The majority of the ratios were measured from photos or figures in lateral view. As exemplified by CV 6 of *Suuwassea* ANS 21122, this approach can yield major differences depending on slight changes in perspective (or left and right lateral views; CV 6 of ANS 21122 has ratios ranging from 0.91-1.27; Tab. S23). Although such differences are partly avoided by using mean ratios, it would be unwise to use closely spaced numerical state boundaries in this case. Therefore, only two steps were regarded as phylogenetically significant, and objective enough. The character left unordered due to diverging evolutionary trends.

PeerJ Reviewing Manuscript

C169: Mid-cervical neural spines, orientation: vertical (0); anteriorly inclined (1) (Rauhut et al., 2005; Fig. 87).

Comments. The neural spine is interpreted to be anteriorly inclined, when the anterior end of the summit reaches further anterior than the posterior-most point of the sprl.

C170: Mid-cervical vertebrae, angle between postzygodiapophyseal and spinopostzygapophyseal laminae: acute (0); right angle (1) (Rauhut et al., 2005; Fig. 85).

Comments. Angles are measured between lines connecting the posterior-most point of podl and spol (often the epipophyses) with their opposing ends.

C171: Mid- and posterior cervical centra, pleurocoels: single without division (0) divided by a bone septum, resulting in an anterior and a posterior lateral excavation (1); divided in three or more lateral excavations, resulting in a complex morphology (2) (Carballido et al., 2012b; modified; Fig. 71).

Comments. The original character (Carballido et al., 2012b) includes a fourth character state, which describes the shallow posterior pneumatic fossa. As such, it overlaps with character 172, introduced by Whitlock (2011a). Furthermore, subdivision of the pleurocoel is not correlated with the depth of the single pneumatic fossae in diplodocids. Therefore, the fourth state was omitted here.

C172: Mid- and posterior cervical vertebrae, pneumatization of lateral surface of centra: large, divided pleurocoel over approximately half of centrum (0); reduced, large fossa but sharp-bordered coel, if present, restricted to area above parapophysis (1) (Whitlock, 2011a; Fig. 75).

Comments. Taxa with single pleurocoels are scored as unknown.

C173: Mid- and posterior cervical vertebrae, pleurocoel extending onto dorsal surface of parapophysis: present (0); absent (1) (Upchurch, 1998; modified by Mannion et al., 2012; based on Whitlock, 2011a; Fig. 71).

C174: Mid- and posterior cervical vertebrae, longitudinal ridge on ventral surface: present (0); absent (1) (New).

C175: Mid- and posterior cervical vertebrae, ventral keel: single (0); bifid, connects posterolaterally to the ventrolateral edges of the centrum (1) (New; Fig. 73).

Comments. Taxa without ventral keels are scored as unknown.

C176: Mid- and posterior cervical vertebrae, paired pneumatic fossae on ventral surface, separated by ventral midline keel: absent (0); present (1) (New; Figs 73, 88).

Comments. Usually, these fossae are situated anteriorly between the parapophyses, separated by a ventral keel. Some apatosaur specimens (e.g. YPM 1861, ET, pers. obs., 2011) show paired

PeerJ Reviewing Manuscript

pneumatic fossae located posterior to the parapophyses, facing ventrolaterally, and not separated by a keel. This morphology is considered different, and accounted for in character 177.

C177: Mid- and posterior cervical vertebrae, lateral edge posterior to parapophysis: continuous (0); marked by a deep groove extending anteroposteriorly along the edge (1) (New; Fig. 88).

Comments. Such a groove was proposed as autapomorphic for *Dinheirosaurus* (Mannion et al., 2012). However, it is also present in *Supersaurus vivianae* WDC DMJ-021, *Apatosaurus laticollis* YPM 1861, and *Dicraeosaurus hansemanni* MB.R.4886. As in most of these specimens, such a groove appears together with more centrally placed ventral pneumatic foramina (see character 176), two different characters are used.

C178: Mid- and posterior cervical vertebrae, rugose tuberosity on anterodorsal corner of lateral side: absent (0); present (1) (Tschopp and Mateus, 2013b; modified; Fig. 87).

Comments. The character description was extended to mid-cervical vertebrae in order to include *Suuwassea emilieae*. In the latter, the distinct rugose tubercles appear in mid-cervical vertebrae, whereas in *Kaatedocus siberi*, mid-cervical vertebrae only have very shallow tubercles. An additional character for serial variation is avoided as it could only be scored for these two taxa, and would thus not be phylogenetically significant.

C179: Mid- and posterior cervical centra with longitudinal flanges in the lateroventral edge on the posterior part of the centrum: absent (0); present (1) (Tschopp and Mateus, 2013b; Fig. 73).

Comments. These flanges are mainly responsible for the posterior portion of the ventral sulcus typical for diplodocines. However, also some apatosaur specimens have weak flanges, but no continuous ventral sulcus marking the ventral surface.

C180: Mid- and posterior cervical prezygapophyses, articular surfaces flat (0); articular surfaces strongly convex transversely (1) (Upchurch, 1995, 1998; Fig. 89).

C181: Mid- and posterior cervical vertebrae, pre-epipophysis: absent (0); present (1) (Remes, 2007; Figs 75, 86).

Comments. The pre-epipophysis is herein defined as a rugose, horizontal ridge laterally below the prezygapophyseal facet, which connects with the prdl anteriorly.

C182: Mid- and posterior cervical vertebrae, spinoprezygapophyseal lamina, anterior end: remains vertical, with the free edge facing dorsally (0); is strongly inclined laterally (sometimes roofing a lateral fossa in the prezygapophyseal process (1) (Tschopp and Mateus, 2013b; modified; Fig. 90).

Comments. At a first glance, it appears possible that this character is correlated with the occurrence of transversely convex prezygapophyseal facets. However, this is not the case, as can

PeerJ Reviewing Manuscript

be seen in the several varying scores for these two characters.

C183: Mid- and posterior cervical neural arches, lateral fossae on the prezygapophysis process: absent (0); present (1) (Harris, 2006b; Tschopp and Mateus, 2013b; Figs 86, 90).

Comments. Where such a lateral fossa is present, it is dorsally roofed by a laterally tilted anterior end of the sprl. However, not all specimens with a laterally tilted lamina also bear these fossae, which justifies the use of two independent characters. The character was first used in a phylogenetic analysis by Tschopp and Mateus (2013b).

C184: Mid- and posterior cervical vertebrae, prezygapophyseal centrodiapophyseal fossa: single cavity (0); subdivided into two cavities by a ridge (1); several accessory laminae subdivide the fossa into various smaller partitions (2) (Gilmore, 1936; Upchurch et al., 2004b; modified; Figs 73, 75).

Comments. A third state was added in order to be able to accurately code the holotype specimen of *Barosaurus lentus* (YPM 429), as well as a few other specimens. The character is treated as ordered, as an increase in lamination is thought to happen step-wise. Two specimens coded as '0' actually only preserve mid-cervical vertebrae (AMNH 7535, CM 3452, ET, pers. obs., 2011). It would thus be possible that more posterior elements of these cervical columns had subdivided prcdf.

C185: Mid- and posterior cervical neural arches, centroprezygapophyseal lamina: single (0); dorsally divided, resulting in a lateral and medial lamina, the medial lamina being linked with the interprezygapophyseal lamina and not with the prezygapophysis (1); divided, resulting in the presence of a “true” divided centroprezygapophyseal lamina, which is dorsally connected to the prezygapophysis (2) (Upchurch, 1995; modified by Carballido et al., 2012b; Fig. 89).

Comments. Usually, taxa with “true” divided cprl also have a lamina connecting from the base of the cprl to the tprl.

C186: Mid- and posterior cervical transverse processes: posterior centrodiapophyseal lamina (pcdl) and postzygodiapophyseal laminae (podl) meet at base of transverse process (0); pcdl and podl do not meet anteriorly, postzygapophyseal centrodiapophyseal fossa extends onto posterior face of transverse process (1) (New; Fig. 91).

C187: Mid- and posterior cervical vertebrae, accessory horizontal lamina in center of spinodiapophyseal fossa, not connected with any surrounding laminae: absent (0); present (1) (New; Fig. 92).

Comments. This accessory lamina could be a vestigial version of the epipophyseal-prezygapophyseal lamina (sensu Wilson, 2012) or the accessory lamina connecting the podl with

PeerJ Reviewing Manuscript

the sprl (as used herein, following Carballido et al., 2012b). However, as no connection exists to any surrounding lamina, this cannot be definitely confirmed in the cases included here. The use of an independent character is thus preferred. The lamina is generally situated in the center of the sdf.

C188: Mid- and posterior cervical vertebrae, posterior centrodiapophyseal lamina: is single (0); bifurcates towards its anterior end (1) (Upchurch et al., 2004b; wording modified; Fig. 92).

Comments. Evidence from SMA 0011 shows that the presence of anteriorly bifurcated pcdl sometimes are a precursor of entirely double pcdl (see above). However, as in various specimens only bifurcated, and no entirely double pcdl exist, the character was retained as independent from the one describing the single or double pcdl (see character 136).

C189: Mid- and posterior cervical vertebrae, centropostzygapophyseal lamina (cpol): single (0); divided, with the medial part contacting the interpostzygapophyseal lamina (1) (Carballido et al., 2012b; Fig. 91).

C190: Mid- and posterior cervical neural arches, interpostzygapophyseal lamina projects beyond the posterior margin of the neural arch (including the centropostzygapophyseal lamina), forming a prominent subrectangular projection in lateral view: absent (0); present (1) (D'Emic, 2012; modified by Mannion et al., 2013; Fig. 75).

Comments. A reduced subrectangular projection is present in mid-cervical vertebrae of *Supersaurus* WDC DMJ-021. Generally, the development of this feature increases in more posterior elements (e.g. in *Diplodocus carnegii* CM 84; Hatcher, 1901). *Supersaurus* WDC DMJ-021 was thus scored as apomorphic, although it is not prominent in the preserved vertebrae. On the other hand, *Apatosaurus louisae* CM 3018, where only CV 13-15 bear weak projections, was coded as plesiomorphic.

C191: Mid- and posterior cervical vertebrae, postzygapophyseal centrodiapophyseal fossa and spinopostzygapophyseal fossa: entirely separated (0); connected by a large foramen (1) (New; Fig. 71).

Comments. The laminae in this area are very thin and might brake easily. In fact, many specimens do show an opening here, but most of them also show broken margins around this opening, making it impossible to decide if the feature is genuine or not. Often, possible foramina are also closed with plaster or similar material during preparation, probably due to stability reasons, and because the presence of such foramina has never been reported before. In fact, only SMA 0011 can be confidently scored as apomorphic to date.

C192: Posterior cervical vertebrae, Elongation Index (cervical centrum length, excluding

PeerJ Reviewing Manuscript

condyle, divided by posterior centrum height): less than 2.0 (0); 2.0 - 2.6 (1); higher than 2.6 (2) (Gauthier, 1986; Mannion et al., 2012; modified; Tab. S24).

Comments. In vertebrae with inclined posterior edges of the anterior condyle, a vertical line is drawn through the posterior-most point of the posterior edge, and the horizontal distance from this vertical line to a second vertical line through the posterior-most extension of the centrum is measured and taken as centrum length in this case. In some cases, only measurements of the complete centrum length were available, and the EI for the centrum length without anterior ball was calculated based on the mean difference between EI with and without condyle. Singular ratios given in table S24 have to be taken with care, as they differ considerably within posterior cervical centra (decreasing towards posterior). Ratios basing only on anterior posterior cervical vertebrae have thus to be corrected to a lower ratio (e.g. in UW 15556, Tab. S24).

C193: Posterior cervical vertebrae, ventral keel: anteriorly placed (0); restricted to posterior portion of centrum (1) (New; Fig. 88).

Comments. Taxa without ventral ridges are scored as unknown.

C194: Posterior cervical prezygapophyses: terminate with or in front of articular ball of centrum (0); terminate well behind articular ball (1) (Upchurch et al., 2004b; modified; Fig. 75).

Comments. The neural canal should be held horizontally, in order to accurately assess the expansion of the prezygapophysis.

C195: Posterior cervical vertebrae, prezygapophysis articular facet posterior margin: confluent with prezygapophyseal process (0); bordered posteriorly by conspicuous transverse sulcus (1) (Tschopp and Mateus, 2013b; Figs 74, 90).

Comments. The distribution of this character is dubious, as it is difficult to observe in photos and drawings. To date, only the holotype specimen of *Kaatedocus siberi* (SMA 0004) was reported to bear such a sulcus. The character in its present state thus does not contribute to the resolution of the tree. It was retained because more work on actual specimens has to be performed in order to confirm or discard this character as an unambiguous autapomorphy of *K. siberi*.

C196: Posterior cervical vertebrae, spinoprezygapophyseal lamina: continuous (0); developing an anterior projection (just beneath but independent from the spine summit) (1) (Tschopp and Mateus, 2013b; Fig. 74).

Comments. Sometimes the spine summit projects anteriorly, which is not what this character describes. Diplodocines often have an anterior projection below the summit, which forms the most anterior point of the spine.

C197: Posterior cervical vertebrae, accessory lateral lamina connecting postzygodiapophyseal

PeerJ Reviewing Manuscript

and spinoprezygapophyseal laminae: absent (0); present (1) (Gallina and Apesteguía, 2005; Fig. 71).

Comments. This lamina was termed epipophyseal-prezygapophyseal lamina by Wilson and Upchurch (2009), but there are different ways of how to unite the epipophysis with the prezygapophysis (Carballido et al., 2012b; Wilson, 2012). Therefore, the description of Carballido et al. (2012b) was preferred herein.

C198: Posterior cervical vertebrae, accessory, subvertical lamina in the postzygapophyseal centrodiapophyseal fossa, with free edge facing laterally: absent (0); present (1) (New; Fig. 91).

Comments. There are two types of accessory laminae present in the pocdf of certain sauropod taxa: 1) laterally facing, relatively broad laminae, which are mostly located posteriorly, marking the lateral wall of the neural canal, and 2) more distinct, posteriorly facing laminae connecting the pcdl and podl anteriorly, at the base of the transverse process. The present character describes the presence of the first type, the second type is accounted for in the character 199.

C199: Posterior cervical vertebrae, accessory, subvertical lamina in the postzygapophyseal centrodiapophyseal fossa, with free edge facing posteriorly: absent (0); present (1) (Gilmore, 1936; Upchurch et al., 2004b; modified; Fig. 71).

Comments. Rarely, these accessory laminae can appear as a parallel pair as in SMA 0011 (Fig. 71). *Jobaria* has posteriorly facing laminae in the posterior portion of the pocdf, connecting to the postzygapophyses. They are herein interpreted as lateral cpol, which are somewhat anteriorly shifted. *Jobaria* is thus scored as plesiomorphic in this character.

C200: Posterior cervical postzygapophyses: terminate at or beyond posterior edge of centrum (0); terminate in front of posterior edge (1) (Upchurch et al., 2004b; modified by Tschopp and Mateus, 2013b; Fig. 92).

C201: Posterior cervical neural arch, interpostzygapophyseal lamina (tpol): connects directly with roof of neural canal (0); vertical lamina connects tpol with neural canal roof (1) (New; Fig. 91).

Comments. Carballido and Sander (2013) termed this vertical lamina 'single intrapostzygapophyseal lamina' (stpol).

C202: Posterior cervical neural arches, epipophyses: transversely compressed (0); dorsoventrally compressed (1) (New; Fig. 77).

Comments. Two different morphologies of the epipophyses are present in diplodocids: 1) dorsoventrally compressed, usually forming a horizontal, rugose ridge above the postzygapophyseal facet, on the lateral side of the spol, and 2) transversely compressed, such that it is formed by a dorsal expansion of the posterior end of the spol, in some cases (e.g. *Diplodocus*

PeerJ Reviewing Manuscript

carnegii CM 84) forming a rugose, vertical plate above the zygapophyseal facet, but never accompanied by a horizontal ridge. Taxa without epipophyses are scored as unknown.

C203: Posterior cervical neural arches, accessory spinal lamina: absent (0); present, running vertically just posterior to spinoprezygapophyseal lamina (1) (Whitlock, 2011a; Fig. 75).

Comments. This lamina could represent a reduced spdl. The presence of a distinct lamina is restricted to advanced diplodocines, but a reduced lamina is present in *Spinophorosaurus* as well (NMB-1699-R, ET, pers. obs., 2011).

C204: Posterior cervical neural spines, dorsoventrally elongate coel on lateral surface: absent (0); present (1) (Mannion et al., 2012; Fig. 88).

C205: Posterior cervical neural spine, horizontal, rugose ridge right below spine summit on lateral surface: absent (0); present, serves as distinct dorsal edge of the spinodiapophyseal fossa (1) (Tschopp and Mateus, 2013b; Fig. 77).

Comments. The ridge can be slightly curved in some taxa. When absent (plesiomorphic state), the sdf fades dorsally.

C206: Posterior bifid, cervical neural spines, medial surface: marked by distinct, dorsoventral ridge from base to spine summit (0); smooth (1) (New; Fig. 93).

C207: Posterior cervical neural and/or anterior-most dorsal neural spines: vertical (0); anteriorly inclined (1) (Rauhut et al., 2005).

Comments. See comments in character 169 for definition of inclined.

C208: Posterior cervical and anterior dorsal vertebrae, roughened lateral aspect of prezygodiapophyseal lamina: absent (0); present (1) (Whitlock, 2011a; Fig. 94).

Comments. The rugose area in the derived taxa lies ventrolateral to the pre-epipophysis, where present.

C209: Posterior cervical and anterior dorsal vertebrae, prespinal lamina: absent (0), present (1) (Salgado et al., 1997; Fig. 95).

Comments. The presence of a prespinal lamina does not imply the presence of a median tubercle or vice versa. However, a dorsally expanded prespinal lamina can form a median tubercle (see below). In anterior dorsal vertebrae of *Diplodocus carnegii* CM 94, the median tubercle leans anteriorly, but no lamina is present connecting it with the base of the notch between the metapophyses (ET, pers. obs., 2011).

C210: Posterior cervical and anterior dorsal bifid neural spines, median tubercle: absent (0); present (1) (McIntosh, 1990b; Upchurch, 1995; Fig. 74).

Comments. The median tubercle can be either an independent structure in the trough between the

PeerJ Reviewing Manuscript

metapophyses, or a dorsal projection of the prespinal lamina.

C211: Posterior cervical and anterior dorsal bifid neural spines, orientation: diverging (0); parallel to converging (1) (Rauhut et al., 2005; modified; Fig. 95).

Comments. Some taxa have diverging neural spines, with only their summits approaching an almost parallel orientation (e.g. CM 11984 or USNM 10865). They are scored as plesiomorphic herein. The character was initially proposed including the rate of divergence (Rauhut et al., 2005). The character was divided as orientation and distance between the metapophyses are not regarded to be dependent characters.

C212: Posterior cervical and anterior dorsal bifid neural spines, divergence: wide (0); narrow, distance between spine summits subequal to neural canal width (1) (Rauhut et al., 2005; modified; Fig. 95).

Comments. This is the second part of the character proposed by (Rauhut et al., 2005; see character 211).

C213: Posterior cervical, and anterior and mid-dorsal vertebrae, anterior projection of diapophysis right lateral to prezygapophysis: absent (0); present (1) (New; Fig. 93).

Comments. The projection described herein is not to be confused with the projection sometimes formed by the pre-epipophysis, which is posteriorly accompanied by a horizontal, rugose ridge.

C214: Cervical ribs, length: long, reaching posterior to posterior end of centrum (0); short, not reaching posterior end of centrum (1) (Russell and Zheng, 1993; modified; Fig. 86).

Comments. An additive binary version describing cervical rib length is preferred herein over the multistate character of Whitlock (2011a).

C215: Cervical ribs, length: overlapping several centra posterior (0); overlapping no more than the next cervical vertebra in sequence (1) (Russell and Zheng, 1993; modified; Fig. 76).

C216: Cervical ribs, position relative to centrum: not projecting far beneath centrum (0); projecting well beneath centrum, such that length of posterior process is subequal in length to fused diapophysis/tuberculum (1) (Wilson, 2002; Whitlock, 2011a; modified; Fig. 75).

Comments. Whitlock (2011a) included two characters describing the length of the ventral projection (from Wilson, 2002) and comparing the length of the posterior process with the length of the fused diapophysis/tuberculum. However, the length of the fused diapophysis and tuberculum depends on how far the cervical ribs project ventrally, and the length of the posterior process is accounted for in the characters defining cervical rib length. Wilson (2002) defined the ventral projection as strong when it leads to a vertebral height that exceeds its length. Such a ratio is also present in dicraeosaurids, but because of their highly elevated neural spines. The ventral

PeerJ Reviewing Manuscript

projection of the cervical rib of dicraeosaurids is minimal as in all taxa other than apatosaurs. Therefore, the two characters of Wilson (2002) and Whitlock (2011a) are herein combined, in order to define ventral projection compared to the length of the posterior process of the cervical rib.

C217: Cervical ribs, posteriorly projecting spur on dorsolateral edge of posterior shaft: absent (0); present (1) (New; Fig. 84).

Comments. The spur was proposed as autapomorphic for *Turiasaurus* (Royo-Torres et al., 2006), but it is also present in some apatosaurs and *Dicraeosaurus* (ET, pers. obs., 2011, 2012).

C218: Anterior and mid-cervical ribs, tuberculum in lateral view: is directed nearly vertically (0); is directed upwards and backwards (1) (Upchurch et al., 2004b; modified; Fig. 85).

Comments. The orientation of the tuberculum tends to become more vertical in more posterior elements. Some apatosaurs scored as plesiomorphic here actually do not have any anterior cervical vertebrae preserved, which means that they could still have inclined tubercula in the anterior elements. However, as others have distinctly inclined tubercula in mid-cervical ribs as well, a differential coding is still justifiable. Taxa that do not preserve cervical ribs were coded based on the relative positions of diapophysis and parapophysis.

C219: Posterior cervical ribs, anterior process: present (0); absent (1) (Upchurch et al., 2004b; modified; Fig. 75).

C220: Posterior cervical ribs, anterior process: distinct, much longer anteroposteriorly than high dorsoventrally (0); reduced to a short bump-like process or absent (1) (New; Fig. 96).

Comments. The last two characters serve as additive binary characters describing the reduction of the anterior process in apatosaurs in general and its complete absence in some apatosaur specimens (e.g. CM 3018; Gilmore, 1936; Wedel and Sanders, 2002).

C221: Posterior cervical ribs, anterior process: is rounded in lateral view (0); has an acute pointed tip in lateral view (1) (Upchurch et al., 2004b; modified; Fig. 96).

Comments. The anterior processes of cervical ribs can be rounded in dorsal view, but dorsoventrally compressed (as in SMA 0011, see above). Therefore, they are still pointed in lateral view.

C222: Posterior cervical ribs, rounded sub-triangular process in lateral view, immediately below tuberculum: absent (0); present (1) (Wedel and Sanders, 2002; Upchurch et al., 2004b; modified; Fig. 96).

Comments. Upchurch et al. (2004b) scored the holotypic cervical vertebra of *Apatosaurus laticollis* YPM 1861 as plesiomorphic. However, as Wedel and Sanders (2002) showed, a process

PeerJ Reviewing Manuscript

3235 is clearly present in this specimen.
3236 C223: Posterior cervical rib shafts: nearly straight and directed backward and a little upwards (0);
3237 initially directed in same direction but turn to run a little downwards toward distal tip (1)
3238 (Upchurch et al., 2004b; Fig. 96).
3239 **Dorsal vertebrae**
3240 C224: Number of dorsal vertebrae: 13 or more (0); 12 (1); 10 (2); 9 (3) (McIntosh, 1990b;
3241 Russell and Zheng, 1993; modified; Tab. S25).
3242 **Comments.** *Amargasaurus* was initially described to have 9 dorsal vertebrae (Salgado and
3243 Bonaparte, 1991), but the putative first dorsal has the parapophysis positioned dorsally to the
3244 pleurocoel, which is highly unusual in sauropods (Carballido et al., 2012a). Generally, this
3245 position marks the second or third dorsal vertebrae, which means that there would be at least ten
3246 dorsal elements, which was the coding used by Mannion et al. (2012). Herein, a coding as
3247 unknown is preferred, following Carballido et al. (2012b).
3248 C225: Dorsal centrum length (excluding articular 'ball'), remains approximately the same along
3249 the sequence (0); shortens from anterior to posterior dorsal vertebrae (1) (Mannion et al., 2012;
3250 Tab. S26).
3251 **Comments.** The exclusion of the articular ball for measuring centrum length for this character is
3252 crucial, as anterior dorsal vertebrae often have considerably larger anterior condyles than
3253 posterior elements. In taxa lacking measurements or good figures to compare between anterior
3254 and posterior elements, scores of Mannion et al. (2012) were used (e.g. *Omeisaurus*).
3255 C226: Dorsal vertebrae, opisthocoely (including a prominent anterior articular 'ball') disappears:
3256 between D2 and D3 (0); between D3 and D4 or more posteriorly (1) (Holland, 1915a; Gilmore,
3257 1936; Upchurch et al., 2004b; Tab. S27).
3258 **Comments.** The definition of 'prominent anterior ball' is somewhat ambiguous. However, a new
3259 definition is not given here, as the character is interpreted to describe a significant change within
3260 the same vertebral column. These changes can be of different absolute size if one compares
3261 between specimens, but are relatively obvious within the same individual. The decrease is thus
3262 relative to its development in more anterior elements, but can be low in an absolute sense.
3263 C227: Dorsal pneumatopores (pleurocoels): present (0); absent (1) (Gauthier, 1986; McIntosh,
3264 1990b; Upchurch, 1995; polarity reversed; Fig. 97).
3265 **Comments.** The dorsal centra of all included sauropod taxa have pleurocoel-like depressions on
3266 their lateral side, but in some taxa they do not bear a foramen.
3267 C228: Dorsal centra, pneumatic structures: absent, dorsal centra with solid internal structure (0);

PeerJ Reviewing Manuscript

present, dorsal centra with simple and big air spaces (1); present, dorsal centra with small and complex air spaces (2) (Carballido et al., 2011; modified by Carballido et al., 2012b; Fig. 72).

C229: Dorsal neural arches, paired, subdivided pneumatic chambers dorsolateral to neural canal: absent (0), present (1) (Sereno et al., 1999; Whitlock, 2011a; Fig. 98).

Comments. Paired pneumatic foramina are present in some diplodocids (e.g. UW 15556, YPM 1840), but they are not subdivided and far less deep than in *Nigersaurus* or *Demandasaurus*. The latter are thus the only taxa with the apomorphic state.

C230: Dorsal transverse processes, orientation: horizontal or only slightly inclined dorsally (0); more than 30° inclined dorsally from the horizontal (1) (Yu, 1993; modified by Upchurch, 1998; Fig. 98).

Comments. The angle of the transverse processes is easily affected by diagenetic distortion, as can be seen in dorsal vertebra 3 of *Suuwassea* ANS 21122, which most probably would actually have horizontal transverse processes.

C231: Dorsal vertebrae, single (not bifid) neural spines, spinoprezygapophyseal laminae: separate along entire length (0); joined distally, forming single prespinal lamina (1) (Upchurch, 1995; modified by Whitlock, 2011a; Fig. 99).

Comments. In some taxa (e.g. *Losillasaurus* or *Camarasaurus*), the sprl unite dorsally with the prsl, but remain separate up to that point. Here, only taxa, where the prsl is formed by the junction of the two sprl, are scored as apomorphic.

C232: Dorsal vertebrae, spinodiapophyseal webbing: laminae follow curvature of neural spine and diapophysis in anterior view (0); laminae 'festooned' from spine, dorsal margin does not closely follow shape of neural spine and diapophysis (1) (Sereno et al., 2007; Fig. 100).

C233: Dorsal vertebrae with single neural spines, middle single fossa projected through midline of neural spine: present (0); absent (1) (Carballido et al., 2012b; Fig. 99).

Comments. The fossa described herein is a distinctly confined area within the sprf, restricted to the anterior edge of the neural spine process.

C234: Dorsal (single) neural spines, postspinal lamina, dorsal end: flat to convex transversely (0); concave transversely (1) (New; Fig. 101).

C235: Dorsal vertebrae, transition from bifid to single neural spines: gradual (0); abrupt (1) (New).

Comments. Gradual transitions go from deeply bifid, to shallowly bifid, to notched, to unsplit, as defined by Wedel and Taylor (2013). If one of the intermediate states is lacking, the taxon is scored as derived. Obviously, only specimens with articulated dorsal vertebrae can be scored for

PeerJ Reviewing Manuscript

this character. Taxa without spine bifurcation are scored as unknown.

C236: Dorsal neural arches, hyposphene-hypantrum articulations: present (0); absent (1) (Gauthier, 1986; Salgado et al., 1997; Tab. S28).

C237: Dorsal vertebrae, hyposphene first appears: on D3 (0); on D4 or more posteriorly (1) (Upchurch et al., 2004b; modified; Tab. S28).

Comments. Both in *Apatosaurus* and *Camarasaurus* there are differences in the appearance of the hyposphene (Ikejiri, 2004; Upchurch et al., 2004b). Since the genotype species, *C. supremus*, appears to show the plesiomorphic state, the genus was scored as such as well. Ikejiri (2004) suggests that the development of the hyposphene might depend on ontogeny, based on observations in the juvenile specimen CM 11338. However, the latter specimen is articulated, and the region with the hyposphene is obliterated, such that its presence or absence is difficult to assess (McIntosh et al., 1996a).

C238: Dorsal vertebrae, single vertical lamina supporting the hyposphene from below: absent (0); present (1) (Gilmore, 1936; Upchurch et al., 2004b; modified; Fig. 98).

Comments. The original character description (Upchurch et al., 2004b) interfered with the character proposed by Wilson (2002) distinguishing between single and double cpol in mid- and posterior dorsal vertebrae (see character 261). The character of Upchurch et al. (2004b) was thus simplified, and polarity was reversed due to the differential taxon sampling. The lamina described herein corresponds to the stpol (Carballido and Sander, 2013). Taxa without hyposphene are scored as unknown.

C239: Dorsal vertebrae 1 and 2, centrum length: DV 1 > DV 2 (0); DV 2 > DV 1 (1) (Upchurch et al., 2004b; modified; Tab. S29).

Comments. The character was originally defined implying that either DV 1 or 2 were the longest in the series (Upchurch et al., 2004b), which is not always the case (see Tab. S29).

C240: First dorsal vertebrae, pleurocoel location: occupy the anterior and middle part of the centrum (0); occupy the posterior part of the centrum (1) (Holland, 1915a; Gilmore, 1936; Upchurch et al., 2004b; modified; Fig. 94).

Comments. The character was restricted to the first dorsal, as also in *Apatosaurus louisae*, for which this character was proposed as species autapomorphy (Holland, 1915a; Gilmore, 1936; Upchurch et al., 2004b), DV 2 and 3 already have a centrally placed pleurocoel (CM 3018, ET, pers. obs., 2011).

C241: Anterior dorsal vertebrae, pleurocoels in first few centra: become larger along the series (0); become smaller (1) (Gilmore, 1936; Upchurch et al., 2004b; wording modified; Tab. S30).

PeerJ Reviewing Manuscript

Comments. Taxa without dorsal pleurocoels are scored as unknown.

C242: Anterior dorsal vertebrae, ventral keel: absent (0); present (1) (Mannion et al., 2012; Fig. 102).

C243: Anterior dorsal transverse process position: high, considerably above dorsal edge of posterior cotyle (0); low, ventral edge about level to dorsal edge of posterior cotyle (1) (Gilmore, 1936; Fig. 103).

Comments. The differing dorsoventral extension of the transverse processes in the anterior-most dorsal vertebrae was proposed as character to distinguish *Apatosaurus louisae* CM 3018 from the supposed *Apatosaurus excelsus* UW 15556 (Gilmore, 1936). It is here applied for the first time in a phylogenetic analysis. In most taxa, position of the transverse process rises considerably in the first few dorsal vertebrae. Therefore, this description applies best for the first element in the series.

C244: Anterior, bifid dorsal vertebrae, base of notch between metapophyses: wide and rounded (0); narrow, V-shaped (1) (Gilmore, 1936; Fig. 103).

Comments. As *Apatosaurus*, also *Camarasaurus* appears to show intrageneric variation: *C. lewisi* has narrow troughs throughout its bifurcated presacral vertebrae, whereas other *Camarasaurus* species have wide bases (Jensen, 1988; McIntosh et al., 1996b). Herein, *Camarasaurus* was scored as plesiomorphic, because new evidence from material at SMA suggests that *C. lewisi*, which was initially described as new genus (*Cathetosaurus*), was actually erroneously referred to *Camarasaurus* (Mateus and Tschopp, 2013).

C245: Anterior dorsal, bifid neural spines, medial surface: gently rounded transversely (0); subtriangular (1) (New; Fig. 95).

Comments. Some diplodocid specimens bear a dorsoventral ridge on the medial surface of the anterior dorsal neural spines, similar to the ridge present in some diplodocid posterior cervical neural spines. The ridge results in a subtriangular shape of the medial surface.

C246: Dorsal vertebra 3, parapophysis: lies at the top of the centrum (0); lies mid-way between the top of the centrum and the level of the prezygapophyses (1) (Gilmore, 1936; Upchurch et al., 2004b; modified; Fig. 97).

C247: Anterior and mid-dorsal centra, pleurocoels: situated entirely on centrum (0); invade neural arch pedicels (1) (Holland, 1915a; Fig. 104).

Comments. Holland (1915a) proposed this morphology as diagnostic for *Apatosaurus louisae*. It is included in a phylogenetic analysis for the first time. Taxa without dorsal pleurocoels are scored as unknown.

PeerJ Reviewing Manuscript

C248: Anterior and mid-dorsal neural arch, hyposphene shape: rhomboid (0); laminar (1) (New; Tab. S28).

Comments. Hyposphene shape can change considerably from front to back, as is seen in specimens of *Camarasaurus* (Osborn and Mook, 1921; McIntosh et al., 1996b). In the present analysis, two different characters are thus used to code for the anterior and mid-dorsal vertebrae, as well as for the posterior elements, which are often less developed (see character 276). See figure 98 for an example of a laminar hyposphene.

C249: Mid-dorsal neural arches, height above postzygapophyses (neural spine) to height below (pedicel): 2.1 or greater (0); < 2.1 (1) (Whitlock, 2011a; modified; Tab. S31).

Comments. Pedicel height is measured from the neural canal floor to the ventral-most point of the postzygapophyseal facets, neural spine height from there to the spine top. Both measurements are taken vertically, ignoring spine inclination. The ratio changes considerably between mid- and posterior dorsal vertebrae, therefore the original character of Whitlock (2011a) was divided in two (see character 272). Furthermore, a numerical boundary was introduced.

C250: Mid-dorsal neural spines, form: single, bifid form (if present) does not extend past second or third dorsal (0); bifid, inclusive of at least fifth dorsal vertebrae (1) (Whitlock, 2011a; Tab. S32).

Comments. Notched and unsplit neural spines (sensu Wedel and Taylor, 2013) are counted as single, shallowly and deeply bifurcated spines as bifid. An additional character is used to account for the notched spines. The taxon scores are thus slightly different from the ones in Whitlock (2011a).

C251: Mid-dorsal neural spines, oblique accessory lamina connecting postspinal lamina with spinopostzygapophyseal lamina: absent (0); present (1) (New; Fig. 104).

Comments. In *Supersaurus* and *Dinheirosaurus*, this accessory lamina extends posterodorsally-anteroventrally from near the dorsal end of the posl to the junction of the spol with the spdl.

C252: Mid- and posterior dorsal vertebrae, lateral pleurocoels present in centra: absent (0); present (1) (Gauthier, 1986; McIntosh, 1990b; Upchurch, 1995; modified by Whitlock, 2011a).

C253: Mid- and posterior dorsal vertebrae, vertically oriented rod-like struts divide the lateral pneumatic foramina: absent (0); present (1) (Mannion et al., 2012; Fig. 104).

Comments. Mannion et al. (2012) proposed the presence of such a strut as synapomorphy for the clade uniting *Supersaurus* and *Dinheirosaurus*. However, similar struts are present as well in some apatosaurs. The pleurocoel is often not completely liberated from matrix during preparation, potentially obscuring the presence or absence of this structure.

PeerJ Reviewing Manuscript

C254: Mid- and posterior dorsal vertebrae, height of neural arch below postzygapophyses (pedicel) divided by posterior cotyle height: <0.8 (0); 0.8 or greater (1) (Gallina and Apesteguía, 2005; modified; Tab. S33).

Comments. Neural arch height is measured from the neural canal floor to where the postzygapophyseal facets meet medially, above the hyposphene, where present.

C255: Mid- and posterior dorsal neural arches, prezygoparapophyseal lamina: present (0); absent (1) (Wilson, 2002; Fig. 105).

C256: Mid- and posterior dorsal parapophyses, location: above centrum, posterior to anterior edge of centrum (0); straight above anterior edge of centrum, or anteriorly displaced (1) (New; Figs 104, 105).

Comments. The anterior edge of the centrum corresponds to the rim of the anterior condyle in opisthocoelous elements. In some taxa, the position of the parapophysis changes from front to back, these taxa are scored for the majority of the elements in the series (e.g. *Haplocanthosaurus*, where DV 10 has a posteriorly placed parapophysis, but the majority of the mid- and posterior dorsal vertebrae have anteriorly displaced parapophyses; Hatcher, 1903).

C257: Mid- and posterior dorsal neural arches, anterior centroparapophyseal lamina: absent (0); present (1) (Upchurch et al., 2004a; Fig. 105).

C258: Mid- and posterior dorsal neural arches, posterior centroparapophyseal lamina: absent (0); present as single lamina (1); present, double (2) (Salgado et al., 1997; modified after Mannion et al., 2013; Figs 105, 106).

Comments. In taxa, where the pcpl is double, the more dorsal branch often connects to the pcdl. Mannion et al. (2013) defined the third state as 'two parallel laminae', but in certain specimens (e.g. *Diplodocus carnegii* CM 84), the dorsal branch becomes more horizontal (Hatcher, 1901). The character is treated as ordered, as it codes for both presence/absence and morphology.

C259: Mid- and posterior dorsal vertebrae, accessory laminae in region between posterior centrodiapophyseal lamina and posterior centroparapophyseal lamina: absent (0); present (1) (Mannion et al., 2012; Fig. 106).

Comments. This character is somewhat ambiguous. Some of these accessory laminae might actually represent dorsal branches of the pcpl (see character 258) or dislocated ppdl. Here, only laminae not directly connecting to any specifying landmark (see Wilson, 1999) are considered accessory. More studies are needed to see if these are homologous to the above mentioned laminae.

C260: Mid- and posterior dorsal vertebrae, accessory lamina linking hyposphene with base of

PeerJ Reviewing Manuscript

posterior centrodiapophyseal lamina: absent (0); present (1) (New; Figs 104, 106).

Comments. The presence of such an accessory lamina was proposed as autapomorphic for *Dinheirosaurus* (Mannion et al., 2012), but is herein interpreted to be present in other diplodocids as well. The accessory lamina can easily be confused with the lateral branch of the cpol, but the latter connects directly with the postzygapophyseal facet, and not with the hyposphene. The accessory lamina described herein is thus situated between the two branches of the cpol.

C261: Mid- and posterior dorsal neural arches, centropostzygapophyseal lamina: single (0); divided, lateral branch connecting to posterior centrodiapophyseal lamina (1) (Wilson, 2002; wording modified; Fig. 105).

Comments. The lateral branch is often only visible in lateral view.

C262: Mid- and posterior dorsal neural arches, infradiapophyseal pneumatopore between anterior and posterior centrodiapophyseal laminae: absent (0); present (1) (Wilson, 2002; Fig. 106).

Comments. Even though the development of pneumatic structures has been shown to depend on the ontogenetic stage (Wedel, 2003; Schwarz et al., 2007c), the early juvenile brachiosaur SMA 0009 already has this pneumatopore.

C263: Mid- and posterior dorsal transverse processes, length: short (0); long (projecting < 1.3 times posterior cotyle width) (1) (Carballido et al., 2012b; modified; Tab. S34).

Comments. The length of a single transverse process is compared to the maximum width of the posterior cotyle. Transverse process length is measured in a horizontal plane. Measurements taken from figures in posterior view generally underestimate the ratio, which has to be accounted for when scoring the taxa. In the case of *Brachiosaurus altithorax* FMNH P25107, true ratios based on the measurements by Riggs (1904) are about 120% of the ratios taken from published figures (Taylor, 2009), whereas in *Apatosaurus* NSMT-PV 20375 or *Diplodocus* CM 84, they are only 103% higher. This percentage depends on the relative position of the transverse processes above the centrum. Ratios generally decrease from anterior to posterior dorsal vertebrae. Taxa or specimens that preserve only posterior elements (e.g. *Amphicoelias altus* AMNH 5764) should thus have higher actual ratios than shown in Tab. S34.

C264: Mid- and posterior dorsal transverse processes, dorsal edge: straight, or curving downwards at distal end (0); developing a distinct dorsal bump or spur (1) (New; Fig. 98).

Comments. Spurs are usually situated at the distal tip, whereas bumps are located more medially.

C265: Mid- and posterior dorsal neural spines, anteroposterior width: approximately constant along height of spine, with subparallel anterior and posterior margins (0); narrows dorsally to form triangular shape in lateral view, with base being approximately twice the width of dorsal tip

PeerJ Reviewing Manuscript

(1) (New; Fig. 106).

C266: Middle and posterior dorsal neural spines, breadth at summit: much narrower (0); equal to or broader (1) transversely than anteroposteriorly (Wilson, 2002; modified).

Comments. Neural spine width can change considerably from the spine bottom to the top. The original character was thus divided in two (see character 265).

C267: Mid- and posterior dorsal neural spines, triangular aliform processes: absent (0); present but do not project far laterally (not as far as postzygapophyses) (1); present, project at least as far laterally as postzygapophyses (2) (Carballido et al., 2012b; Figs 98, 99).

Comments. The character is treated as ordered.

C268: Posterior dorsal centra, total length/height of posterior articular surface: 1.0 or greater (0); short, < 1.0 (1) (New; Tab. S35).

C269: Posterior dorsal centra: subequal width and height, or higher than wide (0); wider than high (1) (Gilmore, 1936; Tab. S35).

Comments. Width and height are measured at the posterior cotyle. The boundary is set between 1.0 and 1.1 in the present study, because it was suggested by Gilmore (1936) to distinguish *Apatosaurus louisae* from *A. ajax* and *A. excelsus*.

C270: Posterior dorsal centra, articular face shape: amphicoelous (0); slightly opisthocoelous (1); strongly opisthocoelous (2) (Yu, 1993; wording modified by Carballido et al., 2012b; Fig. 105).

Comments. Slightly opisthocoelous means that the condyle is either ventrally or dorsally restricted, but still visible in lateral view. Strongly opisthocoelous vertebrae have anterior balls that reach from the dorsal to the ventral edge of the centrum. In *Apatosaurus ajax* YPM 1860, no anterior articulation surface of a posterior dorsal vertebrae is observable, but the posterior articulation surface of a posterior element has a small, but distinct fossa marking its upper half. This indicates a slightly opisthocoelous centrum in the following element.

C271: Posterior dorsal vertebrae, pleurocoel shape: oval to circular (0); subtriangular with apex dorsally (1) (New; Fig. 106).

Comments. Taxa without dorsal pleurocoels are scored as unknown.

C272: Posterior dorsal neural arches, height above postzygapophyses (neural spine) to height below (pedicel): < 3.1 (0); 3.1 or greater (1) (Whitlock, 2011a; modified; Tab. S31).

Comments. See character 249.

C273: Posterior dorsal neural arches, parapophyseal centrodiapophyseal fossa: ventrally open, relatively shallow (0); deep, triangular (1) (Gallina and Apesteguía, 2005; Fig. 106).

Comments. The apomorphic state is applied to specimens with the pcpl connecting to the pcdl or

PeerJ Reviewing Manuscript

acdl, thus creating a ventrally closed, triangular fossa between them and the ppdl or prdl. In plesiomorphic taxa, the pcpl fades out posteroventrally or connects to the centrum anterior to the ventral end of the pcdl.

C274: Posterior dorsal vertebrae, spinoprezygapophyseal lamina: absent or greatly reduced (0); present (1) (Upchurch et al., 2007; modified; Fig. 107).

Comments. Reduced sprl fade out anteroventrally and/or join the prsl at a very ventral level.

C275: Posterior dorsal postzygapophyses: almost horizontal, such that the two articular facets include a wide angle (0); articular facets oblique, including an almost 90° angle (1) (New; Fig. 101).

Comments. Some diplodocine taxa have curved facets. These are interpreted as horizontal.

C276: Posterior dorsal vertebrae, hyposphene-hypantrum system: well developed, rhomboid shape up to last element (0); weakly developed, mainly as a laminar articulation (1) (Carballido et al., 2012b; modified; Fig. 98; Tab. S28).

Comments. Taxa without hyposphenes are scored as unknown.

C277: Posterior dorsal neural arches, spinopostzygapophyseal laminae: single (0); divided near postzygapophyses (1) (Wilson, 2002; Fig. 98).

Comments. The spol can bifurcate in two ways in different taxa: rebbachisaurids have ventrally forked laminae, whereas in some diplodocids the spol bifurcates dorsally, creating a medial and a lateral branch. The presence of a medial spol is accounted for in character 278, the present one describes the ventral bifurcation.

C278: Posterior dorsal vertebrae, medial spinopostzygapophyseal lamina: absent (0); present and forms part of median posterior lamina (1) (Carballido et al., 2012b; Fig. 101).

Comments. The mspol can either be connected with the lspol ventrally or they can remain separated.

C279: Posterior dorsal vertebrae, base of neural spines just above transverse processes: longer than wide (0); subequal in width and length (1) (New).

Comments. This is the second character about spine width to length, inspired by a character from Wilson (2002) (see character 266).

C280: Posterior dorsal neural spines, orientation at its base: vertical (0); anteriorly inclined (1) (New; Fig. 105).

Comments. Anterior inclination can be restricted to the very base of the neural spine, as is the case in *Apatosaurus louisae* CM 3018 (Fig. 105A). The best indication for the inclination is the prsl in lateral view.

PeerJ Reviewing Manuscript

C281: Posterior dorsal neural spines, midline cleft along the dorsal surface: absent (0); present (1) (Mannion et al., 2012; modified; Fig. 100; Tab. S32).

Comments. The midline cleft described herein corresponds to the notched spines of Wedel and Taylor (2013). Not all posterior dorsal spines have to be notched in order to be scored as apomorphic.

C282: Posterior dorsal and/or sacral neural spines (not including arch), height: less than 2 times centrum length (0); 2 to 3 times centrum length (1); more than 3 times centrum length (2) (Mannion et al., 2012; modified; Tab. S36).

Comments. Neural spine height is measured from the top of the postzygapophyses to the highest point of the spine, vertically. Centrum length does not include the anterior ball. The original version (Mannion et al., 2012) was restricted here to posterior dorsal and sacral vertebrae only, as mid-dorsal elements of diplodocids considerably lower the mean ratio in some cases (Tab. S36). Also, state boundaries are adapted. The character is treated as ordered.

C283: Dorsal ribs, rib head: area between capitulum and tuberculum flat (0); oblique ridge present that connects medial and lateral edge at the base of the rib head (1) (New; Fig. 108).

Comments. The ridge marks the posterior surface of the rib head of advanced diplodocines.

C284: Dorsal ribs, proximal pneumatopores: absent (0); present (1) (Wilson, 2002; Fig. 108).

Comments. In some taxa, only one rib of the entire series bears a pneumatopore. However, the ability to develop pneumatized ribs appears to be restricted to certain diplodocid groups, therefore the character was included in this analysis.

C285: Mid-dorsal ribs, orientation of tuberculum: spreading outside from rib shaft (0); following straight direction of rib shaft (1); following medial bend of rib shaft (2) (Gallina and Apesteguía, 2005; Fig. 108).

Sacral vertebrae

C286: Sacral vertebrae, number: 4 (0); 5 (1); 6 (2) (Salgado et al., 1997; modified; Tab. S37).

Comments. Some *Camarasaurus* specimens appear to have six sacral vertebrae, which is usually considered a synapomorphy of advanced titanosauriforms (Tidwell et al., 2005). The addition of a sacral vertebra was suggested to be a sign of very old age (Tidwell et al., 2005). The unusual six sacral vertebrae in the holotype of '*Apatosaurus*' *minimus* AMNH 675 (Mook, 1917) might thus also be ontogenetic.

C287: Sacral vertebral centra, pleurocoels: absent (0); present (1) (Upchurch et al., 2004a; wording modified).

C288: Sacral rib III, ventral surface: smooth (0); with oblique ridge (1) (Mook, 1917; Fig. 109).

PeerJ Reviewing Manuscript

Comments. The presence of an oblique ridge was proposed as synapomorphy of *Apatosaurus* by Mook (1917), but later regarded as ambiguous and thus of little use to diagnose the genus (McIntosh, 1995). The presence of this ridge is herein used for the first time as phylogenetic character, in order to test its utility. According to Mook (1917), the ridge marks the ventral face of sacral rib II. However, as shown in the holotype specimen if *Brontosaurus amplus* YPM 1981 (Ostrom and McIntosh, 1966), among others, the ridge actually lies on sacral rib III. Some *Camarasaurus* specimens bear oblique ridges on their sacral ribs (e.g. AMNH 690; Osborn, 1904), but not the genotype specimen AMNH 5761. In the present analysis, *Camarasaurus* was thus scored as plesiomorphic.

C289: Sacral neural spines, lateral side, towards summit: flat, with only spinodiapophyseal lamina (spdl) well-developed (0); with distinct horizontal accessory laminae that connect spdl to pre- and/or postspinal lamina (1) (New; Fig. 110).

C290: Sacral neural spines, lateral view, spinodiapophyseal lamina: reduced to absent, does not connect summit and diapophysis (0); present and distinct, connects spine summit with diapophysis (1) (New; Fig. 110).

C291: Sacral neural spines, lateral view, spinodiapophyseal laminae (spdl): remain vertical and thus parallel to each other (0); spdl of neighboring spines converge (1) (New; Fig. 110).

Comments. Diplodocinae develop a very distinct dorsal widening of the sacral spdl. Together with the inclination of the spines towards the central portion of the sacrum, this often leads to a fusion of these anteroposteriorly widened dorsal ends of the spdl.

Caudal vertebrae

C292: Caudal neural spines, elliptical depression between lateral spinal lamina and postspinal lamina on dorsolateral surface: absent (0); present (1) (Sereno et al., 2007; modified; Fig. 111).

Comments. Sereno et al. (2007) initially defined the character as follows: 'elliptical depression between spinodiapophyseal lamina and postspinal lamina on lateral neural spine'. However, the spinal lamina they were most probably referring to (herein called lateral spinal lamina) is usually the united spol and sprl (at least in diplodocids). The character description has thus been reworded in order to clarify this. Sereno et al. (2007) recovered the presence of such a depression as synapomorphy of Nigersaurinae, but actually it is present in any taxon with transversely widened posl, and spol that either fuse with the spdl or the posl. Anterior caudal vertebrae of *Diplodocus* are a good example for this, although they were scored as plesiomorphic by Sereno et al. (2007). Taxa without spdl or posl are scored as unknown.

C293: Caudal neural spines with triangular lateral processes: absent (0); present (1) (Sereno et al.,

PeerJ Reviewing Manuscript

2007; Fig. 112).

Comments. These processes correspond to the triangular lateral processes of dorsal neural spines, but do not appear to be correlated.

C294: Posterior dorsal, sacral and anterior caudal neural spines, shape in anterior/posterior view: rectangular through most of length (0); 'petal' shaped, expanding transversely through 75% of its length and then tapering (1) (Calvo and Salgado, 1995; Upchurch, 1998; Fig. 112).

Comments. Plesiomorphic caudal neural spines can still be transversely expanded at their ends. Also, taxa with gradually expanding neural spines that do not taper dorsally are herein scored as plesiomorphic, as without the tapering, the spines do not develop the 'petal' shape typical for rebbachisaurs and dicraeosaurs.

C295: First caudal centrum, articular face shape: flat (0); procoelous (1); opisthocoelous (2) (Wilson, 2002; modified).

Comments. The fourth state (biconvex) of Wilson (2002) was deleted as no used OTU has a biconvex first caudal vertebra. The probable brachiosaurid SMA 0009 and *Demandasaurus* have platycoel first caudal vertebrae (Torcida Fernández-Baldor et al., 2011; Carballido et al., 2012a), and are herein scored as opisthocoelous rather than flat.

C296: Anterior-most caudal centra, transverse cross-section: sub-circular with rounded ventral margin (0); 'heart'-shaped with an acute ventral ridge (1) (Gilmore, 1936; Upchurch et al., 2004b; wording modified; Fig. 113).

Comments. Taxa with ventral hollows in their anterior caudal centra are scored as plesiomorphic, because the presence of the ventral ridge is regarded as the crucial trait this character codes for.

C297: Anterior-most caudal centra, pneumatic fossae: reduced to absent (0); large pleurocoels (1) (New; Fig. 111).

Comments. Some apatosaur specimens and *Supersaurus* have distinct pleurocoels in their anterior-most caudal centra, whereas in anterior centra (as defined in table 10), pleurocoels are reduced to foramina in these taxa (see e.g. Riggs, 1903). The current character is thus added to the usual one coding for pleurocoels in anterior caudal vertebrae in general.

C298: Anterior-most caudal vertebrae, additional pneumatic fossa on posterodorsal corner of centrum: absent (0); present (1) (New; Fig. 111).

Comments. In lateral views, these additional pneumatic foramina are often obscured by the transverse process.

C299: Anterior-most caudal transverse processes, shape: triangular, tapering distally (0); wing-like (1) (McIntosh, 1990b; Yu, 1993; modified; Fig. 112).

PeerJ Reviewing Manuscript

Comments. A transverse process is herein interpreted as wing-like if it has a distinct shoulder, i.e. an angled bump on its dorsolateral edge.

C300: Anterior-most caudal vertebrae, transition from 'fan'-shaped to ' normal' caudal ribs: between Cd 1 and 2 (0); Cd4 and Cd5 (1); Cd5 and Cd6 (2); Cd6 and Cd7 (3); Cd7 and Cd8 or more posteriorly (4) (Upchurch et al., 2004b; modified; Tab. S38).

C301: Anterior-most caudal neural arches, accessory lamina connecting pre- and postzygapophyses: absent (0); present (1) (New; Fig. 111).

Comments. This accessory lamina usually connects the postzygapophysis with the sprl.

C302: Anterior-most caudal neural spine (not including arch), height: less than 1.5 times centrum height (0); 1.5 times centrum height or more (1) (Yu, 1993; modified after Upchurch and Mannion, 2009; Tab. S39).

Comments. Neural spine height is measured from the dorsal edge of the postzygapophyses to the spine top, vertically. Centrum height is measured at the posterior articular surface. Yu (1993) used the entire neural arch height for the ratio, and formulated it as a multistate character, restricted to the first two caudal vertebrae. The ratio is herein adapted following Upchurch and Mannion (2009), but keeping the restriction to the anterior-most elements, instead of including all anterior caudal vertebrae as Upchurch and Mannion (2009).

C303: Anterior-most caudal neural spines, lateral spinal lamina: has the same anteroposterior width ventrally and dorsally (0); expands anteroposteriorly towards its distal end, and becomes rugose (1) (Upchurch et al., 2004a; wording modified; Fig. 111).

Comments. Apatosaurs usually have a more dorsally restricted anteroposterior expansion of the lateral spinal lamina, compared to diplodocines. SMA 0087 appears to show the plesiomorphic state, which could be an autapomorphic reversal. However, due to the bad preservation of the bones, the true morphology of the lateral spinal lamina is difficult to assess, and it might actually turn out to be widened as well, once all the material is prepared.

C304: Anterior caudal centra (excluding the first), articular surface shape: amphiplatyan or amphicoelous (0); procoelous/distoplatyan (1); slightly procoelous (2); procoelous (3) (McIntosh, 1990b; Russell and Zheng, 1993; modified after González Riga et al., 2009; Tab. S38).

Comments. Slightly procoelous is herein defined as the slightly opisthocoelous in posterior dorsal centra (see character 270). In diplodocids, the centra change their shape in anterior to middle caudal vertebrae from slightly procoelous to procoelous/distoplatyan to amphicoelous/amphiplatyan. This change occurs more posteriorly in *Diplodocus* than in *Apatosaurus*, for example, therefore specimens of the former genus have to be scored as slightly

PeerJ Reviewing Manuscript

procoelous for this character, whereas *Apatosaurus* specimens are scored as procoelous/distoplatyan. However, more detailed studies about this transition is needed in order to score this character appropriately, as the specimens used herein generally show some correlation (within Flagellicaudata) of the development of procoely and the presence of wing-like transverse processes, which also mark more caudal vertebrae in *Diplodocus* than in less derived Flagellicaudata.

C305: Anterior caudal centra, ventral surface: without irregularly placed foramina (0); irregular foramina present on some anterior caudal vertebrae (1) (Whitlock, 2011a; Fig. 113).

Comments. Foramina can also be present in anterior caudal vertebrae without concave ventral surfaces (see *Suuwassea emilieae* ANS 21122; Harris, 2006b).

C306: Anterior caudal centra, pneumatopores (pleurocoels): absent (0); present (1) (McIntosh, 1990b; Yu, 1993; modified).

Comments. Small pneumatopores also mark the lateral surfaces of non-diplodocine sauropods (e.g. *Lourinhasaurus alenquerensis* MIGM specimen, ET, pers. obs., 2012). The development of the pneumatopores as foramina or deep coels is described in character 307.

C307: Anterior caudal centra, pneumatopores: restricted to foramina (0); large coels present (1) (Tschopp and Mateus, 2013b; modified; Fig. 114).

Comments. This character only codes for the anterior caudal vertebrae, excluding the anterior-most elements with wing-like transverse processes. The presence of a large coel in the latter is coded for in character 297. Taxa without pneumatopores are scored as unknown.

C308: Anterior caudal centra, pneumatopores: disappear by caudal 15 (0); present until caudal 16 or more (1) (McIntosh, 2005; Tab. S38).

Comments. McIntosh (2005) recognized this as distinguishing character between *Diplodocus* and *Barosaurus*, but it is applied for the first time as phylogenetic character.

C309: Anterior caudal centra, length: subequal amongst first 20 (0); more or less doubling over first 20 (1) (Upchurch, 1998; modified; Tab. S40).

Comments. Lengths were compared between the shortest element among the first three, and the longest preserved vertebrae within Cd 17 and 22 (or if this part of the tail is lacking, the longest element preserved). Taxa with a ratio of 1.5 or more are scored as derived.

C310: Anterior caudal vertebrae, concavo-convex zygapophyseal articulation: absent (0); present (1) (Wilson, 2002; Whitlock, 2011a; Fig. 112).

Comments. This character is similar to the one for cervical vertebrae, which describes the flat versus convex prezygapophyses of diplodocine cervical vertebrae. Wilson (2002) suggested that

PeerJ Reviewing Manuscript

convex prezygapophyses and concave postzygapophyses are diagnostic for *Diplodocus*, but Whitlock (2011a) showed that also *Barosaurus* showed the derived state. During the current study, also some apatosaur specimens were observed to have the apomorphic condition.

C311: Anterior caudal prezygapophyses, pre-epipophysis laterally below articular facet: absent (0); present (1) (New; Fig. 111).

Comments. A rugose horizontal ridge marks the lateral surface of the prezygapophysis of *Diplodocus* and very few other taxa, below the articular facet. The position corresponds to where the pre-epipophysis of cervical vertebrae is located and is thus termed equally here.

C312: Anterior caudal vertebrae, transverse processes: ventral surface directed laterally or slightly ventrally (0); directed dorsally (1) (Whitlock, 2011a; Fig. 112).

Comments. This character describes the orientation of the ventral edge of the transverse process in anterior or posterior view.

C313: Anterior caudal transverse processes, anterior diapophyseal laminae (acdl, prdl): reduced or absent (0); present, well defined (1) (Wilson, 2002; modified; see Fig. 114 for equivalent in posterior diapophyseal laminae).

Comments. The original character (Wilson, 2002) was split in two, as the development of the posterior centrodiapophyseal and the postzygodiapophyseal laminae differs between *Apatosaurus* and *Diplodocus*.

C314: Anterior caudal transverse processes, anterior centrodiapophyseal lamina, shape: single (0); divided (1) (Wilson, 2002; Fig. 111).

Comments. In contrast to dicraeosaurids or more basal diplodocoids, diplodocids have wing-like transverse processes, which are anteriorly supported by two independent laminae, which both originate on the centrum and thus classify as acdl (and the latter thus as divided or double). In advanced diplodocines, the lower of the two acdl is furthermore branching in two towards the transverse process.

C315: Anterior caudal transverse processes, posterior diapophyseal laminae (pcdl, podl): reduced or absent (0); present, well defined (1) (Wilson, 2002; modified; Fig. 114).

C316: Anterior caudal transverse processes, anteroposteriorly expanded lateral extremities: absent (0); present (1) (New; Fig. 113).

Comments. Backwards curving transverse processes are not necessarily anteroposteriorly expanded.

C317: Anterior caudal neural spines, maximum mediolateral width to anteroposterior length ratio: < 1.0 (0); 1.0 or greater (1) (Upchurch, 1998; modified by Mannion et al., 2013; Tab. S39).

PeerJ Reviewing Manuscript

Comments. The anteroposterior length of the spine is measured at the same level as the maximum mediolateral width, perpendicular to the inclination of the neural spine. The unusual plesiomorphic state of SMA 0087 within the apatosaur specimens might be due to diagenetic transverse compression.

C318: Anterior caudal neural spines, spinoprezygapophyseal lamina: absent, or present as small short ridges that rapidly fade out into the anterolateral margin of the spine (0); present, extending onto lateral aspect of neural spine (1) (Wilson, 2002), modified by (Mannion et al., 2012; Fig. 111).

C319: Anterior caudal neural spines, spinopre- and spinopostzygapophyseal laminae contact: absent (0); present (1) (Wilson, 2002; Fig. 111).

C320: Anterior caudal neural arches, prespinal lamina: absent (0); present (1) (Upchurch, 1995; Fig. 111).

Comments. Sauropod anterior caudal neural spines are generally rugose anteriorly and posteriorly, but only derived eusauropods develop distinct ridges or laminae.

C321: Anterior caudal neural spines, thickened anterior rim of prespinal lamina: absent (0); present (1) (Gallina and Apesteguía, 2005; Fig. 111).

Comments. Specimens without prespinal lamina are scored as unknown.

C322: Anterior caudal neural spines, prespinal lamina or rugosity: terminate at or beneath dorsal margin of neural spine (0); project dorsally above neural spine (1) (Whitlock, 2011a; modified; see Fig. 114 for equivalent in postspinal lamina).

Comments. The original character (Whitlock, 2011a) was split in two, because in the anterior caudal vertebrae of *Cetiosauriscus stewarti* NHMUK R.3078 only the postspinal rugosity expands dorsally above the spine summit (Woodward, 1905). The character description was slightly changed in order to include taxa without distinct prsl.

C323: Anterior caudal neural arches, postspinal lamina: absent (0); present (1) (Upchurch, 1995; Fig. 111).

Comments. See character 320. The two characters coding for the presence of pre- or postspinal laminae, are scored equally in the present analysis, as also in Wilson (2002), and might thus prove correlated in future. They were both retained herein as they distinguish between basal and derived non-neosauropod eusauropods and should thus have no influence on the relationships between ingroup diplodocids.

C324: Anterior caudal neural spines, postspinal lamina or rugosity: terminate at or beneath dorsal margin of neural spine (0); project dorsally above neural spine (1) (Whitlock, 2011a; modified;

PeerJ Reviewing Manuscript

Fig. 114).

Comments. See character 322.

C325: Anterior caudal neural arches; hyposphenal ridge on posterior face of neural arch; present (0); absent (1) (Mannion et al., 2012; Fig. 115).

C326: Anterior caudal neural spines, shape: single (0); slightly bifurcate anteriorly (1) (Whitlock, 2011a; Fig. 112).

Comments. Anterior caudal neural spines can be bifid in two ways: anteroposteriorly and transversely. The former is coded for in characters 322 and 324, whereas the latter is described in the present character.

C327: Anterior caudal neural spines, maximum mediolateral width to minimum mediolateral width ratio: < 2.0 (0); 2.0 or greater (1) (Canudo et al., 2008; Taylor, 2009; modified by Mannion et al., 2013; Tab. S39).

C328: Anterior caudal neural spines, lateral expansion at distal end: gradual, expanding through the last third of the neural spine (0); abrupt, restricted to distal fourth of neural spine (1) (New; Fig. 112).

C329: Anterior and mid-caudal vertebrae, ventrolateral ridges: absent (0); present (1) (Upchurch et al., 2004a; Fig. 116).

Comments. There are two horizontal ridges marking some diplodocid caudal centra: the lateral ridge and the ventrolateral ridge. Usually, only one of the two is present, which is interpreted as the lateral ridge. The ventrolateral ridge as used herein does not describe the borders of the ventral longitudinal hollow of advanced diplodocines.

C330: Anterior and mid-caudal centra, ventral longitudinal hollow: absent (0); present (1) (McIntosh, 1990b; Yu, 1993; Fig. 113).

Comments. A ventral hollow is herein interpreted to be longitudinal concavity occupying the entire ventral surface. Various taxa have very distinct posterior chevron facets, with distinct ridges leading to them, thus creating a posteriorly concave ventral surface. However, these ridges often fade anteriorly. In some anterior diplodocine caudal centra, the ventral hollow is subdivided by longitudinal struts (e.g. *Tornieria africana* SMNS 12141a; Remes, 2006).

C331: Anterior- and mid-caudal vertebrae, ventral hollow depth: shallow, 10mm or less (0); deep, >10mm (1) (Curtice, 1996; Tab. S40).

Comments. Ventral hollow depth is used as distinguishing character between *Diplodocus* and *Barosaurus* (Curtice, 1996; McIntosh, 2005). Curtice (1996) showed that a caudal centra with a ventral hollow depth of more than 10 mm can be confidently identified as *Diplodocus*, whereas

PeerJ Reviewing Manuscript

shallower centra are typical for less derived diplodocines. Only very limited measurements were available, and the scoring was mainly based on descriptions and thus the subjective opinion of the respective authors. An interesting case is present in *Tornieria*, where the only preserved caudal vertebra of the holotype specimen (SMNS 12141a, Cd 2) has a deep ventral hollow, whereas the medial caudal vertebra of skeleton k (MB.R.2913) is only shallowly excavated (Remes, 2006). More detailed research is needed in order to sort this out.

C332: Mid-caudal vertebrae, ratio of centrum length to posterior height: < 1,7 (0); 1,7 or greater (1) (Yu, 1993; modified; Tab. S40).

Comments. Usually, this character is included in analyses with its state boundary set at 2. In the present analysis, it was regarded more useful to put the boundary at 1.7, as some diplodocine taxa have ratios between 1.7 and 2. Generally, the ratio increases in more posterior elements, therefore specimens with only anterior mid-caudal vertebrae preserved (e.g. *Diplodocus longus* YPM 1920, see McIntosh and Carpenter, 1998) most probably would have higher ratios than indicated in the table.

C333: Mid-caudal vertebrae, lateral surface of centra: without longitudinal ridge at midheight (0); longitudinal ridge present, centra hexagonal in anterior/posterior view (1) (Upchurch and Martin, 2002; Fig. 116).

Comments. This ridge is not the same as the ventrolateral ridge described above, which is located below midheight.

C334: Mid-caudal centra, articular surface shape: cylindrical (0); quadrangular (1); trapezoidal (2); with flat ventral margin but rounded lateral edges (3) (Wilson, 2002; Gallina and Apesteguía, 2005; modified after Carballido et al., 2012b; Fig. 117).

Comments. The character was modified in order to be able to code for the various intermediate states between cylindrical, quadrangular, and triangular as described by earlier workers.

C335: Mid-caudal centra ventral surface in lateral view: gently curved (0); greater portion straight, with expansions on both ends to form the chevron facets restricted to about last fourth of centrum length (1) (New; Fig. 116).

Comments. This description applies especially for anterior mid-caudal elements, more posterior vertebrae of derived specimens tend to develop a more gentle curvature. This can create problems in taxa preserving only posterior mid-caudal vertebrae, as e.g. *Tornieria* specimen k, which is herein scored as plesiomorphic for this character. Caudal vertebrae from trench dd, however, indicate that *Tornieria* actually might show the derived state, but these have not been found in articulation, and because anatomical overlap with the referred specimens included herein is

PeerJ Reviewing Manuscript

minimal, their attribution to the species should be regarded as doubtful.

C336: Mid-caudal posterior articular surface: concave (0); flat (1); convex (2) (New; Tab. S38).

C337: Mid-caudal neural arches: over the midpoint of the centrum with approximately subequal amounts of the centrum exposed at either end (0); on the anterior half of the centrum (1) (Huene, 1929; Salgado et al., 1997; Fig. 116).

Comments. For this character, the distance between pre- and postzygapophyses and their location above the vertebral centrum is regarded as reference. The pedicels can still be dislocated anteriorly in plesiomorphic taxa. It is generally used as titanosauriform synapomorphy (Salgado et al., 1997; Wilson, 2002), but convergently present in some *Diplodocus* specimens (e.g. AMNH 223, or USNM 10865).

C338: Mid-caudal prezygapophyses: free (0); posteriorly interconnected by a transverse ridge, creating a triangular fossa together with the spinoprezygapophyseal laminae (1) (New; Fig. 118).

Comments. This transverse lamina marks the caudal vertebrae of *Diplodocus longus* YPM 1920, and might prove a valid autapomorphy for the species in future.

C339: Mid-caudal prezygapophyses position: terminate at or behind anterior edge of centrum (0); project considerably beyond anterior edge of centrum (1) (New).

Comments. Only taxa where the prezygapophyses clearly overhang the centrum (i.e. recognizable without any need of measuring) are scored as derived.

C340: Mid-caudal neural spines, orientation: directed posteriorly (0); vertical (1) (McIntosh, 1990a; Salgado et al., 1997; modified after Carballido et al., 2012b; Fig. 116).

C341: Mid-caudal neural arch, anterior extreme of spine summit: smooth (0); developing a short anterior or anterodorsal projection, such that anterior edge of spine becomes slightly concave (1) (New; Fig. 119).

Comments. Such a spur might also be interpreted as pathologic or ontogenetic. However, its presence in the juvenile to subadult *Apatosaurus* (= *Camarasaurus*) *grandis* YPM 1901 suggests that ontogeny can probably be excluded as a cause. More studies are needed in order to confirm or refuse pathological reasons, in the meanwhile the character is kept in the analysis.

C342: Mid- and posterior caudal vertebral centra, articular surfaces: subequal in width and height or higher than wide (0); considerably wider than high (1) (Salgado et al., 1997; modified; Tab. S40).

Comments. A ratio of 1.2 or greater is regarded as considerably wider than high.

C343: Mid- and posterior caudal neural spines: spine summit overhangs postzygapophyses considerably posteriorly (0); posterior end of spine summit more or less straight above

PeerJ Reviewing Manuscript

postzygapophyses (1) (New; Fig. 116).

C344: Mid- and posterior caudal spines: elongate and strongly caudally directed, extending over more than 50% of length of succeeding vertebral centrum (0); short, not extending far beyond caudal articular facet of centrum (1) (Remes et al., 2009; polarity reversed; Fig. 119).

C345: Posterior caudal prezygapophyses position: terminate at or behind anterior edge of centrum (0); project beyond anterior edge of centrum (1) (New).

C346: Distal-most caudal centra, articular face shape: platycoelous (0); biconvex (1) (Wilson et al., 1999; Tab. S38).

Comments. Taxa without distal caudal vertebrae are scored as unknown.

C347: Distal-most caudal centra, length-to-height ratio: < 4.0 (0); 4.0-6.5 (1); > 6.5 (2) (Upchurch, 1998), modified after (Wilson et al., 1999; Tab. S40).

C348: Distal-most caudal centra, number: ten or fewer (0); more than 30 (1) (Wilson, 2002; modified).

Comments. The character was modified such that it was not restricted to distal-most 'biconvex' caudal centra as in Wilson (2002).

C349: Caudal ribs, last occurs on: Cd 12 or more anteriorly (0); Cd 13 (1); Cd 14 (2); Cd 15-17 (3); Cd 18 or more posteriorly (4) (Holland, 1915a; Gilmore, 1936; Upchurch et al., 2004b; modified; Tab. S38).

Comments. Upchurch et al. (2004b), who were the first to include this positional character into a phylogenetic analysis, only distinguished between two states: Cd 14 and/or Cd 12. However, enlarging the taxon list, a higher variety becomes evident (Tab. S38). The state description was thus adapted accordingly. The character is left unordered as no obvious step-like evolution is recognizable.

C350: Anterior, 'fan'-shaped caudal ribs, foramen: present (0); absent (1) (Gilmore, 1936; Upchurch et al., 2004b; polarity reversed; Fig. 112).

Comments. Polarity was reversed herein given the different taxon sampling compared to Upchurch et al. (2004b).

Chevrons

C351: Chevrons, 'crus' bridging haemal canal: absent in some (0); present in all (1) (Yu, 1993; modified after Mannion et al., 2012).

Comments. Additive binary coding is preferred here in order to be able to code incomplete tails (following Mannion et al., 2012).

C352: Chevrons, 'crus' bridging haemal canal: present in some (0); absent in all (1) (Yu, 1993;

PeerJ Reviewing Manuscript

modified after Mannion et al., 2012; Fig. 120).

Comments. See character 351.

C353: Chevrons with anterior and posterior projections: present (0); absent (1) (McIntosh, 1989; Russell and Zheng, 1993; modified; Fig. 121).

Comments. This character describes the often called 'forked chevrons' that inspired Marsh (1878) to name the specimen YPM 1920 *Diplodocus* (= double beam).

C354: Anterior chevrons, longitudinal median ridge on anterior surface: absent (0); present (1) (New; Fig. 120).

Comments. The ridge extends proximodistally.

C355: Anterior chevrons, posterior edge of distal blade in lateral view: continuous (0); posteriorly expanded in a step-like fashion (1) (New; Fig. 120).

C356: Anterior mid-chevrons, lateral surface: smooth (0); marked by a horizontal ridge right below articulation surfaces (1) (New; Fig. 121).

Comments. The ridge can be quite broad, but it is always rugose. Anterior mid-chevrons are meant to be the first elements with anterior projections on the distal blade.

C357: Middle chevrons, distinct fossae on medial surfaces of proximal branches: absent (0); present (1) (New; Fig. 121).

C358: Forked chevrons, anteroposterior length: short, about 50% of relative vertebral centrum length (0); elongate, approaching corresponding vertebral centrum length (1) (McIntosh, 1995).

Comments. The increased relative length of the chevron compared to its corresponding caudal vertebra was proposed as useful character to distinguish *Diplodocus* from *Apatosaurus* by McIntosh (1995), and is herein used for the first time in a phylogenetic analysis.

Pectoral girdle

C359: Scapular length/minimum blade breadth: > 5.5 (0); 5.5 or less (1) (Carballido et al., 2012b; polarity reversed; Tab. S41).

Comments. Measurements are taken from figures in lateral view, ignoring the proximodistal curve of the scapula. Greatest length follows the long axis of the scapula, such that orientation within the articulated skeleton is not taken into account, as this is still debated (see Schwarz et al., 2007a; Remes, 2008; Hohn, 2011). Minimum blade breadth is measured perpendicular to the long axis.

C360: Scapular acromion length/scapular length: > 0.54 (0); 0.46-0.54 (1); < 0.46 (2) (Gallina and Apesteguía, 2005; modified; Tab. S41).

Comments. Measurements were taken from figures in lateral view. Acromion length is measured

PeerJ Reviewing Manuscript

perpendicular to scapular length, between horizontal lines extending through the ventral- and dorsal-most points of the acromion, with the distal blade oriented horizontally. The character is treated as ordered.

C361: Scapula, orientation of scapular, angle with coracoid articulation: > 80° (0); 80° or less (1) (Wilson, 2002; modified; Tab. S41).

Comments. The angle is measured from figures or photos in lateral view.

C362: Scapula, angle between acromial ridge and distal blade: < 70° (0); 70°-81° (1); > 81° (2) (Riggs, 1903; Carpenter and McIntosh, 1994; Upchurch et al., 2004b; modified; Tab. S41).

Comments. The angle to be measured lies between the dorsal half of the acromial ridge, and the long axis of the scapular blade. An additional state was added to the original version (Upchurch et al., 2004b), in order to be able to score specimens with intermediate ratios. The character is left unordered as no obvious evolutionary trend is observable.

C363: Scapular acromion process, dorsal part of posterior margin: convex or straight (0); U-shaped concavity (1) (Wilson, 2002; modified by Whitlock, 2011a; Fig. 122).

C364: Scapular, acromion process position: lies near the glenoid level (0); lies nearly at midpoint of scapular body (1) (Carballido et al., 2012b; Fig. 122).

Comments. The position of the acromion process relative to the glenoid has to be checked with the long axis of the distal blade oriented horizontally.

C365: Scapula, area posterior to acromial ridge and distal blade: is excavated (0); is flat or slightly convex (1) (Upchurch et al., 2004b; Fig. 123).

Comments. This character describes the area posterior to the acromial ridge, and dorsal to the distal blade, where the two meet.

C366: Scapular glenoid, orientation: relatively flat or laterally facing (0); strongly beveled medially (1) (Wilson and Sereno, 1998).

Comments. The medially beveled glenoid surface was proposed as autapomorphy for *Apatosaurus* (Wilson, 2002), but Upchurch et al. (2004b) showed that the orientation was actually variable within *Apatosaurus* specimens, which is confirmed herein.

C367: Scapular blade, acromial edge: straight (0); rounded expansion at distal end (1); racquet-shaped (2) (Wilson, 2002; wording modified; Fig. 122).

C368: Scapular blade, ventral edge in lateral view: is straight (0); curves ventrally towards its distal end (1) (Upchurch et al., 2004b; wording modified; Fig. 122).

Comments. Whereas the original character (Upchurch et al., 2004b) described the entire blade, the derived ventral curving is here restricted to the ventral edge of the blade.

PeerJ Reviewing Manuscript

C369: Scapula: without semi-ovate, flat muscle scar just distal to glenoid on scapular shaft (0); scar present (1) (Whitlock, 2011a; Fig. 123).

Comments. The scar described herein lies on the lateral side of the blade.

C370: Scapular blade, subtriangular projection on anterior portion of ventral edge: absent (0); present (1) (Gallina and Apesteguía, 2005; Fig. 122).

Comments. In *Diplodocus* sp. AMNH 223, there are two eminences close to each other (ET, pers. obs., 2011).

C371: Scapular blade, expansion of distal end: wide (at least 2 times narrowest width of shaft in lateral view) (0); narrow (< 2 times narrowest width of shaft) (1) (Yu, 1993; modified; Tab. S41).

Comments. Measurements are taken perpendicular to the long axis of the blade.

C372: Coracoid, anteroventral margin shape: rounded (0); rectangular (1) (Bakker, 1998; Wilson, 2002; Fig. 124).

C373: Coracoid, infraglenoid groove: reduced to absent (0); present and distinct (1) (Carballido et al., 2012b; modified; Fig. 124).

C374: Sternal plates, shape: subcircular or oval (0); subtriangular with widened posterior border (1); elliptical to crescentic, with concave lateral margin (2) (Calvo and Salgado, 1995; modified; Fig. 125).

Comments. The subtriangular shape was added to the original version of Calvo and Salgado (1995) in order to better describe the difference between typical basal neosauropod or macronarian, and diplodocid shape. The character is treated as unordered, because none of the states can convincingly be interpreted as intermediate.

C375: Sternal plate, ridge on the ventral surface: absent (0); broad and shallow, or elongate and prominent (1) (Upchurch et al., 2004a; wording modified; Fig. 125).

C376: Sternal plate, anterior end: expanded dorsoventrally (0); flat, not expanded (1) (Tschopp and Mateus, 2012; modified; Fig. 125).

C377: Sternal plate, posterior border: convex (0); straight (1) (González Riga, 2002; modified; Fig. 125).

Comments. The true shape of the posterior border can sometimes be obscured due to the presence of fused sternal ribs (Tschopp and Mateus, 2012).

Forelimb

C378: Forelimb: hindlimb length ratio: 0.76 or greater (0); less than 0.76 (1) (Upchurch, 1995, 1998; modified; Tab. S42).

Comments. Forelimb length is the sum of the lengths of the humerus, radius, and metacarpal III,

PeerJ Reviewing Manuscript

hindlimb length the sum of the lengths of femur, tibia, and metatarsal III.

C379: Humerus-to-femur ratio: < 0.7 (0); 0.7-0.76 (1); 0.77-0.89 (2); = or > 0.90 (3) (McIntosh, 1990a; modified; Tab. S43).

Comments. State boundaries are chosen such that the generally accepted genera *Apatosaurus* and *Diplodocus* can be distinguished from *Tornieria* and *Barosaurus*. The character is treated as ordered.

C380: Humerus, RI (sensu Wilson and Upchurch, 2003): gracile (less than 0.27) (0); medium (0.28-0.32) (1); robust (more than 0.33) (2) (Carballido et al., 2012b; Tab. S44).

Comments. The humerus RI was defined as the mean between proximal, distal, and midshaft transverse widths, divided by humerus length (Wilson and Upchurch, 2003). Scores for taxa where no measurements were available were taken from Carballido et al. (2012b). The character is herein treated as ordered.

C381: Humerus, shaft twist: minor to absent (0); high, distal articular surface twisted by at least 30° compared to proximal articular surface (1) (Gilmore, 1932; Tab. S44).

Comments. This angle is difficult to measure due to lacking references. It was proposed as distinguishing feature of *Diplodocus* (Gilmore, 1932) and is here included into a phylogenetic analysis for the first time.

C382: Humerus, midshaft cross-section, shape: circular, transverse diameter: anteroposterior diameter ratio is 1.5 or lower (usually close to 1.3) (0); elliptical, transverse diameter: anteroposterior diameter ratio is greater than 1.5 (usually close to 1.8) (1) (Wilson, 2002; modified by Mannion et al., 2012; Tab. S44).

C383: Humerus, pronounced proximolateral corner: absent (0); present (1) (Upchurch, 1998; Fig. 126).

Comments. A pronounced proximolateral corner forms a weak hump in anterior or posterior view.

C384: Humerus, proximal expansion: more or less symmetrical (0); asymmetrical, proximomedial corner much more pronounced than proximolateral one (1) (Wilhite, 2005; Fig. 126).

Comments. The differing expansions were found to be taxonomically significant (Wilhite, 2005), but have not been previously included in any phylogenetic analysis. This character forms an additive binary character together with character 385.

C385: Humerus, proximal end expanded laterally in anterior/proximal view: expanded, lateral margin concave in anterior/posterior view (0); not expanded (1) (Curry Rogers, 2005; polarity

PeerJ Reviewing Manuscript

reversed; Fig. 126).

Comments. Polarity was reversed compared to the original description (Curry Rogers, 2005), due to the differing taxon sampling.

C386: Humerus, shallow, but distinct rugose tubercle at the center of the concave proximal portion of the anterior surface: absent (0); present (1) (New; Fig. 126).

C387: Ulna to humerus length: < 0.65 (0); 0.66-0.76 (1); > 0.76 (2) (Janensch, 1929b; Tab. S45).

Comments. The states were defined in order to include the majority of diplodocids in the same state. The character is treated as ordered.

C388: Ulna, proximal condylar processes: subequal in length (0); anterior arm longer (1) (Wilson, 2002; Tab. S46).

Comments. The state boundary is here set at 1.1, as this follows best higher-level taxonomy.

C389: Ulna, proximal articular surface, angle between anterior and lateral branch: 90° (0); acute (1) (New; Tab. S46).

Comments. Taxa with angles greater than 83° were scored as plesiomorphic.

C390: Ulna, distal transverse expansion: slight, < 1.3 times minimum shaft width (min sw) (0); wide, 1.3 times min sw or greater (1) (New; Tab. S46).

Comments. Some width measurements published do not state explicitly if they are taken transversely or anteroposteriorly, they just report maximum distal width. Anteroposterior width is often much greater than transverse width in distal surfaces of the sauropod ulnae. This leads to exaggerated ratios, if erroneously included here. Also, especially disarticulated ulnae, where both proximal processes are equally long, are difficult to orient properly. Nonetheless, the differences in these ratios still appear significant.

C391: Radius, maximum diameter of the proximal end divided by greatest length: < 0.3 (0); 0.3 or greater (1) (McIntosh, 1990a; modified by Mannion et al., 2013; Tab. S47).

Comments. Maximum diameter can be width or depth.

C392: Radius, distal articular surface for ulna: reduced and relatively smooth (0); well developed with one or two distinct longitudinal ridges (1) (New; Fig. 127).

C393: Radius, distal condyle orientation in anterior view: perpendicular or beveled less than 15° to long axis of shaft (0); beveled at least 15° to long axis of shaft (1) (Curry Rogers and Forster, 2001; Wilson, 2002; modified; Tab. S47).

Comments. As stated by Mannion et al. (2013), the beveling of the distal surface often only affects the lateral half of the distal end. Given the different scope of the phylogenetic analysis, character state boundaries are different herein compared to Mannion et al. (2013).

PeerJ Reviewing Manuscript

C394: Radius, distal breadth: <1.8 times larger than midshaft breadth (0); at least 1.8 times midshaft breadth (1) (Wilson, 2002; modified).

Comments. Breadth is measured mediolaterally.

C395: Carpus, number of carpal bones: 3 or more (0); 2 (1); 1 or less (2) (McIntosh, 1990b; Upchurch, 1998; modified).

Comments. The character was initially proposed with only two character states (three or more, two or less; Upchurch, 1998). A third state was added here in order to distinguish *Apatosaurus* from the remaining taxa (Bonnan, 2003). Even though SMA 0011 was found with only one carpal preserved, its articulated position directly below the radius, and articulating with the first two to three metacarpals suggest that a second element was present. Such a presence is also indicated by the proximodistal width of the preserved element, which in articulation would create a large gap between the ulna and the lateral metacarpals. A similar case can be seen in the putative *Diplodocus* manus described by Bedell and Trexler (2005). The opposite can be seen in apatosaurs, where the only carpal lies above mc II to IV, is proximodistally flattened, and metacarpals I and V are proximally dislocated in respect to the inner elements (CM 3018, UW 15556; Hatcher, 1902; Gilmore, 1936; Bonnan, 2003). Due to the probable gradual decrease in the number of carpal bones the character is treated as ordered.

C396: Carpals: block-like (0); proximodistally compressed discs (1) (New; Fig. 128).

C397: Metacarpus, shape: spreading (0); bound, with subparallel shafts and articular surfaces that extend half their length (1) (Wilson, 2002).

C398: Metacarpals, shape of proximal surface in articulation: gently curving, forming a 90° arc (0); U-shaped, subtending a 270° arc (1) (Wilson, 2002).

C399: Metacarpus, ratio of longest metacarpal to radius: < 0.40 (0); 0.40 or greater (1) (Calvo and Salgado, 1995; modified by Mannion et al., 2013; Tab. S48).

Comments. The longest metacarpal is usually mc II or mc III.

C400: Metacarpal I, length: shorter than IV (0); longer than IV (1) (Wilson and Sereno, 1998; Tab. S48).

Comments. The state boundary applied herein lies at 1.0.

C401: Metacarpal I, proximal end dorsoventral height to mediolateral width ratio: < 1.8 (0); 1.8 or greater (1) (Apesteguía, 2005; Mannion and Calvo, 2011; Mannion et al., 2013; Tab. S48).

Comments. Mannion et al. (2013) were the first to include this ratio in a phylogenetic analysis.

C402: Metacarpal III, robustness (length/distal transverse width): robust, <2.9 (0); intermediate, 2.9-3.5 (1); slender, > 3.5 (2) (Bedell and Trexler, 2005; Tab. S48).

PeerJ Reviewing Manuscript

Comments. Suggested as distinguishing character between *Diplodocus* and *Apatosaurus*, and especially between WDC-FS001A and *Galeamopus hayi* HMNS 175 (Bedell and Trexler, 2005), which are both probably not *Diplodocus* (see below), metacarpal robustness is herein used for the first time as a character in a phylogenetic analysis. The character is treated as ordered.

C403: Metacarpal V, proximal articular surface: subequal to smaller than (0); or significantly larger than proximal articular surface of mc III and IV (1) (Janensch, 1929b; Fig. 129).

Comments. An enlarged proximal articular surface of mc V can be seen in *Apatosaurus louisae* CM 3018 (Gilmore, 1936). However, this does not seem to be the case in another apatosaur specimen (NSMT-PV 20375; Upchurch et al., 2004b), such that the derived state might prove an autapomorphy of the species *A. louisae*. A similar development can be seen in the manus of *Janenschia robusta* (Janensch, 1922).

C404: Manual phalanx I-1, flange-like sheet of bone projecting from the proximoventral margin: absent (0); present (1) (Hatcher, 1902; Gilmore, 1936; Upchurch et al., 2004b; Fig. 130).

Pelvic girdle

C405: Ilium, ratio of blade height above pubic peduncle to anteroposterior length: <0.40 (0); 0.40 or more (1) (New; Tab. S49).

Comments. Blade height is measured vertically above the base of the pubic pedicel, with the ischiadic tubercle and the anteroventral-most point of the preacetabular process oriented on a horizontal line.

C406: Iliac preacetabular process, shape: sharply pointed (0); blunt to semicircular anterior margin (1) (Salgado et al., 1997; Fig. 131).

Comments. A strict lateral view of the ilium is often misleading, given the anterolateral to lateral orientation of the preacetabular lobe.

C407: Ilium, preacetabular process orientation: anterolateral to body axis (0); perpendicular to body axis (1) (Salgado et al., 1997).

Comments. The perpendicular orientation of the preacetabular process is generally considered synapomorphic for derived titanosauriforms (Salgado et al., 1997; Wilson, 2002), but they also occur in the holotype of '*Apatosaurus*' *minimus* AMNH 675 (Mook, 1917).

C408: Ilium, angle between the ventral edge of anterior iliac lobe and the anterior surface of the pubis process: is ~90° (0); is acute (1) (Gilmore, 1936; Upchurch et al., 2004b).

C409: Ilium, dorsal margin shape: flat to slightly convex (0); semicircular (1) (Wilson, 2002; modified; Fig. 131).

Comments. Derived taxa have uniformly convex dorsal margins, apomorphic ones generally

PeerJ Reviewing Manuscript

have a large straight portion.

C410: Ilium, highest point on dorsal margin: lies posterior to base of pubic process (0); lies anterior to base of pubic process (1) (Upchurch et al., 2004a; Fig. 131).

Comments. The position of the highest point in respect to the pubic peduncle is assessed with the ischiadic tubercle and the anteroventral-most point of the preacetabular process lying on a horizontal line.

C411: Ilium, pubic peduncle (measured at the articular surface), anteroposterior to mediolateral width ratio: > 0.80 (0); 0.80 or less (1) (Taylor, 2009; Mannion et al., 2013; modified; Tab. S49).

Comments. Mannion et al. (2013) was the first to include this character in a phylogenetic analysis, based on observations made by Taylor (2009). State boundaries are adapted herein from 0.5 to 0.8, given the different scope and thus taxon sampling of the present analysis.

C412: Ilium, triangular fossa laterally at base of pubic peduncle: absent (0); present (1) (New; Fig. 131).

Comments. The apex of this fossa is pointing ventrally.

C413: Ilium, distinct tubercle in the postacetabular region: absent (0); present (1) (Carballido et al., 2012a; Fig. 131).

Comments. The herein described tubercle is not the transverse widening of the dorsal edge towards its posterior end, but a second rugose area laterally on the blade (see Schwarz et al., 2007c; Carballido et al., 2012a).

C414: Pubis, ambiens process development: small, confluent, not differentiated from anterior border of the pubis (0); evident, but not especially developed (1); prominent, hook-like (2) (McIntosh, 1990b; Yu, 1993; wording modified; Fig. 132).

Comments. The hook-like ambiens process is interpreted to represent an increased development of the incipient shape. The character is thus treated as ordered.

C415: Pubis, length of puboischial contact: less than 0.41 total length of pubis (0); 0.41 or more of total length of pubis (1) (Salgado et al., 1997; modified; Tab. S50).

Comments. Mannion et al. (2012) used a ratio of 0.45 as state boundary, but as shown in table S50, for the present set of taxa, 0.41 appears more appropriate.

C416: Pubis, participation in acetabulum: subequal to larger, compared to ischium (0); significantly smaller (1) (Janensch, 1961; Tab. S51).

Comments. A state boundary of 0.8 was used herein as the used OTU show a large step from ratios below 0.75 to ratios greater than 0.83. The character was proposed as potentially useful to distinguish taxa by Janensch (1961). It is included in a phylogenetic analysis for the first time.

PeerJ Reviewing Manuscript

C417: Ischium, acetabular articular surface: maintains approximately the same transverse width throughout its length (0); is transversely narrower in its central portion and strongly expanded as it approaches the iliac and pubic articulations (1) (Mannion et al., 2012).

Comments. The narrow acetabular surface is only present in some rebbachisaurids (Mannion et al., 2012).

C418: Ischium, acetabular margin, in lateral view: flat or mildly concave (0); strongly concave, pubic articular surface forms an anterodorsal projection (1) (D'Emic, 2012; modified by Mannion et al., 2013; Fig. 133).

Comments. In some diplodocids (e.g. *Apatosaurus excelsus* YPM 1980, see Fig. 133), the lateroventral edge of the acetabular surface is strongly concave, whereas the mediodorsal margin forms a bony sheet extending straight from the iliac to the pubic articular surfaces. In lateral view, this configuration appears straight and was thus scored as plesiomorphic herein.

C419: Ischium, iliac peduncle: iliac peduncle straight or widening in smooth curve distally (0); narrow, with distinct 'neck' (1) (Sereno et al., 2007; Fig. 133).

C420: Ischia pubic articulation/anteroposterior length of pubic pedicel: < 1.5 (0); 1.5 or greater (1) (Salgado et al., 1997; modified; Tab. S52).

Comments. Anteroposterior length of the pubic pedicel is measured perpendicular to the articular surface, from its ventral-most point, to the point where it intersects with a line following the ventral edge of the distal shaft. A numerical state boundary was added to the original version of Salgado et al. (1997), which separates Macronaria from basal Eusauropoda, and most diplodocines from most apatosaurs (Tab. S52).

C421: Ischium, elongate muscle scar on proximal end: absent (0); present (1) (Sereno et al., 2007; Fig. 133).

Comments. We follow Mannion et al. (2012), in that the presence of a distinct ridge on the dorsolateral edge qualifies for the apomorphic state.

C422: Ischium, lateral fossa at base of shaft: absent (0); present (1) (Wilson, 2002; Fig. 133).

Comments. The fossa is longitudinally oriented, and marks the dorsolateral edge.

C423: Ischial distal shaft, shape: blade-like, medial and lateral depths subequal (0); triangular, depth of ischial shaft increases medially (1) (Wilson, 2002; Fig. 133).

C424: Ischial distal shafts, cross-sectional shape: V-shaped, forming an angle of nearly 50° with each other (0); flat, nearly coplanar (1) (Upchurch, 1998; Wilson and Sereno, 1998; Fig. 133).

C425: Ischial shaft, transverse distal expansion: absent (0); present (1) (Whitlock, 2011a; Fig. 133).

PeerJ Reviewing Manuscript

Comments. Due to the V-shaped distal end of the ischia, 'transverse' and 'posterodorsal' do not apply very well to the ingroup specimens. However, given the twist of the ischial shaft in the taxa with coplanar distal shafts, which results in almost horizontally oriented distal ends, the main expansion of diplodocid ischia should be regarded as transverse, even though in lateral view it would appear rather dorsoventral.

C426: Ischium, posterodorsal expansion of distal end: absent (0); present (1) (Lovelace et al., 2007; Fig. 133).

Comments. See comment on transverse expansion in character 425.

Hindlimb

C427: Femur, robustness index (sensu Wilson and Upchurch, 2003): gracile, <0.22 (0); intermediate, 0.22-0.25 (1); robust, > 0.25 (2) (Janensch, 1961; Tab. S53).

Comments. Due to the gradual increase, this character is treated as ordered.

C428: Femur, lateral bulge (marked by the lateral expansion and a dorsomedial orientation of the laterodorsal margin of the femur, which starts below the femur head ventral margin): absent (0); present (1) (Salgado et al., 1997; modified; Fig. 134).

Comments. The definition of this character changed in different phylogenetic analyses (e.g. Salgado et al., 1997; Mannion et al., 2012). Here, we follow Mannion et al. (2012) in that we also score incipient lateral bulges as apomorphic.

C429: Femoral shaft, lateral margin shape: straight (0); proximal one-third deflected medially (1) (Wilson, 2002; Fig. 134).

Comments. The fact that the probable brachiosaurid juvenile SMA 0009 (in contrast to other brachisaurids) does not show any medial deflection might indicate that this character changes during ontogeny. This might be correlated with the weak development of the articular surface in juvenile specimens (Ikejiri et al., 2005; Schwarz et al., 2007c).

C430: Femur, cross-sectional shape: subequal to anteroposterior diameter (0); 125-150% anteroposterior diameter (1); at least 185% anteroposterior diameter (2) (Wilson and Smith, 1996; Tab. S53).

Comments. The character was added in order to distinguish between titanosauriforms, but it is also useful for the distinction of *Amphicoelias altus* AMNH 5764. Taxa scored but without entries in table S53 are taken from Carballido et al. (2012b). The character is treated as ordered.

C431: Femoral head, position of highest point in anterior view: above point of maximum curvature of ventral edge of femoral head (0); laterally shifted, above main portion of shaft (1) (New; Fig. 134).

PeerJ Reviewing Manuscript

C432: Femur, ventral surface of head: confluent with shaft (0); stepped (1) (New; Fig. 134).

C433: Femur, greatest anteroposterior thickness of shaft: less than or approximately equal to half anteroposterior depth of distal articular condyles (0); much greater than half anteroposterior depth of distal articular condyles (1) (Whitlock, 2011a; Tab. S53).

Comments. The state boundary used herein is 0.6. Taxa scored for this character, but not having any values in table S53 are taken from Whitlock (2011a).

C434: Femur, large nutrient foramen opening midshaft anteriorly on femur: absent (0); present (1) (Wilson, 2002; Fig. 134).

C435: Femur, pronounced ridge on posterior surface between greater trochanter and head: absent (0); present (1) (Sereno et al., 2007).

Comments. The derived state is a synapomorphy for Nigersaurinae, convergently present in *Rapetosaurus* (Sereno et al., 2007; Curry Rogers, 2009).

C436: Femur, fourth trochanter: not visible in anterior view (0); prominent, visible in anterior view (1) (Gallina and Apesteguía, 2005; modified by Whitlock, 2011a; Fig. 134).

Comments. In certain taxa, a small bulge is visible on the medial edge in anterior view, which represents the medially positioned, and prominent fourth trochanter.

C437: Femoral fourth trochanter, present as low rounded ridge (0); greatly reduced so that it is virtually absent (1) (Mannion et al., 2012).

Comments. A reduced fourth trochanter is synapomorphic for rebbachisaurs and some titanosauriforms (Torcida Fernández-Baldor et al., 2011; Mannion et al., 2012). The reduced fourth trochanter of the juvenile *Elosaurus parvus* CM 566 implies that the development of this structure happens during ontogeny.

C438: Femur, fourth trochanter, position: distally displaced (0); on proximal half of shaft (1) (Schwarz-Wings and Böhm, 2012; Tab. S53).

Comments. Distance between femoral head and fourth trochanter is measured to the distal end of the trochanter. Taxa with ratios of 0.4 are scored as apomorphic.

C439: Femur, shape of distal condyles: articular surface restricted to distal portion of femur (0); expanded onto anterior portion of femoral shaft (1) (Wilson and Carrano, 1999; Wilson, 2002; Fig. 134).

C440: Tibia to femur length: < 0.68 (0); 0.68 or greater (1) (New; Tab. S54).

C441: Tibia, proximal articulation surface, shape: subcircular to transversely compressed (0); anteroposteriorly compressed (1) (Wilson, 2002; modified; Fig. 135).

Comments. Character descriptions was slightly changed such that the subcircular surfaces are

PeerJ Reviewing Manuscript

now scored together with the transversely compressed, instead of the anteroposteriorly compressed as in (Wilson, 2002).

C442: Tibia, proximal articular surface, shape: subrectangular (0); subtriangular (1) (Harris and Dodson, 2004; Fig. 135).

Comments. Rhomboid or suboval outlines are scored as plesiomorphic.

C443: Tibia, short transverse ridge on anteromedial surface of distal end: absent (0); present (1) (New; Fig. 136).

C444: Tibia, cnemial crest in anterior view: widely rounded (0); subtriangular (1) (New; Fig. 137).

C445: Tibia, posterior surface of cnemial crest: smooth (0); bears a distinct fibular trochanter (1) (Harris, 2007; Fig. 138).

Comments. A distinct fibular trochanter marks the posterior face of the cnemial crest of *Suuwassea* (Harris, 2007). The character is herein included in a phylogenetic analysis for the first time.

C446: Tibia, lateral edge of proximal end forms a pinched out projection, posterior to cnemial crest (the 'second cnemial crest' of Bonaparte et al., 2000): present (0); absent (1) (Mannion et al., 2013; Fig. 135).

C447: Fibula, proximal end with anteromedially directed crest extending into a notch behind the cnemial crest of the tibia: absent (0); present (1) (Wilson and Upchurch, 2009; D'Emic, 2012; modified by Mannion et al., 2013).

Comments. Most sauropods have ellipsoid proximal articular surfaces of the fibula. However, some diplodocid specimens (as well as some titanosauriforms; Wilson and Upchurch, 2009; D'Emic, 2012; Mannion et al., 2013) develop a distinct, narrow, anteromedial crest.

C448: Fibula, insertion of the M. iliofibularis: located approximately at mid-shaft (0); proximal, located above midshaft (1) (Whitlock, 2011a; Tab. S55).

Comments. Distance from the proximal articular surface to the center of the tubercle was measured and compared to greatest length. Values of 0.4 or lower were scored as derived.

C449: Astragalus, morphology in anterior view: rectangular (0); wedge-shaped, narrowing medially (1) (Upchurch, 1995, 1998; modified by Nair and Salisbury, 2012; Fig. 139).

C450: Astragalus, anteroposterior dimension as seen in dorsal view: widens medially or does not change in width (0); narrows medially (1) (Cooper, 1984; Upchurch, 1998; Fig. 139).

Comments. The taxonomic significance of this character was recognized by Cooper (1984), but included into a phylogenetic analysis for the first time by Upchurch (1998).

PeerJ Reviewing Manuscript

C451: Astragalus, proximodistal length/transverse breadth: < 0.55 (0); 0.55 or greater (1) (McIntosh et al., 1992; Tab. S56).

Comments. This ratio was used by McIntosh et al. (1992) to distinguish *Dyslocosaurus* from *Diplodocus*, but is here included in a phylogenetic analysis for the first time.

C452: Astragalus, mediolateral width to maximum anteroposterior length ratio: 1.6 or greater (0); < 1.6 (1) (Sander et al., 2006; modified; Tab. S56).

C453: Astragalus, ascending process length: limited to anterior two-thirds of astragalus anteroposterior width (0); extends beyond two-thirds of astragalus anteroposterior width (normally to posterior margin of astragalus) (1) (Wilson and Sereno, 1998; Wilson, 2002; modified by Mannion et al., 2012; Fig. 139).

C454: Astragalus, fibular facet: faces laterally (0); faces posterolaterally, anterior margin visible in posterior view (1) (Whitlock, 2011a; Fig. 139).

C455: Astragalus, laterally directed ventral shelf underlies distal end of fibula: present (0); absent (1) (Mannion et al., 2013; based on Wilson and Upchurch, 2009; Fig. 139).

Comments. The ventral shelf only underlies a part of the fibula.

C456: Astragalus, anteromedial corner in posterior view: short and blunt (0); elongate and narrow (1) (New; Fig. 139).

Comments. The short and blunt shape is a somewhat intermediate state between triangular and rectangular outlines, as described in character 449.

C457: Calcaneum: proximodistally compressed (0); globular (1) (Harris and Dodson, 2004).

Comments. *Suuwassea* has a globular calcaneum, whereas most other sauropods that preserve calcanea have dorsoventrally compressed elements. These bones are very rarely preserved, and were even proposed to be absent in diplodocids (McIntosh, 1990b; Upchurch, 1998). However, Bonnan (2000) reported a probable calcaneum from *Diplodocus*, and also an apatosaur specimen from Como Bluff, Wyoming (NHMUK R.3215) appears to show such an element (ET, pers. obs., 2011).

C458: Metatarsals, metatarsal I to metatarsal V proximodistal length ratio: 1.0 or greater (0); < 1.0 (1) (Mannion et al., 2013; polarity reversed; Tab. S57).

Comments. Length is measured between parallel lines through the proximal- and distal-most points of the metatarsals.

C459: Metatarsal I, dorsal/anterior surface: without foramina (0); several foramina present (1) (New; Fig. 140).

C460: Metatarsal I proximal articular surface, transverse axis orientation: angled ventromedially

PeerJ Reviewing Manuscript

approximately 15º to (0); perpendicular to axis of shaft (1) (Wilson, 2002; modified by Carballido et al., 2012b; polarity reversed; Fig. 140).

Comments. The original character (Wilson, 2002) was split into two by Carballido et al. (2012b), because some specimens have one of the two articular surfaces in an angle to the long axis of the shaft, and the other one perpendicular. Herein, polarity was reversed due to the different taxon sampling.

C461: Metatarsal I, robustness (proximal transverse width/greatest length): relatively gracile, < 0.8 (0); robust, 0.8 or more (1) (Upchurch et al., 2004a; modified; Tab. S58).

C462: Metatarsal I distal articular surface, transverse axis orientation: angled dorsomedially to (0); perpendicular to axis of shaft (1) (Wilson, 2002; modified by Carballido et al., 2012b; polarity reversed; Fig. 140).

C463: Metatarsal I distal condyle, posterolateral projection: absent (0); present (1) (Berman and McIntosh, 1978; see Fig. 140).

Comments. All taxa where the posterolateral corner of the distal articular surface can be seen in anterior view are scored as apomorphic.

C464: Metatarsal I, distolateral projection, if present: small and blunt, not projecting considerably lateral to dorsal edge of distal articular surface (0); prominent and pointed, reaching significantly more laterally than dorsal edge of distal articular surface (1) (McIntosh, 1990b; Fig. 140).

Comments. Usually, a prominent posterolateral or distolateral projection exceeds the lateral expansion of the proximal articular surface in anterior view.

C465: Metatarsals I-III, rugosities on dorsolateral margins near distal ends: absent (0); present (1) (Upchurch, 1995).

Comments. A second character (C468) accounts for the strength of the rugosity on mt II (see Fig. 141).

C466: Metatarsal II, robustness (mean proximal and distal transverse breadth /maximum length): slender, <0.53 (0); intermediate, 0.53-0.65 (1); robust, >0.65 (2) (McIntosh et al., 1992; Tab. S58).

Comments. The robustness of metatarsal II was used by McIntosh et al. (1992) to distinguish between diplodocids, but has never been included in a phylogenetic analysis. The character is treated as ordered.

C467: Metatarsal II, lateral margin in proximal view: concave (0); straight (1) (Mannion et al., 2013; Fig. 142).

Comments. The medial margin is usually concave. With the lateral margin being concave as

PeerJ Reviewing Manuscript

4357 well, the outline of the proximal articular surface of mt II becomes somewhat hourglass-shaped.
4358 C468: Metatarsal II, rugosity on dorsolateral margin near distal end (if present): shallow (0);
4359 well-developed, extending to center of shaft (1) (New; Fig. 141).
4360 **Comments.** The development of the rugosities in mt I to III differs within the pes (mt II bearing
4361 the most prominent ridge), but more so between taxa. This is exemplified by the well-developed,
4362 rugose ridge of *Dyslocosaurus polyonychius* AC 663, which extends almost to the center of the
4363 shaft. Taxa without any rugosities are scored as unknown.
4364 C469: Metatarsal II distal condyle, posterolateral projection: absent (0); present (1) (New; Fig.
4365 141).
4366 **Comments.** The distribution of the posterolateral projection in mt II was discussed by Nair and
4367 Salisbury (2012).
4368 C470: Metatarsal IV, proximal articular surface, outline: L- to V-shaped, with distinctly concave
4369 posterolateral edge (0); subtriangular (1) (New; Fig. 143).
4370 C471: Metatarsal V, proximal articular surface, shape: triangular (0); rhomboid (1) (New; Fig.
4371 144).
4372 C472: Metatarsal V proximal end to distal end maximum mediolateral width ratio: 1.6 or greater
4373 (0); < 1.6 (Mannion et al., 2013; Tab. S58).
4374 **Comments.** Transverse width was measured between parallel vertical lines through the medial-
4375 and lateral-most points of the articular surfaces.
4376 C473: Pes, phalanx I-1: proximal and ventral surfaces meet at approximately 90° (0);
4377 proximoventral corner drawn out into thin plate underlying metatarsal I (1) (McIntosh et al.,
4378 1992; Fig. 145).
4379 C474: Pes, phalanx I-1, distal articular surface shape: wide, maximum transverse width > 1.1
4380 times anteroposterior height (0); narrow, maximum transverse width 1.1 times anteroposterior
4381 height or less (1) (New; Tab. S59).
4382 C475: Pes, phalanx II-2: well developed and subrectangular in dorsal view (0); reduced, with an
4383 irregular D-shaped outline and proximal and distal articular surfaces that meet virtually along
4384 dorsal and plantar margins (1) (McIntosh et al., 1992).
4385 C476: Pes, phalanges III-1 and IV-1: equal to longer than wide (0); wider than long (1) (McIntosh
4386 et al., 1992; Tab. S59).
4387 **Comments.** The greatly elongate php IV-1 of the early juvenile SMA 0009 indicates that
4388 phalanges grow allometrically during early ontogeny.
4389 C477: Pedal unguals, groove on lateral surface: follows curvature of claw (0); straight

PeerJ Reviewing Manuscript

horizontally (1) (New; Fig. 146).

Results

The first iteration of the analysis yielded 184 most parsimonious trees with a score of 1897 steps. The second iteration using the command bbreak increased this number to 41000 (more was not possible due to computer limitations). Overall CI and RI were calculated in WinClada (version 1.00.08, www.cladistics.com), and are equal to 27, and 58, respectively. The strict consensus tree had twelve nodes, which are exclusively located outside Diplodocidae, meaning that all ingroup specimens formed one big polytomy (Fig. 147). Deleting the six most unstable taxa a posteriori, the higher-level clades within Flagellicaudata can be observed (Dicraeosauridae, Apatosaurinae, and Diplodocinae; Fig. 148). The equally weighted reduced consensus tree includes 51 from the originally 76 taxa. The classical diplodocid genera as used in earlier phylogenetic analyses (Whitlock, 2011a; Mannion et al., 2012; Tschopp and Mateus, 2013b) are all visible (Fig. 149). Diplodocoidea forms the sister-taxon to Titanosauriformes, with *Camarasaurus* and Turiasauria forming a more basal clade. This result contradicts most of the recent analyses on sauropod, and in particular studies on early macronarian phylogenetic relationships (Carballido et al., 2012b; D'Emic, 2012; Mannion et al., 2013), and appears to corroborate preliminary results from Upchurch (2009) and Mateus et al. (2011), which recovered Macronaria as polyphyletic. However, many important taxa and characters usually defining Macronaria are missing in the present tree, due to the focus on Diplodocoidea. Since diplodocoid synapomorphies are often shared with derived titanosauriforms, these characters probably pulled the entire clade into a closer relationship with Diplodocoidea.

Within Diplodocoidea, Rebbachisauridae forms the most basal clade, followed by Dicraeosauridae (including *Suuwassea emilieae*), and the Diplodocidae. Diplodocidae are divided into Apatosaurinae and Diplodocinae. The newly described genera *Kaatedocus* and *Galeamopus* are deeply nested within Diplodocinae. Taxonomically important specimens not represented in the equally weighted reduced consensus tree are YPM 1920 (genoholotype of *Diplodocus*), YPM 1980 (genoholotype of *Brontosaurus*), and CM 566 (genoholotype of *Elosaurus*).

The single most unstable taxon as recovered by the pruned trees approach was *Diplodocus lacustris* YPM 1922. By excluding this taxon from the strict consensus tree, twelve more nodes were resolved (*Australodocus* in a trichotomy with *Brachiosaurus* and *Giraffatitan*, a polytomous Dicraeosauridae including *Dyslocosaurus* and *Suuwassea, Dinheirosaurus* + *Supersaurus*, an apatosaur clade comprising the new sister arrangement *Elosaurus parvus* CM 566 + UW 15556,

PeerJ Reviewing Manuscript

and a diplodocine clade including a branch with CM 3452, *Barosaurus*, and *Kaatedocus*). *Diplodocus lacustris* YPM 1922 was shown to group with a large number of OTUs, mostly within Flagellicaudata, as exemplified by the large polytomy of the reduced consensus tree including the specimen. As YPM 1922 is a teeth-only specimen, the result mentioned above indicates that flagellicaudatan teeth cannot be distinguished at the present state of knowledge. The analysis done under implied weighting yielded 202 most parsimonious trees of a length of 187.97214, but the number was increased by the second iteration of tree branch swapping to 41000, as in the first analysis with equal weighting. However, the strict consensus tree preserved 24 nodes, the double of the first version (Fig. 150). The pruned tree analysis with implied weights confirmed that the *Diplodocus lacustris* holotype specimen (YPM 1922) is the least stable. Deletion of YPM 1922 results in 29 gained nodes, compared to the strict consensus tree. Omission of the least stable quartet (*D. lacustris* YPM 1922, the diplodocine skulls CM 11161 and USNM 2672, and the braincase SMA O25-8) resulted in a pruned consensus tree with 36 nodes more than the complete strict consensus tree, and 17 nodes more than the pruned tree with equal weighting, where six specimens were deleted a posteriori (Fig. 151). The reduced consensus tree with implied weights includes 66 taxa, 15 more than the equally weighted reduced consensus tree (Fig. 152).

Implied weighting leads to an exclusion of *Cetiosauriscus stewarti* and *Barosaurus affinis* from Diplodocoidea, and even Neosauropoda. '*Apatosaurus*' *minimus* is recovered within Somphospondyli. Inside Diplodocinae, *Dinheirosaurus* is separated from *Supersaurus*, which groups with *Australodocus* instead. The clade *Eobrontosaurus* + *Amphicoelias* is split here, with the latter resolved as most basal diplodocid. Finally, an apatosaurine clade including the genoholotypes of *Brontosaurus*, *Dystrophaeus* and *Elosaurus* is found.

Symmetric resampling did not find much support for ingroup clades (Tab. S60), most probably due to the little anatomical overlap. However, it found support for three clades that were not recovered in any of the six main trees: the grouping of the two diplodocine skulls USNM 2672 and CM 11161 (resampling value of 12), a dichotomy of holotype and paratype of *Diplodocus carnegii* (CM 84 and 94, resampling value 8), and a clade including the holotypes of *Apatosaurus louisae* and *A. laticollis*, as well as the specimen CM 3378 (resampling value of 15). The latter two clades are actually found in trees excluding *D. longus* YPM 1920 or *Brontosaurus amplus* YPM 1981, respectively. The grouping of the two skulls CM 11161 and USNM 2672 indicates that they are more similar to each other than to any other diplodocine skull.

Discussion

PeerJ Reviewing Manuscript

The phylogenetic history of Diplodocidae

Earlier phylogenetic studies of sauropods mostly just included the three genera *Apatosaurus*, *Diplodocus*, and *Barosaurus* (e.g. Upchurch, 1998; Wilson, 2002; Upchurch et al., 2004a). More recent analyses with a narrower focus on diplodocoid intrarelationships included more diplodocid species (Upchurch et al., 2004b; Rauhut et al., 2005; Remes, 2006; Lovelace et al., 2007; Sereno et al., 2007; Whitlock, 2011a; Carballido et al., 2012b; Mannion et al., 2012; Tschopp and Mateus, 2013b). However, other than Upchurch et al. (2004b), all of them included the genera *Apatosaurus* and *Diplodocus* as OTU, and no analysis was ever done with all proposed diplodocid species (Fig. 153). Basic relationships between diplodocid taxa generally remained the same among the studies, which is probably a consequence of the fact that most were based on Wilson (2002), with only minor changes (Rauhut et al., 2005; Remes, 2006; Lovelace et al., 2007; Sereno et al., 2007). The greatest changes between these four phylogenetic analyses occur in the position of *Suuwassea*, which is recovered within Apatosaurinae (Lovelace et al., 2007), in a polytomy with *Apatosaurus* and Diplodocinae (Remes, 2006), just outside Apatosaurinae + Diplodocinae (Rauhut et al., 2005), or in a trichotomy with Diplodocidae and Dicraeosauridae (Sereno et al., 2007). Of the remaining diplodocid taxa other than *Apatosaurus*, *Diplodocus*, or *Barosaurus*, only *Tornieria* was included in more than one of these four analyses, and found within Diplodocinae (Rauhut et al., 2005; Remes, 2006).

Given the strong focus on interspecific relationships of *Apatosaurus*, Upchurch et al. (2004b) had a very reduced dataset, with only 16 taxa and 32 characters. The character list was assembled based on earlier descriptions and diagnoses of the different species (mostly Riggs, 1903; Holland, 1915a; Gilmore, 1936), with some original characters added (Upchurch et al., 2004b). Whitlock (2011a), although basing on Wilson (2002), can be considered a new analysis as well, given the large number of modifications and added characters, and the largely increased number of taxa in order to be able to resolve diplodocoid intrarelationships. Subsequently published analyses (Mannion et al., 2012; Tschopp and Mateus, 2013b) thus consequently based on Whitlock (2011a).

The present analysis further increases both taxon and character list of Whitlock (2011a) by almost 300% and 250%, respectively (76 versus 26 OTUs, 477 versus 189 characters), and can thus be considered independent as well. Nonetheless, most of the positions of the common genera included in the analyses remained the same. The analyses thus generally corroborate each other.

Difficulties and possibilities of a specimen-based analysis

Anatomical overlap. A specimen-based phylogenetic analysis has both drawbacks and

PeerJ Reviewing Manuscript

advantages. One of the major problems is the lacking anatomical overlap, most importantly between incomplete historic holotype specimens. In particular in diplodocid sauropods, the majority of the type specimens was described by Marsh and Cope during the so-called Bone Wars (Cope, 1877a, b; Marsh, 1877a, 1878, 1879, 1881, 1884, 1890, 1899). New species were rushed into press without detailed description, sometimes even lacking illustrations (e.g. Marsh, 1881, 1899). In certain cases, subsequent studies revealed that different species were erected based on different bones of possibly the same skeleton ('*Atlantosaurus*' *immanis* YPM 1840 and *Apatosaurus laticollis* YPM 1861; Marsh, 1877a, 1879; McIntosh, 1995). More complete skeletons were later recovered, but many of these still lack a description, and were identified as a particular genus or species without any detailed study (e.g. '*Diplodocus longus*' DMNS 1494). Lately, more and more nearly complete specimens are becoming available for study (e.g. Harris and Dodson, 2004; Upchurch et al., 2004b; Tschopp and Mateus, 2013b; Barrett et al., 2011). Complete, articulated specimens, or parts of skeletons preserving portions underrepresented in earlier finds (e.g. skulls attached to their necks, transitions from cervical to dorsal vertebrae, articulated manus or pedes), are crucial for a specimen-based phylogenetic analysis. They provide the anchorage with which fragmentary specimens can be compared, thereby allowing for indirect comparisons. Care has to be taken to include articulated specimens and exclude information from portions of the skeleton for which an unambiguous association with the specimen to be studied cannot be ascertained. The most valuable documents to assure genuine association of skeletal parts to one individual are detailed quarry maps and field notes, but these often lack in historic type specimens. However, efforts were made lately to unravel excavation stories and bone associations of the most important holotype specimens (e.g. McIntosh, 1990a, 1995; McIntosh and Carpenter, 1998). The present study heavily relies on these earlier studies to confirm or discard bone associations. However, certain specimens would still need such a detailed overhaul, and their phylogenetic positions has still to be regarded provisional (see below).

Deformation. An additional problem for quantitative characters in particular, are deformed specimens. Whereas brittle deformation can be readily identified due to the introduced cracks, plastic deformation results in unfractured, but distorted fossils (Tschopp et al., 2013). If plastic deformation happens symmetrically, it is almost impossible to identify, and least of all to quantify. Retrodeformation can yield some information on how bones were deformed, but only in bilaterally symmetrical elements (Arbour and Currie, 2012; Tschopp et al., 2013). For species- or genus-level phylogenetic analyses, mean ratios can be taken from different individuals of the same taxon, thereby approaching more closely the ratios generally typical for that taxon. In

PeerJ Reviewing Manuscript

specimen-based analyses, such an approach is not possible. However, if a specimen is deformed in such a way that it would be scored differently from closely related species, or specimens from the same species, it increases homoplasy of this single character, and decreases its consistency index. By using implied weighting, as was done in the second analysis herein, this can be partly accounted for.

Morphological details. During the study of single specimens, one usually records and describes morphological details unique to the animal, which might or might not be taxonomically significant. If the phylogenetic analysis accompanying the description recovers the new specimen on a separate branch and thus as new taxon, these traits are generally interpreted as autapomorphic for the new taxon. The confirmation of such an interpretation can only be made with the discovery of additional specimens of the same species, preserving the same portions of the skeleton. Before that, variation due to any pre- or post-mortem processes (ontogeny, individual variation, sexual dimorphism, or taphonomic deformation) cannot be excluded with certainty as a cause for the morphological disparity found in the fossil. Specimen-based phylogenetic analyses are the only way to test for such variation. As mentioned above, highly homoplastic characters are describing the most variation, in the case of a specimen-based analysis between individuals. They are thus the most probable to code for individual variation, and should thus either be deleted or downweighted compared to the less variable characters, as is done by implied weighting (Goloboff, 1993). Because it cannot be excluded that characters describing individual variation in some groups actually code for taxonomically significant differences in other taxa, downweighting the characters in question appears more accurate than deleting them entirely. Finally, by scoring single specimens of a species, and thereby detecting individual variation in some characters, researchers create a firmer base for how to score species- or even genus-level OTUs.

Validity of recovered diplodocoid subclades

The following discussion includes only the clades recovered within Diplodocoidea, as the present analysis was designed for the study of diplodocid intrarelationships, and is thus not suitable for inferring phylogenetic positions and definitions for clades recovered outside Diplodocoidea. The systematic affinities of single specimens included in the analysis, which are recovered outside Diplodocoidea, are discussed below. Definitions of the clade names follow Taylor and Naish (2005) and Whitlock (2011a).

One of the problems raised in a specimen-based phylogenetic analysis is where to draw the line between individual variation, and differences on species or genus level. The decision for specific

PeerJ Reviewing Manuscript

versus generic separation is somewhat arbitrary, in particular in paleontology, where no tests exist for the biological species concept (Carpenter, 2010). If qualitatively assessing the validity and significance of single characters, subjectivity of the interpretation as separate species or genus is even more increased. In order to avoid subjectivity at least in parts, a quantitative approach was developed. With a numerical approach, personal influence can be minimized, and the process of generic separation can be rendered more repeatable and thus scientifically sound. The herein proposed approach bases on the number and quality of 'synapomorphies' and 'autapomorphies', as found by the software TNT. Because the analysis is specimen-based, one has to keep in mind that these do not conform to real species or genus autapomorphies or synapomorphies, but described unique or shared morphological features of specimens or groups of specimens. In the following, these 'false' apomorphies found by TNT are thus mentioned in quotation marks. The qualitative assessment of the apomorphies, as outlined below, counts for both real and 'false' apomorphies, however.

Synapomorphies are separated into four, qualitatively different categories. Unambiguous synapomorphies are shared by all ingroup members of the respective clade, and only by them. Exclusive synapomorphies only mark ingroup members, but not all of them. Shared synapomorphies are present in all ingroup members, but also occasionally occur in taxa outside the clade in question. Ambiguous synapomorphies are neither exclusive, nor shared by all ingroup members, but still recovered as synapomorphies by at least one analysis with equal and one with implied weighting. Ambiguous synapomorphies recovered by only one type of analysis (equal or implied weighting) are not considered reliable.

Specimen 'autapomorphies' are divided into unambiguous, or ambiguous (shared with other taxa). Autapomorphies found by only reduced consensus trees, but no pruned tree are considered invalid, or at least dubious, as more specimens potentially bearing the same morphology are excluded from reduced trees compared to pruned trees. Also, autapomorphies of apatosaurine specimens, which are shared with other apatosaurine specimens or clades (or diplodocine with diplodocine) are interpreted as inappropriate for species diagnosis.

'Synapomorphies' of diplodocid genera and species generally considered valid were then counted and summed between sister taxa (specimens or clades, in this case). A minimum number of synapomorphies was defined for justifying specific or generic separation. The minimum number of needed differences for generic separation was chosen based on the count obtained from the well-established sister genera *Dinheirosaurus* and *Supersaurus*, which are also geographically separated (Portugal, and USA, respectively). The ten differences obtained here were compared

PeerJ Reviewing Manuscript

with the sum of changes between two species of *Apatosaurus* (*A. ajax* and *A. louisae*) or *Diplodocus* (*D. carnegii* and *D. hallorum*), which were both found to be lower (8 and 9, respectively). Both species were are well established in the literature, and recovered as sister taxa in the present analysis. A third count of changes was made between specimens from the same species (*D. carnegii* CM 84 and CM 94, and *A. louisae* CM 3018 and CM 3378). As for the chosen species, also the used specimens were generally considered the same species in the past, and recovered as such in the present analysis. The sum of changes between these specimens amounts to one. A minimum of ten differences is thus considered enough for genus-level separation, whereas for species, a margin of five changes is given in order to account for individual variation (which is already accounted for by the evaluation of the validity of the autapomorphies, but a wider margin is preferred herein in order to be more cautious). The precise numbers established here (5 and 10 changes) cannot be applied to any other analysis, even of the same clade, as the recovery of 'autapomorphies' and 'synapomorphies' depends on the number of characters included in the analysis, and also on the software used. However, the general approach can be used in other analyses as well.

The discussion of the various clades recovered is done following a bottom-up approach, starting with dichotomies between single specimens. This is preferred over a top-down approach, because it is the specimens that define the taxa, not the taxa that determine the affiliation of the specimen. Based on the validity of the recovered dichotomies between single specimens, species and finally genera and higher-level taxa can be evaluated more accurately.

***Barosaurus lentus* YPM 429 + AMNH 6341.** These two specimens were recovered as sister taxa in all pruned and reduced trees. It has a relatively high resampling value and is supported by four shared 'synapomorphies' (Tabs S60, S61). All four 'synapomorphies' were resulting as such by every analysis recovering this clade. Whereas the two 'synapomorphies' are only shared with taxa outside Diplodocoidea (with the possible exception of *Australodocus bohetii*, see below), the other two are also shared with various specimens within Diplodocidae, or even Diplodocinae. The two specimens are separated by one change only, indicating that they belong to the same species.

CM 11984 + (*Barosaurus lentus* YPM 429 + AMNH 6341). All four trees show this grouping, and found one shared and an ambiguous 'synapomorphy' defining it (Tabs S60, S62). The ambiguous 'synapomorphy' (prezygapophyseal centrodiapophyseal fossa of mid- and posterior cervical vertebrae subdivided into various smaller partitions by several accessory laminae; C184-2) is not present in a mid-cervical vertebra in storage at AMNH, but the determination of

PeerJ Reviewing Manuscript

presence or absence of accessory laminae was not possible for posterior cervical vertebrae on public display. Further studies are needed to clarify this. Both of these 'synapomorphies' are shared with other diplodocine specimens, and do therefore not classify as species autapomorphies. No valid 'autapomorphy' separates CM 11984 from the other two specimens, which are thus interpreted to belong to the same species.

AMNH 7535 + (CM 11984 + (*Barosaurus lentus* YPM 429 + AMNH 6341)). As the two clades discussed above, also the present arrangement was recovered by all four trees. Statistical support for it is lower, and only one shared 'synapomorphy' is found (Tabs S60, S63). This 'synapomorphy' (very elongate mid-cervical vertebrae) is the best known and most widely used trait to distinguish *Barosaurus* from *Diplodocus* (e.g. McIntosh, 2005). The lack of other synapomorphies is probably due to the very restricted overlap in the four specimens of this clade, but also with the closest sister group (*Kaatedocus siberi* SMA 0004 + (SMA D16-3 + AMNH 7530)), which is only known from neck and skull material. Neither delayed nor accelerated transition (DELTRAN and ACCTRAN, respectively) approaches are thus able to find more 'synapomorphies' for either clade, but probably more will be recovered when it will be possible to add more specimens preserving overlapping material. The number of changes does not allow the erection of different species. Since the entire clade only includes the holotype specimen of *Barosaurus lentus* (YPM 429), all specimens are herein referred to that species.

SMA D16-3 + AMNH 7530. This clade is not supported by any 'synapomorphy', but recovered in all four trees. The latter is mainly due to the fact that SMA 0004 (the sister specimen of the current clade) has some morphological features in common with more basal diplodocine specimens, which are not present in SMA D16-3 or AMNH 7530. Given that both specimens of this group do not show any specimen 'autapomorphies', a referral to the same species can be regarded well-supported.

***Kaatedocus siberi* SMA 0004 + (SMA D16-3 + AMNH 7530).** The current triplet constitutes the sister group to the *Barosaurus lentus* clade discussed above. It is found in all four trees, and supported by a resampling value of 14, one higher than the clade CM 11984 + (YPM 429 + AMNH 6341) (Tab. S60). Nine shared 'synapomorphies' are recovered (Tab. S64). One additional unambiguous autapomorphy of the genus was proposed by Tschopp and Mateus (2013b), but not recovered as such by the present analyses: a transverse sulcus bordering the prezygapophyseal facets of posterior cervical vertebrae posteriorly. This feature was impossible to code for in the other two specimens of *Kaatedocus siberi*, which was probably the reason why it was not found as synapomorphy or autapomorphy herein. However, SMA 0004 is the only specimen positively

PeerJ Reviewing Manuscript

scored for its presence in the current analysis, indicating that one more synapomorphy, possibly unambiguous for this clade, might be present. Not counting this, the nine shared 'synapomorphies' of *K. siberi* plus the single 'synapomorphy' of the sister clade *Barosaurus lentus* sum to ten, which is deemed enough for generic separation (see above). Within *Kaatedocus*, one change separates SMA 0004 from the other two specimens, which are thus referred to the type species *K. siberi*.

***Kaatedocus* + *Barosaurus*.** The sister arrangement of *Barosaurus* and *Kaatedocus* is herein recovered by both analyses, supported by three shared synapomorphies (Tab. S65). These traits are somewhat problematical, as they concern anterior and mid-cervical vertebrae. Many specimens within Diplodocidae are not represented by anterior cervical vertebrae, and within *Barosauus*, AMNH 7535 is the only specimen preserving them. Furthermore, overlap between *Kaatedocus* and *Barosaurus* is low. However, differences in height of anterior neural spines are very pronounced when comparing *Kaatedocus* SMA 0004 with *Diplodocus* CM 84 or *Galeamopus* SMA 0011, the two genera most closely related to *Kaatedocus* + *Barosaurus* within Diplodocidae. Dorsoventrally elongate coels on the lateral side of the neural spines are typical for posterior cervical vertebrae of *Diplodocus*, among others, but in this genus, these coels are not present in anterior elements. In *Kaatedocus* and *Barosaurus* AMNH 7535 the serial pattern is inverted, and the coels only mark anterior elements. Additional synapomorphies, in particular from appendicular bones, might be found once a more complete specimen of *Kaatedocus siberi* is described.

CM 3452 + (*Kaatedocus* + *Barosaurus*). Before the description of *Kaatedocus siberi* SMA 0004, the specimen CM 3452 was the only diplodocid preserving an almost complete skull in articulation with the most anterior, postaxial cervical vertebrae. Although generally identified as *Diplodocus* (Holland, 1924; McIntosh and Berman, 1975; Whitlock et al., 2010), CM 3452 is recovered as sister taxon to *Barosaurus* + *Kaatedocus* in all four trees found here. The affiliation of CM 3452 with this group is supported by one unambiguous, nine shared, and one ambiguous synapomorphies. None of these are present in any specimen recovered within the *Diplodocus* clade (Tab. S66). The lateral lacrimal spur recovered as unambiguous synapomorphy for this clade was proposed as autapomorphy of *Kaatedocus* (Tschopp and Mateus, 2013b), and is actually not unambiguous among sauropods: Tschopp and Mateus (2013b) reported a specimen of *Camarasaurus* (SMA 0002), which shows a similar trait, as do some other camarasaur lacrimals (Madsen et al., 1995). However, within Diplodocidae, of the few skulls known, only CM 3452, SMA 0004, and CM 11255 bear such a spur (Tschopp and Mateus, 2013b). If the feature gets

PeerJ Reviewing Manuscript

confirmed to diagnose this group, also CM 11255 would have to be referred to it, instead of being identified as *Diplodocus* (Whitlock et al., 2010). Although tree topologies suggests that CM 3452 constitutes its own genus, the low number of four changes between the specimen and the *Kaatedocus* + *Barosaurus* clade does not support an erection of a new genus nor a species.

DMNS 1494 + USNM 10865. These two specimens traditionally referred to *Diplodocus* (Gilmore, 1932; McIntosh, 2005) are recovered as sister taxa in both trees obtained with implied weighting, as well as the reduced consensus with equal weighting. The equally weighted pruned consensus tree shows a polytomy formed by all putative *Diplodocus* specimens and the clade CM 3452 + mdD. This is probably a consequence of the incompleteness of important specimens like *D. longus* YPM 1920, or the skulls CM 11161 and USNM 2672. The clade DMNS 1494 + USNM 10865 is supported by a resampling value of nine (Tab. S60), and one shared 'synapomorphy' (Tab. S67), which is a single instead of two parallel pcpl in mid- and posterior dorsal neural arches, as present in other *Diplodocus* specimens. As only one change separates DMNS 1494 from USNM 10865, the two specimens are referred to the same species.

***Seismosaurus hallorum* NMMNH 3690 + (DMNS 1494 + USNM 10865).** The current triplet is found in the equally weighted reduced consensus tree, as well as in both pruned and reduced consensus trees when applying implied weights. It has a resampling value of six (Tab. S60), and is supported by one shared 'synapomorphy' (Tab. S68). The four changes separating *S. hallorum* from the clade DMNS 1494 + USNM 10865 are not enough to justify the erection of two different species, therefore the entire triplet is referred to the same species.

AMNH 223 + (*Seismosaurus hallorum* NMMNH 3690 + (DMNS 1494 + USNM 10865)). As the two clades discussed above, the present quartet of specimens is recovered in all trees but the equally weighted pruned tree. It has a resampling value of six (Tab. S60), and one unambiguous and five shared 'synapomorphies', which distinguish it from the other *Diplodocus* specimens (Tab. S69). One of these 'synapomorphies' (a subtriangular process on the scapular blade) also occurs in other diplodocines. Three changes are recovered between AMNH 223 and the remaining triplet, indicating that they belong to the same species, as was already suggested by McIntosh (2005).

Sister specimens recovered as such are *D. longus* YPM 1920 in the reduced consensus using implied weighting, and *D. carnegii* CM 84 + CM 94 in the equally weighted reduced consensus tree with CM 94 added. Nine changes lie between the *D. carnegii* pair and the clade discussed herein, whereas only six changes are recovered between the current clade and *D. longus*. As both of these remain below the ten changes set as sufficient for genus-level separation, *Seismosaurus*

PeerJ Reviewing Manuscript

is here considered a synonym of *Diplodocus*, but as its own species *D. hallorum*, including the specimens AMNH 223, DMNS 1494, NMMNH 3690, and USNM 10865.

***Diplodocus longus* YPM 1920 + *Diplodocus hallorum*.** Of the four main trees, only the reduced consensus tree with implied weighting recovered this arrangement, but by substituting *D. carnegii* CM 84 by *D. longus* YPM 1920 in the equally weighted reduced consensus tree, the same result is obtained. Such a grouping, where *D. longus* + *D. hallorum* form the sister clade to *D. carnegii* CM 84 + CM 94 is not supported by any 'synapomorphy'. In fact, when adding either the holotype or the paratype specimen of *D. carnegii*, a polytomy is recovered between CM 84, CM 94, YPM 1920 and *Diplodocus hallorum*, as can be seen in the pruned consensus tree using implied weighting.

***Diplodocus carnegii* CM 84 + CM 94.** Although not recovered in the four main trees discussed here, symmetric resampling yielded a value of eight for this clade (Tab. S60), and indeed, when deleting YPM 1920 and adding CM 84 and CM 94 to the reduced consensus trees, the clade discussed here forms the sister group to *D. hallorum* as discussed above. The clade is supported by three shared 'synapomorphies', which are all absent in any specimen referred to *D. hallorum* above (Tab. S70). Together with the six synapomorphies of the *D. hallorum* clade, this amounts to nine changes, which allows erection of different species but not genera, following the guidelines established above. The recovery of this clade in the extended reduced consensus trees confirms Hatcher's (1901) assignment of CM 94 as paratype of the species *D. carnegii*. Both specimens were found in the same stratigraphic level of the same quarry (Hatcher, 1901).

***Diplodocus carnegii* + *Diplodocus hallorum*.** The grouping of these two species within the genus *Diplodocus* occurs in all trees excluding the skull specimens CM 11161 and USNM 2672. When including *D. longus* YPM 1920 as well, the grouping of CM 84 and 94 is split, and a polytomy is formed as explained above. All these specimens are united by six shared and one unambiguous 'synapomorphies' (Tab. S71). One of these 'synapomorphies' is shared with one single specimen of *Barosaurus lentus* (anteroposterior width of mid- and posterior dorsal neural spines remains approximately constant along the height of the spine; C265-0, shared with YPM 429), and an additional one is shared with a specimen of *Galeamopus*, the genus forming the sister taxon to *Diplodocus* + mdD (anterior end of the sprl of mid- and posterior cervical vertebrae remains vertical; 182-0, with SMA 0011). As all trees recovered also include *D. longus* YPM 1920 within this clade, and because *D. longus* is currently regarded type species of the genus *Diplodocus* (but see below for a more detailed assessment of YPM 1920), the specimens included in the clade are herein referred to that genus. It is separated from its sister clade CM 3452 + mdD by 18 changes,

PeerJ Reviewing Manuscript

and both groups are diagnosed with an unambiguous synapomorphy. ***S***even synapomorphies of the clade CM 3452 + mdD are based on cranial material, none of which is definitely attributable to the *Diplodocus* clade (2-0, 10-1, 19-1, 48-2, 52-1, 65-1, 67-1). All of these traits are different from the two included skulls CM 11161 and USNM 2672, which probably belong to the genus *Diplodocus* (see below for a discussion of their taxonomic affinities). The synapomorphies are thus tentatively retained in the count for the changes between the clades, and the 17 changes between *Diplodocus* and CM 3452 + mdD (excluding the one shared with YPM 429) still confidently justify generic separation.

***Diplodocus* + mdD.** *Diplodocus* is recovered as sister taxon to the clade with *Kaatedocus* and *Barosaurus* in all four principal trees discussed here. It is diagnosed by 13 synapomorphies, of which one is unambiguous, ten are shared, and two are ambiguous (Tab. S72). Four of the shared synapomorphies are unique within Diplodocidae (69-0, 80-0, 154-0, 440-1), and five more within Diplodocinae (196-1, 269-1, 367-0, 381-1, 405-1).

Galeamopus [redacted] **SMA 0011 + *Galeamopus hayi* HMNS 175.** All four principal trees show this clade, which is supported by one shared 'synapomorphy' (if strictly following the qualitative assignment of synapomorphies mentioned above; Tab. S73). However, all three trees recovering this synapomorphy exclude the skulls CM 11161, SMA O25-8, and USNM 2672, which all share the same position of the frontal-parietal suture as the *Galeamopus* specimens. When added to the reduced consensus trees, these skulls form polytomies with specimens from *Diplodocus* (CM 11161 and USNM 2672), or *Barosaurus* (SMA O25-8). As also the skull CM 3452 shows the same morphology, an interpretation of this synapomorphy as diagnosing the clade *Galeamopus* [redacted] SMA 0011 + *Galeamopus hayi* HMNS 175 is highly questionable. The clade is thus not diagnosable by any synapomorphy. The two specimens are separated from each other by nine changes, including one unambiguous autapomorphy diagnosing *Galeamopus* [redacted] SMA 0011. The high number of differences allows the erection of two species, as suggested in the descriptive part of the thesis: *Galeamopus hayi* as the type species, and *G.* [redacted]

AMNH 969 + (*Galeamopus hayi* + *G.* [redacted] The triplet is recovered in all main trees, and shows a resampling value of two (Tab. S60). It is supported by two unambiguous and two shared 'synapomorphies', which all describe morphological features of the skull, or the atlas-axis complex (Tab. S74). Due to the rare finds of atlantes and axes, these synapomorphies are somewhat dubious, and will have to be assessed in more detail once more complete specimens become available for study. However, the continuous recovery of the same triplet in the same

PeerJ Reviewing Manuscript

position of all four trees, as well as its higher resampling value compared with most other clades indicates that this grouping forms its own genus. Two changes lie between AMNH 969 and the clade with *G. hayi* + *G.* [redacted] therefore not allowing the erection of a third species. The affinities of AMNH 969 will be discussed in more detail below.

***Galeamopus* + mdD.** All four trees show the new genus *Galeamopus* as sister taxon to the clade with *Diplodocus*, *Kaatedocus*, and *Barosaurus*. Two unambiguous, six shared, and two ambiguous synapomorphies diagnose this group (Tab. S75). Only one of the shared synapomorphies is present in other diplodocines as well (posterior dorsal postzygapophyses almost horizontal; C275-0, in ML 418 and *Supersaurus vivianae*), whereas one ambiguous synapomorphy is unique within the sampled Neosauropoda (an accessory spinal lamina in posterior cervical neural arches running vertically just posterior to sprl; C203-1), but *Kaatedocus* autapomorphically bears the reversed state. Between *Galeamopus* and its sister clade *Diplodocus* + mdD, 16 differences are present. One is shared between *Galeamopus* and *Kaatedocus* (47-1), one between *Galeamopus* and the putative *Barosaurus* SMA O25-8 (80-0), a third is present in both SMA 0011 and AMNH 6341 (269-0), and a fourth is shared with CM 94 (367-0). Deleting them from the 16 changes, the remaining twelve are still sufficient for a generic separation.

***Dinheirosaurus* + mdD.** Although *Dinheirosaurus* is recovered in the same relative position in both analyses with equal and implied weighting, the first major difference between the trees of these two analyses is encountered here. Whereas the equally weighted trees show a sister genera arrangement of *Dinheirosaurus* and *Supersaurus*, the analyses using implied weighting results in a more basal position of *Supersaurus*. In this paragraph, only the clade excluding *Supersaurus* will be discussed, recovered by applying implied weights. The more parsimonious position of *Supersaurus* will be assessed below. Only one shared 'synapomorphy' supports such an arrangement to the exclusion of *Supersaurus* (Tab. S76). The equally weighted analysis recovers this feature as synapomorphic for the entire Diplodocidae (in the pruned consensus tree), with a reversal in *Tornieria*. The state is unknown in *Supersaurus*, due to insufficient information in descriptions, and lacking figures in anterior view. Future personal observations of the BYU specimen might clarify its morphology. The present arrangement yields ten changes between *Dinheirosaurus* and its sister clade *Galeamopus* + mdD, four more synapomorphies of *Galeamopus* + mdD are not preserved in the known material from *Dinheirosaurus*.

***Tornieria africana* holotype + skeleton k.** The earlier referral of these two specimens to *Tornieria* (Remes, 2006, 2009) is confirmed by both analyses performed herein. They show a resampling value of four (Tab. S60), and five shared synapomorphies, which all describe

PeerJ Reviewing Manuscript

appendicular morphology (Tab. S77). The apparent lack of vertebral characters is due to the destruction of most putative *Tornieria* vertebrae during World War II (Remes, 2006; Whitlock, 2011a). A series of caudal vertebrae from trench dd from Tendaguru (MB.R.2956), referred to *Tornieria* by Remes (2006) was not included into the analysis as concerns of their attribution to the same individual were raised by Remes (2006). No valid autapomorphies are recovered for either *Tornieria* specimen, confirming the referral of skeleton k to the species *T. africana*.

***Tornieria* + mdD.** A clade with *Tornieria* and more derived Diplodocoidea to the exclusion of other diplodocine specimens was only recovered in the analysis using implied weighting, and including all specimens. With equal weights, or by excluding *Australodocus bohetii* from the analysis with implied weighting a priori, *Tornieria* + mdD corresponds to Diplodocinae. In the following, the find of the main trees by using implied weights is discussed. One unambiguous, one exclusive, and one shared synapomorphy are found for this clade (Tab. S78). Given the more basal position of *Supersaurus* in the implied weight trees, these features are absent in that genus. Two of the synapomorphies proposed for *Tornieria* + mdD by the analysis using implied weighting (131-1, 307-1) are also recovered by the equally weighted trees (for the clade Diplodocinae), with the difference that the unambiguous synapomorphy becomes exclusive. The same happens when excluding *Australodocus bohetii* from the implied weights analysis a priori. In the main trees from the analysis with implied weighting, seven changes separate *Tornieria* from the clade *Dinheirosaurus* + mdD, nine changes are between *Tornieria* and *Dinheirosaurus*, when adding the autapomorphies of *Dinheirosaurus* comparable with their states in *Tornieria*. In the equally weighted trees, where the clade *Tornieria* + mdD corresponds to Diplodocinae, six changes are recovered between *Tornieria* and *Supersaurus* + mdD. This would not allow the erection of a different genus for *Tornieria*, but see below for a more detailed taxonomic assessment.

***Supersaurus vivianae* BYU + WDC DMJ-021.** The unity of the two *Supersaurus* specimens included in the present analysis is well supported. All four trees show this arrangement, and resampling yielded a value of 36, which is the highest value reported within Diplodocidae (Tab. S60). Seven shared 'synapomorphies' define the clade (Tab. S79). Recovery of these 'synapomorphies' highly depends on tree topology, and thus the type of analysis performed. In the main trees obtained through implied weighting, where *Supersaurus* lies outside *Tornieria* + mdD, only one 'synapomorphy' (a deep groove extending anteroposteriorly within the lateral edge posterior to the parapophysis of mid- and posterior cervical vertebrae, C177-1) was found to unite the two specimens. The split ventrolateral edge is shared with *Dinheirosaurus*, with which

PeerJ Reviewing Manuscript

Supersaurus groups in all other trees, including the one obtained by implied weighting, and excluding *Australodocus bohetii* a priori. On the other hand, from the other six 'synapomorphies', three are shared with *Australodocus bohetii* (131-0, 136-1, 172-1), and two of them result as synapomorphies of this clade as recovered by the main implied weights trees (see below). In any case, attribution of the two specimens to *Supersaurus* appears well-supported, and the absence of any valid differences between the specimens confirms the referral of WDC DMJ-021 to the type species *S. vivianae*, and in turn also corroborates the assignment of the single bones in the BYU collection to the same individual, as suggested by Lovelace et al. (2007).

***Dinheirosaurus* + *Supersaurus*.** A sister taxon relationship of these two taxa to the exclusion of others is only recovered by using equal weights, or by pruning *Australodocus bohetii* from the implied weights analysis a priori. In the latter analysis, *Dinheirosaurus* + *Supersaurus* is the sister clade to the specimen ML 418, with which it forms the sister group to *Galeamopus* + mdD. Where *Dinheirosaurus* and *Supersaurus* form a clade, they are located within Diplodocinae, in a position more derived than *Tornieria*. *Dinheirosaurus* + *Supersaurus* is supported by a resampling value of three (Tab. S60), as well as six shared and one unambiguous synapomorphies (Tab. S80). One of the shared synapomorphies (a high ratio of neural spine to pedicel height; C272-1) is present as well in ML 418. *Dinheirosaurus* is separated from *Supersaurus* by ten changes, and was the main pair of genera on which the numerical approach of specific and generic distinction was based, given the geographical distance between the two genera.

***Australodocus bohetii* type + *Supersaurus*.** Such a group was only recovered in the main trees of the analysis with implied weighting. There, it is located basal to *Tornieria*, within Diplodocinae, and thus contrasts with the position of *Supersaurus* when associated with *Dinheirosaurus*. The more basal position of the clade *Australodocus* + *Supersaurus* is probably due to the several traits *Australodocus* shares with titanosauriform sauropods. Resampling does not support the current clade (Tab. S60), which is specified by four shared synapomorphies (Tab. S81). Two of them are shared with brachiosaurid titanosauriforms (172-1, 183-1), and actually diagnose the brachiosaurid clade including *Australodocus* in the pruned tree with equal weighting. The other two synapomorphies recovered for an *Australodocus* + *Supersaurus* clade (136-1 and 162-1) are not shared with any included taxon outside Diplodocidae. The two genera are only separated by six changes, which would not allow generic separation. However, this would only apply if *Australodocus* really would represent the sister taxon to *Supersaurus*, which is highly questionable, as will be discussed in more detail below.

***Supersaurus* + mdD.** Depending on the analysis, this clade includes *Tornieria* or represents its

PeerJ Reviewing Manuscript

sister group. Therefore, also the combination of synapomorphies change in the different trees. Whereas none can be considered valid (based on the guidelines established above) for the main trees recovered with implied weighting – thus including *Tornieria* – one shared synapomorphy describes *Supersaurus* + mdD excluding *Tornieria* in the equally weighted trees (Tab. S82). This synapomorphy is not found in the agreement subtree of the analysis with implied weights excluding *Australodocus bohetii* a priori, where the position of *Supersaurus* + mdD is the same as in the equally weighted trees, but furthermore includes ML 418. In this tree, another shared synapomorphy unites the clade: ratio of the pubic articulation length of the ischium to the anteroposterior length of the pubic pedicel is less than 1.5 (420-0). However, measurements were only obtainable for four specimens within *Supersaurus* + mdD, and the validity of this synapomorphy will have to be addressed in more detail in future. In any case, the only probably valid synapomorphies are found in the trees excluding *Tornieria* from *Supersaurus* + mdD. In the equally weighted trees, *Dinheirosaurus* + *Supersaurus* are separated from *Galeamopus* + mdD by 16 changes. *Australodocus* + *Supersaurus* distinguish only seven changes from their sister clade *Tornieria* + mdD.

Diplodocinae. The composition of Diplodocinae is almost equal in all main trees. The only taxon changing between diplodocine, and non-diplodocine affinities is *Australodocus bohetii*, as already mentioned above. Due to the incompleteness of ML 418, which was recovered as most basal diplodocine in the main trees by using implied weights, the number of synapomorphies for the entire clade is much reduced compared to the main equally weighted trees, where ML 418 was excluded from both the pruned and reduced consensus trees. Applying the guidelines for assessing the significance of synapomorphies, two exclusive and eight shared synapomorphies are found by the two analyses (Tab. S83). Three of these synapomorphies are shared with certain apatosaurine specimens (218-1, 283-1, 330-1). Upwards and backwards directed tubercula of anterior and mid-cervical ribs (218-1) are not present in *Australodocus*, such that in the improbable case of diplodocine affinities of this taxon, this character state would become an ambiguous synapomorphy of Diplodocinae, instead of shared. In the trees, where ML 418 represents the most basal diplodocine taxon, it is separated from the more derived group by just two changes, which does not allow the erection of a new species. This is supported by the fact that ML 418 was among the six most unstable taxa in the equally weighted analysis, and that it switches to a position within the clade *Dinheirosaurus* + *Supersaurus* when excluding *Australodocus* a priori from the analysis applying implied weighting.

***Apatosaurus louisae* CM 3018 + CM 3378.** A clade only including these two specimens is

PeerJ Reviewing Manuscript

recovered in both reduced consensus trees, and supported by a relatively high resampling value of 23 (Tab. S60). The pruned consensus tree of the analysis using implied weighting shows a polytomy with these two specimens and the holotype specimens of *Apatosaurus laticollis* (YPM 1861) and *Brontosaurus amplus* (YPM 1981). When adding these two specimens to the reduced consensus tree of the equally weighted analysis, *A. laticollis* forms a trichotomy with the *A. louisae* specimens, whereas *B. amplus* is recovered more basally within Apatosaurinae. Two shared 'synapomorphies' are considered reliable (Tab. S84). One of these 'synapomorphies' (the presence of a ridge on the dorsal rib head; C283-1) is otherwise typical for diplodocines. One change lies between the two specimens, confirming the previous referrals to the same species (e.g. McIntosh, 1981; Upchurch et al., 2004b).

***Brontosaurus amplus* YPM 1981 + mdA.** This clade is only recovered by the reduced consensus tree obtained applying implied weighting. Adding *A. laticollis* YPM 1861 to the tree, a polytomy is created between *B. amplus*, *A. laticollis*, *A. louisae*, and CM 3378, as visible in the pruned consensus tree with implied weights. In the analysis with implied weights excluding *Australodocus* a priori, *B. amplus* groups with *Apatosaurus ajax* YPM 1860 to form the sister clade to the two *A. louisae* specimens. When excluding *A. laticollis*, only one shared 'synapomorphy' is found (Tab. S85). If *A. laticollis* is added, one unambiguous and three shared synapomorphies are added (Tab. S85). However, it was not possible to score *B. amplus* for any these additional 'synapomorphies'. They thus mostly describe the grouping of *A. laticollis* with the two *A. louisae* specimens. Four changes lie between *B. amplus* YPM 1981 and the two *A. louisae* specimens, two changes separate *A. laticollis* YPM 1861 from the *A. louisae* holotype, and a single change from CM 3378. This would indicate that all four specimens belong to the same species, but see below for a more detailed assessment of the affinities of YPM 1861 and 1981.

***Apatosaurus ajax* YPM 1860 + '*Atlantosaurus*' *immanis* YPM 1840.** The unity of these two specimens is only shown in the equally weighted trees. In the tree obtained with implied weighting, the holotype specimen of '*Atlantosaurus*' *immanis* groups together with NSMT-PV 20375, which was described as belonging to *Apatosaurus ajax* (Upchurch et al. 2004b), but does not group with the holotype YPM 1860 in any of the trees recovered here. Four shared 'synapomorphies' support the clade *Apatosaurus ajax* + '*Atlantosaurus*' *immanis* (Tab. S86). All four 'synapomorphies' are shared with other specimens within Apatosaurinae. Two are shared with the putative *Apatosaurus ajax* specimen NSMT-PV 20375 (168-0, 426-1), and one with the holotype of *Apatosaurus laticollis*, YPM 1861 (198-1). Considering the low overlap index of

PeerJ Reviewing Manuscript

13%, and the inability to recover this group by resampling, support for this clade is very low. Six changes lie between the two specimens, which indicate that they are different species, but not different genera.

***Apatosaurus ajax* + mdA.** Such a clade is found with both methods. It is present in the reduced consensus tree from the equally weighted analysis, and both main trees obtained with implied weighting. The only difference lies in the position of '*Atlantosaurus*' *immanis* YPM 1840, which is included in the equally weighted reduced consensus tree, but excluded in the trees with implied weights. This appears to have an influence on the number of 'synapomorphies' found in the different trees, with the equally weighted reduced consensus tree showing less than half of the 'synapomorphies' recovered by implied weighting. In total, eight shared 'synapomorphies' were found (Tab. S87). Only one of these characters is preserved in YPM 1840 as well (208), but the latter specimen does not show the plesiomorphic state. Consequently, this 'synapomorphy' was only found by the trees obtained with implied weights, and excluding YPM 1840 from the clade *Apatosaurus ajax* + mdA. Three 'synapomorphies' are shared with NSMT-PV 20375 (271-0, 293-0, 365-1), an additional one with UW 15556 (208-0). Three 'synapomorphies' are not present in any other apatosaur specimen (253-1, 328-0, 368-0). In the equally weighted reduced tree, *Apatosaurus ajax* YPM 1860 + '*Atlantosaurus*' *immanis* YPM 1840 is separated from the sister clade *Apatosaurus louisae* CM 3018 + CM 3378 by six changes, whereas *Apatosaurus ajax* YPM 1860 and *Brontosaurus amplus* + mdA are distinguished by a sum of eleven apomorphies. The difference mainly lies in the high number of 'autapomorphies' found for YPM 1860, which contrasts with the low number of 'synapomorphies' of the clade YPM 1860 + YPM 1840. Two of the 'autapomorphies' are from the braincase included in YPM 1860, which cannot definitively be attributed to the same specimen (McIntosh, 1995). Excluding these info, the number of changes between *Apatosaurus ajax* and *Brontosaurus amplus* + mdA drops to nine. At this stage, an assignment to two different species appears thus better supported than an erection of a different genus for the sister clade of *Apatosaurus ajax*.

***Eobrontosaurus* + *Amphicoelias*.** Both the pruned and reduced consensus trees of the equally weighted analysis recover these two genera as sister taxa within Apatosaurinae. If applying implied weighting, *Amphicoelias* results as the most basal diplodocid sauropod, sister taxon to Diplodocinae + Apatosaurinae, whereas *Eobrontosaurus* is still found well within Apatosaurinae. Two shared 'synapomorphies' are found for the clade *Eobrontosaurus* +*Amphicoelias* (Tab. S88). Whereas one does not occur in other apatosaurines (265-1), the other synapomorphy is shared with *Elosaurus parvus* CM 566 and the specimen UW 15556 (279-0). The latter (longer than

PeerJ Reviewing Manuscript

wide bases of the posterior dorsal neural spines) are recovered as autapomorphic for *Amphicoelias* in the trees obtained with implied weighting. The low overlap index of seven percent casts further doubts on the validity of the grouping of *Eobrontosaurus* and *Amphicoelias*. If confirmed, two changes would separate the two specimens, not justifying the erection of two different species.

***Eobrontosaurus* + mdA.** Such a clade is recovered in both main trees with implied weights, as well as the equally weighted reduced consensus tree. It always includes the clade with *Apatosaurus ajax* and *Apatosaurus louisae*, and excludes the specimens NSMT-PV 20375, SMA 0087, and WDC-FS001A. '*Atlantosaurus*' *immanis* YPM 1840 switches positions in the two analyses from *A. ajax* to a sister taxon arrangement with NSMT-PV 20375. When excluding *Australodocus bohetii* from the implied weights analysis a priori, *Eobrontosaurus* + mdA becomes more inclusive as compared to the complete implied weights trees. Without *Australodocus*, it also includes AMNH 460, as well as the clade including the holotype specimens of *Dystrophaeus viaemalae*, *Brontosaurus excelsus*, and *Elosaurus parvus*. The unstable taxa are thus *Eobrontosaurus* and AMNH 460, as the clade with *Brontosaurus* also results sister clade to *Apatosaurus ajax* + *Apatosaurus louisae* if excluding *Eobrontosaurus*. The result of the analysis without *Australodocus* can be neither confirmed nor rejected by the equally weighted reduced consensus tree, as none of the doubtful specimens are recovered there.

Combining the information of the main trees, nine shared synapomorphies are found (Tab. S89). All but one of these synapomorphies are unique within Apatosaurinae: the single lamina supporting the hyposphene (238-1) is also present in AMNH 460. This character, as well as two more (400-1, 452-1) are also found as synapomorphies for the more inclusive clade *Eobrontosaurus* + mdA in the implied weights analysis excluding *Australodocus bohetii* a priori. Three more shared and one unambiguous synapomorphies are found in the tree without *Australodocus*. None of these were possible to code for AMNH 460, with the result that all of them are recovered as synapomorphies for *Brontosaurus* + mdA in the complete implied weights analyses.

In the equally weighted reduced consensus tree, *Eobrontosaurus* + *Amphicoelias* and its sister clade are separated by five changes. The trees obtained by implied weighting yield distances of 15 (pruned) and 14 (reduced) changes from *Eobrontosaurus* to *Apatosaurus ajax* + mdA. The tree without *Australodocus* shows nine changes between *Eobrontosaurus* and AMNH 460 + mdA. Whereas *Eobrontosaurus* or *Eobrontosaurus* + *Amphicoelias* can thus be confidently considered a new species, support for being a different genus is dubious. The taxonomic status of

PeerJ Reviewing Manuscript

Eobrontosaurus and *Amphicoelias* will be assessed with further detail below.

***Dystrophaeus viaemalae* USNM 2364 + UW 15556.** The unity of these two specimens to the exclusion of any other is only seen in the reduced consensus tree applying implied weights. Support from overlap index is extremely low, being only four percent. A single shared 'synapomorphy' is recovered (Tab. S90). The addition of the single specimen FMNH P25112 to the reduced consensus tree with implied weights results in a polytomy between *Dystrophaeus viaemalae*, *Elosaurus parvus*, UW 15556, and FMNH P25112. Six changes are found between *Dystrophaeus viaemalae* USNM 2364 and UW 15556, but the states of all five autapomorphies recovered for UW 15556 are not known in *D. viaemalae.* The apomorphy count thus drops to one, indicating that the two specimens would represent the same species if they truly are sister taxa.

***Elosaurus parvus* CM 566 + UW 15556.** In the equally weighted pruned tree, the specimen UW 15556 is recovered together with the holotype specimen of *Elosaurus parvus* (CM 566), to the exclusion of all other taxa. *Dystrophaeus viaemalae* was excluded from that tree. When added to the equally weighted pruned tree, *Dystrophaeus* creates a large polytomy close to the base of the tree, and the unity of the two specimens CM 566 and UW 15556 remains. This clade was also recovered by Upchurch et al. (2004b), and interpreted as its own species within *Apatosaurus*, introducing the new combination *Apatosaurus parvus*. Seven shared 'synapomorphies' are recovered for this clade, but only supported by the equally weighted pruned tree (Tab. S91). Five of the seven 'synapomorphies' are shared with other apatosaurines (184-0, 238-0, 261-0, 279-0, 408-1), the greatly reduced sprl in posterior dorsal vertebrae (274-0) is unique within Diplodocoidea. The two specimens can be distinguished by a sum of four 'autapomorphies', which are all also observable in the other specimen.

***Elosaurus parvus* CM 566 + (*Dystrophaeus* + UW 15556).** This triplet does only occur in the reduced implied weight trees, excluding the specimen FMNH P25112. In the pruned implied weight tree, where FMNH P25112 is present, the four specimens form a polytomy, with *Brontosaurus excelsus* YPM 1980 as sister taxon. Three shared 'synapomorphies' are found by the reduced consensus tree, and five more are added in the pruned consensus tree with FMNH P25112 (Tab. S92). Due to its incompleteness, *Dystrophaeus* cannot can be scored for any of these 'synapomorphies'. The three 'synapomorphies' found by the reduced implied weights tree are in fact also found by the equally weighted trees for the cluster *E. parvus* + UW 15556. In the reduced implied weight trees, *Elosaurus parvus* CM 566 is separated from the *Dystrophaeus* cluster by four changes, not justifying specific separation.

PeerJ Reviewing Manuscript

***Brontosaurus excelsus* YPM 1980 + (*Elosaurus* + *Dystrophaeus*).** A grouping of the holotype specimen of *Brontosaurus excelsus* with *Elosaurus* and other specimens, as sister clade to a clade including the type specimens of *Apatosaurus ajax* and *A. louisae*, is only found by applying implied weights. The clade always contains three holotype specimens (*B. excelsus* YPM 1980, *E. parvus* CM 566, and *D. viaemalae* USNM 2364), as well as UW 15556. In the pruned consensus tree, also FMNH P25112 was recovered within this group. Five shared and one exclusive 'synapomorphies are recovered (Tab. S93). Two of the shared synapomorphies are also present in other apatosaurs (237-1, 272-1). The transition of fan-shaped to normal caudal ribs between Cd 5 and 6 (300-2) does not appear to be shown in UW 15556, where it is between Cd 4 and 5, according to Gilmore (1936). However, the caudal vertebrae were found disarticulated, and the serial positions proposed by Gilmore (1936) were based on comparisons with the type specimen of *A. louisae* (Gilmore, 1936: p. 251). Therefore, it could be that an anterior-most caudal vertebra is missing, and it would thus probably be more accurate to score UW 15556 as unknown in this character. As with the previous clade, due to the fragmentary state of USNM 2364, it was not possible to score *Dystrophaeus* for any of the characters herein recovered as synapomorphies for *Brontosaurus* + (*Elosaurus* + *Dystrophaeus*). *Brontosaurus excelsus* is separated from the sister clade by twelve changes, justifying the use of two distinct genera (see below).

***Brontosaurus* + mdA.** This clade is found in the implied weights analysis only. Whereas the main trees show the *Brontosaurus* clade to be sister taxon to *Eobrontosaurus* + mdA, the reduced consensus tree obtained by excluding *Australodocus* a priori does show a more basal position for *Eobrontosaurus*. The clade is supported by eight shared and one unambiguous synapomorphies (Tab. S94). Six of the present synapomorphies describe features of appendicular elements, which lack in several specimens included in the present analysis. They diagnose the more inclusive *Eobrontosaurus* + mdA in the reduced consensus tree of the analysis excluding *Australodocus* a priori (380-2, 391-1, 395-2, 396-1, 400-1, 452-1). In the latter analysis, only one, but an unambiguous synapomorphy is found for *Brontosaurus* + mdA: posterior cervical rib shafts are initially directed in the same direction but turn to run a little downwards toward the distal tip (223-1). Including *Australodocus* in the analysis, 15 changes are recovered between the *Brontosaurus* clade and the *Eobrontosaurus* clade, whereas in the other analysis, eleven changes separate *Brontosaurus* from *Apatosaurus ajax* + mdA. Both counts support the use of different genera for the two clades.

WDC-FS001A + SMA 0087. The clustering of these two specimens is only found when using implied weighting. They have a very low overlap, indicated by the index of seven percent. Two

PeerJ Reviewing Manuscript

shared 'synapomorphies' describing tibial morphology characterize the clade (Tab. S95). None of these traits are seen in other apatosaur specimens preserving the tibia. Two changes are separating the two specimens, indicating that they might belong to the same species. More detailed study of the material will be needed in order to definitely assess the systematic position of these two specimens.

SMA 0087 + mdA. As the clades discussed above, also this arrangement is only recovered in the trees obtained with implied weighting. Whereas AMNH 460 is found as sister taxon to the present clade in the trees obtained by the complete analysis, this specimen is included into SMA 0087 + mdA when *Australodocus* is deleted from the matrix a priori. No valid synapomorphies are found with the analysis including *Australodocus*, but one unambiguous synapomorphy characterizes this clade when *Australodocus* is excluded a priori (403-1; Tab. S96). However, only two ingroup specimens (out of twelve) and 14.7 percent of the specimens in the entire analysis were scorable for this character. Support for such an arrangement is thus very low. Nonetheless, eleven changes separate the clade SMA 0087 + WDC-FS001A from *Brontosaurus* + mdA in the main implied weights trees, and eight in the case of the analysis without *Australodocus*. This relatively high number indicates the presence of a new, previously unrecognized taxon.

AMNH 460 + mdA. The composition of this clade as recovered by the implied weight analyses changes depending on in- or exclusion of *Australodocus*. The specimens changing their positions in respect to this clade are *Eobrontosaurus yahnahpin* Tate-001, SMA 0087, and WDC-FS001A. They are nested within the present clade in the main trees, but fall outside when excluding *Australodocus*. A single valid, shared synapomorphy is found with the main, pruned consensus tree (Tab. S97). This trait (174-1) is not identified as synapomorphic for AMNH 460 + mdA in the analysis without *Australodocus*, as it shows the same development in *Eobrontosaurus*, which is recovered as sister taxon to the present clade, instead of being nested within. No changes separate AMNH 460 from the more derived clade SMA 0087 + mdA in the main implied weights trees, and one single change is found between AMNH 460 and *Brontosaurus* + mdA in the implied weights reduced consensus tree without *Australodocus*. Neither specific nor generic separation of AMNH 460 from its sister groups is thus warranted. The taxonomic affinities of AMNH 460 will be addressed below.

'*Atlantosaurus*' *immanis* YPM 1840 + NSMT-PV 20375. The grouping of these two specimens is only recovered with implied weights. Both specimens are usually interpreted as belonging to *Apatosaurus ajax* (McIntosh, 1995; Upchurch et al., 2004b), but are here found as the most basal

PeerJ Reviewing Manuscript

apatosaurines. Whereas NSMT-PV 20375 occupies the same position in the equally weighted trees, '*Atlantosaurus*' *immanis* YPM 1840 switches to a sister arrangement with the *Apatosaurus ajax* holotype YPM 1860. Overlap is low, as indicated by the index of 15%. Four valid, shared 'synapomorphies' are found (Tab. S98). All four 'synapomorphies' are shared with other apatosaurines, and would thus not qualify as species autapomorphies. Two traits are also present in *Apatosaurus ajax* YPM 1860 (168-0, 426-1), which supports the earlier identifications, and casts additional doubt on the position recovered herein. If a true phylogenetic signal, the two specimens would be separated by one single difference, not allowing specific separation.

Apatosaurinae. Whereas an apatosaurine clade was recovered in all four main trees, composition of it changes. Five putative apatosaur specimens are found outside Apatosaurinae, in a polytomy with the latter clade and Diplodocinae in the equally weighted pruned consensus tree: WDC-FS001A, SMA 0087, FMNH P25112, AMNH 460, and NSMT-PV 20375. When adding them one by one to the reduced consensus, only WDC-FS001A and SMA 0087 result in such a position, indicating that they are the main cause for the large polytomy in the pruned tree. *Amphicoelias altus* is found within Apatosaurinae applying equal weights, but remains outside when using implied weighting. Two unambiguous, one exclusive, 20 shared, and one ambiguous synapomorphies add to a total of 24 synapomorphies recovered for the clade (Tab. S99). Seven of these traits result as synapomorphic for Diplodocidae in the equally weighted pruned tree (135-1, 185-2, 186-1, 216-1, 220-1, 256-0, 275-1), but this is because of the apatosaur specimens recovered outside Apatosaurinae in this tree (135-1, 186-1, 216-1, 220-1, 256-0, 275-1), or the changing positions of *Supersaurus* (185-2). Nine synapomorphies are recovered for the less inclusive *Brontosaurus* + mdA in the implied weight trees, and should thus not be used in diagnoses of Apatosaurinae (259-0, 358-0, 380-2, 391-1, 395-2, 396-1, 400-1, 452-1, 466-2). The reason for the discrepancy is that the specimens found basal to *Brontosaurus* are mostly the ones recovered outside Apatosaurinae in the equally weighted pruned tree. Of the latter nine, two result as synapomorphic for *Eobrontosaurus* + mdA in the equally weighted reduced tree (400-1, 452-1), and seven for the same clade in the implied weights analysis without *Australodocus* (380-2, 391-1, 395-2, 396-1, 400-1, 402-0, 452-1). The high number of synapomorphies for Apatosaurinae contrasts with the low number of generally accepted genera this clade includes (*Apatosaurus*, and possibly *Eobrontosaurus*). This is surprising, when compared to its sister clade Diplodocinae, which includes at least six different genera, but does not appear to be much more divers morphologically. An analysis of morphological disparity would probably be able to quantify the difference, but is out of the scope of this paper. In any case, the numerical approach

PeerJ Reviewing Manuscript

as chosen herein also indicates a higher generic diversity within Apatosaurinae, with at least three, possibly up to six valid genera.

The most basal taxon as recovered by this analysis, would be represented by NSMT-PV 20375 (equal weights) or '*Atlantosaurus*' *immanis* YPM 1840 + NSMT-PV 20375. These specimens are separated from more derived apatosaurs by 14 changes in the case of the equally weighted reduced tree, five in the case of the main implied weights trees, as well as the one without *Australodocus*. This difference is mainly due to the fact that many specimens recovered between *Eobrontosaurus* and NSMT-PV 20375 in the implied weight trees, are not present in the equally weighted reduced consensus tree, in which the 14 changes were found. However, the true number also depends on the systematic position of YPM 1840, which will be discussed in more detail below.

Apatosaurinae + Diplodocinae. The unity of these clades usually corresponds to Diplodocidae, but since the definitions of the two clades are stem-based, as is Diplodocidae (Taylor and Naish, 2005), additional taxa can be recovered basal to Apatosaurinae + Diplodocinae, but still within Diplodocidae. This is the case in the implied weights trees, where *Amphicoelias altus* AMNH 5764 is found to be the basal-most diplodocid. Two unambiguous, four exclusive, and two shared synapomorphies are found for this clade (Tab. S100). Seven of these are also recovered as synapomorphies of Diplodocidae (17-1, 23-1, 25-1, 224-2, 259-1, 263-0, 294-0, 314-1). Two traits are scored differently in *Amphicoelias* (characters 259 and 294), and should thus not be used to diagnose Diplodocidae. The sum of synapomorphies for Apatosaurinae and Diplodocinae is 34.

Diplodocidae. As stated above, the implied weight trees recover *Amphicoelias* as sister taxon to Apatosaurinae + Diplodocinae, and thus as the most basal diplodocid genus. Sixteen synapomorphies are supported by the analysis, three unambiguous, six exclusive, five shared, and two ambiguous (Tab. S101). One of the stated synapomorphies actually only occurs in apatosaurine specimens (216-1), and is recovered as a synapomorphy for that clade by all but the equally weighted pruned tree. It is thus more carefully treated as synapomorphy of Apatosaurinae, and should not be used in diagnoses of Diplodocidae. A similar case is character 259, where the derived state is recovered as diplodocid synapomorphy, but *Amphicoelias* is scored for the plesiomorphic state. If the basal position of *Amphicoelias* is confirmed, the derived state would only diagnose the clade Apatosaurinae + Diplodocinae, as already stated above. *Amphicoelias* – in such a position – is separated from more derived diplodocids by a sum of twelve changes, but only six are actually comparable due to the incomplete condition of the type

PeerJ Reviewing Manuscript

specimen of *Amphicoelias*.

Flagellicaudata. The node-based taxon Flagellicaudata includes Diplodocidae and Dicraeosauridae. It is recovered by all four main trees, and supported by eight unambiguous, three exclusive, eight shared, and three ambiguous synapomorphies (Tab. S102). One of the above mentioned synapomorphies was recovered as diagnosing Diplodocimorpha in the implied weight trees, instead (318-1), because the sprl also extends onto the lateral aspect of the caudal neural spines in rebbachisaurs. Since *Cetiosauriscus* and *Haplocanthosaurus* are recovered as diplodocoid sauropods more derived than rebbachisaurs in the equally weighted analysis, but have reduced caudal sprl, it results a shared synapomorphy of rebbachisaurs and flagellicaudatans. If – as in the trees found by using implied weighting – *Cetiosauriscus* and *Haplocanthosaurus* are found to be more basal to rebbachisaurs, the well-developed caudal sprl become a diagnosing feature for Diplodocimorpha as defined by Taylor and Naish (2005). Proximally closed haemal arches (352-0) are present as well in *Cetiosauriscus stewarti* NHMUK R3078. In the equally weighted pruned tree, where *C. stewarti* is recovered as diplodocoid more than Rebbachisauridae, this feature thus appears synapomorphic for a clade *C. stewarti* + mdD. The same occurs in character 463 describing the presence of a posterolateral projection on the distal condyle of metatarsal I, which is also present in *C. stewarti* and thus becomes a synapomorphy for the slightly more inclusive clade *C. stewarti* + mdD. Within Flagellicaudata, Dicraeosauridae and Diplodocidae are separated by 56 changes.

***Cetiosauriscus* + mdD.** Such a clade is only found with equal weighting, where *Cetiosauriscus stewarti* NHMUK R3078 is recovered in a position between Rebbachisauridae and Flagellicaudata. Three shared synapomorphies support this grouping (Tab. S103). All of these synapomorphies are shared with more basal taxa, close to the position where *Cetiosauriscus* is recovered in the implied weights trees, and are thus not conclusive evidence for diplodocoid affinities of *Cetiosauriscus*. The sum of apomorphies between *Cetiosauriscus* and Flagellicaudata is 30.

***Haplocanthosaurus* + mdD.** This clade corresponds to Diplodocoidea in the implied weights trees, but is more restricted when applying equal weighting. In the latter analysis, *Haplocanthosaurus* is recovered more derived than Rebbachisauridae. Such an arrangement is supported by one exclusive synapomorphy (Tab. S104). However, this feature (324-1) is also present in *Cetiosauriscus*. If the true phylogenetic position of *Cetiosauriscus* would be outside Diplodocoidea, it would thus not be useful anymore to define this clade, and indeed was not found as such in the implied weights analysis. *Haplocanthosaurus* is separated from

PeerJ Reviewing Manuscript

Cetiosauriscus + mdD by 14 changes.

Diplodocimorpha. The present clade is often used in the same way as Diplodocoidea, but in fact has a node-based definition, whereas Diplodocoidea is stem-based (Taylor and Naish, 2005). In the present analyses, Diplodocimorpha is only different from Diplodocoidea when using implied weighting, where *Haplocanthosaurus* is recovered more basal to Rebbachisauridae. In these cases, even the complete strict consensus tree finds Diplodocimorpha. One unambiguous, two exclusive, and one ambiguous synapomorphies are found to be reliable in the implied weights trees (Tab. S105). The semicircular dorsal margin of the ilium (409-1) was the only characteristic also recovered as synapomorphic for Diplodocoidea by equal weighting. One of the synapomorphies was found to diagnose Rebbachisauridae in the equally weighted tree (294-1). The latter clade is distinct from Flagellicaudata (which is the sister taxon to Rebbachisauridae in the implied weight trees) by 27 changes.

Diplodocoidea. The clade Diplodocoidea is represented in all consensus trees but the complete strict consensus tree with equal weighting. Due to the more derived position of *Haplocanthosaurus priscus* in the equally weighted analyses compared to the analysis with implied weights, Diplodocoidea is equivalent to Diplodocimorpha in the former analysis. Synapomorphies recovered include 14 unambiguous, five exclusive, five shared, and one ambiguous traits (Tab. S106). Twenty of the synapomorphies mentioned describe cranial features, which are rarely preserved, as exemplified by the low percentage of ingroup specimens scored: nine of them are only known from less than 20% of all specimens included in the analysis, five from less than 15%. Their assignment as synapomorphies should thus be regarded provisional. The distance between *Haplocanthosaurus* and Diplodocimorpha amounts to 17 changes.

Validity and taxonomic assessment of the holotype specimens

Discussion of the taxonomic affinities of the holotype specimens is ordered based on date of description. By doing so, possible synonymy of the species and genera can be assessed in a more intuitive way. The specimens are listed with the initially proposed name.

***Dystrophaeus viaemalae* USNM 2364.** The phylogenetic position of *Dystrophaeus viaemalae* is dubious, mostly due to its fragmentary remains. In the present analysis, the holotype USNM 2364 was among the six most unstable, and thus pruned taxa in the equally weighted trees. The analysis using implied weighting recovered it consistently as sister taxon to UW 15556, closely related with the holotype of *Elosaurus parvus*. Validity and phylogenetic position of *Dystrophaeus viaemalae* is particularly important because it was the first sauropod to be described from North America, and would thus have priority over any possibly synonymous

PeerJ Reviewing Manuscript

taxon. The present study is the first to include the specimen in a phylogenetic analysis. Earlier studies proposed diplodocid affinities (McIntosh, 1997), but that was mainly based on the plesiomorphically short and robust metacarpals (Upchurch et al., 2004a). The latter did not find any diagnostic feature in the fragmentary material, but refrained to classify *Dystrophaeus* as nomen dubium as it was found very low in stratigraphy, possibly even below the Morrison Formation.

One single, ambiguous autapomorphy was recovered for USNM 2364 (Tab. S107), describing the morphology of the distal radius. The identification of the partial radius as distal is debatable, however, as proximal and distal ends of the radius can be highly similar. McIntosh (1997), for example, identified the same piece as proximal radius, which would render the autapomorphy invalid. As recovered herein, it is shared with specimens from all major taxonomic groups included in the analysis. The fact that two specimens of the same diplodocine genus (*Galeamopus*) are scored differently for this character casts further doubt on its validity as autapomorphy. A single character ties *D. viaemalae* to UW 15556 (Tab. S90). This trait (389-0) is shared with *Omeisaurus*, and possibly affected by deformation. Incompleteness of the specimen inhibits a scoring for any character providing synapomorphies of lower-level clades (below Apatosaurinae) recovered including *Dystrophaeus*. The holotype specimen can be scored for a single character producing a shared synapomorphy of Apatosaurinae (robust metacarpal III), but actually results in a controversial coding (intermediate robustness of metacarpal III), not shown in any other apatosaurine specimen. A differential scoring is also present in an ambiguous synapomorphy of Diplodocidae (posterior centroparapophyseal lamina absent instead of single or double in mid- and posterior dorsal neural arches). However, identification of laminae in the preserved partial dorsal vertebra of *Dystrophaeus* is challenging, because distinction of bone from the still adherent matrix is not made without difficulty. The plesiomorphic coding for this character is furthermore shared by the type specimen *Elosaurus*, which groups with *Dystrophaeus* in the implied weights tree. No synapomorphy of higher-level clades as Flagellicaudata, Diplodocimorpha, or Diplodocoidea can be identified in USNM 2364. This implies that either USNM 2364 is not diagnostic, or not a diplodocoid sauropod. As a macronarian affinity appears to be improbable given the relatively short metacarpals (McIntosh, 1997; Upchurch et al., 2004a), the only reasonable identification would be a non-neosauropod eusauropod.

In order to test these interpretations, constrained tree searches with equal weights were performed forcing USNM 2364 into a position with *Elosaurus parvus* CM 566 and UW 15556 as found by

PeerJ Reviewing Manuscript

5280 the implied weight trees, as well as forcing it into a position outside Diplodocoidea. Minimum
5281 tree length obtained by imposing a grouping of USNM 2364 with CM 566 and UW 15556 is
5282 three steps higher (1900) than the most parsimonious trees (1897), and produces one
5283 synapomorphy recognizable in *Dystrophaeus* as well: distal end of the radius much wider than
5284 midshaft (394-1). The same trait has been identified as synapomorphy for Apatosaurinae (equally
5285 weighted pruned tree) or *Jobaria* + mdE (equally weighted reduced tree). The shortest tree
5286 constraining *Dystrophaeus* to a taxon outside Diplodocoidea resulted from a grouping with
5287 *Lourinhasaurus* or *Omeisaurus*, both producing the same tree length as the most parsimonious
5288 trees (1897). A single synapomorphy supports the grouping with *Lourinhasaurus*: presence of a
5289 subtriangular process on the ventral edge of the scapular blade (370-1) – which is present as well
5290 in several diplodocid specimens. The sister group arrangement with *Omeisaurus* yielded three
5291 synapomorphies: 1) a flat or slightly convex area posterior to the acromial ridge and the distal
5292 blade of the scapula (365-1); 2) the right angle between the two arms of the ulnar proximal
5293 articular surface (389-0); and 3) a beveled distal articular surface of the radius (393-1). Any of
5294 these traits are shared with diplodocid specimens as well. Forcing USNM 2364 into a non-
5295 diplodocoid position by using implied weights yielded a minimal tree length of 188.00488 when
5296 grouping with *Lourinhasaurus*, which is an increase of 0.03274 steps, compared to the most
5297 parsimonious trees. If forced to group with *Omeisaurus*, tree length increases to 188.3466. The
5298 synapomorphy found for *Lourinhasaurus* + *Dystrophaeus* is the same as in the equally weighted
5299 tree (370-1). A length increase of 0.16% is thus needed in the equally weighted trees to force
5300 *Dystrophaeus* into the position recovered with implied weighting, whereas a position outside
5301 Diplodocoidea results in the same length. On the other hand, using implied weighting, a tree
5302 length increase of 0.02% already supports a grouping of *Dystrophaeus* with *Lourinhasaurus*. A
5303 position outside Diplodocoidea seems thus better supported. More detailed studies are needed
5304 including basal Macronaria, Neosauropoda, as well as derived, non-neosauropod Eusauropoda, in
5305 order to resolve phylogenetic relationships of *Dystrophaeus viaemalae* and definitively assess its
5306 taxonomic validity.
5307 ***Amphicoelias altus* AMNH 5764.** The holotype of *Amphicoelias altus* is found in two different
5308 positions in the present analysis. Both positions contrast with the position found by Rauhut et al.
5309 (2005), Whitlock (2011a), Mannion et al. (2012) or Tschopp and Mateus (2013b): whereas it was
5310 found within Diplodocidae in the present analysis, all earlier assessments recovered it more basal
5311 than Dicraeosauridae, mostly even outside Diplodocimorpha (Rauhut et al., 2005; Whitlock,
5312 2011a; Mannion et al., 2012). The strict interpretation of the holotype as used in the present

PeerJ Reviewing Manuscript

analysis (only including the dorsal vertebrae and the femur) possibly increased the diplodocid affinities, even though preliminary analyses recovered them in the same position. The positions recovered herein are in a dichotomy with *Eobrontosaurus yahnahpin* within Apatosaurinae, or as basal-most diplodocid, neither apatosaurine nor diplodocine.

Four ambiguous autapomorphies were considered valid for the holotype, two of them for the position within Apatosaurinae (with equal weighting), and two as basal-most diplodocid (with implied weights; Tab. S108). Nearly horizontal postzygapophyses (275-0) are widespread among sauropods, and thus probably not a meaningful autapomorphy. The 'petal' shape in the posterior dorsal of *A. altus* (294-1) is less developed than in rebbachisaurs and dicraeosaurs, and an additional tree search was performed changing this single character state. In both equal and implied weights analyses, length of the MPTs was increased compared to the main trees (1900 and 188.32214 steps, respectively). Position of *Amphicoelias* remained the same, the interpretation of the neural spine shape is thus without influence. The gracile femur, with its mediolateral width subequal to anteroposterior depth (427-0, 430-0) describes the stove-pipe shape of this element, most often used as the best way to distinguish *Amphicoelias* from other sauropods. In fact, these are the autapomorphies least shared with other taxa. On the other hand, the greatly deformed femur of SMA 0087 shows that ratios like transverse width to anteroposterior depth can be considerably distorted. However, in contrast to SMA 0087, the femur of AMNH 5764 does not show any sign of breakage, indicating that the preserved subcircular cross-section might at least approach the true shape in the living animal. The subcircular femoral cross-section, as well as the 'petal'-shaped posterior dorsal neural spines, and the horizontal posterior dorsal postzygapophyses are all traits shared with dicraeosaurids, whereas only one is shared with a single apatosaurine. In fact, the horizontal posterior dorsal postzygapophyses contrast with the state in all other Apatosaurinae, for which the implied weights analysis recovered a low angle as synapomorphy shared by all apatosaurine specimens. Moreover, *Amphicoelias* does not show an additional otherwise shared synapomorphy of Apatosaurinae: mid- and posterior dorsal parapophyses are not located above the centrum, but anteriorly displaced (256-1, instead of 256-0). One exclusive synapomorphy of Apatosaurinae + Diplodocinae, the accessory laminae in the region between the pcdl and the pcpl of mid- and posterior dorsal vertebrae (259-1) is absent in *Amphicoelias*, but also in *Brontosaurus* + mdA, and in *Eobrontosaurus*. *Amphicoelias* shares the diplodocid synapomorphies of short posterior dorsal transverse processes, and the presence of a lateral bulge on the femur, both of which are not present in any other sampled diplodocoid sauropod. A diplodocid affiliation is thus probable.

PeerJ Reviewing Manuscript

This is also supported by constrained searches testing the position of *Amphicoelias altus* recovered in the alternative analysis. When inhibiting a grouping of *Amphicoelias* with *Eobrontosaurus* in the equally weighted analysis, a tree of one step longer than the original is found (0.05% length increase), but relationships of *Amphicoelias* cannot be established beyond Diplodocidae indet. Tree length for a grouping of *Amphicoelias* and *Eobrontosaurus* using implied weights is 188.13188, which corresponds to a tree length increase of 0.08%. Such a constrain pulls *Amphicoelias* into Apatosaurinae, into the position corresponding to the one found in the equally weighted reduced consensus tree. However, given that relative tree length increase is lower when inhibiting instead of forcing such an interrelationship, the two taxa are herein considered distinct. Based on the lacking apatosaurine synapomorphies of *Amphicoelias*, and given that previous analyses agreed in a more basal position within Diplodocoidea, the position outside Apatosaurinae + Diplodocinae is herein interpreted as more reasonable.

***Amphicoelias latus* AMNH 5765.** All analyses performed agreed in a position of AMNH 5765 within Camarasauridae. *Amphicoelias latus* is generally synonymized with *Camarasaurus supremus*, following Osborn and Mook (1921).

No autapomorphies are found for *Amphicoelias latus*. The synapomorphies of *Camarasaurus* + Turiasauria, not shared with AMNH 5765 are a maximum to minimum mediolateral width of anterior caudal neural spines of 2.0 or greater (327-1), and a fourth trochanter on the femur, which is visible in anterior view (436-1). The first of these synapomorphies has actually been shown to be variable within *Camarasaurus* by Ikejiri (2004). The second is somewhat dubious, as AMNH 5765 was only scored based on the drawings in Cope (1877b) and Osborn and Mook (1921). Of the four synapomorphies recovered for *Camarasaurus* (92-0, 333-1, 392-1, 408-0), AMNH 5765 is not scorable for any of these. Furthermore, given that the present analysis is designed to resolve relationships within Diplodocidae, and that AMNH 5765 is highly incomplete (see above), the more basal position compared to the other two *Camarasaurus* OTUs should not be considered significant. The present result can thus be regarded to corroborate the referral of Osborn and Mook (1921) of the holotype material of *Amphicoelias latus* to *Camarasaurus*.

***Apatosaurus ajax* YPM 1860.** As type specimen of the type species of *Apatosaurus*, YPM 1860 has special taxonomic importance. It is herein always recovered in the same tree branch as *Apatosaurus louisae* CM 3018. This is opposite to the finding of Upchurch et al. (2004b), where *Apatosaurus louisae* formed the sister group to all other apatosaur specimens included.

Six autapomorphies are found for YPM 1860, one of which unambiguous (Tab. S109). Even when excluding the information of the putatively assigned braincase, the unambiguous

PeerJ Reviewing Manuscript

synapomorphy would warrant specific separation. The specimen YPM 1860 can thus be regarded diagnostic, and the species *Apatosaurus ajax* valid. YPM 1860 is thus per definition an apatosaurine diplodocid.

***Apatosaurus grandis* YPM 1901.** The specimen YPM 1901 has long been known not to belong to *Apatosaurus*, but to typify its own species within *Camarasaurus* (Marsh, 1878; Osborn and Mook, 1921; McIntosh et al., 1996a, b; Ikejiri, 2004). It is herein consistently recovered as sister taxon to the genus-level OTU *Camarasaurus*, thereby confirming this identification. Four ambiguous autapomorphies are considered valid (Tab. S110). Specific separation from *Camarasaurus* appears thus well-founded, and more detailed work on camarasaur intrarelationships will definitely produce more differences. *Apatosaurus grandis* is thus referred to *Camarasaurus*, as *Camarasaurus grandis*, with the type specimen being YPM 1901.

***Amphicoelias fragillimus* AMNH 5777.** This specimen was the only putative diplodocid holotype specimen not included into the present analysis. Given that it has been lost shortly after publication (Carpenter, 2006), and that no other material has yet been reported reaching anywhere near the same size as proposed in the initial description (Cope, 1878), it seems unwise to speculate about its phylogenetic position solely based on the single drawing and inadequate description of this extremely fragmentary specimen. *Amphicoelias fragillimus* is thus herein considered a nomen dubium.

'*Atlantosaurus*' *immanis* YPM 1840. Generally considered synonymous to *Apatosaurus ajax* (McIntosh, 1995; Upchurch et al., 2004b), findings of this study are controversial (see above). No recovered autapomorphy for the specimen can be considered valid according to the guidelines established above (Tab. S111). Both sister group arrangements with *Apatosaurus ajax* YPM 1860 and the putative *Apatosaurus ajax* NSMT-PV 20375 do not yield any synapomorphy not shared with any other apatosaur specimen. '*Atlantosaurus*' *immanis* YPM 1840 furthermore could not be scored for the single unambiguous autapomorphy found for *Apatosaurus ajax* YPM 1860 (smooth medial face of bifid posterior cervical neural spines). From the eight shared synapomorphies recovered for the clade *Apatosaurus ajax* + mdA (Tab. S87), only one was scored in YPM 1840, but opposite to the remaining ingroup specimens (C208). YPM 1840 unambiguously classifies as Apatosaurinae due to the divided posterior cervical cprl (185-2), the pcdl and podl of mid- and posterior cervical vertebrae that do not meet anteriorly (186-1), the cervical ribs projecting well beneath centrum (216-1), the bump-like anterior process of cervical ribs (220-1), and the high ratio of the pubic articulation of the ischia to the anteroposterior length of the pubic pedicel (420-1). However, placement within Apatosaurinae remains controversial.

PeerJ Reviewing Manuscript

Forcing YPM 1840 to group with NSMT-PV 20375 (as recovered with implied weighting) in the equally weighted analysis yielded minimal tree lengths of 1 step more than the most parsimonious trees, or a relative length increase of 0.05%. The strict reduced consensus tree shows three more taxa compared to the main equally weighted reduced consensus tree. The most important changes are the following: *Dystrophaeus* is found as most basal titanosauriform, thus further corroborating its non-diplodocoid affinities stated above; and *Brontosaurus excelsus*, together with UW 15556, now form the sister clade to *Apatosaurus ajax* + *Apatosaurus louisae*, which is the same arrangement as seen in the implied weights reduced consensus tree. Synapomorphies found for the union of YPM 1840 and NSMT-PV 20375 are the same as in the main implied weight trees. A constrained search with implied weighting, imposing a sister arrangement of YPM 1840 with YPM 1860 (as found by the equally weighted trees) resulted in a minimal tree length of 188.16879, which corresponds to a relative length increase of 0.1%. Apatosaurine intrarelationships changed considerably: NSMT-PV 20375 was found as sister taxon to YPM 1840 + YPM 1860, and together they formed the sister clade to SMA 0087 + mdA. The specimen AMNH 460 was recovered as most basal apatosaurine. The *Elosaurus parvus* group was pulled out of its relationship with *Brontosaurus excelsus*, and recovered as sister taxon to *Brontosaurus* + mdA, including *Brontosaurus excelsus*, *Brontosaurus amplus*, and *Eobrontosaurus yahnahpin* + FMNH P25112 as successive sister groups to a trichotomy with *Apatosaurus louisae*, *A. laticollis*, and CM 3378. Traits uniting NSMT-PV 20375 with *Apatosaurus ajax* + '*Atlantosaurus*' *immanis* are the following: 1) cervical vertebrae that are much wider than high (128-2); 2) mid-cervical neural spines that are shorter than the neural arches (168-0); 3) posterior dorsal centra wider than high (269-1); 4) the posterior edge of anterior chevrons expands in a step-like fashion (355-1); 5) an almost right angle between the scapular blade and the coracoid articular surface (361-0); 6) a flat or slightly convex area posterior to the acromial ridge and distal scapular blade (365-1); and 7) dorsoventrally expanded distal ends of the ischia (426-1). The low mid-cervical neural spines would qualify as unambiguous synapomorphy, and the dorsoventrally expanded distal end of the ischium would be unique within Apatosaurinae. All other traits are shared with other apatosaur specimens.

To summarize, concerning the phylogenetic position of YPM 1840, the present study best supports a grouping with NSMT-PV 20375, with or without participation of *Apatosaurus ajax* remains to be seen. These uncertainties, as well as the lacking autapomorphies for the specimen suggest that YPM 1840 has to be treated as undiagnostic, and classified as an indeterminate Apatosaurinae. '*Atlantosaurus*' *immanis* is thus a nomen dubium. As it has no taxonomic

PeerJ Reviewing Manuscript

preference, and was usually synonymized with *Apatosaurus ajax*, such a treatment has no influence on apatosaur taxonomy.

***Diplodocus longus* YPM 1920.** Being the type specimen of the type species of the genus *Diplodocus*, validity of it is of particular taxonomic importance. Nonetheless, results obtained herein raise considerable doubts about the diagnosability of the specimen.

Diplodocus longus YPM 1920 consistently groups with the other included specimens of *Diplodocus* in both types of analyses (equal and implied weighting). It is found as sister taxon to *Diplodocus hallorum* in the reduced consensus tree obtained by implied weighting, and is recovered in the same position, when added to the equally weighted reduced consensus tree. In all cases, if the tree also includes one or both specimens of *Diplodocus carnegii* (CM 84 or 94), a polytomy is formed with YPM 1920, the included specimen(s) of *D. carnegii*, and the *D. hallorum* clade. If *D. longus* is excluded, but both *D. carnegii* specimens are added, they form the sister clade to *D. hallorum*. This shows that *D. longus* YPM 1920 switches position between the two specimens of *D. carnegii*, and a position closer to *D. hallorum*, indicating that it is not diagnosable on its own. A single autapomorphy (338-1) was recovered from the main trees, but considered invalid as it is shared with the *Diplodocus* specimen AMNH 223 (Tab. S112). Given that no tree recovers this as a synapomorphy for a clade uniting YPM 1920 and AMNH 223 to the exclusion of all other *Diplodocus* specimens, this feature has probably to be interpreted as individual variation. A constrained search uniting these two specimens yielded an equally weighted tree of 1899 steps, and an implied weights tree of 188.14357 steps. Relative length increase thus amounts to 0.11% and 0.09%, respectively.

Although confidently identifiable as belonging to the same genus as the type specimens of *D. carnegii* and *Seismosaurus hallorum*, YPM 1920 does not appear to be diagnosable to the species level. This would mean that *Diplodocus longus* would have to be considered a nomen dubium, and that consequently also the genus name *Diplodocus* would have to be abolished. As *Diplodocus* is probably one of the most iconic dinosaurs, and generally considered to be one of the best known sauropod genera, based on numerous partly to nearly complete skeletons (McIntosh and Carpenter, 1998; Upchurch et al., 2004a), an abolition of the genus just for the sake of strictly following ICZN rules is not advisable. A case to ICZN is thus being prepared to suggest the suppression of *D. longus* as type species of *Diplodocus*, and its replacement by *D. carnegii*. *D. carnegii* is typified by the nearly complete, and articulated type specimen CM 84, which includes a complete vertebral column from the second cervical to the twelfth caudal vertebra, as well as articulated fore- and hindlimb material. CM 84 is the most famous specimen

PeerJ Reviewing Manuscript

of *Diplodocus*, constituting the largest part of the *Diplodocus* cast sent by Andrew Carnegie to various museums around the world in order to promote the activities of the newly founded Carnegie Museum (Nieuwland, 2010). The greater scientific importance of this specimen compared to the holotype specimen of *D. longus*, YPM 1920, is also exemplified by the fact that important studies of diplodocoid interrelationships do not base on personal observations of YPM 1920, but mainly of CM 84 (e.g. Whitlock, 2011a). This shows that even if further studies would reveal YPM 1920 to be diagnosable, and that *D. longus* would therefore be valid, a suppression of the latter species in favor of CM 84 and *D. carnegii* as type for *Diplodocus* would still make sense due to the wider availability for study, as well as the much higher degree of completeness of the specimen. Consequently, and pending a decision on the prepared case to ICZN, it is hereby suggested to use *D. carnegii* as type species for *Diplodocus*. YPM 1920 is considered not diagnostic at species level, and *Diplodocus longus* has therefore to be regarded a nomen dubium. A similar case was announced by Upchurch and Martin (2003) for the substitution of *Cetiosaurus medius* by *C. oxoniensis* as type species, and submitted in 2009 (Upchurch et al., 2009). Their reasoning leading to the case was almost identical to the one presented herein.

***Brontosaurus excelsus* YPM 1980.** Differences between YPM 1980 and *Apatosaurus ajax* YPM 1860 are usually considered not abundant enough to justify generic distinction (Riggs, 1903), leading to a treatment of *Brontosaurus* as junior synonym of *Apatosaurus* (Riggs, 1903; Gilmore, 1936; McIntosh, 1995; Upchurch et al., 2004a, b). The specimen YPM 1980 is the genoholotype of *Brontosaurus*. Where recovered, it forms the sister taxon to a clade including *Apatosaurus ajax* YPM 1860 and *Apatosaurus louisae* CM 3018.

Four ambiguous autapomorphies are found to be reliable (Tab. S113). One was found to be unique within Diplodocidae (443-1). Given the high number of differences with the *Elosaurus* clade, as well as with the *Apatosaurus ajax* clade, generic separation from both of these genera is herein regarded valid.

Additional support for generic separation and thus a resurrection of *Brontosaurus* as a valid genus comes from the equally weighted tree, and the position recovered for *Amphicoelias altus* therein. *Amphicoelias altus* was described before any other putative apatosaurine genus (Cope 1877a), and would thus have priority over any genus recovered as sister taxon and considered to pertain to the same genus. In the equally weighted reduced consensus tree, *Amphicoelias altus* + *Eobrontosaurus yahnahpin* form the sister clade to *Apatosaurus ajax* + *Apatosaurus louisae*. When adding *Brontosaurus excelsus* to the tree, a trichotomy is formed between *Brontosaurus*, *Amphicoelias* + *Eobrontosaurus*, and *Apatosaurus*. If *Brontosaurus* would be considered

PeerJ Reviewing Manuscript

synonymous to *Apatosaurus* in such an arrangement, *Apatosaurus* would have to be synonymized with *Amphicoelias* according to ICZN rules. The specimen YPM 1980 is thus herein considered diagnosable, and distinct enough to justify generic separation from *Apatosaurus*.

***Apatosaurus laticollis* YPM 1861.** Based on a single, fragmentary, mid- to posterior cervical vertebra, this specimen is one of the least complete included in the analysis. McIntosh (1995) suggested it to come from the same individual as YPM 1840, but evidence from two partial femur elements suggest that more than one individual was present in the quarry (McIntosh, 1995). The fact that no tree of the present analysis shows a sister taxon arrangement of YPM 1840 and 1861 casts further doubts on the proposal of McIntosh (1995). *A. laticollis* YPM 1861 is herein consistently found as most closely related to *A. louisae* CM 3018 and CM 3378. If true, and if YPM 1861 is considered diagnosable, this would indicate that the two species would be synonymous, and that *A. laticollis* would therefore have priority over *A. louisae*.

One ambiguous autapomorphy is found for *Apatosaurus laticollis* YPM 1861, which is unique within Apatosaurinae (Tab. S114). However, as only two traits distinguish *A. laticollis* from *A. louisae*, specific separation cannot be justified, and the two traits are more cautiously interpreted as individual variation, at least in the present species. The fact that the two shared synapomorphies for CM 3018 + CM 3378 (and thus YPM 1861 as well) could not be scored in YPM 1861 indicates that the latter specimen does not exhibit any taxonomically significant character for the species it forms together with CM 3018 and CM 3378.

Forcing *Apatosaurus laticollis* YPM 1861 into close relationship with YPM 1840 (following McIntosh, 1995), recovered tree lengths are 1898 (length increase of 0.05%) with equal weighting, and 188.34011 (relative increase of 0.2%) with implied weighting. In both analyses, YPM 1861 is pulled into the clade where YPM 1840 was found in the unconstrained search. The fact that YPM 1861 readily changes position further indicates that it is not diagnosable to species level, and that *A. laticollis* has to be considered a nomen dubium. Pending further detailed studies of the specimens YPM 1840 and 1861, YPM 1861 is herein referred to *A. louisae*.

***Brontosaurus amplus* YPM 1981.** *Brontosaurus amplus* YPM 1981 is often considered synonymous to *Brontosaurus excelsus* (McIntosh, 1995; Upchurch et al., 2004b), although mostly stating that further studies are needed in order to assess its taxonomic affinities. The present study does not allow a much more detailed assessment, mostly because of limited personal observations of the specimen due to time constraints during the collection visit at YPM. However, some conclusions can be drawn from the trees recovered. Although not present in the equally weighted reduced consensus tree, addition of the specimen results in a polytomy with

PeerJ Reviewing Manuscript

Apatosaurus louisae + CM 3378, *Eobrontosaurus* + *Amphicoelias*, and *Apatosaurus ajax* + YPM 1840. In the implied weights trees, *Brontosaurus amplus* does not group with *Brontosaurus excelsus*, but with *Apatosaurus louisae*.

Two ambiguous autapomorphies were recovered for YPM 1981 (Tab. S115). However, the four changes separating YPM 1981 from *Apatosaurus louisae* do not allow specific separation (see above). Also the polytomy recovered when adding *A. laticollis* to the reduced consensus tree obtained by implied weights indicates that all four specimens (CM 3018, CM 3378, YPM 1861, and YPM 1981) might belong to the same species. More detailed studies of YPM 1981 would be needed in order to confirm presence or absence of the five synapomorphies found for the clade uniting these four specimens. Although no apatosaurine synapomorphies can be positively identified in YPM 1981 to date, the robust humerus (380-2) and astragalus (452-1) suggest that an identification of *B. amplus* as apatosaur more derived than *Eobrontosaurus* or *Brontosaurus* can be stated with some confidence.

Constraining the search to trees recovering a clade with *Brontosaurus excelsus* and *B. amplus* expulses both *Apatosaurus ajax* and *A. louisae* from the equally weighted reduced consensus tree. Tree length is 1898 steps, and three major clades are recovered within Apatosaurinae: the previously unrecognized combination of FMNH P25112 + (SMA 0087 + AMNH 460) forms the sister taxon to *Elosaurus* + *Brontosaurus*, which include CM 566 + UW 15556, and YPM 1980 + YPM 1981, respectively. When one of the *Apatosaurus* specimens is added, a large polytomy is formed including many diplodocine specimens as well. The same constraint in the implied weights analysis yields trees of a length of 187.98825 steps, which is only 0.01% longer than the most parsimonious trees. Several changes are introduced to apatosaurine interrelationships: SMA 0087 forms a clade together with AMNH 460, *Elosaurus parvus* CM 566 + UW 15556 are separated from *Brontosaurus*, and form the sister clade to *Apatosaurus ajax* + mdA, the two *Brontosaurus* type specimens form the sister group to *Apatosaurus ajax*, together forming the sister clade to *Eobrontosaurus* + (FMNH P25112 + (*Apatosaurus louisae* + CM 3378)). However, no valid synapomorphies unite YPM 1980 with YPM 1981 in that tree, and only one of the four found synapomorphies for the clade uniting them with *Apatosaurus ajax* is found as well in YPM 1981: the presence of a ridge on the ventral side of the third sacral rib (288-1). The latter trait has been proposed by Mook (1917), but regarded as unreliable for species identification within *Apatosaurus* by Upchurch et al. (2004b). Given this, although tree length is not increased much by the current constraint, morphological support for the recovered arrangement appears low. A closer relationship with *Apatosaurus louisae* seems thus better supported by the present

PeerJ Reviewing Manuscript

analysis, but since YPM 1981 cannot be scored for any of the recovered species autapomorphies, it has to be considered a nomen dubium, pending restudy. It is tentatively referred to *Apatosaurus louisae*.

***Diplodocus lacustris* YPM 1922.** Marsh (1884) established this species based on more slender teeth compared to the ones present in the skull USNM 2672. Whereas this appears to be true (Tab. S16), both specimens are within the minimum and maximum values of the teeth of the skull CM 11161, which was only found after Marsh's death (Holland, 1924). The specimen YPM 1922 was found to be the least stable in both main analyses, being mainly responsible for the large polytomy within Diplodocoidea in the complete strict consensus tree.

Given that no characters are known that would allow an identification of diplodocid teeth at species level, and that both the premaxilla and maxilla referred to the type specimen are not diplodocid (see above), the teeth of the holotype specimen YPM 1922 can only be identified as Diplodocidae indet. *D. lacustris* should thus be regarded as a nomen dubium. It is thus also not available as type specimen for the substitution of the suppressed *D. longus* YPM 1920. The choice of *D. carnegii* and CM 84 to typify *Diplodocus* is thus further supported.

***Elosaurus parvus* CM 566.** The specimen CM 566 is a very juvenile individual, as exemplified by its small size and the lacking neurocentral fusion (Peterson and Gilmore, 1902; McIntosh, 1995; Upchurch et al., 2004b; Schwarz et al., 2007c). Until recently, it was generally referred to *Brontosaurus excelsus*, together with the adult specimen UW 15556, with which it was found (Gilmore, 1936; McIntosh, 1995). By means of a specimen-based phylogenetic analysis, Upchurch et al. (2004b) showed that specific separation of CM 566 and UW 15556 from other apatosaur species is justifiable. Recovered autapomorphies for the species were also shown in the juvenile specimen CM 566, leading Upchurch et al. (2004b) to propose the new combination *Apatosaurus parvus*. The present analysis also consistently recovers CM 566 together with UW 15556, and confirms the validity of the species autapomorphies found by Upchurch et al. (2004b), as well as their presence in CM 566. Position in the trees is generally close to the holotype of *Brontosaurus excelsus* (YPM 1980). Whereas at first sight, this might corroborate synonymy of *Elosaurus parvus* with *Brontosaurus excelsus*, the high number of differences between the two taxa not only allows specific, but also generic distinction (see above). *Elosaurus* is thus considered a valid genus, with *Elosaurus parvus* as its type species, and CM 566 as its genoholotype.

***Gigantosaurus africanus* various specimen numbers.** The holotype specimen of *Gigantosaurus africanus* consists of several bones excavated in the first expedition to Tendaguru, Tanzania, now

PeerJ Reviewing Manuscript

housed at the Staatliches Museum für Naturkunde in Stuttgart, Germany. More elements from the same individual were found later and brought to the Museum für Naturkunde in Berlin, Germany (Remes, 2006). The taxon has a complex taxonomic history: *Gigantosaurus* being preoccupied, it was later renamed *Tornieria* (Sternfeld, 1911), and then synonymized with *Barosaurus* (Janensch, 1922). After a thorough redescription and study of all preserved material, Remes (2006) re-established it as the separate genus *Tornieria*, in the combination *Tornieria africana*, adapting the latinized species name to the female genus. Its generic distinction from *Barosaurus* has been shown to hold in phylogenetic analyses as well (Remes, 2006; Whitlock, 2011a; Mannion et al., 2012). The current study confirms this separation. Skeleton A, from which the holotype material is a part of, consistently clusters with a second specimen referred to the same species by Remes (2006), skeleton k, also from Tendaguru. Both together form a relatively basal clade within Diplodocinae, in many cases the most basal one. Five shared synapomorphies unite the two specimens (Tab. S77), although only one of these qualifies as species autapomorphy (420-1), as all other four are shared with other diplodocine specimens. The holotype specimen is thus diagnosable at species level, and *Tornieria africana* a valid species.

***Apatosaurus louisae* CM 3018.** The type specimen of *A. louisae* is the most complete type specimen of the entire clade of Apatosaurinae. It is also one of the few diplodocid holotypes which has been decently described and figured (Gilmore, 1936). CM 3018 is thus probably the best known and most used reference specimen for *Apatosaurus*, even though it is not its genoholotype. In the recovered main trees, it consistently groups with CM 3378 and *A. laticollis* YPM 1861, with which it forms the sister clade to *A. ajax*.

Even though it is so complete, only one ambiguous 'autapomorphy' was found for the single specimen (Tab. S116). This indicates that the other specimens grouping with CM 3018 belong to the same species. As *Apatosaurus laticollis* is herein considered a nomen dubium, the only available species name for this group is *A. louisae*, as initially proposed for CM 3018 (Holland, 1915a). The specimen CM 3018 shows all the five 'synapomorphies' found for the clade with CM 3018, CM 3378, YPM 1861, and YPM 1981 (see above). Of these, three qualify as valid autapomorphies for the species, not shared with any other apatosaur specimen (see updated diagnosis below). Following the numerical approach, generic separation from *A. ajax* is not justified, corroborating previous referrals of CM 3018 to *Apatosaurus*, as *A. louisae*.

***Apatosaurus minimus* AMNH 675.** *Apatosaurus minimus* was described by Mook (1917), based on a sacrum and pelvic girdle. The specimen has generally been considered misidentified, and its diplodocoid affinities rejected (McIntosh, 1995; Upchurch et al., 2004b). Whereas pubis

PeerJ Reviewing Manuscript

morphology strongly resembles *Camarasaurus*, the presence of six sacral vertebrae and widely splayed preacetabular lobes of the ilium are generally considered titanosauriform characteristics (McIntosh, 1990a; Upchurch et al., 2004a, b). Due to its incompleteness, the true identity of AMNH 675 still remains dubious. Other than confirming the non-flagellicaudatan (and probably non-diplodocoid) affinities of AMNH 675, the present study does not help much in resolving this issue. Whereas the equally weighted trees recovered AMNH 675 as one of the six most unstable taxa (thus deleted from the pruned consensus), implied weighting resolves AMNH 675 as somphospondylian titanosauriform, based on the two characteristics mentioned above. The three autapomorphies found for the specimen indicate that AMNH 675 probably shows a unique combination of features. Addition of AMNH 675 to the equally weighted reduced consensus tree results in a polytomy with *Cetiosauriscus stewarti*, SMA 0009, AMNH 5765, Titanosauriformes, *Camarasaurus* + Turiasauria, Rebbachisauridae, and Flagellicaudata.

Forcing *Apatosaurus minimus* AMNH 675 into a titanosauriform position in the equally weighted analysis results in a tree three steps longer than the most parsimonious tree. *Dystrophaeus* is pulled into Titanosauriformes as well, and *Australodocus* is recovered as basal-most Diplodocinae. The same tree length is found when imposing apatosaurine affinities, with a completely unresolved clade as result. Camarasaurid affinities are much more probable, given that a forcing into this group yields the same tree length as the equally weighted most parsimonious trees (1897 steps). Furthermore, also the presence of six sacral vertebrae has already been reported in a camarasaur (Tidwell et al., 2005), and was interpreted as an ontogenetic feature. Tree length of the implied weight trees increase to 188.23185 steps, or by a percentage of 0.14%, when restricting AMNH 675 to Apatosaurinae (where it grouped with *Dystrophaeus* and *Elosaurus*), and to 188.18066 (0.11%) when forcing it into Camarasauridae. Camarasaurid or titanosauriform affinities are thus the most probable for AMNH 675, but more detailed studies of those clades are needed in order to identify AMNH 675 properly.

***Diplodocus hayi* HMNS 175.** Described by Holland (1924) as *Diplodocus hayi*, HMNS 175 (initially CM 662) was often thought not to belong to *Diplodocus* (e.g. McIntosh, 1990b; Foster, 1998; Harris, 2006c), due to its relatively robust forelimbs, and the widely diverging basipterygoid processes – both traits that are generally interpreted to diagnose apatosaurs (Berman and McIntosh, 1978; McIntosh, 1990a; Upchurch et al., 2004a). The specimen HMNS 175 is one of the most complete specimens known from Diplodocinae, but has never been completely described. It preserves cranial material, cervical, dorsal, sacral, and caudal vertebrae, as well as a nearly complete forelimb and hindlimb (McIntosh, 1981; ET, pers. obs., 2010). The

PeerJ Reviewing Manuscript

current analysis supports a generic separation from *Diplodocus*, as HMNS 175 consistently results in a clade more basal to *Diplodocus*, together with the specimens AMNH 969 and SMA 0011. It is therefore herein referred to the new genus *Galeamopus*, of which it is the genoholotype specimen.

Autapomorphies for HMNS 175 amount to four (Tab. S117), one of which unique within Diplodocidae (392-0), and a second one within Diplodocoidea (387-2). Forcing *Galeamopus hayi* HMNS 175 to group with the classical *Diplodocus* specimens, equally weighted analysis recovers shortest trees of 1904 steps, a length increase of seven steps of 0.37% compared to the unconstrained most parsimonious trees. Applying implied weights, tree length counts 188.70122 steps, corresponding to a relative increase of 0.39%. A generic separation from *Diplodocus* is thus well-supported.

'*Apatosaurus*' *alenquerensis* MIGM various numbers (lectotype). As *Tornieria africana*, also '*Apatosaurus*' *alenquerensis* has had a complicated taxonomic history. After being referred to *Camarasaurus* (McIntosh, 1990b), Dantas et al. (1998) erected the new genus *Lourinhasaurus* for a number of specimens thought to belong to the same species. No specific type specimen was attributed to the name (only a skeleton was mentioned without specimen number; Dantas et al., 1998), until Antunes and Mateus (2003) established the first specimen found at Moinho do Carmo, Alenquer, Lourinhã, as lectotype specimen. In the meantime, the specimen on which Dantas et al. (1998) made most observations of differences between *Lourinhasaurus* and *Camarasaurus* was redescribed and referred to a new species and genus, *Dinheirosaurus lourinhanensis* (Bonaparte and Mateus, 1999). Even so, *Lourinhasaurus* remained accepted, and its generic separation subsequently justified by means of phylogenetic analyses, which did not recover the lectotype specimen in a position close to *Camarasaurus* or *Apatosaurus* (e.g. Upchurch et al., 2004a; Royo-Torres and Upchurch, 2012).

Two ambiguous autapomorphies are found to diagnose *Lourinhasaurus* (Tab. S118). The fact that *Lourinhasaurus* consistently forms its own clade in any recovered tree indicates that it also exhibits a unique combination of traits. The lectotype specimen is thus considered diagnostic, and *Lourinhasaurus alenquerensis* valid.

Forcing *Lourinhasaurus* into the Camarasauridae clade, equal weighting results in a tree only one step longer than the most parsimonious trees. *Lourinhasaurus* is found to be in the turiasaur clade, not supported by any synapomorphy. Implied weighting recovers *Lourinhasaurus* basal to *Camarasaurus* + Turiasauria, with a tree length of 188.03513, an increase of 0.03%. A close relationship with *Camarasaurus* can thus not be excluded, although generic separation is

PeerJ Reviewing Manuscript

probably warranted. Although the precise phylogenetic position of *Lourinhasaurus* cannot be resolved herein, a position at the base of Neosauropoda appears the most supported.

***Cetiosauriscus stewarti* NHMUK R3078.** Phylogenetic position of *Cetiosauriscus stewarti* has been debated (Charig, 1980; McIntosh, 1990b; Heathcote and Upchurch, 2003; Upchurch et al., 2004a). Diplodocid affinities were purported several times (Charig, 1980; McIntosh, 1990b; Upchurch et al., 2004a), but mostly based on a second specimen containing a whip-lash tail, which has no overlapping bones with the holotype (Heathcote and Upchurch, 2003; Upchurch et al., 2004a). Diplodocid affinities of the holotype specimen are thus questionable, and consequently, a closer relationship to *Mamenchisaurus* or *Omeisaurus* was found by Heathcote and Upchurch (2003). The current analysis recovers NHMUK R3078 in two different positions depending on the weighting strategy applied. Equal weighting yields diplodocimorph affinities, more derived than Rebbachisauridae, whereas implied weighting recovers NHMUK R3078 as non-neosauropod eusauropod, close to *Mamenchisaurus* or *Omeisaurus* as proposed by Heathcote and Upchurch (2003).

No autapomorphies were found by the implied weights analysis, probably due to the sister relationship with *Barosaurus affinis* YPM 419. The incompleteness of the latter find inhibited the recovery of autapomorphies in its sister taxon *Cetiosauriscus*, as for many features the two specimens are not comparable. However, the recovered autapomorphies from the equally weighted trees were assessed in two ways, and their validity was tested based on both diplodocoid as well as non-neosauropod eusauropod affinities. Three traits qualified as ambiguous autapomorphy in both cases (Tab. S119). The fact that autapomorphies were found reliable independent from the phylogenetic position indicates that NHMUK R3078 is diagnosable, and *Cetiosauriscus stewarti* thus valid.

Imposing a sister arrangement of *Cetiosauriscus* and *Barosaurus affinis* YPM 419 in the equally weighted tree does not increase length, nor influence the position of *Cetiosauriscus*. Forced sister arrangements with *Omeisaurus* and *Mamenchisaurus* produced tree lengths of 1900 and 1903 steps or length increases of 0.16% and 0.32%, respectively. When forcing *Cetiosauriscus* into Apatosaurinae or Diplodocinae with implied weighting, tree lengths of 188.80886 or 189.29031 steps are recovered (length increase of 0.45% or 0.7%). Imposing dicraeosaurid or rebbachisaurid affinities results in tree lengths of 188.72199 or 188.99738, corresponding to an increase of 0.4% or 0.55%. Consequently, changing the position from diplodocoid to non-neosauropod eusauropod in the equally weighted tree (in particular close to *Omeisaurus*) is easier than imposing diplodocoid affinities of *Cetiosauriscus* in the implied weights analysis. *Cetiosauriscus stewarti*

PeerJ Reviewing Manuscript

5742 is thus herein interpreted as non-diplodocoid eusauropod, possibly closely related to *Omeisaurus*,
5743 as already proposed by Heathcote and Upchurch (2003).
5744 ***Supersaurus vivianae* BYU 12962.** The holotype specimen of *Supersaurus vivianae* is restricted
5745 to a scapula (Jensen, 1985), but other elements from the same quarry most probably belong to the
5746 same individual (Curtice and Stadtman, 2001; Lovelace et al., 2007). A scapula is not present in
5747 the second specimen referred to *Supersaurus vivianae* by Lovelace et al. (2007; WDC DMJ-021),
5748 which inhibited recognition of autapomorphies on the scapula by TNT. However, the fact that
5749 both referred specimens consistently group together in all trees indicates that identification of
5750 additional elements as belonging to the same individual as the type specimen (Curtice and
5751 Stadtman, 2001; Lovelace et al., 2007) was right. Even though the holotype might not be
5752 diagnostic, the individual it is part of definitely is.
5753 No valid autapomorphies separate the type individual from the second specimen, WDC DMJ-
5754 021, indicating that they belong to the same species. Of the seven traits uniting the two specimens
5755 (Tab. S79), only three can be considered valid autapomorphies for the species (231-0, 296-1, 307-
5756 0), as the other four also occur in other diplodocine specimens.
5757 *Supersaurus vivianae* forms a clade together with *Dinheirosaurus* when applying equal
5758 weighting, whereas implied weighting recovers it together with *Australodocus*, in a position more
5759 basal to *Dinheirosaurus*, and even *Tornieria*. The fact that trees excluding *Australodocus* a priori,
5760 or restricting it to Titanosauriformes, show *Supersaurus* again as sister taxon to *Dinheirosaurus*,
5761 in its more derived position, indicates that the change is mainly due to the instability of
5762 *Australodocus*. Furthermore, when restricting *Supersaurus* to *Dinheirosaurus* in the implied
5763 weights trees, *Australodocus* is again recovered within Titanosauriformes. Tree length in this case
5764 is 188.02344, which is even shorter than the trees recovered when forcing *Australodocus* directly
5765 into Titanosauriformes (188.09844). The former tree length equals a length increase of 0.03%,
5766 which corresponds to less than a one-step increase in the equally weighted trees. The position
5767 more derived than *Tornieria* appears thus better supported by the present analysis, even though
5768 this is contrary to the findings of Whitlock (2011a), Mannion et al. (2012), or Tschopp and
5769 Mateus (2013b).
5770 ***Dystylosaurus edwini* BYU 4503.** The holotype specimen of *Dystylosaurus edwini* was
5771 previously proposed to belong to the same individual as the *Supersaurus vivianae* holotype
5772 scapula (Curtice and Stadtman, 2001), a view supported by Lovelace et al. (2007), as well as
5773 preliminary analyses of the present study (see above). Therefore, *Dystylosaurus edwini* is herein
5774 considered a junior synonym of *Supersaurus vivianae*. Its type specimen BYU 4503 has thus not

PeerJ Reviewing Manuscript

been included in the final analysis as separate slot, but was incorporated into the OTU called *Supersaurus vivianae* BYU+.

***Seismosaurus halli* NMMNH 3690.** Gillette (1991) named this new genus based on the specimen NMMNH 3690, and later changed to species name to *hallorum*, in order to correct it for wrongly applied latin grammar (Gillette, 1994). *Seismosaurus* was later synonymized with *Diplodocus* (Lucas et al., 2006; Lovelace et al., 2007), with uncertainties if it can be retained as separate species or if it should be regarded synonymous to *Diplodocus longus* (Lovelace et al., 2007). The latter statement was most probably based on previous identifications of the more complete specimens AMNH 223 and USNM 10865 as *Diplodocus longus* (Osborn, 1899; Gilmore, 1932), which was herein showed to be erroneous, or at least questionable. *Seismosaurus hallorum* NMMNH 3690 is consistently recovered in a group with AMNH 223, USNM 10865, and DMNS 1494, which has been shown to constitute its own species. Showing four of the six shared traits of the group, *Seismosaurus hallorum* NMMNH 3690 can be considered diagnostic. As it is the only type specimen in this cluster, and since the number of changes does not allow generic separation (see above), *Diplodocus hallorum* is the only valid, available name for this taxon.

***Dyslocosaurus polyonychius* AC 663.** Being based on very fragmentary appendicular material, assessment of the phylogenetic position is difficult for this taxon. Although initially described as diplodocid (McIntosh et al., 1992), the high number of probable pedal unguals resembles basal sauropods, as the loss of pedal phalanges and unguals is usually considered typical for Eusauropoda and more derived forms (Wilson, 2002; Upchurch et al., 2004a). However, almost no complete and articulated pes is known from any diplodocid, and of the included specimens, only few preserve pedal material. A positive confirmation of the absence of vestigial phalanges or unguals is very difficult, if not impossible. The true distribution of a high number of pedal phalanges can thus not be assessed with the present analysis.

Although reduced consensus trees omit *Dyslocosaurus polyonychius*, both pruned trees find it as dicraeosaurid. Five synapomorphies found for Dicraeosauridae are present in *Dyslocosaurus*, but four of them are only shared with one other dicraeosaurid taxon (431-1, 443-1, and 452-1 are shared with *Dicraeosaurus*; 477-1 is shared with *Suuwassea*; and 461-0 is shared with *Dicraeosaurus* and *Suuwassea*). None of these traits could be coded in *Amargasaurus* or *Brachytrachelopan*, and all of them are also present in certain diplodocid taxa. If *Dyslocosaurus* should not be a dicraeosaurid, only the gracility of the metatarsal I (461-0) would possibly remain as dicraeosaurid synapomorphy, pending further finds of dicraeosaurid hindlimb material.

PeerJ Reviewing Manuscript

Five ambiguous autapomorphies are found for AC 663 when considered a dicraeosaurid (Tab. S120). Three of these autapomorphies are shared with apatosaur specimens (442-1, 468-1, 470-1), four also occur in diplodocines (442-1, 446-0, 456-1, 468-1). The fact that this specimen appears to unite apatosaur, diplodocine, and dicraeosaurid traits indicates that AC 663 – even though highly incomplete – is diagnostic, and *Dyslocosaurus polyonychius* thus a valid taxon. Forcing *Dyslocosaurus* into a position within Apatosaurinae produced shortest trees of a length of 1902 (equal weighting) and 188.17813 (implied weighting) steps, an increase of 0.26% and 0.11%, respectively. When imposing diplodocine affinities, tree lengths of 1910 and 189.51146 steps are recovered, corresponding to length increases of 0.69% and 0.82%. Diplodocine affinities are thus the least parsimonious, followed by an identification as Apatosaurinae, which still appears improbable. Despite the shared characters with both diplodocid clades, an identification of *Dyslocosaurus* as dicraeosaurid diplodocoid is considerably better supported.

***Apatosaurus yahnahpin* Tate-001.** *Apatosaurus yahnahpin* Tate-001 has been renamed *Eobrontosaurus yahnahpin* (Bakker, 1998), but it was never included in any phylogenetic analysis, and no detailed description has yet been published. Based on purportedly primitive conditions in the pectoral girdle and the cervical ribs, Bakker (1998) interpreted *Eobrontosaurus* as the basal-most apatosaurine. Upchurch et al. (2004a) stated that the specimen Tate-001 is practically indistinguishable from *Camarasaurus*, but personal comments of R. Wilhite (cited in Taylor et al., 2011) and P. Mannion (2012) implied that the taxon might be a valid diplodocid. The present analysis confirms this: Tate-001 is consistently recovered as apatosaurine diplodocid. Whereas it forms the sister taxon to *Amphicoelias altus* in the equally weighted tree, its position within the clade is less clear when applying implied weighting: *E. yahnahpin* is found as sister taxon to *Apatosaurus ajax* + mdA in the main trees, whereas an a priori deletion or forced titanosauriform affinities of *Australodocus* result in a more basal position of *E. yahnahpin*, as sister taxon to AMNH 460 + mdA.

Eight ambiguous autapomorphies are considered valid for Tate-001 (Tab. S121). Whereas this already justifies specific separation, support for generic separation depends on the position where it is recovered (see above). The least support for generic distinction is found if recovered as sister taxon to *Amphicoelias* (five changes), followed by the tree without *Australodocus* (nine changes). As *Amphicoelias* is more parsimoniously considered the basal-most diplodocid genus, instead of an Apatosaurinae, distance between *Eobrontosaurus* and its sister clade *Apatosaurus ajax* + mdA in the equally weighted tree increases to 16. Given that it is generally found as single slot, *Eobrontosaurus* is herein accepted as valid genus within Apatosaurinae.

PeerJ Reviewing Manuscript

Forcing *Eobrontosaurus* to lie outside AMNH 460 + mdA in the implied weight trees resulted in tree lengths of 188.00659 steps, an increase of 0.02%. Position of *Eobrontosaurus* is thus not very clear to date, and has to await publication of the promised detailed description.

***Dinheirosaurus lourinhanensis* ML 414.** *Dinheirosaurus lourinhanensis* ML 414 was first described as *Lourinhasaurus alenquerensis* (Dantas et al., 1998), but a more detailed redescription showed that it constitutes its own genus within Diplodocidae (Bonaparte and Mateus, 1999). Such a position was later confirmed by phylogenetic analyses, and refined to Diplodocinae (Rauhut et al., 2005; Whitlock, 2011a; Mannion et al., 2012). The present analysis supports this assignment, but recovered *Dinheirosaurus* in an even more derived position than Whitlock (2011a) or Mannion et al. (2012). Both analyses find *Dinheirosaurus* in a position within Diplodocinae, more derived than *Tornieria*. Differences occur in the relative position of *Supersaurus*, although a position as sister genus of *Dinheirosaurus* appears more probable, as discussed above.

Four ambiguous autapomorphies are found for ML 414, and thus for *Dinheirosaurus lourinhanensis* (Tab. S122). The ten changes found between *Dinheirosaurus* and *Supersaurus* or (in the case of a more basal position of the latter) *Galeamopus* + mdD are considered enough to justify generic separation, especially given that *Dinheirosaurus* is a Portuguese taxon, and thus also geographically separated from its closest relatives.

***Losillasaurus giganteus* MCNV Lo-5.** Whereas the holotype is restricted to an anterior caudal vertebrae, it actually belongs to a more complete individual (Casanovas et al., 2001) and was included as such in the present analysis. Initially regarded a basal diplodocoid (Casanovas et al., 2001), *Losillasaurus* was soon found to represent a non-diplodocoid, probably non-neosauropod eusauropod (Rauhut et al., 2005; Harris, 2006c). With the description of *Turiasaurus* (Royo-Torres et al., 2006), which has since been consistently recovered as sister genus to *Losillasaurus* (Royo-Torres et al., 2006, 2009; Barco, 2009; Carballido et al., 2012b; Royo-Torres and Upchurch, 2012), the more basal position has been generally accepted. The present study supports this view as well.

Two ambiguous autapomorphies are found (Tab. S123). Despite the low number of autapomorphies, the numerical approach is not applied here, as non-diplodocid OTUs have not been sampled with enough detail to apply the same standards as established for Diplodocidae. *Losillasaurus* is thus considered herein a valid, non-diplodocoid genus, probably a non-neosauropod eusauropod.

***Suuwassea emilieae* ANS 21122.** *Suuwassea emilieae* was initially described as indeterminate

PeerJ Reviewing Manuscript

PeerJ Reviewing Manuscript

flagellicaudatan (Harris and Dodson, 2004). Whereas earlier studies showed more diplodocid affinities (Gallina and Apesteguia, 2005; Rauhut et al., 2005; Remes, 2006; Lovelace et al., 2007), the discovery of the dentary of the holotype specimen (Whitlock and Harris, 2010) subsequently resulted in an identification as dicraeosaurid (Whitlock, 2011a; Mannion et al., 2012; Tschopp and Mateus, 2013b). The present analysis supports the latter assignment: *Suuwassea emilieae* ANS 21122 is consistently found as basal-most dicraeosaurid sauropod. *Suuwassea emilieae* ANS 21122 is herein diagnosed by 35 ambiguous autapomorphies (Tab. S124). The high number of autapomorphies for *Suuwassea emilieae* reflect not only its diagnosability, but also the fact that the main dicraeosaurid OTUs were not studied in the same detail as the diplodocid sauropods. Given that the majority of the found autapomorphies are shared with certain diplodocid specimens, the difficulties in determining its dicraeosaurid affinities are not surprising. However, forcing *Suuwassea* into an apatosaurine clade (as found by Lovelace et al., 2007) yields trees of 1907 or 189.58814 steps (relative length increases of 0.53% and 0.86%, respectively). Diplodocine relationships are found in shortest trees of 1903 and 189.21056 steps, corresponding to increases in tree length of 0.32% and 0.66%. Apatosaurine or diplodocine affinities are thus much less parsimonious than an identification as dicraeosaurid.

***Australodocus bohetii* MB.R.2455.** Whereas the holotype only includes the single cervical vertebra MB.R.2455, a second, probably adjacent cervical vertebrae most probably belongs to the same animal (MB.R.2454; Remes, 2007). *Australodocus* was first described as diplodocid (Remes, 2007), but later found to represent a titanosauriform (Whitlock, 2011a, c; Mannion et al., 2012, 2013). The present analysis shows ambiguous results, with the equal weights analysis recovering it as brachiosaurid titanosauriform, but implied weighting finding diplodocine affinities. The incompleteness of the type individual complicates the recovery of a stable position for *Australodocus*.

Of the autapomorphies recovered for *Australodocus*, only two were found by both analyses (Tab. S125). Both of these autapomorphies are shared with diplodocine specimens. In general, autapomorphies recovered for a brachiosaurid position are shared with diplodocines, and autapomorphies found for a diplodocine position with titanosauriforms. This indicates that the combination of traits is unique in *Australodocus*, which is thus regarded valid.

As mentioned in the discussion of *Supersaurus*, *Australodocus* pulls the former genus into a more basal position in the main implied weight trees. When forcing *Supersaurus* into a monophyletic group with *Dinheirosaurus*, *Australodocus* is recovered again as a brachiosaurid titanosauriform. The latter constrained search produced shortest trees of 188.02344 (a 0.03% length increase),

whereas diplodocine affinities for *Australodocus* in the equally weighted trees finds trees of a length of 1898 steps, one more compared to the most parsimonious trees (an increase of 0.05%). In this case, however, *Supersaurus* remains united with *Dinheirosaurus*, instead of grouping with *Australodocus* as in the most parsimonious implied weight trees. The low number of titanosauriform OTUs in the present specimen lowers the capability of the analysis to recover *Australodocus* as belonging to that taxon, such that convergences found with Diplodocinae tend to become more important. Given that *Australodocus* is still recovered as titanosauriform in many trees, and that relative tree length increase to impose diplodocine affinities is slightly higher than the inverse direction in the implied weight trees, indicates that an identification as titanosauriform is more probable. Addition of titanosauriform specimens preserving cervical vertebrae would help to resolve this problem, but is not the scope of this analysis.

***Kaatedocus siberi* SMA 0004.** *Kaatedocus siberi* was initially described as diplodocine less derived than *Tornieria*, *Diplodocus*, and *Barosaurus* (Tschopp and Mateus, 2013b). In the present analysis, *Kaatedocus* is consistently recovered in a more derived position, as sister taxon to *Barosaurus lentus*.

The type specimen SMA 0004 bears one ambiguous 'autapomorphy' (a transverse ridge on the basal tubera; Tab. S126). As no 'synapomorphy' was found for the sister clade AMNH 7530 + SMA D16-3, only one change separates SMA 0004 from the latter. The presence of such a transverse ridge is thus better interpreted as individual variation. Four of the nine 'synapomorphies' found for the entire group of *Kaatedocus siberi* qualify as species autapomorphies, not shared with other diplodocine specimens (178-1, 202-1, 211-1, and 212-1; Tab. S64).

***Galeamopus* [redacted] SMA 0011.** *Galeamopus* [redacted] is herein reported and described for the first time and thus no comparisons with earlier studies exist. The holotype specimen SMA 0011 consistently groups with the holotype of *Galeamopus hayi*, HMNS 175, and the skull previously identified as *Diplodocus*, AMNH 969 (Holland, 1906).

The specimen SMA 0011 shows four ambiguous and three unambiguous autapomorphies, justifying specific separation from *Galeamopus hayi* (Tab. S127). One of these, the horizontal canal connecting the preantorbital and the antorbital fenestra (12-1) was not recovered by the analysis, as the state in AMNH 969 or HMNS 175 cannot be discerned due to incomplete preservation. The trait could thus also be diagnostic for a more inclusive taxon, possibly the genus *Galeamopus*.

Taxonomic affinities and identification of diplodocid non-type specimens

PeerJ Reviewing Manuscript

AMNH 223. Described as *Diplodocus longus* (Osborn, 1899), AMNH 223 readily became the reference specimen for this species (Hatcher, 1901; Gilmore, 1932). However, the present analysis does not recover AMNH 223 together with the holotype specimen YPM 1920, but as most basal OTU of a clade including the holotype of *Seismosaurus hallorum*.

Two ambiguous 'autapomorphies' are found for this specimen (Tab. S128), which describe scapular morphology. The fact that only one of the other three specimens in the same clade preserves a scapula, and the low number of differences between AMNH 223 and the remaining triplet, indicates that these might represent individual variation, and that AMNH 223 is most parsimoniously identified as belonging to the same species, which would be *Diplodocus hallorum*.

AMNH 460. The specimen AMNH 460 has never been described, but was included in the specimen-level phylogenetic analysis of Upchurch et al. (2004b). In the latter, it has been identified as *Apatosaurus ajax*, which is not supported by the most parsimonious trees of the present analysis. In the equally weighted pruned tree, AMNH 460 is pulled outside Apatosaurinae due to unresolved relationships with SMA 0087 and WDC-FS001A. When applying implied weights, AMNH 460 is found within Apatosaurinae, as single slot between YPM 1840 + NSMT-PV 20375 and SMA 0087 + WDC-FS001A. When excluding *Australodocus* from Diplodocidae, AMNH 460 changes position within Apatosaurinae, and forms the sister taxon to *Brontosaurus* + *Apatosaurus*, still as single slot. The found positions would imply that AMNH 460 represent a different taxon, but the fact that no found 'autapomorphy' is unique within Apatosaurinae (Tab. S129) makes such an assignment questionable.

A constrained search forcing AMNH 460 into the clade including *Apatosaurus ajax* YPM 1860 yielded trees of a length of 1902 or 188.54847 steps, corresponding to relative length increases of 0.26% or 0.31%. AMNH 460 continues to be found as a single slot, more basal to *Apatosaurus ajax* YPM 1860. Imposed brontosaur affinities for AMNH 460 result in tree lengths of 1903 and 188.31076 steps, or relative increases of 0.32% and 0.18%. A sister clade arrangement with *Eobrontosaurus* produces tree lengths of 1900 and 188.10509 steps, relative increases of 0.16% and 0.07%. In both cases, the pair is recovered basal to the clade *Brontosaurus* + mdA. When forced into a triplet with SMA 0087 and WDC-FS001A, tree length stayed the same (1897) or increased by 0.01%, to 187.98825 steps. Equal weighting finds trees of 1903 steps (0.32% longer) if constrained by a unity of AMNH 460 with NSMT-PV 20375, whereas implied weighting results in trees 0.05% longer (188.06943 steps) if constraining the triplet AMNH 460, NSMT-PV 20375, and YPM 1840. A closer relationship with the specimens SMA 0087 and

PeerJ Reviewing Manuscript

WDC-FS001A can thus not be excluded by the present analysis. Such a triplet would be supported by the following three ambiguous synapomorphies: 1) posterior dorsal centra longer than high (268-0, unique within Apatosaurinae); 2) a widely rounded cnemial crest of the tibia, in anterior view (444-0, unique within Apatosaurinae); and 3) the posterior surface of the tibial cnemial crest bears a distinct fibular trochanter (445-1, unique within Apatosaurinae). It thus possibly represents a yet unknown, apatosaurine taxon. However, none of the specimens included have yet been completely described, and it thus refrained herein to establish a new name at the moment. Relative positions are considered too unstable to confidently suggest a new taxon.

AMNH 969. This skull was generally considered to belong to *Diplodocus* (Holland, 1906, 1924; Berman and McIntosh, 1978), probably due to strong resemblances with the purported skulls of *Diplodocus longus* USNM 2672 and 2673. However, the latter two specimens cannot be confidently referred to the type species, as there is no overlap with the type specimen YPM 1920 (McIntosh and Carpenter, 1998). Furthermore, given the few differences in skull morphology between diplodocine and apatosaurine species, even less can be expected within one of the two clades only. Indeed, the present analysis recovers AMNH 969 consistently with the two type specimens of *Galeamopus hayi* and *G.* [redacted] indicating that it belongs to this genus. Constrained searches support this assignment, as a forced inclusion in *Diplodocus* yields shortest trees of 1901 or 188.61461 steps, a relative increase of 0.21% or 0.34%, respectively.

One ambiguous 'autapomorphy' is found that distinguishes AMNH 969 from the other two specimens (Tab. S130). As the clade formed by the other two *Galeamopus* specimens does only show one shared synapomorphy, differences between the species are not enough to justify erection of a third species. When forcing AMNH 969 to group with either of the two species of *Galeamopus*, tree lengths for a *G. hayi* assignment are 1900 (equal weighting) and 188.21024 (implied weighting) steps, whereas affinities with *G.* [redacted] are found with trees of a length of 1898 (equal weighting) and 188.1269 (implied weighting) steps. The skull and first two cervical vertebrae of AMNH 969 are thus herein tentatively referred to *Galeamopus* [redacted] The more squared snout of AMNH 969, compared to SMA 0011 might indicate a higher individual age of AMNH 969 (Whitlock et al., 2010).

AMNH 6341. The specimen AMNH 6341 is the most complete specimen generally considered to be a *Barosaurus lentus*. As it is completely prepared, and appears largely undeformed (in contrast to the type specimen YPM 429), AMNH 6341 has generally been used as reference specimen for the genus (see Whitlock, 2011a). Although it was found early after the discovery of the Carnegie Quarry at what was later to be named Dinosaur National Monument (McIntosh, 2005), it was

PeerJ Reviewing Manuscript

6006 only described by McIntosh (2005), but still not in a very detailed way.
6007 In the present analysis, AMNH 6341 was consistently found as sister taxon to the holotype
6008 specimen of *Barosaurus lentus*, YPM 429. Given that all the recovered 'autapomorphies' cannot
6009 be considered valid (Tab. S131), AMNH 6341 is most parsimoniously interpreted to belong to the
6010 same species as YPM 429. Previous assignments to *Barosaurus lentus* are thus corroborated by
6011 the current analysis.
6012 **AMNH 7530.** The specimen AMNH 7530 was never described but is labeled *Barosaurus* sp. on
6013 display at AMNH. It is herein consistently recovered together with *Kaatedocus siberi* SMA 0004.
6014 No autapomorphies are found for the specimen, probably due to the fragmentary preservation of
6015 the specimen with which it forms a dichotomy (the partial skull SMA D16-3). Differences
6016 between AMNH 7530 and SMA 0004 exist in the shape of the dorsal edge of the parietal (C62),
6017 in the orientation of the longest axes of the basal tubera (C87), and in the development of the pre-
6018 epipophyseal anterior spur (C167). However, the sum of recovered 'autapomorphies' between the
6019 specimens is too low to justify specific separation. The mentioned differences are thus interpreted
6020 as individual variation, contrary to the interpretation in Tschopp and Mateus (2013b), where the
6021 anterior spur of the pre-epipophysis was stated as autapomorphic for the species *Kaatedocus*
6022 *siberi*.
6023 Forcing AMNH 7530 in a position with the other sampled *Barosaurus* specimens increased tree
6024 length by 0.42% (equal weighting) and 0.4% (implied weighting), to 1905 and 188.73208 steps,
6025 respectively. Such an assignment is thus considerably less parsimonious than an referral to
6026 *Kaatedocus siberi*.
6027 **AMNH 7535.** As AMNH 7530, also AMNH 7535 was tentatively identified as *Barosaurus* in the
6028 AMNH data base, but was never described. In contrast to the specimen AMNH 7530, here
6029 identified as *Kaatedocus*, AMNH 7535 consistently groups with other *Barosaurus* specimens in
6030 the present analysis.
6031 No autapomorphies were recovered for the specimen, and as stated above, the sum of differences
6032 between AMNH 7535 and its sister clade CM 11984 + mdD is too low to establish specific
6033 separation. Obvious differences between AMNH 7535 and the holotype specimen YPM 429 (as
6034 transverse width, or size of the cervical vertebrae) are herein interpreted to represent a
6035 combination of ontogenetic variation, deformation, and serial variation within the cervical
6036 column. AMNH 7535 is thus referred to *Barosaurus lentus*.
6037 **CM 94.** This specimen was designated the paratype of *Diplodocus carnegii* (Hatcher, 1901). It
6038 complements the knowledge of *Diplodocus carnegii* in crucial parts as the mid-caudal vertebrae

PeerJ Reviewing Manuscript

(thus allowing comparisons with the holotype specimen of *D. longus* YPM 1920), and appendicular elements. When pruning YPM 1920 from the complete consensus trees, CM 94 is consistently recovered as sister taxon to the holotype specimen of *D. carnegii*, CM 84.

Three 'autapomorphies' are found reliable for the specimen CM 94 (Tab. S132). Of these, only one (366-1) can be compared with CM 84, as the other two describe pedal morphology, and CM 84 does not preserve a pes. The sum of comparable differences thus amounts to one (no valid 'autapomorphies' were found for CM 84), and referral to the same species and thus an assignment of CM 94 as paratype for *Diplodocus carnegii* is justified.

CM 3378. The specimen CM 3378 was found together with the holotype of *Apatosaurus louisae* at Dinosaur National Monument, and preserves the most complete vertebral column of any of the specimens included herein (McIntosh, 1981). Nonetheless, it has only been described and figured in parts (Holland, 1915b; Gilmore, 1936). It was included into the specimen-based phylogenetic analysis of Upchurch et al. (2004b), and resulted as specimen of *Apatosaurus louisae*. As none of the recovered 'autapomorphies' for CM 3378 can be considered valid (Tab. S133), the present analysis confirms this interpretation.

CM 3452. The specimen CM 3452 is one of very few preserving an almost complete skull in articulation with the first few cervical vertebrae. It was reported as juvenile to subadult *Diplodocus* specimen (Holland, 1924; McIntosh and Berman, 1975; Whitlock et al., 2010), but never described in detail. A referral to *Diplodocus* is questionable, as almost no overlapping material exists between CM 3452 and any type specimen of *Diplodocus*. Now that generic separation from *Diplodocus* is confirmed for *Galeamopus hayi*, the only *Diplodocus* type specimen preserving anterior cervical vertebrae is CM 84. With the description of two additional specimens preserving articulated skulls and cervical vertebrae (SMA 0004 and 0011), affinities of CM 3452 can be assessed more accurately. The present analysis consistently recovers CM 3452 as sister taxon to *Kaatedocus siberi* + *Barosaurus lentus*.

A single 'autapomorphy' was found valid for CM 3452 (Tab. S134). Summed differences between CM 3452 and its sister clade amount to four, not justifying specific separation. Constrained searches were thus performed in order to evaluate the most parsimonious identification. Forcing CM 3452 into *Diplodocus*, following earlier identifications, equal weighting finds shortest trees of 1905 steps, and implied weighting 188.82961 steps – relative length increases of 0.42% and 0.46%, respectively. Imposed affinities with *Kaatedocus* yield trees with a length of 1903 and 188.44375 steps, corresponding to an increase in length of 0.32% and 0.25%. A forced inclusion into the *Barosaurus* clade results in length increases of 0.11% and 0.04%, to 1899 and 188.04743

PeerJ Reviewing Manuscript

steps, respectively.

In the case of affinities to *Barosaurus*, CM 3452 is recovered as the basal-most specimen, united with the remaining quartet by the presence of an accessory horizontal lamina in the center of the spinodiapophyseal fossa of mid- and posterior cervical vertebrae, not connected with any surrounding lamina (187-1). This trait is shared with all included *Barosaurus* specimens but AMNH 7535, which was not scorable for this character. The only other diplodocine specimen showing the same development is *Diplodocus carnegii* CM 94. Distance between CM 3452 and the more derived clade amounts to a single difference, which does not allow specific separation. Therefore, CM 3452 is herein tentatively referred to *Barosaurus lentus*.

CM 11161. This skull-only specimen is generally referred to *Diplodocus* (Holland, 1915b, 1924; McIntosh and Berman, 1975; Berman and McIntosh, 1978; Whitlock et al., 2010; Whitlock and Lamanna, 2012), and has been used in numerous publications as model for feeding strategies or other ecological or behavioral studies concerning this genus (e.g. Haas, 1963; Barrett and Upchurch, 1994; Calvo, 1994; Upchurch and Barrett, 2000; Whitlock, 2011b; Young et al., 2012). However, as no overlap exists with any of the type specimens of *Diplodocus*, referral to that genus remains controversial. Given that all skulls with articulated vertebrae are herein identified as other diplodocine species (AMNH 969 and SMA 0011 as *Galeamopus* [redacted] CM 3452 as *Barosaurus lentus*, SMA 0004 as *Kaatedocus siberi*), only indirect evidence can be used for such an assignment, as exemplified by the present analysis, which is not able to resolve the position of CM 11161 due to the lacking overlap.

Two ambiguous 'autapomorphies' are found for the specimen (Tab. S135). One of these traits (61-0) was scored as unknown in the other putative *Diplodocus* skull, USNM 2672, due to lacking measurements. In another skull not included in the present analysis, the mean ratio is 1.4 (USNM 2673), thus resembling CM 11161. The short posteroventral process of the jugal, however, is not present in USNM 2672 (ET, pers. obs., 2011) and CM 11255, a putative juvenile *Diplodocus* skull (Whitlock et al., 2010; but see above).

Constrained searches were performed forcing CM 11161 to group with diplodocine taxa preserving articulated skull material. Imposed relationships with *Galeamopus* produced trees 0.16% and 0.18% longer than the most parsimonious trees, with lengths of 1900 and 188.31381 steps, respectively. A forced assignment to *Kaatedocus* yielded shortest trees of 1911 and 189.77095 steps, a relative increase in length of 0.74% and 0.96%. When constraining CM 11161 to group with *Barosaurus*, tree length increases by 0.58% and 0.62%, reaching 1908 and 189.12979 steps. Given that all these alternative assignments increase tree length by at least three

PeerJ Reviewing Manuscript

steps (or almost the equivalent to it in implied weight trees), a referral to *Diplodocus* still remains the most parsimonious identification. However, given that nearly complete specimens including articulated skulls, vertebrae from anterior cervical to distal caudal elements, as well as appendicular elements including manual and pedal material are known from *Galeamopus*, the latter genus appears more appropriate as representative of the diplodocine clade in phylogenetic analyses.

CM 11984. The specimen CM 11984 was partly described as *Barosaurus lentus* by McIntosh (2005), but is largely unprepared. The present analysis finds CM 11984 in all most parsimonious trees as sister taxon to *Barosaurus lentus* YPM 429 + AMNH 6341.

'Autapomorphies' recovered for the specimen were all shared with other diplodocine specimens, and thus not considered reliable (Tab. S136). The four 'synapomorphies' found for the sister clade *Barosaurus lentus* YPM 429 + AMNH 6341 (Tab. S61) are thus not enough to erect a new species within *Barosaurus*. Therefore, McIntosh's (2005) referral of this specimen to *Barosaurus lentus* is herein corroborated.

DMNS 1494. Although undescribed, DMNS 1494 is often considered a *Diplodocus longus* (McIntosh, 1981; Gillette, 1991), probably based on similarities with AMNH 223, the specimen described as *D. longus* by Osborn (1899). As the latter identification was herein rejected, also the referral of DMNS 1494 to *D. longus* appears questionable. In the present analysis DMNS 1494 is consistently found as sister taxon to USNM 10865.

A single ambiguous 'autapomorphy' was found for the specimen (Tab. S137). As this is the only valid difference between DMNS 1494 and USNM 10865 (Tab. S67), the two are considered to belong to the same species. Following the reasoning stated above, this species will be *Diplodocus hallorum*.

FMNH P25112. The current specimens is one of the few non-type specimens, which was described (Riggs, 1903). Riggs (1903) referred it to *Apatosaurus excelsus* (herein reinterpreted as *Brontosaurus excelsus*), an identification which was accepted by Gilmore (1936). Upchurch et al. (2004b) recovered FMNH P25112 as a single OTU, proposing that it might belong to its own species within *Apatosaurus*. In the present analysis, FMNH P25112 is recovered in the same position as *Brontosaurus excelsus* when adding it to the equally weighted reduced consensus tree, whereas it groups with *Elosaurus* and *Dystrophaeus* in the implied weights pruned consensus tree.

Forcing FMNH P25112 into the clade with *Apatosaurus ajax* YPM 1860 (together with YPM 1840 in the equally weighted analysis, but alone when using implied weighting), tree lengths

PeerJ Reviewing Manuscript

increase by 0.47% with equal weighting and 0.19% in the analysis with implied weights, to 1906 and 188.38266 steps, respectively. Imposing a dichotomy with *Brontosaurus excelsus* YPM 1980, shortest trees measure 1903 and 188.17315 steps, an increase of 0.32% and 0.11%. A grouping with *Elosaurus parvus* as proposed by the implied weights trees increases equally weighted tree lengths by 0.11%, to 1899 steps. When restricting FMNH P25112 to *Eobrontosaurus*, trees lengthen by 0.16% or 0.02%, to a length of 1900 or 188.01343 steps. A forced relationship with the putative new taxon including AMNH 460, SMA 0087, and WDC-FS001A (see above) is supported by trees of a length of 1897 or 188.11135 steps, a relative increase of 0% or 0.07% compared to the most parsimonious trees. Finally, imposing a relationship with NSMT-PV 20375 in the equally weighted trees, or with NSMT-PV 20375 and YPM 1840 in the implied weights trees produces shortest trees of 1897 or 187.99160 steps, respectively, corresponding to increases of 0% or 0.01%. According to these values, several different referrals appear similarly parsimonious: an identification as *Elosaurus*, as belonging to the same taxon as AMNH 460, SMA 0087, and WDC-FS001A, or as NSMT-PV 20375, possibly together with YPM 1840.

A single synapomorphy supports an assignment to *Elosaurus* (274-0). The quartet FMNH P25112, AMNH 460, SMA 0087, and WDC-FS001A would be united by the two synapomorphies diagnosing SMA 0087 + WDC-FS001A (444-0, 445-1). However, both FMNH P25112 and AMNH 460 could not have been scored for these two characters. The unity of FMNH P25112 with NSMT-PV 20375 in the equally weighted tree would yield one synapomorphy (420-0). The triplet FMNH P25112, NSMT-PV 20375, and YPM 1840 in the implied weight trees is not supported by any valid synapomorphy. Taking all this together, an assignment to *Elosaurus* appears to be the best supported. Therefore, pending further studies on the involved specimens, FMNH P25112 is tentatively referred to *Elosaurus parvus*.

MB.R. skeleton k. Skeleton k is the second individual referred to *Tornieria africana* by Remes (2006). The individual includes a braincase (MB.R.2386), which was interpreted to not belong to that taxon by Harris (2006a). However, based on preserved quarry maps, referral to the same individual appears justified (Heinrich, 1999; Remes, 2006). The present analysis consistently recovers skeleton k with the holotype individual of *Tornieria africana*. As no autapomorphy was found distinguishing skeleton k from skeleton A, Remes' (2006) referral to the same species is herein corroborated.

ML 418. Consisting of very fragmentary material, ML 418 was identified as one of the six most unstable taxa in the equally weighted analysis. It was referred to *Dinheirosaurus* by Antunes and Mateus (2003), and later assigned to *Apatosaurus* sp. by Mateus (2005). Mannion et al. (2012)

PeerJ Reviewing Manuscript

noted that it cannot be confidently identified as either of these two taxa, as it lacks their autapomorphic traits, and identified it as indeterminate diplodocid. When added to the equally weighted reduced consensus tree, ML 418 produces a polytomy at the base of Diplodocinae, together with SMA 0011, *Galeamopus hayi* HMNS 175, AMNH 969, the two *Tornieria* skeletons, the clade uniting *Dinheirosaurus* with *Supersaurus*, and *Diplodocus* + mdD. In the most parsimonious implied weights trees, ML 418 occupies the most basal position within Diplodocinae, but switches to a position within the clade of *Dinheirosaurus* and *Supersaurus* when excluding *Australodocus* or restricting it to Titanosauriformes.

One ambiguous 'autapomorphy' is found for the specimen (Tab. S138). The fact that the sum of differences between ML 418 and the remaining diplodocines is just two does not allow an identification as separate species. Constrained searches forcing ML 418 into a dichotomy with *Dinheirosaurus* (as suggested by Antunes and Mateus, 2003) produce equally weighted trees of a length of 1900 steps, whereas implied weighting finds shortest trees of 188.09487 steps, corresponding to length increases of 0.16% and 0.07%, respectively. In both cases, no synapomorphies are found for the clade uniting them. This implies that Mannion et al. (2012) were right in considering it a possible second diplodocid taxon, although not diagnosable based on the preserved material. As ML 418 shows two shared synapomorphies of Diplodocinae (218-1, 283-1) and does not exhibit any of Apatosaurinae (275-0 instead of 275-1), it is herein considered an indeterminate Diplodocinae.

NSMT-PV 20375. The specimen NSMT-PV 20375 was described by Upchurch et al. (2004b) and identified as *Apatosaurus ajax*, by means of a specimen-based phylogenetic analysis. In the present analysis, it is never found in close relationship with the holotype specimen of *Apatosaurus ajax*. In fact, NSMT-PV 20375 consistently occupies the most basal position within Apatosaurinae, alone in the equally weighted trees, or together with YPM 1840 in the implied weights trees. A single, ambiguous 'autapomorphy' is recovered for NSMT-PV 20375 (Tab. S139).

Forcing NSMT-PV 20375 into a dichotomy together with YPM 1840 with the equally weighted analysis yielded trees one step longer (1898; 0.05%) than the most parsimonious trees. The resulting reduced consensus tree recovered *Elosaurus parvus*, *Apatosaurus ajax*, and *Apatosaurus louisae* in the same relative positions as the shortest implied weights trees. Imposing a grouping with *Apatosaurus ajax*, as found by Upchurch et al. (2004b) produced trees of 1899 and 188.10818 steps, a relative increase of 0.11% and 0.07%. In both cases, it has YPM 1840 as sister taxon, and the triplet is positioned relatively basal within Apatosaurinae, detached from

PeerJ Reviewing Manuscript

Apatosaurus louisae. The same results are obtained when forcing the entire triplet (NSMT-PV 20375, YPM 1840 and YPM 1860) to cluster together, thus not imposing a sister taxon relationship between NSMT-PV 20375 and YPM 1860 a priori. The most parsimonious interpretation thus seems the arrangement found by the implied weights trees, with NSMT-PV 20375 and YPM 1840 forming the basal-most taxon within Apatosaurinae. It thus seems that two more, previously unrecognized taxa are present within Apatosaurinae. However, support for such a separation is low, and more detailed studies are needed to confirm such a hypothesis. No additional taxa shall thus be named herein.

SMA 0087. The specimen SMA 0087, yet unreported, but from the same quarry as SMA 0011, forms a clade together with WDC-FS001A – in the cases when the analysis is able to resolve their position. In the equally weighted pruned tree, SMA 0087 is found outside Apatosaurinae, as also if added to the equally weighted reduced consensus tree. On the other hand, implied weighting finds SMA 0087 + WDC-FS001A within Apatosaurinae, more derived than NSMT-PV 20375 + YPM 1840.

No valid 'autapomorphy' is found by the present analysis (Tab. S140), but both shared synapomorphies between SMA 0087 and WDC-FS001A would qualify as species autapomorphies (444-0, 445-1), given that they are not shared with any other apatosaurine specimen. Apatosaurine affinities are indicated for SMA 0087 by the presence of two shared (256-0, 275-1) and two ambiguous synapomorphies (235-1, 250-0) of the clade. The absence of one exclusive (307-0 instead of 1) and three shared synapomorphies of Diplodocinae (283-0, 330-0, 332-0 instead of 283-1, 330-1, and 332-1) implies that an identification as apatosaurine is more probable.

When forcing SMA 0087 into a dichotomy with WDC-FS001A in the equally weighted trees, tree length does not increase, but SMA 0087 + WDC-FS001A remains in a trichotomy with Apatosaurinae and Diplodocinae. Imposing apatosaurine affinities, two large polytomies are found to form the clade, with SMA 0087, WDC-FS001A, FMNH P25112, and AMNH 460 being the sister clade to a polytomy with all other apatosaurine specimens. Tree length is 1898, one step more than in the most parsimonious trees. When forcing SMA 0087 into Diplodocinae, tree length stays the same, and SMA 0087 is recovered together with WDC-FS001A as the most basal diplodocine taxon. Five synapomorphies are found for Diplodocinae in such a case, but only one of these would be shared by all diplodocines, and not be present in any apatosaurine specimen: a subtriangular proximal articular surface of the tibia. However, the latter trait is not recognizable in the badly distorted tibia of SMA 0087. Given that previously established synapomorphies of

PeerJ Reviewing Manuscript

Apatosaurinae and Diplodocinae favor an apatosaurine identification of SMA 0087, the latter is herein preferred over an assignment to Diplodocinae.

SMA D16-3. This partial skull has not been described in detail yet. It is herein consistently found as *Kaatedocus siberi*. No autapomorphies were found in any of the trees. A referral to *Kaatedocus siberi* is thus warranted.

SMA O25-8. The second isolated partial skull (besides SMA D16-3) from Howe Quarry exhibits both internal and external differences in braincase morphology, compared with the *Kaatedocus siberi* specimens (Schmitt et al., 2013). Being identified as one of the four most unstable taxa, it was excluded from all most parsimonious pruned and reduced consensus trees. When added, it consistently groups within the *Kaatedocus* + *Barosaurus* clade, but outside *Kaatedocus siberi*. The specimen SMA O25-8 can be confidently identified as Diplodocidae due to the hook-shaped posterior process of the prefrontal and the slightly concave posterior face of the basal tubera, and as Diplodocinae given the box-like basal tubera and the presence of a basipterygoid recess. It is included in the *Kaatedocus* + *Barosaurus* clade based on the distinct nuchal fossae on the parietal, and the ridge on the posterior face of the paroccipital process.

Forcing SMA O25-8 into *Barosaurus lentus* does not increase tree length, but a confident assignment to this taxon is hampered by the lack of overlap with definitive *Barosaurus lentus* specimens. Indeed, recovered consensus trees show one large polytomy including all of the specimens. When further including CM 3452 into *Barosaurus lentus* (following the identification of CM 3452 above), tree lengths increase by 0.42% (equal weighting) and 0.31% (implied weighting), to 1905 and 188.55338 steps, respectively. Imposing a clustering with *Kaatedocus siberi* also does not increase tree length, but no synapomorphies are found for an inclusion into *Kaatedocus siberi*. Taking all the information into account, SMA O25-8 can be confidently identified as derived diplodocine, most closely related to either *Kaatedocus* or *Barosaurus*. The fact that a unity of CM 3452, SMA O25-8 and the definitive *Barosaurus* specimens is relatively unparsimonious indicates that a third taxon might be present, or that morphological variety within *Kaatedocus* might be higher than acknowledged at present. Pending further studies, and given the differences found between SMA O25-8 and the known *Kaatedocus* braincases, SMA O25-8 is herein still tentatively referred to *Barosaurus*.

USNM 2672. The specimen USNM 2672 is the second skull usually identified as *Diplodocus* included in the study. It also preserves a partial atlas. The problem for a confident identification of USNM 2672 remains the same as in CM 11161, as no definitive *Diplodocus* specimen is known with either atlas or skull.

PeerJ Reviewing Manuscript

No 'autapomorphy' was found in the equally weighted pruned consensus tree, the only tree to include USNM 2672. Nonetheless, the specimen can be confidently identified as diplodocid due to the broad contact between maxilla and quadratojugal, the large preantorbital fenestra, the concave dorsal margin of the antorbital fenestra, the medially curving anteromedial corner of the prefrontal, the hook-shaped posterior process of the prefrontal, the slightly concave posterior face of the basal tubera, the absence of a coronoid eminence, as well as absence of direct crown-to-crown occlusion in the teeth. Diplodocine affinities are confirmed by the box-like basal tubera. The same constrained searches are performed as for CM 11161, in order to test affinities with species for which cranial material is known. Affinities with *Galeamopus* are found in trees of a length of 1900 or 188.43524 steps (an increase of 0.16% or 0.25%). Forcing an inclusion into the *Kaatedocus* clade yields trees of a length of 1911 and 189.61024 steps, corresponding to a 0.74% and 0.87% length increase. When imposing an assignment to the clade uniting *Kaatedocus*, *Barosaurus*, and CM 3452, the trees are lengthened by 0.11% and 0.13%, reaching 1899 and 188.21381 steps. Taking everything together, USNM 2672 appears to be most parsimoniously referred to *Diplodocus*, but it remains unknown to what species.

USNM 10865. On display at USNM, the specimen USNM 10865 is the second, relatively complete skeleton referred to *Diplodocus longus* after AMNH 223 (Osborn, 1899; Gilmore, 1932). It has been partially described by Gilmore (1932). In the present analysis, USNM 10865 consistently forms a dichotomy with DMNS 1494.

No valid 'autapomorphy' is found for the present specimen (Tab. S141), and as stated above, specific distinction from DMNS 1494, AMNH 223, and most importantly the holotype of *Seismosaurus hallorum*, NMMNH 3690, is not warranted. As *Seismosaurus* was synonymized with *Diplodocus*, the specimen USNM 10865 is herein referred to the species *Diplodocus hallorum*.

UW 15556. Described in detail by Hatcher (1902) and Gilmore (1936), the specimen UW 15556 (previously CM 563) is one of the best known apatosaur specimens. It was often referred to *Apatosaurus excelsus* (Hatcher, 1902; Gilmore, 1936; McIntosh, 1981, 1995), but recently found to constitute its own species within *Apatosaurus*, together with the holotype of *Elosaurus parvus*, CM 566 (Upchurch et al., 2004b). Upchurch et al. (2004) thus proposed the new combination *Apatosaurus parvus.* However, as showed earlier, generic separation of the two specimens can be justified due to several differences with the recovered sister taxon *Brontosaurus excelsus*. The specimen UW 15556 is thus herein referred to *Elosaurus parvus*.

WDC DMJ-021. The specimen WDC DMJ-021 was described by Lovelace et al. (2007), and

PeerJ Reviewing Manuscript

identified as *Supersaurus vivianae*. Herein, it is always found together with the BYU specimen of *Supersaurus vivianae*, thus confirming the assignment of Lovelace et al. (2007).

No valid 'autapomorphies' for the specimen are found by any of the trees (Tab. S142), but seven shared synapomorphies unite the two specimens of *Supersaurus* (Tab. S79). Three of them are unique within Diplodocinae, and can be considered autapomorphies of the species.

WDC-FS001A. Only the manus of the present specimen has been described in detail (Bedell and Trexler, 2005). The specimen was identified as *Diplodocus* cf. c*arnegii*, based on morphology of a caudal vertebra, which was different from the specimens generally considered '*Diplodocus longus*', and the general slenderness of the appendicular bones (Bedell and Trexler, 2005). The implied weights analysis finds WDC-FS001A together with SMA 0087, for which apatosaurine affinities are more probable than diplodocine (see above). On the other hand, equal weighting is not able to resolve the relationships of WDC-FS001A, finding affinities with both Apatosaurinae and Diplodocinae.

Two ambiguous 'autapomorphies' are found for WDC-FS001A, both of them shared with *Diplodocus* specimens (Tab. S143). Apatosaurinae affinities are ambiguous, as WDC-FS001A shares one shared synapomorphy (476-1), but does not exhibit an ambiguous synapomorphy of the clade (402-1 instead of 0). The first of these is shared with *Diplodocus hallorum* USNM 10865, whereas the second is also present in the basal apatosaurine NSMT-PV 20375.

Information is also ambiguous concerning diplodocine synapomorphies: whereas WDC-FS001A shows one shared synapomorphy (330-1), a second one is absent (332-0 instead of 1). Here, the first trait also occurs in apatosaurine specimens, but the second one is not shared by any diplodocine. Morphological evidence therefore slightly favors an assignment to Apatosaurinae.

A forced clustering with the two *Diplodocus carnegii* specimens (as proposed by Bedell and Trexler, 2005) produces tree lengths of 1903 and 188.65885 steps, an increase of 0.32% and 0.37%. Diplodocine affinities are found with shortest trees of 1898 and 188.28028 steps, corresponding to a lengthening of 0.05% and 0.16%, respectively. Imposing a grouping within Apatosaurinae (as found by the implied weight analysis) did not result in longer trees. Both morphological evidence as well as constrained searches thus indicate that apatosaurine affinities are more parsimonious for WDC-FS001A. Therefore, and following also the reasoning in the earlier paragraphs about the affinities of SMA 0087 and AMNH 460, WDC-FS001A is herein referred to one of the putative new apatosaurine taxa, together with the specimens mentioned before.

Combined cladogram

PeerJ Reviewing Manuscript

Based on the identifications stated above, a combined cladogram was created to summarize the results (Fig. 154). The cladogram represents the most up-to-date species-level taxonomy of Diplodocidae. Diagnoses of the proposed clades, genera, and species are given below. Outgroup taxa are reduced considerably compared to the trees recovered by the main analyses, in order to increase the intended focus on Diplodocidae.

Biostratigraphic and paleobiogeographical implications

The present analysis rejects diplodocid affinities of the only putative Middle Jurassic and Cretaceous diplodocid species, i.e. *Cetiosauriscus stewarti*, *Losillasaurus giganteus*, *Dystrophaeus viaemalae*, and *Dyslocosaurus polyonychius*. A single anterior caudal vertebra previously identified as Cretaceous diplodocid (Upchurch and Mannion, 2009) was subsequently shown to belong to Titanosauriformes (Whitlock et al., 2011), and therefore not included in the present analysis. Diplodocidae thus appear restricted to the Late Jurassic, with a caudal vertebra from the Oxfordian of Georgia being the first representative of the clade (Gabunia et al., 1998; Mannion et al., 2012). Given the high diversity, such a temporal restriction is remarkable. The Morrison Formation, from where the majority of diplodocids are known, is interpreted to represent a time span of about seven (Swierc and Johnson, 1996; Kowallis et al., 1998) to eleven million years (Platt and Hasiotis, 2006). Therefore, even though morphologically similar, at least two diplodocid species appear to have lived contemporaneously throughout the entire duration of the sedimentation of the Morrison Formation, and besides non-diplodocid sauropods like *Camarasaurus*, *Haplocanthosaurus*, *Brachiosaurus*, or others. If precise stratigraphical levels and geological ages would be known for all the sites where diplodocids were found, the present analysis would provide a good phylogenetic foundation on which hypotheses of speciation or niche partitioning within diplodocids from the Morrison Formation could be based. However, exact geological dating was rarely done, or has provided controversial results (in particular for the Howe Ranch sites, Tschopp and Mateus, 2013b). Therefore, and because no reliable marker beds appear to be present throughout the entire extent of the Morrison Formation (Trujillo, 2006; contra Turner and Peterson, 1999), long distance correlation between Morrison Formation quarries is nearly impossible at present. Proposed biostratigraphical zones within the formation (Bakker, 1998; Turner and Peterson, 1999; Foster, 2003; Ikejiri, 2004) have thus to be regarded questionable and provisional. Their validity is furthermore debatable because they heavily rely on species and genus referrals that have not been tested by means of phylogenetic analyses. Given that diversity appears to have been underestimated, as indicated by the present analysis, these referrals will have to be reconsidered. Notwithstanding the lack of knowledge concerning such

PeerJ Reviewing Manuscript

specific stratigraphy and phylogeny, Diplodocidae as a whole appears to be a good candidate to serve for relative geological dating. Their presence in at least three continents, and restriction in time to the Late Jurassic, and more precisely the period of the Oxfordian to Tithonian qualifies them as age index fossils.

Diplodocidae is most divers in North America, but the earliest finds from Georgia suggest that the origin of the clade lies in Europe (Mannion et al., 2012). As the Georgian caudal vertebra, also the non-American diplodocid OTU included herein (ML 418, *Dinheirosaurus lourinhanensis*, *Tornieria africana*) can be referred to Diplodocinae (Mannion et al., 2012; this study). The fact that the latter two species lie at the base of the diplodocine radiation (Fig. 154) furthermore corroborates a hypothesis of an extra-American origin of this clade. Interestingly, apatosaurine specimens have only been recovered from North America to date, so that interpretations of their origin are more dubious.

Diagnoses

Updated diagnoses of the main diplodocoid subclades

The following lists of synapomorphies only includes the named nodes and stems in the recovered phylogenetic tree, which directly lead to Diplodocidae, as well as its sister clade Dicraeosauridae (Fig. 154). Synapomorphies are divided into their qualitative states as defined above, and ordered based on anatomical regions. Where conflicting interpretations exist between the analyses using equal or implied weighting, the synapomorphy is attributed to the less inclusive clade. Additional synapomorphies are added to the diagnoses following earlier studies, if supported by the data set, also in cases where the analysis did not recognize them as such. References for the synapomorphies credit the first recognition of the respective trait as synapomorphic for the taxon in question. Finally, previously proposed synapomorphies are discussed in the light of the new analysis.

Diplodocoidea Marsh, 1884.

Definition: *Diplodocus*, not *Saltasaurus* (stem-based; Wilson and Sereno, 1998).

Unambiguous synapomorphies:

premaxilla is a single elongate unit with nearly no distinction between the body and the nasal process (3-1; Upchurch et al., 2004a);

posteroventral edge of the ascending process of the premaxilla is straight in lateral view, and directed posterodorsally (5-2; Upchurch, 1995);

the dorsal process of the maxilla extends posterior to the posterior process (13-1; Wilson, 2002)

PeerJ Reviewing Manuscript

maximum diameter of the antorbital fenestra is subequal (greater than 90%) to the orbital maximum diameter (18-1; Wilson, 2002);

the external nares are retracted to a position between the orbits, facing dorsally or dorsolaterally (21-1; Marsh, 1898);

a large contribution of the jugal to the antorbital fenestra, bordering approximately one-third of its perimeter (40-1; Upchurch, 1995);

the anterior terminus of the quadratojugal lies below the anterior margin of the orbit or beyond (45-1; Rauhut et al., 2005);

angle between anterior and dorsal processes of the quadratojugal is greater than 90°, approaching 130°, so that the quadrate shaft slants posterodorsally (46-1; McIntosh, 1990b);

the basipterygoid processes are angled less than 75° to the skull roof (normally approximately 45°) (93-1; Calvo and Salgado, 1995);

the transverse flange (i.e. ectopterygoid process) of the pterygoid lies anterior to the antorbital fenestra (102-1; Upchurch, 1998);

four or more replacement teeth per alveolus (115-1; Wilson, 2002);

planar wear facets of the teeth (117-1);

cylindrical cross-sectional shape of the teeth at midcrown (121-1; Marsh, 1884);

the fibular facet of the astragalus faces posterolaterally, such that the anterior margin is visible in posterior view (454-1).

Exclusive synapomorphies:

external surface of the premaxilla is marked by vascular grooves (2-1);

the anterior maxillary foramen lies on the medial edge of the maxilla, opening medially into the premaxillary-maxillary boundary (11-1);

the articular surface of the quadrate is roughly triangular in shape (49-1);

SI values for tooth crowns are 3.4 or greater (119-1; McIntosh, 1990b);

short cervical ribs, not reaching the posterior end of the centrum (214-1; Berman and McIntosh, 1978).

Shared synapomorphies:

the posterolateral process of the premaxilla and the lateral process of the maxillary are without any midline contact (6-0; Wilson, 2002);

maximum diameter of the external nares is shorter than the orbital maximum diameter (22-0);

the articular surface of the occipital condyle is continuously grading into the condylar neck (77-1);

PeerJ Reviewing Manuscript

cervical ribs overlap no more than the next cervical vertebra in sequence (215-1);
the proximal expansion of the humerus is more or less symmetrical (384-0).
Ambiguous synapomorphies:
the dorsal transverse processes are inclined dorsally more than 30° from the horizontal (230-1).
Previously suggested synapomorphies:
A very acute angle between medial and lateral margins of the premaxilla (Upchurch et al., 2004a). The character describing the angle between medial and lateral borders of the premaxilla was redefined herein, and the numeric boundary changed as to be able to distinguish between Dicraeosauridae and Diplodocidae. An angle lower than 17° would thus be synapomorphic for both Rebbachisauridae and Diplodocidae, but not for Dicraeosauridae. The same character was further found by Whitlock (2011a) to diagnose Diplodocimorpha.
An elongate subnarial foramen (Upchurch et al., 2004a). The character describing the elongation of the subnarial foramen was not included in the present analysis, as it is impossible to code in most specimens. Even when rostral skull elements are preserved, the fossa containing the subnarial and the anterior maxillary foramina is often obliterated with matrix (e.g. USNM 2672), and only CT scanning would reveal the true shape.
A strongly reduced anteroposterior diameter of the supratemporal fenestra (Upchurch et al., 2004a). The relation of anteroposterior diameter of the supratemporal to occipital width was not included in the present analysis, as it was not well explained what was measured for obtaining a value for the occiput width (Upchurch et al., 2004a). Also, anteroposterior diameter of supratemporal fenestrae seems to be variable within diplodocids, and relatively easily deformed (compare the two putative *Diplodocus* skulls CM 11161 and 11255).
Elongate basipterygoid processes (McIntosh, 1990b; Upchurch, 1998). This trait is recovered as diplodocimorph synapomorphy by Wilson (2002) and Whitlock (2011a). In fact, the difference is inexistent as Diplodocimorpha describes the same clade as Diplodocoidea in McIntosh (1990b) and Upchurch (1998). Whitlock (2011a) resolved it as diplodocimorph synapomorphy due to the basal diplodocoid position of *Haplocanthosaurus*, which does not preserve cranial bones, and applying the character state optimization strategy DELTRAN. In the present analysis, definition of the character was slightly changed, which lead to varying scores for diplodocid taxa. It can thus not be considered a synapomorphy for any clade herein.
A rectangular snout (Upchurch et al., 2004a). The rectangular snout was herein included as diagnosing Diplodocimorpha, following Whitlock (2011a).
Dentary with ventrally projecting 'chin' (Wilson and Sereno, 1998). At the time Wilson and

PeerJ Reviewing Manuscript

Sereno's (1998) monograph was published, no dentary was known from diplodocoids more basal than Flagellicaudata. The recovery of *Nigersaurus* and *Demandasaurus* dentaries showed that such a 'chin' was absent in rebbachisaurids (Sereno et al., 1999; Sereno and Wilson, 2005; Torcida Fernández-Baldor et al., 2011). Consequently, its presence was later found as synapomorphy for Flagellicaudata (Whitlock 2011a; this study).

The anterior restriction of the tooth row (McIntosh, 1990a). The length of the tooth row is recovered as diplodocimorph synapomorphy by Whitlock (2011a), applying DELTRAN. In the present analysis, the number of states has been increased, compared to the definition of Whitlock (2011a), due to the recognition of a higher diversity within diplodocids. Also, brachiosaurid skulls have anteriorly restricted tooth rows (Janensch, 1935; Wilson and Sereno, 1998), which shows that this feature is present in diplodocoid outgroups as well.

Atlantal intercentrum with anteroventral lip (Wilson and Sereno, 1998). The same doubts apply here as for the presence of a 'chin' in the dentary (see above). The question is furthermore complicated as no rebbachisaurid atlas has been described to date. With the present dataset it is thus more cautious to add this trait as synapomorphy of Flagellicaudata.

Cervical and anterior dorsal vertebrae opisthocoelous (McIntosh, 1990a). Opisthocoel cervical and anterior dorsal vertebrae are actually widespread among sauropod dinosaurs, and represent the plesiomorphic condition. No phylogenetic analysis was thus able to support this trait as a synapomorphy of Diplodocoidea.

Deeply divided V-shaped posterior cervical and anterior dorsal neural spines (McIntosh, 1990b). Subdivided cervical and dorsal neural spines are known from a variety of sauropod dinosaurs from different clades (Upchurch et al., 2004a; Wedel and Taylor, 2013). The shape of the subdivision was proposed as distinguishing feature between diplodocids and camarasaurs (V- versus U-shaped; McIntosh, 1990a), but has rarely been used in phylogenetic analyses. In the present analysis, a character is used to describe the base of the notch. Reducing the description to the base of the notch, occurrence of U-shaped notches is not restricted to camarasaurs, but also present in diplodocoid species (e.g. *Amargasaurus cazaui* or *Apatosaurus ajax* YPM 1860). It should thus not be used to diagnose Diplodocoidea.

Dorsal junction of the spinoprezygapophyseal laminae of dorsal vertebra (Whitlock, 2011a). Here, this feature is recovered as diagnosing a more inclusive clade, SMA 0009 + mdE, in the equally weighted reduced consensus tree, as well as in both main implied weights trees. The difference is a result of the addition of the titanosauriform species *Giraffatitan brancai*, *Ligabuesaurus leanzai*, and *Isisaurus colberti*, where spinoprezygapophyseal and prespinal

PeerJ Reviewing Manuscript

laminae join dorsally (Janensch, 1950; Jain and Bandyopadhyay, 1997; Bonaparte et al., 2006).
Posterior dorsal centra are amphicoelous (McIntosh, 1990a). Detailed study of diplodocine posterior dorsal centra showed that most of them are actually slightly opisthocoelous (e.g. *Diplodocus carnegii* CM 84) to distinctly so (*Supersaurus vivianae*). The amphicoelous condition was thus herein recovered as synapomorphic for Apatosaurinae or less inclusive clades.
Arches of dorsal and caudal vertebrae tall (more than two and one-half times length of dorsoventral centrum height) (Wilson and Sereno, 1998). The present synapomorphy actually includes two characters as used by Whitlock (2011a) as well as in this study. They were both interpreted to diagnose Diplodocimorpha by Whitlock (2011a). In the present study, state boundaries for the dorsal neural arch height were changed, leading to differently scored diplodocid specimens, which actually show variable ratios. A detailed study of the ratio of diplodocid caudal neural spines showed that many specimens do not have neural spines that are 1.5 times taller than the posterior articular surface. Therefore, neither of the two characters was recovered as diplodocid or diplodocimorph synapomorphy.
Proximal caudal vertebrae with procoelous centra (McIntosh, 1990b). Procoelous centra were shown to have a much wider distribution than just Diplodocoidea (Carballido et al., 2012b; D'Emic, 2012; Mannion et al., 2013). Herein, the character describing caudal articular surface shape, is subdivided into four states, including slight and strong procoely (following Carballido et al., 2012b). Whereas most diplodocines have slightly procoelous anterior caudal centra, many other diplodocid specimens actually have flat posterior articular surfaces. To state that all diplodocoid taxa have procoelous centra would thus over simplify the variety of morphologies found.
Caudal vertebrae with wing-like transverse processes (McIntosh, 1990b). The same trait was found to diagnose Diplodocimorpha by Whitlock (2011a). Many non-diplodocid sauropod species do have dorsally expanded caudal transverse processes on their first caudal vertebra. These are herein interpreted as wing-like, but they do not have the same shape as diplodocoid taxa. The problem is best exemplified by a putative diplodocid anterior caudal from the Cretaceous of China (PMU R263; Upchurch and Mannion, 2009), which was later reidentified as somphospondylan titanosauriform (Whitlock et al., 2011). A more precise definition of wing-like would be beneficial for future analyses.
Presence of a whiplash tail (at least 30 elongate, biconvex posterior caudal vertebrae) (McIntosh, 1990a; Wilson and Sereno, 1998). Even though probably valid, the present analysis is not able to identify this feature as synapomorphic for any clade, due to the incompleteness of the included

PeerJ Reviewing Manuscript

specimens. Only the two specimens of *Apatosaurus louisae* (CM 3018 and 3378) preserve a tail complete enough to confidently score them for this character. The trait was thus not included into any clade diagnosis.

Presence of forked chevrons (McIntosh, 1990b). Although named for this peculiar morphology (Marsh, 1878), *Diplodocus*, as well as its higher-level clades are not the only taxa to have forked chevrons. In fact, recent studies and discovery of new basal sauropods show that it might actually be a retained plesiomorphy (Zhang et al., 1988; Ouyang and Ye, 2002; Remes et al., 2009).

Short metacarpals (McIntosh, 1990a). The same as for the forked chevrons accounts here: relatively short metacarpals are plesiomorphic for Sauropoda, whereas the elongate metacarpals diagnose macronarian and titanosauriform taxa (Wilson, 2002; Upchurch et al., 2004a; Tschopp, 2008).

Ischia have expanded distal ends (McIntosh, 1990b). The expanded distal ends of the ischia are in fact typical for all diplodocoid sauropods from which ischia were known in 1990. Now, rebbachisaurs are known to have distally unexpanded ischia, restricting this trait to diagnose Flagellicaudata.

Diplodocimorpha Calvo and Salgado, 1995.

Definition: *Diplodocus* + *Rebbachisaurus* (node-based; Taylor and Naish, 2005).

Unambiguous synapomorphies:

the anterior margin of the premaxilla does not have a step (1-0; Wilson, 2002. This synapomorphy was not found by the present analysis, but recovered as such by Wilson (2002) and Whitlock (2011a). As the data matrix indeed supports an identification of this trait as unambiguous synapomorphy for Diplocimorpha, it has been included in the present list);

squared (111-2) or blunted snout (111-1; Berman and McIntosh, 1978. As the first synapomorphy, also this one was found by Whitlock (2011a), but not directly confirmed by the present analysis, although supported by the data matrix);

sprl extend onto lateral aspect of anterior caudal neural spines (318-1).

Exclusive synapomorphies:

posterior dorsal, sacral and anterior caudal neural spines are 'petal' shaped in anterior/posterior view, expanding transversely through 75% of its length and then tapering (294-1);

transition from 'fan'-shaped to 'normal' caudal ribs occurs between Cd4 and Cd5 (300-1).

Ambiguous synapomorphies:

a semicircular dorsal margin of the ilium (409-1).

Previously suggested synapomorphies:

PeerJ Reviewing Manuscript

the analysis of Whitlock (2011a) produced a high number of synapomorphies for Rebbachisauridae + Flagellicaudata. Several of these are herein recovered as synapomorphic for Diplodocoidea: the straight, and posterodorsally directed nasal process of the premaxilla, the absence of a sharp distinction between the premaxillary main body and the nasal process, the lacking midline contact of the posterolateral process of the premaxilla and the lateral process of the maxilla, the dorsal process of the maxilla that extends posterior to the posterior process, the subequal diameters of the antorbital and orbital fenestra, the retracted external nares, the large contribution of the jugal to the antorbital fenestra, the anterior ramus of the quadratojugal that reaches anterior to the orbit, the wide angle between the anterior and the dorsal process of the quadratojugal, the low angle between basipterygoid processes and skull roof, the transverse flange of the pterygoid that reaches anterior to the antorbital fenestra, and the four or more replacement teeth per alveolus. As no skull is known for *Haplocanthosaurus*, the recovery of these synapomorphies for Diplodocidea or Diplodocimorpha depends on the method used. With ACCTRAN, they result synapomorphic for Diplodocoidea, whereas DELTRAN recovers them diagnosing Diplodocimorpha. Additional synapomorphies previously recovered for Diplodocimorpha are the following:

parietal excluded from margin of posttemporal foramen (Calvo and Salgado, 1995; Upchurch, 1998; Wilson, 2002). The exclusion of the parietal from the posttemporal foramen is not recovered as synapomorphy for any clade herein, although the data set would support one for Flagellicaudata, as proposed by Whitlock (2011a) as well.

Squamosal extends anteriorly past posterior margin of orbit (Whitlock, 2011a). The anterior extension of the squamosal is restricted in *Kaatedocus* (Tschopp and Mateus, 2013b), which inhibited an identification of the anteriorly reaching squamosal as diplodocimorph synapomorphy in the present analysis.

Tooth crowns aligned along jaw axis, not overlapping (Wilson, 2002). Lacking overlap of tooth crowns is not restricted to Diplodocoidea, but also present in *Giraffatitan brancai*, for example (Janensch, 1935; Wilson and Sereno, 1998). It was thus not recovered as synapomorphy of any clade in the present analysis.

Mid-caudal vertebral centra length at least twice its height (Upchurch et al., 2004a). The mid-caudal centra are generally more elongate in diplodocoids, compared to other taxa. However, they only reach ratios of two times centrum height in advanced diplodocines, as a more detailed assessment of this character shows. It can thus not be regarded synapomorphic for Diplodocimorpha.

PeerJ Reviewing Manuscript

Biconvex distal-most caudal centra (Upchurch, 1998). Biconvex distal caudal vertebrae are exclusive to Diplodocimorpha in the present analysis (but absent in *Suuwassea*, Harris 2006a), which would favor an identification as synapomorphy, as in Whitlock (2011a). However, biconvex caudal vertebrae also occur in titanosauriforms (Wilson et al., 1999), and would thus only qualify for an ambiguous synapomorphy. Therefore, it was not included as such in the present diagnosis.

Distal-most caudal centra at least five times longer than tall (Wilson et al., 1999). The elongation of these distal caudal vertebrae was coded differently in Whitlock (2011a) and here, which resulted in *Apatosaurus* specimens being scored different than *Diplodocus*. The value of greater than five, as proposed by Whitlock (2011a) might thus still be valid, but cannot be recovered as synapomorphic with the present analysis due to varying state boundaries.

Proximal margin of humerus expanded, lateral margin concave in anterior/posterior view (Janensch, 1961). The last diplodocimorph synapomorphy recovered by Whitlock (2011a) describes the concave lateral border of the humerus. This feature is actually present as well in most of the basal sauropods used as outgroups herein. It is thus a plesiomorphic trait and cannot be used as synapomorphy of Diplodocimorpha.

Flagellicaudata Harris and Dodson, 2004.

Definition: *Dicraeosaurus* + *Diplodocus* (node-based; Harris and Dodson, 2004).

Unambiguous synapomorphies:

subnarial foramen and anterior maxillary foramen are separated by a narrow bony isthmus (8-1; Wilson, 2002);

presence of a preantorbital fossa (15-1);

an elongate and slender posterior end of the quadrate (posterior to posterior-most extension of pterygoid ramus) (54-1);

the absence of any squamosal-quadratojugal contact (56-1);

the absence of a parietal contribution to the post-temporal fenestra (59-1; Whitlock, 2011a);

vomer articulates with maxilla (103-1; Wilson, 2002. The recovery of this trait as synapomorphy for Flagellicaudata is supported by the present analysis but not recovered as such, probably due to the very low percentage of specimens scorable for the character);

the anteroventral margin of the dentary bears a sharply projecting triangular process or 'chin' (104-1; Wilson and Smith, 1996);

anteriorly oriented, procumbent teeth (122-1);

atlantal intercentrum bears an anteroventral lip (144-1. Recovered as diplodocoid synapomorphy

PeerJ Reviewing Manuscript

by Wilson and Sereno (1998), the presence of the anteroventral lip can actually only be confirmed for Flagellicaudata, as no rebbachisaurid atlas has yet been reported. The data matrix supports an identification of the derived as diagnostic for Flagellicaudata, even though it was not recovered as such);

the distal shaft of the ischium is triangular, with its depth increasing medially (423-1).

Exclusive synapomorphies:

the longest axes of the basal tubera are oriented in an angle to each other, pointing towards the occipital condyle (87-1);

the lateral spinal lamina of anterior-most caudal neural spines expands anteroposteriorly towards its distal end, and becomes rugose (303-1);

the posterior edge of the distal blade of anterior chevrons is posteriorly expanded in a step-like fashion (355-1).

Shared synapomorphies:

a shallow quadrate fossa (51-0);

absence of longitudinal grooves on the lingual aspect of the teeth (123-0);

anterior diapophyseal laminae (acdl, prdl) are well defined in in anterior caudal vertebrae (313-1);

a 'crus' bridging the haemal canal is present in some chevrons (352-0; Wilson, 2002);

the cross-sectional shape of ischial distal shafts is V-shaped, forming an angle of nearly 50° with each other (424-0; Upchurch, 1998);

the ischial shaft is transversely expanded distally (425-1; Upchurch, 1998);

the distal condyle of metatarsal I bears a posterolateral projection (463-1; Berman and McIntosh, 1978).

Ambiguous synapomorphies:

presacral neural spine bifurcation present (126-1; McIntosh, 1990b; this synapomorphy was not found by the main analyses, but included in the list as it readily distinguishes derived diplodocoids from more basal forms as rebbachisaurs or *Haplocanthosaurus*);

mid- and posterior dorsal neural arches have divided centropostzygapophyseal lamina, with the lateral branch connecting to the pcdl (261-1);

the hyposphene-hypantrum system is well developed in posterior dorsal vertebrae, having a rhomboid shape up to last element (276-0);

the ventral surface is marked by irregular foramina on some anterior caudal centra (305-1).

Previously suggested synapomorphies:

PeerJ Reviewing Manuscript

quadrate articular surface roughly triangular in shape (Whitlock, 2011a). The triangular articular surface of the quadrate was recovered as exclusive diplodocoid synapomorphy herein, with rebbachisaurids developing crescent-shaped surfaces. This is most probably due to the fact that the character was herein treated as ordered, thus assuming that a common ancestor of rebbachisaurs and flagellicaudatans must have had triangular articular surfaces.

Distance between supratemporal fenestrae twice the length of the longest axis of the supratemporal fenestrae (Salgado and Calvo, 1992). A detailed assessment of this ratio showed that most diplodocids do not reach a ratio of two. Even after redefining the state boundaries, variation between diplodocid specimens results in differential scorings. A high ratio, and thus wide distance between the supratemporal fenestrae can thus not be regarded synapomorphic for Flagellicaudata.

Ventrally directed occipital condyle (Upchurch, 1998). The orientation of the occipital condyle was not included in the present analysis, as it was found to be very difficult to define a character in an unambiguous way.

Single planar occlusal facet on teeth (Wilson, 2002). This synapomorphy includes two characters as used in the present analysis, the distinction between single and double occlusal facets, as well as the planar versus V-shaped facets. The planar facets were found herein as synapomorphy for Diplodocoidea, whereas the single facets are not found to be typical for any clade.

17 dentary teeth or fewer (Wilson, 2002). Whereas it is true that flagellicaudatans have less than 17 teeth, the same is true for basal macronarian dinosaurs (e.g. *Camarasaurus* or *Giraffatitan*; Gilmore, 1925; Janensch, 1935), as well as for the rebbachisaurid *Demandasaurus*. It thus seems more parsimonious to interpret the less than 17 dentary teeth as ancestral to all neosauropods, with subsequent reversal to a higher number of teeth in *Nigersaurus* (Sereno and Wilson, 2005).

Low-angled, planar wear facets on the teeth (Calvo, 1994). The angulation of the wear facets was not included as character in the present analysis, as an acute angle only characterizes rebbachisaurids, and enough characters were already used to resolve the position and relationship of that clade. Low angles are not restricted to diplodocids either, being also present as late stages in the wear of camarasaur teeth (e.g. SMA 0002; Wiersma, 2013).

Anterior cervical neural spines bifid (McIntosh, 1990b). Anterior neural spines are rarely preserved in cervical vertebrae, even in nearly complete specimens like the holotypes of *Apatosaurus louisae* or *Diplodocus carnegii* (CM 3018 and 84, respectively; Wedel and Taylor, 2013). Diplodocid specimens preserving anterior neural spines actually all show the bifurcation to initiate posterior to CV 5 or 6, and thus not in the anterior elements. The only group positively

PeerJ Reviewing Manuscript

confirming bifid neural spines in anterior cervical vertebrae are the Dicraeosauridae. Indeed, the present analysis recovered bifid anterior neural spines as synapomorphic for this taxon.

Presence of a median tubercle in bifurcated cervical and dorsal neural spines (Wilson, 2002). Although generally present in Flagellicaudata, some specimens do not show such a tubercle (e.g. *Amargasaurus cazaui*, or UW 15556). Also, the probable non-diplodocoid *Australodocus* does have a median tubercle, such that its presence could at most be interpreted as ambiguous synapomorphy. Since it was not recovered as such by the present analysis, it was not included in the diagnosis.

Anterior dorsal vertebrae with divided centropostzygapophyseal laminae (Wilson, 2002). A divided centropostzygapophyseal lamina was only positively identified in mid- and posterior dorsal vertebrae, but not in anterior ones. Therefore, the character was restricted to mid- and posterior elements.

Height of sacral neural spines nearly four times length of centrum (Wilson, 2002). This ratio was redefined and posterior dorsal vertebrae were included into the description. The apomorphic state of the new character (282-1) was found to diagnose Dicraeosauridae in the present analysis.

Anterior caudal neural arches with spinoprezygapophyseal lamina (sprl) on lateral aspect of neural spine (Wilson, 2002). The extension of the caudal spinoprezygapophyseal lamina onto the lateral side of the neural spine is actually a diplodocimorph synapomorphy, as it is also present in rebbachisaurids, but absent in *Haplocanthosaurus* (Hatcher, 1903; Sereno et al., 2007).

Procoelous first caudal centrum (Wilson, 2002). The first caudal centrum is actually flat posteriorly in many flagellicaudatan specimens (e.g. CM 84, ET, pers. obs., 2011), and only more posterior elements develop a slight convexity, if at all. This trait is thus not included as synapomorphic for any clade herein.

Pubis with prominent ambiens process (McIntosh, 1990b). In the present analysis, a distinction is made between the hook-like ambiens process as present in *Diplodocus* and *Dicraeosaurus* (Hatcher, 1901; Janensch, 1961), for example, and the less developed, but still prominent process of apatosaurines (Ostrom and McIntosh, 1966). The presence of a prominent ambiens process can thus still be confirmed as synapomorphic for Flagellicaudata, but as the morphology is different, it was not recovered as such in the present analysis.

Dicraeosauridae Huene, 1927.

Definition: *Dicraeosaurus*, not *Diplodocus* (stem-based; Sereno, 1998).

Unambiguous synapomorphies:

the crista prootica is expanded laterally into dorsolateral process (76-1; Salgado and Calvo,

PeerJ Reviewing Manuscript

1992);
basipterygoid processes are narrowly diverging (< 31°) (92-2; Wilson, 2002);
the area between the basipterygoid processes and parasphenoid rostrum forms a deep slot-like cavity that passes posteriorly between the bases of the basipterygoid processes (95-1; Upchurch et al., 2004a);
subtriangular cross-sectional shape of the symphysis of the dentary, tapering sharply towards its ventral extreme (105-1; Whitlock and Harris, 2010);
presence of a tuberosity on the labial surface of the dentary, near the symphysis (106-1; Whitlock and Harris, 2010);
the first bifid cervical neural spine is in CV 3 (140-0).

Shared synapomorphies:

frontal symphysis is fused in adult individuals (26-1; Salgado and Calvo, 1992);
presence of a pineal (parietal) foramen between frontals and parietals (36-0);
presence of a postparietal foramen (66-1; Salgado and Calvo, 1992);
the sagittal nuchal crest of the supraoccipital is narrow, sharp, and distinct (74-1);
the supraoccipital bears a foramen close to its contact with the parietal (75-1);
absence of a basioccipital depression between foramen magnum and basal tubera (80-0);
the anterolateral corner of the tooth row is displaced labially (112-1);
the width to height ratio of cervical vertebrae is less than 0.5 (128-0; Upchurch et al., 2004a);
the total height to centrum length ratio of anterior cervical vertebrae is greater than 1.2 (usually around 1.5) (154-2);
the pleurocoels of anterior cervical centra are undivided (157-0);
presence of paired pneumatic fossae on the ventral surface of anterior cervical centra (160-1);
mid-cervical neural spines are anteriorly inclined (169-1; Rauhut et al., 2005);
posterior cervical and anterior dorsal bifid neural spines are parallel to converging (211-1; Rauhut et al., 2005);
absence of an anterior, middle single fossa projected through the midline of single dorsal neural spines (233-1);
the transition from bifid to single dorsal neural spines is abrupt (235-1);
mid-dorsal neural spines are bifid, inclusive of at least the fifth dorsal vertebrae (250-1);
lateral pleurocoels are absent in mid- and posterior dorsal centra (252-0; Janensch, 1929a);
posterior dorsal centra are amphicoelous (270-0);
the ratio of height above postzygapophyses (neural spine) of posterior dorsal neural arches to

PeerJ Reviewing Manuscript

height below (pedicel) is 3.1 or greater (272-1);
the height of posterior dorsal and/or sacral neural spines (not including arch) is more than 3 times centrum length (282-2; McIntosh, 1990a);
absence of pleurocoels in sacral vertebral centra (287-0);
the ventral surface of anterior caudal transverse processes is directed dorsally (312-1);
a ratio of blade height above pubic peduncle of the ilium to its anteroposterior length of 0.40 or more (405-1);
the position of the highest point of the femoral head is laterally shifted in anterior view, and lies above the main portion of the shaft (431-1);
presence of a short transverse ridge on the anteromedial surface of the distal end of the tibia (443-1);
a ratio of mediolateral width of the astragalus to maximum anteroposterior length of less than 1.6 (452-1);
metatarsal I is relatively gracile, proximal transverse width to greatest length is less than 0.8 (461-0);
the groove on the lateral surface of pedal unguals extends straight horizontally (477-1).

Ambiguous synapomorphies:

postzygodiapophyseal and spinopostzygapophyseal laminae of mid-cervical vertebrae form a right angle (170-1);
mid- and posterior cervical neural arches bear lateral fossae on the prezygapophysis process (183-1);
absence of dorsal pneumatopores (pleurocoels) (227-0);
the base of the notch between the metapophyses of anterior, bifid dorsal vertebrae is narrow and V-shaped (244-1);
the parapophysis of DV 3 lies mid-way between the top of the centrum and the level of the prezygapophyses (246-1).

Previously suggested synapomorphies:

premaxilla with anteroventrally orientated vascular grooves originating from an opening in the maxillary contact (Wilson, 2002). The grooves are shown to be present as well in some diplodocid specimens (see above). An identification of this trait as dicraeosaurid synapomorphy is thus questionable.
Frontal contributes to margin of supratemporal fenestra (reversal; Wilson and Sereno, 1998). Although this is true for *Dicraeosaurus* and *Amargasaurus*, *Suuwassea* does not show any

PeerJ Reviewing Manuscript

participation of the frontal in the supratemporal fenestra. Therefore, the present analysis was not able to recover this reversal as synapomorphic for the entire clade Dicraeosauridae.

Supratemporal fenestra smaller than foramen magnum (Salgado and Calvo, 1992). The reduced size of the supratemporal fenestra has been found as synapomorphic for *Amargasaurus* + *Dicraeosaurus* by the equally weighted reduced consensus tree. However, this trait is shared with *Limaysaurus*, and it remains thus unclear how to interpret it (diplodocoid or diplodocimorph synapomorphy with reversals, or as convergently acquired traits of Rebbachisauridae and Dicraeosauridae).

Ventrally directed prong on squamosal (Whitlock, 2011a). A ventrally directed process is present in some diplodocids as well, and very similar to the state in *Dicraeosaurus* (see above). An enlarged prong-like structure is only present in *Amargasaurus*, which does not allow an identification of this feature as synapomorphic for Dicraeosauridae.

Basal tubera narrower than occipital condyle (Wilson, 2002). As shown by Mannion (2011), the ratio between basal tubera and occipital condyle width is highly variable. The state boundaries used herein do not allow to identify the lowest ratio as synapomorphic for Dicraeosauridae, although the ratios themselves indicate that it might be taxonomically significant.

'Petal' shaped posterior dorsal neural spines (Wilson, 2002). The peculiar 'petal' shape of dorsal, and sacral neural spines of dicraeosaurids is also present in rebbachisaurids, which led to an identification of this feature as diplodocimorph synapomorphy herein.

Cervical vertebrae with longitudinal ridge on ventral surface (Sereno et al., 2007). The presence of a longitudinal ridge is a plesiomorphic feature within sauropods, and present as well in some diplodocid specimens (e.g. SMA 0004, YPM 429; Lull, 1919; Tschopp and Mateus, 2013b).

Dicraeosaurids have well-developed keels in anterior cervical centra, shared with *Shunosaurus*, but also with *Galeamopus* [redacted] SMA 0011 (see above). The presence of ventral ridges and keels is thus too variable as that a reversal to the plesiomorphic state could be recovered as synapomorphic for any clade.

Anterior caudal centra with irregularly placed foramina on ventral surface (Harris, 2007). The presence of ventral foramina in anterior caudal vertebrae is herein recovered as flagellacaudatan synapomorphy, as it is shared with numerous diplodocid specimens.

Mid-caudal vertebral centra with mid-height longitudinal ridge on lateral surface, centra hexagonal in anterior/posterior view (Whitlock, 2011a). Longitudinal ridges also mark the mid-caudal vertebrae of *Camarasaurus*, as well as many apatosaurine specimens (Gilmore, 1925, 1936). Their presence could thus only be interpreted as shared synapomorphy for

PeerJ Reviewing Manuscript

Dicraeosauridae. Since it was not recovered as such, it is not included in the diagnosis herein.
Humerus with pronounced proximolateral corner (Wilson, 2002). This trait was recovered as neosauropod synapomorphy in the implied weights trees. As definition of 'pronounced' is somewhat vague, interpretation of this character might have been different in Wilson (2002). The herein used definition is explained and figured above.

Diplodocidae Marsh, 1884.

Definition: *Diplodocus*, not *Dicraeosaurus* (stem-based; Sereno, 1998).

Unambiguous synapomorphies:

maxilla-quadratojugal contact broad (14-1; Rauhut et al., 2005; not recovered by the present analysis, it is still supported by the data matrix. The reason why it was not recovered is probably the low percentage of specimens preserving these two bones);

antorbital fenestra with concave dorsal margin (20-1; Wilson, 2002; also this trait was not recovered as diplodocid synapomorphy, although supported by the specimens for which a scoring was possible. The reason is probably the same as in the previous synapomorphy);

posterior process of the prefrontal is hooked (25-1; Berman and McIntosh, 1978);

mandible without strong coronoid eminence (108-1; Whitlock, 2011a; as in the previous characters, the low number of specimens preserving the mandible probably precluded an identification of this character as synapomorphy for Diplodocidae, although supported by the data set);

direct crown-to-crown occlusion absent (116-1; Wilson, 2002; yet another trait not found as synapoorphic, probably due to low percentage of preservation, but supported by the dataset);

14 to 15 cervical vertebrae (127-1; Huene, 1929);

anterior centrodiapophyseal lamina (acdl) of anterior caudal vertebrae is divided (314-1; Wilson, 2002).

Exclusive synapomorphies:

preantorbital fenestra occupies at least 50% of the preantorbital fossa (17-1);

medial margin of the prefrontal is curving distinctly medially at its anterior end to embrace the anterolateral corner of the frontal (23-1);

ten dorsal vertebrae (224-2; Huene, 1929);

anterior and mid-caudal vertebrae bear ventrolateral ridges (329-1).

Shared synapomorphies:

shape of the posterior face of the basal tubera flat (85-1) or slightly concave (85-2);

short mid- and posterior dorsal transverse processes (263-0);

PeerJ Reviewing Manuscript

posterior dorsal, sacral and anterior caudal neural spines rectangular through most of their length (294-0; Whitlock, 2011a; the current state represents a reversal to the plesiomorphic condition, and it was scored differently in *Amphicoelias altus* AMNH 5764, which has a dorsally expanded neural spine, somewhat resembling a 'petal' shape, although not to the extent as in dicraeosaurs or rebbachisaurs)

anterior caudal transverse processes with anteroposteriorly expanded lateral extremities (316-1);

spinoprezygapophyseal laminae (sprl) and spol contact each other on anterior caudal neural spines (319-1; Wilson, 1999);

presence of a lateral bulge on the femur (428-1).

Ambiguous synapomorphies:

dorsal transverse processes horizontal or only slightly inclined dorsally (230-0);

posterior centroparapophyseal lamina of mid- and posterior dorsal neural arches present as single lamina (258-1; Wilson, 2002).

Previously suggested synapomorphies:

antorbital fenestra subequal to orbital maximum diameter (Wilson, 2002). The large antorbital fenestrae are recovered as diplodocid synapomorphy herein, as *Nigersaurus* also shows the apomorphic state (Sereno et al., 1999, 2007).

Prefrontal posterior process elongate (Wilson, 2002). Determination of the length of the posterior process of the prefrontal is highly influenced by the orientation of the skull roof, as shown previously. Taking this into account, elongated posterior processes of the prefrontal are not present in all diplodocid specimens. This trait was thus excluded from the diagnosis.

No internarial bar (Upchurch et al., 2004a). An internarial bar also appears to be absent in dicraeosaurids (Janensch, 1935; Harris, 2006b). It would thus more appropriately be interpreted as flagellicaudatan synapomorphy, but was not included in the present analysis, because in most specimens it is difficult to distinguish true absence from incomplete preservation.

Frontal contribution to dorsal margin of orbit roughly equal to contribution of prefrontal (Whitlock, 2011a). Remeasuring the contribution of the frontal and prefrontal in various diplodocid skulls showed that variation occurs both within but also outside Diplodocidae. Neither one nor the other state can thus be confidently considered synapomorphic for any clade.

Quadrate fossa shallow (Wilson, 2002). A shallow quadrate fossa was later found in *Suuwassea* as well (Harris, 2006a), showing that this trait is not restricted to Diplodocidae. Consequently, it has here been found as flagellicaudatan synapomorphy.

PeerJ Reviewing Manuscript

Squamosal-quadratojugal contact absent (Wilson, 2002). Tschopp and Mateus (2013b) showed that a contact between the squamosal and the quadratojugal was also absent in *Suuwassea* (contrary to Harris, 2006a). Therefore, the present trait was herein recovered as flagellicaudatan synapomorphy.

The jugal forms a substantial part of the caudoventral margin of the antorbital fenestra (Upchurch, 1998). The contribution of the jugal to the antorbital fenestra was recovered as diplodocoid synapomorphy, as *Nigersaurus* shows the same morphology (Sereno and Wilson, 2005).

An angle between the rostra1 and dorsal quadratojugal processes of 130° (Upchurch et al., 2004a). A wide angle between rostral and dorsal processes of the quadratojugal also occurs in *Nigersaurus* (Sereno and Wilson, 2005), leading to a recovery of this feature as diplodocoid synapomorphy herein.

The distal end of the paroccipital process rounded and tongue-like (Upchurch et al., 2004a). This character was not used in the present analysis as it was unclear what tongue-like precisely means. It was substituted by a character describing dorsoventral expansion towards the distal ends of the paroccipital processes, which varies within Diplodocidae and does thus not qualify as reliable synapomorphy.

The parasphenoid rostrum is a laterally compressed, thin spike lacking the longitudinal dorsal groove (Upchurch et al., 2004a). A dorsal groove is actually present on many diplodocid parasphenoid rostra (e.g. CM 11161, ET, pers. obs., 2011). Transverse compression of the parasphenoid rostrum is also apparent in *Camarasaurus* (Madsen et al., 1995). Generally, diplodocid parasphenoid rostra are more spike-like, or dorsoventrally compressed, compared to *Giraffatitan* or *Camarasaurus* (Janensch, 1935; Madsen et al., 1995), but that is difficult to translate into a valid phylogenetic character, and was thus not used as such herein.

The ectopterygoid process of the pterygoid located below the antorbital fenestra (Upchurch et al., 2004a). Such an anterior position of the ectopterygoid process is shared with rebbachisaurs (Whitlock, 2011a) , and thus recovered as diplodocoid synapomorphy herein.

The ectopterygoid process of the pterygoid reduced, so that it cannot be seen below the ventral margin of the skull in lateral view (Upchurch et al., 2004a). No such character was included in the present analysis. However, given the rareness of palatal complexes preserved in their true position, it remains doubtful if the analysis would have been capable to confidently resolve character state distributions.

PeerJ Reviewing Manuscript

The breadth of the main body of the pterygoid at least 33% of pterygoid length (Upchurch et al., 2004a). Given that only one disarticulated diplodocid pterygoid was available for direct study (SMA 0011), no character was included in the present analysis to test the distribution of this trait. Generally, diplodocid pterygoids do appear more elongate compared to non-diplodocid taxa, but only rarely measurements can be taken directly from the specimen. It is thus not included in the diagnosis herein.

Cervical vertebrae with longitudinal sulcus on ventral surface (Upchurch, 1998). Presence of a ventral longitudinal sulcus in cervical vertebrae is uncommon in apatosaurs, if one does not consider the concave area between the strongly ventrally projecting parapophyses. Consequently, the sulcus is herein recovered as diplodocine synapomorphy.

Bifurcated centroprezygapophyseal lamina in cervical vertebrae, with a medial and a lateral ramus connecting to the zygapophysis (Wilson, 2002). As *Supersaurus* does not seem to have divided cprl, the current analysis recovered this trait as synapomorphic for both Apatosaurinae and Diplodocinae more derived than *Supersaurus*.

70-80 caudal vertebrae (Upchurch et al., 2004a). The high number of caudal vertebrae is difficult to score in a specimen-based phylogenetic analysis, because only very few specimens preserve reasonably complete caudal series. In the present analysis, only CM 3018 and 3378 positively confirm such a statement. Indirect evidence for an elongated tail also comes from the rod-like distal caudal vertebrae in some dicraeosaurid specimens, as well as in *Limaysaurus*. The number of caudal vertebrae is thus not included in the diagnosis here.

Presence of diapophyseal laminae on anterior caudal vertebrae (Upchurch, 1998). This character has been divided in the present analysis, distinguishing between anterior and posterior diapophyseal laminae. Apatosaurs, as well as *Supersaurus* tend to have much broader posterior diapophyseal laminae compared to diplodocines, thus not qualifying to be scored as 'distinct'. On the other hand, well-developed anterior diapophyseal laminae also occur in dicraeosaurs. Therefore, the latter were recovered as flagellicaudatan synapomorphy, whereas distinct posterior diapophyseal laminae were found to diagnose *Galeamopus* + mdD.

Humero-femoral length ratio is approximately 0.66 (Huene, 1927). Due to the lack of specimens preserving both complete fore- and hindlimbs, the distribution of this character state cannot be assessed in enough detail with the present analysis. While generally supporting the identification as diplodocid synapomorphy, the low number of only two specimens positively confirming this ratio for the entire clade Diplodocidae does not allow a well-founded inclusion of the trait into a diagnosis.

PeerJ Reviewing Manuscript

Insertion of the M. iliofibularis on the fibula located above midshaft (Wilson and Sereno, 1998). In fact, insertion of this muscle on the fibula is located further distally in apatosaurines and *Tornieria* than in more derived diplodocines, as a detailed assessment showed (see above). The proximal location of the insertion is thus recovered as synapomorphic for *Supersaurus* + mdD herein.

An absence of a calcaneum (McIntosh, 1990b). The absence of a calcaneum as diplodocid synapomorphy is most probably a preservational artifact. As shown by Bonnan (2000), at least one pes of *Diplodocus* preserves a calcaneum, and personal observations in two putative apatosaur pedes (CM 30766 and NHMUK R3215) reveal the probable presence of such an element in apatosaurs as well. It is thus not included in the diagnosis of any clade.

Pedal phalanx I-1 having a proximoventral margin drawn out into a thin plate or heel that underlies the distal end of metatarsal I (Upchurch et al., 2004a). The distribution of this trait is more complicated: it is also present in the non-diplodocid *Turiasaurus* and *Cetiosauriscus stewarti*, and absent in *Apatosaurus louisae* CM 3018. Its presence would thus only qualify for an ambiguous synapomorphy, but was not recovered as such by the present analysis.

Pedal phalanx II-2 reduced in craniocaudal length and having an irregular shape (Upchurch et al., 2004a). Whereas all included diplodocid specimens preserving this element show a reduced craniocaudal length in php II-2, the same is also present in *Mamenchisaurus* (Ouyang and Ye, 2002). As no complete pes is known from any dicraeosaur or rebbachisaur, true distribution of this trait cannot be assessed to date, and it is thus excluded from the updated diagnosis of Diplodocidae.

Apatosaurinae Huene, 1927.

Definition: *Apatosaurus*, not *Diplodocus* (stem-based; Taylor and Naish, 2005).

Unambiguous synapomorphies:

cervical ribs projecting well beneath centrum, such that the length of the posterior process is subequal in length to the fused diapophysis/tuberculum (216-1).

Exclusive synapomorphies:

posterior cervical rib shafts are initially directed in the same direction but turn to run a little downwards toward the distal tip (223-1).

Shared synapomorphies:

dorsoventral height of the occipital process of the parietal is low, subequal to less than the diameter of the foramen magnum (63-0);

presence of a foramen in the notch that separates the two basal tubera (90-1);

PeerJ Reviewing Manuscript

centroprezygapophyseal lamina of mid- and posterior cervical neural arches is divided, resulting in the presence of a 'true' divided centroprezygapophyseal lamina, which is dorsally connected to the prezygapophysis (185-2);
posterior centrodiapophyseal lamina (pcdl) and postzygodiapophyseal laminae (podl) of mid- and posterior cervical transverse processes do not meet anteriorly, such that the postzygapophyseal centrodiapophyseal fossa extends onto the posterior face of the transverse process (186-1);
anterior process of posterior cervical ribs is reduced to a short bump-like process or absent (220-1);
mid- and posterior dorsal parapophyses lie posterior to the anterior edge of centrum (256-0);
posterior dorsal postzygapophyses are oblique, including an almost 90° angle (275-1);
ratio of the pubic articulation of the ischia to the anteroposterior length of the pubic pedicel of 1.5 or greater (420-1);
pedal phalanges III-1 and IV-1 are wider than long (476-1).

Ambiguous synapomorphies:

posterior centrodiapophyseal lamina in cervical vertebrae reaches below the posterior end of the neural canal (135-1);
abrupt transition from bifid to single dorsal neural spines (235-1);
bifid dorsal neural spines (if present) do not extend past the second or third dorsal (250-0);
ratio of metacarpal III length to distal transverse width of less than 2.9 (402-0).

Previously suggested synapomorphies:

To our knowledge, only one phylogenetic study is published recognizing an apatosaurine clade including more than just the genus *Apatosaurus*: Lovelace et al. (2007) also recover *Supersaurus* and *Suuwassea* as apatosaurine diplodocids, but do not provide a diagnosis for the clade. The current diagnosis is thus the first for Apatosaurinae based on a cladistic analysis.

Diplodocinae Marsh, 1884.

Definition: *Diplodocus*, not *Apatosaurus* (stem-based; Taylor and Naish, 2005).

Exclusive synapomorphies:

cervical vertebrae bear a small, shallow, anteroposteriorly elongate fossa posteroventral to the pleurocoel (131-1);
large coels mark the anterior caudal centra (307-1; Wilson, 2002).

Shared synapomorphies:

box-like basal tubera (82-1);
presence of a basisphenoid/basipterygoid recess (91-1);

PeerJ Reviewing Manuscript

a longitudinal sulcus marks the ventral surface of the cervical vertebrae (133-1);
the tuberculum of anterior and mid-cervical ribs is directed upwards and backwards in lateral view (218-1);
an oblique ridge connects the medial and lateral edges at the base of the rib head in dorsal ribs (283-1);
presence of a ventral longitudinal hollow in anterior and mid-caudal centra (330-1; Marsh, 1895);
a ratio of centrum length to posterior height in mid-caudal vertebrae of 1.7 or greater (332-1);
the scapular acromial process that lies nearly at midpoint of the scapular body (364-1).

Previously suggested synapomorphies:

EI of mid-cervical vertebrae greater than 4.0 (Upchurch, 1998). State boundaries were changed herein in comparison to Upchurch (1998). However, a mean value of four or more is not reached by several diplodocine specimens, but convergently acquired by various outgroup taxa (Tab. S22). It is thus excluded from the diagnosis of Diplodocinae.

Quadrangular anterior articular surface of anterior caudal centra (Wilson, 2002). There is a wide range of articular surface shapes in these elements, and it is difficult to describe them qualitatively or divide them into only two categories, as was done by Wilson (2002: circular or quadrangular). Most of the diplodocine anterior caudal centra have a flat ventral edge (e.g. *Barosaurus lentus* YPM 429; Lull, 1919), but this is accounted for in other characters. The shape becomes gradually more quadrangular towards middle caudal vertebrae in *Diplodocus* (e.g. AMNH 223; Osborn, 1899), but not in *Barosaurus*, which keeps its rounded lateral edges (e.g. AMNH 6341; ET, pers. obs., 2011). Although anterior caudal centra with flat ventral border can still be confidently assigned to Diplodocinae, more rounded centra cannot be excluded just based on this morphology. The 'quadrangular' shape of the anterior face should thus not be regarded a true synapomorphy of Diplodocinae.

Caudal centrum length doubles over first 20 vertebrae (Wilson, 2002). Caudal centra that are nearly doubling their length within the first 20 elements is not restricted to Diplodocinae. It is shared by *Cetiosauriscus stewarti* (NHMUK R3078, ET, pers. obs., 2011), *Zapalasaurus bonapartei* (Salgado et al., 2006), as well as *Suuwassea emilieae* (Harris, 2006a) and the apatosaur FMNH P25112 (Gilmore, 1936). It is therefore not considered a diplodocine synapomorphy herein.

Middle caudal neural spines vertical (Wilson, 2002). Actually, the majority of diplodocine specimens preserving mid-caudal vertebrae have posterodorsally directed neural spines. The only species with vertical mid-caudal neural spines is *Diplodocus hallorum*.

PeerJ Reviewing Manuscript

Updated diagnoses of valid diplodocid genera and species

The following diagnoses include autapomorphies found by the analysis as well as additional traits found to be unique at least within the respective higher-level clade (Apatosaurinae or Diplodocinae). Autapomorphies found only in one specimen are marked by an asterisk. Referred specimens as well as localities and horizons only include information from the present analysis. Specific or generic identification of other specimens is often not done with enough detail (i.e. without phylogenetic analysis or accurate description of the material), such that earlier referrals require a reappraisal before definitely including them in the species lists. Geographical and temporal distribution of the genera and species proposed herein have thus to be regarded as smallest possible ranges.

Systematic Paleontology

Dinosauria Owen, 1842.

Sauropoda Marsh, 1878.

Neosauropoda Bonaparte, 1986.

Diplodocoidea Marsh, 1884.

Flagellicaudata Harris and Dodson, 2004.

Diplodocidae Marsh, 1884.

***Amphicoelias* Cope, 1877a.**

Type and only referred species: *Amphicoelias altus* Cope, 1877a.

Invalid proposed species: *Amphicoelias latus* Cope, 1877a (= *Camarasaurus*); *Amphicoelias fragillimus* Cope, 1878 (nomen dubium).

Revised diagnosis: *Amphicoelias* is diagnosed by the following autapomorphies: posterior dorsal postzygapophyses almost horizontal, such that the two articular facets include a wide angle (275-0*, shared with Diplodocinae); posterior dorsal neural spines 'petal' shaped, expanding transversely through 75% of its length and then tapering (294-1*, unique within Diplodocidae); a gracile femur, with a robustness index (sensu Wilson and Upchurch, 2003) of less than 0.22 (427-0*, only shared with USNM 10865 within Diplodocidae); and a mediolateral width of the femur which is subequal to the anteroposterior diameter (430-0*, only shared with CM 566 and *Dicraeosaurus* within Diplodocoidea).

Comments: The characters initially used by Cope (1877a) to diagnose the genus are now known to be more widespread among sauropods, as the amphicoelous dorsal centra, or the weak development of the greater trochanter on the femur. Osborn and Mook (1921) first recognized the extreme slenderness of the femur of *Amphicoelias*, compared to other sauropods. Wilson and

PeerJ Reviewing Manuscript

Smith (1996) reported two autapomorphies for the skull, based on a second specimen referred to the genus. However, no detailed description nor figures of the material have yet been published, such that the validity of these traits as autapomorphic features for *Amphicoelias* are herein regarded questionable. The assignment of the specimen to *Amphicoelias* was mainly based on the circular cross section of the femur midshaft (Wilson and Smith, 1996), which has been recovered as autapomorphic herein as well. Upchurch et al. (2004a) proposed the unusual, slightly posterodorsal orientation of the posterior dorsal neural spine as an autapomorphy of the genus. Although characters were included in the present analysis to code for this morphology (C265 and 280), none of them was found as autapomorphic for *Amphicoelias*, and both are shared with specimens from both Apatosaurinae and Diplodocinae.

Locality and horizon: Cope Quarry 12, Garden Park Area, Fremont County, Colorado. Uppermost Brushy Basin Member, Morrison Formation (probably Tithonian). Dinosaur zone 4 (Turner and Peterson, 1999), Zone 6 (Foster, 2003).

***Amphicoelias altus* Cope, 1877a.**

Type specimen: AMNH 5764.

Referred specimens: -

Diagnosis, locality, and horizon as genus.

Apatosaurinae Huene, 1927.

***Apatosaurus* Marsh, 1877a.**

Syn. *Brontosaurus amplus* Marsh, 1881.

Type species: *Apatosaurus ajax* Marsh, 1877a.

Referred species: *Apatosaurus louisae* Holland, 1915a.

Invalid proposed species: *Apatosaurus grandis* Marsh, 1877a (= *Camarasaurus grandis*), *A. laticollis* Marsh, 1879 (nomen dubium; =*A. louisae*), *A. minimus* Mook, 1917 (non-diplodocoid neosauropod), *A. alenquerensis* Lapparent and Zbyzewski, 1957 (= *Lourinhasaurus alenquerensis*), *A. yahnahpin* Filla and Redman, 1994 (= *Eobrontosaurus yahnahpin*).

Revised diagnosis: *Apatosaurus* is diagnosed by the following autapomorphies: presence of an accessory horizontal lamina in the spinodiapophyseal fossa of mid- and posterior cervical vertebrae, not connected to any surrounding lamina (187-1, unique within Apatosaurinae), vertical struts divide lateral pneumatic foramen of mid- and posterior dorsal centra (253-1, unique within Apatosaurinae); gradual transverse expansion of anterior caudal neural spines (328-0, unique within Diplodocidae); absence of ventrolateral ridges (329-0, unique within Apatosaurinae); and a straight scapular blade in lateral view (368-0, unique within Diplodocidae).

PeerJ Reviewing Manuscript

Comments: Berman and McIntosh (1978) proposed the relative positions of ectopterygoid and pterygoid as distinguishing character between the skulls CM 11161 and 11162. It was used as a phylogenetic character by Wilson (2002). However, there are only very few diplodocid skulls available, with the palatal complex articulated and complete. One of these is the juvenile probable *Diplodocus* skull CM 11255, which was interpreted to have an morphology more similar to the state in *Apatosaurus* than to *Diplodocus* (Whitlock et al., 2010). However, recent studies appear to show that actually *Apatosaurus* CM 11162 has the same arrangement as *Diplodocus* CM 11161 (Whitlock and Lamanna, 2012). The distribution of this character thus seems very difficult to interpret. The fact that there are so few specimens preserving this area also decreases the phylogenetic value of this character. Therefore, until a more numerous sample of diplodocid skulls with articulated palatal complex is found, this feature should not be used in diagnoses. In general, autapomorphies previously proposed for the genus *Apatosaurus* most often describe a more inclusive clade in the present analysis, as many taxa previously included in the genus are actually forming their own genera (e.g. *Brontosaurus*, or *Elosaurus*). These traits are thus not further discussed here.

Locality and horizon: various sites in Colorado, Wyoming, and Utah. Middle to upper part of the Upper Jurassic Morrison Formation, Late Kimmeridgian to Early Tithonian. Apatosaurine intervals 2 and 3 (Bakker, 1998); Dinosaur zone 3B upper (Turner and Peterson, 1999); Zone 5 (Foster, 2003).

***Apatosaurus ajax* Marsh, 1877a.**

Syn.? *Brontosaurus amplus* Marsh, 1881

Type specimen: YPM 1860.

Referred specimens: ?YPM 1981

Revised diagnosis: *A. ajax* is diagnosed by the following autapomorphies: a shallow, second fossa marks the quadrate shaft medially to the pterygoid flange (not the quadrate fossa) (52-1*, unique within Apatosaurinae), box-like basal tubera (81-1*, unique within Apatosaurinae), longest axes of the basal tubera oriented parallel to each other (87-0*, unique within Apatosaurinae), medial surface of posterior bifid, cervical neural spines is smooth (206-1*, unambiguous), presence of an accessory lamina linking the hyposphene of mid- and posterior dorsal vertebrae with the base of the posterior centrodiapophyseal lamina (260-1*, unique within Apatosaurinae), and presence of an elliptical depression between the lateral spinal lamina of caudal neural spines and the postspinal lamina (292-1*, unique within Apatosaurinae).

Comments: In the most recent revised diagnosis of the species, Upchurch et al. (2004b)

PeerJ Reviewing Manuscript

proposed four more autapomorphies of the species, which are not found in the present analysis, due to the differing set of referred specimens to the species. Upchurch et al. (2004b) also recovered the specimens AMNH 460, NSMT-PV 20375, YPM 1840, and 1861 within *A. ajax*, whereas the present analysis finds the first three specimens as more basal, possibly new apatosaurine taxa, and YPM 1861 as *Apatosaurus louisae*. Wide cervical vertebrae, and low cervical neural spines are thus variable within Apatosaurinae. The dorsolateral process of the distal condyle of mt I, as well as the flange-like proximoventral process of php II-1might diagnose NSMT-PV 20375 instead.

Locality and horizon: Lakes' Quarry 10, Morrison, Gunnison County, Colorado (YPM 1860), and possibly Reed's Quarry 11, Como Bluff, Albany County, Wyoming (YPM 1981). Upper middle to upper-most Morrison Formation, Late Kimmeridgian to Early Tithonian. Apatosaurine intervals 2 and 3 (Bakker, 1998); Dinosaur zone 3B upper (Turner and Peterson, 1999); Zone 5 (Foster, 2003).

***Apatosaurus louisae* Holland, 1915a.**

Syn.? *Brontosaurus amplus* Marsh, 1881

Type specimen: CM 3018.

Referred specimens: CM 3378, CM 11162, YPM 1861, ?YPM 1981.

Revised diagnosis: *A. louisae* can be diagnosed by the following autapomorphies: presence of a dorsoventrally elongate coel on anterior and mid-cervical neural spines (165-1*, unique within Apatosauridae), posterior cervical prezygapophyses terminate well behind anterior ball (194-1, unique within Flagellicaudata), absence of a subvertical lamina in the postzygapophyseal centrodiapophyseal fossa of posterior cervical vertebrae, with the free edge facing posteriorly (199-0, unique within Apatosaurinae), presence of a rounded, subtriangular process on posterior cervical ribs, below the tuberculum (222-1, unambiguous), DV 2 is longer than DV 1 (239-1, unique within Diplodocoidea), pleurocoel on the first dorsal centra located posteriorly (240-1, unique within Apatosaurinae), parapophysis of DV 3 lies mid-way between centrum and prezygapophyses (246-1, unique among Diplodocidae), presence of an oblique ridge on the rib head of some dorsal ribs (283-1, unique within Apatosaurinae), slightly bifid anterior caudal neural spines (326-1*, unique within Apatosaurinae), and presence of a subtriangular projection on the ventral edge of the scapular blade (370-1*, unique among Apatosaurinae).

Comments: In their revised diagnosis, Upchurch et al. (2004b) also proposed the presence of pneumatopores in the dorsal ribs as autapomorphic for *A. louisae*. However, pneumatized dorsal ribs were already figured by Marsh (1896) from the holotype of *Brontosaurus excelsus*, YPM

PeerJ Reviewing Manuscript

1980, and are also present in YPM 1981 (ET, pers. obs., 2011). The anterior restriction of the sacral ribs as interpreted to be present in the holotype specimen by Upchurch et al. (2004b) is herein regarded a questionable autapomorphy, as original matrix was left filling the space between the sacral ribs, which might thus partly be obliterated. Two more autapomorphies put forward by Upchurch et al. (2004b) are actually also present in other apatosaurine specimens: the heart-shaped anterior caudal centra, and the medially beveled glenoid surface of the scapula.

Locality and horizon: Dinosaur National Monument, Jensen, Uintah County, Utah (CM 3018, 3378, and 11162), and Lakes' Quarry 10, Morrison, Gunnison County, Colorado (YPM 1861). Upper middle to upper-most Morrison Formation, Late Kimmeridgian to Early Tithonian. Apatosaurine intervals 2 and 3 (Bakker, 1998); Dinosaur zone 3B upper (Turner and Peterson, 1999); Zone 5 (Foster, 2003).

***Brontosaurus* Marsh, 1879.**

Type and only species: *Brontosaurus excelsus* Marsh, 1879.

Invalid proposed species: *Brontosaurus amplus* Marsh, 1881 (= *Apatosaurus*).

Revised diagnosis: *Brontosaurus* can be diagnosed by the following autapomorphies: orientation of the tuberculum of mid-dorsal ribs follows the straight direction of the rib shaft (285-1*, unique among Apatosaurinae), the posterior end of mid- and posterior caudal neural spine summits lies more or less straight above the postzygapophyses (343-1*, unique among Apatosaurinae); presence of a large nutrient foramen opening on midshaft anteriorly on the femur (434-1*, unique among Apatosaurinae); presence of a short transverse ridge on the anteromedial surface of the distal end of the tibia (443-1*, unique among Diplodocidae).

Comments: The autapomorphies proposed for '*Apatosaurus*' *excelsus* by Upchurch et al. (2004b) are questionable. Cervical ribs that terminate in front of the posterior end of the centrum are widespread among Diplodocoidea, and are recovered as synapomorphic for that clade herein. The ventromedially projecting process on the anterior end of the cervical ribs is here reinterpreted as shortened anterior process of the cervical rib. The spine summits in anterior dorsal vertebrae are actually longer than wide (Ostrom and McIntosh, 1966: plates 17 and 18), and the slight medial widening is due to the presence of a medial ridge on the metapophyses, which is also present on other apatosaurine specimens (e.g. CM 3018, UW 15556; Gilmore, 1936).

Locality and horizon: Reed's Quarry 10, Como Bluff, Albany County, Wyoming. Middle (Bakker, 1998) to upper (Foster, 1998) Morrison Formation, Late Kimmeridgian to ?Early Tithonian. Dinosaur zone 3B upper (Turner and Peterson, 1999), Zone 5 (Foster, 2003).

***Brontosaurus excelsus* Marsh, 1879.**

PeerJ Reviewing Manuscript

Type specimen: YPM 1980.

Referred specimens: -

Diagnosis, locality, and horizon as genus.

***Elosaurus* Peterson and Gilmore, 1902.**

Type and only species: *Elosaurus parvus* Peterson and Gilmore, 1902.

Revised diagnosis: *Elosaurus* is diagnosed by the following autapomorphies: greatly reduced spinoprezygapophyseal laminae in posterior dorsal vertebrae (274-0, unique within Diplodocoidea), and absence of a shallow, but distinct rugose tubercle at the center of the concave proximal portion of the anterior surface of the humerus (386-0*, unique within Apatosaurinae).

Comments: In their revised diagnosis of '*Apatosaurus*' *parvus*, Upchurch et al. (2004b) further mentioned wider than high posterior dorsal centra, a right angle between acromial ridge and scapular blade, differences in length of the ulnar proximal branches, a constriction in the distal half of mc III, and subequal width and depth of the distal articular surface of mc V. Wider than high dorsal centra are also present in NSMT-PV 20375 (Upchurch et al., 2004b), an almost right angle between acromial ridge and distal blade can be seen in *Apatosaurus ajax* as well as in *Eobrontosaurus yahnahpin* (Filla and Redman, 1994), and different lengths of the ulnar branches also mark *Apatosaurus ajax* (Tab. S46). The characters from the manus could not have been positively identified in the specimens included, and were thus omitted from the revised diagnosis.

Locality and horizon: Sheep Creep Quarry E, Albany County, Wyoming, and possibly Riggs' Quarry 15, Dinosaur Hill, Mesa County, Colorado. Middle Morrison Formation, probably Late Kimmeridgian. Dinosaur zone 3B lower (Turner and Peterson, 1999), Zone 4 (Foster, 2003).

***Elosaurus parvus* Peterson and Gilmore, 1902.**

Type specimen: CM 566.

Referred specimens: UW 15556 (previously CM 563), FMNH P25112 (provisionally).

Diagnosis, locality, and horizon as genus.

***Eobrontosaurus* Bakker, 1998.**

Type and only species: *Eobrontosaurus yahnahpin* (Filla and Redman, 1994). The species was initially described as belonging to *Apatosaurus*.

Revised diagnosis: *Eobrontosaurus* can be diagnosed by the following autapomorphies: presence of a longitudinal sulcus on the ventral surface of cervical vertebrae (133-1*, unique among Apatosaurinae), total height of anterior cervical vertebrae to centrum length ratio is greater than 1.2 (usually around 1.5) (154-2*, unique among Apatosaurinae), the medial surface of anterior

PeerJ Reviewing Manuscript

dorsal, bifid neural spines is gently rounded transversely (245-0*, unique within Apatosaurinae), mid- and posterior dorsal neural spines narrow dorsally to form a triangular shape in lateral view, with the base approximately twice the width of the dorsal tip (265-1*, unique among Apatosaurinae), absence of a thickened anterior rim of anterior caudal prespinal lamina (321-0*, unique among Apatosaurinae), a rounded anteroventral margin of the coracoid (372-0*, unique among Apatosaurinae), a ratio of the longest metacarpal to radius length of 0.40 or greater (399-1*, unique among Diplodocoidea), and the distal articular surface of the metatarsal I being perpendicular to the axis of the shaft (462-1*, unique among Flagellicaudata).

Comments: Bakker (1998) mentioned three more diagnosing features: long cervical ribs, distal scapular blade expanded, and coracoid suture at right angle with the long axis of the scapular blade. The presence of long cervical ribs could not have been confirmed based on the available pictures of the type specimen. The distally expanded scapular blade is actually shared with many apatosaur specimens (e.g. CM 3018, UW 15556, Gilmore, 1936). The unexpanded state is primarily based on the type specimen of *Apatosaurus ajax*, YPM 1860, but personal observations showed that the edges of the distal end are broken, and that the true expansion can therefore not be assessed in its entirety. The angle between the coracoid articulation and the distal blade, measured from photographs, is 74° (Tab. S41). Even if that should be wrong, the specimen described by Upchurch et al. (2004b), NSMT-PV 20375 shows an almost right angle, which would thus impede an interpretation as autapomorphy for *Eobrontosaurus*.

Locality and horizon: Bertha Quarry, Como Bluff, Albany County, Wyoming. Lower Morrison Formation, Kimmeridgian. Apatosaurine interval 1 (Bakker, 1998), Dinosaur zone 2 (Turner and Peterson, 1999), Zone 2 (Foster, 2003).

***Eobrontosaurus yahnahpin* (Filla and Redman, 1994).**

Type specimen: Tate-001.

Referred specimens: -

Diagnosis, locality, and horizon as genus.

Diplodocinae Marsh, 1884.

***Diplodocus* Marsh, 1878.**

Syn. *Seismosaurus* Gillette, 1991

Type species: *Diplodocus carnegii* Hatcher, 1901 (suppressing the *D. longus* Marsh, 1878, see above).

Referred species: *Diplodocus hallorum* (Gillette, 1991).

Invalid proposed species: *Diplodocus longus* Marsh, 1878 (nomen dubium, previous type

PeerJ Reviewing Manuscript

species, case to ICZN in preparation to propose *D. carnegii* as substitute), *D. lacustris* Marsh, 1884 (nomen dubium), *D. hayi* Holland, 1924 (= *Galeamopus hayi*).

Revised diagnosis: *Diplodocus* can be diagnosed by the following autapomorphies: base of posterior dorsal neural spines anteriorly inclined (280-1, unique within Diplodocinae), pneumatopores of anterior caudal centra persist until caudal 16 or more posteriorly (308-1, unambiguous), well-developed rugosity on dorsolateral margin of metatarsal II, near the distal end, extending to the center of the shaft (468-1, unique among Diplodocidae).

Comments: Whitlock (2011a) proposes three cranial traits as autapomorphies of *Diplodocus*: a well-defined preantorbital fossa, the pterygoid that lies medial to the ectopterygoid, and the anteriorly inclined, procumbent teeth. As no skull can be definitely attributed to *Diplodocus*, these suggestions are questionable. Furthermore, distinct preantorbital fossae, and procumbent teeth are also present on other diplodocine taxa (e.g. *Galeamopus, Kaatedocus*), and the relative positions of the pterygoid and ectopterygoid are not established with enough certainty to use it as diagnostic character (see above). Upchurch et al. (2004a) also defines *Diplodocus* solely based on cranial traits, most of which are actually shared with other diplodocine species that were not described or recognized at the time (*Galeamopus*, *Kaatedocus*). Wilson (2002) proposed the anteriorly expanded femoral distal condyles as autapomorphic for *Diplodocus*, as shared characteristic with advanced titanosauriforms. However, although the distal condyles are accompanied anteriorly by two distinct vertical ridges, the articular surface does not extend onto them as in *Rapetosaurus krausei* FMNH PR 2209, for example (Curry Rogers, 2009).

Locality and horizon: various sites in Colorado, New Mexico, Utah, and Wyoming. Middle Morrison Formation, probably Late Kimmeridgian. Apatosaurine interval 2 (Bakker, 1998), Dinosaur zones 3A to 3B upper (Turner and Peterson, 1999), Zones 3 to 5 (Foster, 2003).

***Diplodocus carnegii* Hatcher, 1901.**

Type specimen: CM 84.

Paratype: CM 94.

Referred specimens: -

Revised diagnosis: *Diplodocus carnegii* is diagnosed by the following autapomorphies: spinopostzygapophyseal laminae (spol) of posterior dorsal neural arches divided near the postzygapophyses (277-1, unique among Flagellicaudata), and slender metatarsal II (mean proximal and distal transverse breadth/maximum length <0.53) (465-0*, unique among Diplodocoidea).

Comments: Hatcher (1901) proposed two different characters to distinguish *D. carnegii* from *D.*

PeerJ Reviewing Manuscript

longus: shorter cervical ribs, and more posteriorly directed caudal neural spines. However, comparisons were not based on the holotype of *D. longus*, but on two referred specimens (USNM 4712 and AMNH 223), which are now known not to belong to the species: the cervical vertebra Hatcher (1901) mentions (USNM 4712) actually has apatosaurine affinities (Hatcher, 1903), whereas the specimen AMNH 223, on which Hatcher (1901) based his comparisons, is herein interpreted to belong to *Diplodocus hallorum*. The short cervical ribs are widespread among Diplodocinae, and do thus not qualify as species autapomorphy. Caudal neural spine orientation is one of the main features distinguishing *D. carnegii* from *D. hallorum*, but the vertical spines from the latter species are herein found to be the derived state, such that the more posteriorly inclined spines in *D. carnegii* cannot be used to diagnose the species.

Locality and horizon: Sheep Creek Quarries D (CM 94) and D(3) (CM 84), Albany County, Wyoming. Middle Morrison Formation, Late Kimmeridgian. Dinosaur zone 3B lower (Turner and Peterson, 1999), Zone 4 (Foster, 2003).

***Diplodocus hallorum* (Gillette, 1991).**

Syn. *Seismosaurus hallorum*, *Seismosaurus halli*.

Type specimen: NMMNH 3690.

Referred specimens: AMNH 223, DMNS 1494, USNM 10865.

Revised diagnosis: *Diplodocus hallorum* can be diagnosed by the following autapomorphies: dorsal end of the postspinal lamina of single dorsal neural spines concave transversely (234-1, unique among Diplodocoidea), mid-caudal neural arches are situated on the anterior half of the centrum (337-1, unique among Diplodocoidea), vertical mid-caudal neural spines (340-1, unambiguous), posterior end of mid- and posterior caudal neural spine summits lies more or less straight above the postzygapophyses (343-1, unique among Diplodocinae), presence of distinct fossae on the medial surfaces of the proximal branches of middle chevrons (357-1, unique among Diplodocinae), a gracile femur (robustness index (sensu Wilson and Upchurch, 2003) <0.22) (427-0*, unique among Diplodocinae), and the groove on the lateral surface of pedal unguals extends straight horizontally (477-1*, unique among Diplodocinae).

Comments: Lucas et al. (2006) in their taxonomic reappraisal of *Seismosaurus hallorum* proposed two more characters that distinguish the type specimen of *D. hallorum* from other species of *Diplodocus*: a more robust pubis, and paddle-shaped distal blades of the chevrons. Whereas the first is difficult to quantify and is thus provisionally omitted from the present diagnosis, the paddle shape of the chevrons is partly included in the character coding the posterior expansion of the chevron blade (C355), which is not present in the other specimens

PeerJ Reviewing Manuscript

referred to *D. hallorum*. The specific chevron shape of NMMNH 3690 is thus herein regarded as individual variation.

Locality and horizon: *Seismosaurus* Quarry, Sandoval County, New Mexico (NMMNH 3690), Dinosaur National Monument Quarry, Uintah County, Utah (DMNS 1494, USNM 10865), and AMNH 223 Quarry, Como Bluff, Albany County, Wyoming (AMNH 223). Middle Morrison Formation, Late Kimmeridgian. Apatosaurine interval 2 (Bakker, 1998), Dinosaur zones 3B lower to upper (Turner and Peterson, 1999), Zones 4 to 5 (Foster, 2003).

***Barosaurus* Marsh, 1890.**

Type and only species: *Barosaurus lentus* Marsh, 1890.

Invalid proposed species: *Barosaurus affinis* Marsh, 1899 (nomen dubium), *Barosaurus gracilis* Russell et al., 1980 (nomen nudum).

Revised diagnosis: *Barosaurus* can be diagnosed by the following autapomorphies: pleurocoel not extending onto parapophysis in anterior cervical vertebrae (158-1*, unique among Diplodocidae), elongation index of posterior cervical vertebrae (without anterior condyle) greater than 2.6 (192-2*, unique among Diplodocoidea), an anterior projection on the prdl of posterior cervical, or anterior and mid-dorsal vertebrae, right lateral to the prezygapophysis (213-1, unique among Diplodocoidea), nine dorsal vertebrae (224-3*, unambiguous), transition from 'fan'-shaped to 'normal' caudal ribs occurs between Cd 6 and Cd 7 (300-3*, unique among Diplodocinae), pneumatopores of anterior caudal centra disappear by Cd 15 (308-0*, unique within Diplodocinae), depth of ventral hollow increasing from anterior to posterior caudal centra (the present trait could not have been assessed in the current analysis, but is provisionally included in the diagnosis of *Barosaurus* following Upchurch et al., 2004a).

Comments: Whitlock (2011a) does not list any autapomorphies for *Barosaurus*. McIntosh (2005) states four more diagnosing features for the genus: bifurcation of cervical neural spines restricted to the posterior half of the neck, summits of caudal neural spines undivided, a proportionally shorter tail, and a less prominent ventral hollow in anterior and mid-caudal centra. However, all of these traits represent the basal diplodocid morphology, and are shared e.g. with *Kaatedocus* or *Supersaurus* (Lovelace et al., 2007; Tschopp and Mateus, 2013b). Upchurch et al. (2004a) suggested an additional autapomorphy: the parapophysis of DV 2 is situated at the bottom of the centrum. Such a low position of the parapophysis is also present in DV 2 of *Galeamopus* [redacted] and can thus not be regarded diagnostic for *Barosaurus*.

Locality and horizon: various sites in South Dakota, Utah, and Wyoming. Lower to middle Morrison Formation, Kimmeridgian. Apatosaurine intervals ?1 to 2 (Bakker, 1998), Dinosaur

PeerJ Reviewing Manuscript

zones 2 to 3B upper (Turner and Peterson, 1999), Zones 2 to 5 (Foster, 2003).

***Barosaurus lentus* Marsh, 1890.**

Type specimen: YPM 429.

Referred specimens: AMNH 6341, AMNH 7535, CM 11984.

Diagnosis, locality, and horizon as genus.

***Tornieria* Sternfeld, 1911.**

Type and only species: *Tornieria africana* (Fraas, 1908). The species was originally assigned to *Gigantosaurus africanus* (Fraas, 1908).

Invalid proposed species: *Tornieria robustus* (Fraas, 1908) (=*Janenschia robusta*).

Revised diagnosis: *Tornieria* is diagnosed by the following autapomorphies: mid-caudal prezygapophyses terminate at or behind the anterior edge of the centrum (339-0*, unique among Diplodocinae), a straight posterior border of the sternal plate (377-1*, unique among Neosauropoda), and distal femoral condyles expand onto the anterior portion of the femoral shaft (439-1*, unambiguous).

Comments: Whitlock (2011a) listed a single autapomorphy for the genus: the absence of a ventral hollow in anterior and mid-caudal centra. Contrary to Whitlock (2011a), a ventral hollow is present in the preserved caudal vertebrae of both specimens included herein (Remes, 2006). In his revision of *Tornieria*, Remes (2006) proposed additional autapomorphies: frontal forms the entire dorsal margin of the orbit, prefrontal with a short posterior process, elongate cervical vertebrae, relatively long anterior caudal vertebrae, pleurocoel located on the upper third of the caudal centra, caudal transverse processes situated high on the centrum, caudal neural spines single, and lacking lateral processes, the distal blade of the scapula is only slightly expanded, unequal lengths of the proximal ulnar processes, robust ischial shaft, and a low tibia to femur length ratio. The traits of the frontal and prefrontal were later shown to be present in *Kaatedocus* as well (Tschopp and Mateus, 2013b). Elongate cervical vertebrae were developed several times within Diplodocinae (e.g. *Barosaurus*, *Supersaurus*; McIntosh, 2005; Lovelace et al., 2007). Centrum length increases from anterior-most towards middle caudal vertebrae in all diplodocines, making relative length a serially variable character. It was thus not included in the present analysis, and a detailed assessment of the relative position of the anterior caudal vertebrae in the *Tornieria* specimens would be needed before including relative centrum length as diagnosing trait for the genus. The position of the pleurocoel in the preserved anterior-most caudal vertebra of the holotype individual (SMNS 12141a) does not appear to be restricted to the upper third (Remes, 2006: fig. 4C). Pneumatic foramina are dorsally located in the referred caudal vertebrae from

PeerJ Reviewing Manuscript

trench dd (MB.R.2956 to MB.R.2958; Remes, 2006), but as this trait appears different in the holotype, it should not be used in a diagnosis. The same accounts for the dorsal location of the transverse processes, which is most probably influenced by the position of the pleurocoel. Single caudal neural spines without lateral processes can only be observed in the referred caudal vertebrae, which were not included in the present analysis. However, these traits also occur in other diplodocine species, and are thus not reliable characters to distinguish *Tornieria*. A slight expansion of the scapular blade as well as robustness of the ischial shaft are difficult to quantify, but ratios do not appear to be significantly different from other diplodocine taxa. Unequally long ulnar proximal processes are shared with *Galeamopus* [redacted] (Tab. S46), as is the low tibia to femur ratio (Tab. S54).

Locality and horizon: localities A and k, Upper Saurian Beds, Tendaguru, District of Lindi, Tanzania. Tithonian.

***Tornieria africana* (Fraas, 1908).**

Type specimen: SMNS 12141a, 12145a, 12143, 12140, and 12142. The individual also contains the specimens SMNS 12145c, MB.R.2672, 2713, and 2728 (Remes, 2006).

Referred specimens: MB.R.2386, 2572, 2586, 2669, 2673, 2726, 2730, 2733, 2913, and 3816 (all belonging to a single individual; Heinrich, 1999; Remes, 2006).

Diagnosis, locality, and horizon as genus.

***Supersaurus* Jensen, 1985.**

Syn. *Dystylosaurus* Jensen, 1985; *Ultrasauros* Olshevsky, 1991.

Type and only species: *Supersaurus vivianae* Jensen, 1985.

Revised diagnosis: *Supersaurus* can be diagnosed by the following autapomorphies: spinoprezygapophyseal laminae in single dorsal neural spines separate along their entire length (231-0, unique among Diplodocoidea), presence of an infradiapophyseal pneumatopore between the acdl and the pcdl of mid- and posterior dorsal neural arches (262-1*, unique among Diplodocinae), opisthocoelous posterior dorsal centra (270-2, unique among Diplodocoidea), 'heart'-shaped anterior-most caudal centra with an acute ventral ridge (296-1, unique among Diplodocinae), pneumatopores on anterior caudal centra restricted to foramina (307-0, unique among Diplodocinae), and an angle between the acromial ridge and the distal blade greater than 81° (362-2*, unique among Diplodocinae).

Comments: Lovelace et al. (2007) listed several additional diagnosing traits for *Supersaurus*: elongate cervical vertebrae, an extreme narrowing of the ventral surface of cervical centra, well-developed parallel keels that mark the ventral surface of cervical centra, pneumatic foramina

PeerJ Reviewing Manuscript

present on the ventral surface of cervical centra, lateral pneumatopores on cervical centra small, located within a shallow coel, anterior dorsal vertebrae with a ventral keel, tall posterior dorsal neural spines, relatively low posterior dorsal neural arch, pneumatized dorsal ribs, and a dorsally expanded scapular blade. Most of these traits are actually shared with other diplodocine species: the elongate cervical vertebrae (e.g. *Tornieria*), the well-developed parallel keels (herein called posteroventral flanges), the ventral pneumatic foramina (e.g. in *Dinheirosaurus*), the restricted and small lateral pneumatic foramina of cervical vertebrae (e.g. *Galeamopus* [redacted] the ventral keel in anterior dorsal centra, the low dorsal neural arches, and the pneumatized dorsal ribs (e.g. *Dinheirosaurus*), the tall dorsal neural spines (typical for diplodocids in general), as well as the expanded scapular blade (e.g. *Galeamopus*). The extreme narrowing of the ventral surface of cervical centra is herein interpreted as a consequence of the centrum elongation, as a narrowing is generally seen relative to the centrum length.

Locality and horizon: Dry Mesa Quarry, Montrose County, Colorado, and Jimbo Quarry, Converse County, Wyoming. Middle Morrison Formation, Late Kimmeridgian to ?Early Tithonian. Dinosaur zone 3B lower (Turner and Peterson, 1999), Zone 4 (Foster, 2003).

***Supersaurus vivianae* Jensen, 1985.**

Syn. *Dystylosaurus edwini* Jensen, 1985; *Ultrasauros macintoshi* (Jensen, 1985).

Type specimen: BYU 12962. Individual probably also contains the specimens BYU 4503, 4839, 9024-25, 9044-45, 9085, 10612, 12424, 12555, 12639, 12819, 12861, 12946, 13016, 13018, 13981, 16679, and 17462 (Lovelace et al., 2007).

Referred specimens: WDC DMJ-021.

Diagnosis, locality, and horizon as genus.

***Dinheirosaurus* Bonaparte and Mateus, 1999.**

Type and only species: *Dinheirosaurus lourinhanensis* Bonaparte and Mateus, 1999.

Revised diagnosis: *Dinheirosaurus* can be diagnosed by the following autapomorphies: single posterior cervical and anterior dorsal neural spines (126-0*, unique among Flagellicaudata), the ventral keel is restricted to the posterior portion of the posterior cervical centrum (193-1*, unique within Flagellicaudata), three small fossae on the lateral face of the posterior cervical neural spine, posterior to the elongated coel (unambiguous; this trait was not included as character, as unambiguous autapomorphies of single OTUs do not bear any phylogenetic information), dorsal centrum length (excluding articular 'ball') remains approximately the same along the sequence (225-0*, unique among Diplodocinae), dorsal transverse processes are more than 30° inclined dorsally from the horizontal (230-1*, unique among Diplodocidae), and the ventral surface of

PeerJ Reviewing Manuscript

anterior caudal centra is without irregularly placed foramina (305-0*, unique within Flagellicaudata).

Comments: In their redescription of the species, Mannion et al. (2012) mention two additional autapomorphies: an accessory, subvertical lamina in the postzygapophyseal centrodiapophyseal fossa, and an accessory lamina linking the hyposphene to the posterior centrodiapophyseal lamina in mid- and posterior dorsal neural arches. A subvertical accessory lamina actually subdivides the pocdf in a variety of diplodocid and diplodocine taxa (e.g. *Galeamopus hayi*), whereas a lamina connecting hyposphene and pcdl is also present in posterior dorsal neural arches of *Supersaurus vivianae*.

Locality and horizon: Praia de Porto Dinheiro, Lourinhã, Portugal. Amoreira-Porto Novo Member, Lourinhã Formation, Late Kimmeridgian.

***Dinheirosaurus lourinhanensis* Bonaparte and Mateus, 1999.**

Type specimen: ML 414.

Referred specimens: -

Diagnosis, locality, and horizon as genus.

***Kaatedocus* Tschopp and Mateus, 2012.**

Type and only species: *Kaatedocus siberi* Tschopp and Mateus, 2012.

Revised diagnosis: *Kaatedocus* can be diagnosed by the following autapomorphies: anteriorly restricted squamosals (55-0*, unique among Diplodocoidea), a rugosity on the anterodorsal corner of the lateral side of mid- and posterior cervical centra (178-1, unique among Diplodocidae), posterior cervical prezygapophyseal facets are posteriorly followed by a transverse sulcus (195-1*, unambiguous), posterior cervical epipophyses are dorsoventrally compressed (202-1, unique among Flagellicaudata), posterior cervical neural spines parallel to converging (211-1, unique among Diplodocidae), and the distance between the bifid posterior cervical neural spine summits is subequal to neural canal width (212-1, unique among Diplodocidae).

Comments: The species and genus reference given above ('Tschopp and Mateus, 2012') does not refer to the publication listed in the references as Tschopp and Mateus (2012), but to Tschopp and Mateus (2013b). This is because the online version of the description of *K. siberi* was published in 2012, and thus the name is valid since that year. The printed version of the paper, however, was only published in 2013.

Tschopp and Mateus (2013b) list several other autapomorphies as well: a U-shaped notch between the frontals, presence of a post-parietal foramen, a sharp, narrow sagittal nuchal crest, a

PeerJ Reviewing Manuscript

straight anterior edge of the basal tubera, and the cervical pre-epipophysis that forms a distinct anterior spur. The notch is herein shown to be shared with *Galeamopus* [redacted] The presence of a post-parietal foramen is difficult to interpret in most diplodocid skulls, due to often fractured surfaces in this area of the skull. Moreover, it is present as well in another braincase from the Howe Quarry, SMA O25-8, which was tentatively referred to *Barosaurus* (Schmitt et al., 2013; this study). A relatively sharp sagittal nuchal crest is present as well in the skull of *Galeamopus hayi* HMNS 175 (Holland, 1906). Straight to convex anterior margins of the basal tubera are shared with CM 3452 and *Galeamopus* [redacted] The development of the cervical pre-epipophysis is actually different in the holotype and the referred specimen AMNH 7530, where no distinct anterior spur is present. The presence or absence of a spur is thus better interpreted as individually variable within *Kaatedocus*, and thus not diagnostic for the present genus.

Locality and horizon: Howe Quarry, Shell, Bighorn County, Wyoming. Lower Morrison Formation, Kimmeridgian. Dinosaur zone 2 (Turner and Peterson, 1999), Zone 2 (Foster, 2003).

***Kaatedocus siberi* Tschopp and Mateus, 2012.**

Type specimen: SMA 0004.

Referred specimens: AMNH 7530, SMA D16-3.

Diagnosis, locality, and horizon as genus.

***Galeamopus* gen. nov.**

Type species: *Galeamopus hayi* (Holland, 1924). The type species was originally assigned to *Diplodocus hayi*.

Diagnosis: *Galeamopus* is diagnosed by the following autapomorphies: portion of the parietal contributing to the skull roof is practically inexistent (60-2, unique among Flagellicaudata), a foramen in the notch that separates the two basal tubera (90-1, unique among Diplodocinae), well-developed anteromedial processes on the atlantal neurapophyses, which are distinct from the posterior wing (146-1, unique among Diplodocoidea), the posterior wing of atlantal neurapophyses remains of subequal width along most of its length (148-1, unambiguous), and the axial prespinal lamina develops a transversely expanded, knob-like tuberosity at its anterior end (151-1, unambiguous).

Locality and horizon: various sites in Wyoming. Lower to Middle Morrison Formation, Kimmeridgian. Apatosaurus interval 1 (Bakker, 1998), Dinosaur zone 2 to possibly 3 (Turner and Peterson, 1999), Zones 2 to possibly 3 or 4 (Foster, 2003).

***Galeamopus hayi* (Holland, 1924).**

Type specimen: HMNS 175 (previously CM 662).

PeerJ Reviewing Manuscript

Referred specimens: -

Diagnosis: *Galeamopus hayi* is diagnosed by the following autapomorphies: dorsoventral height of the parietal occipital process is low, subequal to less than the diameter of the foramen magnum (63-0*, unique among Diplodocinae), basipterygoid processes widely diverging (> 60°; 92-0*, unique among Diplodocinae), an ulna to humerus length of more than 0.76 (387-2*, unique within Diplodocoidea), distal articular surface for the ulna on the radius is reduced and relatively smooth (392-0*, unique within Diplodocidae), and the distal condyle of the radius is beveled at least 15° to the long axis of the shaft (393-1*, unique within Diplodocinae).

Locality and horizon: Quarry A, Red Fork of the Powder River, Johnson County, Wyoming. Lower Morrison Formation, Kimmeridgian. Apatosaurine interval 1 (Bakker, 1998).

[redacted]

Conclusions

The present paper increases knowledge about the morphology and the phylogenetic relationships of diplodocid sauropods. One new, partially complete specimen is described, including a nearly complete skull, and represents a new diplodocine species: *Galeamopus* [redacted] In order to resolve its exact systematic position within Diplodocidae, a specimen-based phylogenetic analysis was performed, which included all holotypes that have been identified as belonging to a

PeerJ Reviewing Manuscript

diplodocid sauropod at some point in history.

By doing so, one of the main challenges was, where to decide if specific or generic separation of the included specimens is warranted. Given that the only applicable species concept in paleontology is based on morphological differences, the sum of differences can be the only way how to approach this issue. Basing on the assumption that the rate of evolution was similar in the two temporally as well as spatially coexisting taxa Diplodocinae and Apatosaurinae, accumulation of individually varying traits is assumed to lead to speciation with the same speed in both taxa. Thus, a numerical approach was introduced, including a three-step approach to account for individual variation: first, phylogenetic software does not find all potential autapomorphies for single specimens or synapomorphies for recovered clades, because the sister clades (specimens or taxa in the case of a specimen-based analysis) often do not preserve the same bones, and are thus not comparable. Second, the quality and thus validity of found apomorphies was assessed based on the number of taxa they were shared with, as well as the relative phylogenetic positions of these taxa with the specimen or clade in question. Finally, the number of valid apomorphies was summed between sister clades (sometimes specimens). Based on the relationship between *Supersaurus* and *Dinheirosaurus*, which have been continuously found as sister taxa (Mannion et al., 2012; Tschopp and Mateus, 2013b; this study), and where generic separation is further supported by the geographical separation (North America versus Portugal), a sum of ten steps was considered enough for generic separation. By comparing the sum of differences between generally accepted species of the same genus with the sum of differences between specimens usually identified as belonging to the same species, a sum of five steps was established as being enough for specific separation. Given the three-step approach to reduce influence of individual variation, the true sum of differences between specimens or clades would even be higher in most cases. By applying these rules to all sister group arrangements found in the tree, validity of the included taxa was assessed in a more objective way.

The numerical approach established in the present analysis allowed a reassessment of the validity of the numerous taxonomic names proposed within Diplodocidae. Thereby, it was found that apatosaurine diversity was particularly underestimated in the past. Two genera previously synonymized with *Apatosaurus* resulted valid based on the sum of differences with their recovered sister taxa: *Brontosaurus* and *Elosaurus*, which together form the sister clade to *Apatosaurus* in the present analysis. *Eobrontosaurus* was found to be valid as well, and two more clusters of specimens were recovered at the base of Apatosaurinae, which might even represent two additional apatosaurine genera. However, more detailed work has to be done on the

PeerJ Reviewing Manuscript

specimens forming these clades before being able to confirm such an extraordinary increase in the number of apatosaurine genera. *Apatosaurus* was found to be the only apatosaurine genus with more than one species: *A. ajax*, and *A. louisae*. This results in four to six genera and five to seven species belonging to Apatosaurinae. In a less inclusive and less detailed specimen-based analysis of *Apatosaurus*, Upchurch et al. (2004b) found five species as probably valid, but did not include *Eobrontosaurus yahnahpin*. The species count thus remained more or less the same in the two analyses.

The intrarelationships of Diplodocinae were already well established before (Whitlock, 2011a; Mannion et al., 2012; Tschopp and Mateus, 2013b). However, by including single specimens, it became possible to furthermore assess the validity of the various species proposed in *Diplodocus*. Thereby, the type species *D. longus* was considered a nomen dubium, given the undiagnostic, fragmentary holotype specimen. This would lead to an abolishment of the famous and popular generic name *Diplodocus*. As this was not considered reasonable, a case is being prepared for submission to ICZN proposing *D. carnegii* as new type species, and suppressing *D. longus*. Furthermore, the holotype specimen of '*Diplodocus*' *hayi*, often mentioned to probably not belong to *Diplodocus* (Holland, 1924; McIntosh, 1990a; Curtice, 1996; Foster, 2003), was found to form its own genus (herein named *Galeamopus*), together with the newly described specimen SMA 0011, and the diplodocine skull AMNH 969 – also the latter having previously been identified as *Diplodocus* (Holland, 1906, 1924; McIntosh and Berman, 1978). Interestingly, no diplodocine specimen preserving articulated skulls and postcranial elements was herein found to group with *Diplodocus*: AMNH 969 and '*Diplodocus*' hayi are referred to *Galeamopus*, and CM 3452, on which Holland (1924), McIntosh and Berman (1975), and Berman and McIntosh (1978) based their identification of the skull-only specimens as *Diplodocus*, is recovered as more closely related to *Barosaurus* and *Kaatedocus*, and provisionally referred to *Barosaurus*. Although essentially complete and well-preserved, skulls like CM 11161, or USNM 2672 can thus not be definitely identified as *Diplodocus*. However, their recovered intermediate position between *Galeamopus* and *Kaatedocus* + *Barosaurus* indicates that a referral to *Diplodocus* might be justifiable, even though direct evidence for it is lacking. In any case, given the completeness and articulation of the two *Galeamopus* specimens HMNS 175 and SMA 0011, as well as the presence of at least an additional, referred skull, the morphology of *Galeamopus* can be considered better preserved than *Diplodocus*, where information on skull, forelimb, or distal tail morphology is not available from type specimens. In total, nine different species in seven genera are recognized within Diplodocinae. Together with the probable non-apatosaurine, non-

PeerJ Reviewing Manuscript

diplodocine diplodocid *Amphicoelias altus*, this amounts to a total of 15 to 17 valid diplodocid species, 13 to 15 of which from the Morrison Formation of the Western United States.

Acknowledgment

Being part of ET's dissertation, first thanks go to the members of the doctoral committee, which are Octávio Mateus, Martin Sander (Bonn, Germany), João Pais, Rogerio de Rocha (both GeoBioTec), and Louis Jacobs (Dallas, USA). They were there when I needed further advice or help with administrative things. Besides them, most importantly, we thank Hans-Jakob Siber and anybody else from the SMA, for the possibility to study material under their care, for logistical and organizational help. In particular, we appreciate the help of Esther Premru for the drawing of the quarry maps, Ben Pabst for the stunning reconstruction of the holotypic skull of *Galeamopus* [redacted] and Martin Kistler and his team for aiding opening boxes for the study of SMA 0011. Preparation of that specimen was led by Yoli Schicker, together with Maya Siber, Esther Wolfensberger, and ET back in 2001 and 2002. Further thanks go to Simão Mateus (ML) for the beautiful reconstruction of the skull of SMA 0011.

Christophe Hendrickx (GeoBioTec), Steve Brusatte (Univ. of Edinbourgh), Jay Nair (Univ. of Queensland), and Mike Taylor (Univ. of Bristol) reviewed an earlier version of portions of this paper and provided corrections for the English. Remo Forster (Zürich, Switzerland) helped with some figures of the specimen SMA 0011.

A specimen-based phylogenetic analysis as performed herein is highly dependent on personal observations of the specimens included. Although it was not possible to see all of them, many collection visits were possible thanks to the help and hospitality from the following people: Kate Wellspring (AC), Carl Mehling, Mark Norell, and Alana Gishlick (AMNH), Ted Daeschler and Ned Gilmore (ANS), Amy Henrici, Matthew Lamanna, and Dan Pickering (CM), Rafael Royo-Torres and Edoardo Espilez (CPT), Daniela Schwarz-Wings (MB.R.), Virginia Tidwell and Logan Ivy (DMNS), David Temple (HMNS), Margarita Belinchón (MCNV), Paul Barrett and Sandra Chapman (NHMUK), Hans-Jakob Siber and Thomas Bolliger (SMA), Matt Carrano and Mike Brett-Surman (USNM), Ralf Kosma, Achim Ritter, and Ulrich Joger (Staatl. Naturhist. Mus. Braunschweig), Bill Wahl and Malcolm Bedell (WDC), and Dan Brinkman and Marilyn Fox (YPM). Several people shared numerous pictures of specimens we were not able to see ourself: Christophe Hendrickx, Carl Mehling, Dave Lovelace (Univ. of Wisconsin), Henry Galiano (Dinosauria International), Heiner Mallison (MB.R.), José Carballido (MPEF), Jean Le Loeuff (Esperaza, France), Jay Nair, John Whitlock, Kelli Trujillo (Univ. of Wyoming), Larry

PeerJ Reviewing Manuscript

Witmer (Ohio Univ.), Mattia Baiano (Inst. Cat. Pal, Barcelona), Mike Brett-Surman, Matt Wedel (West. Univ. of Health Sciences, Pomona), Nils Knötschke (Dinopark Münchehagen), Phil Mannion, Pong Suteethorn (Univ. of Mahasarakham, Thailand), Regina Fechner, Ralf Kosma, Spencer Lucas (NMMNH), Takehito Ikejiri (Univ. of Alabama), Virginia Tidwell, William Gearty (YPM), and William Simpson (FMNH).

We thank the Willy Hennig Society for making the phylogeny software TNT freely accessible, and Andrea Cau (Museo Geologico "Cappellini", Bologna), Jay Nair, and especially José Carballido for invaluable help with phylogenetic techniques.

References

Antunes, M. T., and O. Mateus. 2003. Dinosaurs of Portugal. Comptes Rendus Palevol 2:77–95.

Apesteguía, S. 2005. Evolution of the titanosaur metacarpus; pp. 321–346 in V. Tidwell and K. Carpenter (eds.), Thunder-Lizards: The Sauropodomorph Dinosaurs. Indiana University Press, Bloomington.

Arbour, V. M., and P. J. Currie. 2012. Analyzing taphonomic deformation of ankylosaur skulls using retrodeformation and Finite Element Analysis. PLoS ONE 7:e39323.

Ayer, J. 2000. The Howe Ranch Dinosaurs. Sauriermuseum Aathal, Aathal, Switzerland, 96 pp.

Bakker, R. T. 1998. Dinosaur mid-life crisis; the Jurassic-Cretaceous transition in Wyoming and Colorado. Bulletin of the New Mexico Museum of Natural History and Science 14:67–77.

Balanoff, A. M., G. S. Bever, and T. Ikejiri. 2010. The braincase of *Apatosaurus* (Dinosauria: Sauropoda) based on Computed Tomography of a new specimen with comments on variation and evolution in sauropod neuroanatomy. American Museum Novitates 3677:1–32.

Barco, J. 2009. Sistemática e implicaciones filogenéticas y paleobiogeográficas del saurópodo *Galvesaurus herreroi* (Formación Villar del Arzobispo, Galve, España). 405 pp.

Barrett, P. M., and P. Upchurch. 1994. Feeding mechanisms of *Diplodocus*. Gaia 10:195–203.

Barrett, P. M., G. W. Storrs, M. T. Young, and L. M. Witmer. 2011. A new skull of *Apatosaurus* and its taxonomic and palaeobiological implications. 1606.

Bedell, M. W. J., and D. L. Trexler. 2005. First articulated manus of *Diplodocus carnegii*; pp. 302–320 in V. Tidwell and K. Carpenter (eds.), Thunder-Lizards: The Sauropodomorph Dinosaurs. Indiana University Press, Bloomington.

Berman, D. S., and J. S. McIntosh. 1978. Skull and relationships of the Upper Jurassic sauropod *Apatosaurus* (Reptilia, Saurischia). Bulletin of the Carnegie Museum of Natural History 8:1–35.

PeerJ Reviewing Manuscript

PeerJ Reviewing Manuscript

7717 Bird, R. T. 1985. Bones for Barnum Brown: Adventures of a Dinosaur Hunter. Texas Christian
7718 University Press, Fort Worth, 225 pp.
7719 Birkemeier, T. 2011. Neurocentral suture closure in *Allosaurus* (Saurischia: Theropoda):
7720 sequence and timing. Journal of Vertebrate Paleontology, Program and Abstracts 2011:72A.
7721 Bonaparte, J. F. 1986. The early radiation and phylogenetic relationships of the Jurassic sauropod
7722 dinosaurs, based on vertebral anatomy; pp. 247–258 in K. Padian (ed.), The Beginning of
7723 the Age of Dinosaurs. Cambridge University Press, Cambridge.
7724 Bonaparte, J. F., and O. Mateus. 1999. A new diplodocid, *Dinheirosaurus lourinhanensis* gen. et
7725 sp. nov., from the Late Jurassic beds of Portugal. Revista Del Museo Argentino de Ciencias
7726 Naturales 5:13–29.
7727 Bonaparte, J. F., B. J. González Riga, and S. Apesteguía. 2006. *Ligabuesaurus leanzai* gen. et sp.
7728 nov. (Dinosauria, Sauropoda), a new titanosaur from the Lohan Cura Formation (Aptian,
7729 Lower Cretaceous) of Neuquén, Patagonia, Argentina. Cretaceous Research 27:364–376.
7730 Bonaparte, J. F., W.-D. Heinrich, and R. Wild. 2000. Review of *Janenschia* Wild, with the
7731 description of a new sauropod from the Tendaguru beds of Tanzania and a discussion on the
7732 systematic value of procoelous caudal vertebrae in the Sauropoda. Palaeontographica
7733 Abteilung A 256:25–76.
7734 Bonnan, M. F. 2000. The presence of a calcaneum in a diplodocid sauropod. Journal of Vertebrate
7735 Paleontology 20:317–323.
7736 Bonnan, M. F. 2001. The evolution and functional morphology of sauropod dinosaur locomotion.
7737 Ph.D. dissertation, Northern Illinois University., Dekalb, Illinois, 759 pp.
7738 Bonnan, M. F. 2003. The evolution of manus shape in sauropod dinosaurs: implications for
7739 functional morphology, forelimb orientation, and phylogeny. Journal of Vertebrate
7740 Paleontology 23:595–613.
7741 Bonnan, M. F. 2005. Pes anatomy in sauropod dinosaurs: Implications for functional morphology,
7742 evolution, and phylogeny; pp. 346–380 in V. Tidwell and K. Carpenter (eds.), Thunder-
7743 lizards: the Sauropodomorph dinosaurs. Indiana University Press, Bloomington.
7744 Bonnan, M. F. 2007. Linear and geometric morphometric analysis of long bone scaling patterns
7745 in Jurassic neosauropod dinosaurs: their functional and paleobiological implications. The
7746 Anatomical Record: Advances in Integrative Anatomy and Evolutionary Biology
7747 290:1089–1111.
7748 Bonnan, M. F., and M. J. Wedel. 2004. First occurrence of *Brachiosaurus* (Dinosauria:
7749 Sauropoda) from the Upper Jurassic Morrison Formation of Oklahoma. PaleoBios 24:13–

7750 21.
7751 Brinkmann, W., and H.-J. Siber. 1992. Dinosaurier in Aathal. Sauriermuseum Aathal, Aathal, 37
7752 pp.
7753 Brochu, C. A. 1996. Closure of neurocentral sutures during crocodilian ontogeny: Implications
7754 for maturity assessment in fossil archosaurs. Journal of Vertebrate Paleontology 16:49–62.
7755 Brown, B. 1935. Sinclair dinosaur expedition, 1934. Natural History 36:2–15.
7756 Calvo, J. O. 1994. Jaw mechanics in sauropod dinosaurs. Gaia 10:183–193.
7757 Calvo, J. O., and L. Salgado. 1995. *Rebbachisaurus tessonei* sp. nov. A new sauropod from the
7758 Albian-Cenomanian of Argentina; new evidence on the origin of the Diplodocidae. Gaia
7759 11:13–33.
7760 Canudo, J. I., R. Royo-Torres, and G. Cuenca-Bescós. 2008. A new sauropod: *Tastavinsaurus*
7761 *sanzi* gen. et sp. nov. from the Early Cretaceous (Aptian) of Spain. Journal of Vertebrate
7762 Paleontology 28:712–731.
7763 Carballido, J. L., and P. M. Sander. 2013. Postcranial axial skeleton of *Europasaurus holgeri*
7764 (Dinosauria, Sauropoda) from the Upper Jurassic of Germany: implications for sauropod
7765 ontogeny and phylogenetic relationships of basal Macronaria. Journal of Systematic
7766 Palaeontology. 1–53.
7767 Carballido, J. L., J. S. Marpmann, D. Schwarz-Wings, and B. Pabst. 2012a. New information on a
7768 juvenile sauropod specimen from the Morrison Formation and the reassessment of its
7769 systematic position. Palaeontology 55:567–582.
7770 Carballido, J. L., L. Salgado, D. Pol, J. I. Canudo, and A. Garrido. 2012b. A new basal
7771 rebbachisaurid (Sauropoda, Diplodocoidea) from the Early Cretaceous of the Neuquén
7772 Basin; evolution and biogeography of the group. Historical Biology 24:631–654.
7773 Carballido, J. L., O. W. M. Rauhut, D. Pol, and L. Salgado. 2011. Osteology and phylogenetic
7774 relationships of *Tehuelchesaurus benitezii* (Dinosauria, Sauropoda) from the Upper Jurassic
7775 of Patagonia. Zoological Journal of the Linnean Society 163:605–662.
7776 Carpenter, K. 2010. Species concept in North American stegosaurs. Swiss Journal of Geosciences
7777 103:155–162.
7778 Carpenter, K., and J. McIntosh. 1994. Upper Jurassic sauropod babies from the Morrison
7779 Formation. Dinosaur Eggs and Babies 265–278.
7780 Carpenter, K., and V. Tidwell. 1998. Preliminary description of a *Brachiosaurus* skull from Felch
7781 quarry 1, Garden Park, Colorado. Modern Geology 23:69–84.
7782 Casanovas, M. L., J. V. Santafé, and J. L. Sanz. 2001. *Losillasaurus giganteus* , un nuevo

PeerJ Reviewing Manuscript

7783 saurópodo del tránsito Jurásico-Cretácico de la cuenca de“ Los Serranos”(Valencia,
7784 España). Paleontologia i Evolució 99–122.
7785 Charig, A. J. 1980. A diplodocid sauropod from the Lower Cretaceous of England; pp. 231–244
7786 in L. L. Jacobs (ed.), Aspects of Vertebrate History. Essays in Honor of Edwin Harris
7787 Colbert. Museum of Northern Arizona Press, Flagstaff.
7788 Chatterjee, S., and Z. Zheng. 2002. Cranial anatomy of *Shunosaurus*, a basal sauropod dinosaur
7789 from the Middle Jurassic of China. Zoological Journal of the Linnean Society 136:145–
7790 169.
7791 Chatterjee, S., and Z. Zheng. 2005. Neuroanatomy and dentition of *Camarasaurus lentus*; pp.
7792 199–211 in V. Tidwell and K. Carpenter (eds.), Thunder-lizards. The sauropodomorph
7793 dinosaurs. Indiana University Press, Bloomington.
7794 Christiansen, N. A., and E. Tschopp. 2010. Exceptional stegosaur integument impressions from
7795 the Upper Jurassic Morrison Formation of Wyoming. Swiss Journal of Geosciences
7796 103:163–171.
7797 Chure, D. J., R. Litwin, S. T. Hasiotis, E. Evanoff, and K. Carpenter. 2006. The fauna and flora of
7798 the Morrison Formation: 2006. Paleontology and Geology of the Upper Jurassic Morrison
7799 Formation. New Mexico Museum of Natural History and Science Bulletin 36:233–249.
7800 Chure, D., B. Britt, J. Whitlock, and J. Wilson. 2010. First complete sauropod dinosaur skull from
7801 the Cretaceous of the Americas and the evolution of sauropod dentition.
7802 Naturwissenschaften 97:379–391.
7803 Claessens, L. P. A. M. 2004. Dinosaur gastralia; origin, morphology, and function. Journal of
7804 Vertebrate Paleontology 24:89–106.
7805 Cooper, M. R. 1984. A reassessment of *Vulcanodon karibaensis* Raath (Dinosauria: Saurischia)
7806 and the origin of the Sauropoda. Palaeontologia Africana 25:203–231.
7807 Cope, E. D. 1877a. On *Amphicoelias*, a genus of saurians from the Dakota Epoch of Colorado.
7808 Paleontology Bulletin 27:1–5.
7809 Cope, E. D. 1877b. On a dinosaurian from the Trias of Utah. Proceedings of the American
7810 Philosophical Society 16:579–584.
7811 Cope, E. D. 1878. A new species of *Amphicoelias*. American Naturalist 12:563–564.
7812 Curry, K. A. 1999. Ontogenetic histology of *Apatosaurus* (Dinosauria: Sauropoda): new insights
7813 on growth rates and longevity. Journal of Vertebrate Paleontology 19:654–665.
7814 Curry Rogers, K. A. 2005. Titanosauria: a phylogenetic overview; pp. 51–103 in K. A. Curry
7815 Rogers and J. A. Wilson (eds.), The Sauropods: Evolution and Paleobiology. University of

PeerJ Reviewing Manuscript

California Press, Berkeley, CA.
Curry Rogers, K. A. 2009. The postcranial osteology of *Rapetosaurus krausei* (Sauropoda: Titanosauria) from the Late Cretaceous of Madagascar. Journal of Vertebrate Paleontology 29:1046–1086.
Curry Rogers, K. A., and C. A. Forster. 2001. The last of the dinosaur titans: a new sauropod from Madagascar. Nature 412:530–534.
Curry Rogers, K. A., and C. A. Forster. 2004. The skull of *Rapetosaurus krausei* (Sauropoda: Titanosauria) from the Late Cretaceous of Madagascar. Journal of Vertebrate Paleontology 24:121–144.
Curtice, B. 1996. Codex of diplodocid caudal vertebrae from the Dry Mesa dinosaur quarry. Master Thesis, Brigham Young University. Department of Geology., 156 pp.
Curtice, B. D., and K. L. Stadtman. 2001. The demise of *Dystylosaurus edwini* and a revision of *Supersaurus vivianae*. Mesa Southwest Museum Bulletin 8:33–39.
Curtice, B. D., K. L. Stadtman, and L. J. Curtice. 1996. A reassessment of *Ultrasauros macintoshi* (Jensen, 1985). Museum of Northern Arizona Bulletin 60:87–95.
D'Emic, M. D. 2012. The early evolution of titanosauriform sauropod dinosaurs. Zoological Journal of the Linnean Society 166:624–671.
D'Emic, M. D., P. D. Mannion, P. Upchurch, R. B. J. Benson, Q. Pang, and C. Zhengwu. 2013. Osteology of *Huabeisaurus allocotus* (Sauropoda: Titanosauriformes) from the Upper Cretaceous of China. PLoS ONE 8:e69375.
Dantas, P., J. Sanz, C. Marques da Silva, F. Ortega, V. Santos, and M. Cachão. 1998. *Lourinhasaurus* n. gen. novo dinossáurio saurópode do Jurássico superior (Kimeridgiano superior-Titoniano inferior) de Portugal. Actas Do V Congresso Nacional de Geologia.-Com. Inst. Geol. Mineiro 84:91–94.
Filla, J., and P. D. Redman. 1994. *Apatosaurus yahnahpin*: a preliminary description of a new species of diplodocid dinosaur from the Late Jurassic Morrison Formation of Southern Wyoming, the first sauropod dinosaur found with a complete set of "belly ribs."159–178.
Foster, J. R. 1998. Aspects of vertebrate paleoecology, taphonomy, and biostratigraphy of the Morrison Formation (Upper Jurassic), Rocky Mountain region, western United States. University of Colorado, 466 pp.
Foster, J. R. 2003. Paleoecological analysis of the vertebrate fauna of the Morrison Formation (Upper Jurassic), Rocky Mountain Region, U.S.A. New Mexico Museum of Natural History and Science Bulletin 23:2–100.

PeerJ Reviewing Manuscript

7849 Fraas, E. 1908. Ostafrikanische Dinosaurier. Palaeontographica 15:105–144.
7850 Gabunia, L. K., G. Mchedlidze, V. M. Chkhikvadze, and S. G. Lucas. 1998. Jurassic sauropod
7851 dinosaur from the Republic of Georgia. Journal of Vertebrate Paleontology 18:233–236.
7852 Galiano, H., and R. Albersdörfer. 2010. *Amphicoelias* "Brontodiplodocus", a New Sauropod,
7853 from the Morrison Formation, Big Horn Basin, Wyoming, with Taxonomic Reevaluation of
7854 *Diplodocus*, *Apatosaurus*, *Barosaurus* and Other Genera. Dinosauria International, LLC, 50
7855 pp.
7856 Gallina, P. A. 2011. Notes on the axial skeleton of the titanosaur *Bonitasaura salgadoi*
7857 (Dinosauria-Sauropoda). Anais Da Academia Brasileira de Ciências 83:235–246.
7858 Gallina, P. A. 2012. Histología ósea del titanosaurio *Bonitasaura salgadoi*(Dinosauria:
7859 Sauropoda) del Cretácico Superior de Patagonia. Ameghiniana 49:289–302.
7860 Gallina, P. A., and S. Apesteguía. 2005. *Cathartesaura anaerobica* gen. et sp. nov., a new
7861 rebbachisaurid (Dinosauria, Sauropoda) from the Huincul Formation (Upper Cretaceous),
7862 Río Negro, Argentina. Revista Museo Argentino Ciencias Naturales Nueva Serie 7:153–
7863 166.
7864 Gauthier, J. 1986. Saurischian monophyly and the origin of birds. Memoirs of the California
7865 Academy of Sciences 8:55.
7866 Gillette, D. D. 1991. *Seismosaurus halli*, gen. et sp. nov., a new sauropod dinosaur from the
7867 Morrison Formation (Upper Jurassic/Lower Cretaceous) of New Mexico, USA. Journal of
7868 Vertebrate Paleontology 11:417–433.
7869 Gillette, D. D. 1994. *Seismosaurus*: The Earth Shaker. Columbia University Press, New York,
7870 205 pp.
7871 Gillette, D. D. 1996a. Origin and early evolution of the sauropod dinosaurs of North America: the
7872 type locality and stratigraphic position of *Dystrophaeus viaemalae* Cope 1877. Utah
7873 Geological Association Guidebook 25:313–324.
7874 Gillette, D. D. 1996b. Stratigraphic position of the sauropod *Dystrophaeus viaemalae* Cope 1877
7875 and its evolutionary implications. Museum of Northern Arizona, Bulletin 60:59–68.
7876 Gilmore, C. W. 1925. A nearly complete articulated skeleton of *Camarasaurus*, a saurischian
7877 dinosaur from the Dinosaur National Monument, Utah. Memoirs of the Carnegie Museum
7878 10:347–384.
7879 Gilmore, C. W. 1932. On a newly mounted skeleton of *Diplodocus* in the United States National
7880 Museum. Proceedings of the United States National Museum 81:1–21.
7881 Gilmore, C. W. 1936. Osteology of *Apatosaurus*: with special reference to specimens in the

PeerJ Reviewing Manuscript

7882 Carnegie Museum. Memoirs of the Carnegie Museum 11:175–300.
7883 Goloboff, P. A. 1993. Estimating character weights during tree search. Cladistics 9:83–91.
7884 Goloboff, P. A., J. S. Farris, and K. C. Nixon. 2008. TNT, a free program for phylogenetic
7885 analysis. Cladistics 24:774–786.
7886 Goloboff, P. A., J. S. Farris, M. Källersjö, B. Oxelman, M. J. Ramírez, and C. A. Szumik. 2003.
7887 Improvements to resampling measures of group support. Cladistics 19:324–332.
7888 González Riga, B. J. 2002. Estratigrafía y Dinosaurios del Cretácico Tardío en el extremo sur de
7889 la provincia de Mendoza, Argentina. Ph.D. dissertation, National University of Córdoba,
7890 Argentina, 280 pp.
7891 González Riga, B. J., E. Previtera, and C. A. Pirrone. 2009. *Malarguesaurus florenciae* gen. et sp.
7892 nov., a new titanosauriform (Dinosauria, Sauropoda) from the Upper Cretaceous of
7893 Mendoza, Argentina. Cretaceous Research 30:135–148.
7894 Haas, G. 1963. A proposed reconstruction of the jaw musculature of *Diplodocus*. Annals of
7895 Carnegie Museum 36:139–157.
7896 Harris, J. D. 2006a. Cranial osteology of *Suuwassea emilieae* (Sauropoda: Diplodocoidea:
7897 Flagellicaudata) from the Upper Jurassic Morrison Formation of Montana, USA. Journal of
7898 Vertebrate Paleontology 26:88–102.
7899 Harris, J. D. 2006b. The axial skeleton of the dinosaur *Suuwassea emilieae* (Sauropoda:
7900 Flagellicaudata) from the Upper Jurassic Morrison Formation of Montana, USA.
7901 Palaeontology 49:1091–1121.
7902 Harris, J. D. 2006c. The significance of *Suuwassea emilieae* (Dinosauria: Sauropoda) for
7903 flagellicaudatan intrarelationships and evolution. Journal of Systematic Palaeontology
7904 4:185–198.
7905 Harris, J. D. 2007. The appendicular skeleton of *Suuwassea emilieae* (Sauropoda:
7906 Flagellicaudata) from the Upper Jurassic Morrison Formation of Montana (USA). Geobios
7907 40:501–522.
7908 Harris, J. D., and P. Dodson. 2004. A new diplodocoid sauropod dinosaur from the Upper Jurassic
7909 Morrison Formation of Montana, USA. Acta Palaeontologica Polonica 49:197–210.
7910 Hatcher, J. B. 1901. *Diplodocus* (Marsh): its osteology, taxonomy, and probable habits, with a
7911 restoration of the skeleton. Memoirs of the Carnegie Museum 1:1–63.
7912 Hatcher, J. B. 1902. Structure of the forelimb and manus of *Brontosaurus*. Annals of the Carnegie
7913 Museum 1:356–376.
7914 Hatcher, J. B. 1903. Osteology of *Haplocanthosaurus*, with description of a new species and

PeerJ Reviewing Manuscript

remarks on the probable habits of the Sauropoda and the age and origin of the *Atlantosaurus* beds: Additional remarks on *Diplodocus*. Memoirs of the Carnegie Museum 2:1–72.

He, X., K. Li, and K. Cai. 1988. The Middle Jurassic Dinosaur Fauna from Dashanpu, Zigong, Sichuan. Vol. IV. Sauropod Dinosaurs (2) *Omeisaurus tianfuensis*. Sichuan Publishing House of Science and Technology, Chengdu, China, 143 pp.

He, X., K. Li, K. Cai, and Y. Gao. 1984. *Omeisaurus tianfuensis*—a new species of *Omeisaurus* from Dashanpu, Zigong, Sichuan. Journal of Chengdu College Geology, Supplement 2:13–32.

He, X., S. Yang, K. Cai, K. Li, and Z. Liu. 1996. A new species of sauropod, *Mamenchisaurus anyuensis* sp. nov. Proceedings of the 30th International Geological Congress 12:83–86.

Heathcote, J., and P. Upchurch. 2003. The relationships of *Cetiosauriscus stewarti* (Dinosauria; Sauropoda): implications for sauropod phylogeny. Journal of Vertebrate Paleontology 23:60A.

Hedrick, B., A. R. Tumarkin-Deratzian, and P. Dodson. 2012. Bone microstructure and relative age of the holotype specimen of the diplodocoid sauropod dinosaur *Suuwassea emilieae*. Acta Palaeontologica Polonica.

Heinrich, W.-D. 1999. The taphonomy of dinosaurs from the Upper Jurassic of Tendaguru (Tanzania) based on field sketches of the German Tendaguru Expedition (1909-1913). Fossil Record 2:25–61.

Herne, M. C., and S. G. Lucas. 2006. *Seismosaurus hallorum*: osteological reconstruction from the holotype. Bulletin of the New Mexico Museum of Natural History and Science 36:139–148.

Hohn, B. 2011. Walking with the shoulder of giants: biomechanical conditions in the tetrapod shoulder girdle as a basis for sauropod shoulder reconstruction; pp. 182–196 in N. Klein, K. Remes, C. T. Gee, and P. M. Sander (eds.), Biology of the Sauropod Dinosaurs: Understanding the Life of Giants., Life of the Past Indiana University Press, Bloomington.

Hohn-Schulte, B. 2010. Form and function of the shoulder girdle in sauropod dinosaurs: a biomechanical investigation with the aid of finite elements. Ruhr-Universität Bochum, Universitätsbibliothek, Bochum, 233 pp.

Holland, W. J. 1906. The osteology of *Diplodocus* Marsh. Memoirs of the Carnegie Museum 2:225–264.

Holland, W. J. 1915a. A new species of *Apatosaurus*. Annals of the Carnegie Museum 10:143–

PeerJ Reviewing Manuscript

145.
Holland, W. J. 1915b. Heads and tails: a few notes relating to the structure of the sauropod dinosaurs. Annals of the Carnegie Museum 9:272–278.
Holland, W. J. 1924. The skull of *Diplodocus*. Memoirs of the Carnegie Museum 9:378–403.
Holliday, C. M., and L. M. Witmer. 2008. Cranial kinesis in dinosaurs: intracranial joints, protractor muscles, and their significance for cranial evolution and function in diapsids. Journal of Vertebrate Paleontology 28:1073–1088.
Huene, F. 1904. *Dystrophaeus viaemalae* Cope in neuer Beleuchtung. Separat-Abdruck Aus Dee Neuen Jahrbuch Fur Mineralogie, Geologie Und Palaeontologie, Stuttgart, Germany.
Huene, F. 1927. Sichtung der Grundlagen der jetzigen Kenntnis der Sauropoden. Eclogae Geologicae Helvetiae 20:444–470.
Huene, F. 1929. Los Saurisquios y Ornithisquios de Cretaceo Argentine. Annales de Museo de La Plata 3 (Series 2):1–196.
Ikejiri, T. 2004. Anatomy of *Camarasaurus lentus* (Dinosauria: Sauropoda) from the Morrison Formation (Late Jurassic), Thermopolis, central Wyoming, with determination and interpretation of ontogenetic, sexual dimorphic, and individual variation in the genus. Master Thesis, Fort Hays State University, Kansas, UMI pp.
Ikejiri, T. 2012. Histology-based morphology of the neurocentral synchondrosis in *Alligator mississippiensis* (Archosauria, Crocodylia). Anatomical Record 295:18–31.
Ikejiri, T., V. Tidwell, and D. L. Trexler. 2005. New adult specimens of *Camarasaurus lentus* highlight ontogenetic variation within the species; pp. 154–179 in Thunder-lizards: the Sauropodomorph dinosaurs. Indiana University Press, Bloomington.
Irmis, R. B. 2007. Axial skeleton ontogeny in the Parasuchia (Archosauria: Pseudosuchia) and its implications for ontogenetic determination in archosaurs. Journal of Vertebrate Paleontology 27:350–361.
Jain, S. L., and S. Bandyopadhyay. 1997. New titanosaurid (Dinosauria: Sauropoda) from the Late Cretaceous of Central India. Journal of Vertebrate Paleontology 17:114–136.
Janensch, W. 1922. Das Handskelett von *Gigantosaurus robustus* und *Brachiosaurus brancai* aus den Tendaguru-Schichten Deutsch-Ostafrikas. Centralblatt Für Mineralogie, Geologie Und Paläontologie 15:464–480.
Janensch, W. 1929a. Die Wirbelsäule der Gattung *Dicraeosaurus*. Palaeontographica Supplement 7:38–133.
Janensch, W. 1929b. Material und Formengehalt der Sauropoden in der Ausbeute der Tendaguru-

PeerJ Reviewing Manuscript

Expedition. Palaeontographica-Supplementbände 1–34.

Janensch, W. 1935. Die Schädel der Sauropoden *Brachiosaurus*, *Barosaurus* und *Dicraeosaurus* aus den Tendaguruschichten Deutsch-Ostafrikas. Palaeontographica Supplement 7:145–298.

Janensch, W. 1950. Die Wirbelsäule von *Brachiosaurus brancai*. Palaeontographica Supplement 7:27–93.

Janensch, W. 1961. Die Gliedmassen und Gliedmassengürtel der Sauropoden der Tendaguru-Schichten. Palaeontographica-Supplementbände 177–235.

Jensen, J. A. 1985. Three new sauropod dinosaurs from the Upper Jurassic of Colorado. Western North American Naturalist 45:697–709.

Jensen, J. A. 1987. New brachiosaur material from the Late Jurassic of Utah and Colorado. Western North American Naturalist 47:592–608.

Jensen, J. A. 1988. A fourth new sauropod dinosaur from the Upper Jurassic pf the Colorado Plateau and sauropod bipedalism. Western North American Naturalist 48:121–145.

Klein, N., and M. Sander. 2008. Ontogenetic stages in the long bone histology of sauropod dinosaurs. Paleobiology 34:247-263.

Klein, N., A. Christian, and P. M. Sander. 2012. Histology shows that elongated neck ribs in sauropod dinosaurs are ossified tendons. Biology Letters 8:1032–1035.

Knoll, F., L. M. Witmer, F. Ortega, R. C. Ridgely, and D. Schwarz-Wings. 2012. The braincase of the basal sauropod dinosaur *Spinophorosaurus* and 3D reconstructions of the cranial endocast and inner ear. PLoS ONE 7:e30060.

Kowallis, B. J., E. H. Christiansen, A. L. Deino, F. Peterson, C. E. Turner, M. J. Kunk, and J. D. Obradovich. 1998. The age of the Morrison Formation. Modern Geology 22:235–260.

Ksepka, D. T., and M. A. Norell. 2006. *Erketu ellisoni*, a long-necked sauropod from Bor Guvé (Dornogov Aimag, Mongolia). American Museum Novitates 3508:1–16.

Lapparent, A. F. de, and G. Zbyszewski. 1957. Les dinosauriens du Portugal. Memoires Des Services Géologiques Du Portugal 2:1–63.

Lovelace, D. M., S. A. Hartman, and W. R. Wahl. 2007. Morphology of a specimen of *Supersaurus* (Dinosauria, Sauropoda) from the Morrison Formation of Wyoming, and a re-evaluation of diplodocid phylogeny. Arquivos Do Museu Nacional 65:527–544.

Lucas, S. G., J. A. Spielman, L. A. Rinehart, A. B. Heckert, M. C. Herne, A. P. Hunt, J. R. Foster, and R. M. Sullivan. 2006. Taxonomic status of *Seismosaurus hallorum*, a Late Jurassic sauropod dinosaur from New Mexico. New Mexico Museum of Natural History and

PeerJ Reviewing Manuscript

8014 Science Bulletin 36:149–162.
8015 Lull, R. S. 1919. The sauropodous dinosaur *Barosaurus* Marsh. Memoirs of the Connecticut
8016 Academy of Arts and Sciences 6:1–42.
8017 Madsen, J. H., J. S. McIntosh, and D. S. Berman. 1995. Skull and atlas-axis complex of the
8018 Upper Jurassic sauropod *Camarasaurus* Cope (Reptilia: Saurischia). Bulletin of Carnegie
8019 Museum of Natural History 31:1–115.
8020 Mannion, P. D. 2009. A rebbachisaurid sauropod from the Lower Cretaceous of the Isle of Wight,
8021 England. Cretaceous Research 30:521–526.
8022 Mannion, P. D. 2010. Environmental and geological controls on the diversity and distribution of
8023 the sauropodomorpha. Ph.D. Dissertation, University College London, London, 349 pp.
8024 Mannion, P. D. 2011. A reassessment of *Mongolosaurus haplodon* Gilmore, 1933, a titanosaurian
8025 sauropod dinosaur from the Early Cretaceous of Inner Mongolia, People's Republic of
8026 China. Journal of Systematic Palaeontology 9:355–378.
8027 Mannion, P. D., and J. O. Calvo. 2011. Anatomy of the basal titanosaur (Dinosauria, Sauropoda)
8028 *Andesaurus delgadoi* from the mid-Cretaceous (Albian–early Cenomanian) Río Limay
8029 Formation, Neuquén Province, Argentina: implications for titanosaur systematics.
8030 Zoological Journal of the Linnean Society.
8031 Mannion, P. D., P. Upchurch, O. Mateus, R. N. Barnes, and M. E. H. Jones. 2012. New
8032 information on the anatomy and systematic position of *Dinheirosaurus lourinhanensis*
8033 (Sauropoda: Diplodocoidea) from the Late Jurassic of Portugal, with a review of European
8034 diplodocoids. Journal of Systematic Palaeontology 10:521–551.
8035 Mannion, P. D., P. Upchurch, R. N. Barnes, and O. Mateus. 2013. Osteology of the Late Jurassic
8036 Portuguese sauropod dinosaur *Lusotitan atalaiensis* (Macronaria) and the evolutionary
8037 history of basal titanosauriforms. Zoological Journal of the Linnean Society 168:98–206.
8038 Marsh, O. C. 1877a. Notice of some new dinosaurian reptiles from the Jurassic Formation.
8039 American Journal of Science (series 3) 14:514–516.
8040 Marsh, O. C. 1877b. A new order of extinct Reptilia (Stegosauria) from the Jurassic of the Rocky
8041 Mountains. American Journal of Science, 3rd Series 14:34–35.
8042 Marsh, O. C. 1878. Principal characters of American Jurassic dinosaurs, Part I. American Journal
8043 of Science (series 3) 16:411–416.
8044 Marsh, O. C. 1879. Notice of new Jurassic reptiles. American Journal of Science (series 3)
8045 18:510–505.
8046 Marsh, O. 1880. The sternum in dinosaurian reptiles. American Journal of Science (Series 3)

PeerJ Reviewing Manuscript

19:395–396.
Marsh, O. C. 1881. Principle characters of American Jurassic dinosaurs. Part V. American Journal of Science (Series 3) 21:417–437.
Marsh, O. C. 1883. Principal characters of American Jurassic dinosaurs. Restoration of *Brontosaurus*. Geological Magazine (Decade II) 10:385–388.
Marsh, O. C. 1884. Principal characters of American Jurassic dinosaurs. Part VII. On the Diplodocidae, a new family of the Sauropoda. American Journal of Science (series 3) 27:160–168.
Marsh, O. C. 1890. Description of new dinosaurian reptiles. American Journal of Science (series 3) 39:81–86.
Marsh, O. C. 1895. On the affinities and classification of the dinosaurian reptiles. American Journal of Science 483–498.
Marsh, O. C. 1896. The dinosaurs of North America. US Geological Survey Annual Report 16:142–230.
Marsh, O. C. 1898. On the families of sauropodous Dinosauria. American Journal of Science 6:487–488.
Marsh, O. C. 1899. Footprints of Jurassic dinosaurs. American Journal of Science s4-7:227–232.
Mateus, O. 2005. Dinossauros do Jurássico Superior de Portugal, com destaque para os saurísquios. Ph.D. dissertation, Universidade Nova de Lisboa, Lisboa 381 pp.
Mateus, O. and E. Tschopp. 2013. *Cathetosaurus* as a valid sauropod genus and comparisons with *Camarasaurus*. Journal of Vertebrate Paleontology, Programs and Abstracts: 173.
Mateus, O., L. L. Jacobs, A. S. Schulp, M. J. Polcyn, T. S. Tavares, A. Buta Neto, M. L. Morais, and M. T. Antunes. 2011. *Angolatitan adamastor*, a new sauropod dinosaur and the first record from Angola. Anais Da Academia Brasileira de Ciências 83:221–233.
Matthew, W. D. 1905. The mounted skeleton of *Brontosaurus*. American Museum Journal 5:63–71.
McIntosh, J. S. 1981. Annotated catalogue of the dinosaurs (Reptilia, Archosauria) in the collections of Carnegie Museum of Natural History. Bulletin of Carnegie Museum of Natural History 18:1–67.
McIntosh, J. S. 1989. The sauropod dinosaurs: a brief survey; pp. 85–99 in K. Padian and D. J. Chure (eds.), The Age of Dinosaurs., Short Courses in Paleontology Paleontological Society, Saint-Louis.
McIntosh, J. S. 1990a. Species determination in sauropod dinosaurs with tentative suggestions for

PeerJ Reviewing Manuscript

their classification; pp. 53–69 in K. Carpenter and P. J. Currie (eds.), Dinosaur Systematics: Perspectives and Approaches. Cambridge University Press, New York.

McIntosh, J. S. 1990b. Sauropoda; pp. 345–401 in D. B. Weishampel, P. Dodson, and H. Osmólska (eds.), The Dinosauria. University of California Press, Berkeley, CA.

McIntosh, J. S. 1995. Remarks on the North American sauropod *Apatosaurus* Marsh. Short Papers 119–123.

McIntosh, J. S. 1997. The saga of a forgotten sauropod dinosaur. Dinofest International Proceedings 7–12.

McIntosh, J. S. 2005. The genus *Barosaurus* Marsh (Sauropoda, Diplodocidae); pp. 38–77 in V. Tidwell and K. Carpenter (eds.), Thunder-lizards: the Sauropodomorph dinosaurs. Indiana University Press, Bloomington.

McIntosh, J. S., and D. S. Berman. 1975. Description of the palate and lower jaw of the sauropod dinosaur *Diplodocus* (Reptilia: Saurischia) with remarks on the nature of the skull of *Apatosaurus*. Journal of Paleontology 49:187–199.

McIntosh, J. S., and K. Carpenter. 1998. The holotype of *Diplodocus longus*, with comments on other specimens of the genus. Modern Geology 23:85–110.

McIntosh, J. S., C. A. Miles, K. A. Cloward, and J. R. Parker. 1996a. A new nearly complete skeleton of *Camarasaurus*. Bulletin of the Gunma Museum of Natural History 1:1–87.

McIntosh, J. S., W. E. Miller, K. L. Stadtman, and D. D. Gillette. 1996b. The osteology of *Camarasaurus lewisi* (Jensen, 1988). Brigham Young University Geology Studies 41:73–116.

McIntosh, J. S., W. P. Coombs, and D. A. Russell. 1992. A new diplodocid sauropod (Dinosauria) from Wyoming, USA. Journal of Vertebrate Paleontology 12:158–167.

Michelis, I. 2004. Taphonomie des Howe Quarry's (Morrison-Formation, Oberer Jura), Bighorn County, Wyoming, USA. Ph.D. dissertation, Institute of Palaeontology, University of Bonn, Bonn, Germany, 41 pp.

Mocho, P., R. Royo-Torres, and F. Ortega. 2014. Phylogenetic reassessment of *Lourinhasaurus alenquerensis*, a basal Macronaria (Sauropoda) from the Upper Jurassic of Portugal. Zoological Journal of the Linnean Society.

Mook, C. C. 1917. Criteria for the determination of species in the Sauropoda, with description of a new species of *Apatosaurus*. Bulletin of the American Museum of Natural History 37:355–358.

Mossbrucker, M. T., and R. T. Bakker. 2013. Missing muzzle found: new skull material referrable

PeerJ Reviewing Manuscript

8113 to *Apatosaurus ajax* (Marsh 1877) from the Morrison Formation of Morrison, Colorado.
8114 Geological Society of America Abstracts with Programs 45:111.
8115 Nair, J. P., and S. W. Salisbury. 2012. New anatomical information on *Rhoetosaurus brownei*
8116 Longman, 1926, a gravisaurian sauropodomorph dinosaur from the Middle Jurassic of
8117 Queensland, Australia. Journal of Vertebrate Paleontology 32:369–394.
8118 Nieuwland, I. 2010. The colossal stranger. Andrew Carnegie and *Diplodocus* intrude European
8119 culture, 1904–1912. Endeavour 34:61–68.
8120 Nopcsa, F. B. 1902. Notizen über die Cretacischen Dinosaurier. Pt. 3. Wirbel eines
8121 südamerikanischen Sauropoden. Sitzungsberichte der Berliner Akademie der
8122 Wissenschaften 3:108–114.
8123 Olshevsky, G. 1991. A revision of the parainfraclass Archosauria Cope, 1869, excluding the
8124 advanced Crocodylia. Mesozoic Meanderings 2:1–196.
8125 Osborn, H. F. 1898. Additional characters of the great herbivorous dinosaur *Camarasaurus*.
8126 Bulletin of the American Museum of Natural History 10:219–233.
8127 Osborn, H. F. 1899. A skeleton of *Diplodocus*. Memoirs of the American Museum of Natural
8128 History 5:191–214.
8129 Osborn, H. F. 1904. Manus, sacrum, and caudals of Sauropoda. Bulletin of the American
8130 Museum of Natural History 20:181–190.
8131 Osborn, H. F., and C. C. Mook. 1921. *Camarasaurus*, *Amphicoelias*, and other sauropods of
8132 Cope. Memoirs of the American Museum of Natural History, New Series 3:249–387.
8133 Ostrom, J. O., and J. S. McIntosh. 1966. Marsh's Dinosaurs: The Collection from Como Bluff.
8134 Vol. 1. Yale University Press, New Haven, 388 pp.
8135 Ouyang, H., and Y. Ye. 2002. The First Mamenchisaurian Skeleton with Complete Skull,
8136 *Mamenchisaurus youngi*. Sichuan Publishing House of Science and Technology, Chengdu,
8137 China, 138 pp.
8138 Owen, R. 1842. Report on British Fossil Reptiles Pt. II. Report of the British Association for the
8139 Advancement of Science 1841:60–204.
8140 Paul, G. S. 1988. The brachiosaur giants of the Morrison and Tendaguru with a description of a
8141 new subgenus, *Giraffatitan*, and a comparison of the world's largest dinosaurs. Hunteria 2
8142 (3):1–14.
8143 Pereda Suberbiola, X., F. Torcida, L. A. Izquierdo, P. Huerta, D. Montero, and G. Pérez. 2003.
8144 First rebbachisaurid dinosaur (Sauropoda, Diplodocoidea) from the early Cretaceous of
8145 Spain: paleobiogeographical implications. Bulletin de La Societe Geologique de France

PeerJ Reviewing Manuscript

174:471–479.

Peterson, O. A., and C. W. Gilmore. 1902. *Elosaurus parvus*; a new genus and species of the Sauropoda. Annals of the Carnegie Museum 1:490–499.

Platt, B. F., and S. T. Hasiotis. 2006. Newly discovered sauropod dinosaur tracks with skin and foot-pad impressions from the Upper Jurassic Morrison Formation, Bighorn Basin, Wyoming, U.S.A. PALAIOS 21:249–261.

Raath, M. A., and J. S. McIntosh. 1987. Sauropod dinosaurs from the central Zambezi Valley, Zimbabwe, and the age of the Kadzi Formation. South African Journal of Geology 90:107–119.

Rauhut, O. W. M., K. Remes, R. Fechner, G. Cladera, and P. Puerta. 2005. Discovery of a short-necked sauropod dinosaur from the Late Jurassic period of Patagonia. Nature 435:670–672.

Remes, K. 2006. Revision of the Tendaguru sauropod dinosaur *Tornieria africana* (Fraas) and its relevance for sauropod paleobiogeography. Journal of Vertebrate Paleontology 26:651–669.

Remes, K. 2007. A second Gondwanan diplodocid dinosaur from the Upper Jurassic Tendaguru beds of Tanzania, East Africa. Palaeontology 50:653–667.

Remes, K. 2008. Evolution of the pectoral girdle and forelimb in Sauropodomorpha (Dinosauria, Saurischia). Ph.D. dissertation, Fakultät für Geowissenschaften, LMU München, München, 355 pp.

Remes, K. 2009. Taxonomy of Late Jurassic diplodocid sauropods from Tendaguru (Tanzania). Fossil Record 12:23–46.

Remes, K., F. Ortega, I. Fierro, U. Joger, R. Kosma, J. M. M. Ferrer, O. A. Ide, and A. Maga. 2009. A new basal sauropod dinosaur from the Middle Jurassic of Niger and the early evolution of Sauropoda. PLoS ONE 4:e6924.

Riggs, E. S. 1901. The fore leg and pectoral girdle of *Morosaurus*: with a note on the genus *Camarosaurus*. Field Columbian Museum, Geological Series 2 275–281.

Riggs, E. S. 1903. Structure and relationships of opisthocoelian dinosaurs: *Apatosaurus* Marsh. Field Columbian Museum, Geological Series 2 4:165–196.

Riggs, E. S. 1904. Structure and relationships of opisthocoelian dinosaurs: the Brachiosauridae. Field Columbian Museum, Geological Series 2 2:229–247.

Royo-Torres, R., A. Cobos, L. Lurque, A. Aberasturi, E. Espílez, I. Fierro, A. González, L. Mampel, and L. Alcalá. 2009. High European sauropod dinosaur diversity during Jurassic–Cretaceous transition in Riodeva (Teruel, Spain). Palaeontology 52:1009–1027.

Royo-Torres, R., A. Cobos, and L. Alcalá. 2006. A giant European dinosaur and a new sauropod

PeerJ Reviewing Manuscript

clade. Science 314:1925–1927.
Royo-Torres, R., and A. Cobos. 2004. Estudio sistemático de un ilion de Sauropoda del yacimiento Pino de Jarque 2 en Riodeva (Teruel). Geo-Temas 6:59–62.
Royo-Torres, R., and P. Upchurch. 2012. The cranial anatomy of the sauropod *Turiasaurus riodevensis* and implications for its phylogenetic relationships. Journal of Systematic Palaeontology 1–31.
Russell, D. A., and Z. Zheng. 1993. A large mamenchisaurid from the Junggar Basin, Xinjiang, People's Republic of China. Canadian Journal of Earth Sciences 30:2082–2095.
Russell, D. A., P. Béland, and J. S. McIntosh. 1980. Paleoecology of the dinosaurs of Tendaguru (Tanzania). Mémoires de La Société Géologique de France 139:169–175.
Salgado, L. 1999. The macroevolution of the Diplodocimorpha (Dinosauria; Sauropoda): a developmental model. Ameghiniana 36:203–216.
Salgado, L., and J. Calvo. 1992. Cranial osteology of *Amargasurus cazaui* Salgado & Bonaparte (Sauropoda, Dicraeosuridae) from the Neocomian of Patagonia. Ameghiniana 29:337–346.
Salgado, L., and J. F. Bonaparte. 1991. Un nuevo saurópodo Dicraeosauridae, *Amargasaurus cazaui* gen. et sp. nov., de la Formación La Amarga, Neocomiano de la provincia del Neuquén, Argentina. Ameghiniana 28:333–346.
Salgado, L., I. S. Carvalho, and A. C. Garrido. 2006. *Zapalasaurus bonapartei*, un nuevo dinosaurio saurópodo de la Formación La Amarga (Cretácico Inferior), noroeste de Patagonia, Provincia de Neuquén, Argentina. Geobios 39:695–707.
Salgado, L., J. I. Canudo, A. C. Garrido, and J. L. Carballido. 2012. Evidence of gregariousness in rebbachisaurids (Dinosauria, Sauropoda, Diplodocoidea) from the Early Cretaceous of Neuquén (Rayoso Formation), Patagonia, Argentina. Journal of Vertebrate Paleontology 32:603–613.
Salgado, L., R. A. Coria, and J. O. Calvo. 1997. Evolution of titanosaurid sauropods: Phylogenetic analysis based on the postcranial evidence. Ameghiniana 34:3–32.
Sander, P. M., and C. Tückmantel. 2003. Bone lamina thickness, bone apposition rates, and age estimates in sauropod humeri and femora. Paläontologische Zeitschrift 77:161–172.
Sander, P. M., O. Mateus, T. Laven, and N. Knötschke. 2006. Bone histology indicates insular dwarfism in a new Late Jurassic sauropod dinosaur. Nature 441:739–741.
Schmitt, A., D. 2012. The inner ear of diplodocoid and basal macronarian sauropods: vestibular adaptations and paleobiological implications. Master, Rheinische Friedrich-Wilhelms-Universität, Bonn, Germany, 82 pp.

PeerJ Reviewing Manuscript

8212 Schmitt, A., D., E. Tschopp, F. Knoll, and P. M. Sander. 2013. Paleoneuroanatomy and braincase
8213 morphology indicate the presence of at least two diplodocine taxa (Dinosauria: Sauropoda)
8214 at the Howe Ranch (Wyoming, USA). Journal of Vertebrate Paleontology, Program and
8215 Abstracts 206.
8216 Schwarz, D., E. Frey, and C. A. Meyer. 2007a. Novel reconstruction of the orientation of the
8217 pectoral girdle in sauropods. The Anatomical Record: Advances in Integrative Anatomy and
8218 Evolutionary Biology 290:32–47.
8219 Schwarz, D., E. Frey, and C. A. Meyer. 2007b. Pneumaticity and soft-tissue reconstructions in the
8220 neck of diplodocid and dicraeosaurid sauropods. Acta Palaeontologica Polonica 52:167–
8221 188.
8222 Schwarz, D., T. Ikejiri, B. H. Breithaupt, P. M. Sander, and N. Klein. 2007c. A nearly complete
8223 skeleton of an early juvenile diplodocid (Dinosauria: Sauropoda) from the Lower Morrison
8224 Formation (Late Jurassic) of north central Wyoming and its implications for early ontogeny
8225 and pneumaticity in sauropods. Historical Biology 19:225–253.
8226 Schwarz-Wings, D. 2009. Reconstruction of the thoracic epaxial musculature of diplodocid and
8227 dicraeosaurid sauropods. Journal of Vertebrate Paleontology 29:517–534.
8228 Schwarz-Wings, D., and N. Böhm. 2012. A morphometric approach to the specific separation of
8229 the humeri and femora of *Dicraeosaurus* from the Late Jurassic of Tendaguru,Tanzania.
8230 Acta Palaeontologica Polonica.
8231 Sereno, P. C. 1998. A rationale for phylogenetic definitions, with application to the higher-level
8232 taxonomy of Dinosauria. Neues Jahrbuch Für Geologie Und Paläontologie Abhandlungen
8233 210:41–83.
8234 Sereno, P. C., A. L. Beck, D. B. Dutheil, H. C. . Larsson, G. H. Lyon, B. Moussa, R. W. Sadleir,
8235 C. A. Sidor, D. J. Varricchio, and G. P. Wilson. 1999. Cretaceous sauropods from the Sahara
8236 and the uneven rate of skeletal evolution among dinosaurs. Science 286:1342–1347.
8237 Sereno, P. C., and J. A. Wilson. 2005. Structure and evolution of a sauropod tooth battery; pp.
8238 157–177 in K. Curry Rogers and J. A. Wilson (eds.), The Sauropods: Evolution and
8239 Paleobiology. University of California Press, Berkeley, CA.
8240 Sereno, P. C., J. A. Wilson, L. M. Witmer, J. A. Whitlock, A. Maga, O. Ide, and T. A. Rowe. 2007.
8241 Structural extremes in a Cretaceous dinosaur. PLoS ONE 2:e1230.
8242 Siber, H. J., and U. Möckli. 2009. The Stegosaurs of the Sauriermuseum Aathal. Sauriermuseum
8243 Aathal, Aathal, 56 pp.
8244 Sternfeld, R. 1911. Zur Nomenklatur der Gattung *Gigantosaurus* Fraas. Sitzungsberichte Der

PeerJ Reviewing Manuscript

8245 Gesellschaft Naturforschender Freunde Zu Berlin 8:398.
8246 Swierc, J. E., and G. D. Johnson. 1996. A local chronostratigraphy for the Morrison Formation,
8247 Northeastern Bighorn Basin, Wyoming. Wyoming Geological Association, 47th Annual
8248 Field Conference Guidebook 47:315–327.
8249 Taylor, M. P. 2009. A re-evaluation of *Brachiosaurus altithorax* Riggs 1903 (Dinosauria,
8250 Sauropoda) and its generic separation from *Giraffatitan brancai* (Janensch 1914). Journal
8251 of Vertebrate Paleontology 29:787–806.
8252 Taylor, M. P. 2010. Sauropod dinosaur research: a historical review. Geological Society, London,
8253 Special Publications 343:361.
8254 Taylor, M. P., and D. Naish. 2005. The phylogenetic taxonomy of Diplodocoidea (Dinosauria:
8255 Sauropoda). PaleoBios 25:1–7.
8256 Taylor, M. P., and M. J. Wedel. 2013. Why sauropods had long necks; and why giraffes have
8257 short necks. PeerJ 1:e36.
8258 Taylor, M. P., M. J. Wedel, and R. L. Cifelli. 2011. A new sauropod dinosaur from the Lower
8259 Cretaceous Cedar Mountain Formation, Utah, USA. Acta Palaeontologica Polonica 56:75–
8260 98.
8261 Tidwell, V., K. L. Stadtman, and A. Shaw. 2005. Age-related characteristics found in a partial
8262 pelvis of *Camarasaurus*; pp. 180–186 in V. Tidwell and K. Carpenter (eds.), Thunder-
8263 Lizards: The Sauropodomorph Dinosaurs. Indiana University Press, Bloomington.
8264 Torcida Fernández-Baldor, F., J. I. Canudo, P. Huerta, D. Montero, and X. Pereda Suberbiola.
8265 2011. *Demandasaurus darwini*, a new rebbachisaurid sauropod from the Early Cretaceous
8266 of the Iberian Peninsula. Acta Palaeontologica Polonica 56:535–552.
8267 Trujillo, K. C. 2006. Clay mineralogy of the Morrison Formation (Upper Jurassic-? Lower
8268 Cretaceous), and its use in long distance correlation and paleoenvironmental analysis. New
8269 Mexico Museum of Natural History and Science Bulletin 36:17–23.
8270 Trujillo, K., D. Demar, J. Foster, and S. A. Bilbey. 2011. An exceptionally large juvenile
8271 *Camarasaurus* from the Morrison Formation (Upper Jurassic) of Albany County, WY,
8272 USA. Journal of Vertebrate Paleontology, Program and Abstracts Suppl. 2:205.
8273 Tschopp, E. 2008. The complete set of autopodia of the *Camarasaurus* SMA 0002 and what it
8274 can tell about systematics, taphonomy, ontogeny, and footprint shape. Master Thesis,
8275 Paläontologisches Institut und Museum, Zürich, 185 pp.
8276 Tschopp, E., and G. Dzemski. 2012. 3-dimensional reproduction techniques to preserve and
8277 spread paleontological material – a case study with a diplodocid sauropod neck. Journal of

PeerJ Reviewing Manuscript

8278 Paleontological Techniques 10:1–8.
8279 Tschopp, E., and O. Mateus. 2012. A sternal plate of a large-sized sauropod dinosaur from the
8280 Late Jurassic of Portugal. ¡Fundamental! 20:263–266.
8281 Tschopp, E., and O. Mateus. 2013a. Clavicles, interclavicles, gastralia, and sternal ribs in
8282 sauropod dinosaurs: new reports from Diplodocidae and their morphological, functional
8283 and evolutionary implications. Journal of Anatomy 222:321–340.
8284 Tschopp, E., and O. Mateus. 2013b. The skull and neck of a new flagellicaudatan sauropod from
8285 the Morrison Formation and its implication for the evolution and ontogeny of diplodocid
8286 dinosaurs. Journal of Systematic Palaeontology 11:853–888.
8287 Tschopp, E., J. Russo, and G. Dzemski. 2013. Retrodeformation as a test for the validity of
8288 phylogenetic characters: an example from diplodocid sauropod vertebrae. Palaeontologia
8289 Electronica 16:1–23.
8290 Turner, C. E., and F. Peterson. 1999. Biostratigraphy of dinosaurs in the Upper Jurassic Morrison
8291 Formation of the Western Interior, USA; pp. 77–114 in Vertebrate Paleontology in Utah.,
8292 Utah Geological Survey Miscellaneous Publication Salt Lake City.
8293 Upchurch, P. 1995. The evolutionary history of sauropod dinosaurs. Philosophical Transactions of
8294 the Royal Society of London. Series B: Biological Sciences 349:365.
8295 Upchurch, P. 1998. The phylogenetic relationships of sauropod dinosaurs. Zoological Journal of
8296 the Linnean Society 124:43–103.
8297 Upchurch, P. 1999. The phylogenetic relationships of the Nemegtosauridae (Saurischia,
8298 Sauropoda). Journal of Vertebrate Paleontology 19:106–125.
8299 Upchurch, P. 2009. The sauropodomorph supermatrix: towards a global phylogeny of the largest
8300 terrestrial animals. Journal of Vertebrate Paleontology Suppl 1:194A.
8301 Upchurch, P., and J. Martin. 2002. The Rutland *Cetiosaurus*: the anatomy and relationships of a
8302 Middle Jurassic British sauropod dinosaur. Palaeontology 45:1049–1074.
8303 Upchurch, P., and P. D. Mannion. 2009. The first diplodocid from Asia and its implications for
8304 the evolutionary history of sauropod dinosaurs. Palaeontology 52:1195–1207.
8305 Upchurch, P., and P. M. Barrett. 2000. The evolution of sauropod feeding mechanisms; pp. 79–
8306 122 in Evolution of herbivory in terrestrial vertebrates: perspectives from the fossil record.,
8307 Cambridge University Press. Sues, H.-D., Cambridge.
8308 Upchurch, P., P. M. Barrett, and P. Dodson. 2004a. Sauropoda; pp. 259–322 in D. B. Weishampel,
8309 P. Dodson, and H. Osmólska (eds.), The Dinosauria. Second edition. University of
8310 California Press, Berkeley, CA.

PeerJ Reviewing Manuscript

8311 Upchurch, P., P. M. Barrett, and P. M. Galton. 2007. A phylogenetic analysis of basal
8312 sauropodomorph relationships: implications for the origin of sauropod dinosaurs. Evolution
8313 and Palaeobiology of Early Sauropodomorph Dinosaurs 57–90.
8314 Upchurch, P., Y. Tomida, and P. M. Barrett. 2004b. A new specimen of *Apatosaurus ajax*
8315 (Sauropoda: Diplodocidae) from the Morrison Formation (Upper Jurassic) of Wyoming,
8316 USA. National Science Museum Monographs 26:1–118.
8317 Varricchio, D. J. 1997. Growth and embryology; pp. 282–288 in Encyclopedia of Dinosaurs.
8318 Academic Press, London.
8319 Wedel, M. J. 2003. The evolution of vertebral pneumaticity in sauropod dinosaurs. Journal of
8320 Vertebrate Paleontology 23:344–357.
8321 Wedel, M. J. 2009. Another mystery: embossed laminae and "unfossae." Sauropod Vertebra
8322 Picture of the Week. http://svpow.com/2009/12/07/another-mystery-embossed-laminae-and-
8323 unfossae/
8324 Wedel, M. J., and M. P. Taylor. 2013. Neural spine bifurcation in sauropod dinosaurs of the
8325 Morrison Formation: ontogenetic and phylogenetic implications. PalArch's Journal of
8326 Vertebrate Palaeontology 10:1–34.
8327 Wedel, M. J., and R. K. Sanders. 2002. Osteological correlates of cervical musculature in Aves
8328 and Sauropoda (Dinosauria: Saurischia), with comments on the cervical ribs of
8329 *Apatosaurus*. PaleoBios 22:1–12.
8330 Wedel, M. J., R. L. Cifelli, and R. K. Sanders. 2000. Osteology, paleobiology, and relationships
8331 of the sauropod dinosaur Sauroposeidon. Acta Palaeontologica Polonica 45:343–388.
8332 Wellik, D. M., and M. R. Capecchi. 2003. Hox10 and Hox11 genes are required to globally
8333 pattern the mammalian skeleton. Science 301:363–367.
8334 Whitlock, J. A. 2011a. A phylogenetic analysis of Diplodocoidea (Saurischia: Sauropoda).
8335 Zoological Journal of the Linnean Society 161:872–915.
8336 Whitlock, J. A. 2011b. Inferences of diplodocoid (Sauropoda: Dinosauria) feeding behavior from
8337 snout shape and microwear analyses. PLoS ONE 6:e18304.
8338 Whitlock, J. A. 2011c. Re-evaluation of *Australodocus bohetii*, a putative diplodocoid sauropod
8339 from the Tendaguru Formation of Tanzania, with comment on Late Jurassic sauropod
8340 faunal diversity and palaeoecology. Palaeogeography, Palaeoclimatology, Palaeoecology
8341 309:333–341.
8342 Whitlock, J. A., and J. D. Harris. 2010. The dentary of *Suuwassea emilieae* (Sauropoda:
8343 Diplodocoidea). Journal of Vertebrate Paleontology 30:1637–1641.

PeerJ Reviewing Manuscript

8344 Whitlock, J. A., and M. C. Lamanna. 2012. A reanalysis of CM 11162, a skull of *Apatosaurus*
8345 (Sauropoda: Diplodocidae). Journal of Vertebrate Paleontology Program and Abstracts:192.
8346 Whitlock, J. A., J. A. Wilson, and M. C. Lamanna. 2010. Description of a nearly complete
8347 juvenile skull of *Diplodocus* (Sauropoda: Diplodocoidea) from the Late Jurassic of North
8348 America. Journal of Vertebrate Paleontology 30:442–457.
8349 Whitlock, J. A., M. D. D'Emic, and J. A. Wilson. 2011. Cretaceous diplodocids in Asia? Re-
8350 evaluating the phylogenetic affinities of a fragmentary specimen. Palaeontology 54:351–
8351 364.
8352 Wiersma, K. 2013. Morphology and function of the dentition of *Camarasaurus*. Bachelor Thesis,
8353 Universität Bonn, Bonn, Germany, 66 pp.
8354 Wilhite, D. R. 2003. Biomechanical reconstruction of the appendicular skeleton in three North
8355 American Jurassic sauropods. Ph.D. dissertation, Graduate Faculty of the Louisiana State
8356 University and Agricultural and Mechanical College 232 pp.
8357 Wilhite, D. R. 2005. Variation in the appendicular skeleton of North American sauropod
8358 dinosaurs: taxonomic implications; pp. 268–301 in V. Tidwell and K. Carpenter (eds.),
8359 Thunder-lizards: the Sauropodomorph dinosaurs. Indiana University Press, Bloomington.
8360 Wilson, J. A. 1999. A nomenclature for vertebral laminae in sauropods and other saurischian
8361 dinosaurs. Journal of Vertebrate Paleontology 19:639–653.
8362 Wilson, J. A. 2002. Sauropod dinosaur phylogeny: critique and cladistic analysis. Zoological
8363 Journal of the Linnean Society 136:215–275.
8364 Wilson, J. A. 2005. Overview of sauropod phylogeny and evolution; pp. 15–49 in K. A. Curry
8365 Rogers and J. A. Wilson (eds.), The Sauropods: Evolution and Paleobiology. University of
8366 California Press, Berkeley, CA.
8367 Wilson, J. A. 2012. New vertebral laminae and patterns of serial variation in vertebral laminae of
8368 sauropod dinosaurs. Contributions from the Museum of Paleontology, University of
8369 Michigan 32:91–110.
8370 Wilson, J. A., and M. B. Smith. 1996. New remains of *Amphicoelias* Cope (Dinosauria:
8371 Sauropoda) from the Upper Jurassic of Montana and diplodocoid phylogeny. Journal of
8372 Vertebrate Paleontology 16:73A.
8373 Wilson, J. A., and M. T. Carrano. 1999. Titanosaurs and the origin of "wide-gauge" trackways: a
8374 biomechanical and systematic perspective on sauropod locomotion. Paleobiology 25:252–
8375 267.
8376 Wilson, J. A., and P. C. Sereno. 1998. Early evolution and higher-level phylogeny of sauropod

PeerJ Reviewing Manuscript

8377 dinosaurs. Journal of Vertebrate Paleontology 18:1–79.
8378 Wilson, J. A., and P. Upchurch. 2003. A revision of *Titanosaurus* Lydekker (Dinosauria-
8379 Sauropoda), the first dinosaur genus with a "Gondwanan"distribution. Journal of
8380 Systematic Palaeontology 1:125–160.
8381 Wilson, J. A., and P. Upchurch. 2009. Redescription and reassessment of the phylogenetic
8382 affinities of *Euhelopus zdanskyi* (Dinosauria: Sauropoda) from the Early Cretaceous of
8383 China. Journal of Systematic Palaeontology 7:199–239.
8384 Wilson, J. A., R. N. Martinez, and O. Alcober. 1999. Distal tail segment of a titanosaur
8385 (Dinosauria: Sauropoda) from the Upper Cretaceous of Mendoza, Argentina. Journal of
8386 Vertebrate Paleontology 19:591–594.
8387 Wilson, J. A., M. D. D'Emic, T. Ikejiri, E. M. Moacdieh, and J. A. Whitlock. 2011. A
8388 nomenclature for vertebral fossae in sauropods and other saurischian dinosaurs. PLoS ONE
8389 6:e17114.
8390 Witmer, L. M., R. C. Ridgely, D. L. Dufeau, and M. C. Semones. 2008. Using CT to Peer into the
8391 Past: 3D Visualization of the Brain and Ear Regions of Birds, Crocodiles, and Nonavian
8392 Dinosaurs; pp. 67–87 in H. Endo and R. Frey (eds.), Anatomical Imaging. Springer Japan,
8393 Tokyo.
8394 Woodruff, D. C., and D. W. Fowler. 2012. Ontogenetic influence on neural spine bifurcation in
8395 Diplodocoidea (Dinosauria: Sauropoda): a critical phylogenetic character. Journal of
8396 Morphology 273:754–764.
8397 Woodward, A. S. 1905. On parts of the skeleton of *Cetiosaurus leedsi*, a sauropodous dinosaur
8398 from the Oxford Clay of Peterborough. Proceedings of the Zoological Society of London
8399 1:232–243.
8400 Young, C.-C. 1939. On a new sauropoda, with notes on other fragmentary reptiles from
8401 Szechuan. Bulletin of the Geological Society of China 19:279–315.
8402 Young, C.-C. 1958. New sauropods from China. Vertebrata PalAsiatica 2:1–28.
8403 Young, C.-C., and X. Zhao. 1972. Description of the type material of *Mamenchisaurus*
8404 *hochuanensis*. Institute of Vertebrate Paleontology and Paleoanthropology Monograph
8405 Series I 8:1–30.
8406 Young, M. T., E. J. Rayfield, C. M. Holliday, L. M. Witmer, D. J. Button, P. Upchurch, and P. M.
8407 Barrett. 2012. Cranial biomechanics of *Diplodocus* (Dinosauria, Sauropoda): testing
8408 hypotheses of feeding behaviour in an extinct megaherbivore. Naturwissenschaften 1–7.
8409 Yu, C. 1993. The skull of *Diplodocus* and the phylogeny of the Diplodocidae. Ph.D. dissertation,

PeerJ Reviewing Manuscript

Faculty of the Division of Biological Sciences and the Pritzker School of Medicine, University of Chicago, Chicago, 154 pp.

Zaher, H., D. Pol, A. B. Carvalho, P. M. Nascimento, C. Riccomini, P. Larson, R. Juarez-Valieri, R. Pires-Domingues, N. J. da Silva, and C. D. de Almeida. 2011. A complete skull of an Early Cretaceous sauropod and the evolution of advanced titanosaurians. PLoS ONE 6:e16663.

Zhang, Y. 1988. The Middle Jurassic Dinosaur Fauna from Dashanpu, Zigong, Sichuan, Vol. 1: Sauropod Dinosaur (I): *Shunosaurus*. Sichuan Publishing House of Science and Technology, Chengdu, China, 114 pp.

Zheng, Z. 1996. Cranial anatomy of *Shunosaurus* and *Camarasaurus* (Dinosauria: Sauropoda) and the phylogeny of the Sauropoda. Ph. D. dissertation, Texas Tech University, Lubbock, TX, USA, 208 pp.

PeerJ Reviewing Manuscript

PeerJ Reviewing Manuscript

Figure 1

Locality of the Howe Ranch

Figure 1: Locality of the Howe Ranch in the vicinity of Shell, Wyoming (lower left, star), with a detailed map of the three most important sites on the Ranch (lower right). Left inlet modified from Christiansen and Tschopp, 2010, right inlet courtesy of the Sauriermuseum Aathal.

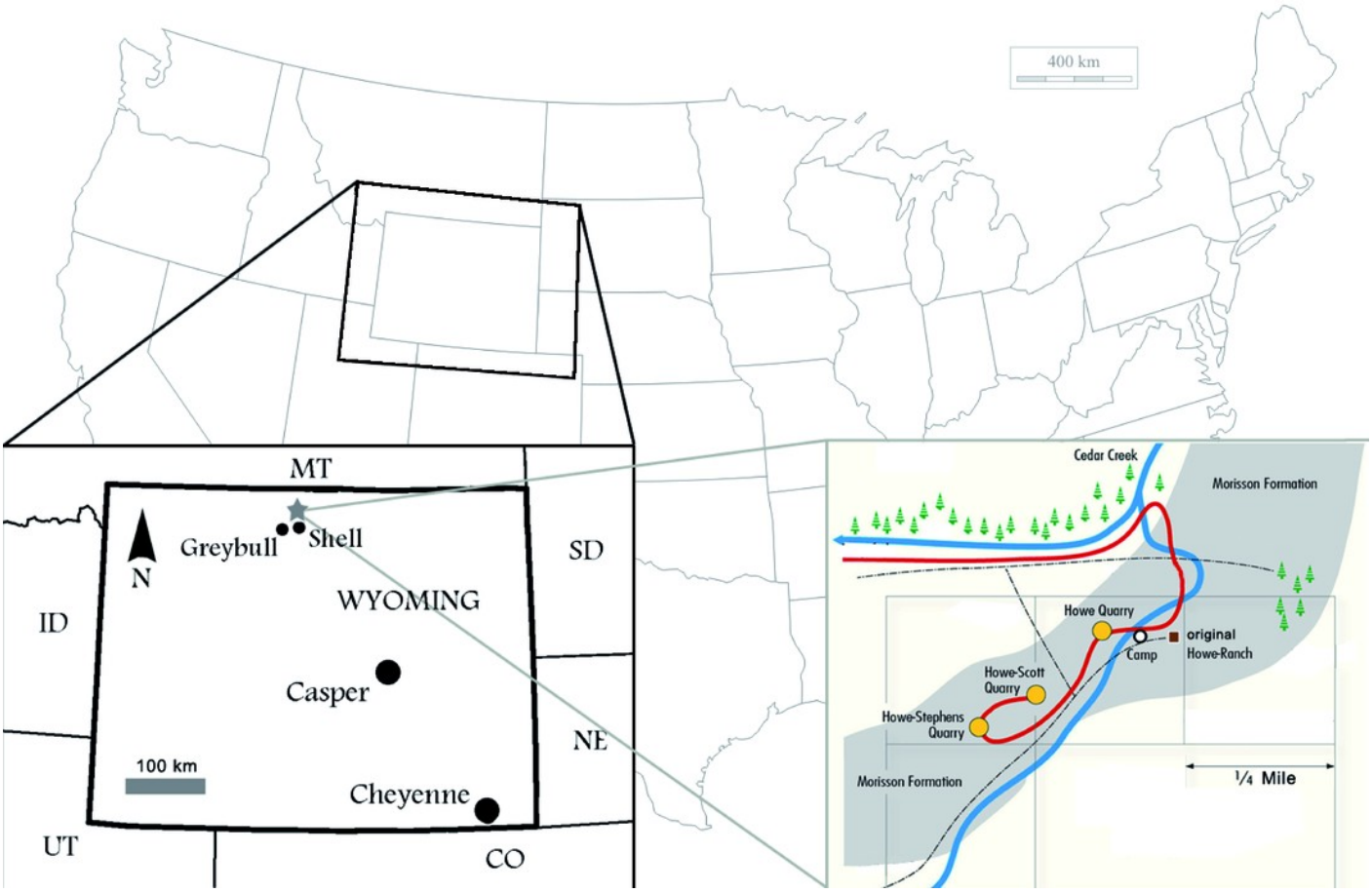


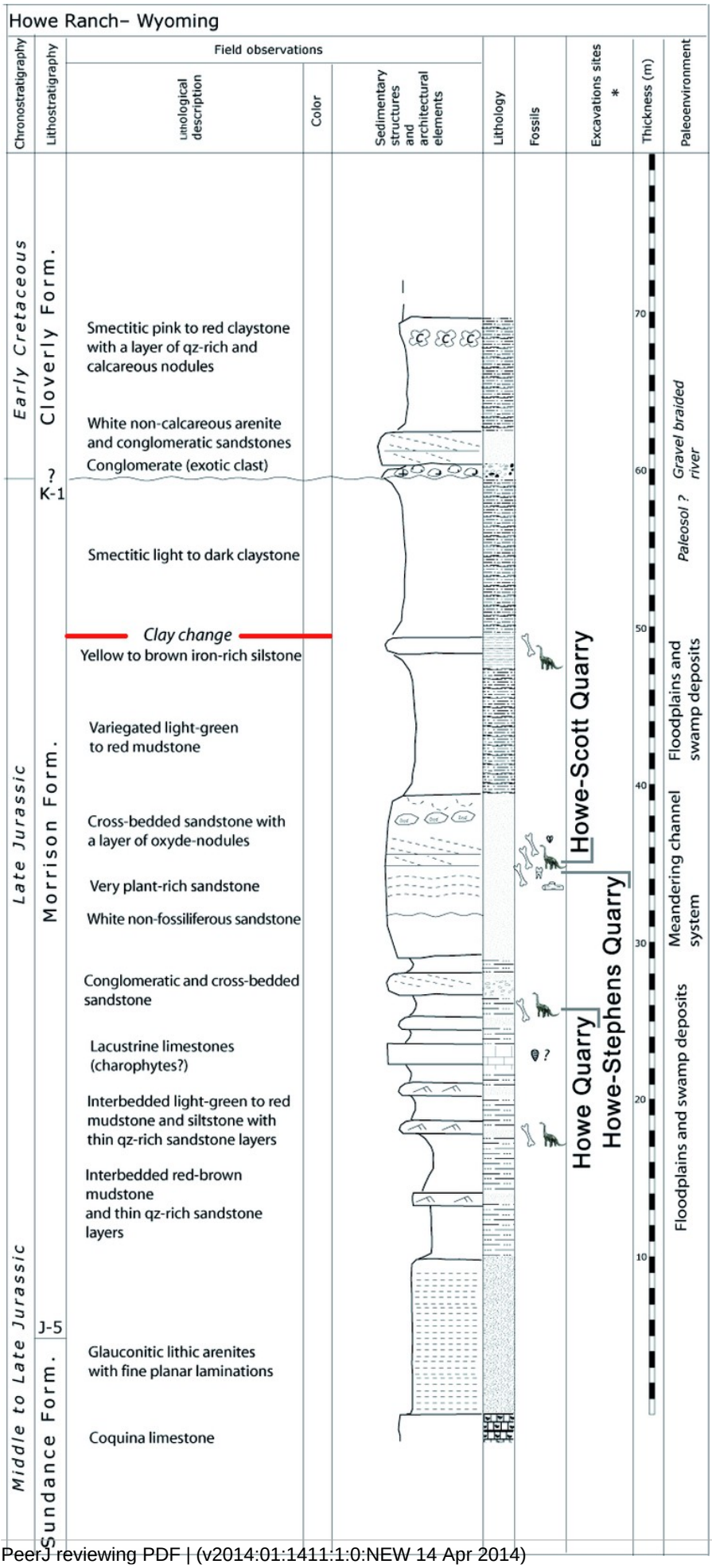
Figure 2

Stratigraphic log of the Howe Ranch sites

Figure 2: Stratigraphic log of the Howe Ranch sites showing the levels of the three most important quarries. The red line marks the clay change which has been proposed as marker bed to correlate sites across the Morrison Formation. Copyright by Jacques Ayer.

PeerJ Reviewing Manuscript

PeerJ Reviewing Manuscript



PeerJ Reviewing Manuscript

Figure 3

Quarry maps of the Howe Ranch sites

Figure 3: Quarry maps of the Howe-Stephens Quarry (a), Howe Quarry (b), and the Howe-Scott Quarry (c), highlighting the specimens included in the phylogenetic analysis (A, light blue: SMA 0009; B, red: SMA 0004; C, green: SMA 0011; C, dark blue: SMA 0087). Quarry maps drawn by Esther Premru, copyright by Sauriermuseum Aathal.

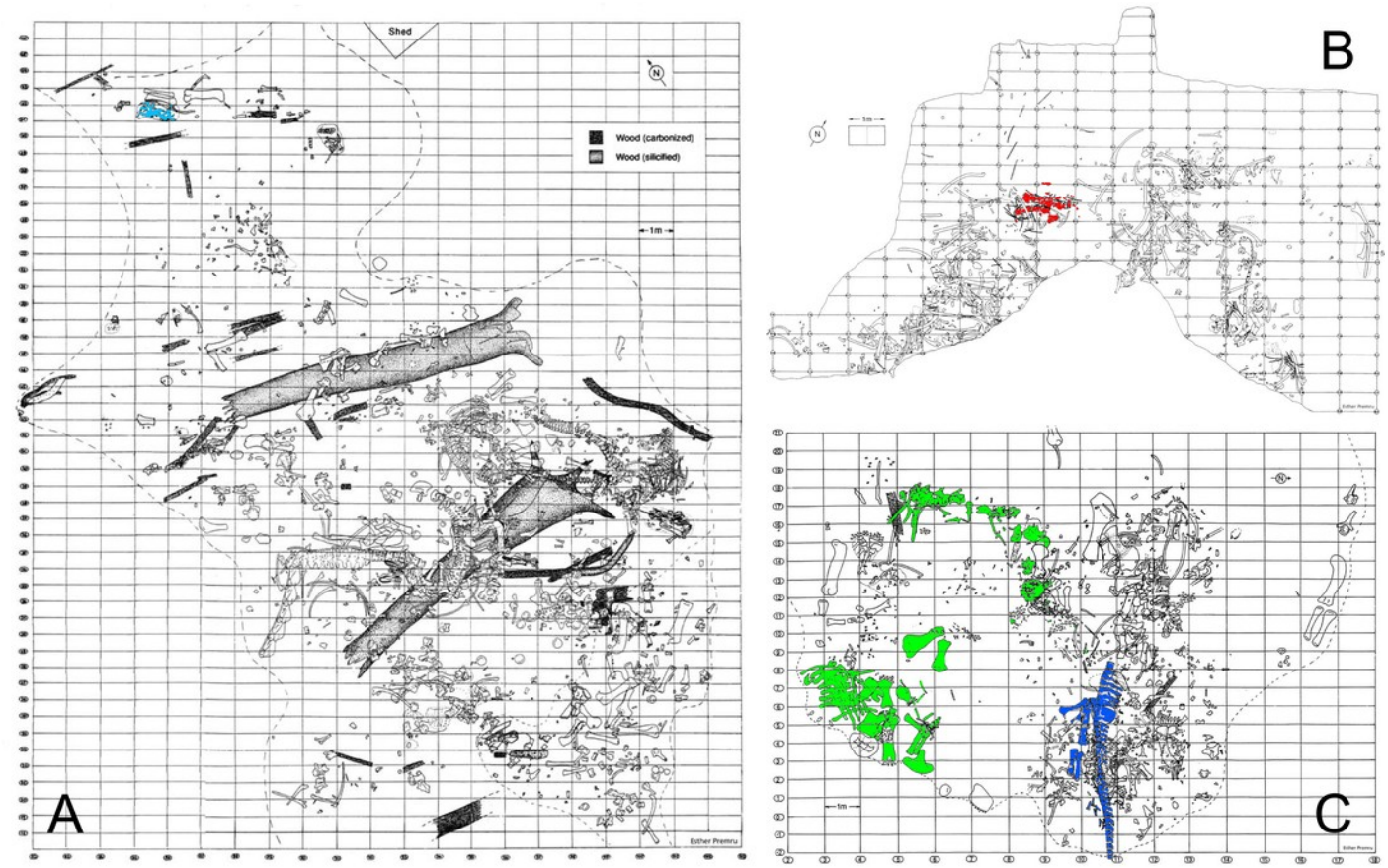


Figure 4

Quarry map of SMA 0011

Figure 4: Quarry map of SMA 0011, indicating the single bones found. Note the separation of the cervical series and the skull from the dorsal column and the appendicular skeleton. Color code: skull (orange), CV (red), DV (violet), DR and SR (yellow), PcG (light green), PvG (dark green), Fl (light blue), Hl (dark blue). Abb.: Bc, braincase; co, coracoid; CR, cervical rib; CV, cervical vertebra; DR, dorsal ribs; DV, dorsal vertebra; fe, femur; fi, fibula; Fl, forelimb; h, humerus; Hl, hindlimb; il, ilium; is, ischium; Ma, manus; PcG, pectoral girdle; Pe, pes; pu, pubis; PvG, pelvic girdle; r, radius; sc, scapula; SR, sternal ribs; SV, sacral vertebrae; tb, tibia; u, ulna. Map drawn by Esther Premru.

PeerJ Reviewing Manuscript

PeerJ Reviewing Manuscript

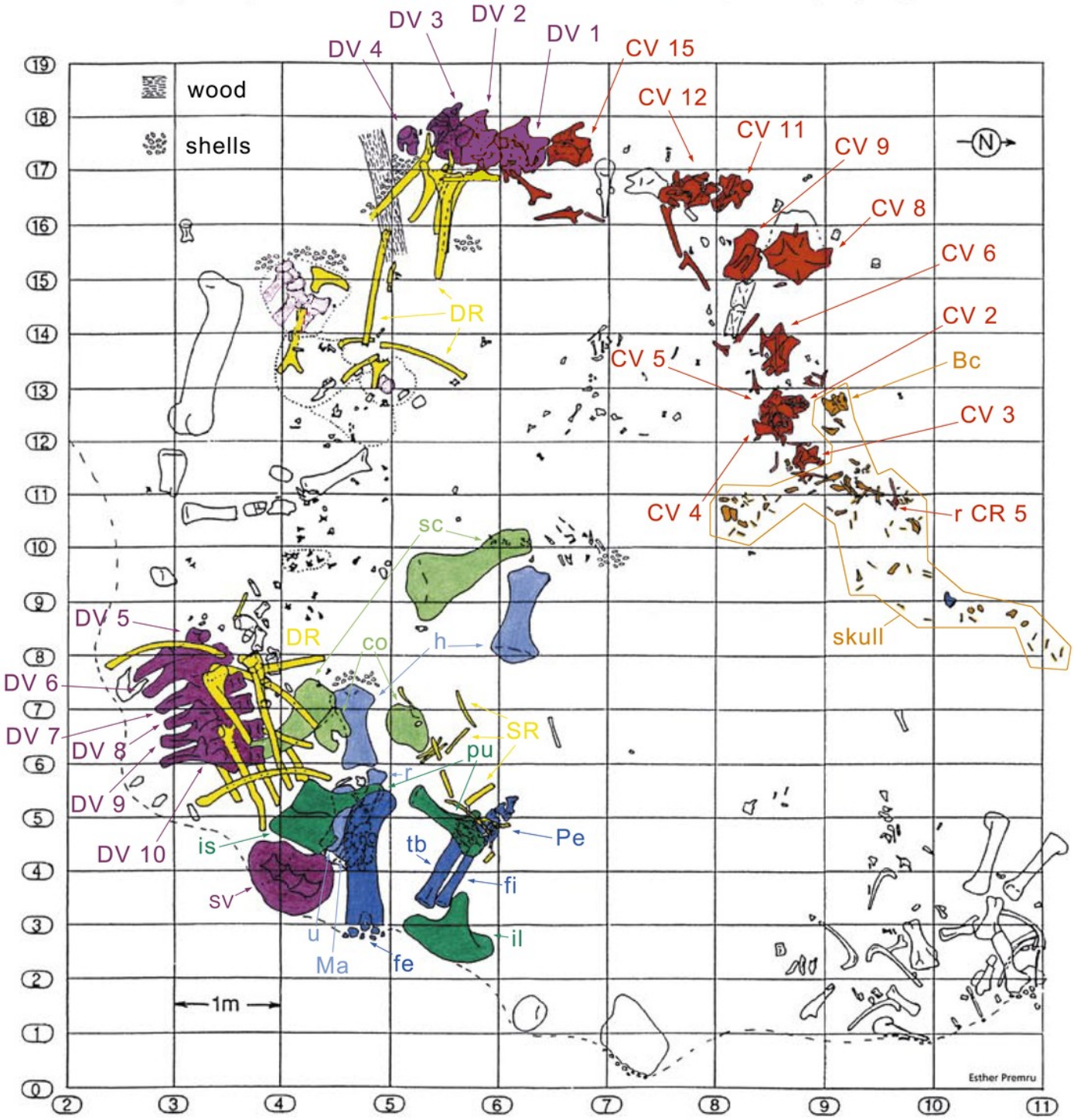


Figure 5

Skull bones of *Galeamopus* [redacted] SMA 0011 before mounting.

Figure 5: Skull bones of *Galeamopus* [redacted] SMA 0011 before mounting. Black elements were lacking and reconstructed for the mounted skull. Abb.: an, angular; aof, antorbital fenestra; at, atlas; Bc, braincase; d, dentary; f, frontal; j, jugal; la, lacrimal; m, maxilla; na, nasal; pf, prefrontal; pm, premaxilla; pra, proatlas; q, quadrate; qj, quadratojugal; sa, surangular; T, teeth. Scale bar = 10 cm. Photo by Urs Möckli.

PeerJ Reviewing Manuscript

PeerJ Reviewing Manuscript



PeerJ Reviewing Manuscript

Figure 6

Skull of *Galeamopus* [redacted] SMA 0011 as usually figured

Figure 6: Skull of *Galeamopus* [redacted] SMA 0011 as usually figured in anterodorsal (top), posterodorsal (left), right lateral (bottom center), and rostral views (right). Dark elements were lacking and reconstructed for the mounted skull. Abb.: an, angular; aof, antorbital fenestra; bo, basioccipital; bpr, basipterygoid process; d, dentary; ex, exoccipital; f, frontal; j, jugal; ltf, laterotemporal fenestra; m, maxilla; n, external nares; na, nasal; o, orbit; os, orbitosphenoid; p, parietal; paof, preantorbital fossa; pf, prefrontal; pm, premaxilla; po, postorbital; popr, paroccipital process; pro, prootic; q, quadrate; qj, quadratojugal; sa, surangular; so, supraoccipital; sq, squamosal; stf, supratemporal fenestra. Scale bar = 10 cm.

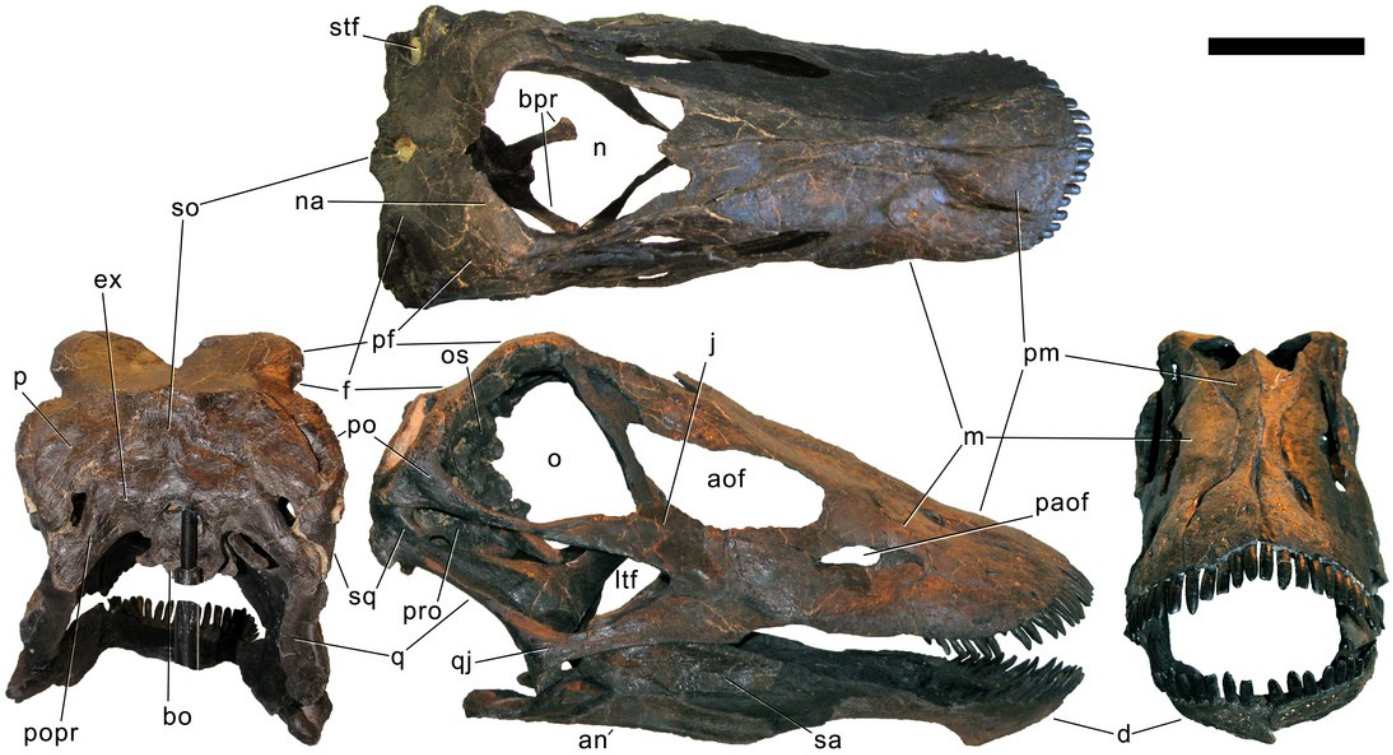
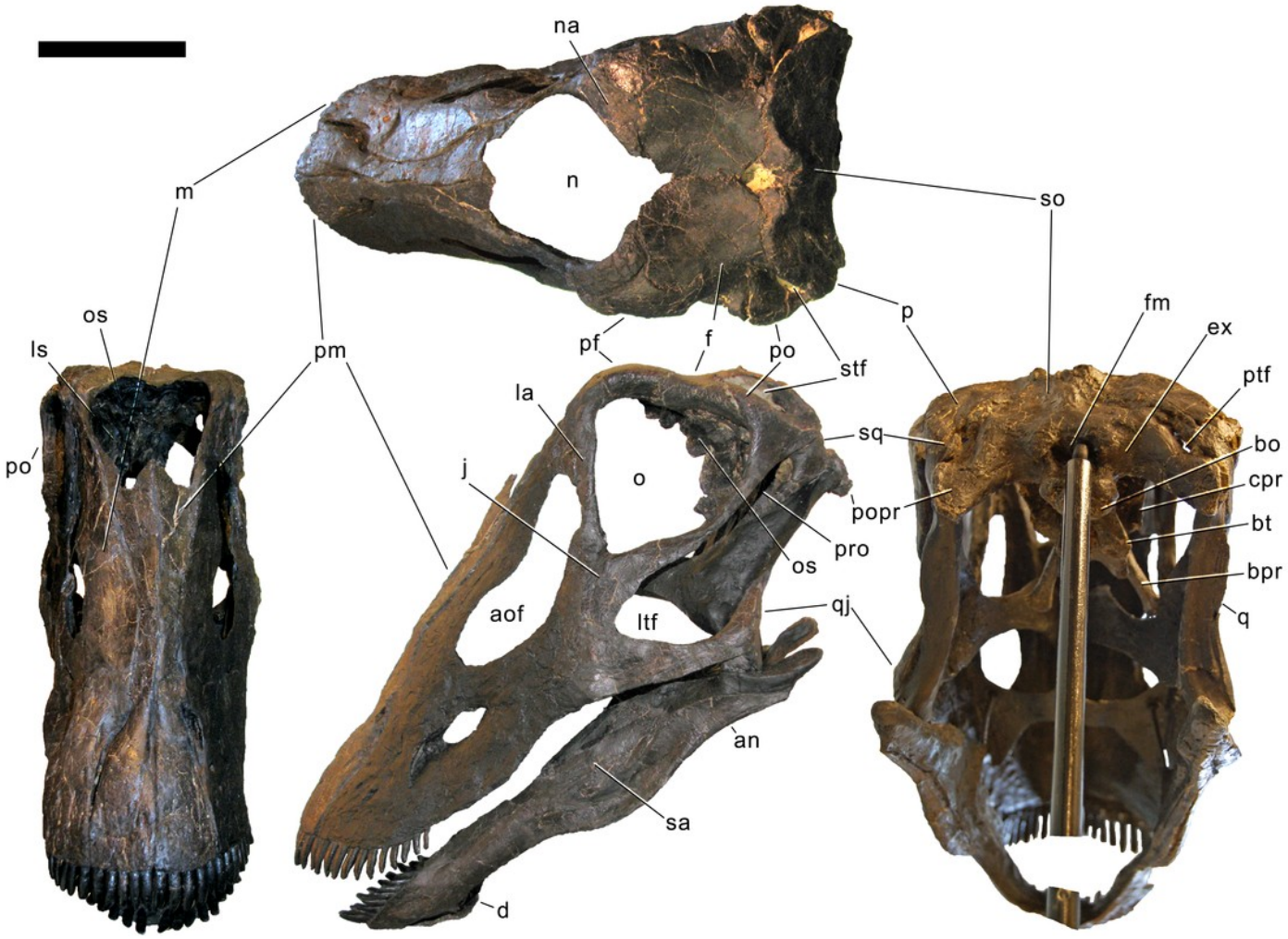


Figure 7

Skull of *Galeamopus* [redacted] SMA 0011 in supposed habitual pose

Figure 7: Skull of *Galeamopus* [redacted] SMA 0011 in supposed habitual pose in dorsal (top), anterior (left), left lateral (bottom center), and posterior views (right). Dark elements were lacking and reconstructed for the mounted skull. Abb.: an, angular; aof, antorbital fenestra; bo, basioccipital; bpr, basipterygoid process; bt, basal tubera; cpr, crista prootica; d, dentary; ex, exoccipital; f, frontal; fm, foramen magnum; j, jugal; ltf, laterotemporal fenestra; m, maxilla; n, external nares; na, nasal; o, orbit; os, orbitosphenoid; p, parietal; pf, prefrontal; pm, premaxilla; po, postorbital; popr, paroccipital process; pro, prootic; ptf, posttemporal fenestra; q, quadrate; qj, quadratojugal; sa, surangular; so, supraoccipital; sq, squamosal; stf, supratemporal fenestra. Scale bar = 10 cm.



PeerJ Reviewing Manuscript

Figure 8

Skull reconstruction of *Galeamopus* [redacted]

Figure 8: Skull reconstruction of *Galeamopus* [redacted] in dorsal and lateral view, created by Simão Mateus (ML), and based on the holotypic skull of SMA 0011. Lacking bones were reconstructed after *Diplodocus* (Whitlock, 2011b).

PeerJ Reviewing Manuscript

PeerJ Reviewing Manuscript

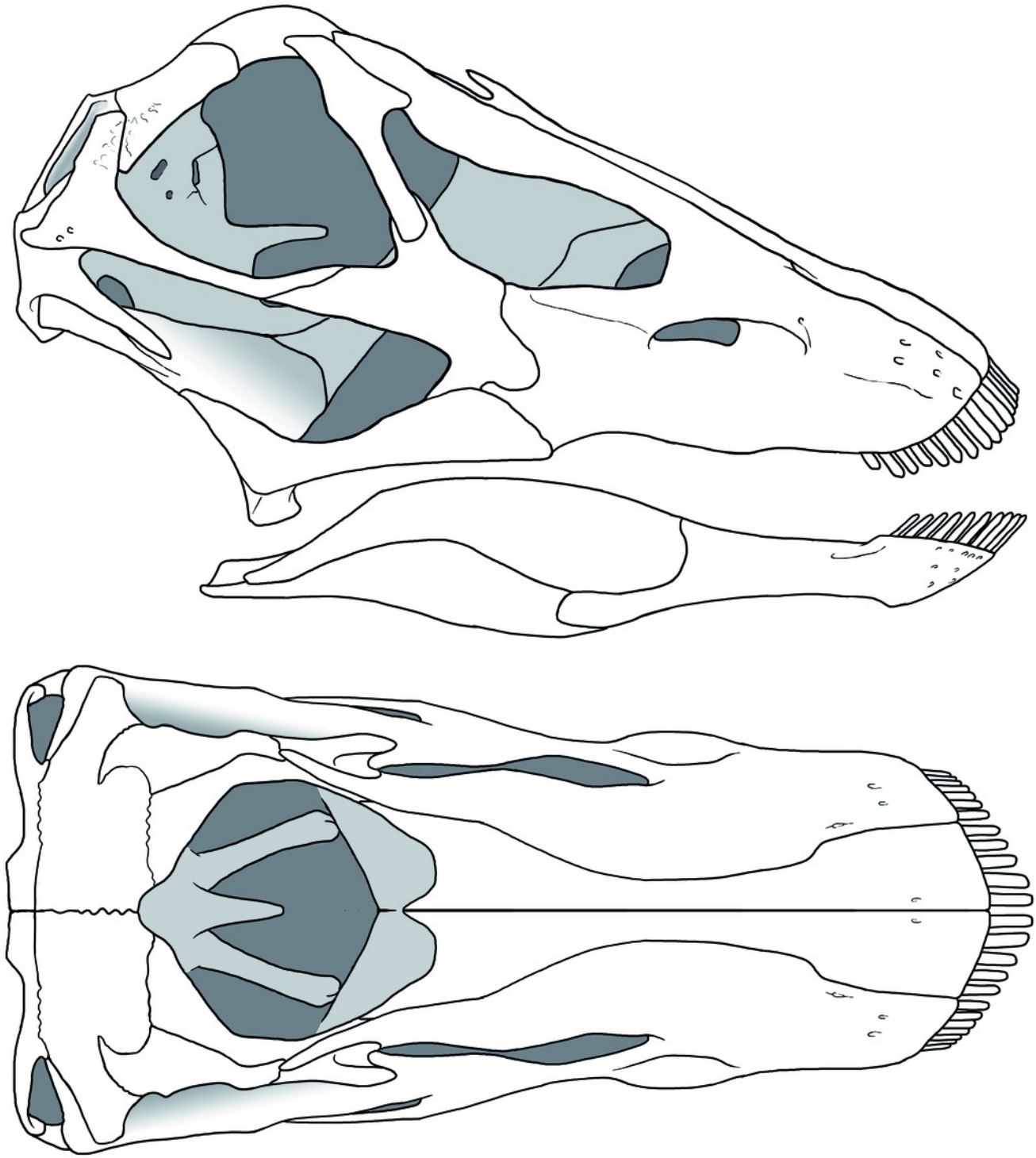


Figure 9

Maxillary canal in the skull of *Galeamopus* [redacted] SMA 0011

Figure 9: Maxillary canal in the skull of *Galeamopus* [redacted] SMA 0011 (arrow in the inlet) in right lateral view. The canal is herein interpreted as an autapomorphy of *G.* [redacted] Abb.: aof, antorbital fenestra; j, jugal; m, maxilla; paof, preantorbital fossa. Scale bar in skull overview = 10 cm.



PeerJ Reviewing Manuscript

Figure 10

Unusual development of sagittal nuchal crest in the skull of Galeamopus [redacted] SMA 0011

Figure 10: Unusual development of sagittal nuchal crest in the skull of Galeamopus [redacted] SMA 0011 (arrow in the inlet) in posterodorsal view. The complex structure indicates that there might have been an additional element lacking, but no such bone has yet been described in any sauropod skull. Abb.: f, frontal; p, parietal; so, supraoccipital. Scale bar in skull overview = 10 cm.

PeerJ Reviewing Manuscript

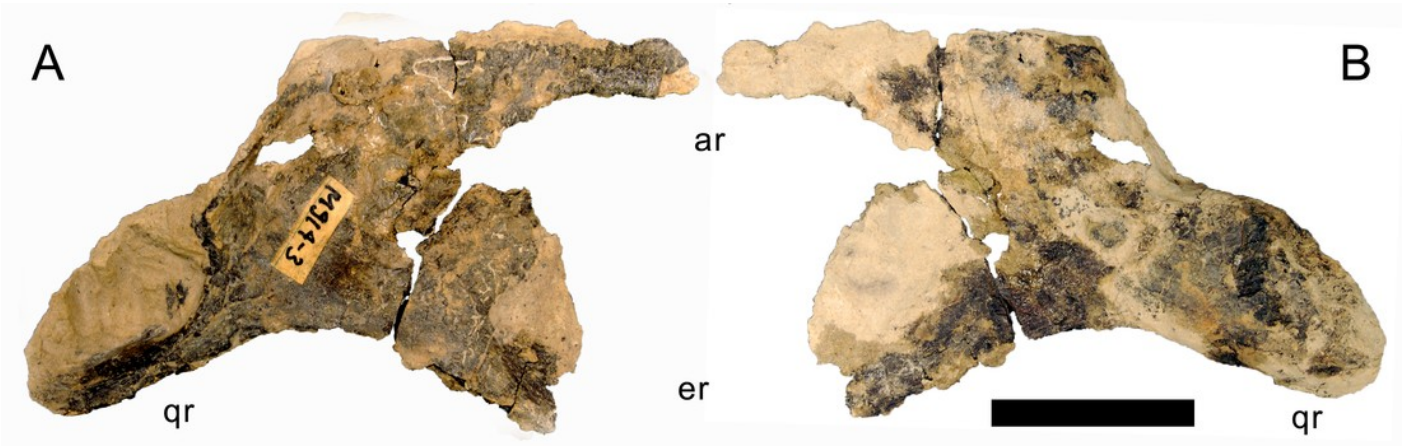
PeerJ Reviewing Manuscript



Figure 11

Right pterygoid of Galeamopus [redacted] SMA 0011

Figure 11: Right pterygoid of Galeamopus [redacted] SMA 0011 in lateral (A) and medial (B) views. The element is only partly prepared, the lighter color is matrix adhered to the darker bone. Abb.: ar, anterior ramus; er, ectopterygoid ramus; qr, quadrate ramus. Scale bar = 5 cm.



PeerJ Reviewing Manuscript

Figure 12

Right hyoid of *Galeamopus* [redacted] SMA 0011

Figure 12: Right hyoid of *Galeamopus* [redacted] SMA 0011 in medial (A) and lateral (B) views. Abb.: ar, anterior ramus; sqr, squamosal ramus. Scale bar = 10 cm.

PeerJ Reviewing Manuscript

PeerJ Reviewing Manuscript



Figure 13

Right ?prearticular of *Galeamopus* [redacted] SMA 0011

Figure 13: Right ?prearticular of *Galeamopus* [redacted] SMA 0011 in lingual view. Note the shallow longitudinal canal (arrows). Scale bar = 5 cm.



PeerJ Reviewing Manuscript

Figure 14

Teeth of *Galeamopus* [redacted] SMA 0011

Figure 14: Teeth of *Galeamopus* [redacted] SMA 0011. They were found disarticulated from the skull. Abb.: tc, tooth crown; tr, tooth root. Scale bar = 2 cm.

PeerJ Reviewing Manuscript

PeerJ Reviewing Manuscript



Figure 15

Right proatlas of *Galeamopus* [redacted] SMA 0011

Figure 15: Right proatlas of *Galeamopus* [redacted] SMA 0011 in lateral (A) and medial (B) views. Note the elongate and narrow distal tip. Scale bar = 2 cm.

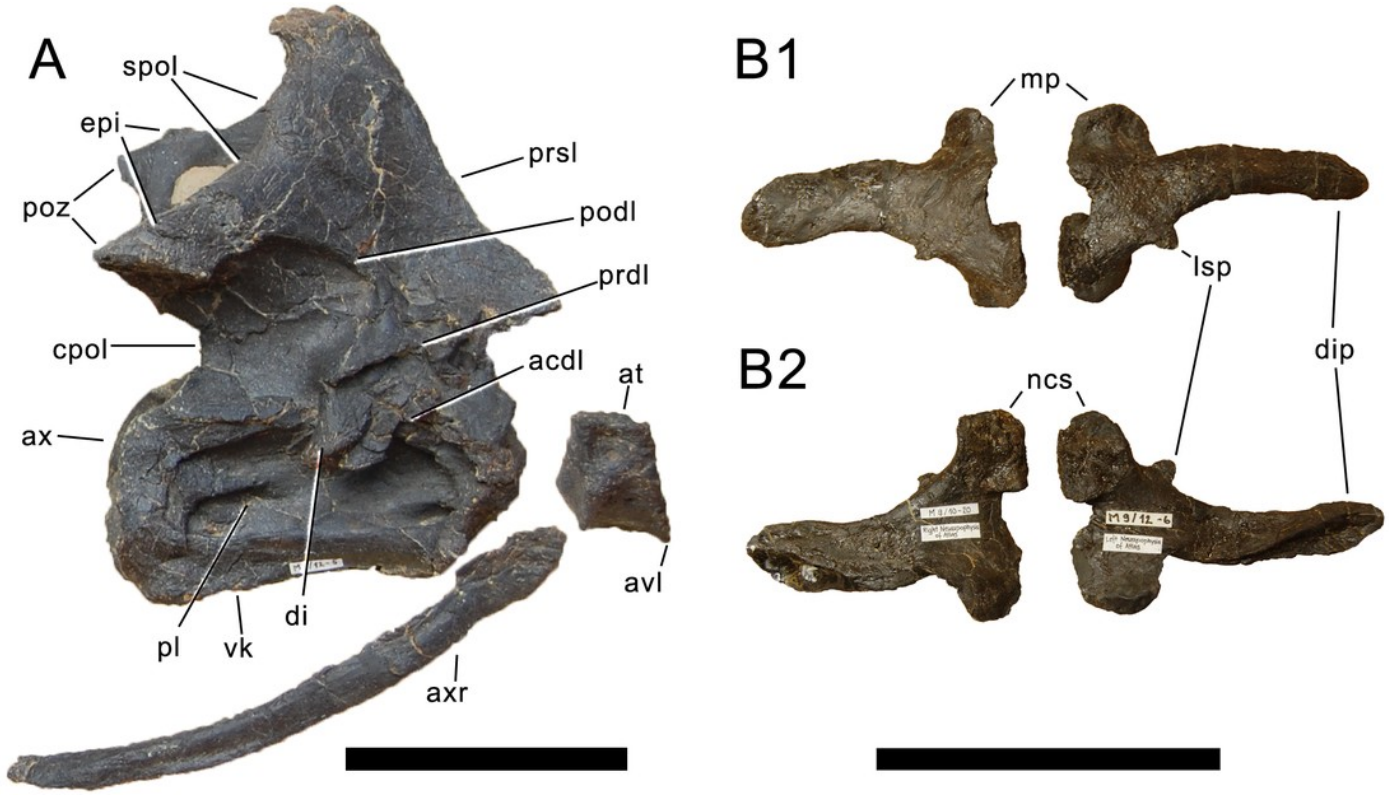


PeerJ Reviewing Manuscript

Figure 16

Atlas and axis of *Galeamopus* [redacted] SMA 0011

Figure 16: Atlas and axis of *Galeamopus* [redacted] SMA 0011. A shows the two elements in an articulated state, B shows the neurapophyses in lateral (B1) and medial (B2) views. Abb.: acdl, anterior centrodiapophyseal lamina; at, atlas; avl, anteroventral lip; ax, axis; axr, axial rib; cpol, centropostzygapophyseal lamina; di, diapophysis; dip, distal process; epi, epipophyses; lsp, lateral spur; mp, medial process; ncs, neurocentral synostosis; pl, pleurocoel; podl, postzygodiapophyseal lamina; poz, postzygapophysis; prdl, prezygodiapophyseal lamina; prsl, prespinal lamina; spol, spinopostzygapophyseal lamina; vk, ventral keel. Scale bars = 10 cm.

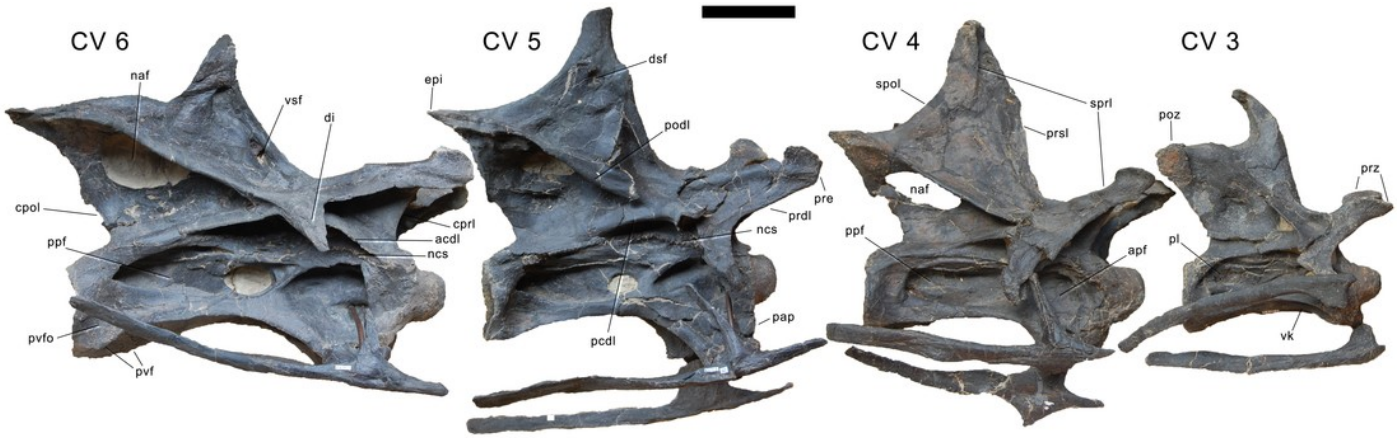


PeerJ Reviewing Manuscript

Figure 17

Cervical vertebrae 3 to 6 of *Galeamopus* [redacted] SMA 0011

Figure 17: Cervical vertebrae 3 to 6 of *Galeamopus* [redacted] SMA 0011 in right lateral view. Abb.: acdl, anterior centrodiapophyseal lamina; apf, anterior pneumatic fossa; cpol, centropostzygapophyseal lamina; cprl, centroprezygapophyseal lamina; di, diapophysis; dsf, dorsal spinal fossa; epi, epipophysis; naf, neural arch foramen; ncs, neurocentral synostosis; pap, parapophysis; pcdl, posterior centrodiapophyseal lamina; pl, pleurocoel; podl, postzygodiapophyseal lamina; poz, postzygapophysis; ppf, posterior pneumatic fossa; prdl, prezygodiapophyseal lamina; pre, pre-epipophysis; prsl, prespinal lamina; prz, prezygapophysis; pvf, posteroventral flange; pvfo, posteroventral fossa; spol, spinopostzygapophyseal lamina; sprl, spinoprezygapophyseal lamina; vk, ventral keel; vsf, ventral spinal fossa. Scale bar = 10 cm.

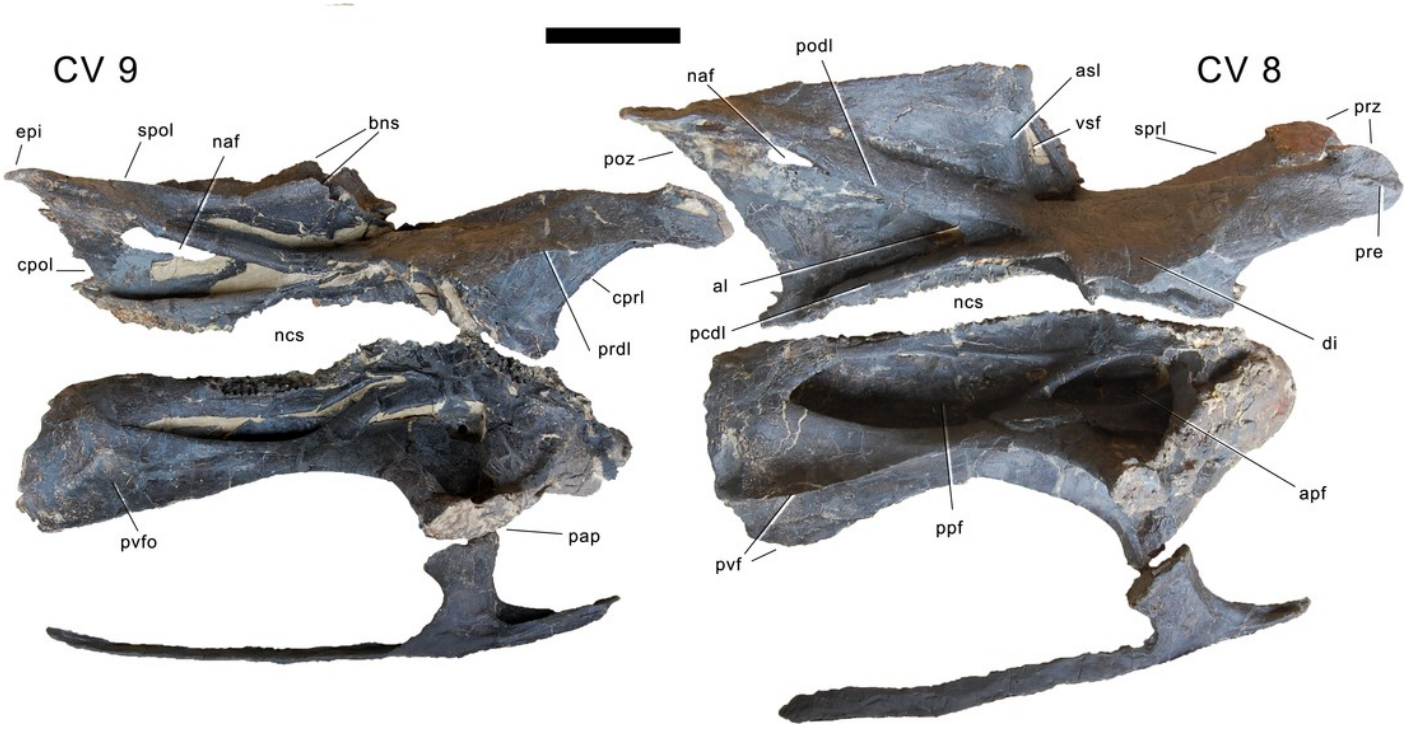


PeerJ Reviewing Manuscript

Figure 18

Cervical vertebrae 8 and 9 of *Galeamopus* [redacted] SMA 0011

Figure 18: Cervical vertebrae 8 and 9 of *Galeamopus* [redacted] SMA 0011 in right lateral view. Note the open neurocentral synchondrosis. Abb.: acdl, anterior centrodiapophyseal lamina; al, accessory lamina; apf, anterior pneumatic fossa; asl, accessory spinal lamina; bns, bifid neural spine; cpol, centropostzygapophyseal lamina; cprl, centroprezygapophyseal lamina; di, diapophysis; epi, epipophysis; naf, neural arch foramen; ncs, neurocentral synostosis; pap, parapophysis; pcdl, posterior centrodiapophyseal lamina; podl, postzygodiapophyseal lamina; poz, postzygapophysis; ppf, posterior pneumatic fossa; prdl, prezygodiapophyseal lamina; pre, pre-epipophysis; prz, prezygapophysis; pvf, posteroventral flange; pvfo, posteroventral fossa; spol, spinopostzygapophyseal lamina; sprl, spinoprezygapophyseal lamina; vsf, ventral spinal fossa. Scale bar = 10 cm.

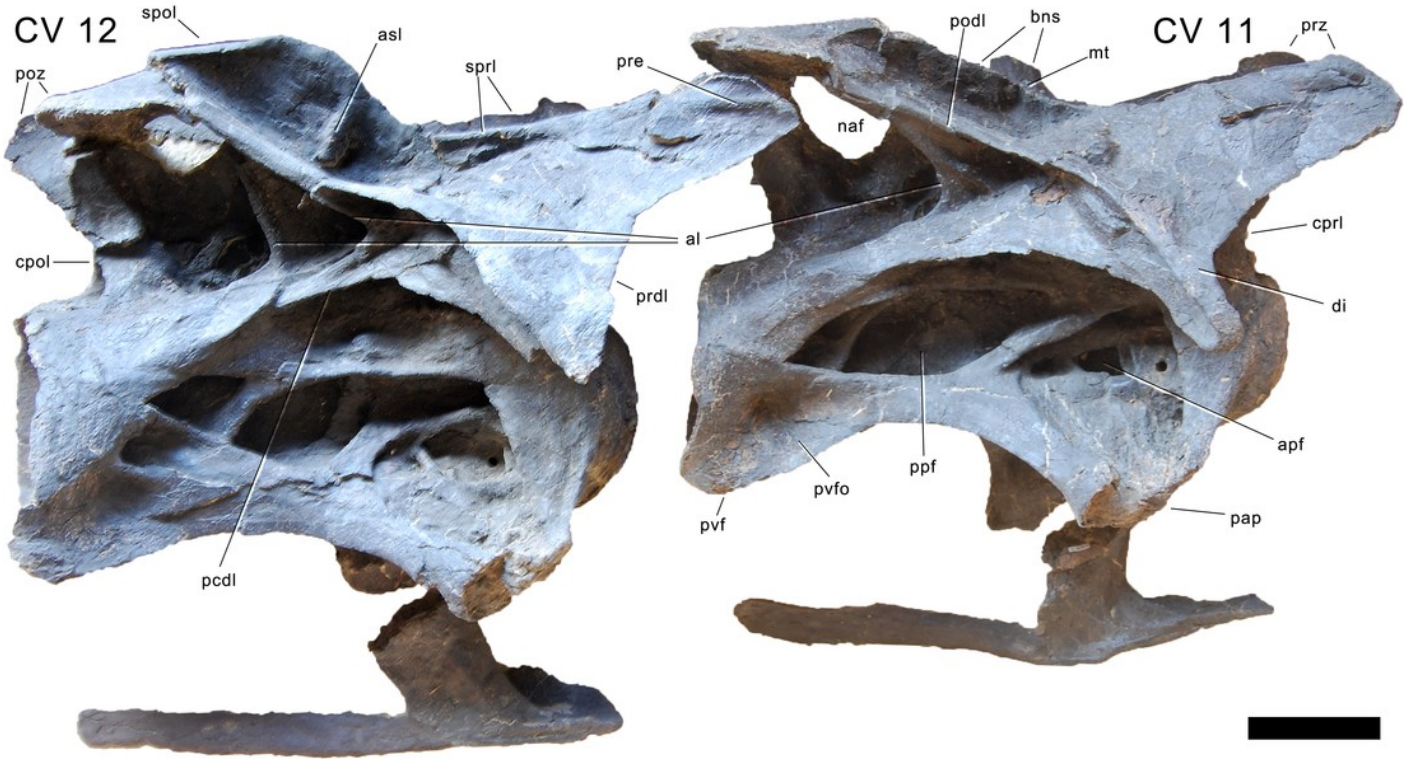


PeerJ Reviewing Manuscript

Figure 19

Cervical vertebrae 11 and 12 of *Galeamopus* [redacted] SMA 0011

Figure 19: Cervical vertebrae 11 and 12 of *Galeamopus* [redacted] SMA 0011 in right lateral view. Abb.: al, accessory lamina; apf, anterior pneumatic fossa; asl, accessory spinal lamina; bns, bifid neural spine; cpol, centropostzygapophyseal lamina; cprl, centroprezygapophyseal lamina; di, diapophysis; mt, median tubercle; naf, neural arch foramen; pap, parapophysis; pcdl, posterior centrodiapophyseal lamina; podl, postzygodiapophyseal lamina; poz, postzygapophysis; ppf, posterior pneumatic fossa; prdl, prezygodiapophyseal lamina; pre, pre-epipophysis; prz, prezygapophysis; pvf, posteroventral flange; pvfo, posteroventral fossa; spol, spinopostzygapophyseal lamina; sprl, spinoprezygapophyseal lamina. Scale bar = 10 cm.



PeerJ Reviewing Manuscript

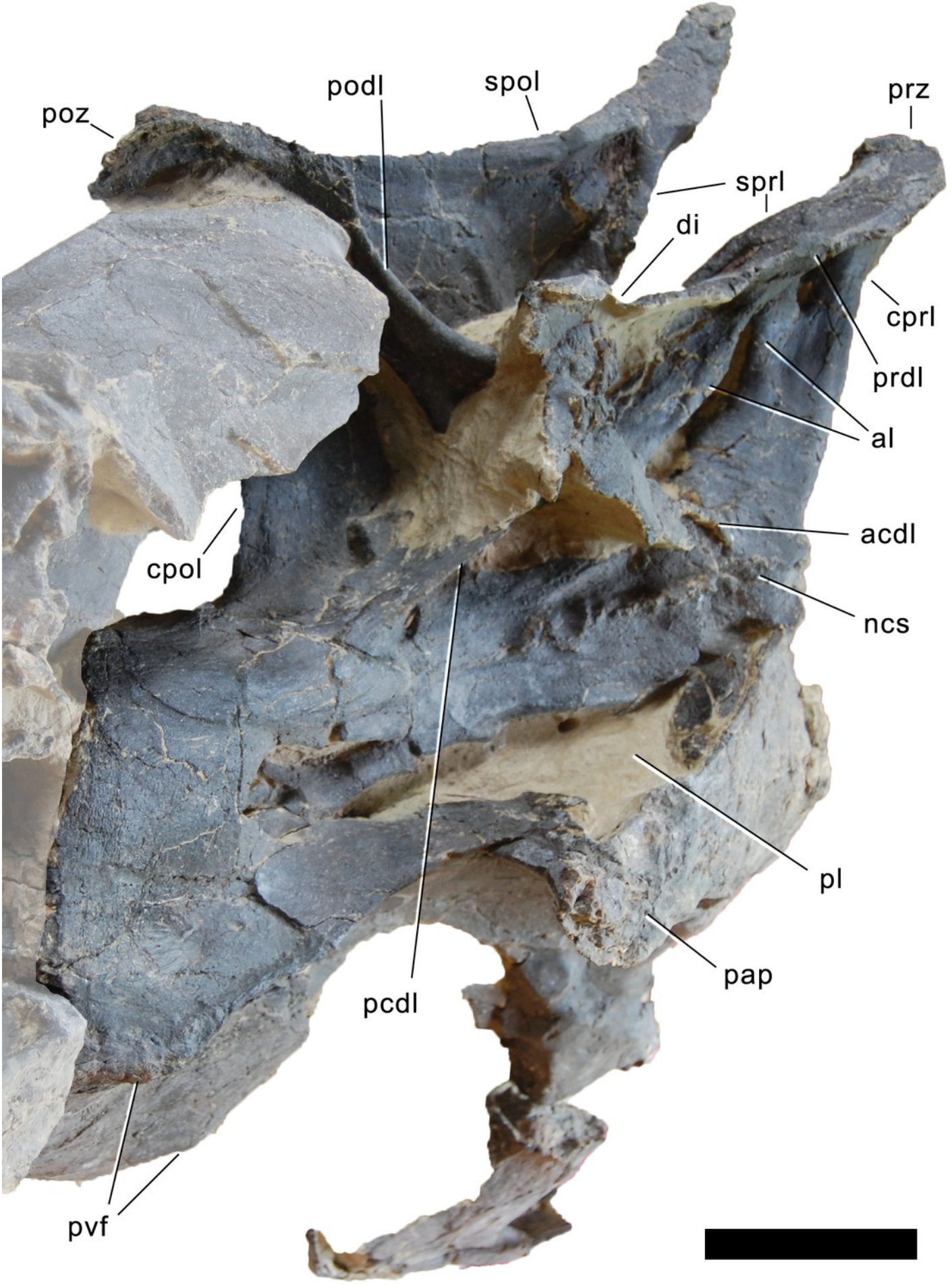
Figure 20

Cervical vertebra 15 of *Galeamopus* [redacted] SMA 0011

Figure 20: Cervical vertebra 15 of *Galeamopus* [redacted] SMA 0011 in right lateral view. Articulated DV 1 shaded. Abb.: acdl, anterior centrodiapophyseal lamina; al, accessory lamina; cpol, centropostzygapophyseal lamina; cprl, centroprezygapophyseal lamina; di, diapophysis; ncs, neurocentral synostosis; pap, parapophysis; pcdl, posterior centrodiapophyseal lamina; pl, pleurocoel; podl, postzygodiapophyseal lamina; poz, postzygapophysis; prdl, prezygodiapophyseal lamina; prz, prezygapophysis; pvf, posteroventral flange; spol, spinopostzygapophyseal lamina; sprl, spinoprezygapophyseal lamina. Scale bar = 10 cm.

PeerJ Reviewing Manuscript

PeerJ Reviewing Manuscript



PeerJ Reviewing Manuscript

Figure 21

Neurocentral synostosis in CV 5 of *Galeamopus* [redacted] SMA 0011

Figure 21: Neurocentral synostosis in CV 5 of *Galeamopus* [redacted] SMA 0011. Detail of the vertebra in right lateral view. Note the higher degree of fusion in the posterior portion compared to the anterior part (arrows). Abb.: apf, anterior pneumatic fossa; cpol, centropostzygapophyseal lamina; di, diapophysis; pcdl, posterior centrodiapophyseal lamina; podl, postzygodiapophyseal lamina; poz, postzygapophysis; ppf, posterior pneumatic fossa; pvfo, posteroventral fossa.

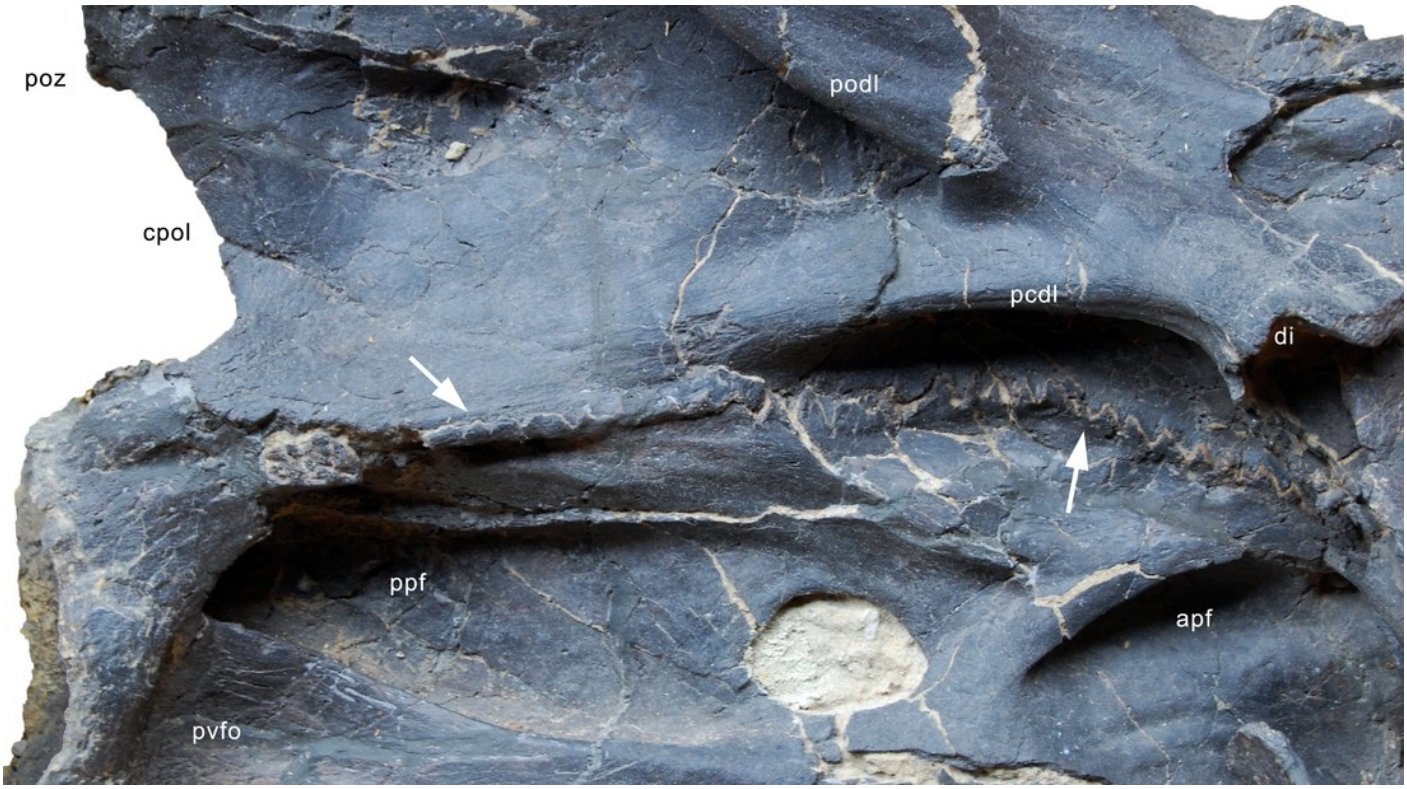


Figure 22

Neural arch foramina in CV 9 of *Galeamopus* [redacted] SMA 0011

Figure 22: Neural arch foramina in CV 9 of *Galeamopus* [redacted] SMA 0011, in posterodorsal view. The foramina are highlighted with the semi-transparent overlay. Abb.: bns, bifid neural spine; epi, epipophysis; mt, median tubercle; naf, neural arch foramen; pap, parapophysis; poz, postzygapophysis; ppf, posterior pneumatic fossa; prdl, prezygodiapophyseal lamina; prz, prezygapophysis; pvfo, posteroventral fossa; spol, spinopostzygapophyseal lamina; sprl, spinoprezygapophyseal lamina. Scale bar = 10 cm.

PeerJ Reviewing Manuscript

PeerJ Reviewing Manuscript

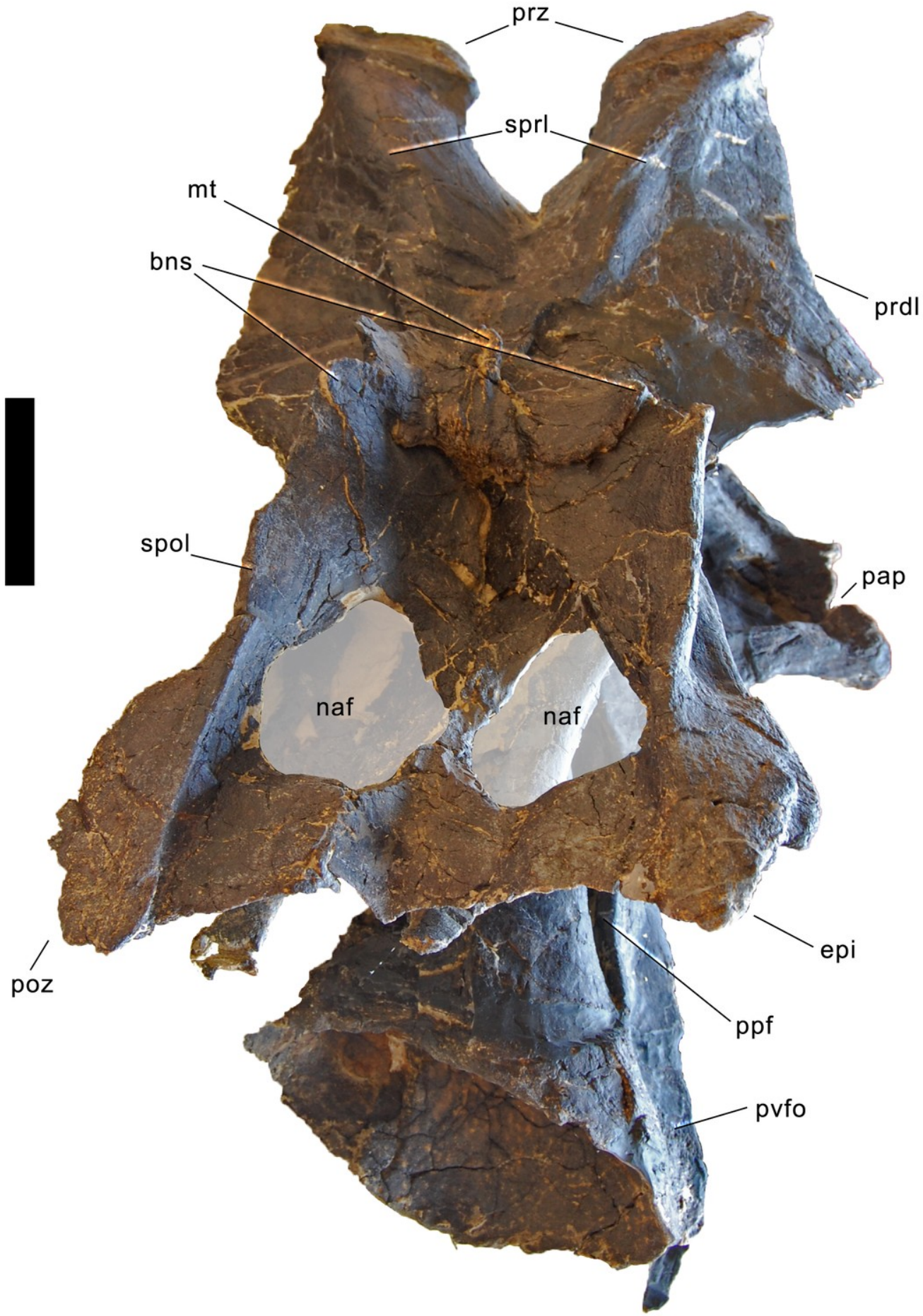


Figure 23

Dorsal vertebra 1 of *Galeamopus* [redacted] SMA 0011

Figure 23: Dorsal vertebra 1 of *Galeamopus* [redacted] SMA 0011 in right lateral view. Articulated CV 15 and DV 2 shaded. Abb.: acdl, anterior centrodiapophyseal lamina; al, accessory lamina; cpol, centropostzygapophyseal lamina; cprl, centroprezygapophyseal lamina; pap, parapophysis; pcdl, posterior centrodiapophyseal lamina; pl, pleurocoel; podl, postzygodiapophyseal lamina; poz, postzygapophysis; prdl, prezygodiapophyseal lamina; prz, prezygapophysis; pvf, posteroventral flange; spol, spinopostzygapophyseal lamina; sprl, spinoprezygapophyseal lamina. Scale bar = 10 cm.

PeerJ Reviewing Manuscript

PeerJ Reviewing Manuscript



Figure 24

Dorsal vertebra 2 of *Galeamopus* [redacted] SMA 0011

Figure 24: Dorsal vertebra 2 of *Galeamopus* [redacted] SMA 0011 in right lateral view. Articulated DV 1 and DV 3 shaded. The right metapophysis is lacking, only the medial face of the left one is visible. Note the broken diapophysis that reveals the inner structure. Abb.: cpol, centropostzygapophyseal lamina; cprl, centroprezygapophyseal lamina; di, diapophysis; pap, parapophysis; pl, pleurocoel; poz, postzygapophysis; prdl, prezygodiapophyseal lamina; prz, prezygapophysis; spol, spinopostzygapophyseal lamina; sprl, spinoprezygapophyseal lamina. Scale bar = 10 cm.

PeerJ Reviewing Manuscript

PeerJ Reviewing Manuscript

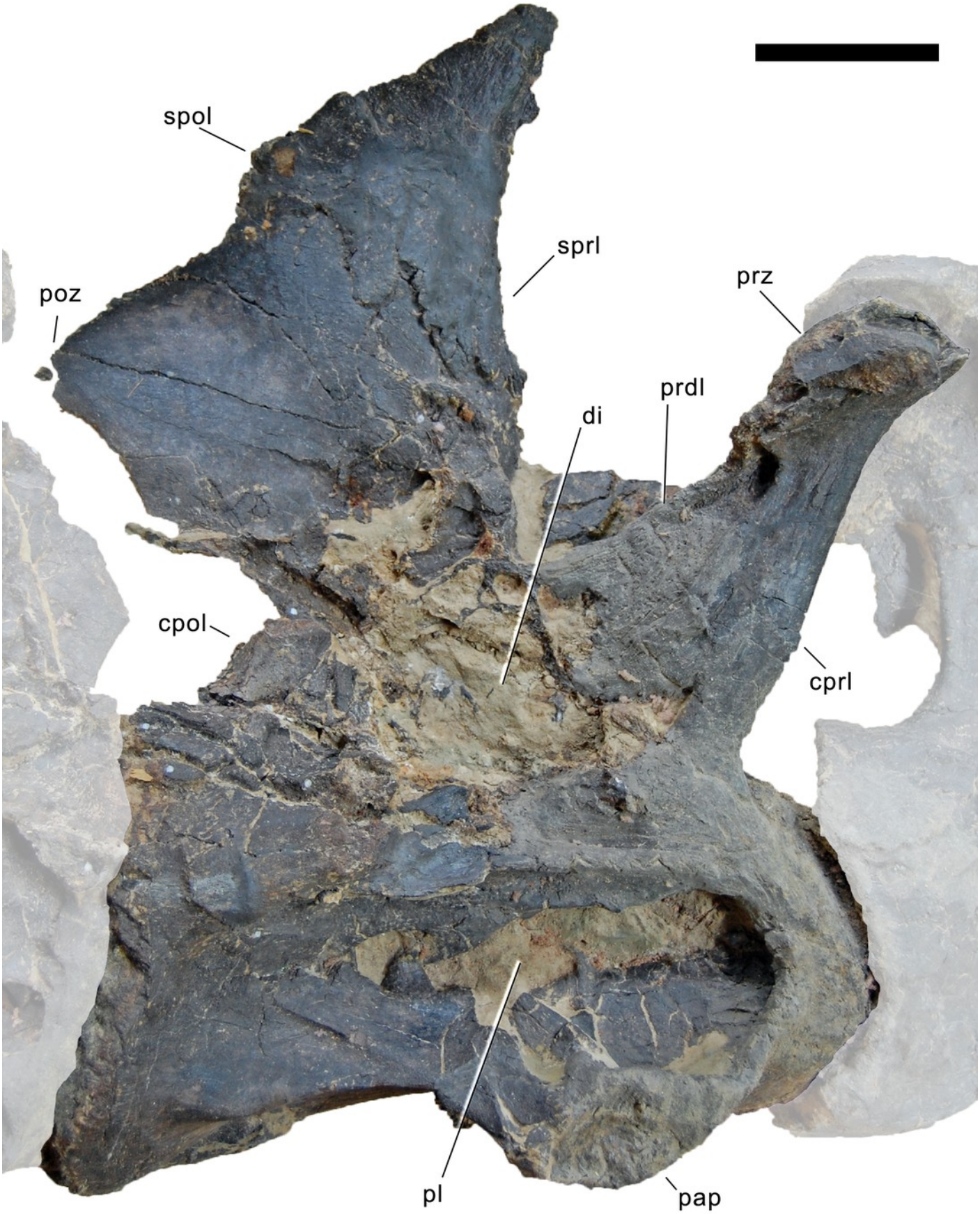


Figure 25

Dorsal vertebra 3 of *Galeamopus* [redacted] SMA 0011

Figure 25: Dorsal vertebra 3 of *Galeamopus* [redacted] SMA 0011 in right lateral view. Articulated DV 2 and partial DV 4 shaded. The right metapophysis is lacking, only the medial face of the left one is visible. The broken right prezygapophysis is present on top of the broken diapophysis. Abb.: DV, dorsal vertebra; ncs, neurocentral synostosis; pap, parapophysis; pl, pleurocoel; prz, prezygapophysis; spol, spinopostzygapophyseal lamina; sprl, spinoprezygapophyseal lamina; vk, ventral keel. Scale bar = 10 cm.

PeerJ Reviewing Manuscript

PeerJ Reviewing Manuscript

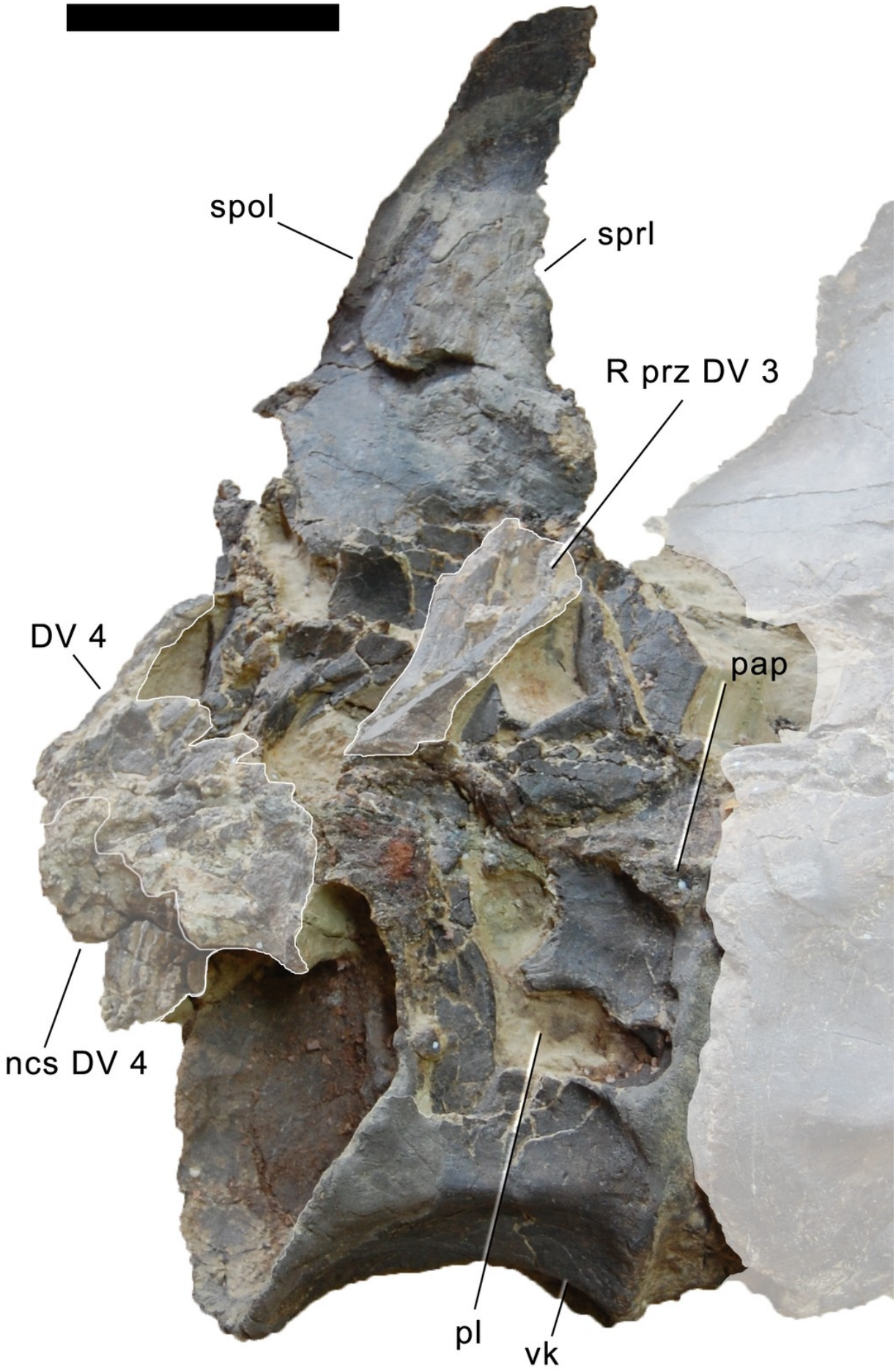
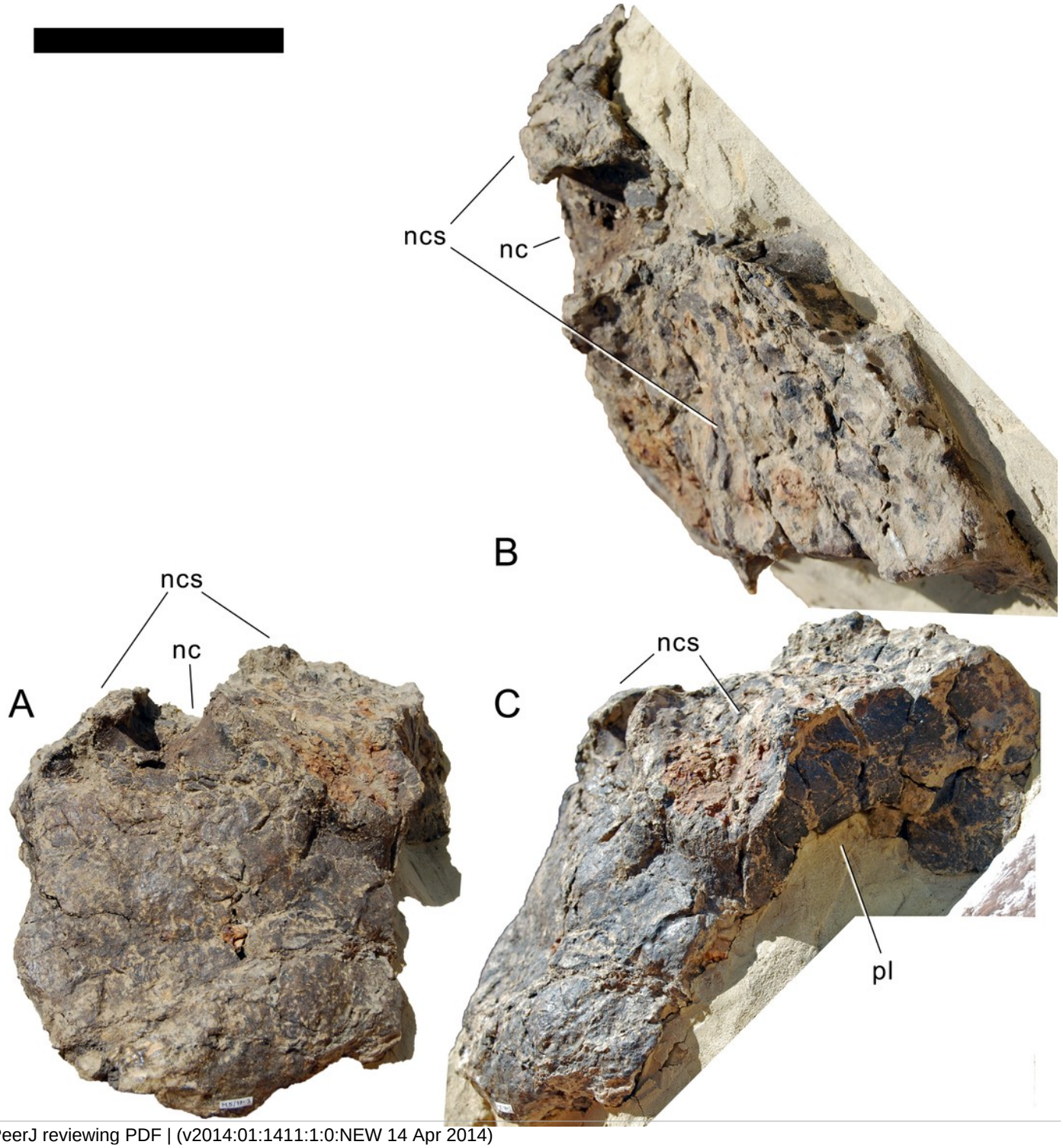


Figure 26

Dorsal vertebral centrum 4 of *Galeamopus* [redacted] SMA 0011

Figure 26: Dorsal vertebral centrum 4 of *Galeamopus* [redacted] SMA 0011 in anterior (A), dorsal (B), and left lateral (C) views. The element is still partly preserved within matrix. Abb.: nc, neural canal; ncs, neurocentral synchondrosis; pl, pleurocoel. Scale bar = 10 cm.



PeerJ Reviewing Manuscript

Figure 27

Dorsal vertebra 5 of *Galeamopus* [redacted] SMA 0011

Figure 27: Dorsal vertebra 5 of *Galeamopus* [redacted] SMA 0011 in posterolateral (A) and right lateral view (B). The element lacks the right half of the neural spine, and is partly mounted in matrix. Grey lines indicate the probable extensions of the right half. Note that the tip of the left diapophysis is reconstructed. Abb.: di, diapophysis; nc, neural canal; pap, parapophysis; pl, pleurocoel; poz, postzygapophysis; prz, prezygapophysis; spdl, spinodiapophyseal lamina; spol, spinopostzygapophyseal lamina; sprl, spinoprezygapophyseal lamina. Scale bar = 10 cm.

PeerJ Reviewing Manuscript

PeerJ Reviewing Manuscript

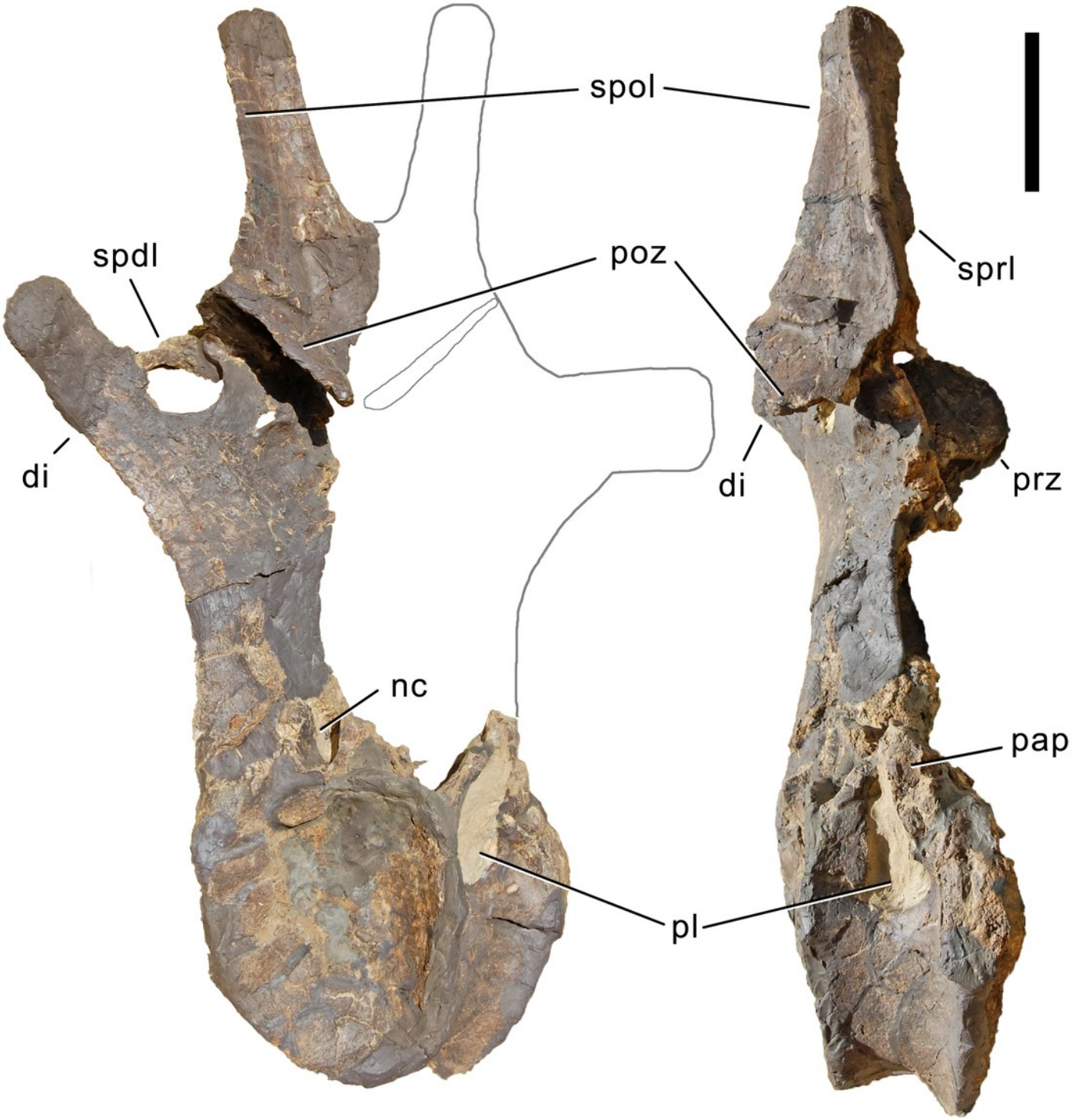


Figure 28

Dorsal vertebrae 6 to 10 of *Galeamopus* [redacted] SMA 0011

Figure 28: Dorsal vertebrae 6 to 10 of *Galeamopus* [redacted] SMA 0011 in right lateral (A), posterolateral (B), and anterolateral view (C). The elements are partly preserved in matrix. Note the open neurocentral synchondrosis in DV 7 to DV 10. Abb.: cpol, centropostzygapophyseal lamina; DV, dorsal vertebra; lspol, lateral spinopostzygapophyseal lamina; pap, parapophysis; pcdl, posterior centrodiapophyseal lamina; pcpl, posterior centroparapophyseal lamina; pl, pleurocoel; podl, postzygodiapophyseal lamina; posl, postspinal lamina; poz, postzygapophysis; prdl, prezygodiapophyseal lamina; prpl, prezygoparapophyseal lamina; prsl, prespinal lamina; spdl, spinodiapophyseal lamina; sprl, spinoprezygapophyseal lamina. Scale bar in A = 10 cm, DV 6 in A and C, and DV 10 in A and B are scaled to the same vertebral height.

PeerJ Reviewing Manuscript

PeerJ Reviewing Manuscript

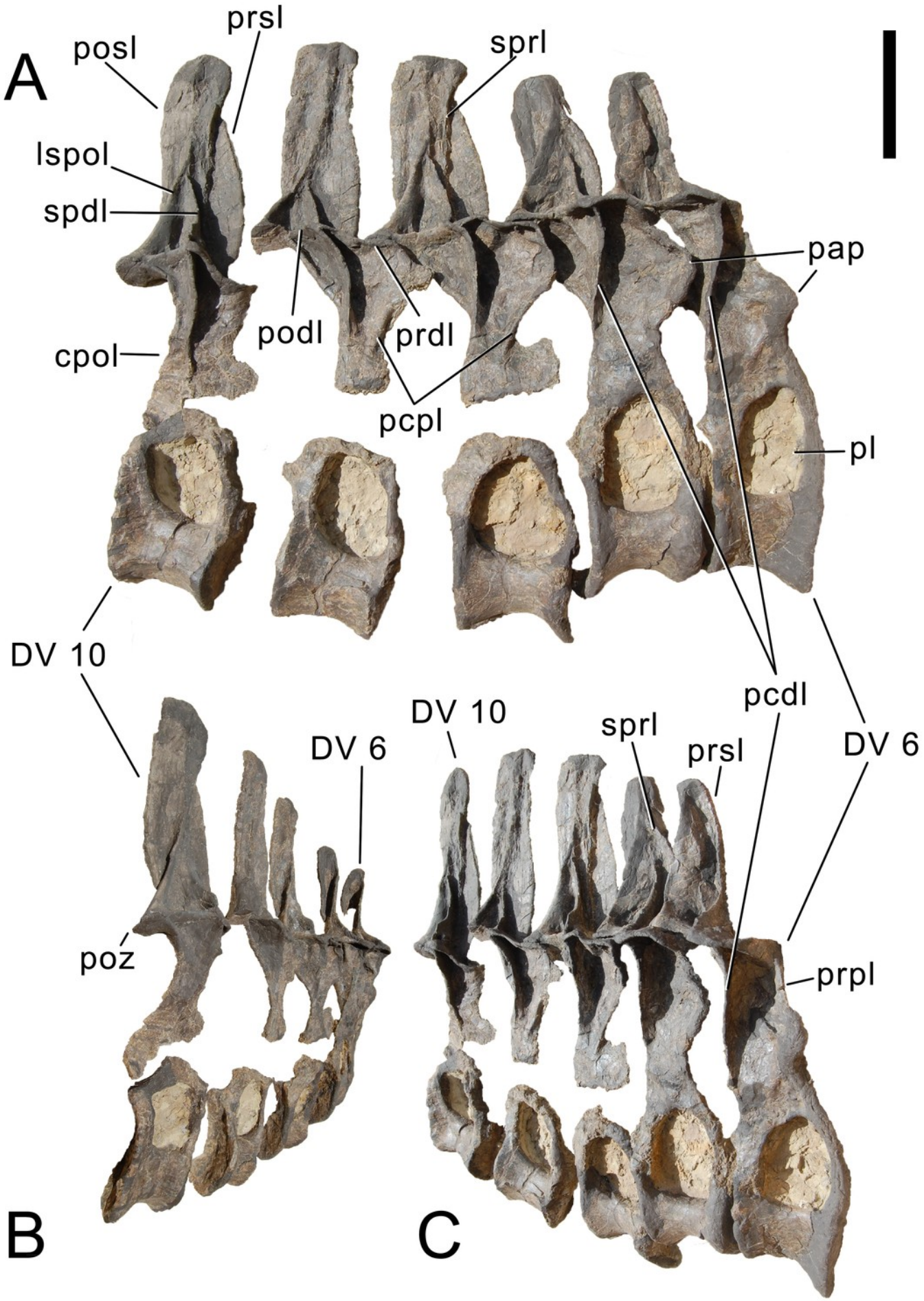
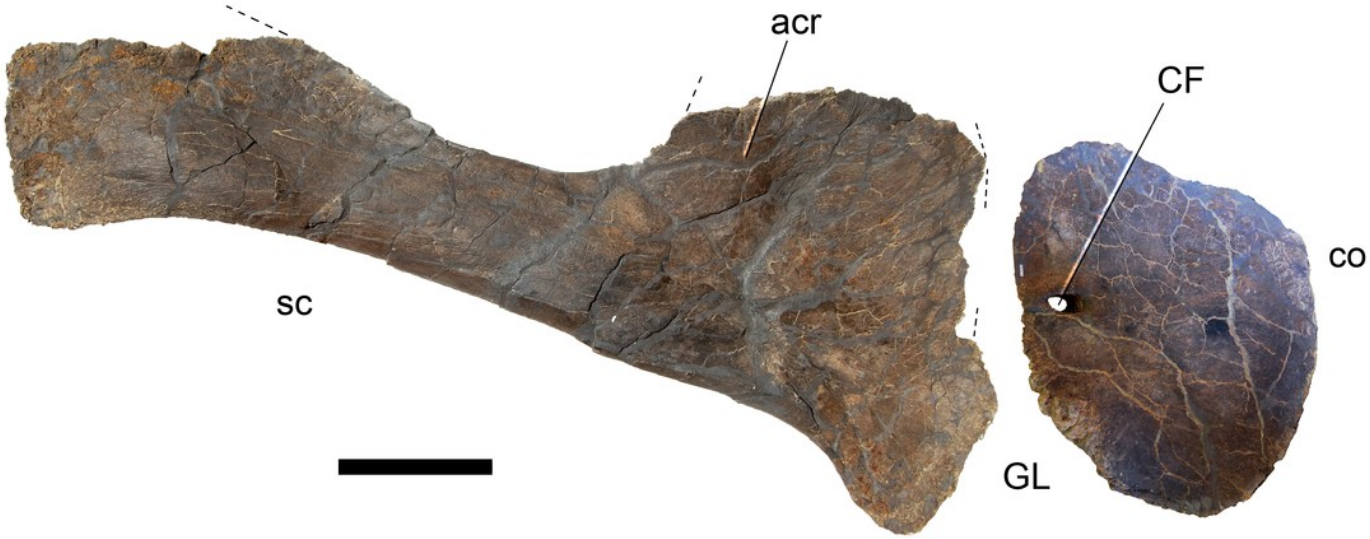


Figure 29

Scapula and coracoid of *Galeamopus* [redacted] SMA 0011

Figure 29: Scapula and coracoid of *Galeamopus* [redacted] SMA 0011 in right lateral view. Lacking parts indicated with dashed lines. Abb.: acr, acromion ridge; CF, coracoid foramen; co, coracoid; GL, glenoid; sc, scapula. Scale bar = 20 cm.



PeerJ Reviewing Manuscript

Figure 30

Forelimb of *Galeamopus* [redacted] SMA 0011 in anterior view

Figure 30: Forelimb of *Galeamopus* [redacted] SMA 0011 in anterior view: A) humerus, B) antebrachium and manus (as mounted within matrix). Note that the carpal was probably mounted upside down. Abb.: c, carpal; dpc, deltopectoral crest; hh, humeral head; lr, lateral ridge; mc, metacarpal; mr, medial ridge; phm, manual phalanx; r, radius; rt, tubercle for articulation with radius; u, ulna; ut, tubercle for articulation with ulna. Scale bar (valid for both A and B) = 20 cm.

PeerJ Reviewing Manuscript

PeerJ Reviewing Manuscript

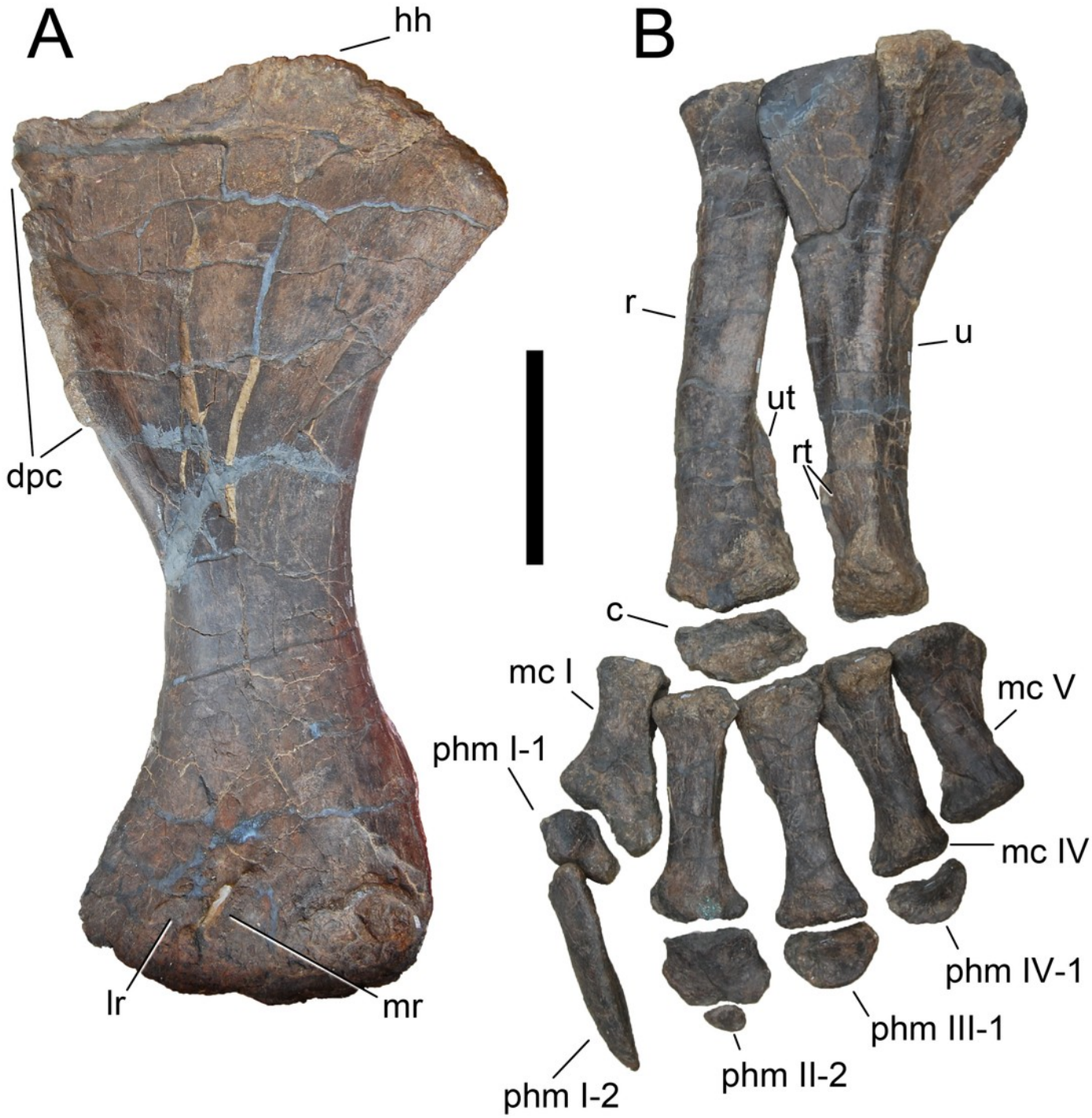
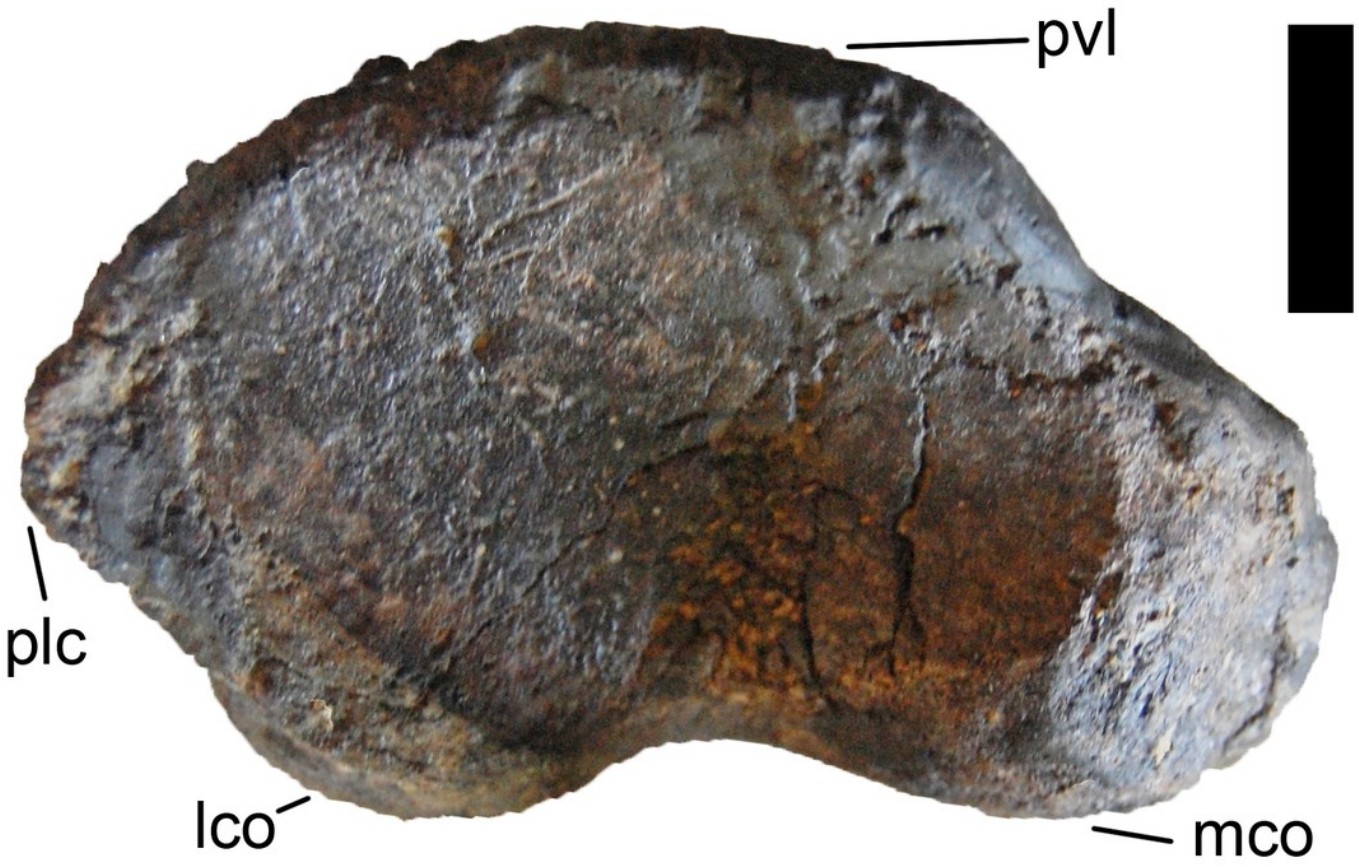


Figure 31

Left manual phalanx I-1 of *Galeamopus* [redacted] SMA 0011

Figure 31: Left manual phalanx I-1 of *Galeamopus* [redacted] SMA 0011 in posterior view. Note the distinct posteroventral lip and posterolateral crest. Abb.: lco, lateral condyle; mco, medial condyle; plc, posterolateral crest; pvl, posteroventral lip. Scale bar = 2 cm.

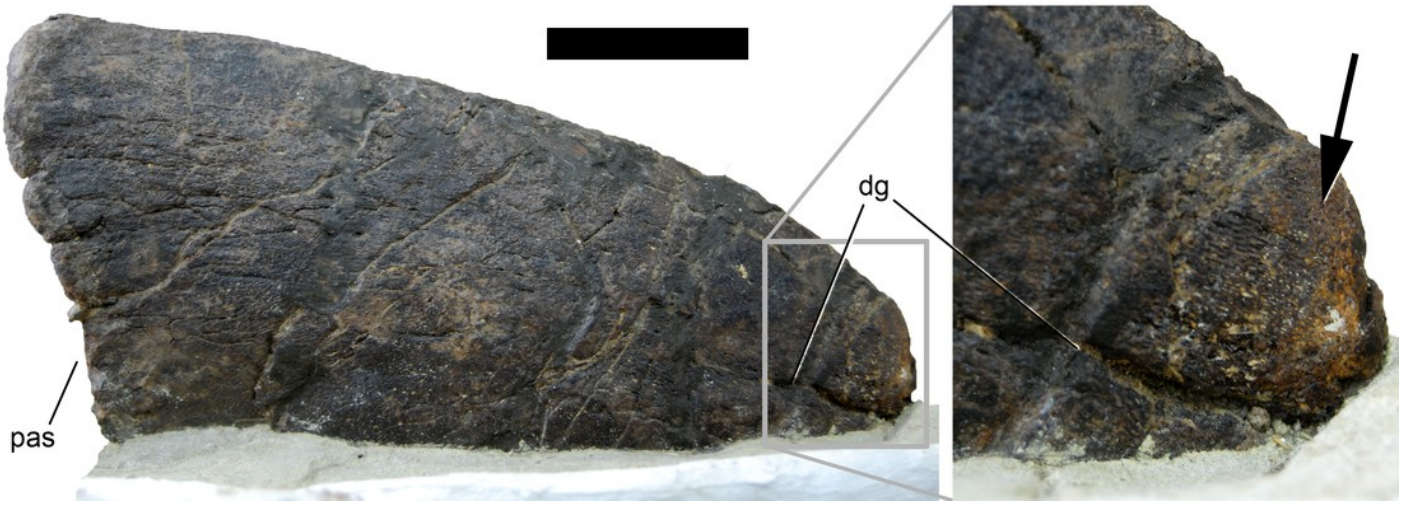


PeerJ Reviewing Manuscript

Figure 32

Possible preservation of keratinous sheet on left manual ungual I-2 of *Galeamopus* [redacted] SMA 0011

Figure 32: Possible preservation of keratinous sheet on left manual ungual I-2 of *Galeamopus* [redacted] SMA 0011 (medial view). Note the different surface texture at the tip (arrow), compared to more posterior portions. Abb.: dg, distal groove; pas, proximal articular surface. Scale bar = 5 cm.

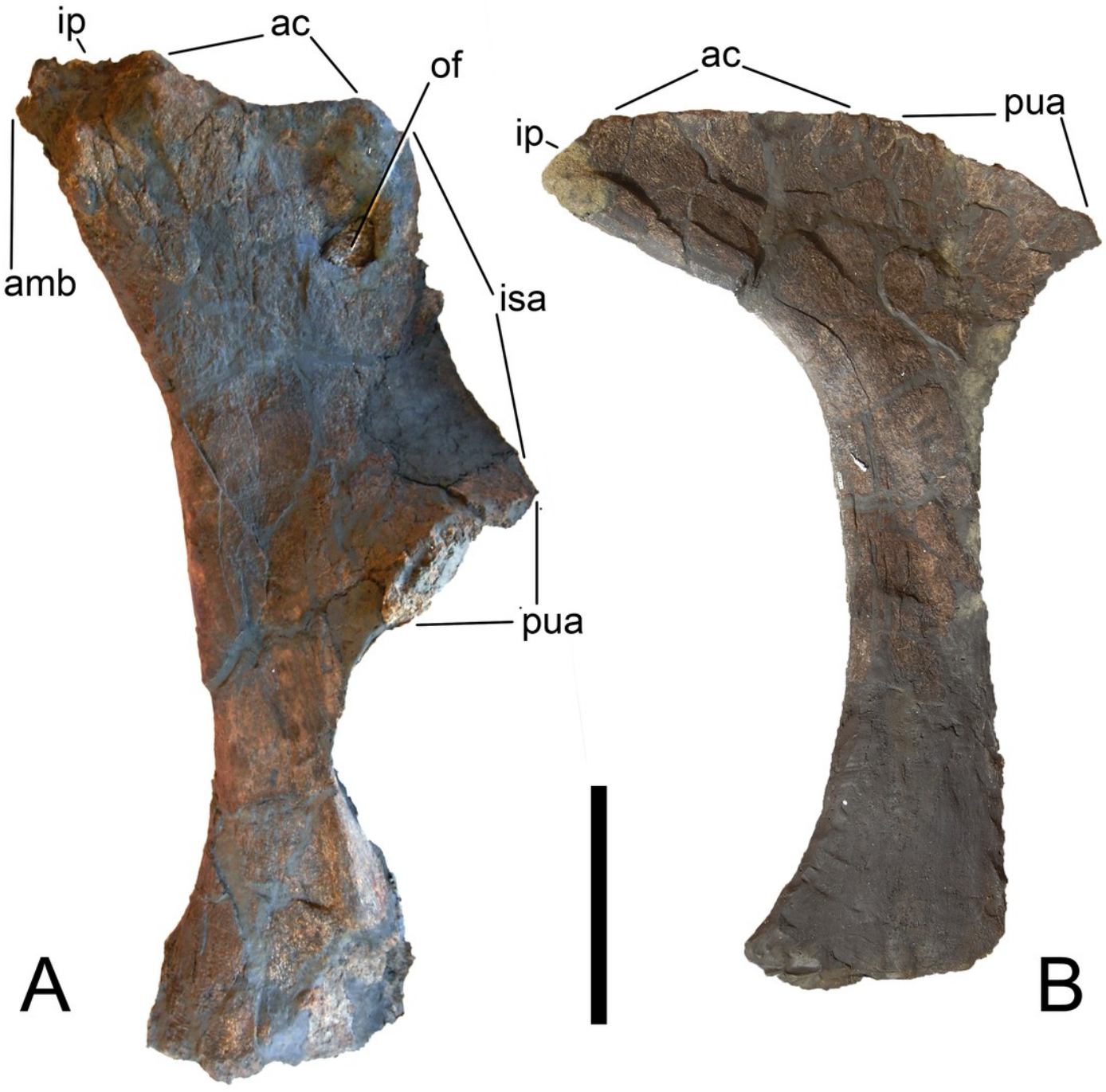


PeerJ Reviewing Manuscript

Figure 33

Pubis and ischium of *Galeamopus* [redacted] SMA 0011

Figure 33: Right pubis (A) and left ischium (B) of *Galeamopus* [redacted] SMA 0011 in medial view. The distal end of the ischium is reconstructed. Abb.: ac, acetabular surface; amb, ambiens process; ip, iliac peduncle; isa, ischial articular surface; of, obturator foramen; pua, pubic articulation. Scale bar = 20 cm.



PeerJ Reviewing Manuscript

Figure 34

Left hindlimb of *Galeamopus* [redacted] SMA 0011

Figure 34: Left hindlimb of *Galeamopus* [redacted] SMA 0011: A) femur in posterior view; B) tibia and fibula in anterior view, as mounted. The lacking greater trochanter of the femur is indicated by the dashed line. Abb.: cc, cnemial crest; ec, epicondyle; fh, femoral head; fi, fibula; fic, fibular condyle; icg, intercondylar groove; tb, tibia; tic, tibial condyle. Scale bar = 20 cm.

PeerJ Reviewing Manuscript

PeerJ Reviewing Manuscript

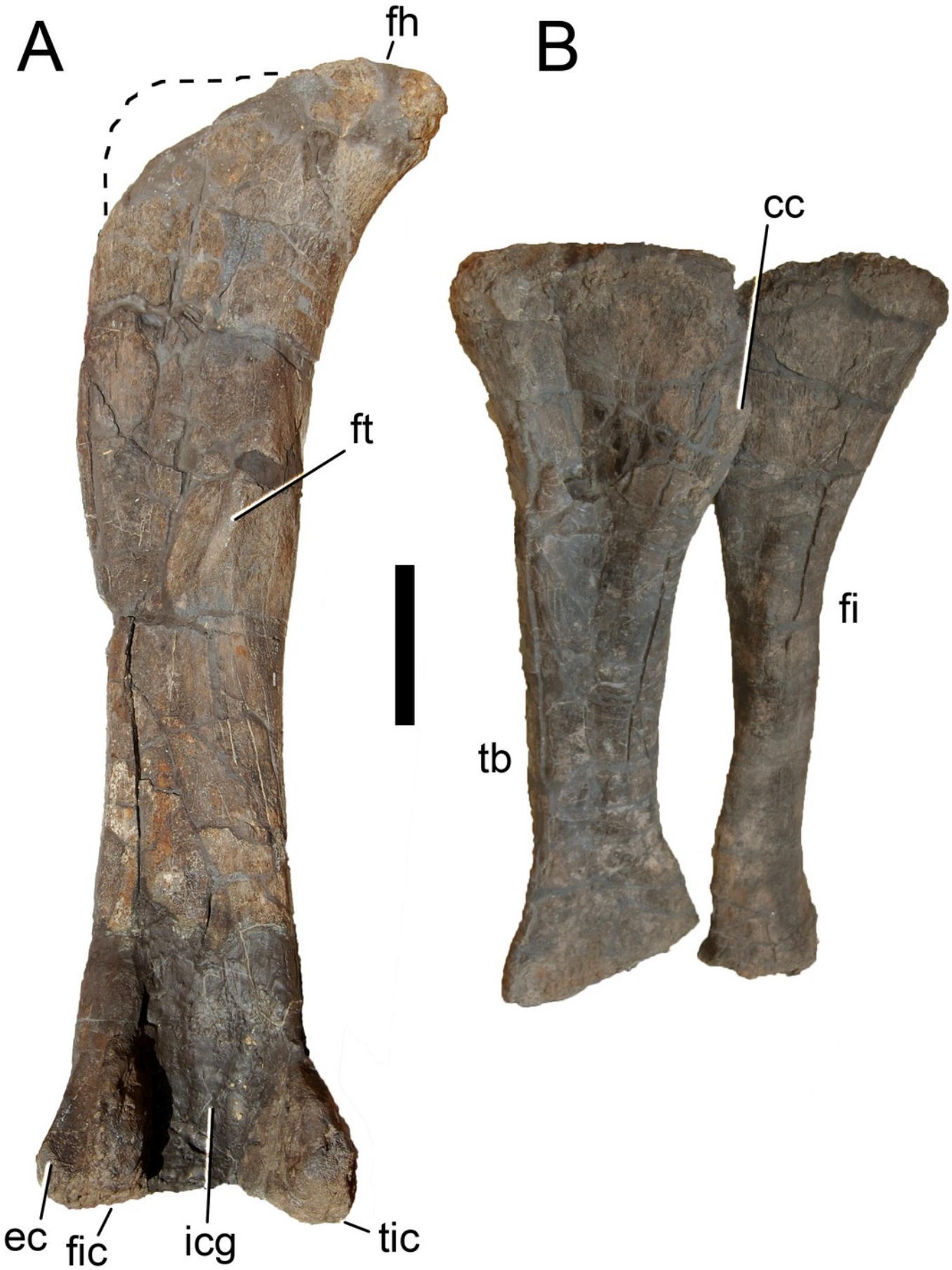


Figure 35

Left pes of *Galeamopus* [redacted] SMA 0011

Figure 35: Left pes of *Galeamopus* [redacted] SMA 0011: A) astragalus in anterior and lateral view (left to right); B) metatarsals I to V (left to right) in anterior/dorsal view; C) pedal phalanges in dorsal view, as mounted. Due to the mounted state, a portion of the tibia, obscuring a posterodorsal part of the astragalus is masked as semitransparent in A. Elements partially overlapping metatarsals are marked by a black line in B. Php IV-1 could actually also be php III-2 or php V-1 (see text). Abb.: asp, ascending process; dlr, dorsolateral ridge; dro, distal roller; fif, fibular facet; icg, intercondylar groove; mts, metatarsal; nf, nutrient foramen; php, pedal phalanx; plp, posterolateral process; tb, tibia; tif, tibial facet; ung, ungual. Scale bar = 10 cm.

PeerJ Reviewing Manuscript

PeerJ Reviewing Manuscript

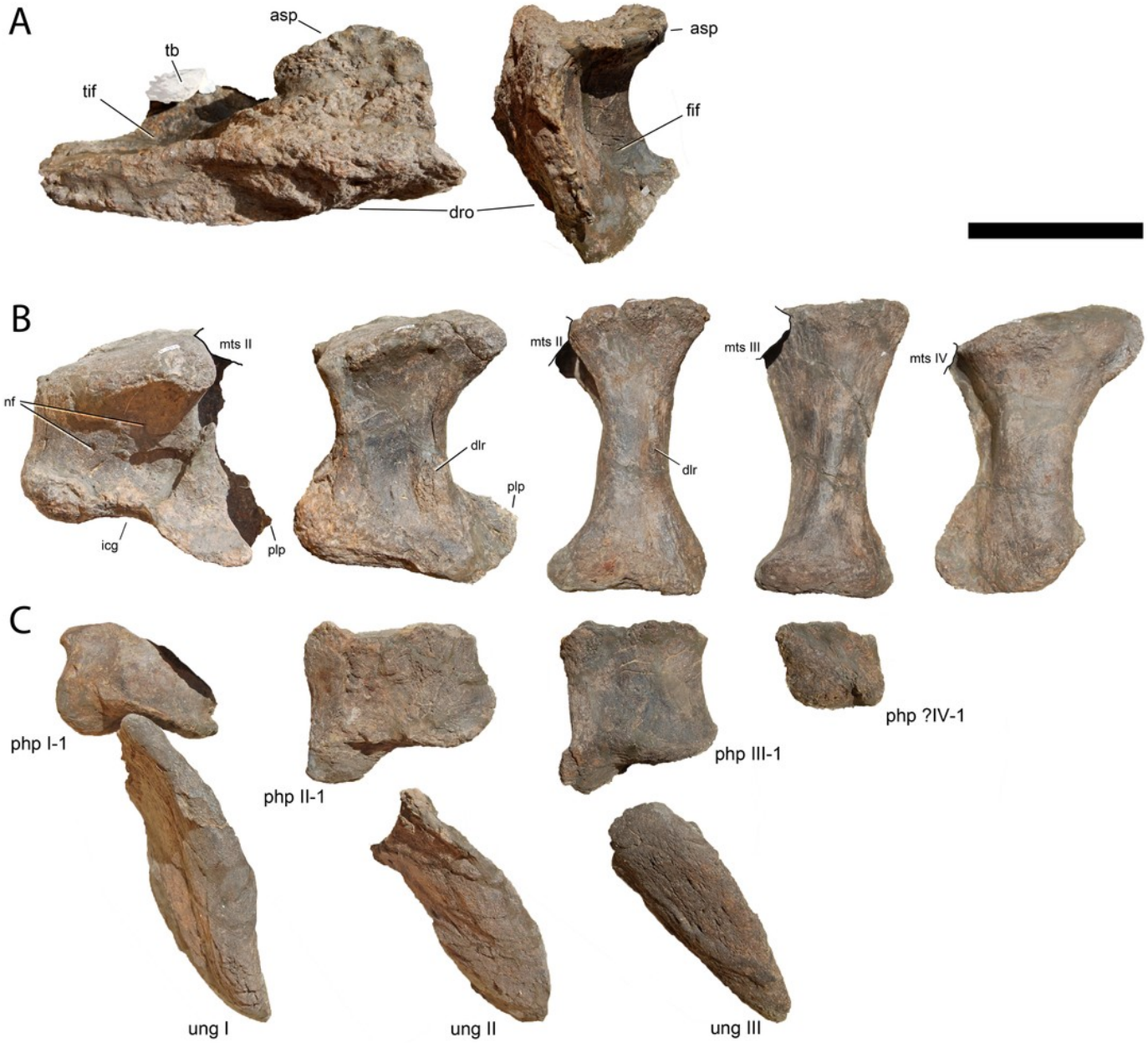
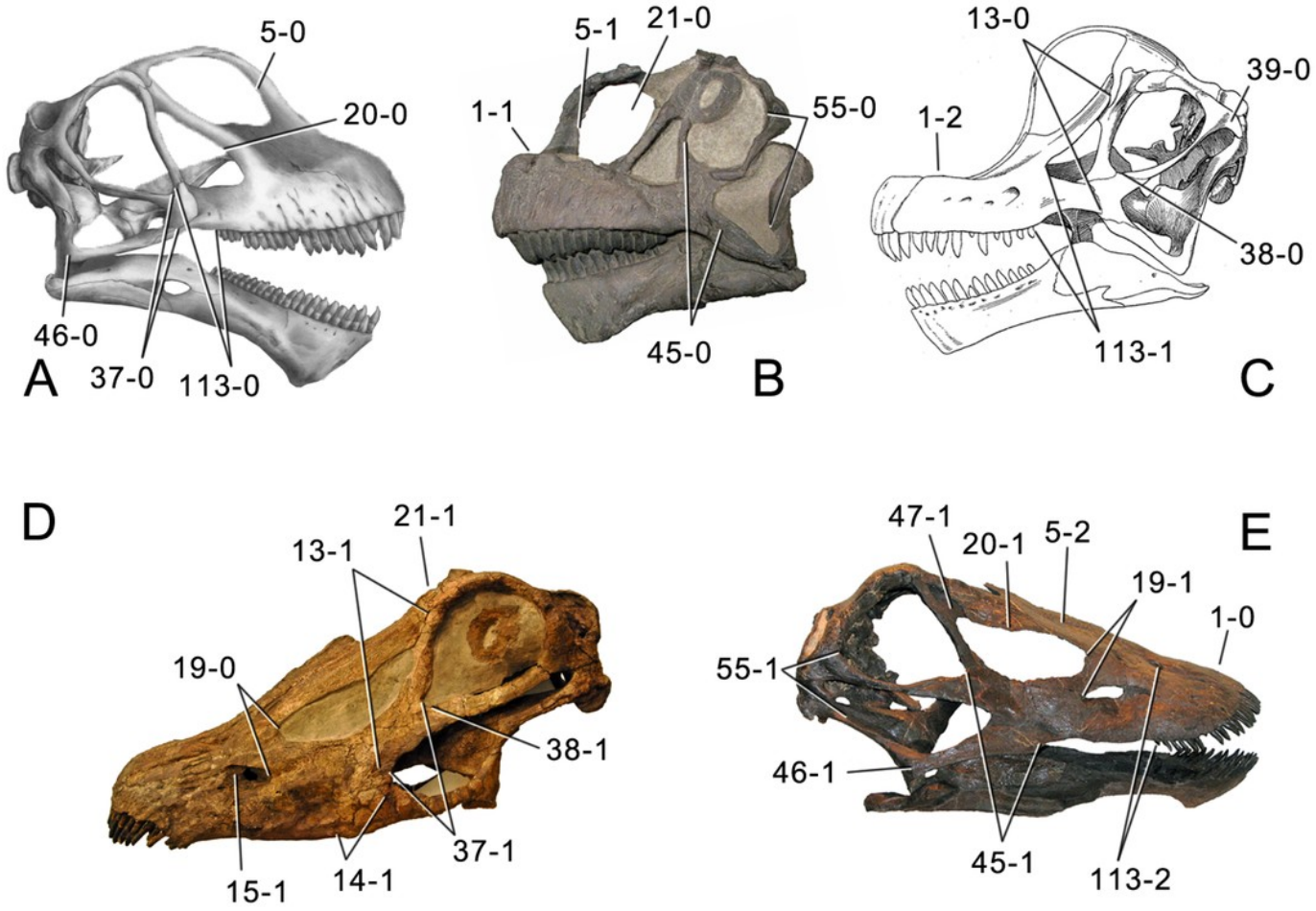


Figure 36

Sauropod skulls

Figure 36: Skulls of *Mamenchisaurus youngi* (A; modified from Ouyang and Ye, 2002), *Camarasaurus* sp. USNM 13786 (B), *Giraffatitan brancai* (C; modified from Janensch, 1935), *Diplodocus* sp. CM 11161 (D), and *Galeamopus* [redacted] SMA 0011 (E) in lateral view, illustrating the states of the characters 1, 5, 13, 14, 15, 19, 20, 21, 37, 38, 39, 45, 46, 55, 113. Not to scale.

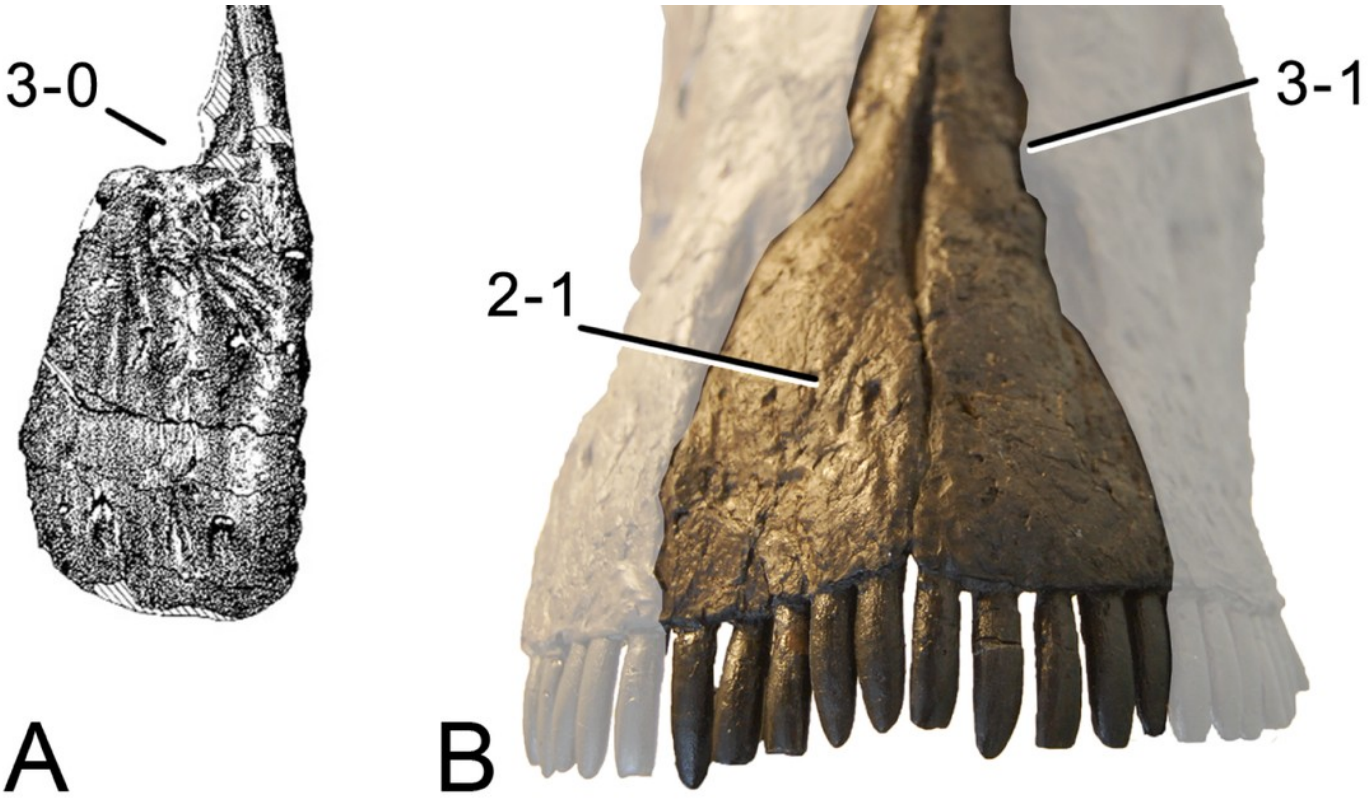


PeerJ Reviewing Manuscript

Figure 37

Anterior portions of sauropod premaxillae

Figure 37: Anterior portions of premaxillae of *Camarasaurus* (A; modified from Madsen et al., 1995) and *Galeamopus* [redacted] SMA 0011 (B) in anterodorsal view, illustrating the states of characters 2 and 3. Not to scale.

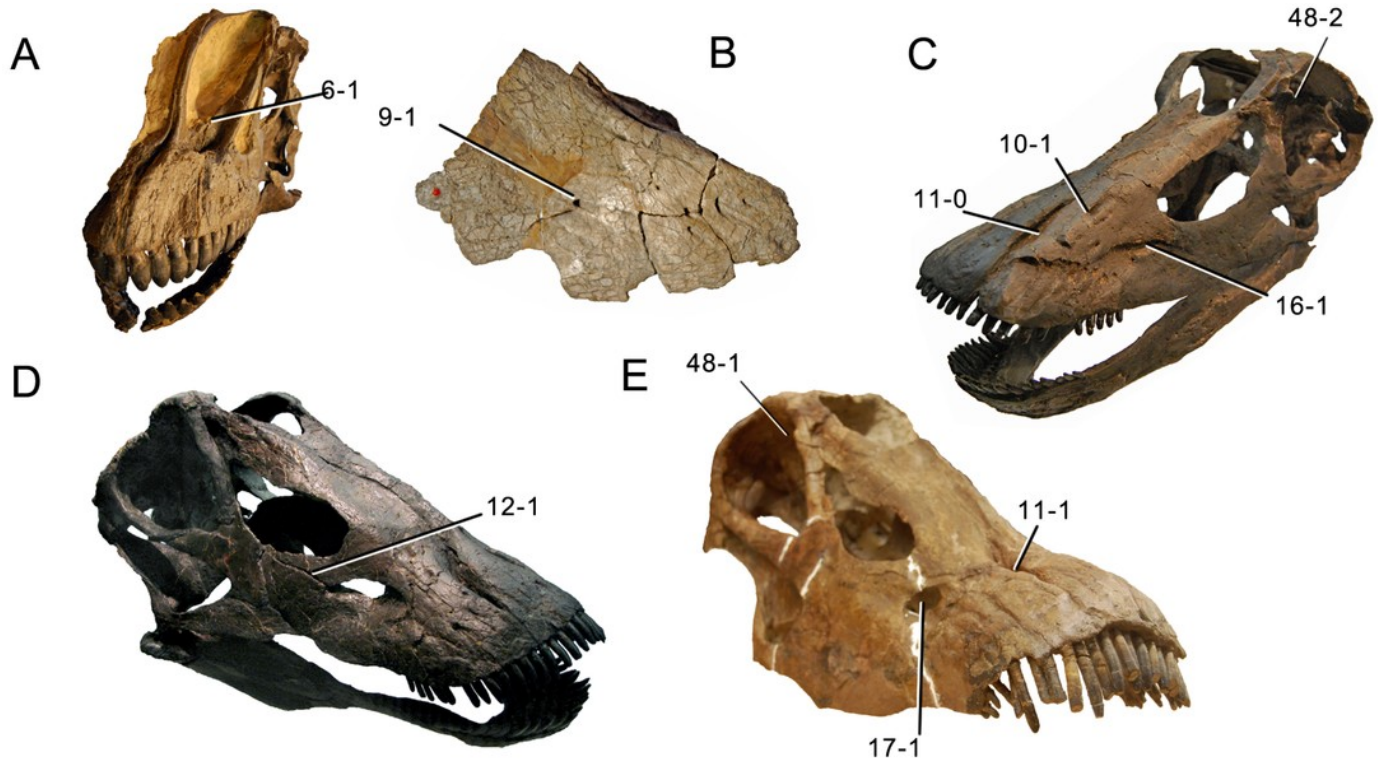


PeerJ Reviewing Manuscript

Figure 38

Sauropod skulls

Figure 38: Skulls (A, C-E) or maxilla (B) of *Camarasaurus* sp. SMA 0002 (A), *Dicraeosaurus hansemanni* MB.R.2336 (B), *Kaatedocus siberi* SMA 0004 (C), *Galeamopus* [redacted] SMA 0011 (D), and *Diplodocus* sp. CM 11161 (E) in anterolateral view, illustrating the states of the characters 6, 9, 10, 11, 12, 16, 17, 48. Not to scale.

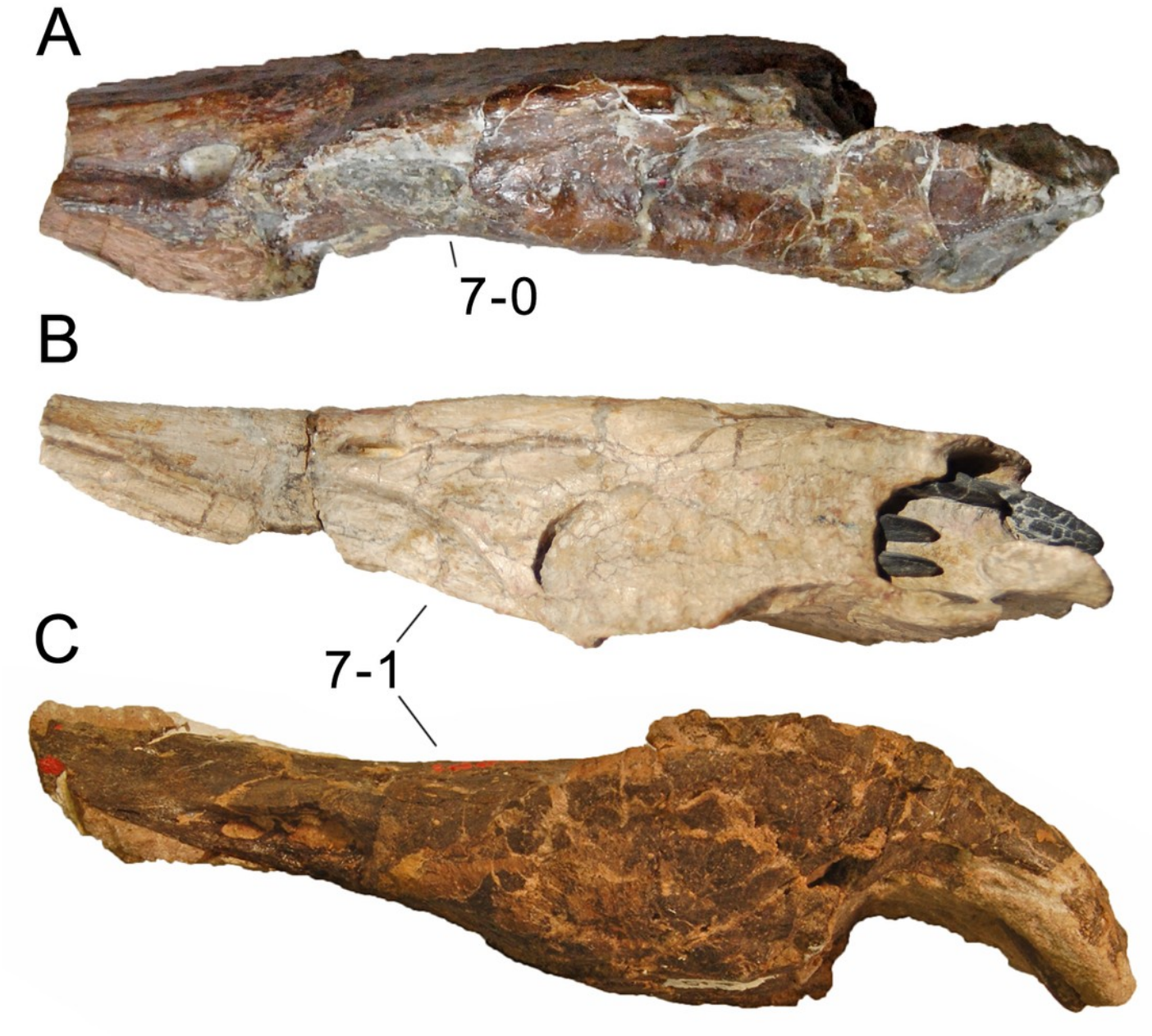


PeerJ Reviewing Manuscript

Figure 39

Sauropod premaxillae

Figure 39: Premaxillae of *Suuwassea emilieae* ANS 21122 (A), *Dicraeosaurus hansemanni* MB.R.2337 (B), and *Diplodocus* sp. USNM 2673 (C, left element reversed) in lateral view, illustrating the states of character 7. Not to scale.

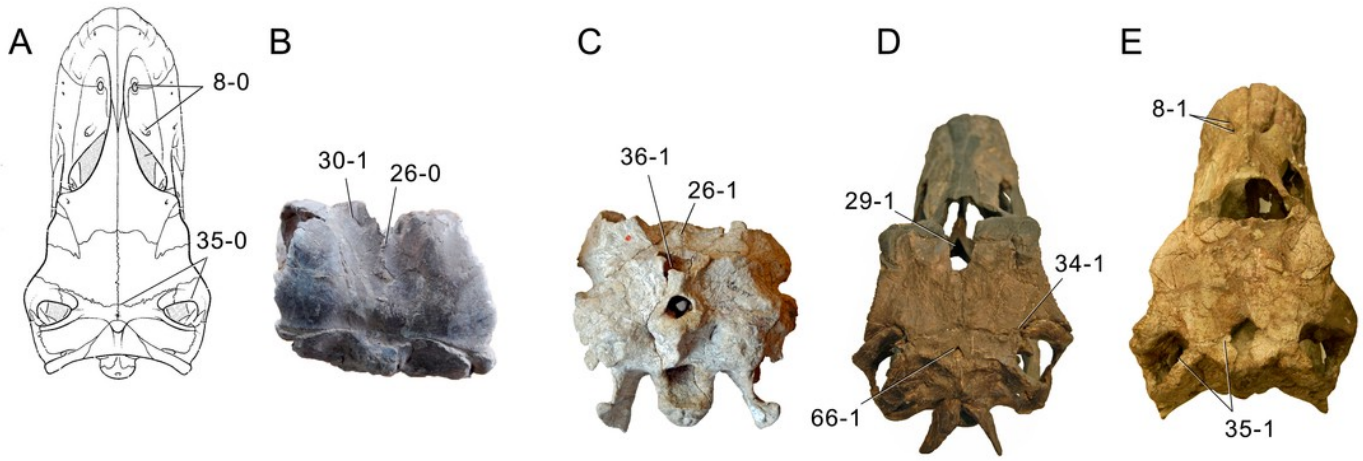


PeerJ Reviewing Manuscript

Figure 40

Sauropod skulls

Figure 40: Skulls of *Camarasaurus* (A; modified from Wilson and Sereno, 1998), *Limaysaurus tessonei* MUCPv-205 (B; photo by J. Whitlock), *Dicraeosaurus hansemanni* MB.R.2379 (C), *Kaatedocus siberi* SMA 0004 (D) and *Diplodocus* sp. CM 11161 (E) in dorsal view, illustrating the states of the characters 8, 26, 29, 30, 34, 35, 36, 66. Not to scale.



PeerJ Reviewing Manuscript

PeerJ Reviewing Manuscript

Figure 41

Diplodocoid skull roofs

Figure 41: Skull roof of *Diplodocus* sp. CM 11161 (A; based on Wilson and Sereno, 1998) and *Limaysaurus tessonei* MUCPv-205 (B; based on Calvo and Salgado, 1995) in dorsal view. Note the anteromedial hook in the prefrontal of CM 11161 (A; C23-1), and the differently shaped frontal-nasal suture (straight to anteriorly bowed in A, C28-0; bowed posteriorly in B, C28-1). Abb.: f, frontal; na, nasal; pf, prefrontal. Scaled to the same skull roof length.

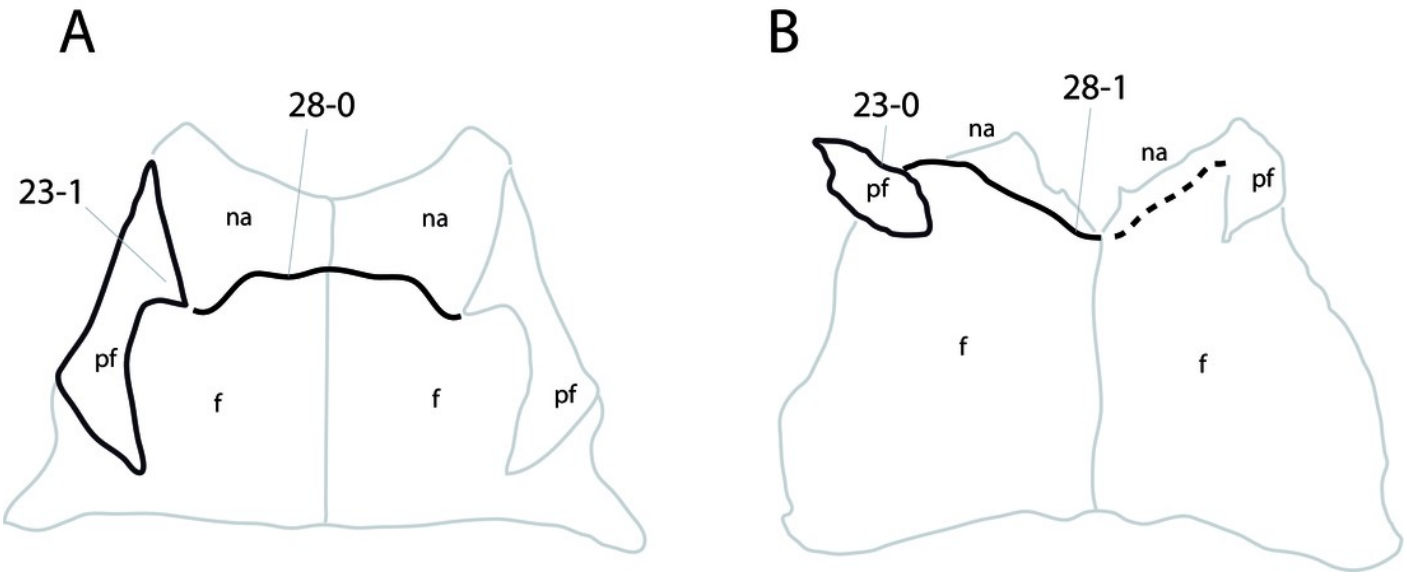
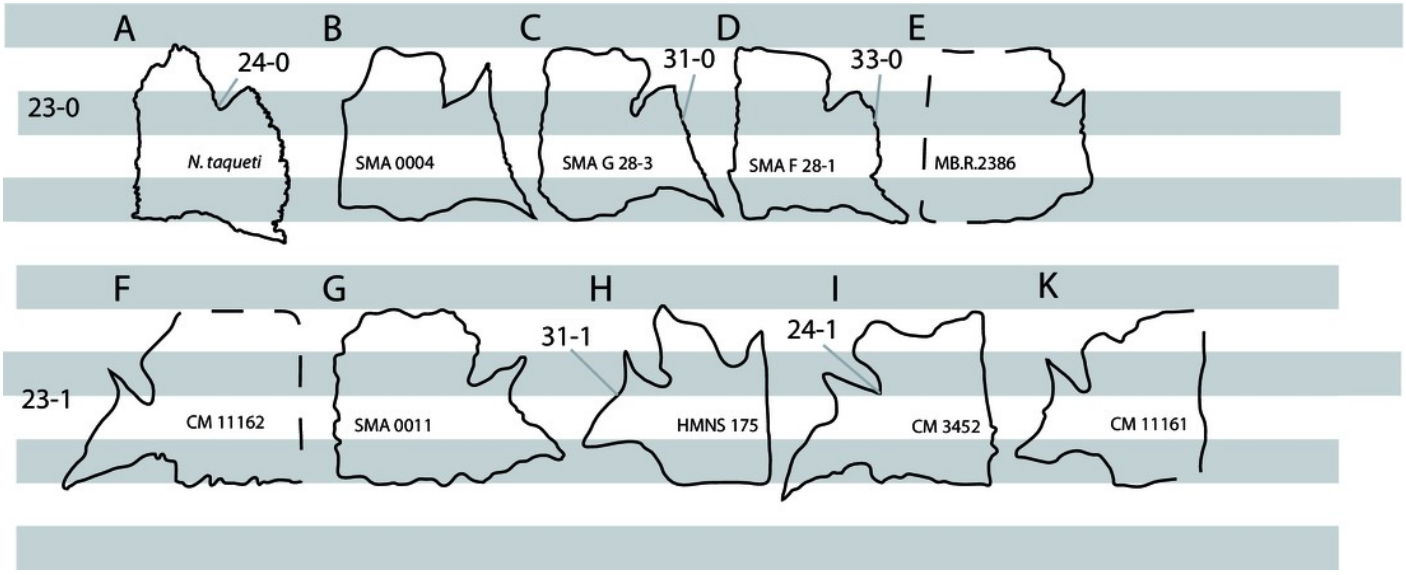


Figure 42

Diplodocid frontals

Figure 42: Left (F, H-K) and right (A-E, G) diplodocoid frontals in dorsal view, anterior to the top. The upper row shows elements with an anteriorly restricted posterior process of the prefrontal (C23-0), the lower row have elongated posterior processes (C23-1). Additional states are illustrated from the characters 24, 31, 33. Frontals figured in strict perpendicular view, and scaled to the same anteroposterior length.



PeerJ Reviewing Manuscript

PeerJ Reviewing Manuscript

Figure 43

Left jugal of *Diplodocus* USNM 2672

Figure 43: Left jugal of *Diplodocus* USNM 2672 in lateral view, illustrating the large contribution of the jugal to the antorbital fenestra (C40-1), the narrow and elongate posteroventral process (C42-1), the dorsal process of the jugal (C43-0), and the anterior spur (C44-1). Abb.: aof, antorbital fenestra; j, jugal; la, lacrimal; ltf, laterotemporal fenestra; m, maxilla; o, orbit; po, postorbital; qj, quadratojugal.

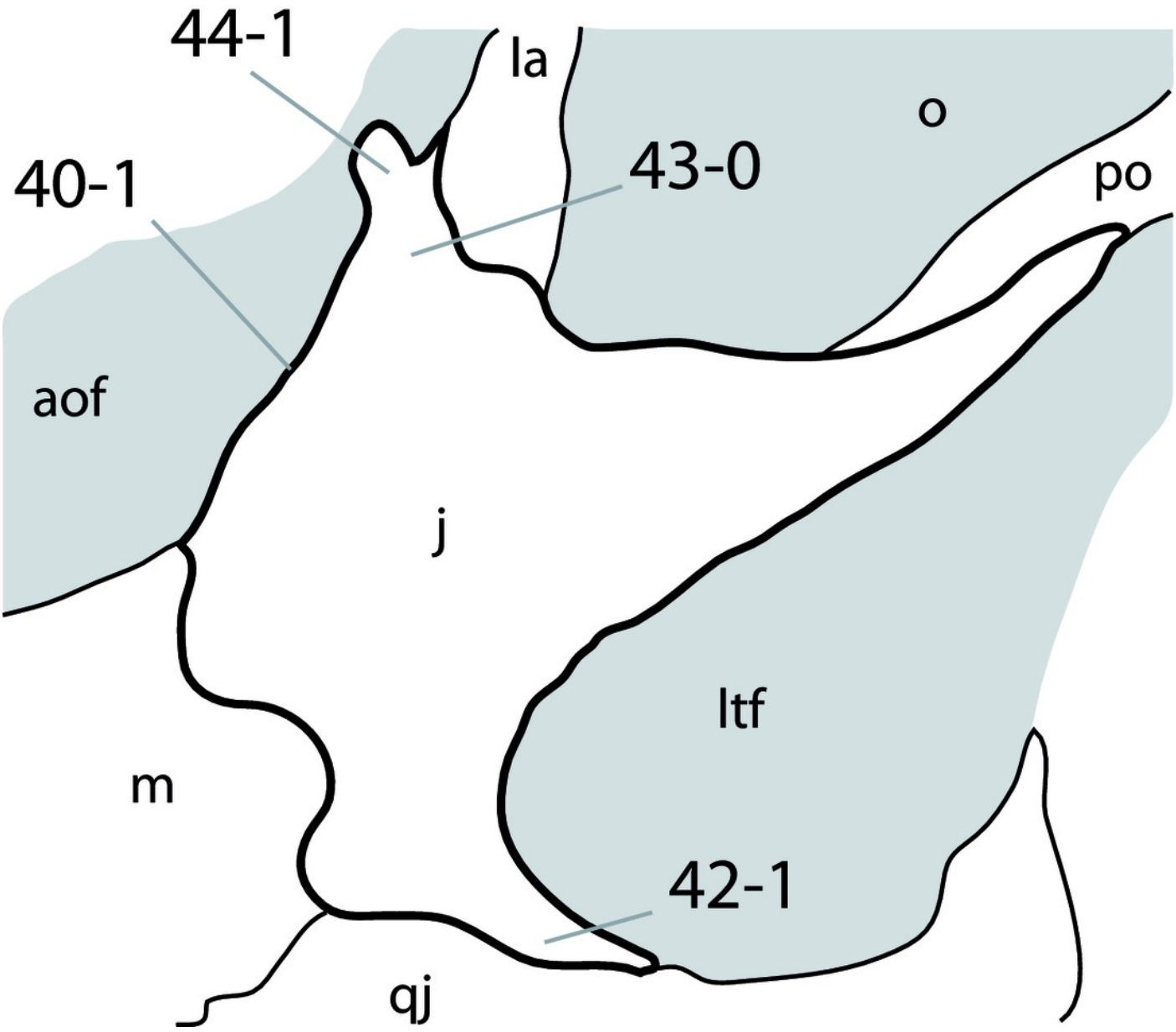


Figure 44

Eusauropod skulls

Figure 44: Skulls of *Shunosaurus lii* ZDM 65430 (A; modified from Chatterjee and Zheng, 2002) and *Diplodocus* sp. CM 11161 (B) in ventral view. Note the anteriorly displaced position of the ectopterygoid ramus of the pterygoid, and the ectopterygoid itself, in *Diplodocus* (B; C41-1 and C102-1), as well as the vomer that articulates with the premaxilla in *Shunosaurus* (A; C103-0), but with the maxilla in *Diplodocus* (B; C103-1). Abb.: aof, antorbital fenestra; bo, basioccipital; bpr, basipterygoid process; bt, basal tuber; ep, ectopterygoid; er, ectopterygoid ramus; j, jugal; m, maxilla; pa, palate; pm, premaxilla; popr, paroccipital process; pt, pterygoid; qj, quadratojugal; v, vomer. Pictures scaled to the same skull length.

PeerJ Reviewing Manuscript

PeerJ Reviewing Manuscript

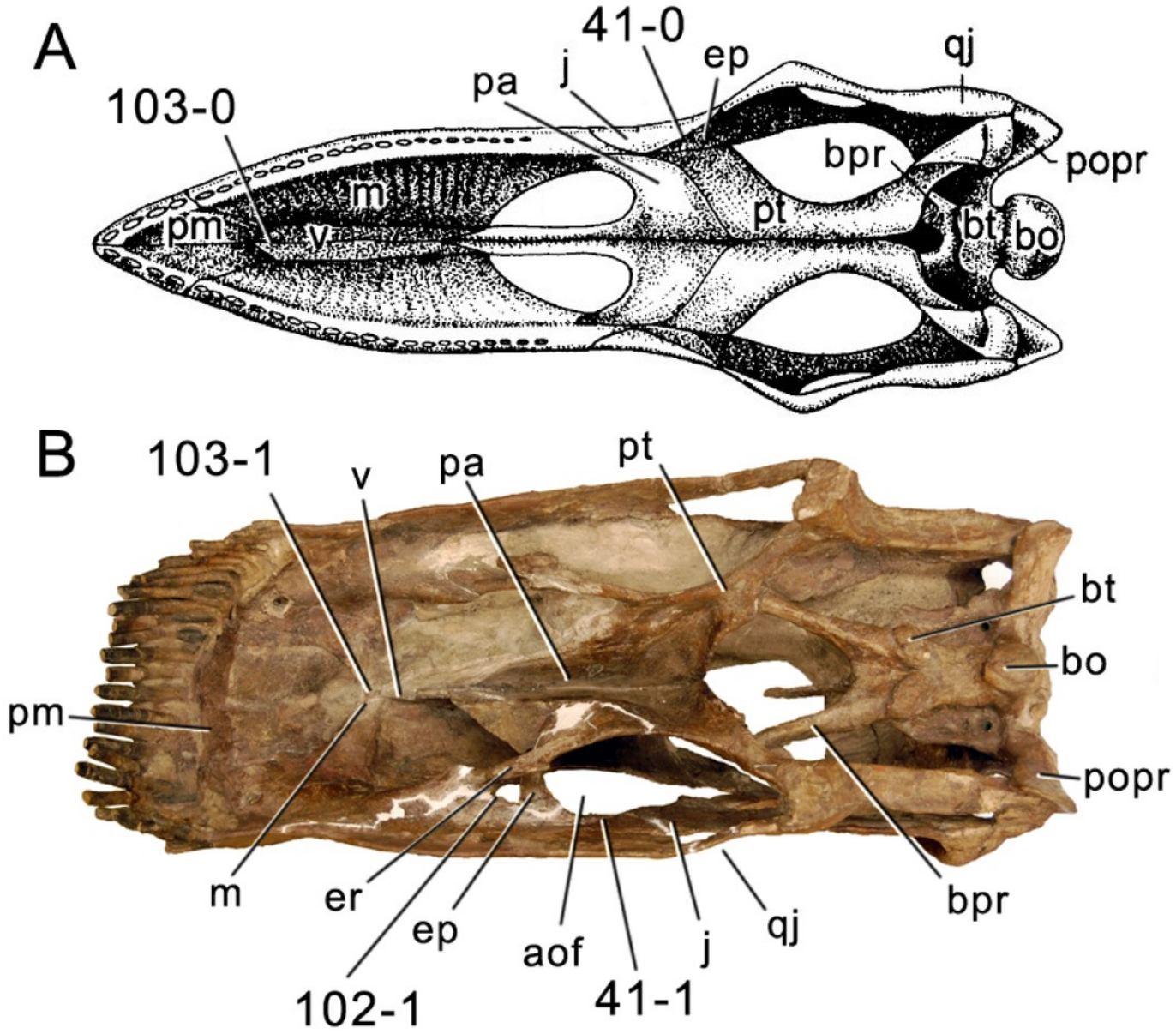
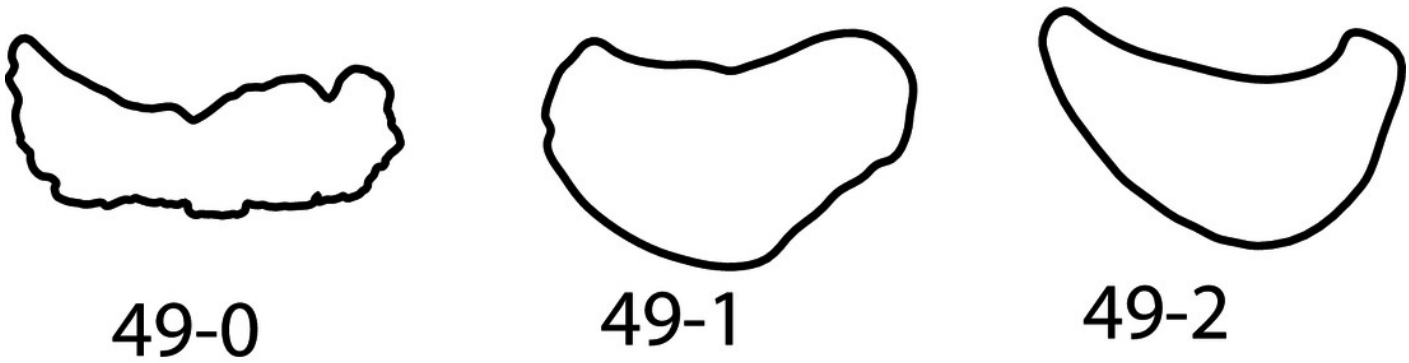


Figure 45

Articular surfaces of neosauropod quadrates

Figure 45: Quadrate articular surface shapes of *Cathetosaurus* sp. SMA 0002 (left, quadrangular, C49-0), *Suuwassea emilieae* ANS 21122 (center, roughly triangular, C49-1), and *Nigersaurus taqueti* MNN GAD512-7 (right, crescent-shaped, C49-2). Figures of *Suuwassea* and *Nigersaurus* traced from Harris (2006a) and Sereno et al. (2007), respectively.

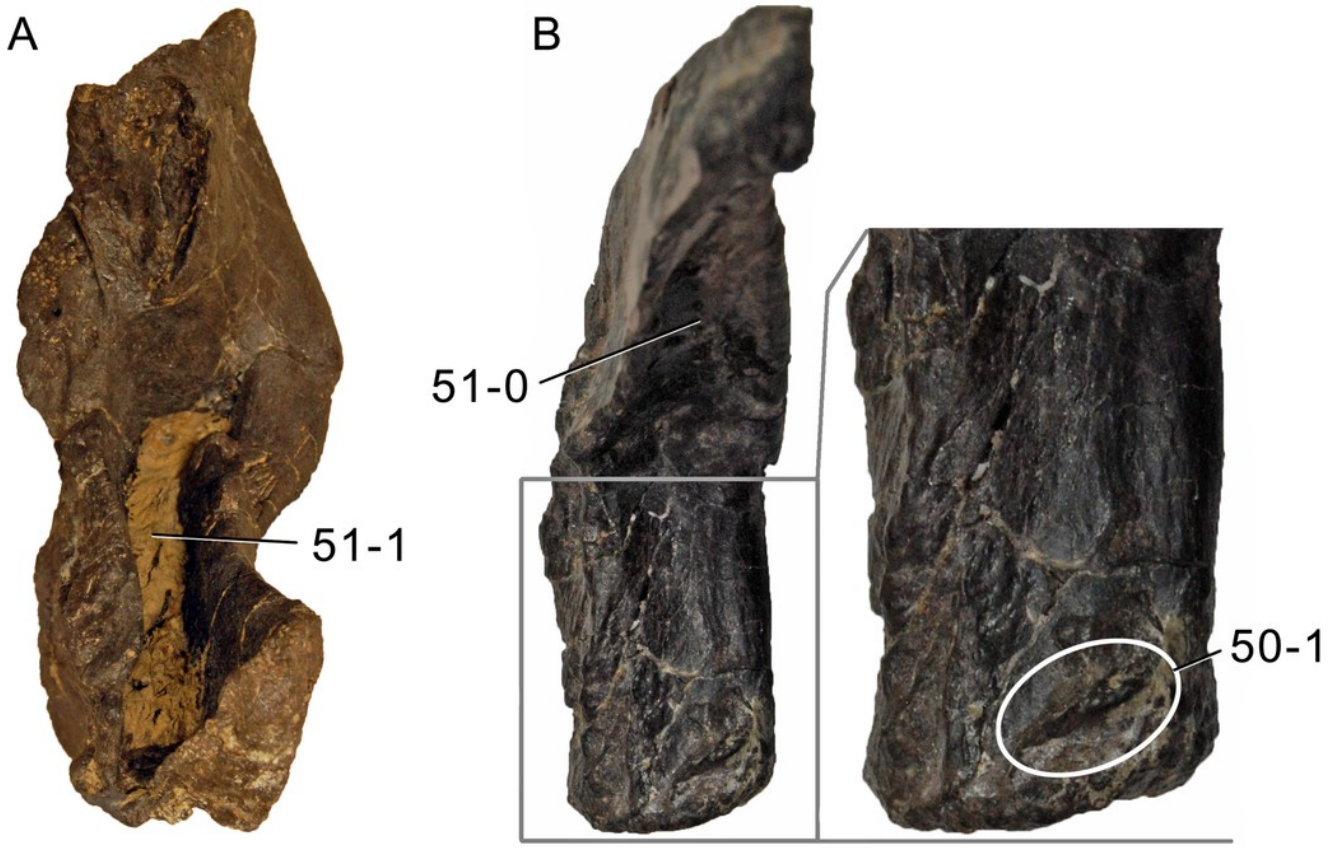


PeerJ Reviewing Manuscript

Figure 46

Neosauropod quadrates

Figure 46: Quadrates of *Cathetosaurus* sp. SMA 0002 (A) and Diplodocidae indet. SMA D27-7 (B) in posterior view, illustrating the transverse ridge (B, inlet; C50-1), and the deep (A; C51-0) versus shallow (B; C51-1) quadrate fossa. Not to scale.



PeerJ Reviewing Manuscript

Figure 47

Neosauropod quadrates

Figure 47: Quadrates of *Cathetosaurus* sp. SMA 0002 (A) and Diplodocidae indet. SMA D27-7 (B) in medial view, illustrating the second medial fossa (B; C52-1), the shape of the dorsal margin (C53, concave versus convex), and the stocky versus slender posterior ramus (C54). Scaled to the same height.

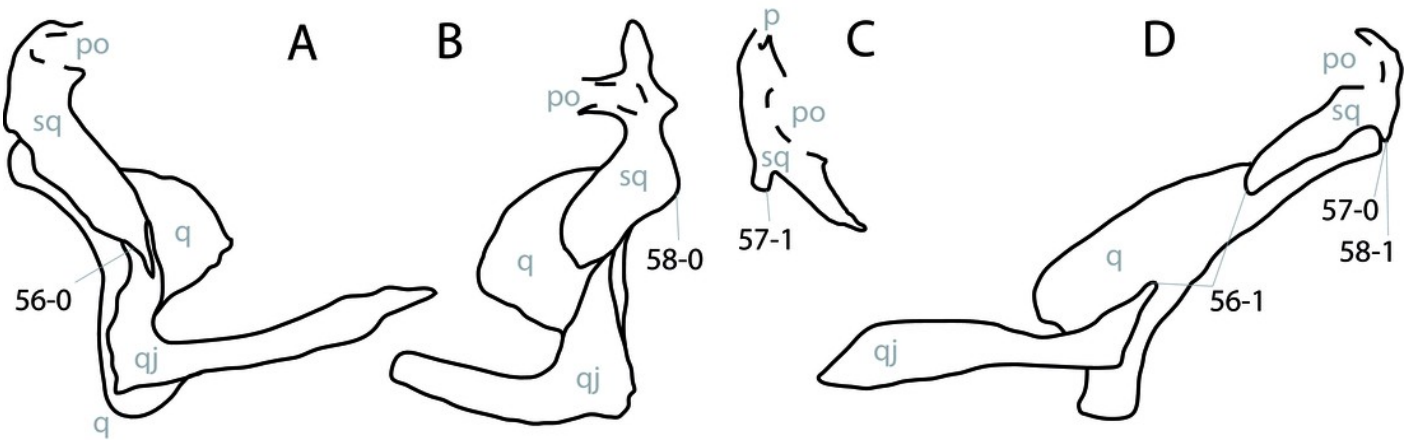


PeerJ Reviewing Manuscript

Figure 48

Temporal region in eusauropod skulls

Figure 48: Squamosal and adjacent bones in *Mamenchisaurus youngi* (A; traced from Ouyang and Ye, 2002), *Camarasaurus lentus* CM 11338 (B; traced from Madsen et al., 1995), *Amargasaurus cazaui* MACN-N15 (C; traced from Salgado and Bonaparte, 1991), and Diplodocinae indet. CM 3452 (D; traced from a 3D model from L. Witmer), in right (A, C) and left (B, D) lateral view; illustrating the states of the characters 56, 57, and 58. Abb.: po, postorbital; q, quadrate; qj, quadratojugal; sq, squamosal. Not to scale.



PeerJ Reviewing Manuscript

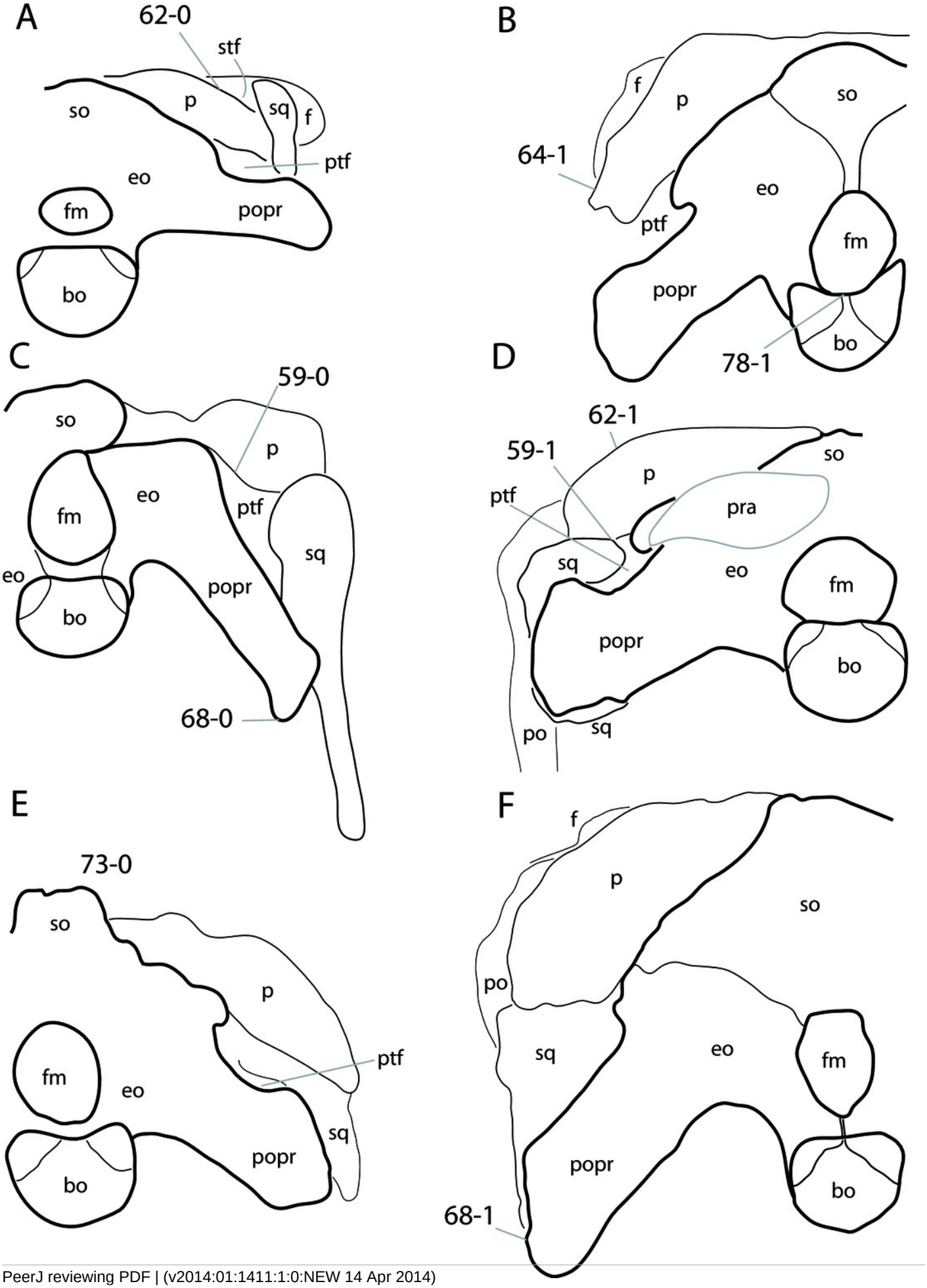
Figure 49

Sauropod skulls in posterior view

Figure 49: Sauropod skulls of *Spinophorosaurus nigerensis* GCP-CV-4229 (A; traced from Knoll et al. 2012); *Suuwassea emilieae* ANS 21122 (B; traced from Harris, 2006a); *Limaysaurus tessonei* MUCPv-205 (C; after Calvo and Salgado, 1995); *Kaatedocus siberi* SMA 0004 (D); *Apatosaurus louisae* CM 11162, (E, reversed); *Diplodocus* sp. CM 11161 (F) in posterior view. Note the participation (C; C59-0) or exclusion (D; C59-1) of the parietal to the posttemporal fenestra; the straight (A; C62-0) or convex (D; C62-1) dorsal edge of the posterolateral process of the parietal; the outwards curve of the distal end of the posterolateral process of the parietal (B; C64-1); the distally expanded (C; C68-0) or straight paroccipital processes (F; C68-1); the dorsally vaulted supraoccipital (E; C73-0); and the narrow contribution of the basioccipital to the dorsal surface of the condyle (B; C78-1). Skulls scaled to the same occipital condyle width.

PeerJ Reviewing Manuscript

PeerJ Reviewing Manuscript



PeerJ Reviewing Manuscript

Figure 50

Parietal of *Kaatedocus siberi* SMA 0004

Figure 50: Transverse ridge of the parietal (arrow, C65-1) of *Kaatedocus siberi* SMA 0004 in posterolateral view. Abb.: anp, antotic process; bo, basioccipital; f, frontal; p, parietal; po, postorbital; popr, paroccipital process; ppfo, postparietal foramen; pra, proatlas; snc, sagittal nuchal crest; so, supraoccipital; stf, supratemporal fenestra.

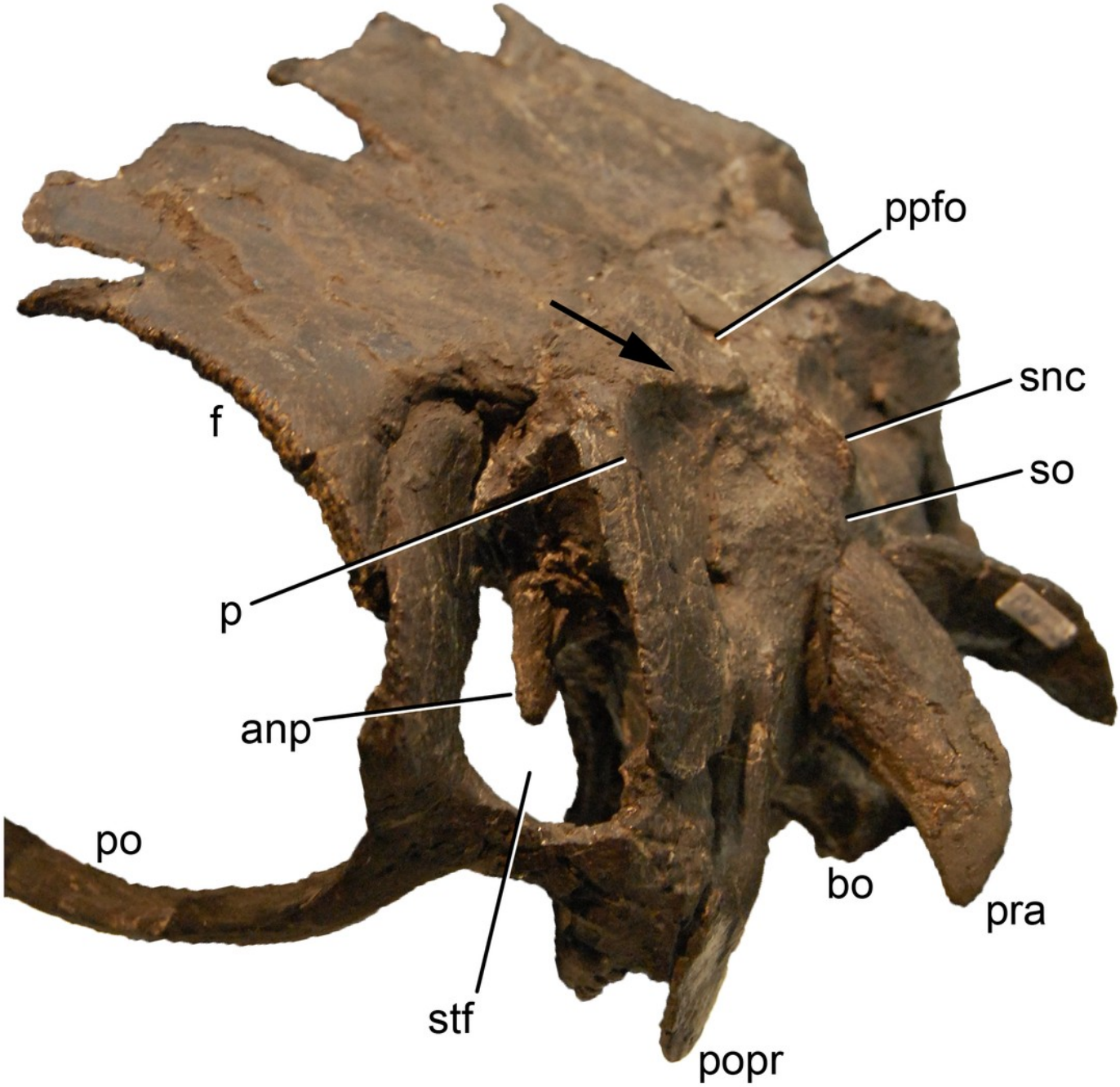


Figure 51

Paroccipital process of *Kaatedocus siberi* SMA 0004

Figure 51: Oblique ridge on paroccipital process (arrow, C67-1) of *Kaatedocus siberi* SMA 0004 in posterior view. Abb.: CV, cervical vertebrae; f, frontal; p, parietal; po, postorbital; popr; paroccipital process; ppfo, postparietal foramen; pra, proatlas; ptf, posttemporal fenestra; q, quadrate; qj, quadratojugal; so, supraoccipital; sq, squamosal; stf, supratemporal fenestra.

PeerJ Reviewing Manuscript

PeerJ Reviewing Manuscript

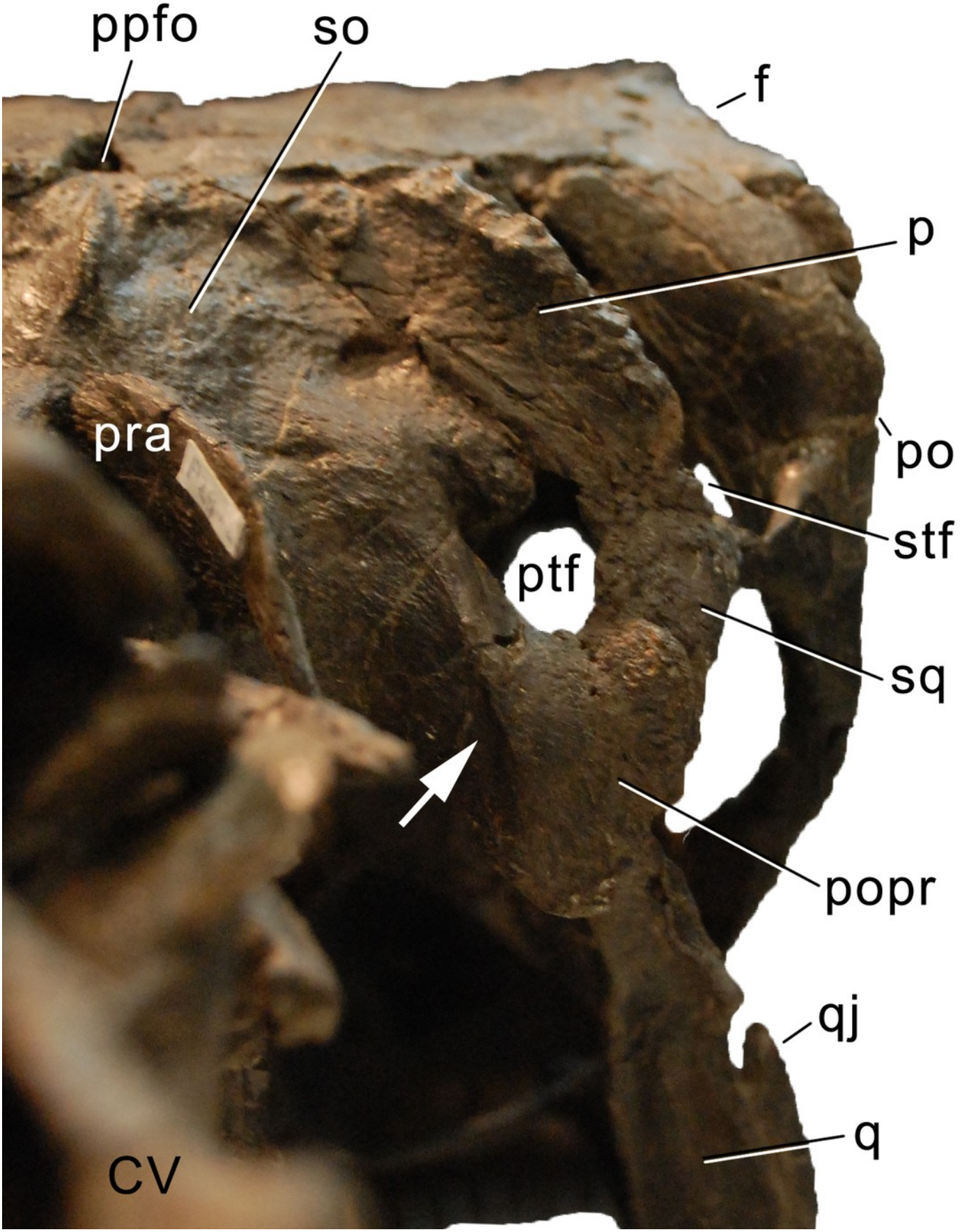
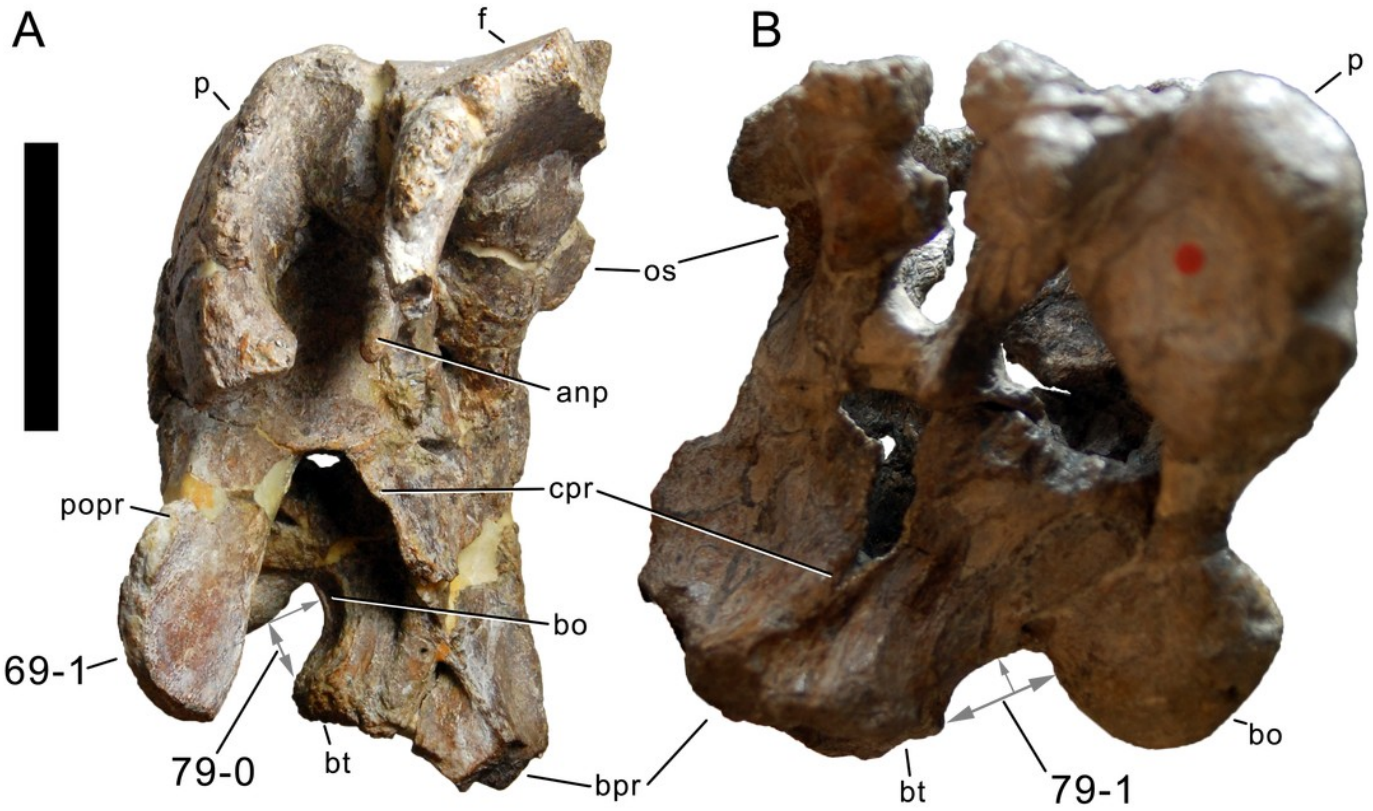


Figure 52

Flagellicaudatan braincases

Figure 52: Braincase of *Suuwassea emilieae* ANS 21122 (A) and *Tornieria africana* MB.R.2386 (B) in right (A) and left (B) lateral view, illustrating the curved lateral end of the paroccipital process (A; C68-1), and the short (A; C79-0) and elongate basioccipital (B; C79-1). Abb.: anp, antotic process; bo, basioccipital; bpr, basipterygoid process; bt, basal tuber; cpr, crista prootica; f, frontal; os, orbitosphenoid; p, parietal; popr, paroccipital process. Scale bar = 5 cm.

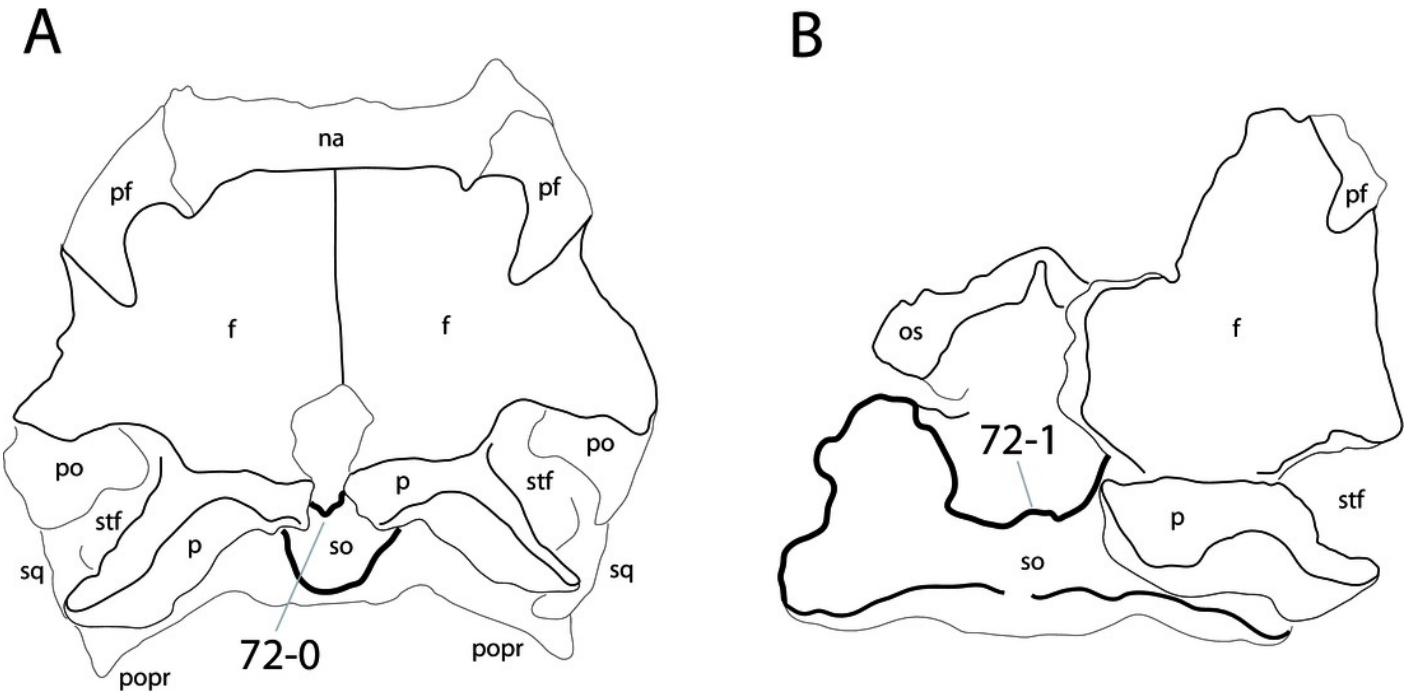


PeerJ Reviewing Manuscript

Figure 53

Diplodocine braincases in dorsal view

Figure 53: Braincase of *Diplodocus* sp. CM 11161 (A) and *Tornieria africana* MB.R.2386 (B) in dorsal view. Note the concave anterior margin of the supraoccipital in *Diplodocus* (A; C72-0), in contrast to the convex edge of *Tornieria* (B; C72-1). The left frontal of MB.R.2386 is lacking. Abb.: f, frontal; na, nasal; os, orbitosphenoid; p, parietal; pf, prefrontal; po, postorbital; popr, paroccipital process; so, supraoccipital; sq, squamosal; stf, supratemporal fenestra. Not to scale.



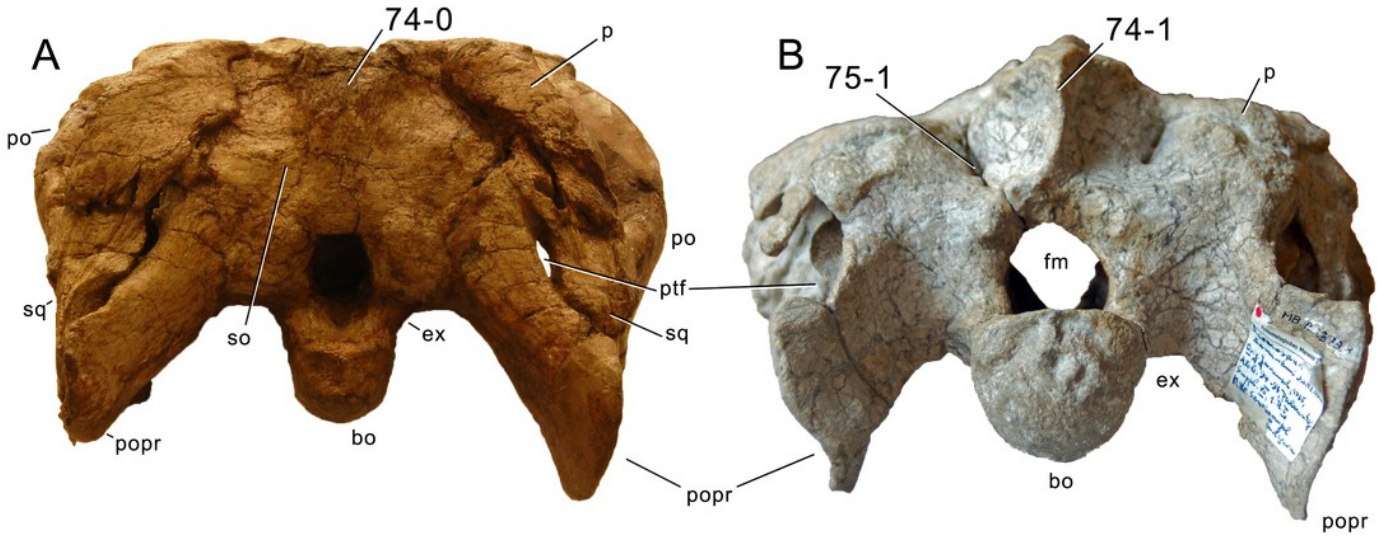
PeerJ Reviewing Manuscript

PeerJ Reviewing Manuscript

Figure 54

Flagellicaudatan skulls in posterior view

Figure 54: Skulls of *Diplodocus* sp. CM 11161 (A) and *Dicraeosaurus hansemanni* MB.R.2379 (B) in posterior view, illustrating the development of the sagittal nuchal crest (C74), and the supraoccipital foramina (C75). Abb.: bo, basioccipital; ex, exoccipital; fm, foramen magnum; p, parietal; po, postorbital; popr, paroccipital process; ptf, posttemporal fenestra; so, supraoccipital; sq, squamosal. Skulls scaled to the same skull width.



PeerJ Reviewing Manuscript

Figure 55

Basal tubera and basisphenoid of *Dicraeosaurus hansemanni* MB.R.2379

Figure 55: Basal tubera and basisphenoid of *Dicraeosaurus hansemanni* MB.R.2379 in posteroventral (A), left lateral (B), and anterodorsal view (C). Note the lateral expansion of the anteroventral end of the crista prootica (C76-1), the narrowly diverging, and elongate basipterygoid processes (C92-2 and C94-2, respectively), the deep slot-like cavity separating the bases of the processes (A, arrowhead; C95-1), and the groove on the dorsal surface of the parasphenoid rostrum (C; C99-1). Abb.: bt, basal tuber; bpr, basipterygoid process; cpr, crista prootica; psr, parasphenoid rostrum. Scale bar = 5 cm.

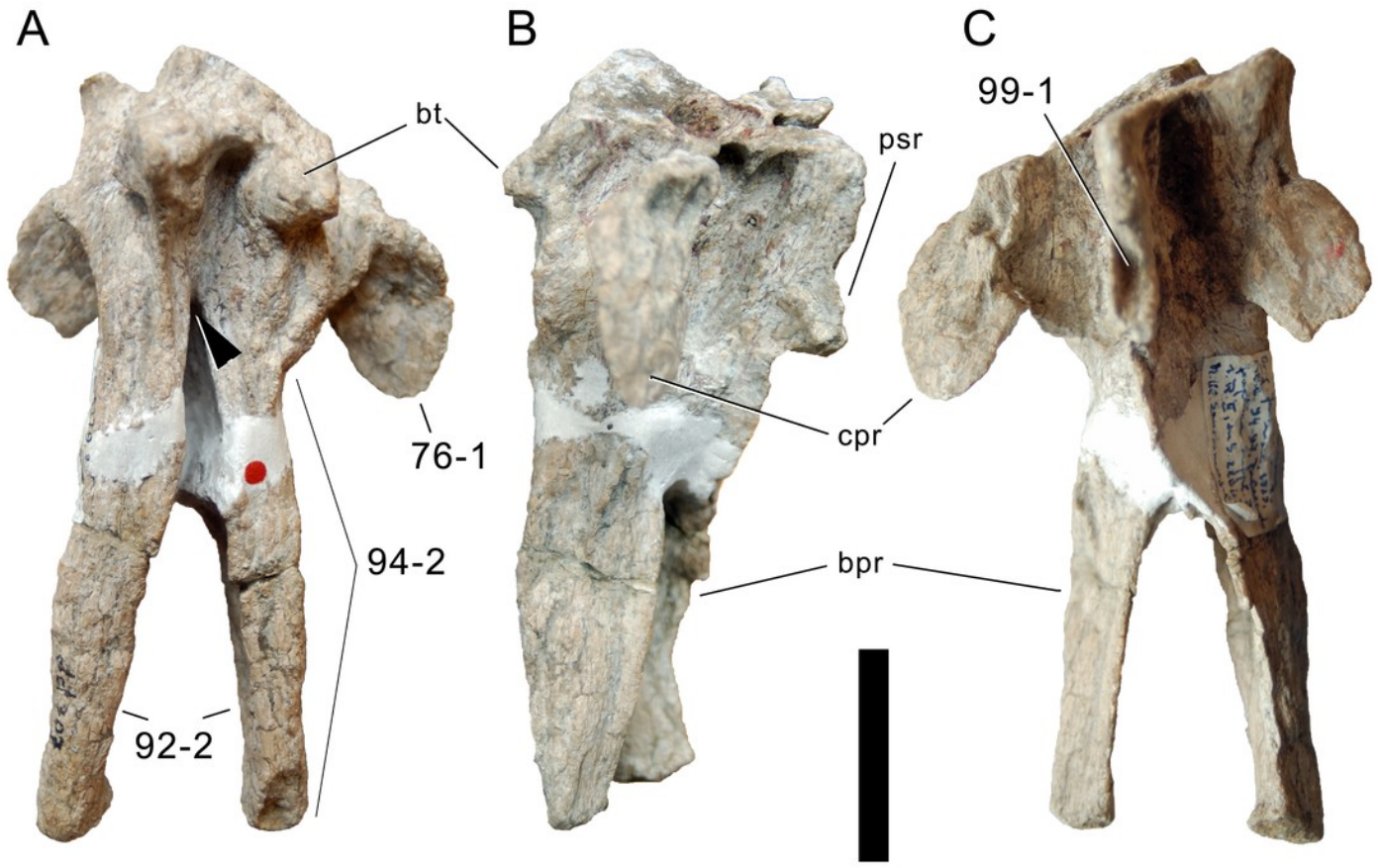
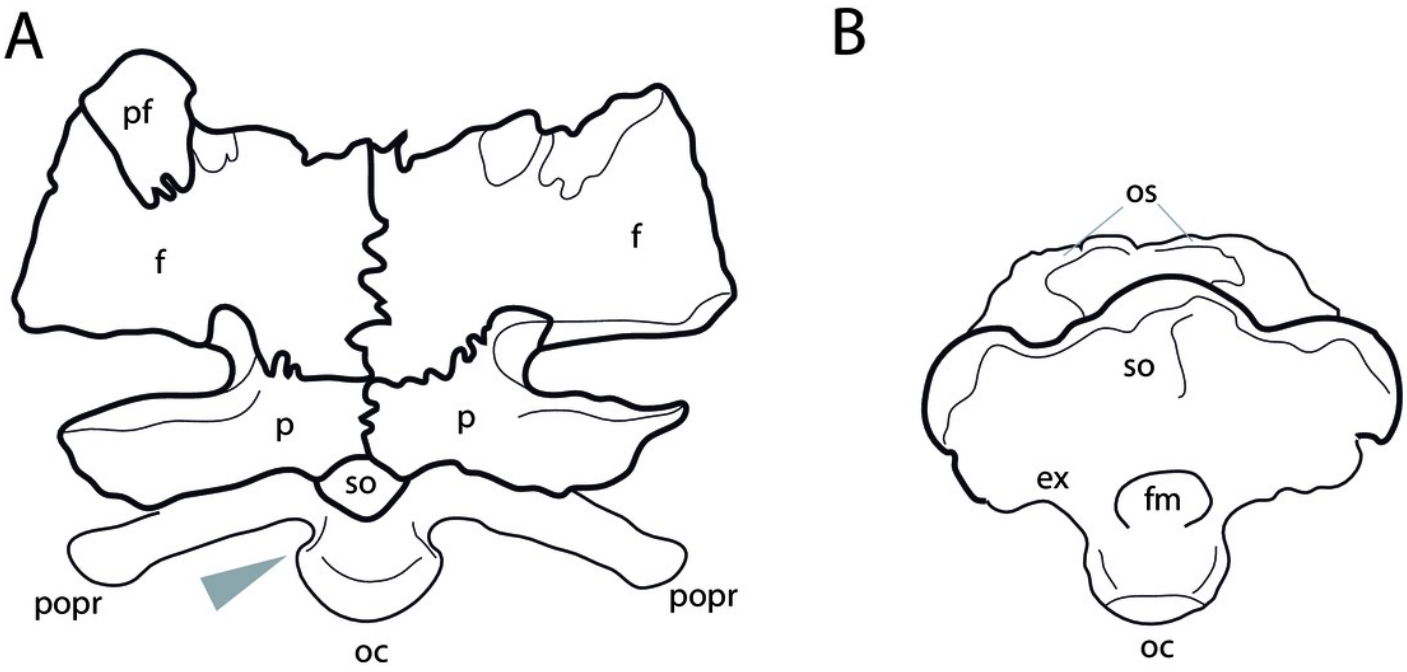


Figure 56

Neosauropod braincases

Figure 56: Braincase of *Camarasaurus* sp. UUVP 4286 (A; modified from Madsen et al., 1995) and *Tornieria africana* MB.R.2386 (B) in a view perpendicular to the dorsal surface of the occipital condyle, illustrating the distinctly offset articular surface (arrow in A; C77-0), in contrast to the derived condition of diplodocoids (B; C77-1). Abb.: ex, exoccipital; f, frontal; fm, foramen magnum; oc, occipital condyle; os, orbitosphenoid; p, parietal; pf, prefrontal; popr, paroccipital process. Skulls scaled to same breadth of occipital condyle.



PeerJ Reviewing Manuscript

PeerJ Reviewing Manuscript

Figure 57

Braincase of *Losillasaurus giganteus* MCNV Lo-26

Figure 57: Braincase of *Losillasaurus giganteus* MCNV Lo-26 in posterolateral (A) and posterior (B) view. Note the lateral basioccipital depression between the foramen magnum and the basal tubera (A; C80-1); the laterally curving distal ends of the basipterygoid processes (B; C97-1), as well as their distinct transverse expansion (B; 98-1). Abb.: bo, basioccipital; bpr, basipterygoid process; bt, basal tuber; ex, exoccipital; fm, foramen magnum; popr, paroccipital process; psr, parasphenoid rostrum; so, supraoccipital. Scale bar = 10 cm.

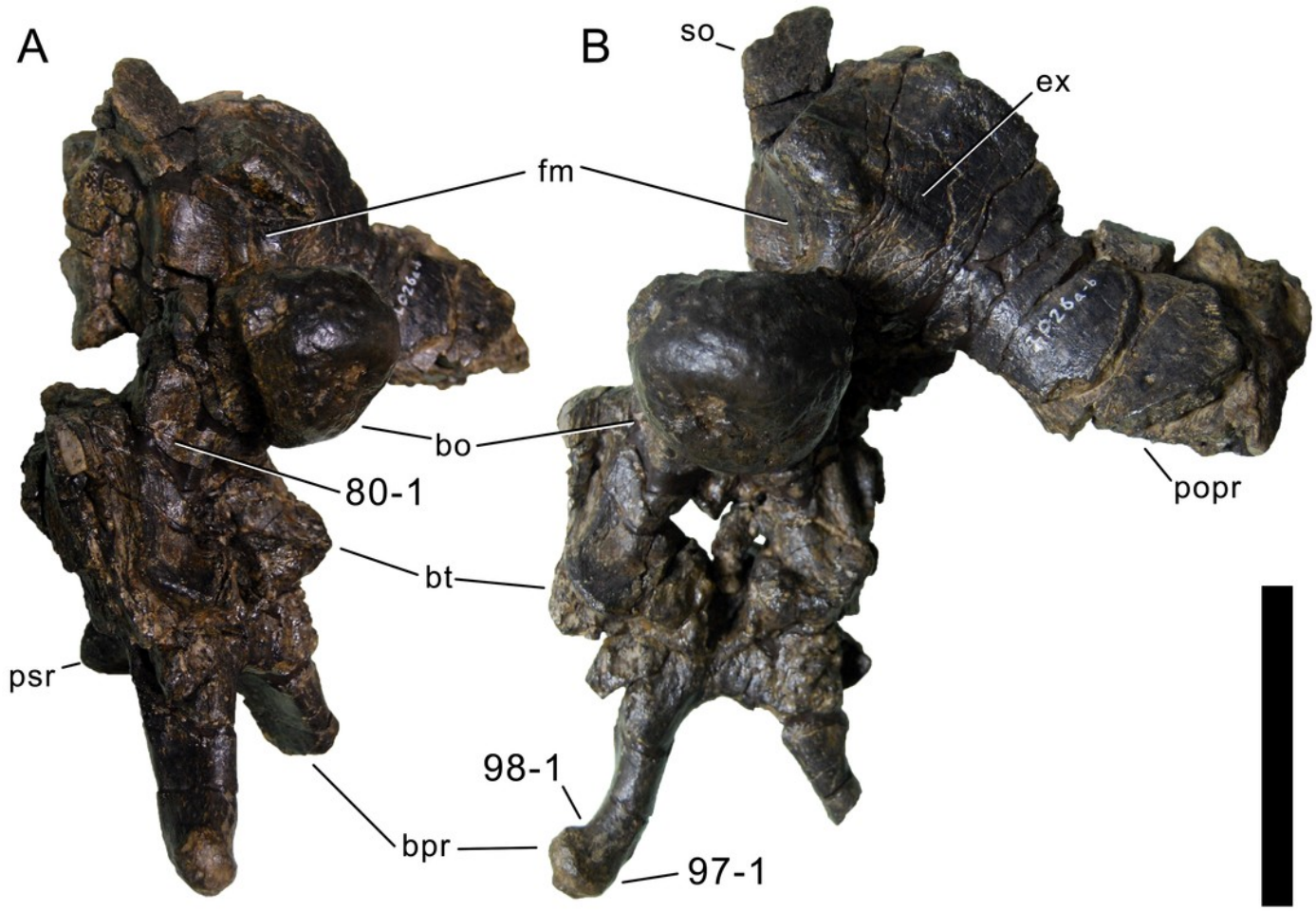


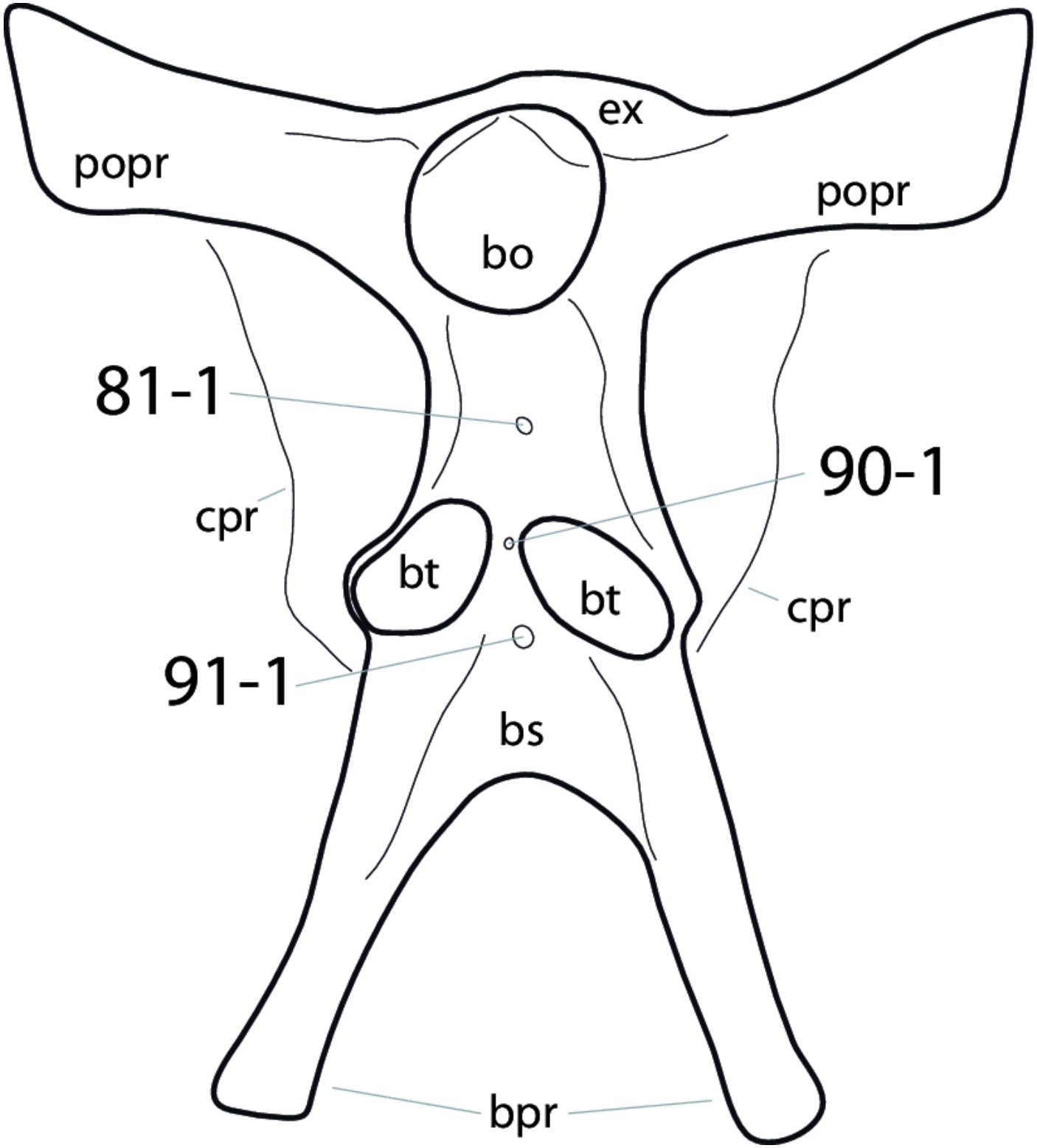
Figure 58

Hypothetical diplodocid basioccipital-basisphenoid complex

Figure 58: Hypothetical diplodocid basioccipital-basisphenoid complex in posteroventral view, showing the locations of pits sometimes present in diplodocid specimens: between occipital condyle and basal tubera (C81-1), in the notch between basal tubera (C90-1), and on the basisphenoid, between the bases of the basipterygoid processes (termed 'basipterygoid recess' by Wilson, 2002; C91-1). Abb.: bo, basioccipital; bpr, basipterygoid process; bs, basisphenoid; bt, basal tuber; cpr, crista prootica; ex, exoccipital; popr, paroccipital process.

PeerJ Reviewing Manuscript

PeerJ Reviewing Manuscript

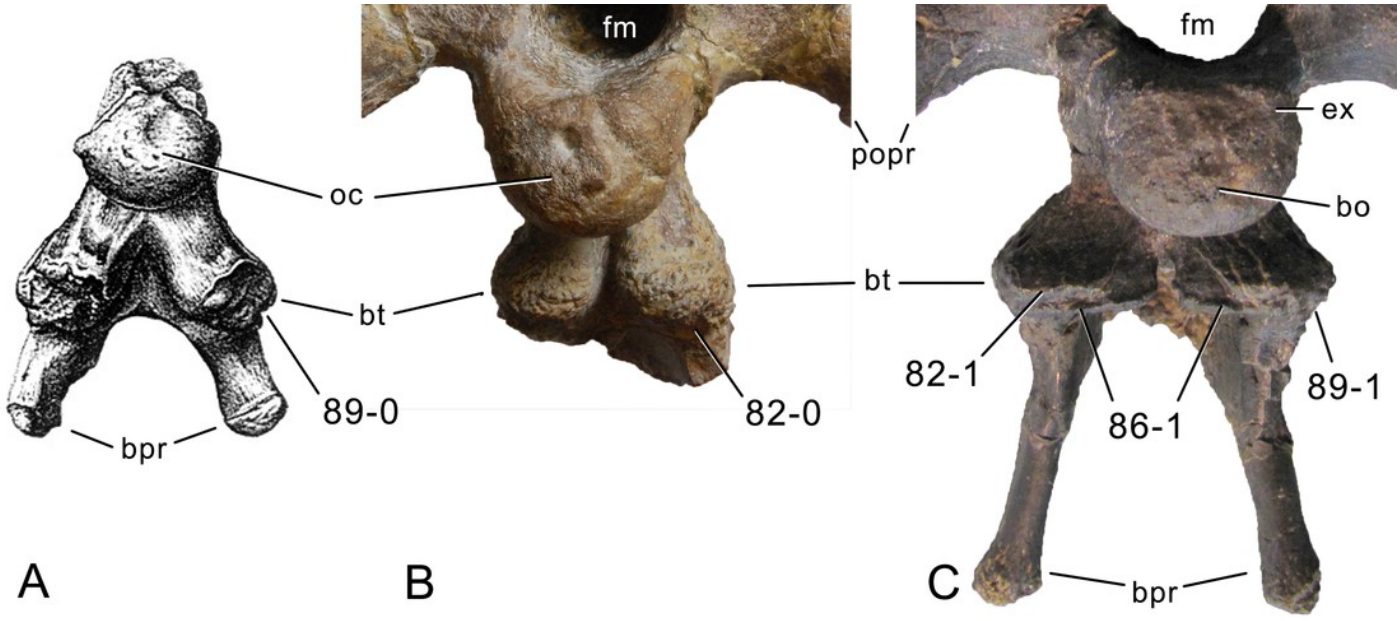


PeerJ Reviewing Manuscript

Figure 59

Neosauropod basal tubera

Figure 59: Basal tubera of *Camarasaurus grandis* YPM 1905 (A; modified from Madsen et al., 1995), *Suuwassea emilieae* ANS 21122 (B), and *Kaatedocus siberi* SMA 0004 (C; photo by J. Marinheiro) in posterior view. Note the globose (B; C82-0) compared to the box-like shape (C; C82-1) of the tubera, the transverse ridge on their posterior face (C; C86-1), and the ventrolateral (A; C89-0) in contrast to ventral orientation (C; C89-1). Abb.: bo, basioccipital; bpr, basipterygoid process; bs, basisphenoid; bt, basal tuber; ex, exoccipital; fm, foramen magnum; oc, occipital condyle; popr, paroccipital process. Pictures scaled to same distance between dorsal face of occipital condyle and basal tubera.

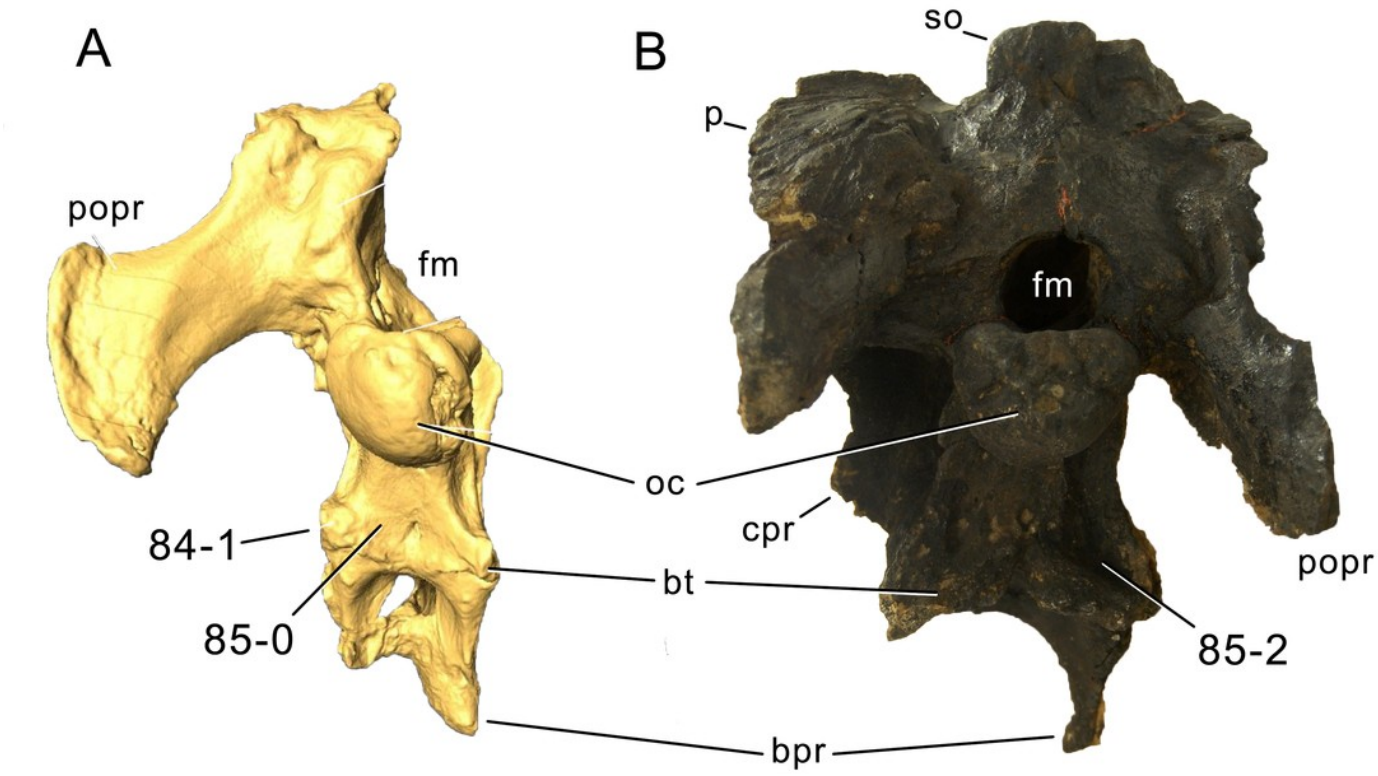


PeerJ Reviewing Manuscript

Figure 60

Diplodocimorph skulls in occipital view

Figure 60: Skulls of *Nigersaurus taqueti* (A; modified from Schmitt, 2012) and *Diplodocus* sp. USNM 2673 (B) in occipital view. Note the reduced basal tubera in *Nigersaurus* (A; C84-1), and the convex (A; C 85-0), or concave (B; C85-2) posterior face of the tubera. Abb.: bpr, basipterygoid process; bt, basal tuber; cpr, crista prootica; fm, foramen magnum; oc, occipital condyle; popr, paroccipital process; so, supraoccipital. Skulls scaled to same occipital condyle height.



PeerJ Reviewing Manuscript

Figure 61

Diplodocid basioccipital-basispenoid complex

Figure 61: Basioccipital-basispenoid complex of *Apatosaurus louisae* CM 11162 (A), *Kaatedocus siberi* SMA 0004 (B; traced from a photo by J. Marinheiro), and *Diplodocus* sp. CM 11161 (C) in posteroventral view. Note the differing orientations of the longest axes of the basal tubera (B; C87-0; in contrast to C; C87-1), as well as the concave (A; C88-1) versus the straight to slightly convex anterior edge of the tubera (B; C88-0). Abb.: bo, basioccipital; bpr, basipterygoid process; bs, basisphenoid; bt, basal tuber; ex, exoccipital. Drawings not to scale.

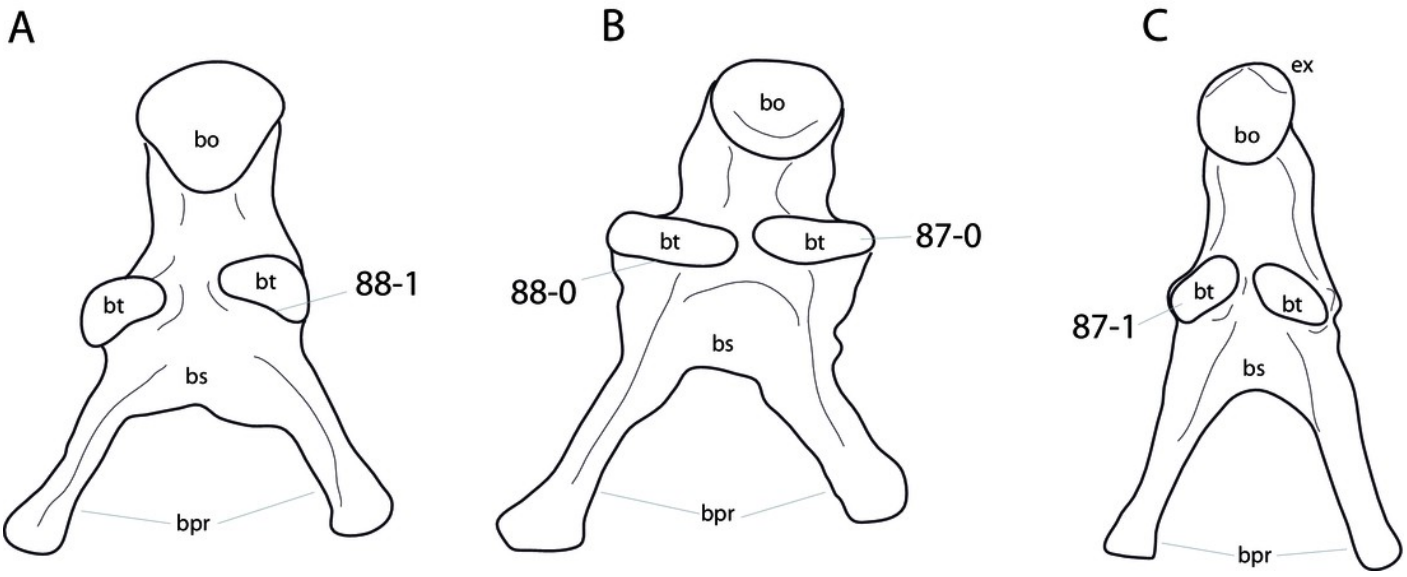
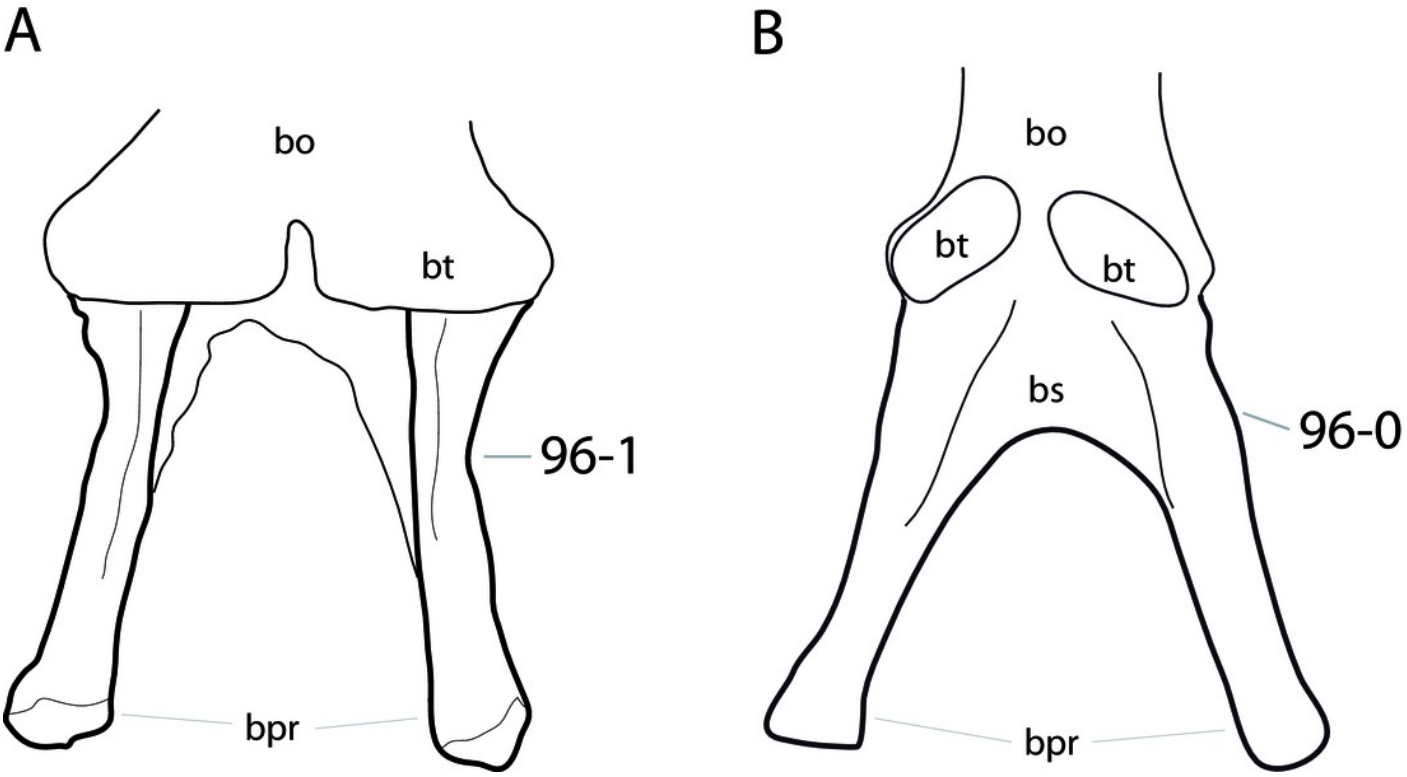


Figure 62

Diplodocine basisphenoids

Figure 62: Basisphenoid of *Kaatedocus siberi* SMA 0004 (A; traced from a photo by J. Marinheiro), and *Diplodocus* sp. CM 11161 (B) in posteroventral view. Note the parallel proximal portion of the basipterygoid processes and the accompanying outwards curve in *Kaatedocus* (A; C96-1), in contrast to the straight processes of CM 11161 (B; C96-0). Abb.: bo, basioccipital; bpr, basipterygoid process; bs, basisphenoid; bt, basal tuber. Scaled to the same process length.



PeerJ Reviewing Manuscript

PeerJ Reviewing Manuscript

Figure 63

Flagellicaudatan braincases

Figure 63: Braincases of *Suuwassea emilieae* ANS 21122 (A), and *Tornieria africana* MB.R.2386 (B; traced from Janensch, 1935) in anterior view. Note the unpaired optic foramen of *Suuwassea* (A; C100-1), in contrast to the paired foramen in *Tornieria* (B; C100-0). Abb.: anp, antotic process; bs, basisphenoid; can, crista antotica; cpr, crista prootica; ls, laterosphenoid; olf, olfactory foramen; opf, optic foramen; os, orbitosphenoid; popr, paroccipital process; pro, prootic. Scaled to the same width of the orbitosphenoids.

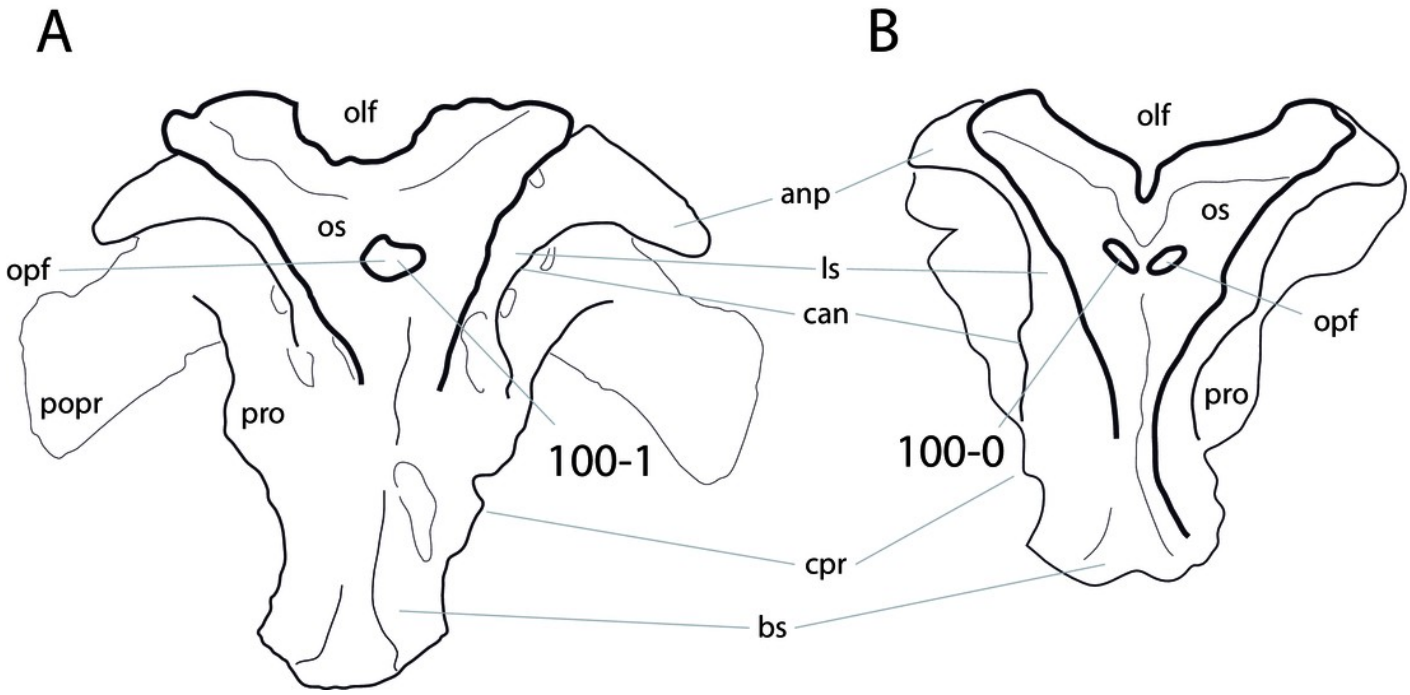
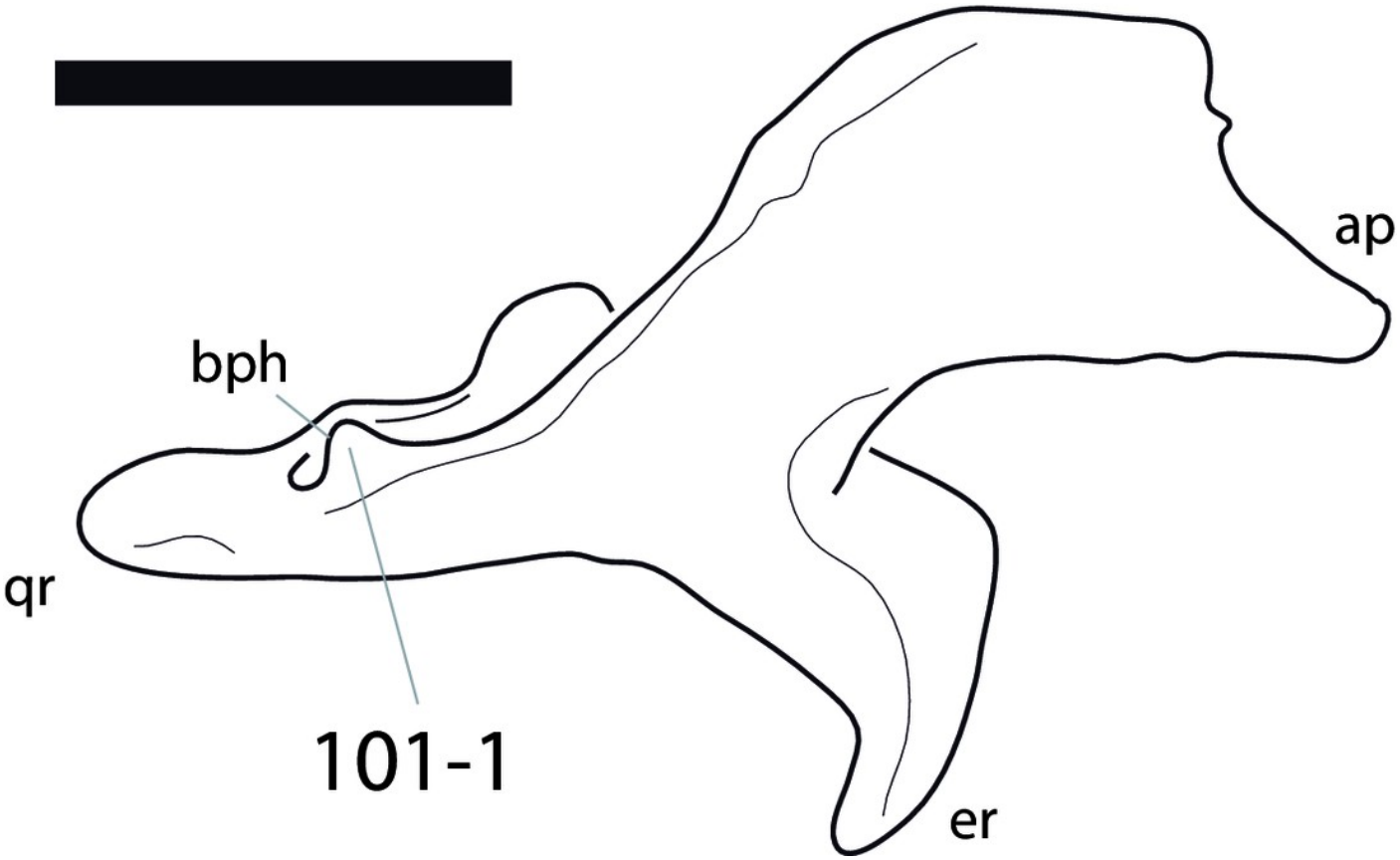


Figure 64

Pterygoid of *Camarasaurus lentus* DNM 28

Figure 64: Left pterygoid of *Camarasaurus lentus* DNM 28 in medial view. Note the presence of a hook-like process at the articulation surface for the basipterygoid process (C101-1). Diplodocidae, on the other hand, only have shallow articular facets without hooks. Abb.: ap, anterior process; bph, basipterygoid hook; er, ectopterygoid ramus; qr, quadrate ramus. Picture traced from Madsen et al. (1995). Scale bar = 10 cm.



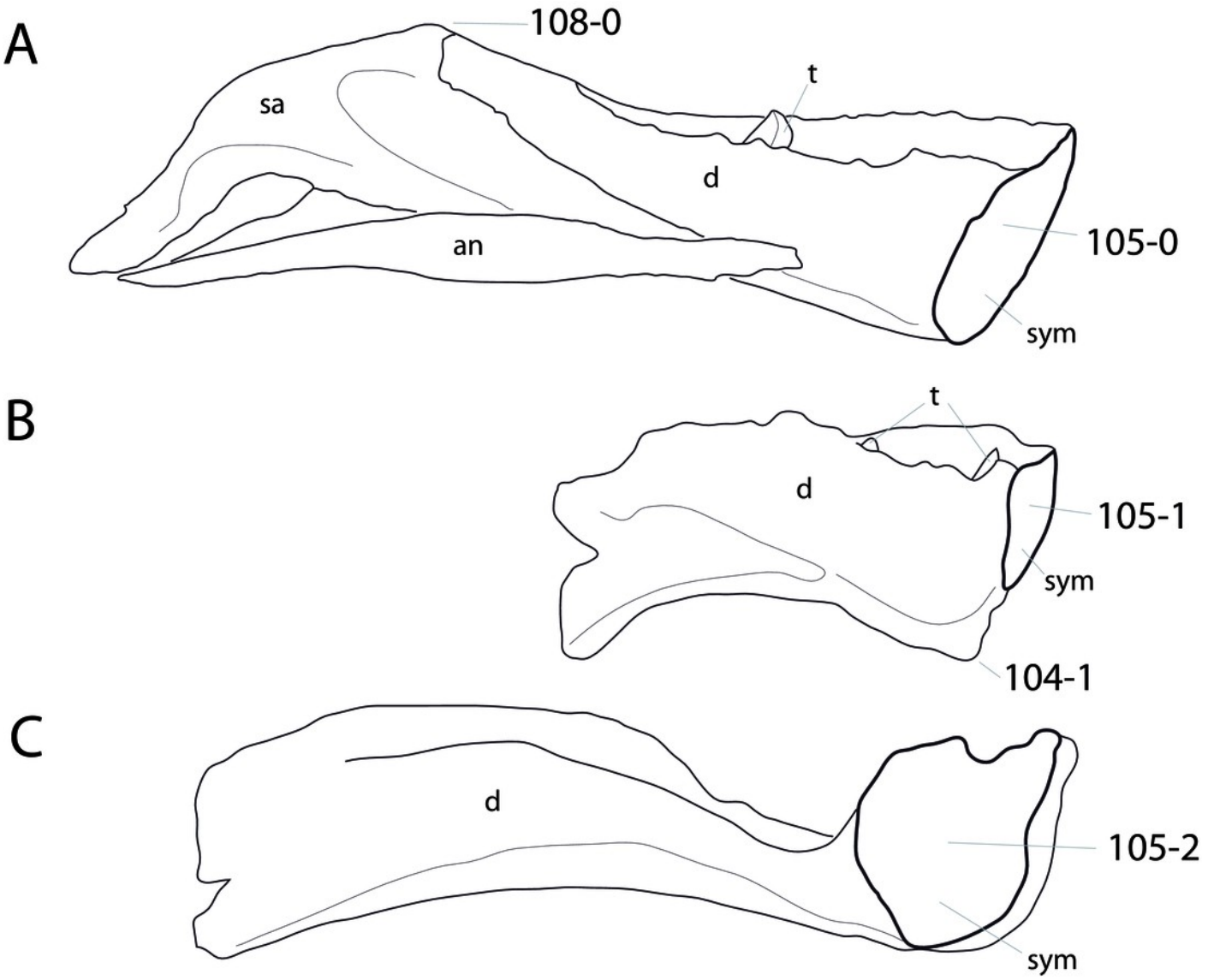
PeerJ Reviewing Manuscript

PeerJ Reviewing Manuscript

Figure 65

Neosauropod dentaries

Figure 65: Left dentary of *Camarasaurus lentus* DNM 28 (A; traced from Madsen et al., 1995), *Dicraeosaurus hansemanni* MB.R.2372 (B; traced from Janensch, 1935), and *Nigersaurus taqueti* MNN GAD512-10 (C; traced from Sereno et al., 2007) in lingual view. Note the chin-like ventral process in *Dicraeosaurus* (B; C104-1), the different shapes of the symphysis (C105-1 to 3), and the high elevation of the coronoid eminence in *Camarasaurus* (A; C108-0). Abb.: an, angular; d, dentary; sa, surangular; sym, symphysis; t, tooth. Scaled to the same anteromedial height of the dentary.



PeerJ Reviewing Manuscript

Figure 66

Diplodocimorph dentaries

Figure 66: Left dentary of *Dicraeosaurus hansemanni* MB.R.2372 (A), and *Nigersaurus taqueti* MNN GAD512-10 (B; traced from Sereno et al., 2007) in dorsal view. Note the labial tubercle in *Dicraeosaurus* (A; C106-1), the dentigerous portion that expands laterally in *Nigersaurus* (B; C107-1), and the anterolaterally displaced tooth row, compared to the usual curvature in both taxa (C112-1). Abb.: sym, symphysis; t, tooth. Scaled to the same anteroposterior length.

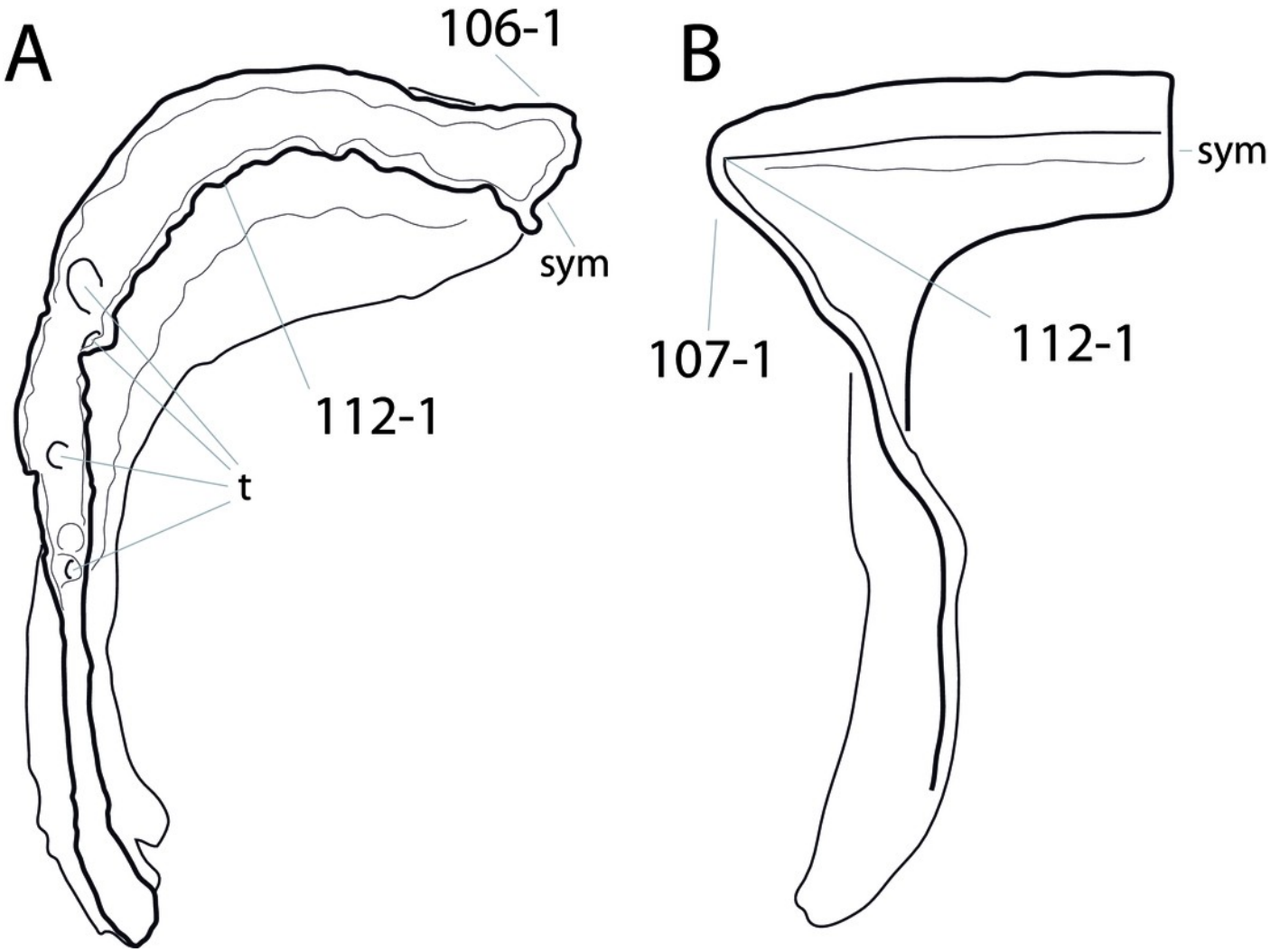


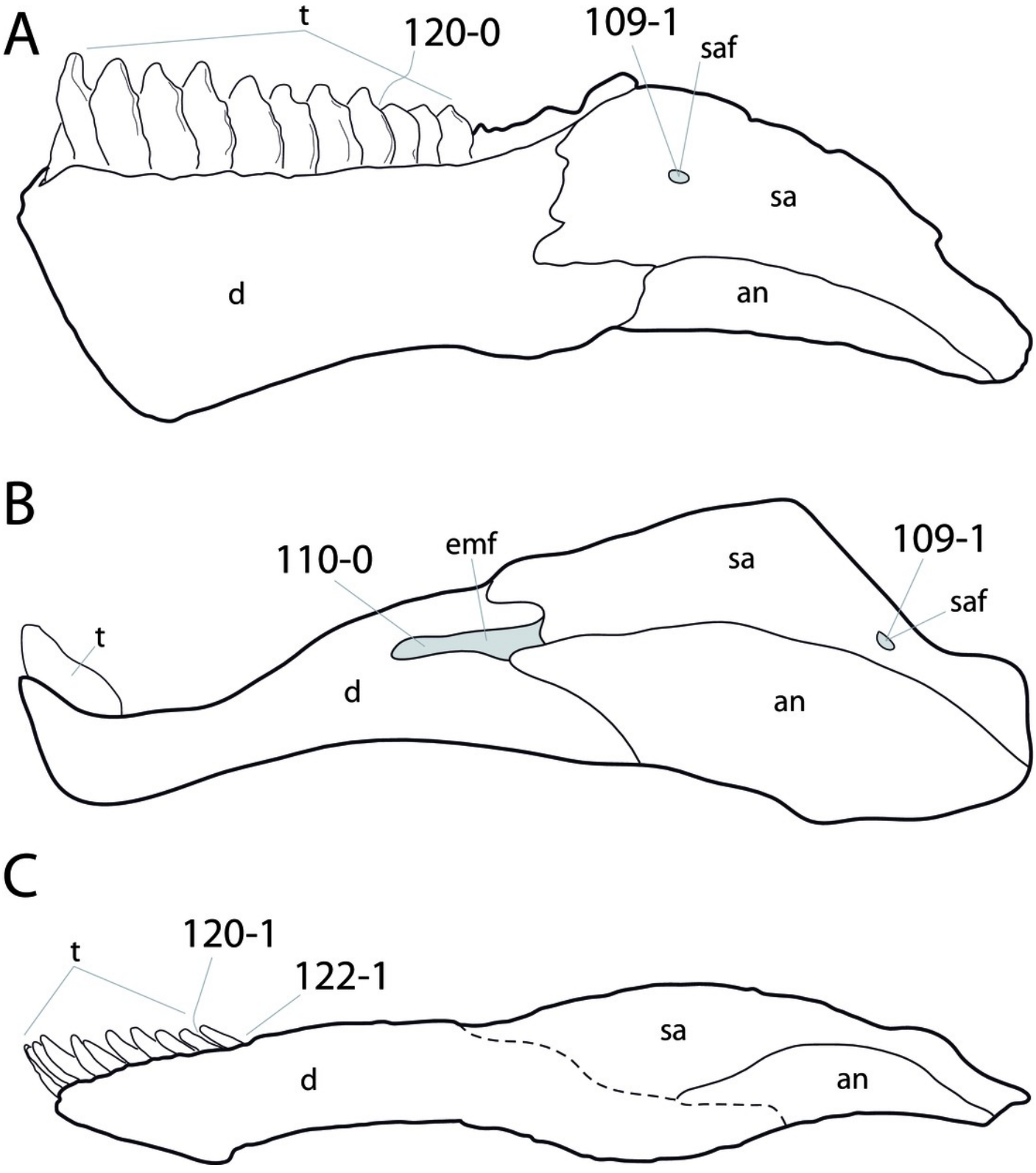
Figure 67

Neosauropod lower jaw

Figure 67: Left lower jaw of *Camarasaurus lentus* CM 11338 (A; modified from Madsen et al., 1995), *Nigersaurus taqueti* MNN GAD-512 (B; traced from Sereno et al., 2007), and *Galeamopus* [redacted] SMA 0011 (C) in lateral view. Note the surangular foramen in A and B (C109-1), the external mandibular fenestra in *Nigersaurus* (B; C110-0), the strongly overlapping teeth of *Camarasaurus* (A; C120-0) in contrast to the more widely spaced teeth of diplodocids (C; C120-1), and the anterior inclination of the the diplodocid teeth in respect to the jaw axis (C; C122-1). Abb.: an, angular; d, dentary; emf, external mandibular fenestra; sa, surangular; saf, surangular foramen; t, tooth. Scaled to the same mandibular length.

PeerJ Reviewing Manuscript

PeerJ Reviewing Manuscript



PeerJ Reviewing Manuscript

Figure 68

Eusauropod teeth

Figure 68: Tooth of *Omeisaurus tianfuensis* ZDM T5705 (A; traced from He et al., 1988), *Cathetosaurus* sp. SMA 0002 (B), and Diplodocinae indet. CM 3452 (C) in lingual view. Note the V-shaped wear facets in *Cathetosaurus* (B; C117-0), in contrast to the single, planar facet in diplodocids (C; C117-1), the longitudinal grooves in *Omeisaurus* and *Cathetosaurus* (A, B; C123-1), and the marginal tooth denticles in *Omeisaurus* (A; C125-0). Abb.: ato, anterior tooth; dt, denticles; pto, posterior tooth; tc, tooth crown; tr, tooth root; wf, wear facet. Teeth scaled to the same crown length.

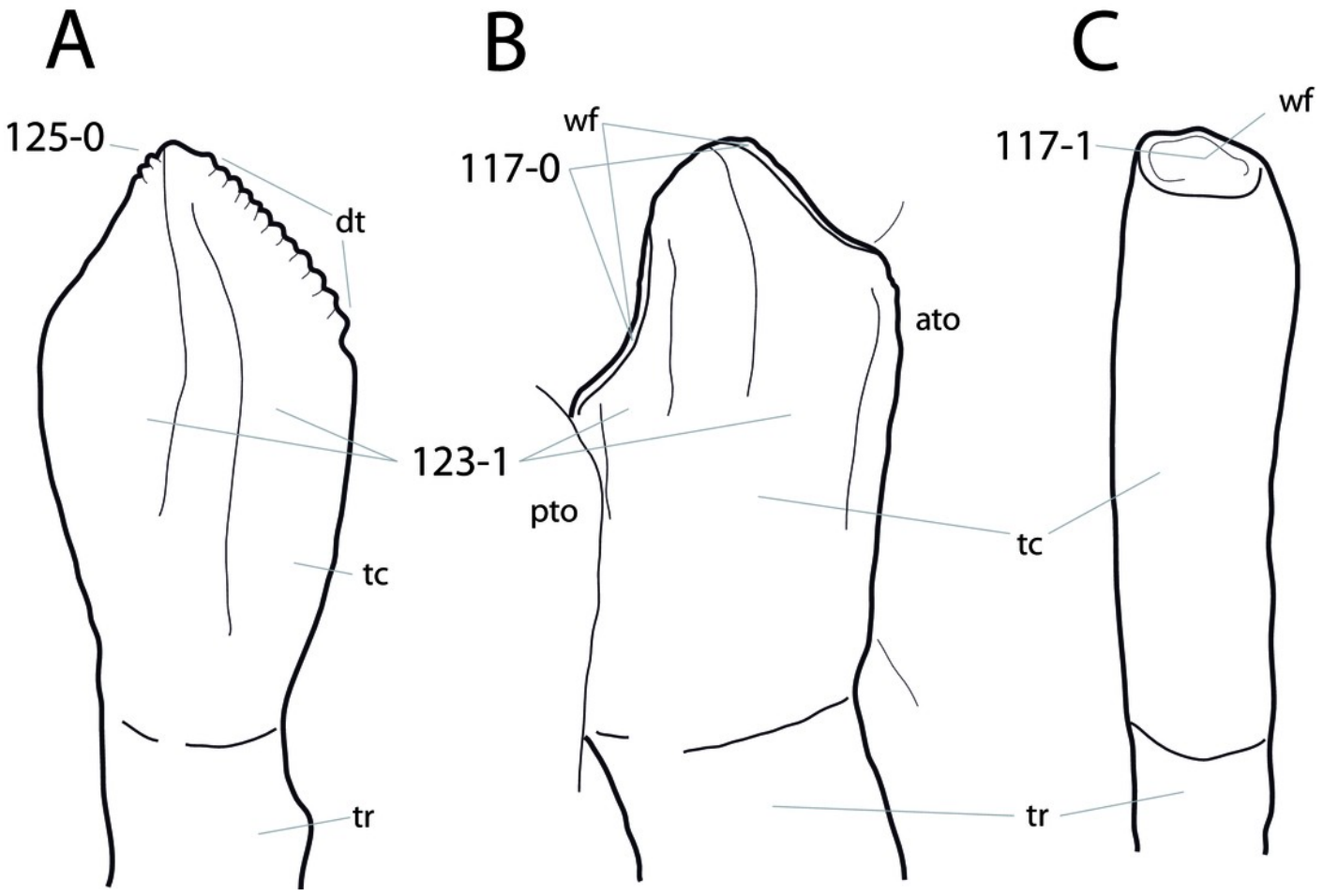


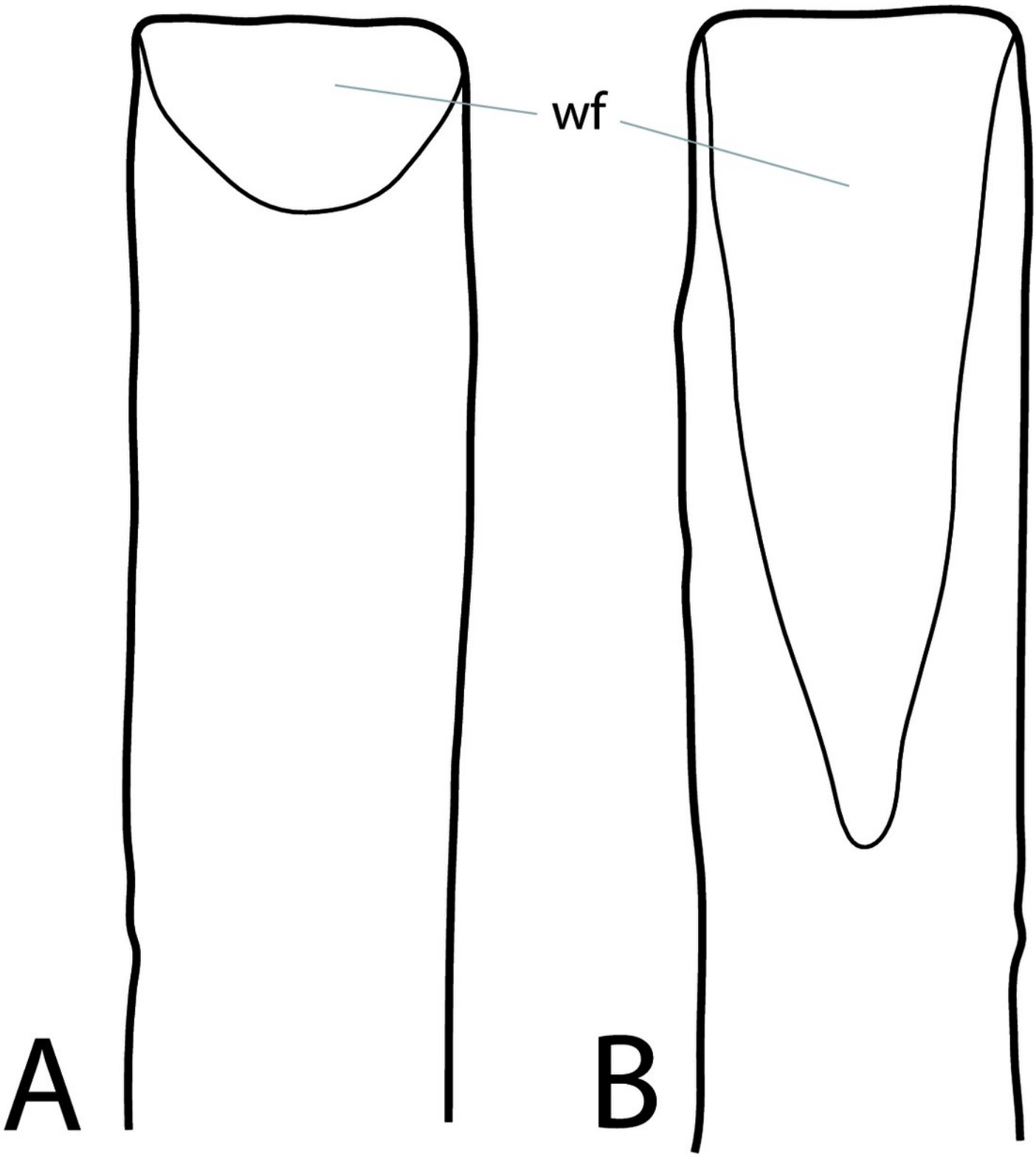
Figure 69

Tooth of Nigersaurus

Figure 69: Tooth of *Nigersaurus* in labial (A) and lingual (B) view, showing the paired, planar wear facets typical for Rebbachisauridae (C117-1; C118-0). Abb.: wf, wear facet. Figure traced from Whitlock (2011b).

PeerJ Reviewing Manuscript

PeerJ Reviewing Manuscript



PeerJ Reviewing Manuscript

Figure 70

Neosauropod tooth cross-sections

Figure 70: Tooth cross-section of *Camarasaurus* sp. AMNH 5764 (A), and *Demandasaurus darwini* MDS-RVII,438 (B; traced from Torcida Fernández-Baldor et al., 2011). Note the D-shaped crown of *Camarasaurus* (A; C121-0) in contrast with the rounded cross-section of diplodocoids (B; C121-0), and the asymmetric disposition of the enamel typical for rebbachisaurids (B; C124-1). The camarasaur tooth has the same specimen number as the *Amphicoelias altus* holotype, but does not belong to the same individual (see text). Abb.: de, dentin; en, enamel. Scaled to the same mesiodistal width.

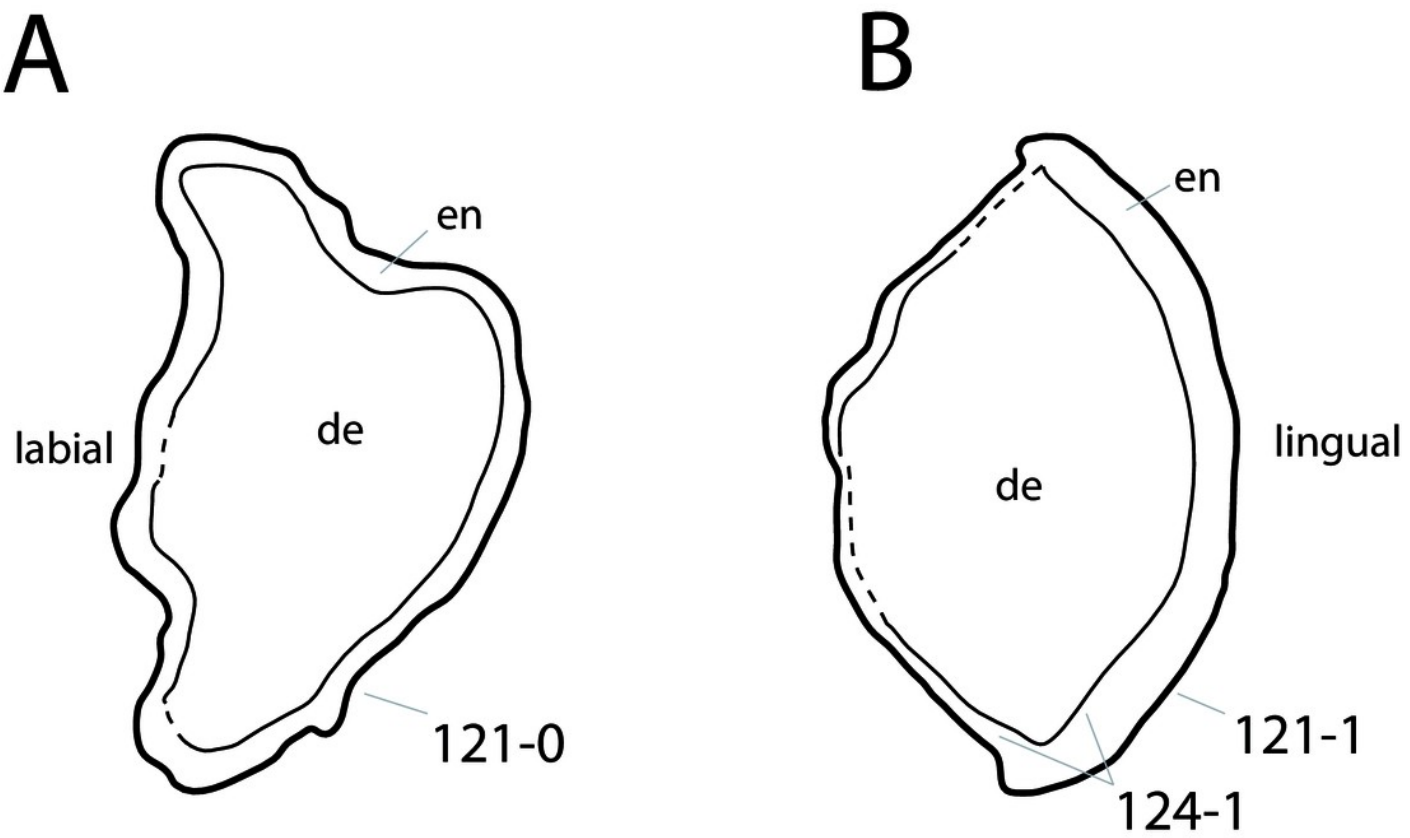


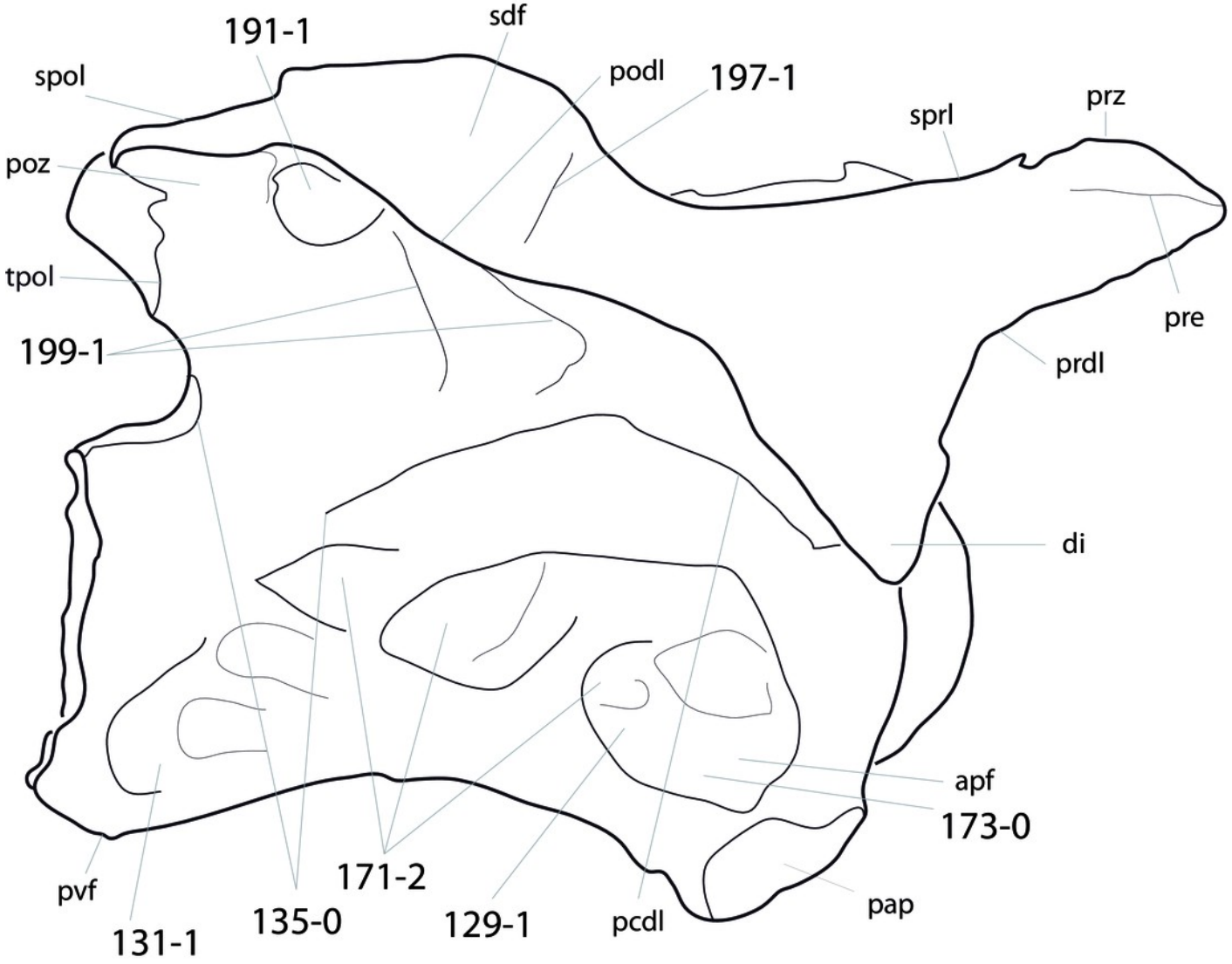
Figure 71

Posterior cervical vertebra (CV ?12) of *Galeamopus* [redacted] SMA 0011

Figure 71: Posterior cervical vertebra (CV ?12) of *Galeamopus* [redacted] SMA 0011 in right lateral view, showing the pleurocoel typical for advanced eusauropods (C129-1), but highly subdivided (C171-2), the elongate posteroventral fossa present in diplodocines (C131-1), the anteriorly restricted pcdl (C135-0), in contrast to the more posteriorly reaching pcdl of *Apatosaurus*, the dorsally excavated parapophysis (C173-0), the large foramen connecting the pocdf and the spof (C191-1), and the accessory laminae connecting the podl and the sprl (C197-1), and the pcdl and the podl (C199-1). Abb.: apf, anterior pneumatic fossa; di, diapophysis; pap, parapophysis; pcdl, posterior centrodiapophyseal lamina; pocdf, postzygapophyseal centrodiapophyseal fossa; podl, postzygodiapophyseal lamina; poz, postzygapophysis; prdl, prezygodiapophyseal lamina; pre, pre-epipophysis; prz, prezygapophysis; pvf, posteroventral flange; sdf, spinodiapophyseal fossa; spof, spinopostzygapophyseal fossa; spol, spinopostzygapophyseal lamina; sprl, spinoprezygapophyseal lamina; tpol, interpostzygapophyseal lamina.

PeerJ Reviewing Manuscript

PeerJ Reviewing Manuscript

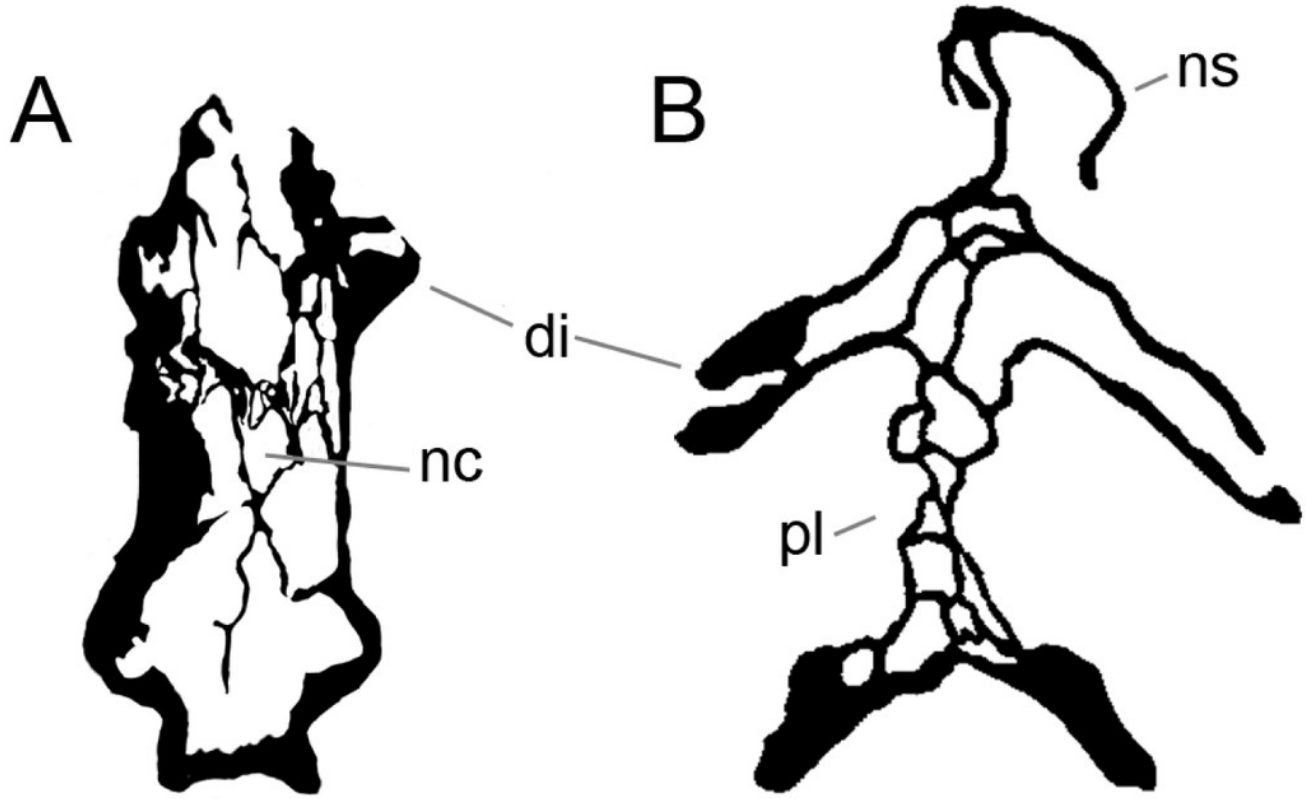


PeerJ Reviewing Manuscript

Figure 72

Cross-section of neosauropod cervical vertebrae

Figure 72: Mid- to posterior cervical vertebrae cross-section of *Supersaurus vivianae* WDC DMJ-021 (A; modified from Lovelace et al., 2007), and *Brachiosaurus* sp. BYU 12866 (B; modified from Wedel, 2009). Sections at base of diapophysis. Note the different internal pneumatic structure, with few but large cavities in *Supersaurus* (A; C128-1), in contrast to the many irregularly small fossa typical for titanosauriforms (B; C128-2). The differences shown here in cervical vertebrae apply as well for dorsal vertebrae (C228). Pictures scaled to the same centrum height. Abb: di, diapophysis; nc, neural canal; ns, neural spine; pl, pleurocoel.



PeerJ Reviewing Manuscript

Figure 73

Flagellicaudatan mid- to posterior cervical vertebrae

Figure 73: Mid- to posterior cervical vertebrae of *Dicraeosaurus hansemanni* MB.R.4886 (A; photo by J. Harris), *Kaatedocus siberi* SMA 0004 (B), and *Barosaurus lentus* YPM 429 (C) in ventral view (anterior to the top). Note the different developments of the ventral keels (prominent in *Dicraeosaurus*, A, C132-0; shallow, single in *Kaatedocus*, B, C132-1 and 175-0; double in *Barosaurus*, C, C175-1), the ventral sulcus typical for diplodocines (B, C; C133-1), the pneumatic foramina accompanying the ventral keel in *Dicraeosaurus* (A; C176-1), the posteroventral flanges (C179-1), and the numerous accessory laminae subdividing the prezygapophyseal centrodiapophyseal fossa in *Barosaurus* (C; C184-2). Vertebrae scaled to same centrum length. Abb: acdl, anterior centrodiapophyseal lamina; CR, cervical rib; di, diapophysis; pap, parapophysis; pcdl, posterior centrodiapophyseal lamina; podl, postzygodiapophyseal lamina; poz, postzygapophysis, prdl, prezygodiapophyseal lamina; prz, prezygapophysis; pvf, posteroventral flange.

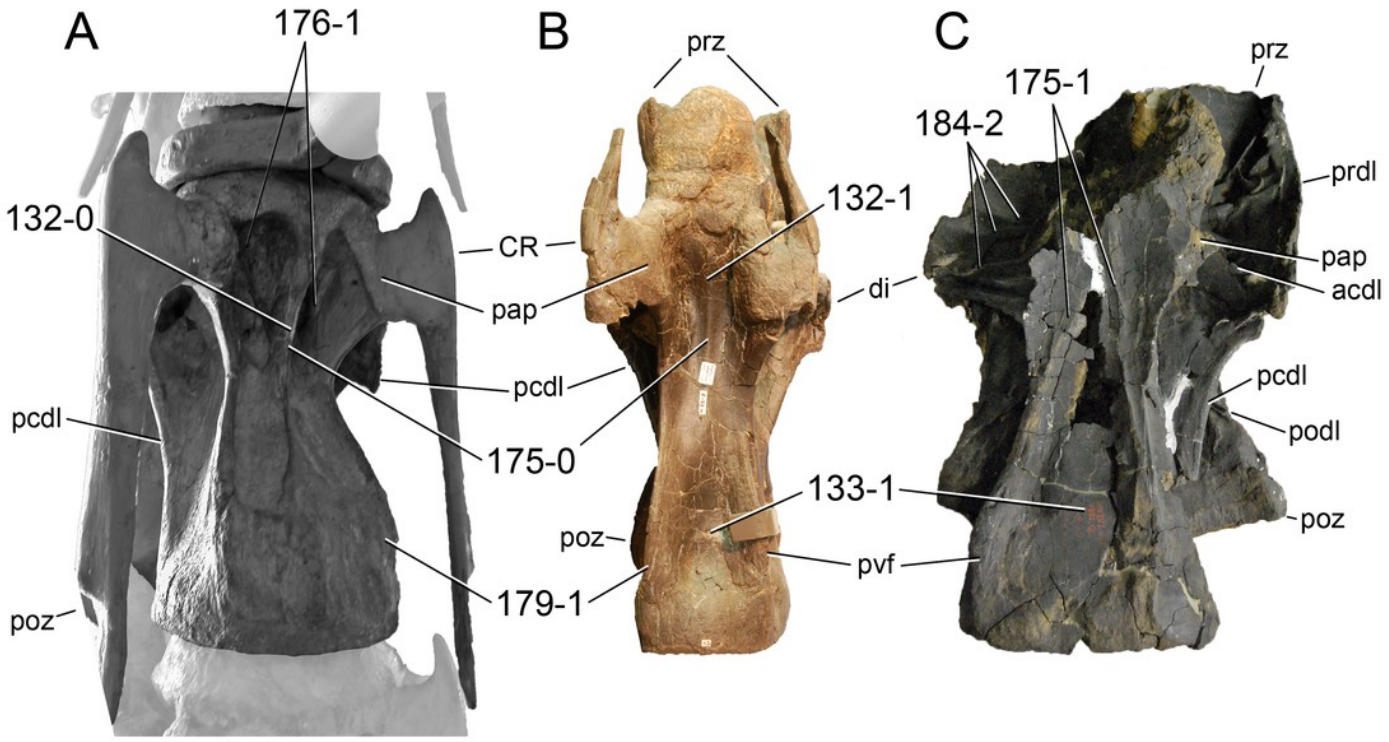
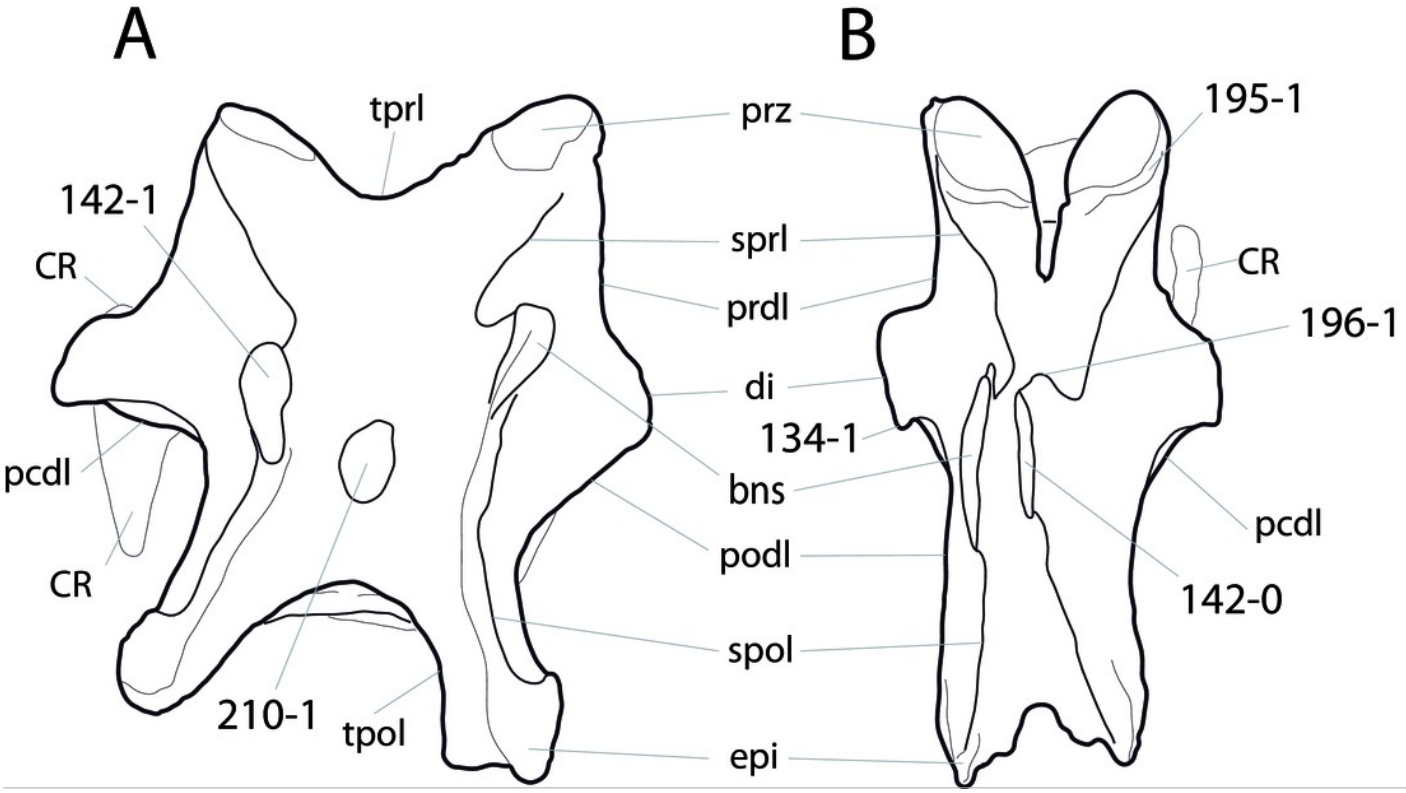


Figure 74

Diplodocid mid- to posterior cervical vertebrae

Figure 74: Mid- to posterior cervical vertebrae of *Apatosaurus ajax* YPM 1860 (A; traced from a photo by M. Taylor), and *Kaatedocus siberi* SMA 0004 (B; CV 13, traced from Tschopp and Mateus, 2013b) in dorsal view (anterior to the top). Note the triangular posterior projection on the diapophysis in *Kaatedocus* (B; C134-1), the transversely compressed (B; C142-0) in contrast to rounded (A; C142-1) neural spine summits, the transverse sulcus accompanying the prezygapophyseal facet posteriorly in *Kaatedocus* (B; C195-1), the anterior bulge of the sprl, just below the spine summit, characterizing most diplodocines (B; C196-1), and the median tubercle visible in *Apatosaurus* (A; C210-1). Abb.: bns, bifid neural spine; CR, cervical rib; di, diapophysis; epi, epipophysis; pcdl, posterior centrodiapophyseal lamina; podl, postzygodiapophyseal lamina; prdl, prezygodiapophyseal lamina; prz, prezygapophysis; spol, spinopostzygapophyseal lamina; sprl, spinoprezygapophyseal lamina; tpol, interpostzygapophyseal lamina; tprl, interprezygapophyseal lamina. Vertebrae scaled to same total length.



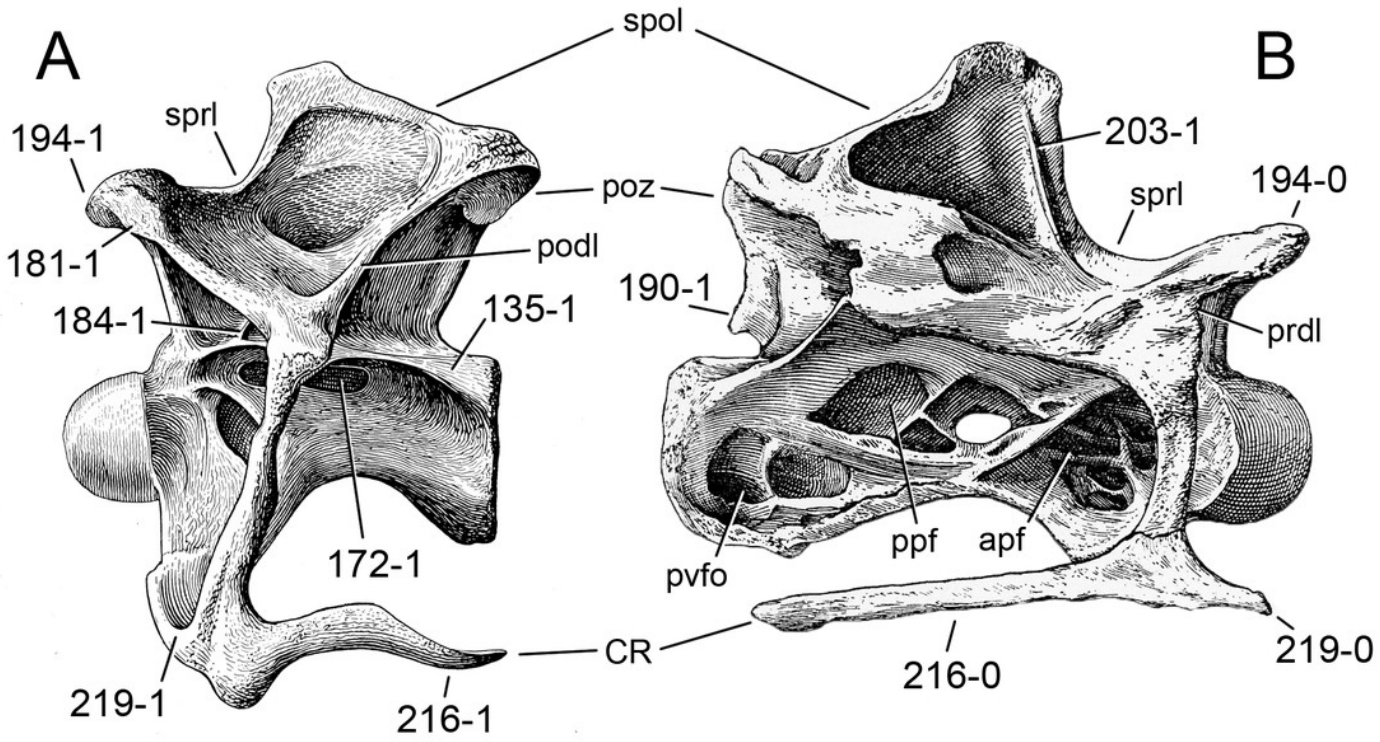
PeerJ Reviewing Manuscript

Figure 75

Cervical vertebra 11 of diplodocids

Figure 75: Cervical vertebra 11 of *Apatosaurus louisae* CM 3018 (A; modified from Gilmore, 1936) and *Diplodocus carnegii* CM 84 (B; modified from Hatcher, 1901) in left (A) and right (B) lateral view. Note the posteriorly extending posterior centrodiapophyseal lamina in *Apatosaurus* (A; C135-1), the anteriorly restricted pneumatic foramen typical for most apatosaurs (A; C172-1), the pre-epipophysis (A; C181-1), the subdivided prezygapophyseal centrodiapophyseal fossa, characterizing *A. louisae* (A; C184-1), the posteriorly expanded interpostzygapophyseal lamina of *Diplodocus* (B; C190-1), the posteriorly restricted prezygapophysis of *A. louisae* (A; C194-1), compared to the state in *Diplodocus*, where it reaches the anterior edge of the condyle (B; C194-0), the vertical accessory spinal lamina marking *Diplodocus* (B; C203-1), the different positions of the cervical ribs (ventrally projecting, A, C216-1; or level with centrum, B, C216-0), and the absence (A; C219-1) or presence (B; C219-0) of the anterior process of the cervical rib. Vertebrae scaled to same posterior cotyle height. Abb: apf, anterior pneumatic fossa; CR, cervical ribs; podl, postzygodiapophyseal lamina; poz, postzygapophysis; ppf. Posterior pneumatic fossa; prdl, prezygodiapophyseal lamina; pvfo, posteroventral fossa; spol, spinopostzygapophyseal lamina; sprl, spinoprezygapophyseal lamina.

PeerJ Reviewing Manuscript



PeerJ Reviewing Manuscript

PeerJ Reviewing Manuscript

Figure 76

Cervical vertebra 6 of neosauropods

Figure 76: Cervical vertebra 6 of *Australodocus bohetii* MB.R.2455 (A) and *Galeamopus* [redacted] SMA 0011 (B) in left (A) and right (B) lateral view. Note the short second pcdl in *Australodocus* (A; C136-1), the foramen piercing the podl (A; C137-1), the projection formed by the epipophysis (B; C138-1), the low (A; C164-0), and high (B; C164-1) neural spines, and the cervical rib, which is slightly longer than the centrum in *Galeamopus* (B; C215-1). Abb.: acdl, anterior centrodiapophyseal lamina; apf, anterior pneumatic fossa; cpol, centropostzygapophyseal lamina; cprl, centroprezygapophyseal lamina; CR, cervical rib; naf, neural arch foramen; pcdl, posterior centrodiapophyseal lamina; podl, postzygodiapophyseal lamina; poz, postzygapophysis; ppf, posterior pneumatic fossa; prz, prezygapophysis; spol, spinopostzygapophyseal lamina; sprl, spinoprezygapophyseal lamina; tpol, interpostzygapophyseal lamina. Vertebrae scaled to the same centrum length.

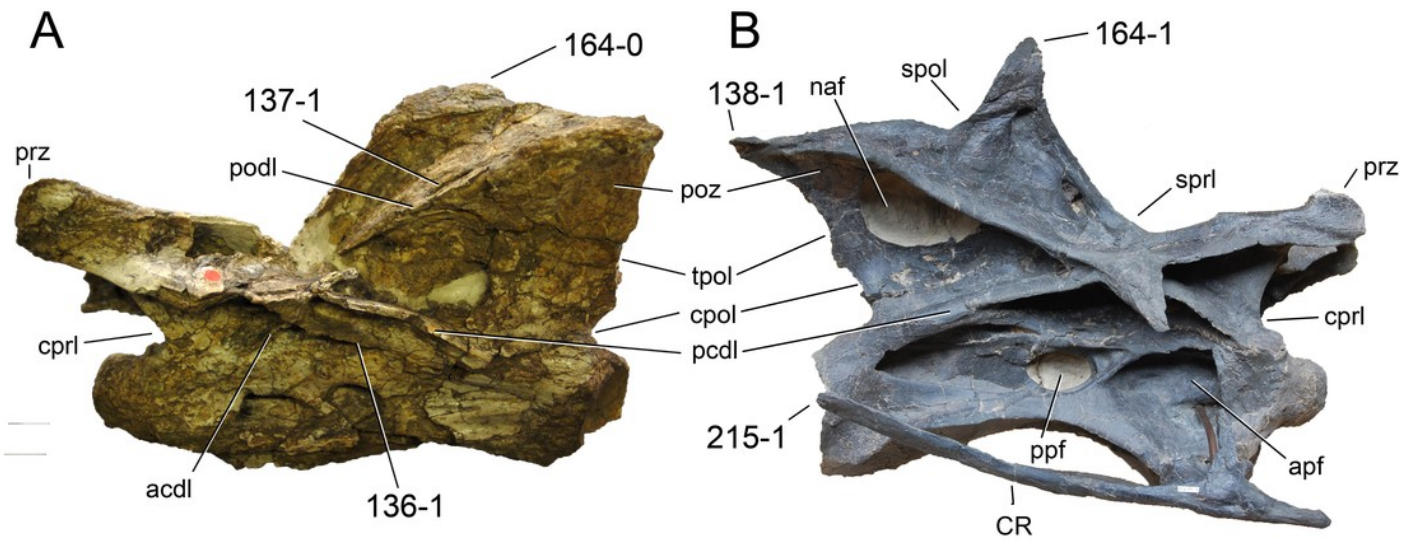


Figure 77

Diplodocine mid- to posterior cervical vertebrae

Figure 77: Mid- to posterior cervical vertebrae of *Barosaurus lentus* YPM 429 (A) and *Diplodocus carnegii* CM 84 (B) in left posterolateral (A) and left dorsolateral view (B). Note the differently pneumatized epipophyses (C139-1), the transversely compressed epipophysis (B; C202-1), and the horizontal ridge below the neural spine summit in *Diplodocus* (B; C205-1). The cervical vertebra of *B. lentus* is partly covered by matrix and plaster. Abb.: apf, anterior pneumatic fossa; CR, cervical rib; pap, parapophysis; pcdl, posterior centrodiapophyseal lamina; ppf, posterior pneumatic fossa; prdl, prezygodiapophyseal lamina; prz, prezygapophysis; pvf, posteroventral flange; pvfo, posteroventral fossa; spol, spinopostzygapophyseal lamina; sprl, spinoprezygapophyseal lamina. Vertebrae scaled to the same posterior cotyle height.

PeerJ Reviewing Manuscript

PeerJ Reviewing Manuscript

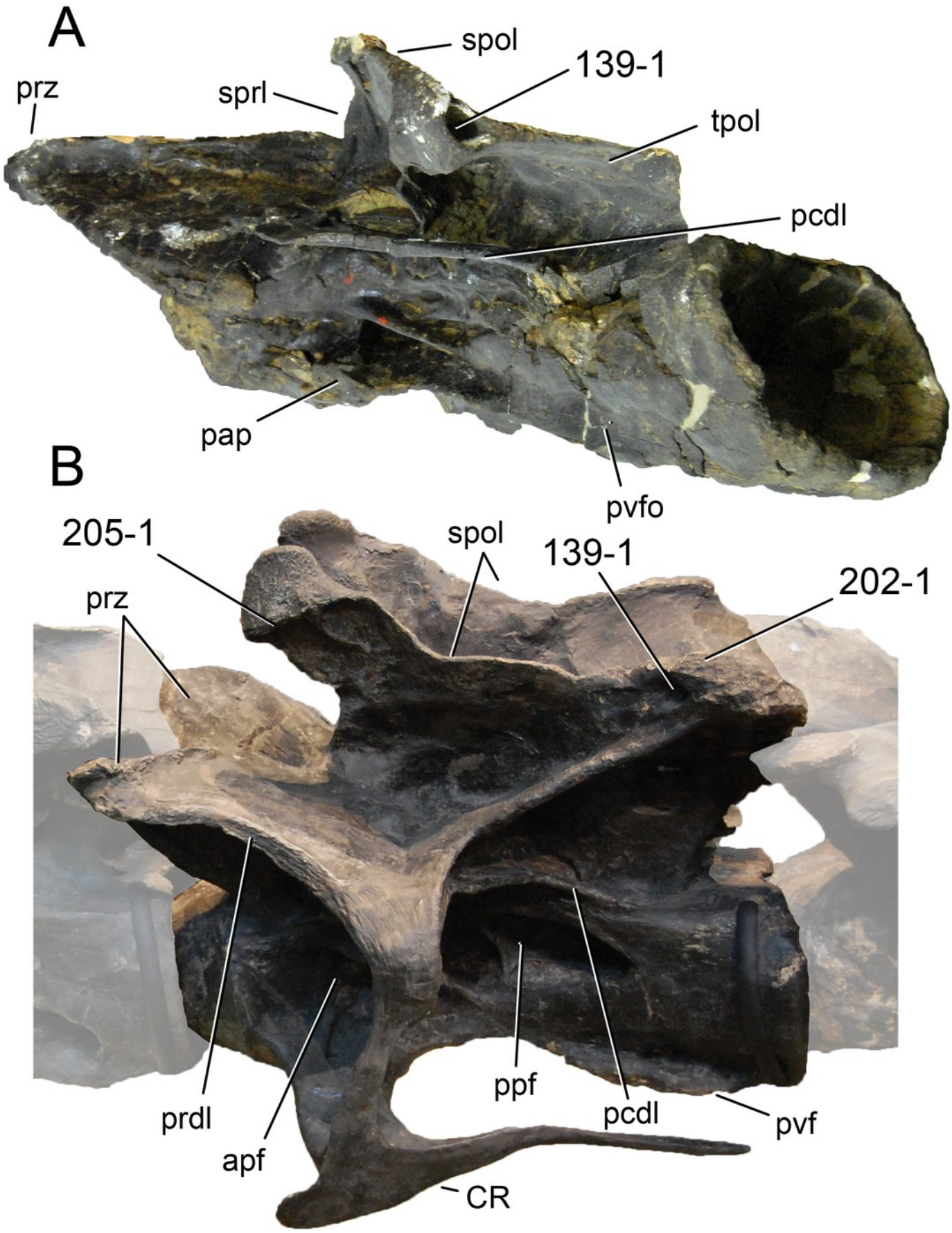


Figure 78

Cervical vertebra 5 of flagellicaudatans

Figure 78: Cervical vertebra 5 of *Suuwassea emilieae* ANS 21122 (A) and *Kaatedocus siberi* SMA 0004 (B; modified from Tschopp and Mateus, 2013b) in anterior view. Note the transversely widening (A; C141-1) instead of straight (B; C141-0) neural spine, and the presence of a prespinal lamina in *Kaatedocus* (B; C161-1). The neural spine of *Suuwassea* (A) is not bifurcated, but broken (as indicated by the dashed line). Abb.: cprl, centroprezygapophyseal lamina; pap, parapophysis; poz, postzygapophysis; prdl, prezygodiapophyseal lamina; prz, prezygapophysis; sprl, spinoprezygapophyseal lamina. Vertebrae scaled to the same anterior condyle length.

PeerJ Reviewing Manuscript

PeerJ Reviewing Manuscript

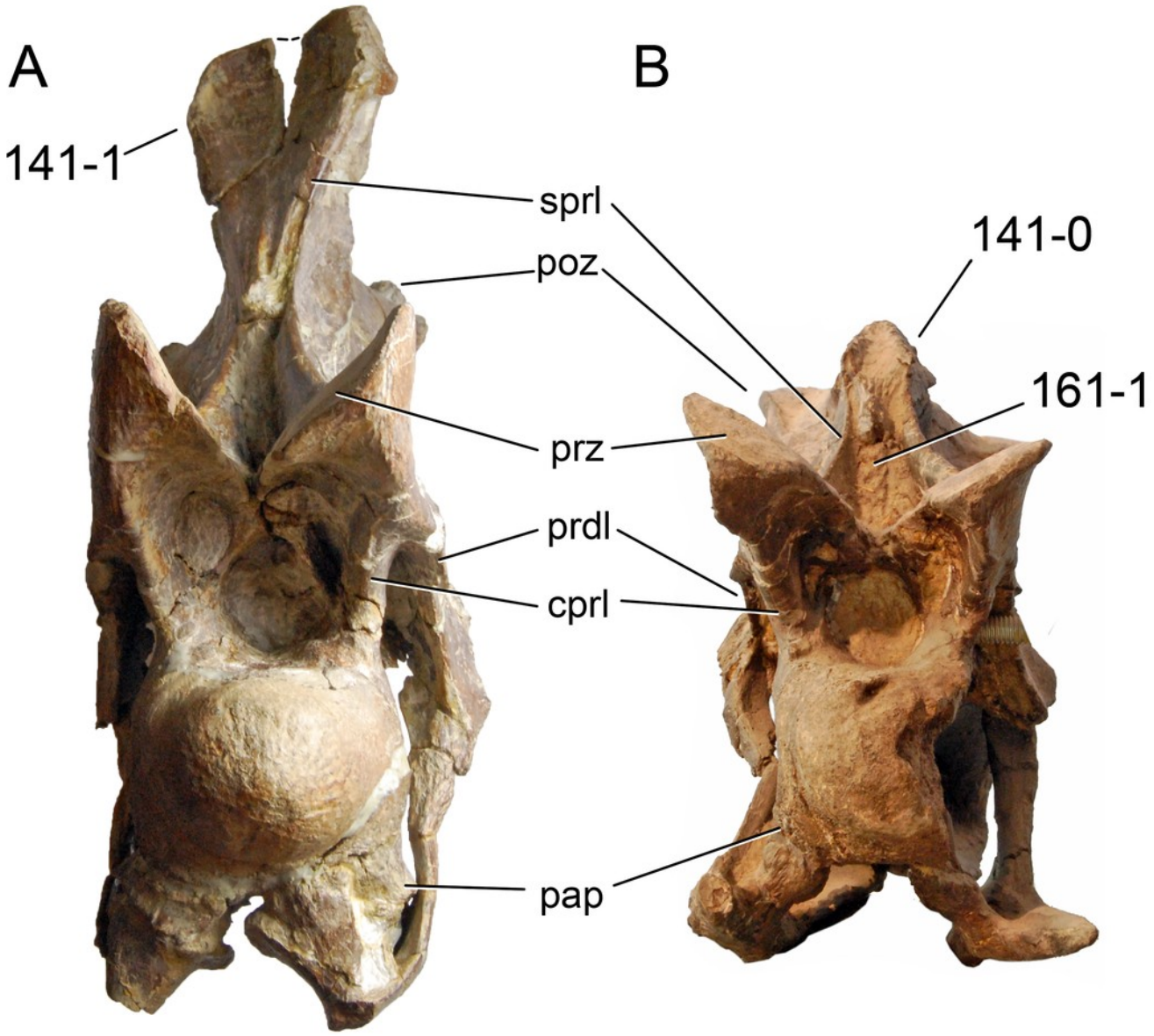
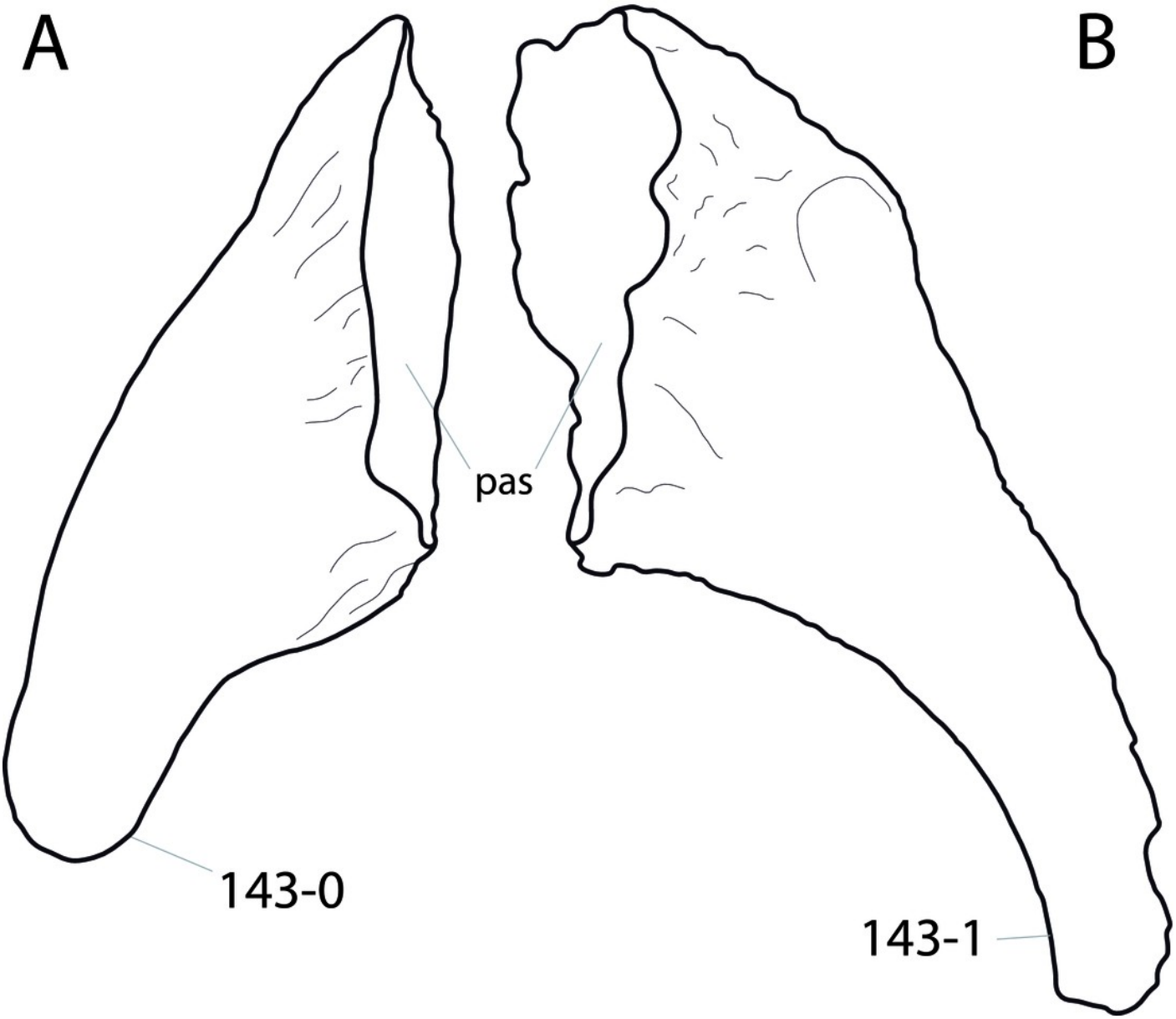


Figure 79

Diplodocine proatlases

Figure 79: Proatlas of ?*Kaatedocus* SMA P29-1 (A) and *Galeamopus* [redacted] SMA 0011 (B) in medial view, illustrating the broad (A; C143-0) and narrow distal tips (B; C143-1). Abb.: pas, proximal articular surface. Scaled to the same articular surface height.

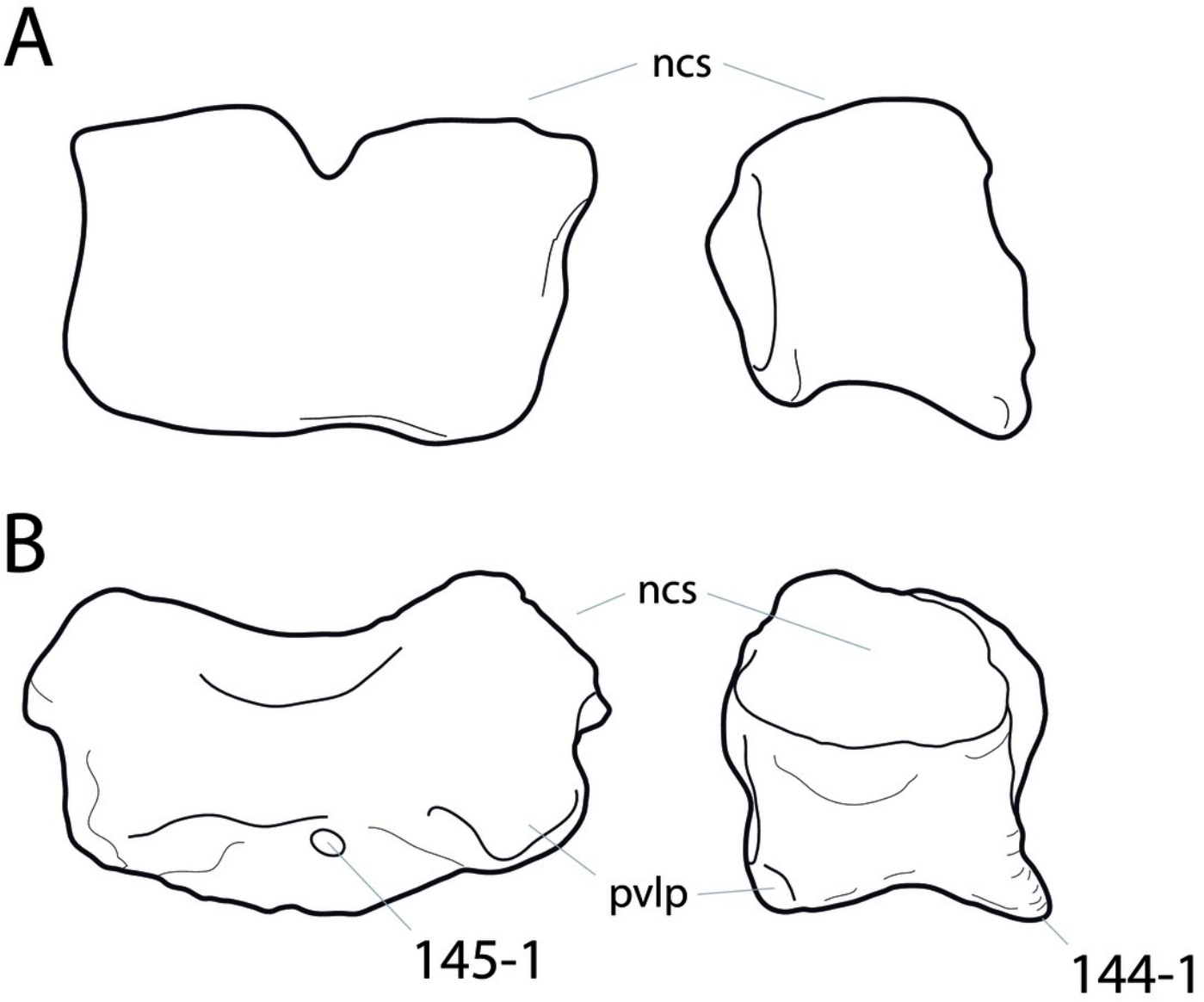


PeerJ Reviewing Manuscript

Figure 80

Neosauropod atlantes

Figure 80: Atlas of *Camarasaurus* sp. UUVP 10070 (A; modified from Madsen et al., 1995), and *Galeamopus* [redacted] AMNH 969 (B) in posterior (left) and right lateral view (right, A shows left side reversed). Note the distinct anteroventral lip characterizing diplodocids (B; C144-1), and the foramen between the posterior ventrolateral processes in AMNH 969 (B; C144-1). Abb.: ncs, neurocentral synchondrosis; pvlp, posterior ventrolateral process. Scaled to the same centrum height.



PeerJ Reviewing Manuscript

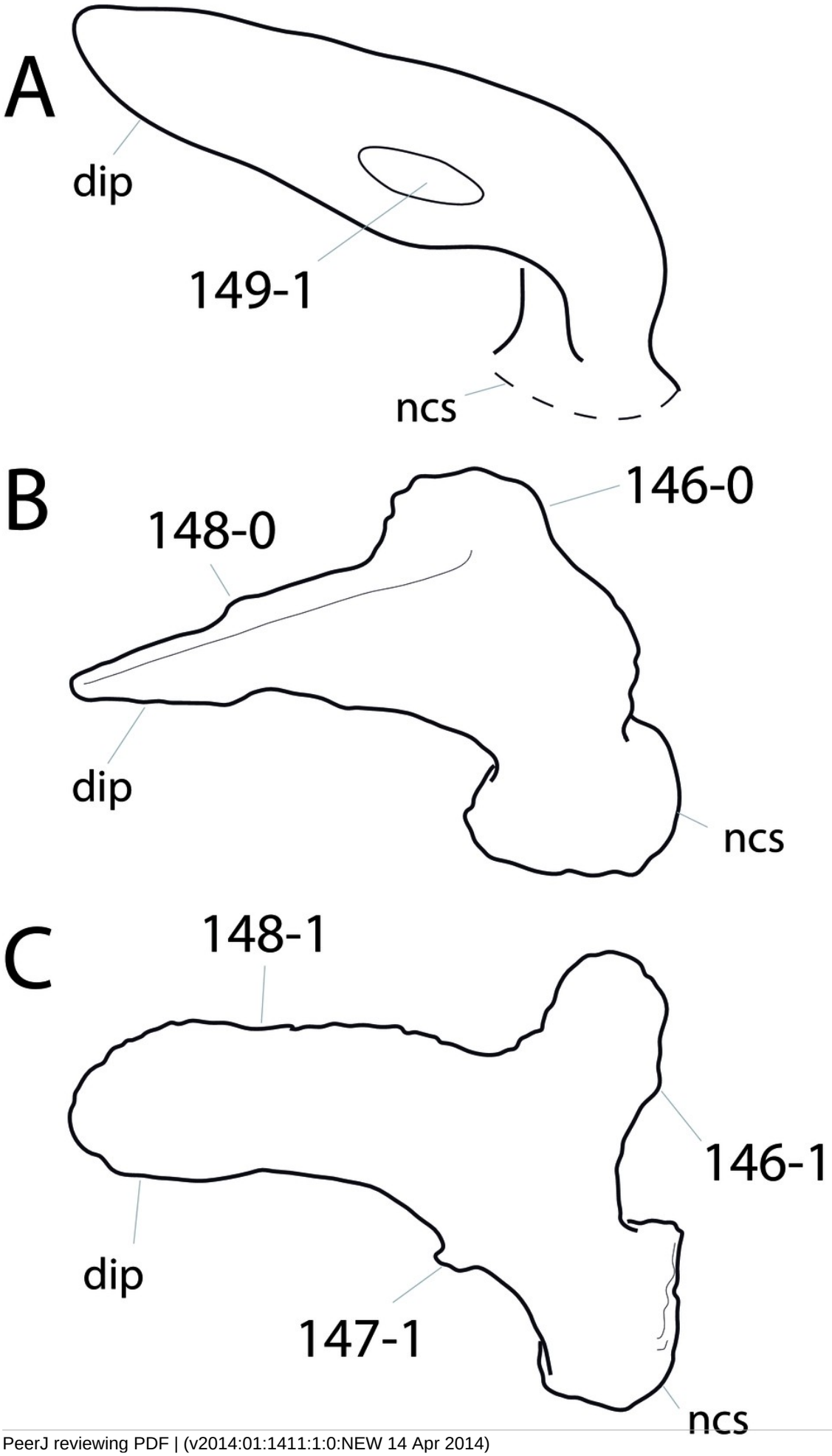
Figure 81

Diplodocid atlantal neurapophyses

Figure 81: Neurapophyses of *Apatosaurus louisae* CM 3018 (A; modified from Gilmore, 1936), *Kaatedocus siberi* SMA 0004 (B; traced from 3D model provided by G. Dzemski), and *Galeamopus* [redacted] SMA 0011 (C) in lateral (A; left side reversed), and dorsolateral view (B, C). Note the weak (B; C146-0) in contrast to well-developed medial process (C; C146-1), the subtriangular lateral spur in *G.* [redacted] (C; C147-1), the different shapes of the distal process (tapering, B, C148-0; wide, C, C148-1), and the foramen characterizing *A. louisae* (A; C149-1). Abb.: dip, distal process; ncs, neurocentral synchondrosis. Scaled to the same anteroposterior length.

PeerJ Reviewing Manuscript

PeerJ Reviewing Manuscript



PeerJ Reviewing Manuscript

Figure 82

Axis of *Diplodocus carnegii* CM 84

Figure 82: Axis of *Diplodocus carnegii* CM 84 in posterolateral view, illustrating the pneumatic slot-like fossa posterior to the parapophysis (C150-1), and the presence of a postspinal lamina (C152-1). Abb.: at, atlas; CV 3, cervical vertebra 3; pap, parapophysis; pl, pleurocoel; poz, postzygapophysis; prdl, prezygodiapophyseal lamina; prsl, prespinal lamina; spol, spinopostzygapophyseal lamina.

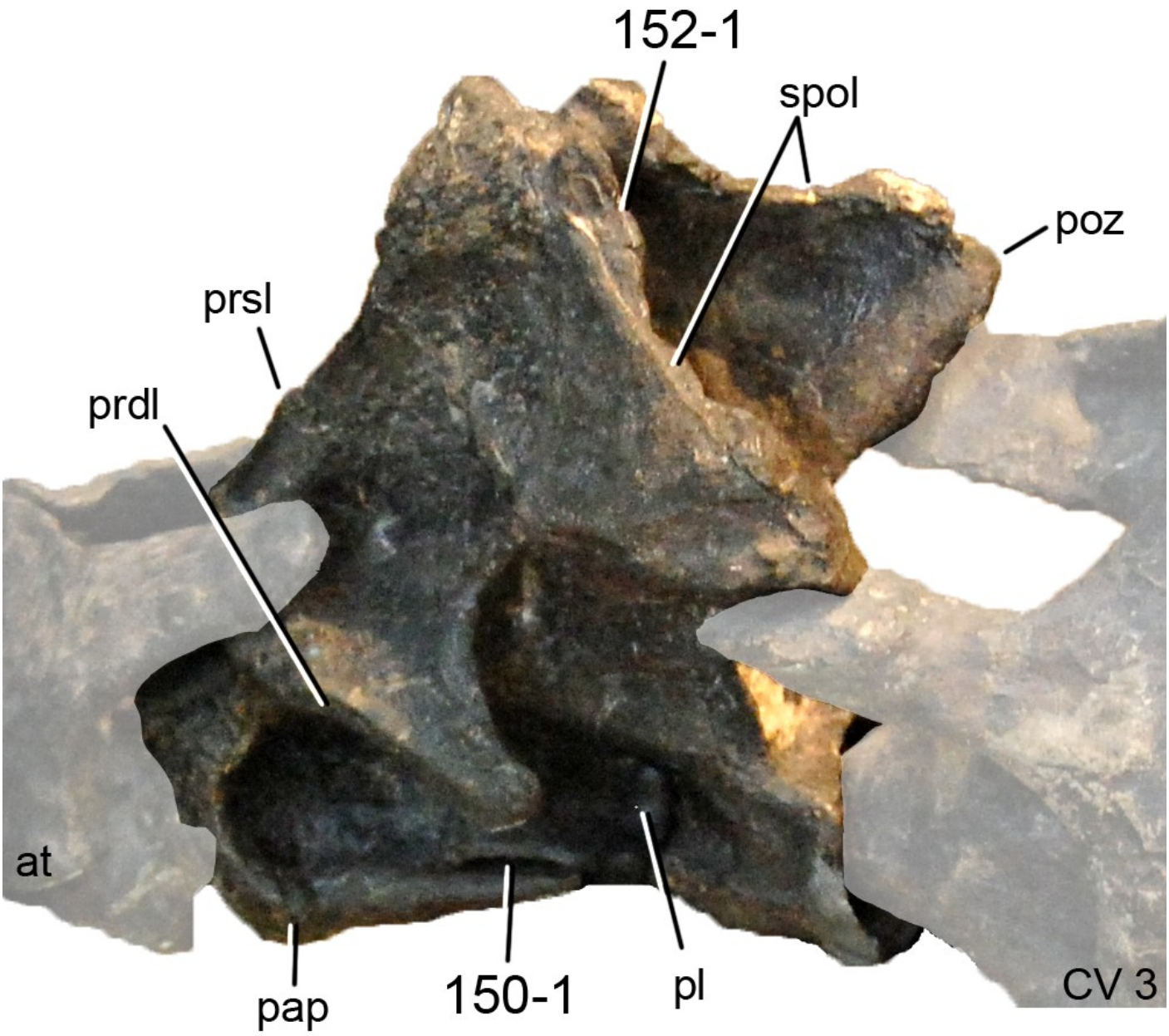


Figure 83

Axis of *Galeamopus* [redacted] AMNH 969

Figure 83: Axis of *Galeamopus* [redacted] AMNH 969 in dorsal (top), right lateral (bottom left), and anterior (bottom right) view, illustrating the anteriorly expanded prespinal lamina (C151-1), and the anteriorly restricted neural spine summit (C153-2). Abb.: di, diapophysis; epi, epipophysis; pap, parapophysis; pcdl, posterior centrodiapophyseal lamina; pl, pleurocoel; poz, postzygapophysis; prsl, prespinal lamina; prz, prezygapophysis. Scale bar = 10 cm.

PeerJ Reviewing Manuscript

PeerJ Reviewing Manuscript

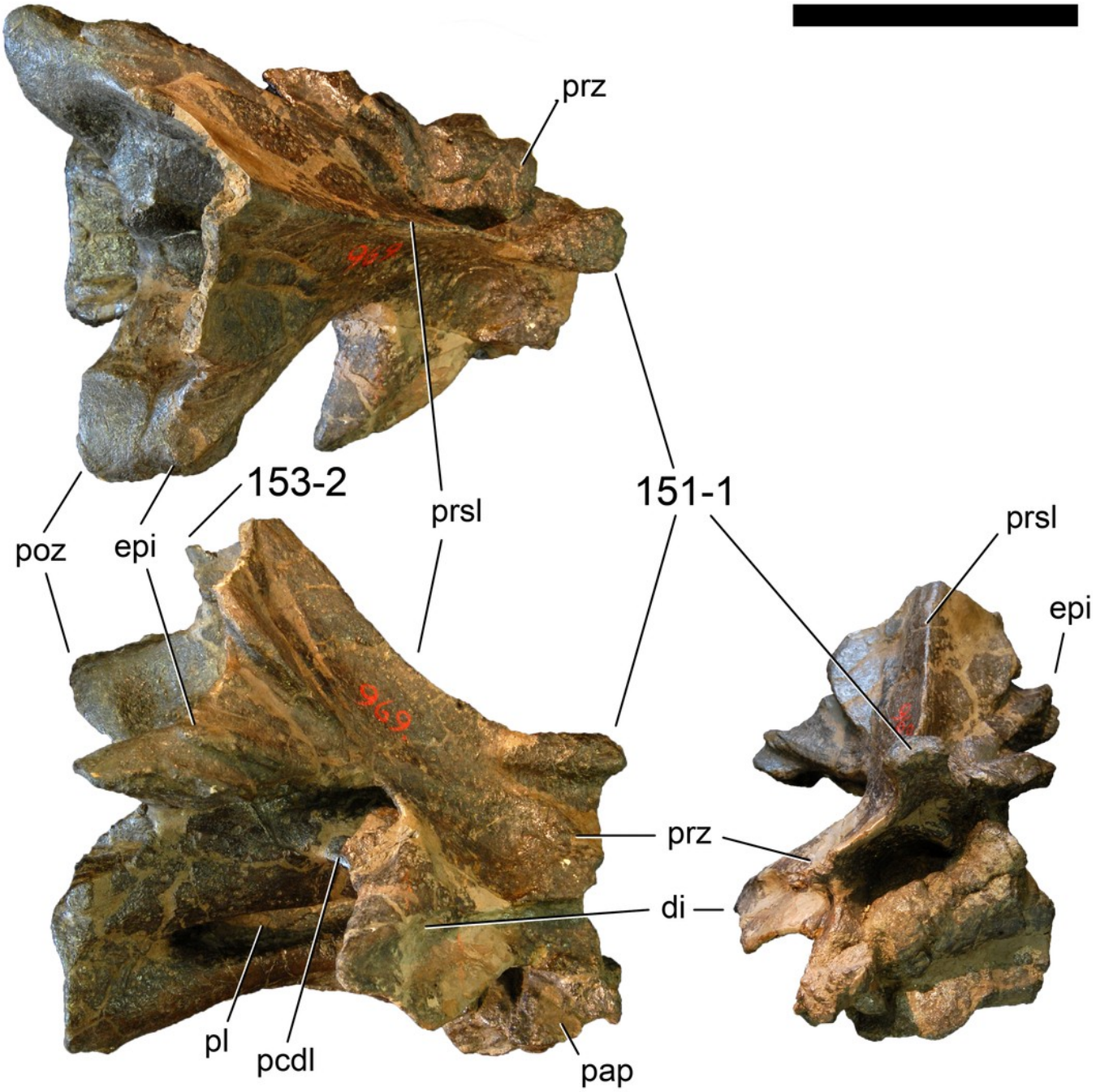
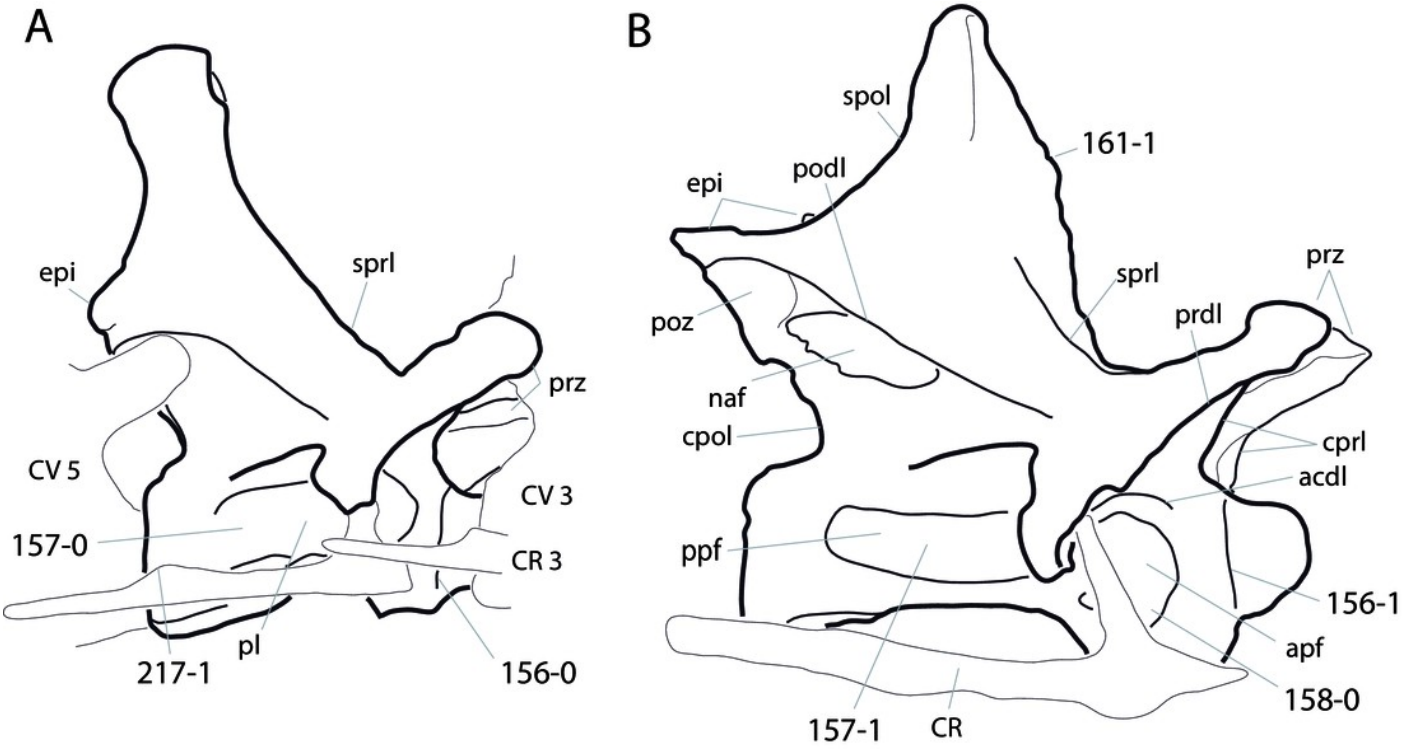


Figure 84

Cervical vertebra 4 of flagellicaudatans

Figure 84: Cervical vertebra 4 of *Dicraeosaurus hansemanni* MB.R.4886 (A) and *Galeamopus* [redacted] SMA 0011 (B) in right lateral view. Note the differently inclined posterior border of the anterior condyle (A, C156-0; B, C156-1), the subdivision of the pleurocoel in *G.* [redacted] (B; C157-1), which is absent in anterior cervical vertebrae of *D. hansemanni* (A; C157-0), the anterior pneumatic fossa that extends onto the parapophysis (B; C158-0), the presence of a prespinal lamina in *G.* [redacted] (B; C161-1), and the posteriorly projecting spur on the dorsal edge of the posterior process of the cervical rib of *D. hansemanni* (A; C217-1). Abb.: acdl, anterior centrodiapophyseal lamina; apf, anterior pneumatic fossa; cprl, centroprezygapophyseal lamina; CR 3, cervical rib 3; CV 3, cervical vertebra 3; epi, epipophysis; naf, neural arch foramen; pl, pleurocoel; podl, postzygodiapophyseal lamina; poz, postzygapophysis; ppf, posterior pneumatic fossa; prdl, prezygodiapophyseal lamina; prz, prezygapophysis; spol, spinopostzygapophyseal lamina; sprl, spinoprezygapophyseal lamina. Vertebrae scaled to the same cotyle height.



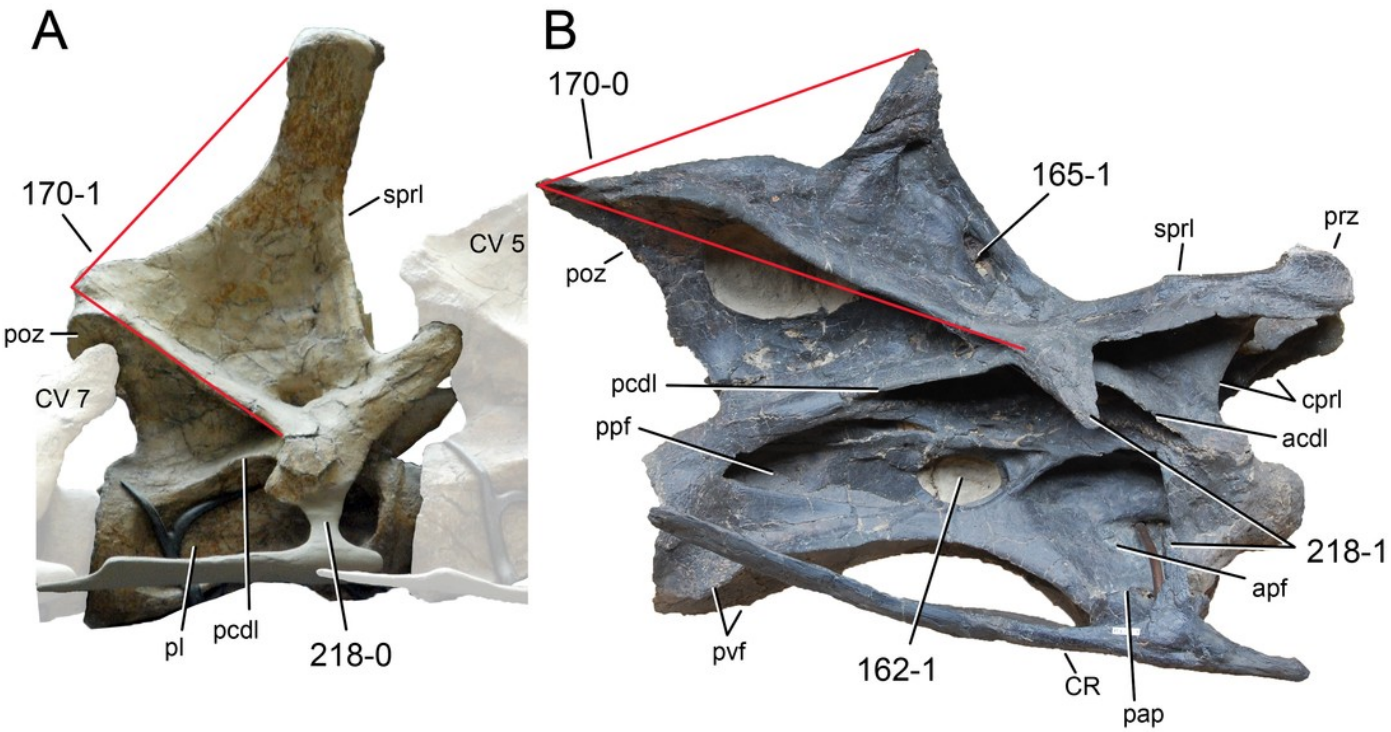
PeerJ Reviewing Manuscript

PeerJ Reviewing Manuscript

Figure 85

Cervical vertebra 6 of flagellicaudatans

Figure 85: Cervical vertebra 6 of *Dicraeosaurus hansemanni* MB.R.4886 (A) and *Galeamopus* [redacted] SMA 0011 (B) in right lateral view. Note the large, rounded pneumatic foramen marking the anterior end of the posterior pneumatic fossa in *G.* [redacted] (B; C162-1), the elongate foramen in the neural spine (B; C165-1), the right (A; C170-1), or acute angles (B; C170-0) between the spinopostzygapophyseal and the postzygodiapophyseal laminae, and the vertical (A; C218-0) or posteriorly inclined tuberculum (B; C218-1). Abb.: acdl, anterior centrodiapophyseal lamina; apf, anterior pneumatic fossa; cprl, centroprezygapophyseal lamina; CR, cervical rib; CV 5, cervical vertebra 5; pap, parapophysis; pl, pleurocoel; poz, postzygapophysis; ppf, posterior pneumatic fossa; prz, prezygapophysis; pvf, posteroventral flanges; sprl, spinoprezygapophyseal lamina. Scaled to the same cotyle height.



PeerJ Reviewing Manuscript

Figure 86

Diplodocine mid-cervical vertebrae

Figure 86: Mid-cervical vertebrae of *Kaatedocus siberi* SMA 0004 (A; CV 10, modified from Tschopp and Mateus, 2013b) and *Diplodocus carnegii* CM 84 (B; CV 8) in right lateral (A) and left laterodorsal view (B). Note the reduced spinoprezygapophyseal lamina (B; C163-1), the pre-epipophysis (C181-1), which is anteriorly expanded in *K. siberi* (A; C167-1), the distinct fossa posterolaterally to the prezygapophysis (A; C183-1), which is absent in CM 84 (B; C183-0), and the short cervical ribs (B; 214-1). Abb.: apf, anterior pneumatic fossa; cprl, centroprezygapophyseal lamina; CR, cervical rib; CV 7, cervical vertebra 7; podl, postzygodiapophyseal lamina; poz, postzygapophysis; ppf, posterior pneumatic fossa; prz, prezygapophysis; pvf, posteroventral flanges; spol, spinopostzygapophyseal lamina; sprl, spinoprezygapophyseal lamina. Not to scale.

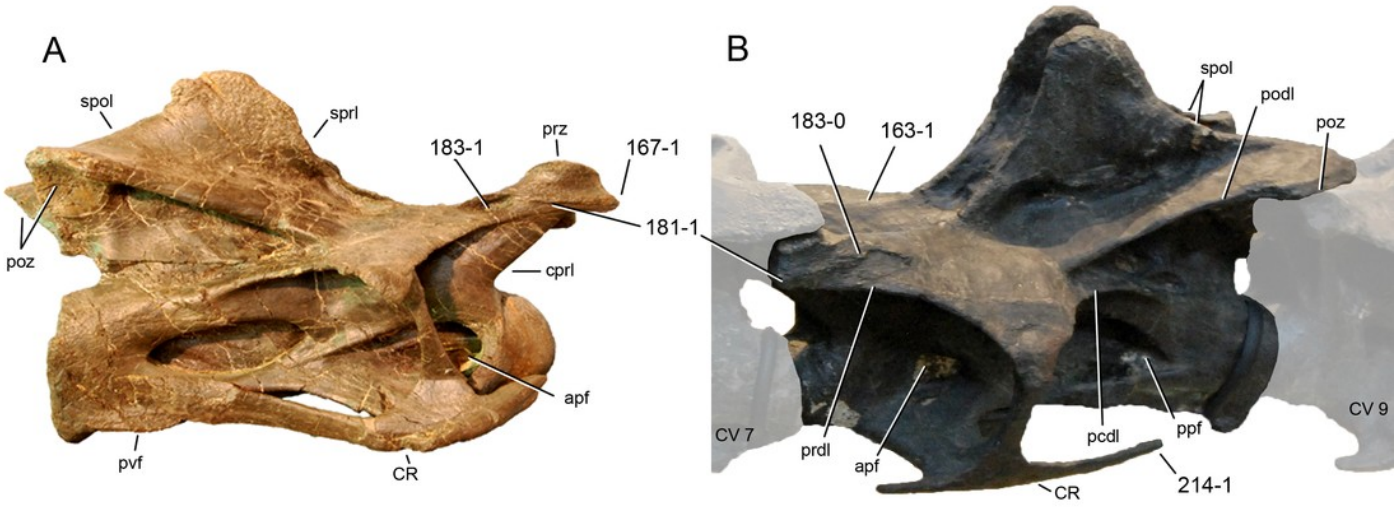
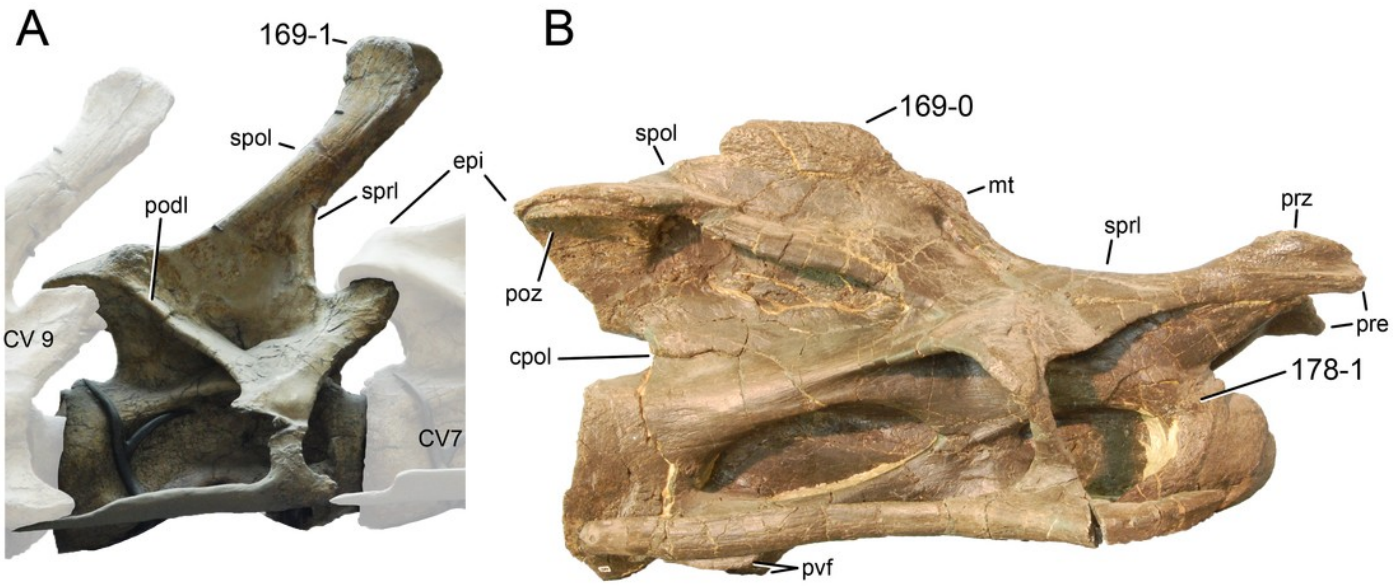


Figure 87

Cervical vertebra 8 of flagellicaudatans

Figure 87: Cervical vertebra 8 of *Dicraeosaurus hansemanni* MB.R.4886 (A) and *Kaatedocus siberi* SMA 0004 (B) in right lateral view. Note the different inclinations of the neural spine (C169), and the small tuberosity marking the anterodorsal corner of the centrum in *Kaatedocus* (B; C178-1). Abb.: cpol, centropostzygapophyseal lamina; CV 7, cervical vertebra 7; epi, epipophysis; mt, median tubercle; podl, postzygodiapophyseal lamina; poz, postzygapophysis; pre, pre-epipophysis; prz, prezygapophysis; pvf, posteroventral flanges; spol, spinopostzygapophyseal lamina; sprl, spinoprezygapophyseal lamina. Scaled to the same cotyle height.



PeerJ Reviewing Manuscript

PeerJ Reviewing Manuscript

Figure 88

Cervical vertebra 14 of *Dinheirosaurus lourinhanensis* ML 414

Figure 88: Cervical vertebra 14 of *Dinheirosaurus lourinhanensis* ML 414 in lateroventral view, illustrating the particular ventral morphology with posteriorly located paired pneumatic foramina (C176-1), lateral grooves posterior to the parapophyses (C177-1), a posteriorly restricted ventral keel (C193-1), and the elongated lateral spinal cavity (C204-1). Abb.: acdl, anterior centrodiapophyseal lamina; CR, cervical rib; pap, parapophysis; poz, postzygapophysis; prz, prezygapophysis; pvf, posteroventral flanges; pvfo, posteroventral fossa.

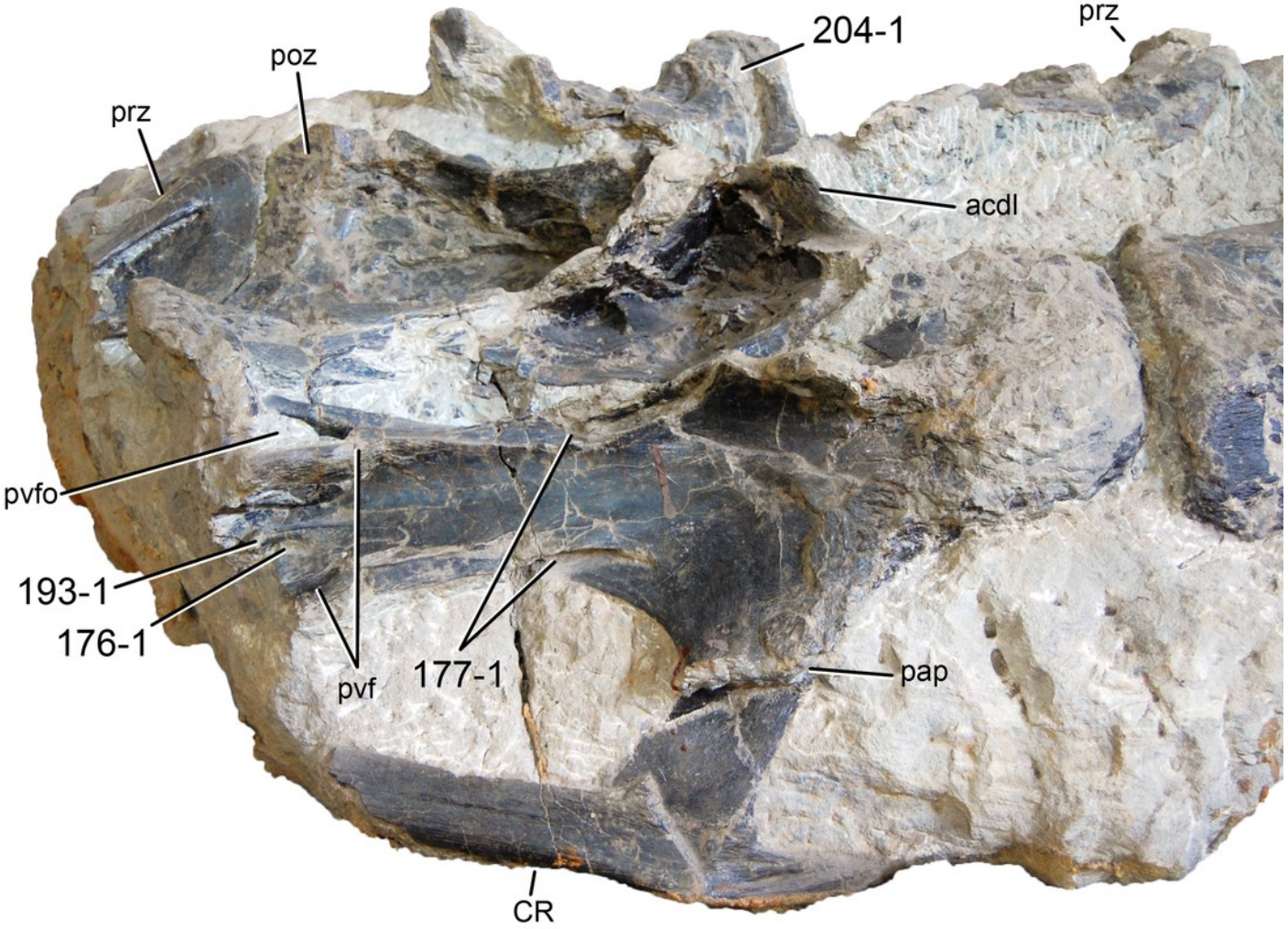
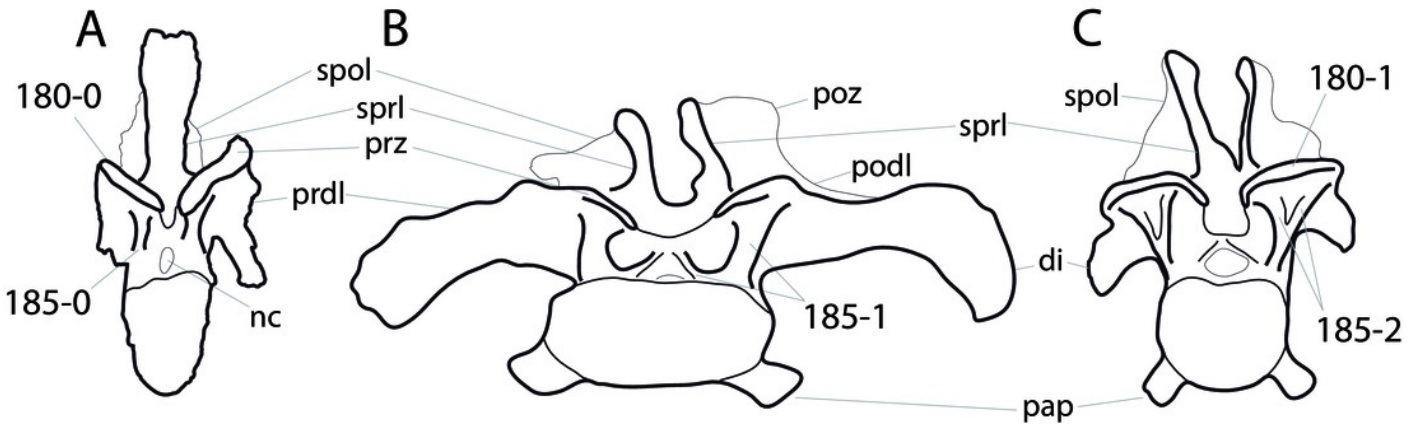


Figure 89

Cervical vertebra 11 of eusauropods

Figure 89: Cervical vertebra 11 of *Jobaria tiguidensis* MNN TIG (A; traced from photo by J. Carballido), *Camarasaurus supremus* AMNH 5671 (B; based on Osborn and Mook, 1921), and *Diplodocus carnegii* CM 84 (C; based on Hatcher, 1901) in anterior view. Note the straight (A; C180-0), in contrast to convex prezygapophyseal facet (C; C180-1), and the different morphologies of the centroprezygapophyseal lamina (single, A, C185-0; divided, and connecting to tprl, B, C185-1; divided with both branches connecting to prezygapophysis, C, C185-2). Abb.: di, diapophysis; nc, neural canal; pap, parapophysis; podl, postzygodiapophyseal lamina; poz, postzygapophysis; prdl, prezygodiapophyseal lamina; prz, prezygapophysis; spol, spinopostzygapophyseal lamina; sprl, spinoprezygapophyseal lamina. Scaled to the same condyle height.



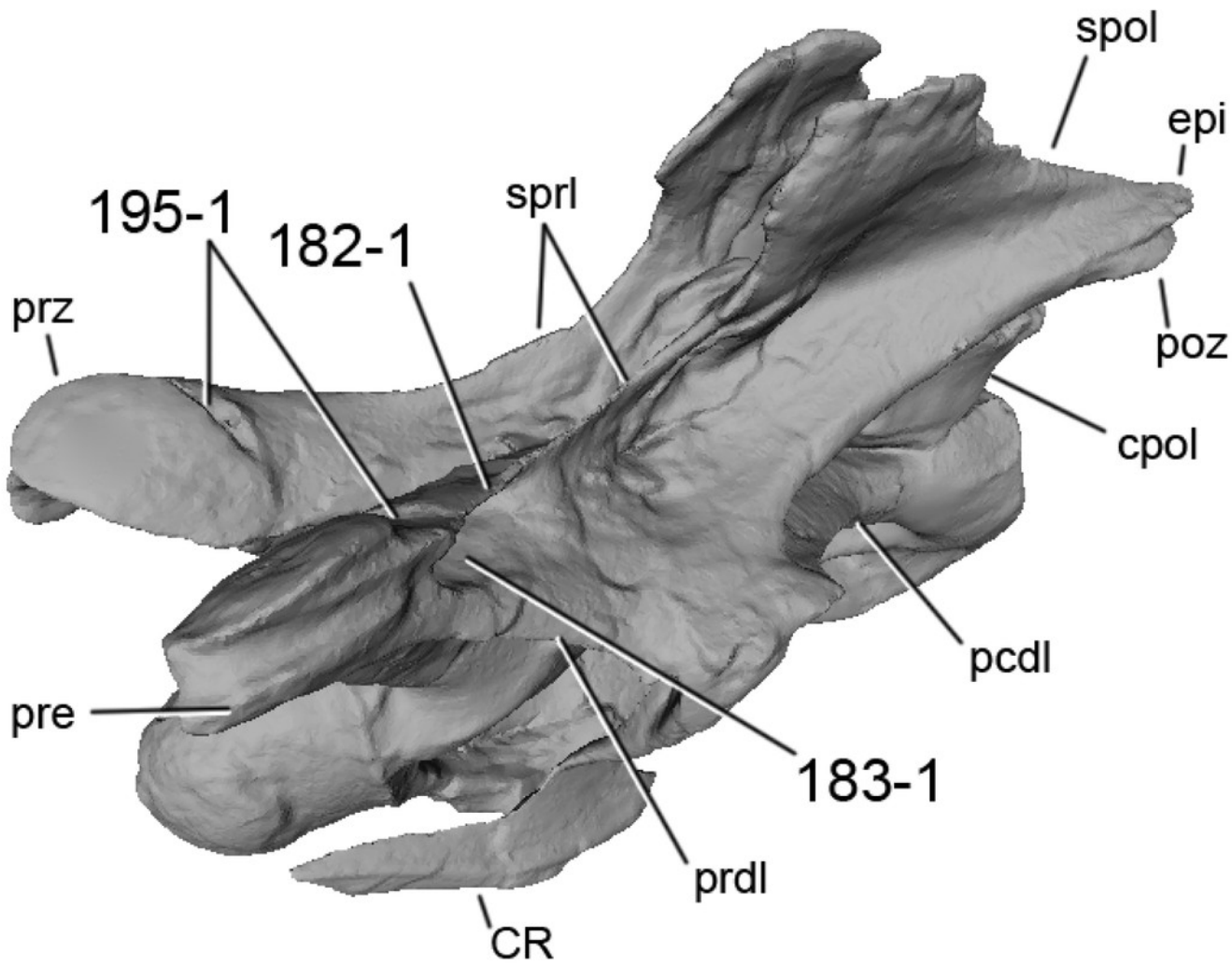
PeerJ Reviewing Manuscript

PeerJ Reviewing Manuscript

Figure 90

Cervical vertebra 12 of *Kaatedocus siberi* SMA 0004

Figure 90: Cervical vertebra 12 of *Kaatedocus siberi* SMA 0004 in lateral anterodorsal view. Note the laterally tilted anterior portion of the sprl (C182-1), the lateral fossa marking the anterior end of the spinodiapophyseal fossa (C183-1), and the transverse sulcus accompanying the prezygapophyseal facet posteriorly (C195-1). Abb.: cpol, centropostzygapophyseal lamina; CR, cervical rib; epi, epipophysis; poz, postzygapophysis; prdl, prezygodiapophyseal lamina; pre, pre-epipophysis; prz, prezygapophysis; spol, spinopostzygapophyseal lamina; sprl, spinoprezygapophyseal lamina. 3D digital model provided by G. Dzemski.

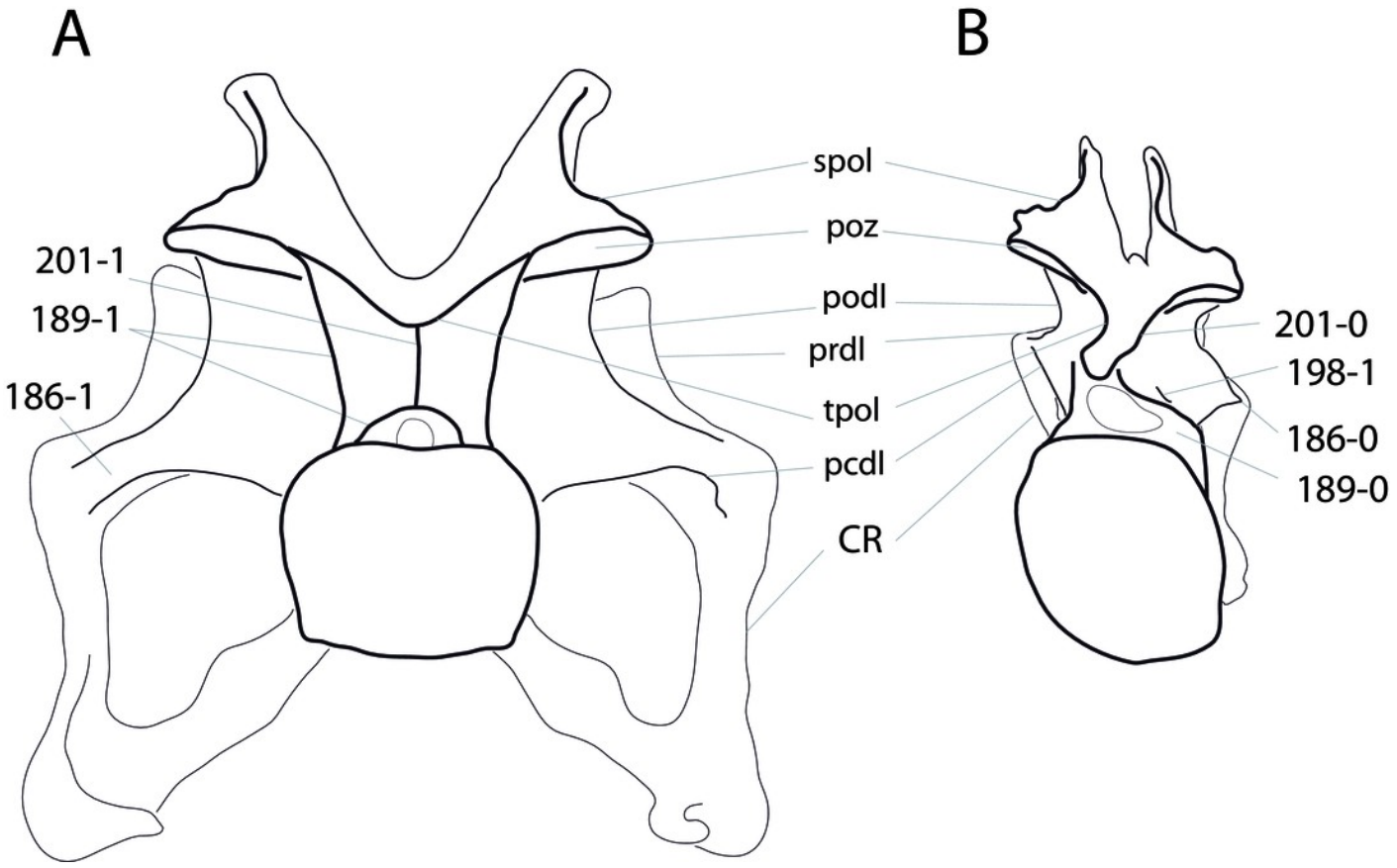


PeerJ Reviewing Manuscript

Figure 91

Cervical vertebra 12 of diplodocids

Figure 91: Cervical vertebra 12 of *Apatosaurus louisae* CM 3018 (A; based on Gilmore, 1936), and *Kaatedocus siberi* SMA 0004 (B; based on Tschopp and Mateus, 2013b) in posterior view. Note the separated (A; C186-1) or connected pcdl and podl (B; C186-0), the divided (A; C189-1) or single cpol (B; C189-0), the accessory lamina in the postzygapophyseal centrodiapophyseal fossa (B; C198-1), and the tpol that connects directly (B; C201-0) or indirectly with the neural canal roof (A; C201-1). Abb.: CR, cervical rib; pcdl; posterior centrodiapophyseal lamina; podl, postzygodiapophyseal lamina; poz, postzygapophysis; prdl, prezygodiapophyseal lamina; spol, spinopostzygapophyseal lamina; tpol, interpostzygapophyseal lamina. Scaled to the same posterior cotyle height.



PeerJ Reviewing Manuscript

Figure 92

Posterior cervical vertebra of *Barosaurus lentus* YPM 429

Figure 92: Posterior cervical vertebra of *Barosaurus lentus* YPM 429 in right lateral view, illustrating the short horizontal accessory lamina within the spinodiapophyseal fossa (C187-1), the anteriorly bifurcated posterior centrodiapophyseal lamina (C188-1), and the anteriorly restricted postzygapophyses (C200-1). Abb.: cpol, centropostzygapophyseal lamina; pap, parapophysis; podl, postzygodiapophyseal lamina; prdl, prezygodiapophyseal lamina; prz, prezygapophysis; pvf, posteroventral flanges; spol, spinopostzygapophyseal lamina; sprl, spinoprezygapophyseal lamina. Scale bar = 10 cm.

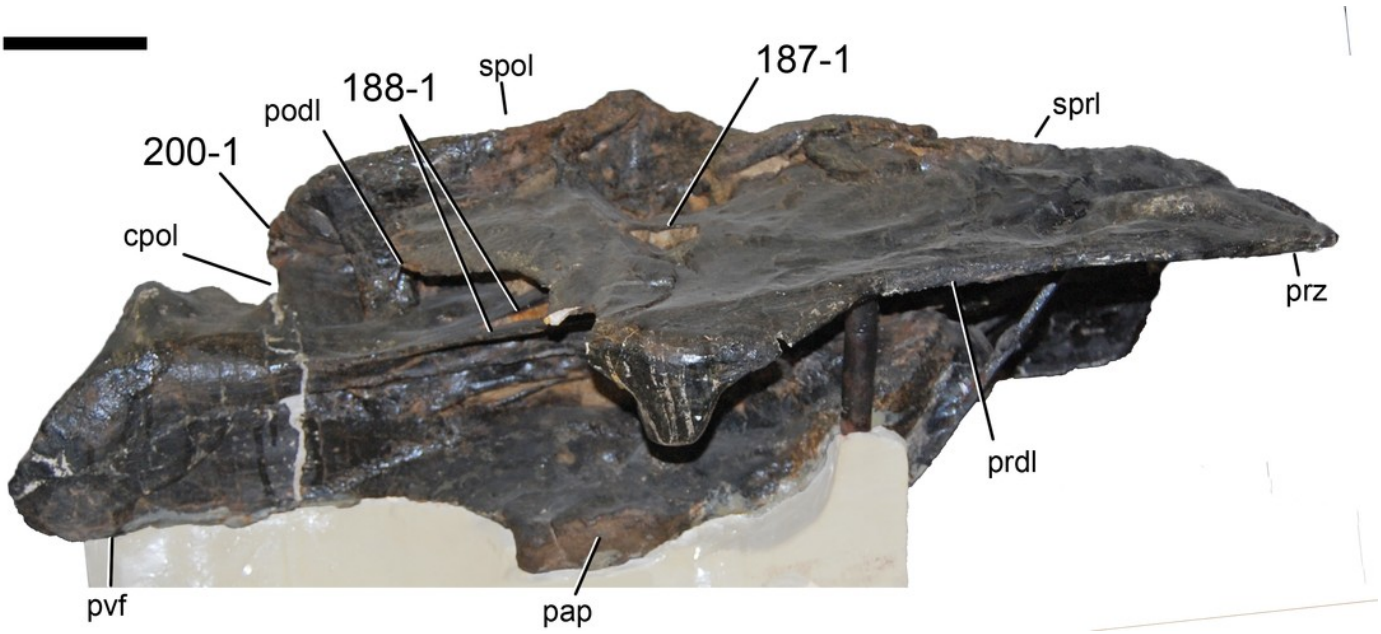


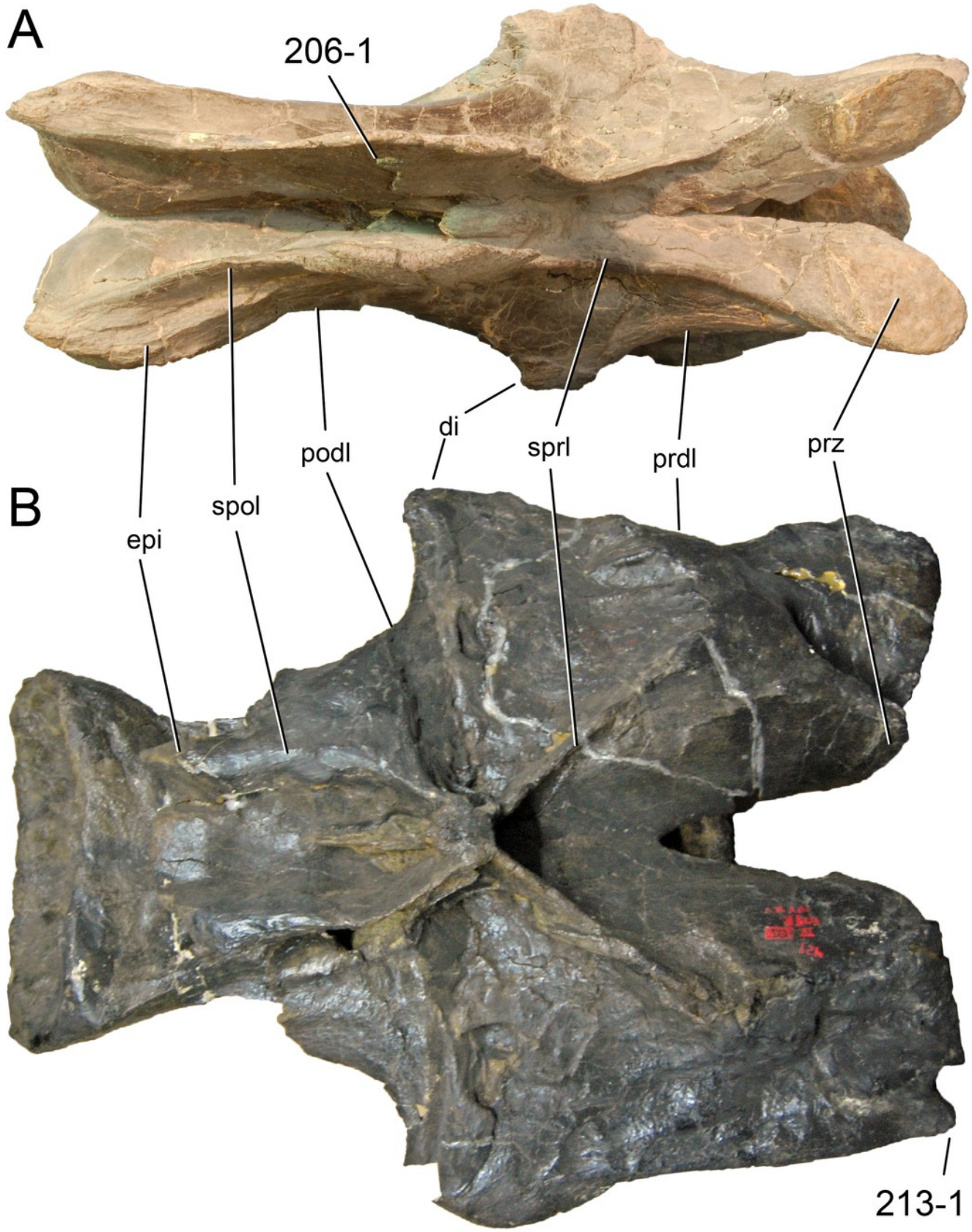
Figure 93

Diplodocine posterior cervical vertebrae

Figure 93: Posterior cervical vertebrae of *Kaatedocus siberi* SMA 0004 (A), and *Barosaurus lentus* YPM 429 (B) in dorsal view. Note the dorsoventral ridge on the medial side of the metapophysis (A; C206-1) and the anterior projection lateral to the prezygapophyseal facet (B; C213-1). Abb.: di, diapophysis; epi, epipophysis; podl, postzygodiapophyseal lamina; prdl, prezygodiapophyseal lamina; prz, prezygapophysis; spol, spinopostzygapophyseal lamina; sprl, spinoprezygapophyseal lamina. Scaled to the same total length.

PeerJ Reviewing Manuscript

PeerJ Reviewing Manuscript



PeerJ Reviewing Manuscript

Figure 94

Dorsal vertebra 1 of diplodocids

Figure 94: Dorsal vertebra 1 of *Apatosaurus louisae* CM 3018 (A; modified from Gilmore, 1936), and *Diplodocus carnegii* CM 84 (B; modified from Hatcher, 1901) in left and right lateral view, respectively. Note the roughened prdl (B; C208-1), and the different location of the pleurocoels (C240). Abb.: cpol, centropostzygapophyseal lamina; di, diapophysis; pap, parapophysis; pcdl; posterior centrodiapophyseal lamina; pl, pleurocoel; poz, postzygapophysis; spol, spinopostzygapophyseal lamina. Scaled to same posterior cotyle height.

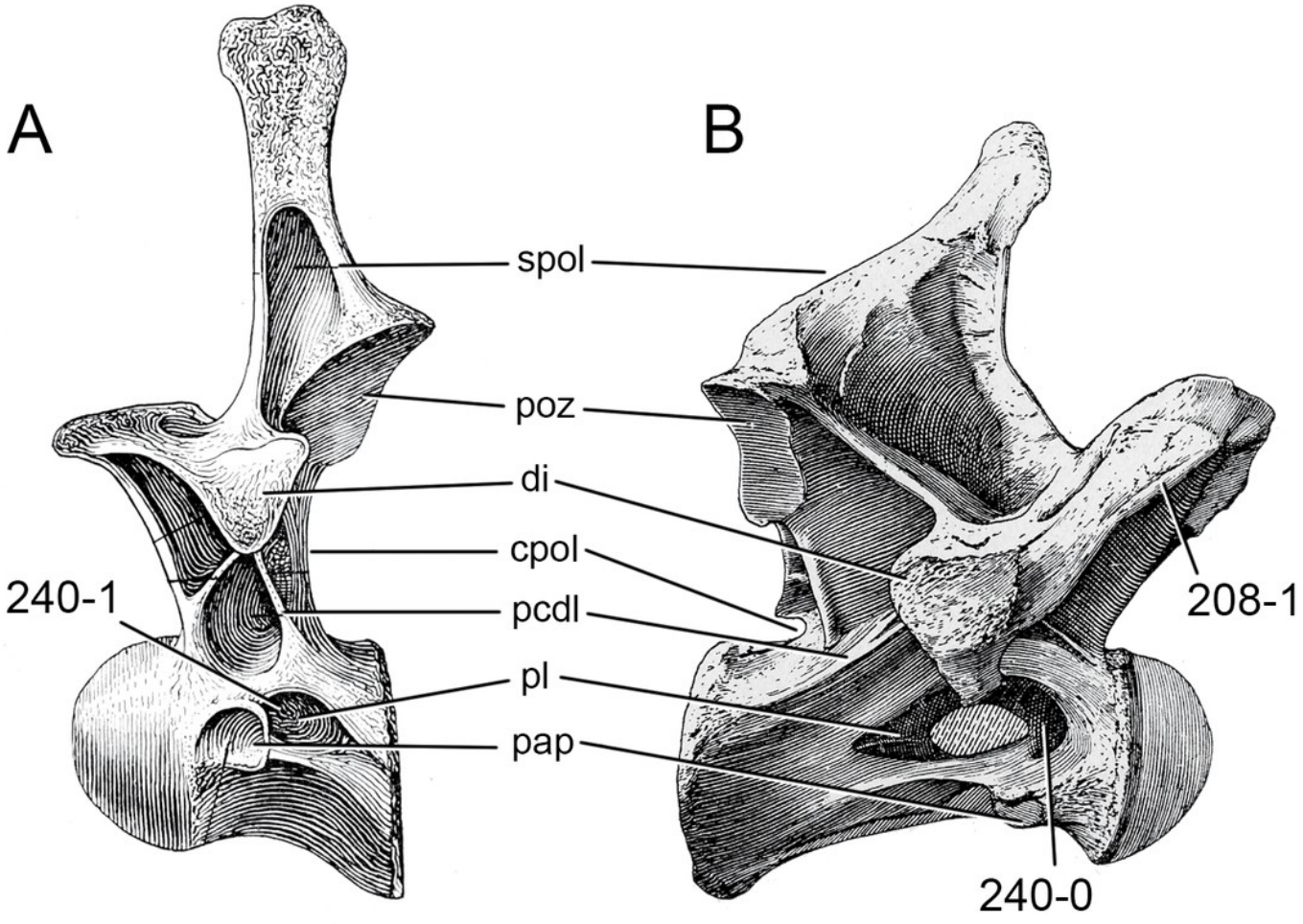
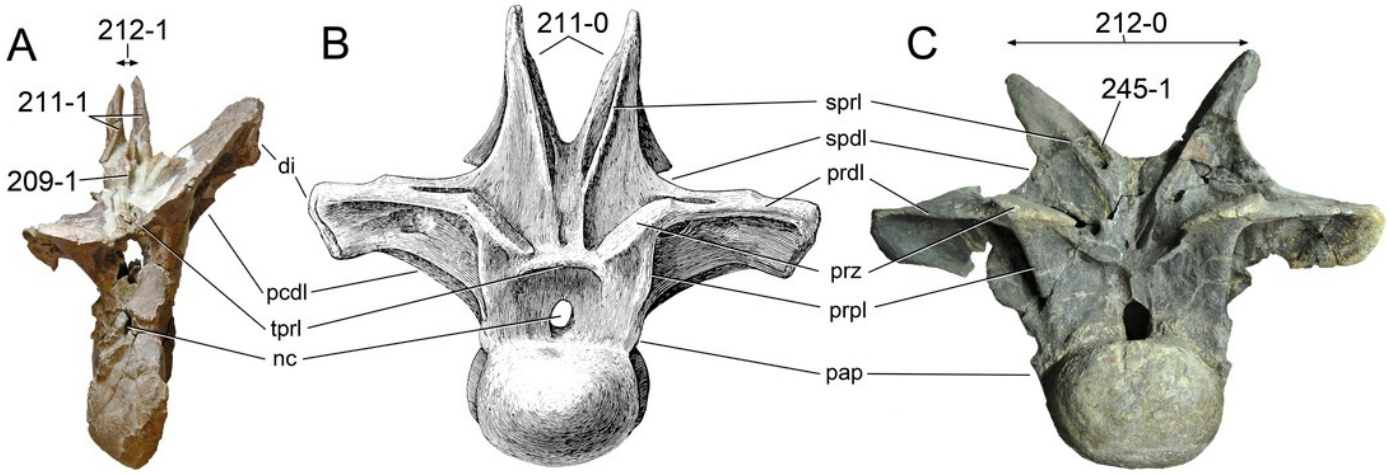


Figure 95

Flagellicaudatan anterior dorsal vertebrae

Figure 95: Anterior dorsal vertebrae of *Suuwassea emilieae* ANS 21122 (A), '*Apatosaurus*' *parvus* UW 15556 (B; modified from Gilmore, 1936), and *Apatosaurus ajax* YPM 1860 (C) in anterior view. Note the prespinal lamina (A and C; C209-1), the diverging (B; C211-0) or parallel neural spines (A; C211-1), the wide (C; C212-0) or narrow (A; C212-1) distance between the spine tops, and the ridge on the medial side of the neural spine (C; C245-1). Abb.: di, diapophysis; nc, neural canal; pap, parapophysis; pcdl; posterior centrodiapophyseal lamina; prdl, prezygodiapophyseal lamina; prpl, prezygoparapophyseal lamina; prz, prezygapophysis; sprl, spinoprezygapophyseal lamina; tprl, interprezygapophyseal lamina. Scaled to same anterior condyle height.



PeerJ Reviewing Manuscript

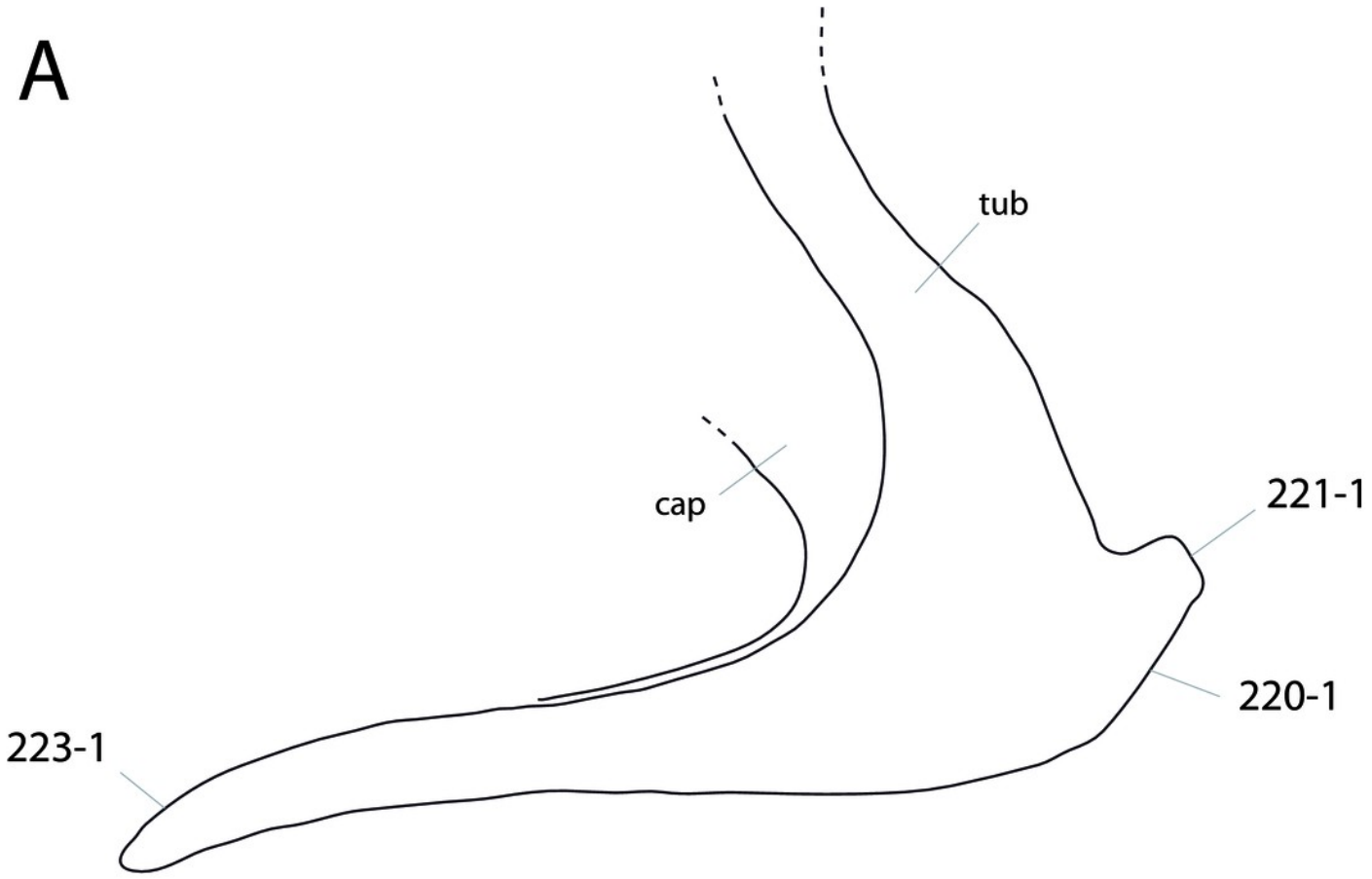
Figure 96

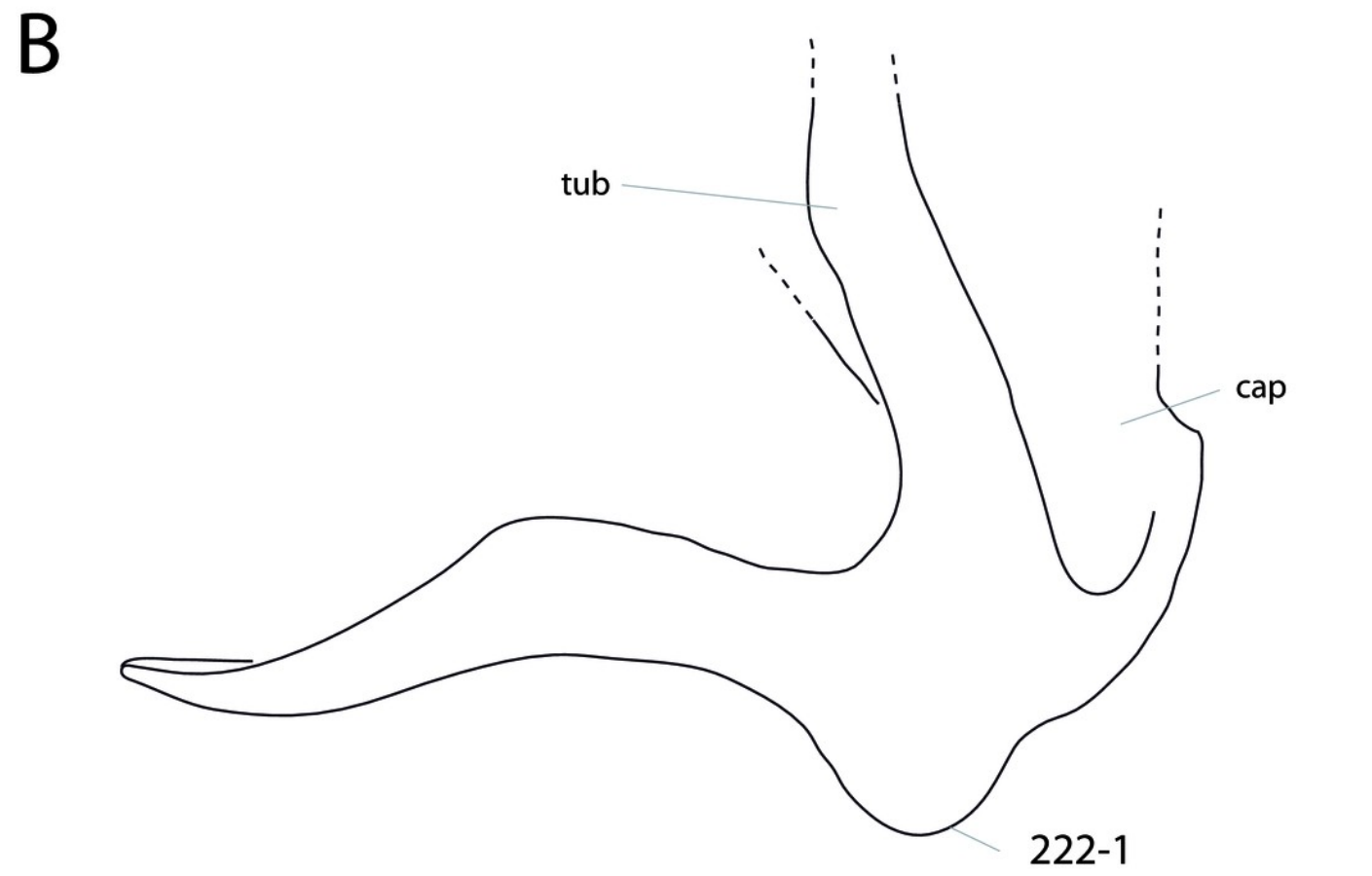
Apatosaurine posterior cervical ribs

Figure 96: Posterior cervical ribs of '*Apatosaurus*' *parvus* UW 15556 (A; after Gilmore, 1936) and *A. louisae* CM 3018 (B; after Gilmore, 1936) in right lateral view (B inverted). Note the short, reduced anterior projection (A; C220-1), the pointed anterior process (A; C221-1), the ventrolateral process (B; C222-1), and the downwards curving posterior process (A; C223-1). Abb.: cap, capitulum; tub, tuberculum. Scaled to same length.

PeerJ Reviewing Manuscript

PeerJ Reviewing Manuscript





PeerJ Reviewing Manuscript

Figure 97

Dorsal vertebra 3 of eusauropods

Figure 97: Dorsal vertebra 3 of *Shunosaurus lii* ZDM T5401 (A; modified from Zhang, 1988), and '*Apatosaurus*' *parvus* UW 15556 (B; modified from Gilmore, 1936) in left (A) and right (B) lateral view. Note the slightly concave lateral surface of the centrum in *Shunosaurus* (A; C227-0), in contrast to the well-defined pneumatopore in UW 15556 (B; C227-1), and the different locations of the parapophyses (C246). Abb.: cpol, centropostzygapophyseal lamina; di, diapophysis; pcdl, posterior centrodiapophyseal lamina; poz, postzygapophysis. Scaled to the same total vertebral height.

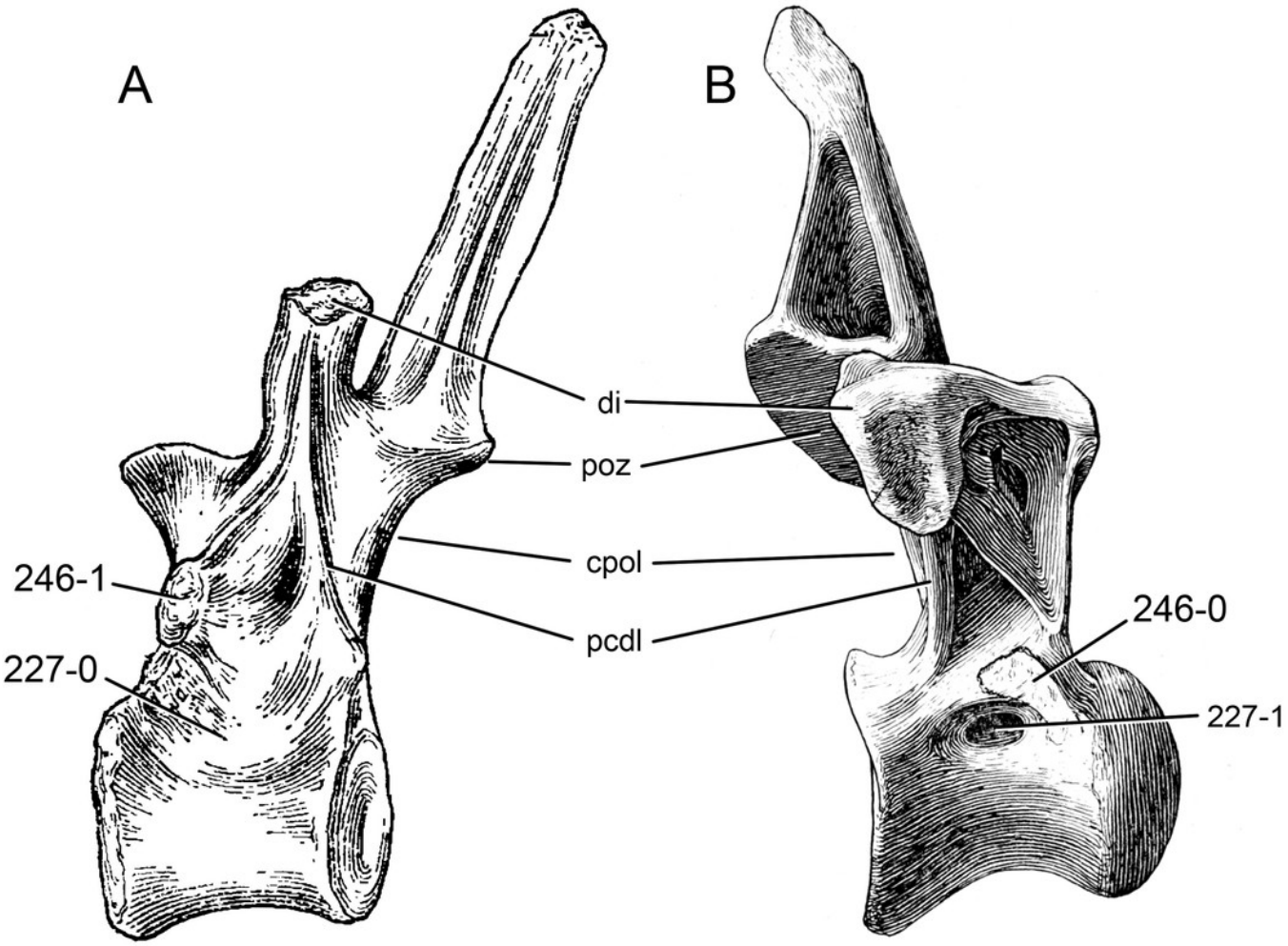


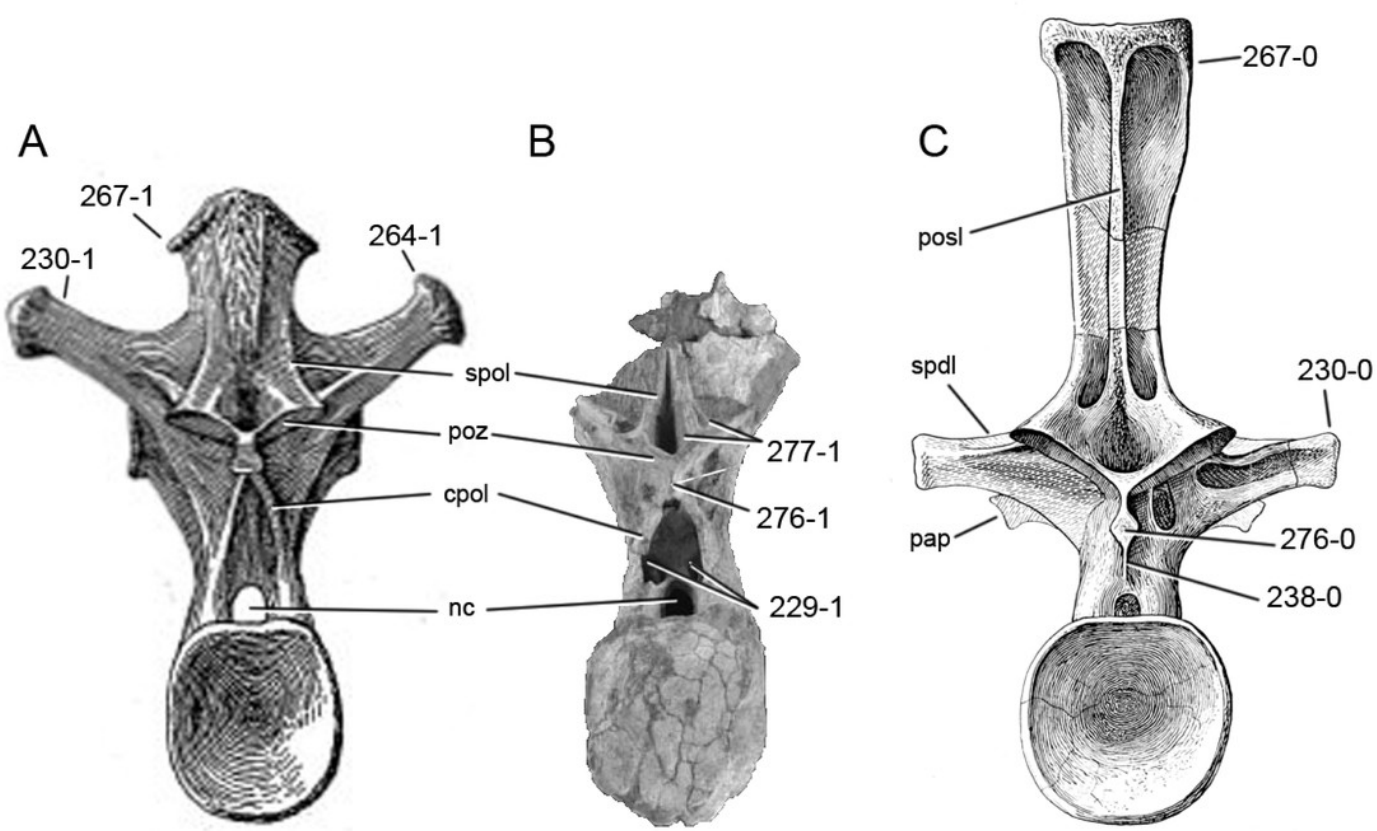
Figure 98

Diplodocoid posterior dorsal vertebrae

Figure 98: Posterior dorsal vertebrae of *Haplocanthosaurus priscus* CM 572 (A; modified from Hatcher, 1903), *Demandasaurus darwini* MDS-RVII 798 (B; modified from Torcida Fernández-Baldor et al., 2011), and *Apatosaurus louisae* CM 3018 (C; modified from Gilmore, 1936) in posterior view. Note the paired pneumatic foramen dorsolateral to the neural canal in *Demandasaurus* (B; C229-1), the different orientations of the diapophyses in *Haplocanthosaurus* (A; C230-1) and *Apatosaurus* (C; C230-0), the single lamina that supports the hyposphene from below (C; C238-0), the dorsal spur on the tip of the transverse process (A; C264-1), the small triangular lateral projections at the spine top (A; C267-1), or their absence (C; C267-0), the rhomboid (C; C276-0) in contrast to laminar (B; C276-1) hyposphene, and the ventrally forked spol (B; C277-1). Abb.: cpol, centropostzygapophyseal lamina; nc, neural canal; pap, parapophysis; posl, postspinal lamina; poz, postzygapophysis; spdl, spinodiapophyseal lamina; spol, spinopostzygapophyseal lamina. Scaled to same posterior centrum height.

PeerJ Reviewing Manuscript

PeerJ Reviewing Manuscript

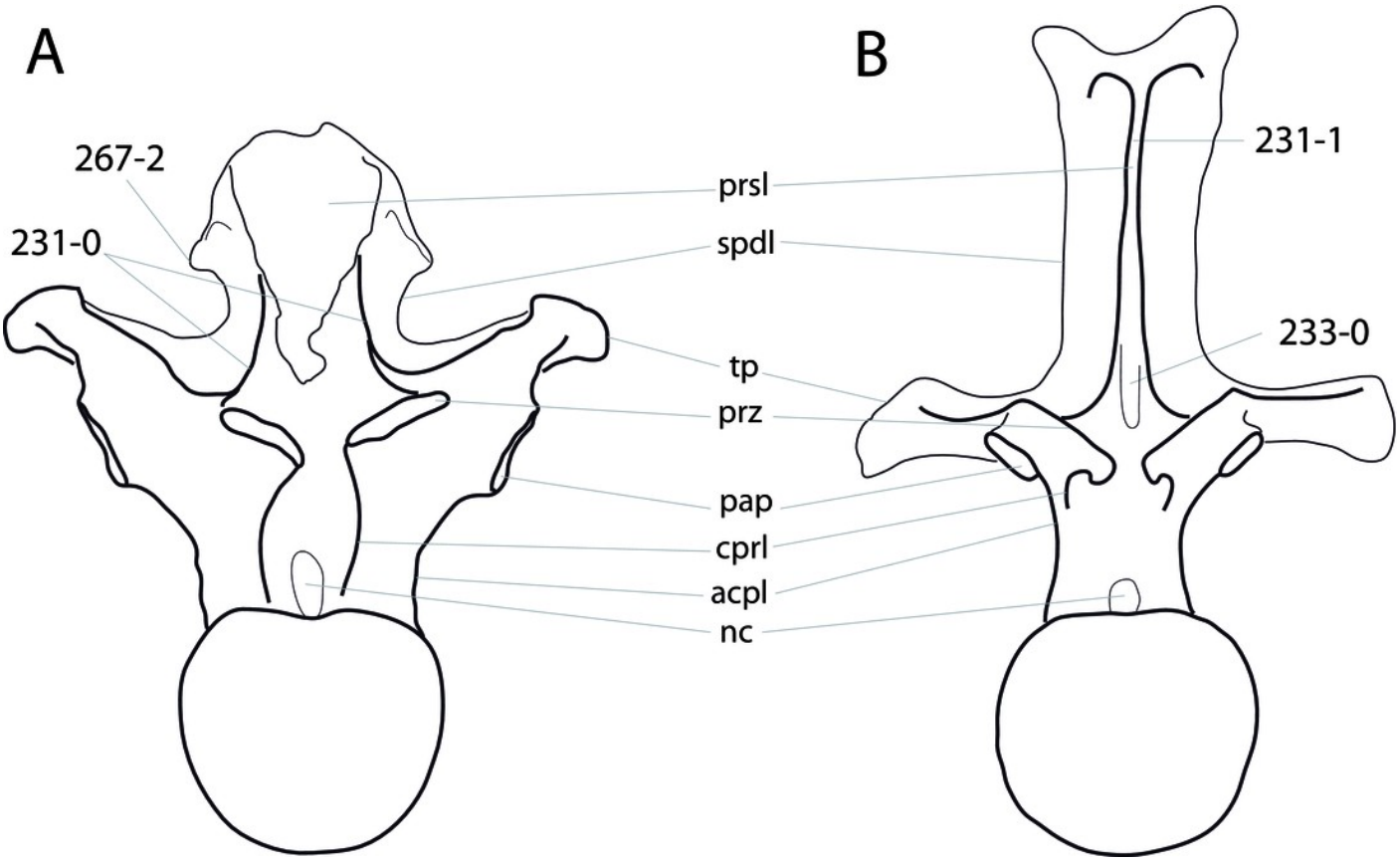


PeerJ Reviewing Manuscript

Figure 99

Dorsal vertebra 8 of neosauropods

Figure 99: Dorsal vertebra 8 of *Camarasaurus supremus* AMNH 5760 (A; traced from Osborn and Mook, 1921) and *Apatosaurus louisae* CM 3018 (B; traced from Gilmore, 1936) in anterior view. Note the separated (A; C231-0) or dorsally united spinoprezygapophyseal laminae (B; C231-1), the fossa between them (B; C233-0), and the triangular processes of the neural spine, that project further than the zygapophyses (A; C267-2). Abb.: acpl, anterior centroparapophyseal lamina; cprl, centroprezygapophyseal lamina; nc, neural canal; pap, parapophysis; prsl, prespinal lamina; prz, prezygapophysis; spdl, spinodiapophyseal lamina; tp, transverse process. Scaled to same anterior condyle height.



PeerJ Reviewing Manuscript

Figure 100

Diplodocimorph dorsal neural arches

Figure 100: Dorsal neural arches of *Diplodocus carnegii* CM 84 (A; traced from Hatcher, 1901) and *Nopcsaspondylus alarconensis* holotype specimen (B; traced from Nopcsa, 1902) in anterior view. Note the festooned spdl typical for rebbachisaurids (B; C232-1), in contrast to the plesiomorphic state (A; C232-0), and the notched (A; C281-1), or straight to convex spine summits (B; C281-0). Abb.: cprl, centroprezygapophyseal lamina; prdl, prezygodiapophyseal lamina; prsl, prespinal lamina; tp, transverse process. Not to scale.

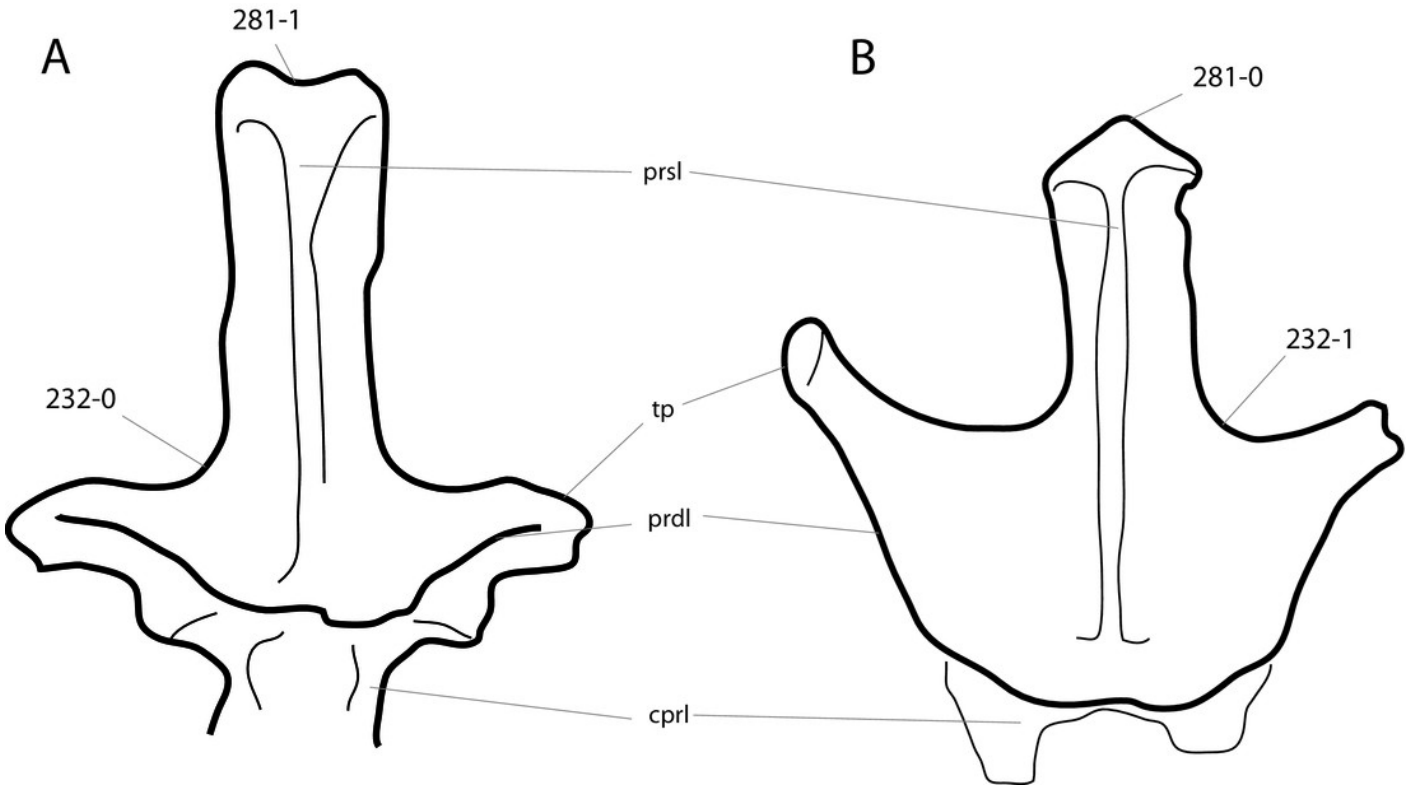


Figure 101

Eusauropod posterior dorsal vertebrae

Figure 101: Posterior dorsal vertebrae of *Losillasaurus giganteus* MCNV Lo-11 (A), and *Apatosaurus louisae* CM 3018 (B; modified from Gilmore, 1936) in posterior view. Note the concave dorsal end of the posl (A; C234-1), the horizontal (A; C275-0), instead of angled (B; C275-1) postzygapophyseal facets, and the medial spinopostzygapophyseal lamina (B; C278-1). Abb.: cprl, centroprezygapophyseal lamina; hys, hyposphene; lspol, lateral spinopostzygapophyseal lamina; posl, postspinal lamina; poz, postzygapophysis; spdl, spinodiapophyseal lamina. Scaled to same posterior cotyle height.

PeerJ Reviewing Manuscript

PeerJ Reviewing Manuscript

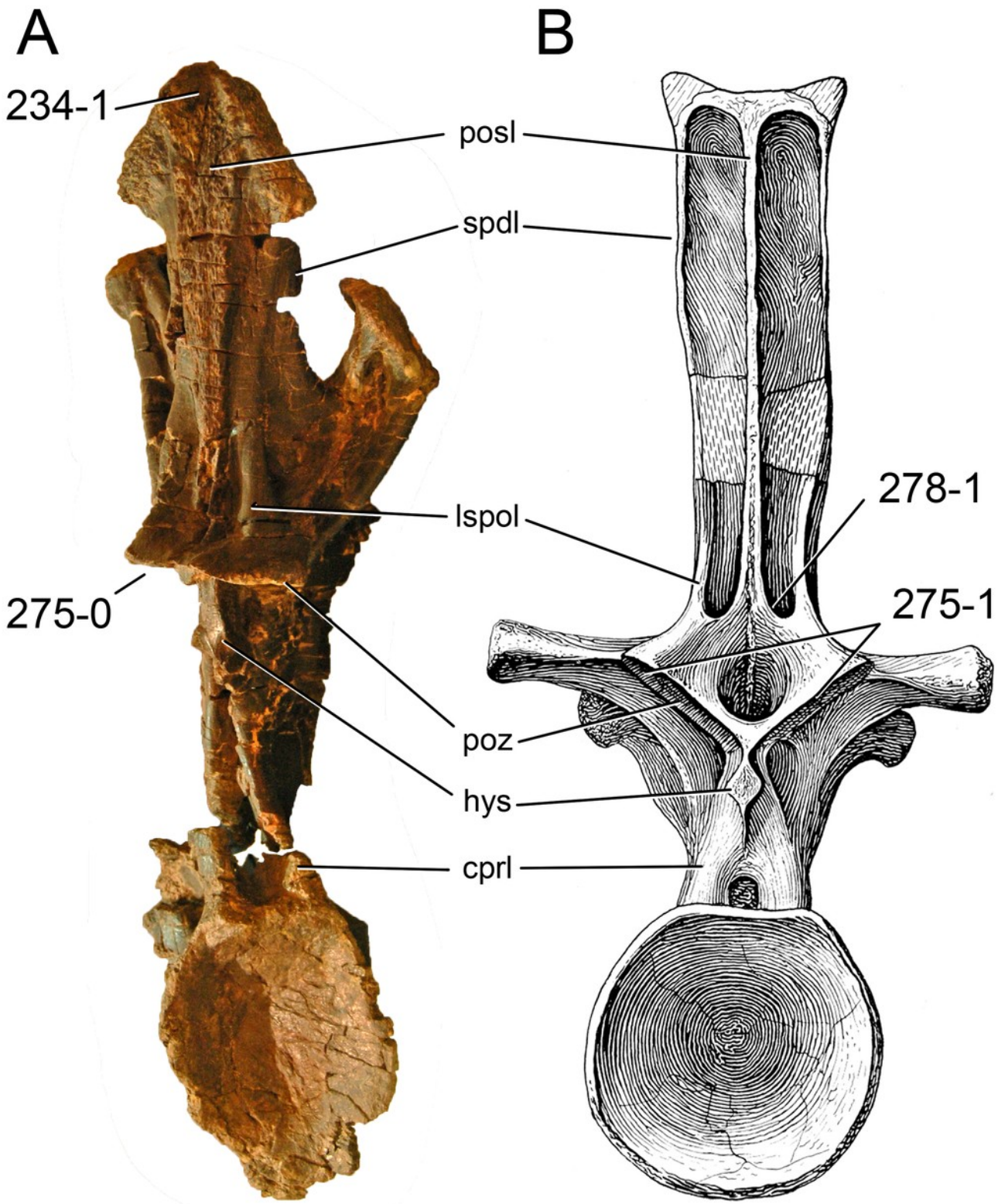


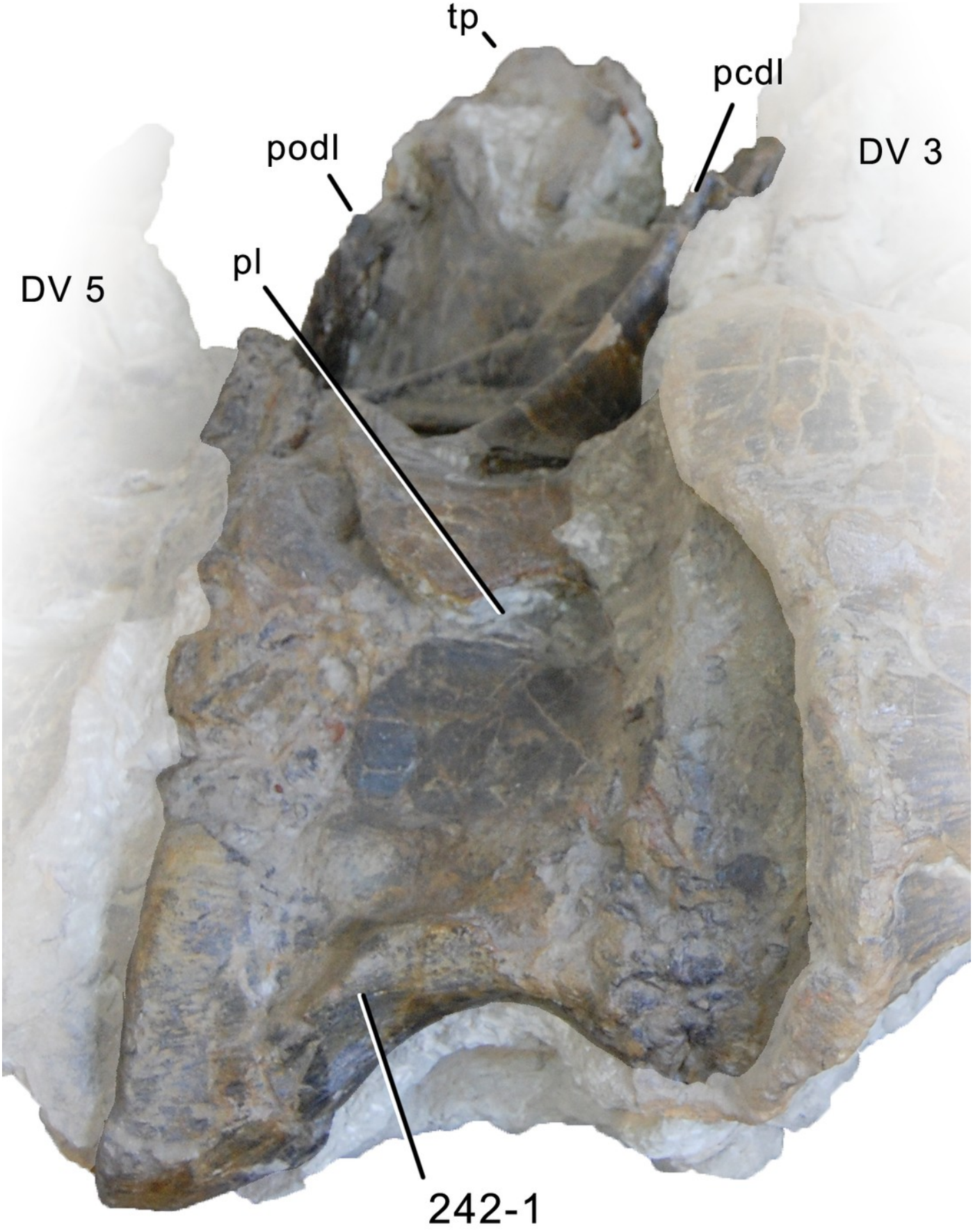
Figure 102

Dorsal vertebra 4 of *Dinheirosaurus lourinhanensis* ML 414

Figure 102: Dorsal vertebra 4 of *Dinheirosaurus lourinhanensis* ML 414 in ventral view, illustrating the ventral keel (C242-1) in anterior dorsal vertebrae. Abb.: DV, dorsal vertebra; pcdl, posterior centrodiapophyseal lamina; pl, pleurocoel; podl, postzygodiapophyseal lamina; tp, transverse process.

PeerJ Reviewing Manuscript

PeerJ Reviewing Manuscript



PeerJ Reviewing Manuscript

Figure 103

Dorsal vertebra 1 of apatosaurines

Figure 103: Dorsal vertebra 1 of *Apatosaurus louisae* CM 3018 (A) and '*Apatosaurus*' *parvus* UW 15556 (B; both traced from Gilmore, 1936) in posterior view. Note the different positions of the transverse processes (high, A, C243-0; low, B, C243-1), and the varying width of the base of the bifurcated spines (wide, A, C244-0; narrow, B, C244-1). Abb.: di, diapophysis; pcdl, posterior centrodiapophyseal lamina; podl, postzygodiapophyseal lamina; poz, postzygapophysis; prz, prezygapophysis. Scaled to same posterior cotyle height.

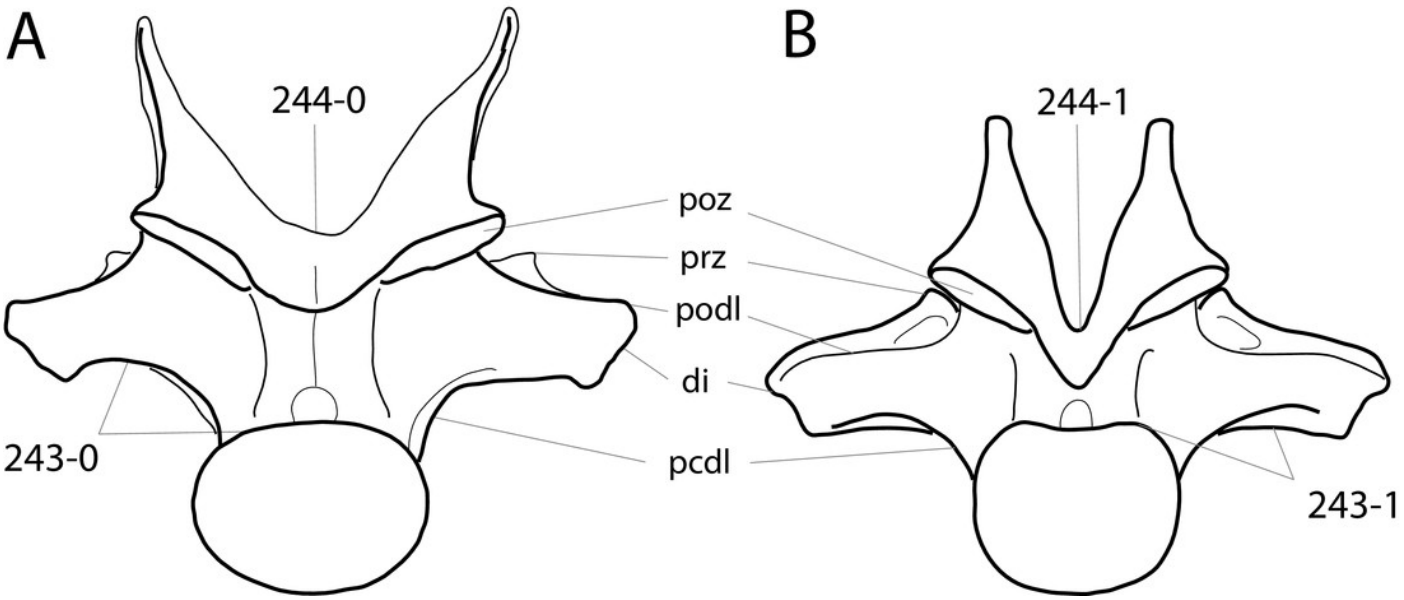


Figure 104

Diplodocine mid-dorsal vertebrae

Figure 104: Mid-dorsal vertebrae of *Dinheirosaurus lourinhanensis* ML 414 (A) and *Galeamopus* [redacted] SMA 0011 (B) in lateral view. Note the pleurocoels that are entirely situated on the centrum (A; C247-0), or invade the neural arch (B; C247-1), the accessory spinal lamina connecting to the junction of spol and spdl (A; C251-1), the vertical lamina subdividing the pleurocoel (A; C253-1), the anteriorly displaced parapophysis (A; C256-1) in contrast to its usual position above the anterior edge (B; C256-0), and the horizontal accessory lamina connecting the hyposphene with the pcdl (A; C260-1). Abb.: cpol, centropostzygapophyseal lamina; pcdl, posterior centrodiapophyseal lamina; pcpl, posterior centroparapophyseal lamina; podl, postzygodiapophyseal lamina; spol, spinopostzygapophyseal lamina. Scaled to same vertebral height.

PeerJ Reviewing Manuscript

PeerJ Reviewing Manuscript

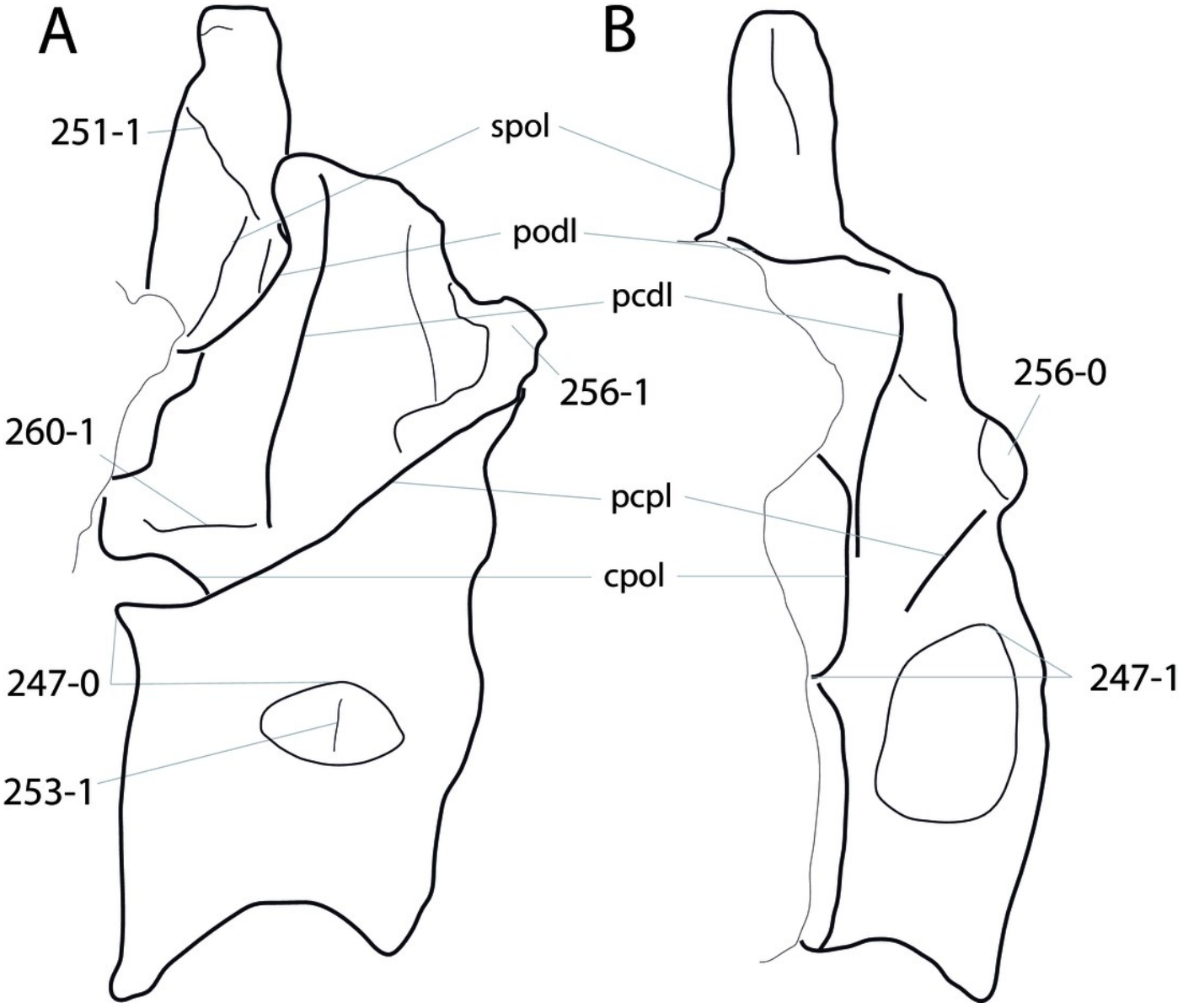


Figure 105

Diplodocid posterior dorsal vertebrae

Figure 105: Posterior dorsal vertebrae of *Apatosaurus louisae* CM 3018 (A; traced from Gilmore, 1936) and *Supersaurus vivianae* BYU 9044 (B; traced from Jensen, 1985) in left (A) and right (B) lateral view. Note the prpl (A; C255-1), the anteriorly displaced parapophysis (B; C256-1), the acpl (A; C257-1), the pcpl (B; C258-1), the lateral branch of the cpol (B; C261-1), the pronounced opisthocoely (B; C270-2), and the anteriorly inclined base of the neural spine (A; C280-1). Abb.: cpol, centropostzygapophyseal lamina; hys, hyposphene; pl, pleurocoel; posl, postspinal lamina; poz, postzygapophysis; spdl, spinodiapophyseal lamina. Scaled to same posterior cotyle height.

PeerJ Reviewing Manuscript

PeerJ Reviewing Manuscript

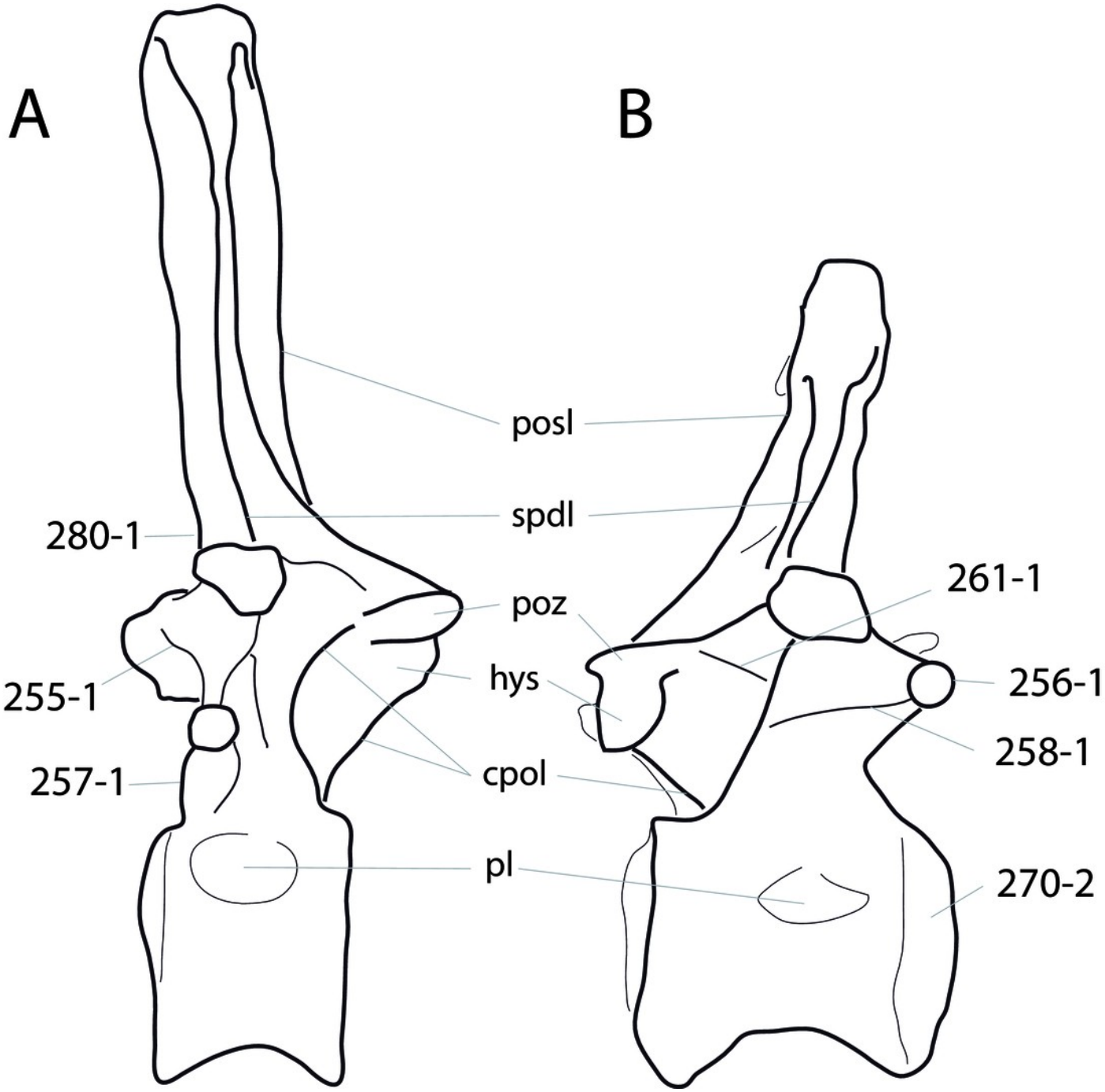


Figure 106

Neosauropod posterior dorsal vertebrae

Figure 106: Posterior dorsal vertebrae of *Giraffatitan brancai* MB.R.3822 (A), *Apatosaurus louisae* CM 3018 (B; traced from Gilmore, 1936), and *Diplodocus carnegii* CM 84 (C; traced from Hatcher, 1901) in right lateral view. Note the double pcpl (C; C258-2), the accessory lamina in the parapophyseal centrodiapophyseal fossa (C; C259-1), the accessory lamina connecting the hyposphene with the pcdl (C; C260-1), the infradiapophyseal pneumatic foramen (A; C262-1), the dorsally tapering neural spine (A; C265-1), the different shapes of the pleurocoels (C271), and the ventrally open parapophyseal, centrodiapophyseal fossa (B; C273-0). Abb.: cprl, centroprezygapophyseal lamina; lspol, lateral spinopostzygapophyseal lamina; posl, postspinal lamina; poz, postzygapophysis; prsl, prespinal lamina; prz, prezygapophysis; spdl, spinodiapophyseal lamina; tp, transverse process. Scaled to same total height.

PeerJ Reviewing Manuscript

PeerJ Reviewing Manuscript

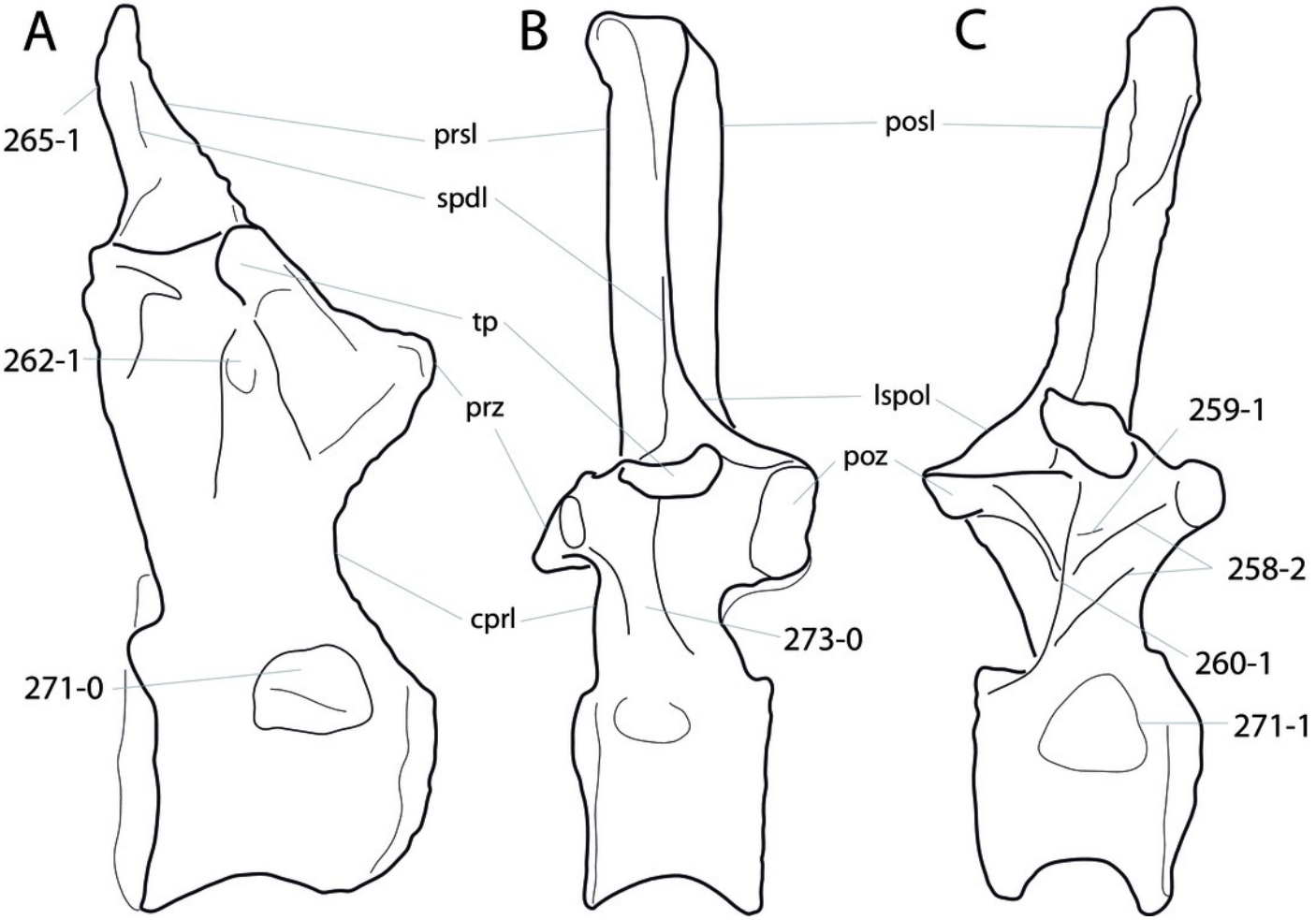


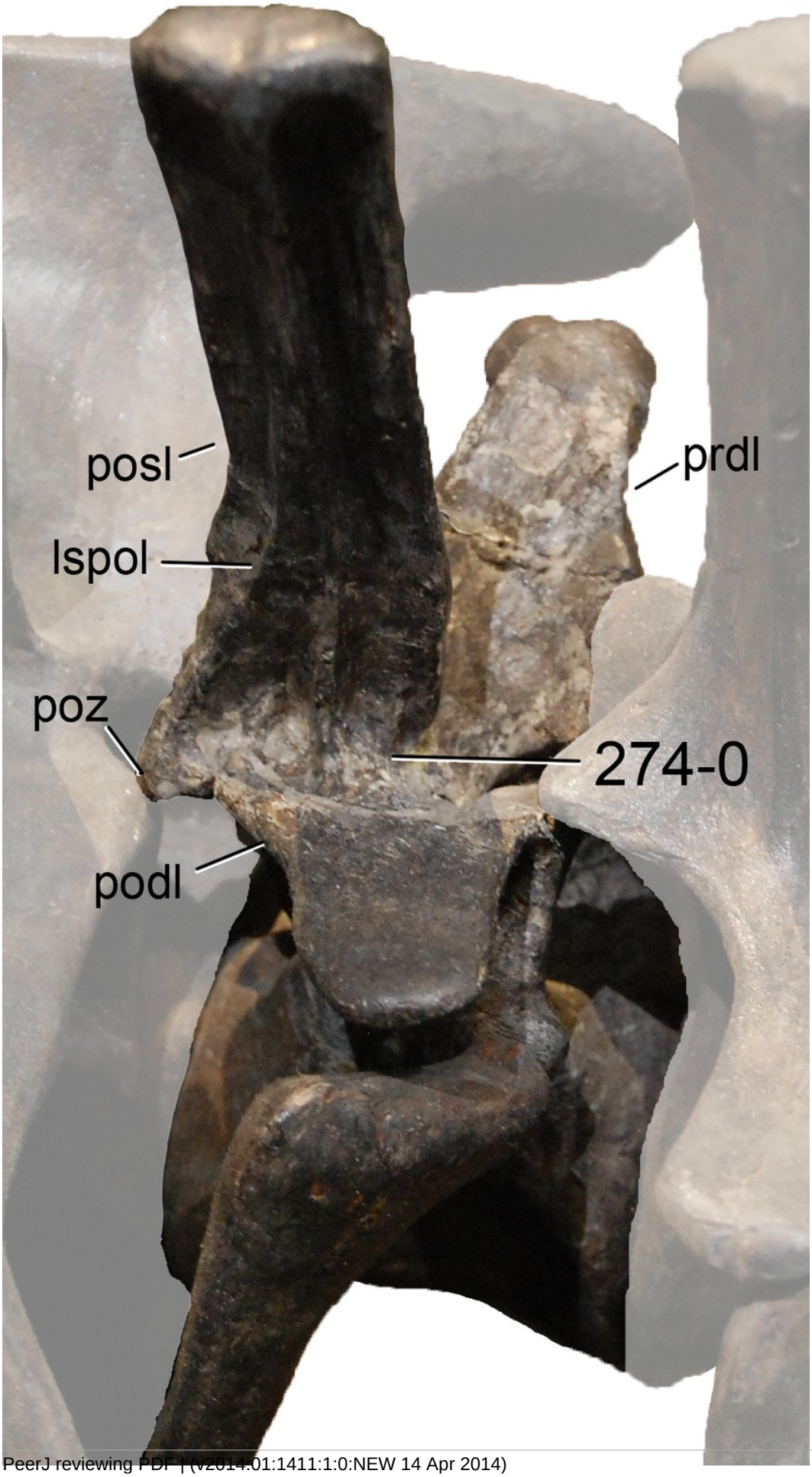
Figure 107

Posterior dorsal vertebra of *Elosaurus parvus* CM 566

Figure 107: Posterior dorsal vertebra of *Elosaurus parvus* CM 566 in lateral anterodorsal view. Note the greatly reduced spinoprezygapophyseal lamina, which does not reach the prezygapophysis (C274-0). Only the base of the neural arch is preserved (see Peterson and Gilmore, 1902). Abb.: lspol, lateral spinopostzygapophyseal lamina; podl, postzygodiapophyseal lamina; posl, postspinal lamina; poz, postzygapophysis; prdl, prezygodiapophyseal lamina.

PeerJ Reviewing Manuscript

PeerJ Reviewing Manuscript



PeerJ Reviewing Manuscript

Figure 108

Flagellicaudatan dorsal rib heads

Figure 108: Dorsal rib heads of *Suuwassea emilieae* ANS 21122 (A; modified from Harris, 2006b), *Apatosaurus louisae* CM 3018 (B; modified from Gilmore, 1936) and *Barosaurus lentus* AMNH 6341 (C, fragment) in anterior (A, B) and posterior (C) view. Note the transverse ridge (C; C283-1), the pneumatic foramen (B; C284-1), and two of three different orientations of the tuberculum in respect to the rib shaft (C285). Grey lines in C indicate the continuation of the rib if complete. Abb.: cap, capitulum; tub, tuberculum. Not to scale.

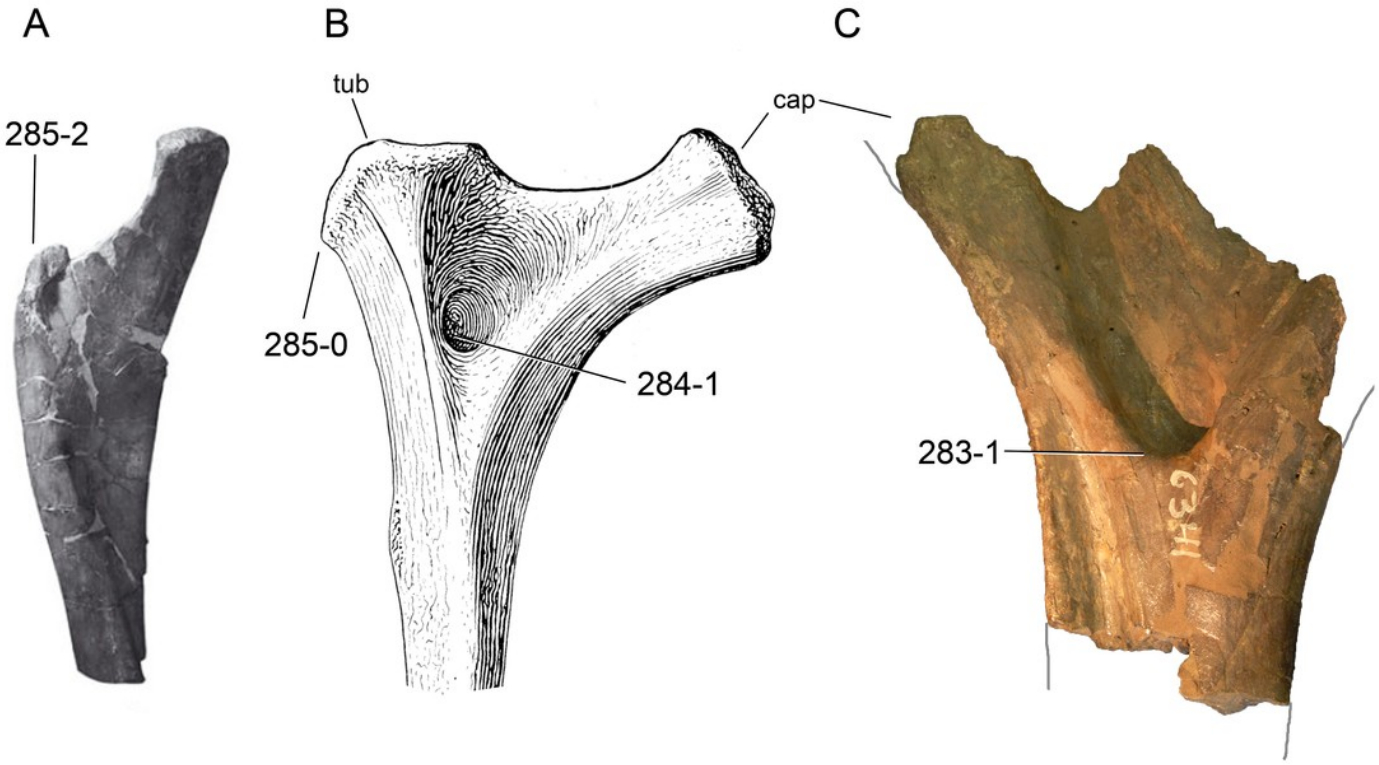


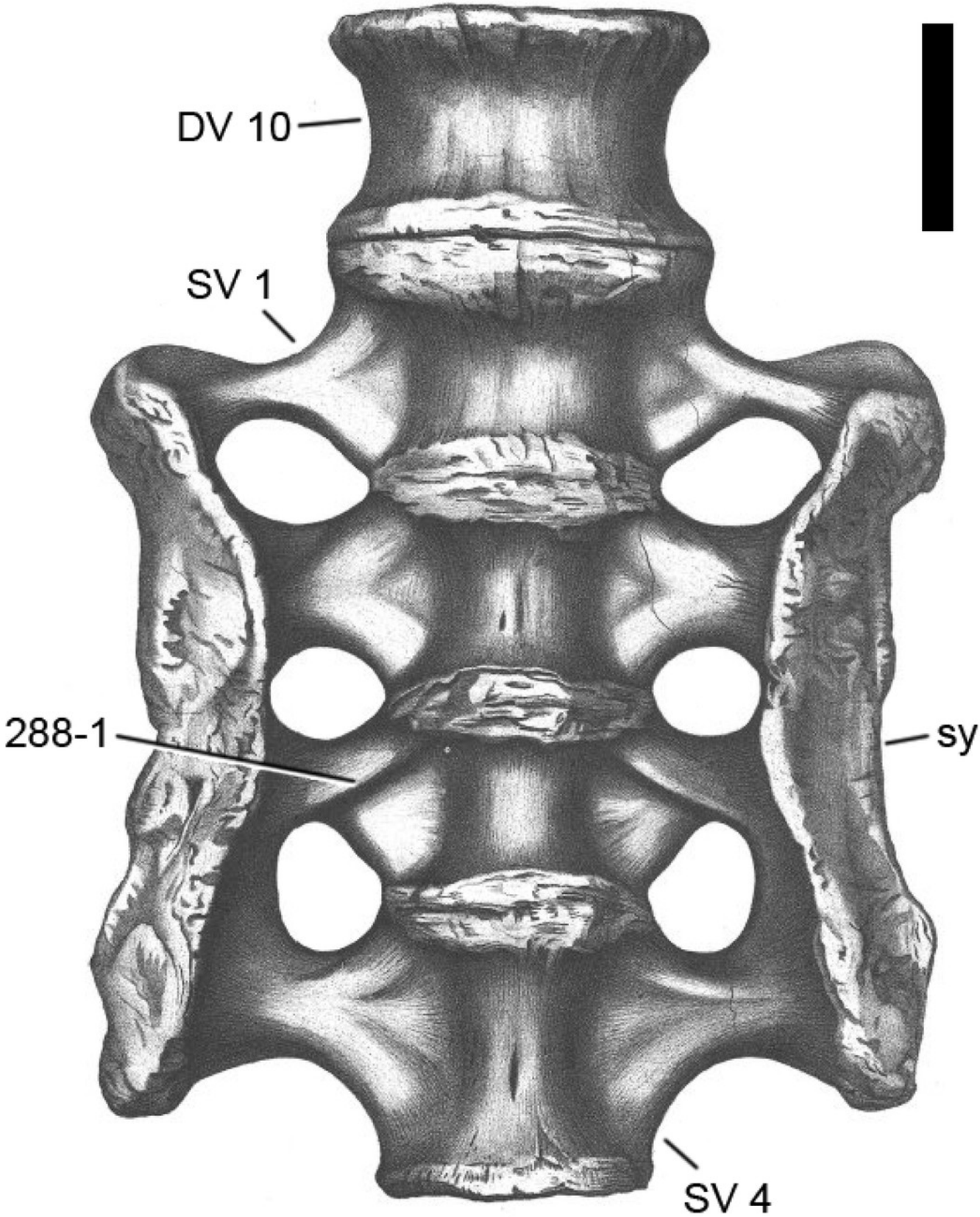
Figure 109

Sacrum of *'Brontosaurus' amplus* YPM 1981

Figure 109: Sacrum of *'Brontosaurus' amplus* YPM 1981 in ventral view (modified from Ostrom and McIntosh 1966), illustrating the oblique ridge on sacral rib III (C288-1). Abb.: DV, dorsal vertebra; SV, sacral vertebra; sy, sacricostal yoke. Scale bar = 20 cm.

PeerJ Reviewing Manuscript

PeerJ Reviewing Manuscript



PeerJ Reviewing Manuscript

Figure 110

Diplodocid sacra

Figure 110: Sacra of '*Apatosaurus*' *parvus* UW 15556 (A; modified from Hatcher, 1903) and *Diplodocus hallorum* AMNH 223 (B; modified from Osborn, 1899) in left lateral view. Note the flat (A; C289-0) instead of ornamented sacral neural spine top (B; C289-1), the spdl that extends ventrally to the diapophysis (A; C290-1), and the parallel (A; C291-0) in contrast to converging neural spines (B; C291-1). Abb.: DR, dorsal rib; il, ilium; SV, sacral vertebra. Scaled to the same height.

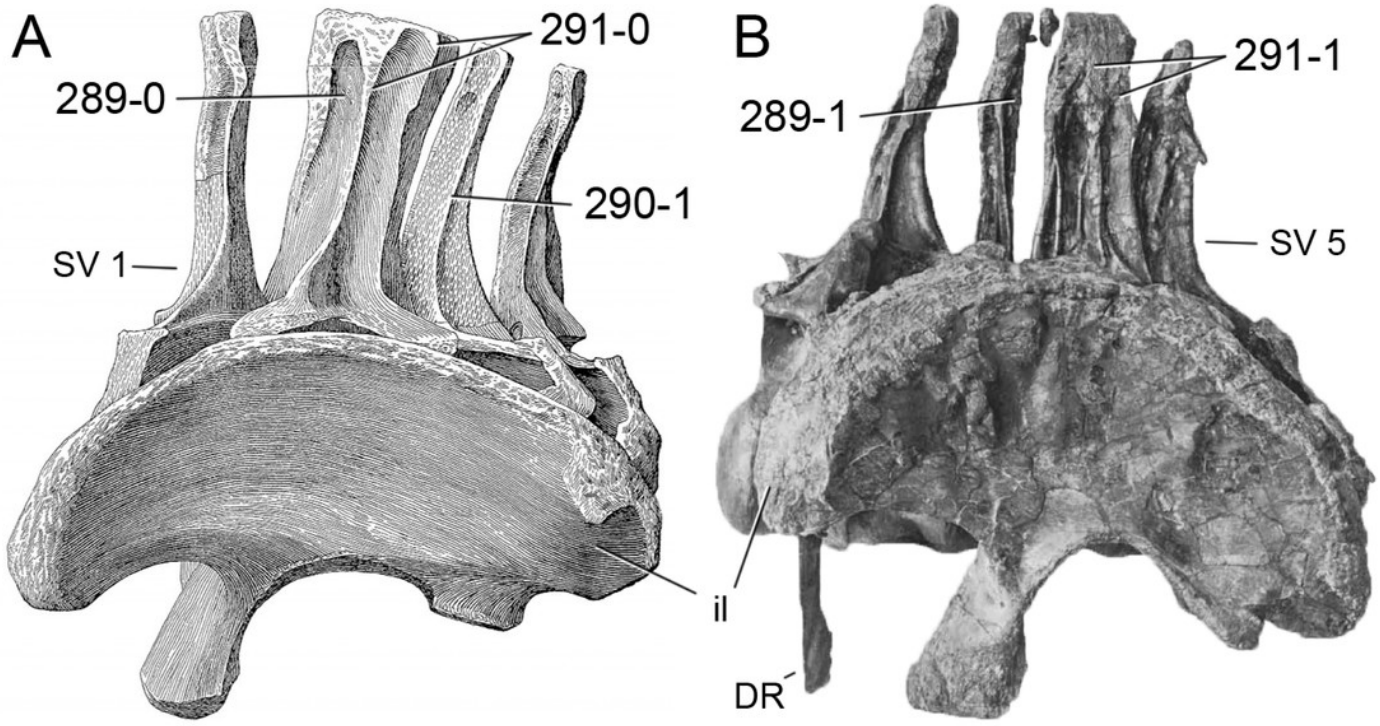


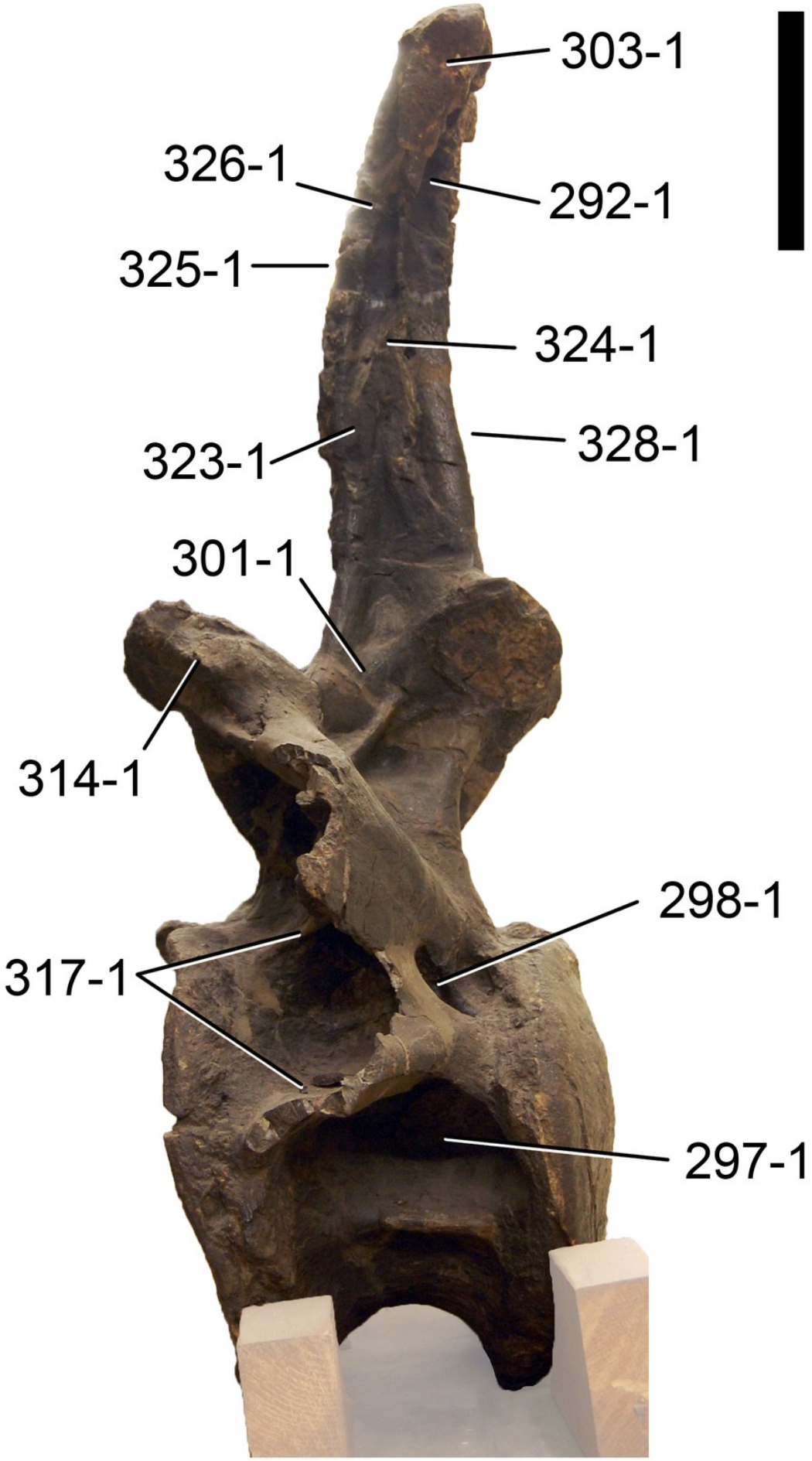
Figure 111

Anterior caudal vertebra of Diplodocus carnegii CM 94

Figure 111: Anterior caudal vertebra of Diplodocus carnegii CM 94 in left lateral view, illustrating various characters typical for the genus: a depression between the lateral spinal lamina and the postspinal lamina (C292-1), the large pleurocoel (C297-1), an additional pneumatic foramen posterodorsally in the caudal centrum (C298-1), the accessory lamina between pre- and postzygapophysis (C301-1), a dorsally widened lateral spinal lamina (C303-1), a pre-epipophysis (C311-1), the double anterior centrodiapophyseal lamina (C314-1), the distinct spinoprezygapophyseal lamina that extends onto the lateral surface of the spine (C318-1) and contacts the spinopostzygapophyseal lamina (C319-1), the presence of a prespinal lamina (C320-1) with a thickened anterior rim (C321-1), and the presence of a postspinal lamina (C323-1). Scale bar = 10 cm.

PeerJ Reviewing Manuscript

PeerJ Reviewing Manuscript



PeerJ Reviewing Manuscript

Figure 112

Diplodocimorph anterior caudal vertebrae

Figure 112: Anterior caudal vertebrae of *Demandasaurus darwini* MDS-RVII,610 (A; traced from Torica Fernandéz-Baldor et al., 2011), *Brontosaurus excelsus* YPM 1980 (B; traced from Ostrom and McIntosh, 1966), and *Diplodocus carnegii* CM 84 (C; traced from Hatcher, 1901) in anterior view. Note the lateral triangular processes (B; C293-1), the mostly rectangular outline of the spine (B; C294-0), the wing-like transverse processes (A; C299-1), the convex prezygapophyses (B; C310-1), the laterally (C; C312-0) or dorsally directed ventral surface of the transverse process (A; C312-1), the notched neural spine top (C; C326-1), the gradual (C; C328-0) or abrupt distal expansion of the spine (B; C328-1), and the foramen piercing the transverse process (B; C350-0). Abb.: prsl, prespinal lamina; prz, prezygapophysis; sprl, spinoprezygapophyseal lamina; tp, transverse process. Scaled to same total height.

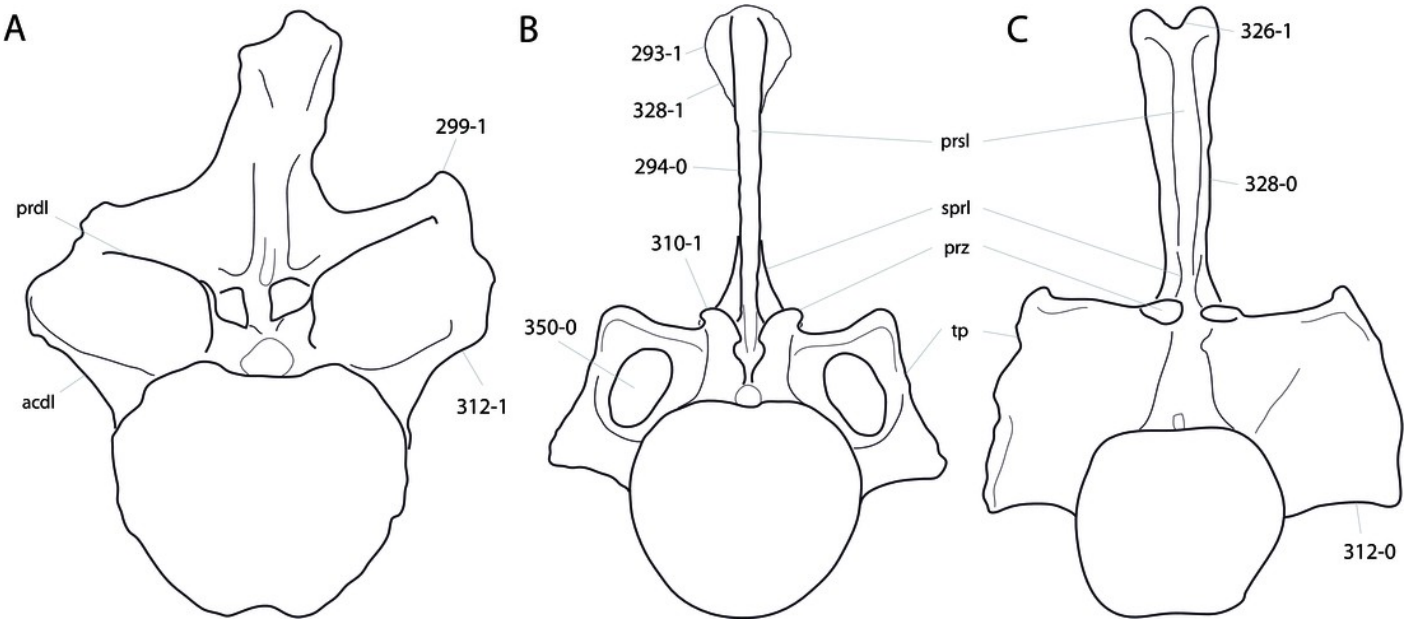
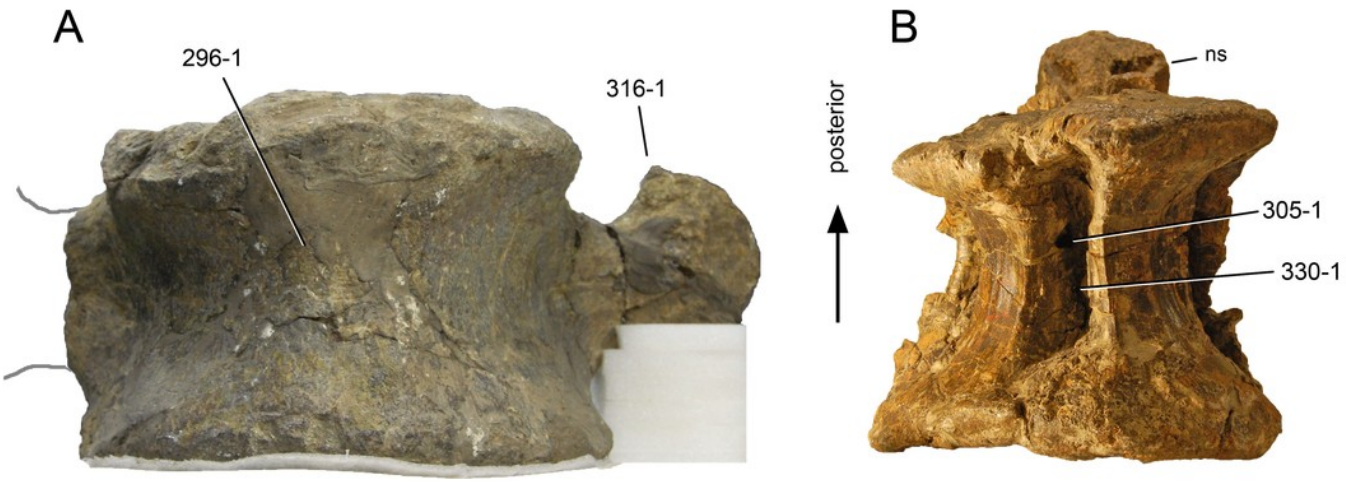


Figure 113

Diplodocid anterior caudal vertebrae

Figure 113: Anterior caudal vertebrae of *Apatosaurus ajax* YPM 1860 (A) and *Diplodocus* sp. DMNS 462 (B) in ventral view. Note the ventral keel (A; C296-1), the ventral foramen (B; C305-1) within the ventral longitudinal hollow (B; C330-1), and the anteroposteriorly expanded distal end of the transverse process (A; C316-1). Abb.: ns, neural spine. Scaled to same centrum length.



PeerJ Reviewing Manuscript

PeerJ Reviewing Manuscript

Figure 114

Flagellicaudatan anterior caudal vertebrae

Figure 114: Anterior caudal vertebrae of *Dicraeosaurus hansemanni* MB.R.3774 (A), *Apatosaurus* sp. NHMUK R.3211 (B), and *Barosaurus lentus* YPM 429 (C) in left lateral view. Note the reduced (B; C307-0) or large pneumatopores (C; C307-1), the distinct posterior centrodiapophyseal and postzygodiapophyseal laminae (C; C315-1), and the postspinal lamina that projects dorsally (A; C324-1). Abb.: prz, prezygapophysis; sprl, spinoprezygapophyseal lamina; tp, transverse process. Scaled to same posterior centrum height.

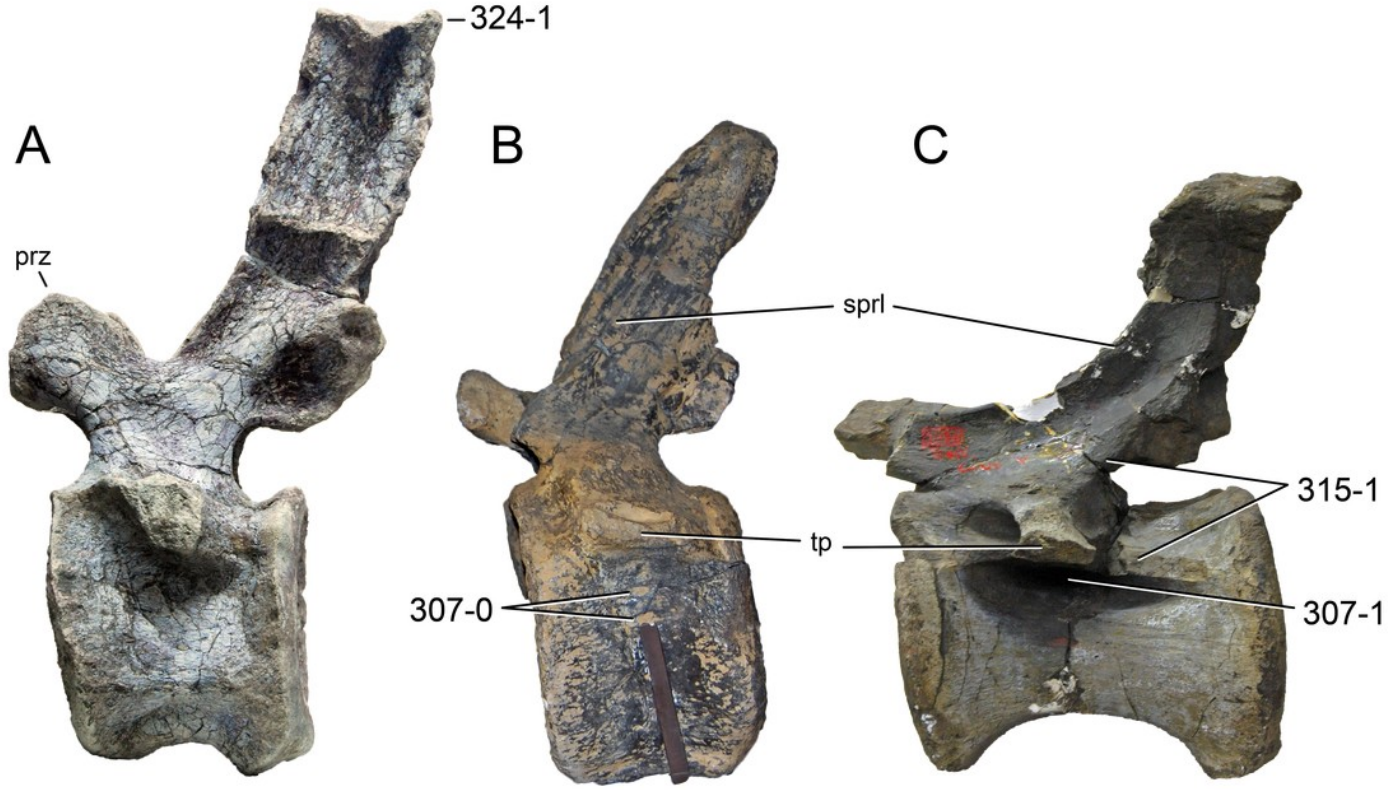


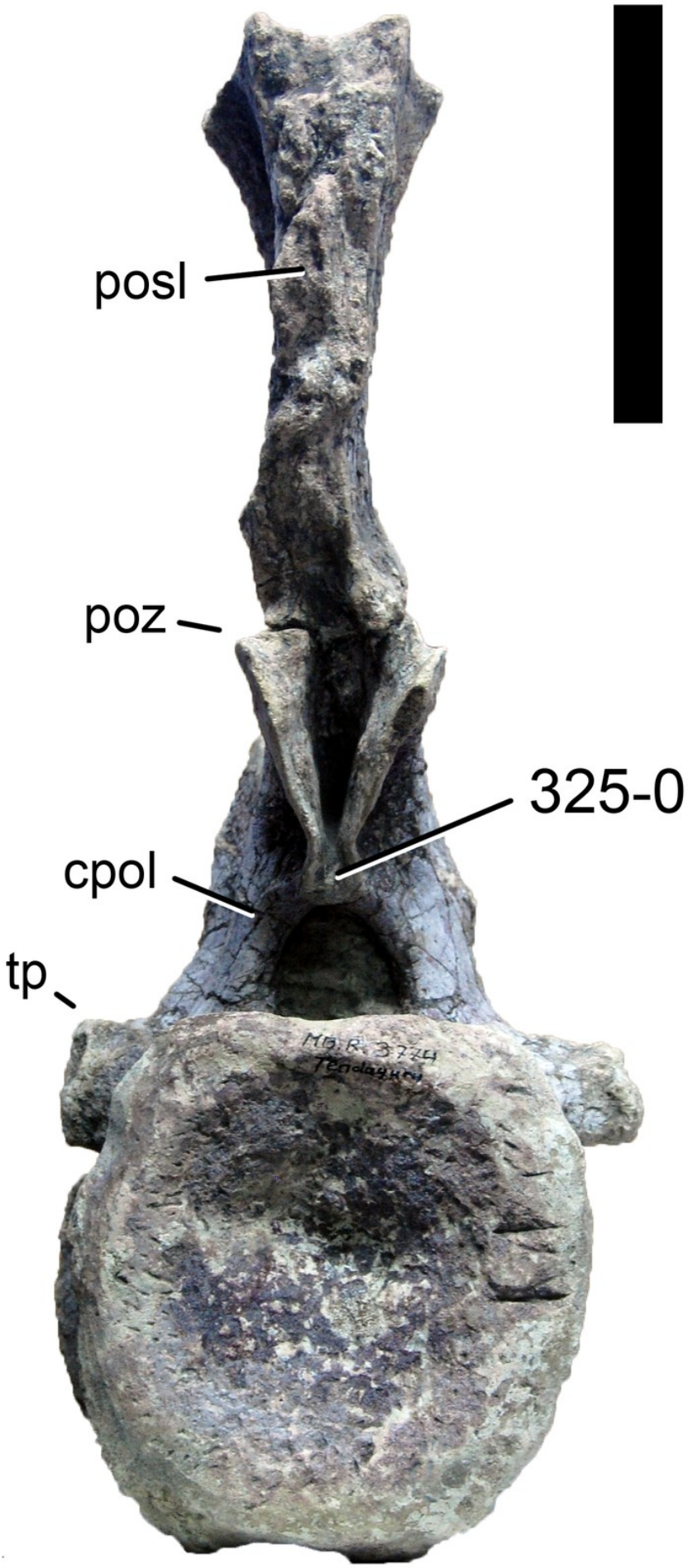
Figure 115

Anterior caudal vertebra of *Dicraeosaurus hansemanni* MB.R.3774

Figure 115: Anterior caudal vertebra of *Dicraeosaurus hansemanni* MB.R.3774 in posterior view, illustrating the hyposphenal ridge (C325-0). Abb.: cpol, centropostzygapophyseal lamina; posl, postspinal lamina; poz, postzygapophysis; tp, transverse process. Scale bar = 10 cm.

PeerJ Reviewing Manuscript

PeerJ Reviewing Manuscript



PeerJ Reviewing Manuscript

Figure 116

Diplodocid mid-caudal vertebrae

Figure 116: Mid-caudal vertebra of Apatosaurinae indet. SMA 0087 (A) and *Diplodocus hallorum* AMNH 223 (B) in right (A) and left (B) lateral view. Note the ventrolateral (A; C329-1) and lateral ridges (A; C333-1), the flat ventral border of the centrum (B; 335-1), the anteriorly shifted neural arch (B; C337-1), the differing inclinations of the neural spine (C340), which overhang the postzygapophyses (A; C343-0), or not (B; C343-1). Abb.: ns, neural spine; prz, prezygapophysis. Scaled to the same anterior articular surface height.

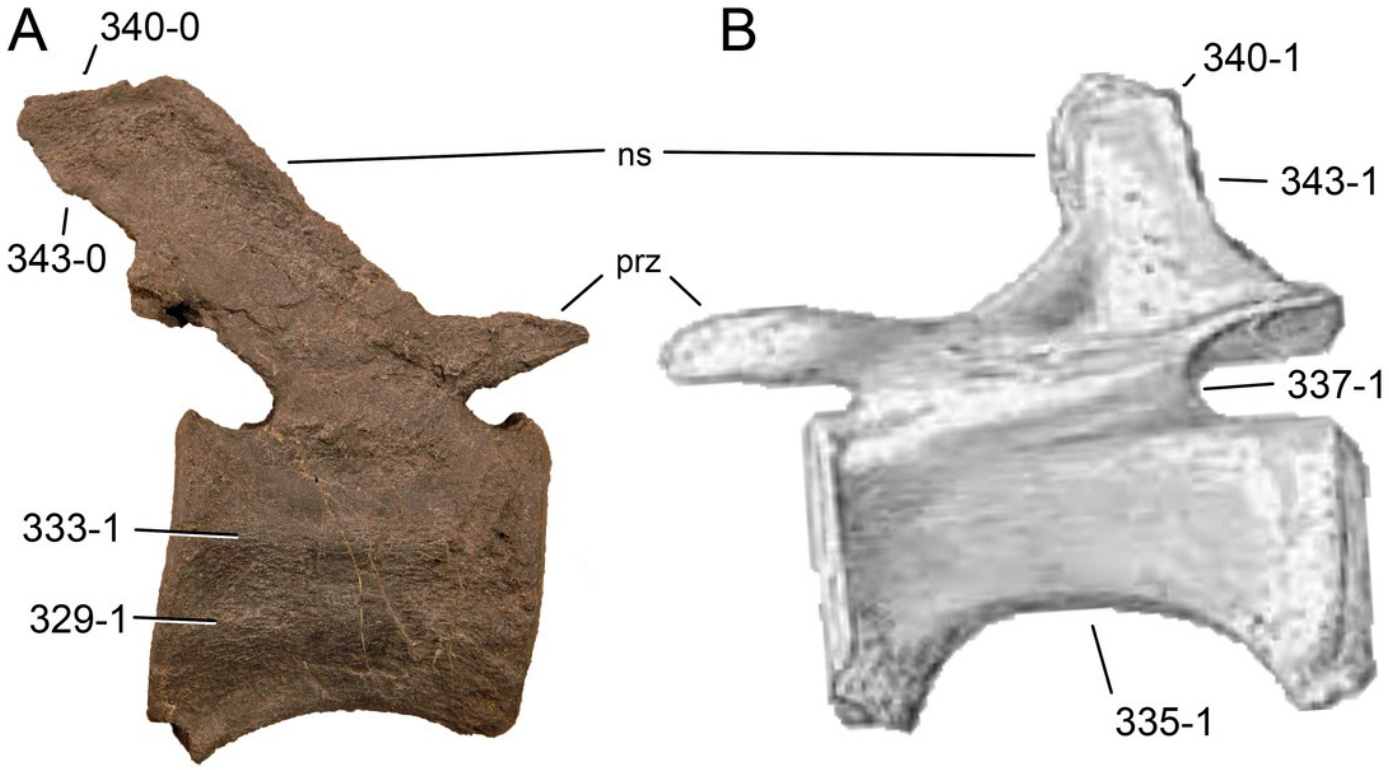
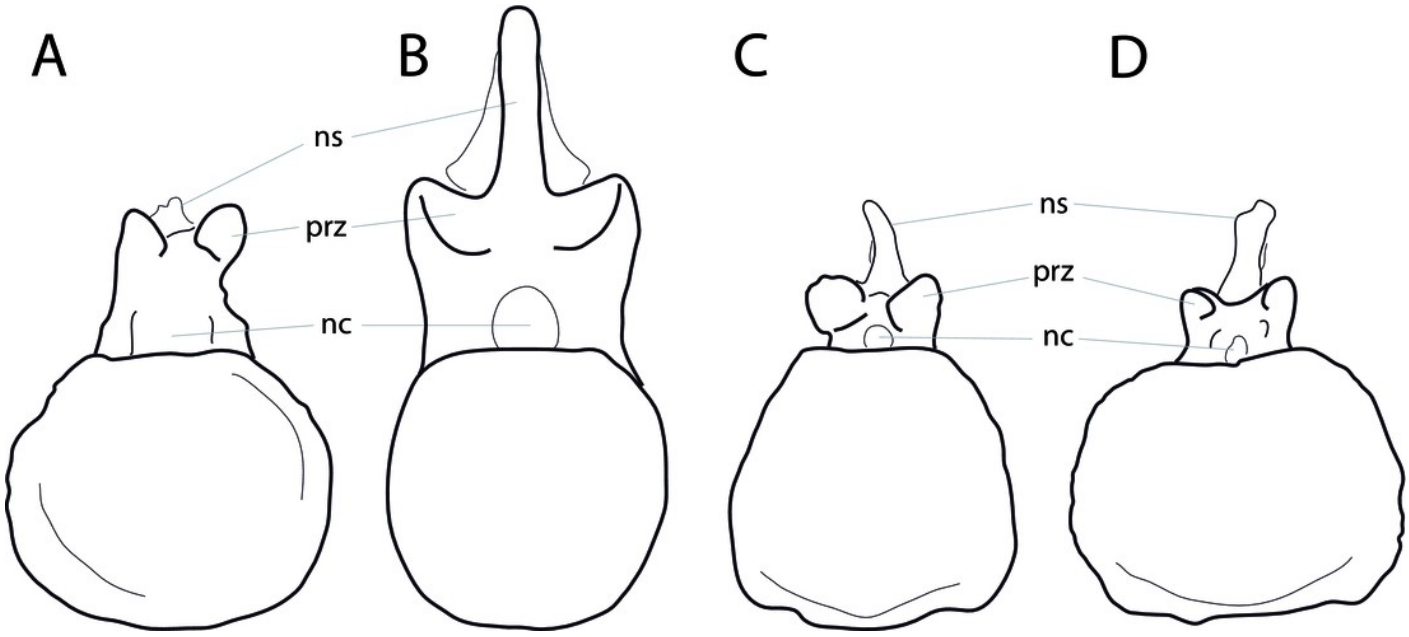


Figure 117

Eusauropod mid-caudal vertebrae

Figure 117: Mid-caudal vertebrae of *Losillasaurus giganteus* MCNV Lo-32 (A), *Isisaurus colberti* ISIR335/42 (B; traced from Jain and Bandyopadhyay, 1997), *Diplodocus* sp. AMNH 655 (C), and *Barosaurus lentus* AMNH 6341 (D) in anterior view, illustrating the four states of character 334 (A, circular; B, quadrangular; C, trapezoidal; D, flat ventral margin with rounded lateral edges). Abb.: nc, neural canal; ns, neural spine; prz, prezygapophysis. Scaled to same anterior surface height.

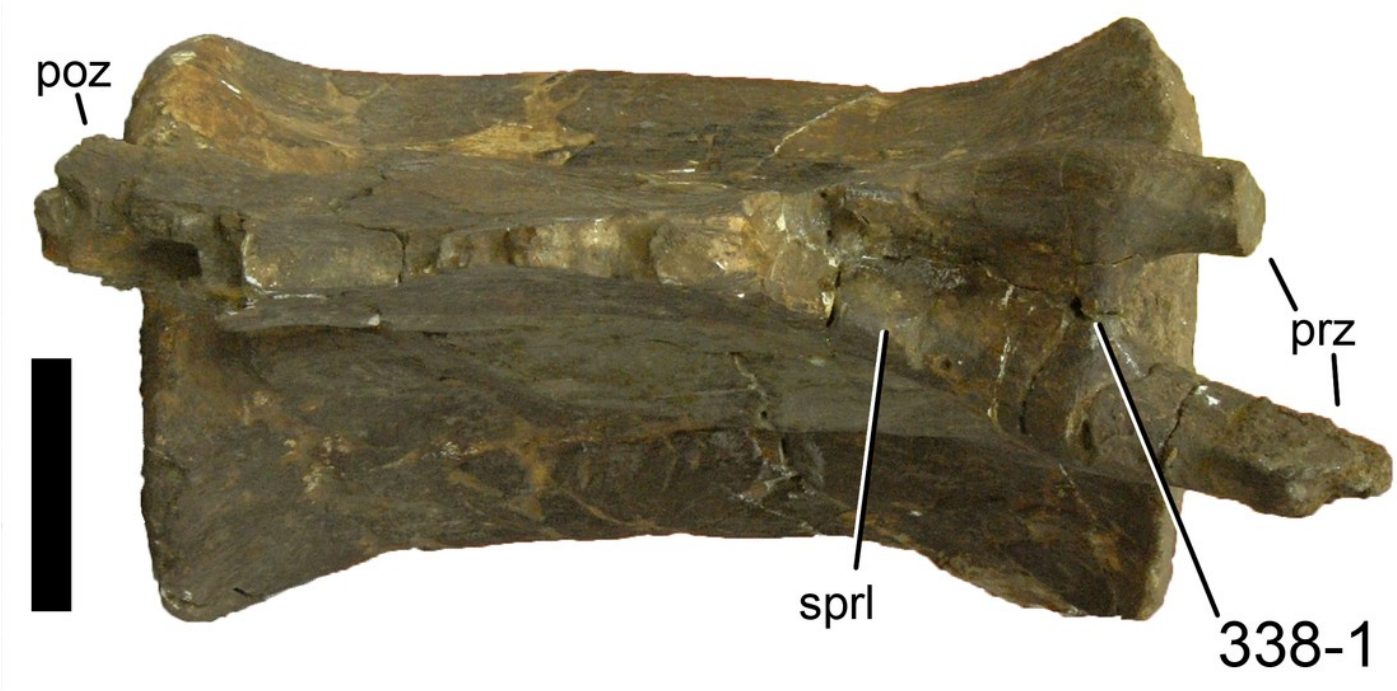


PeerJ Reviewing Manuscript

Figure 118

Mid-caudal vertebra of *Diplodocus longus* YPM 1920

Figure 118: Mid-caudal vertebra of *Diplodocus longus* YPM 1920 in dorsal view, illustrating the transverse ridge connecting the prezygapophyses posteriorly (C338-1). Abb.: poz, postzygapophysis; prz, prezygapophysis; sprl, spinoprezygapophyseal lamina. Scale bar = 5 cm.

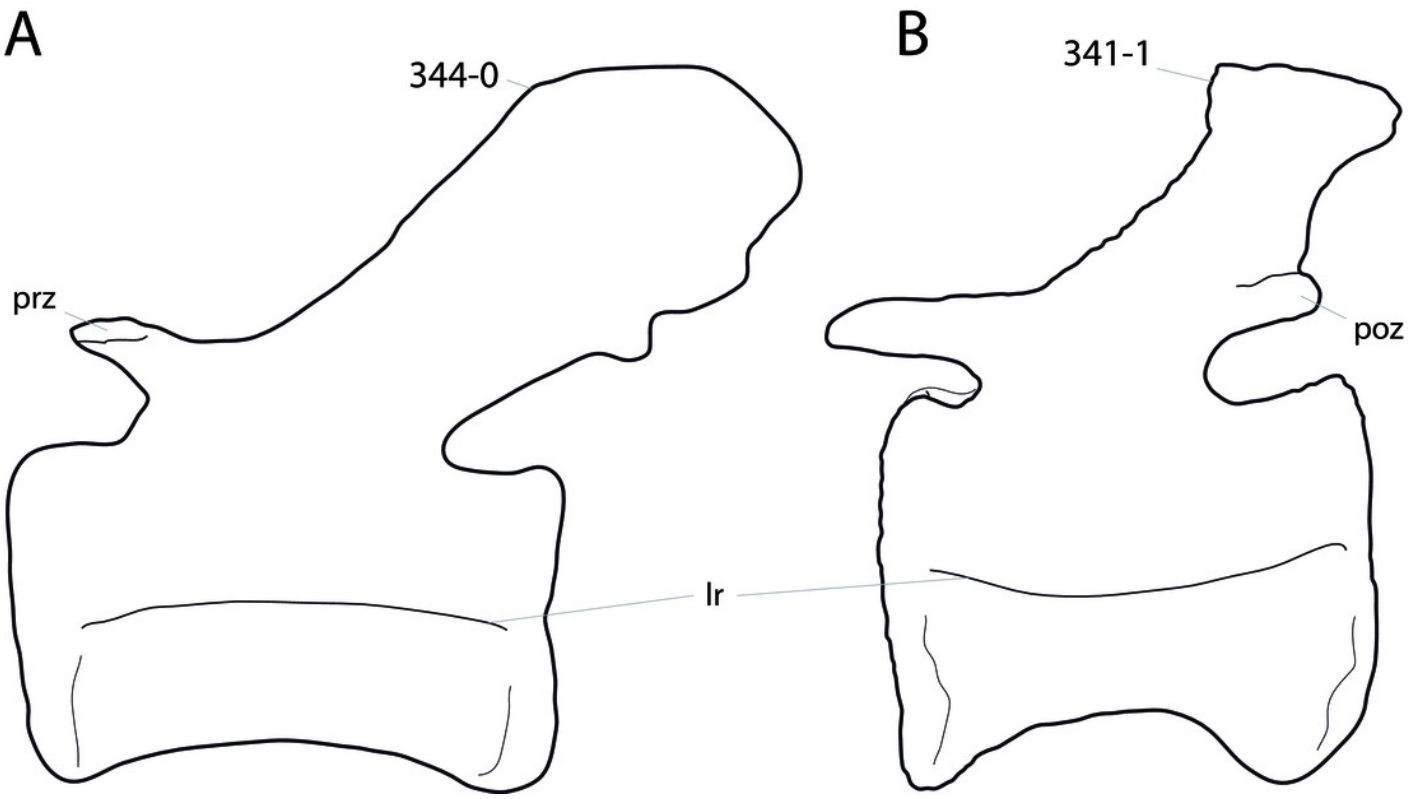


PeerJ Reviewing Manuscript

Figure 119

Eusauropod mid-caudal vertebrae

Figure 119: Mid-caudal vertebrae of *Cetiosauriscus stewarti* NHMUK R.3078 (A; traced from Woodward, 1905) and *Supersaurus vivianae* WDC DMJ-021 (B; traced from a photo by D. Lovelace) in left lateral view, illustrating the anterodorsal projection on the spine top (B; C341-1), and the posteriorly elongated neural spine (A; C344-0). Abb.: lr, lateral ridge; poz, postzygapophysis; prz, prezygapophysis. Scaled to same total vertebral height.



PeerJ Reviewing Manuscript

Figure 120

Anterior chevron of *Apatosaurus ajax* YPM 1860

Figure 120: Anterior chevron of *Apatosaurus ajax* YPM 1860 in anterior, right lateral, and posterior view (left to right). Note the crus bridging the haemal canal dorsally (broken here; C352-0), the anterior, longitudinal median ridge (C354-1), and the step-like posterior expansion of the distal blade (C355-1). Abb.: db, distal blade; hc, haemal canal. Scale bar = 10 cm.



PeerJ Reviewing Manuscript

Figure 121

Mid-chevron of *Diplodocus hallorum* AMNH 223

Figure 121: Mid-chevron of *Diplodocus hallorum* AMNH 223 in dorsal, left lateral, and ventral view (top-bottom). Note the anterior and posterior projections (C353-1), the rugose horizontal ridge (C356-1), and the medial fossa (C357-1). Abb.: pas, proximal articular surface. Scale bar = 5 cm.

PeerJ Reviewing Manuscript

PeerJ Reviewing Manuscript



PeerJ Reviewing Manuscript

Figure 122

Diplodocoid scapulae

Figure 122: Scapula outlines of *Haplocanthosaurus priscus* CM 879 (A), *Limaysaurus tessonei* MUCPv-205 (B), *Apatosaurus louisae* CM 3018 (C; all traced from Mannion, 2009), and *Diplodocus hallorum* AMNH 223 (D; traced from Osborn, 1899). Note the concave dorsal border of the acromion process (B; C363-1), the acromion process that reaches almost half the scapular length (D; C364-1), the different shapes of the acromial edge (straight, C, C367-0; with rounded expansion distally, A, C367-1; raquet-shaped, B, C367-2), the ventrally curving ventral margin (A; C368-1), and the subtriangular process (D; C370-1). Abb.: acm, acromion; ca, coracoid articulation; db, distal blade. Scaled to same scapular length.

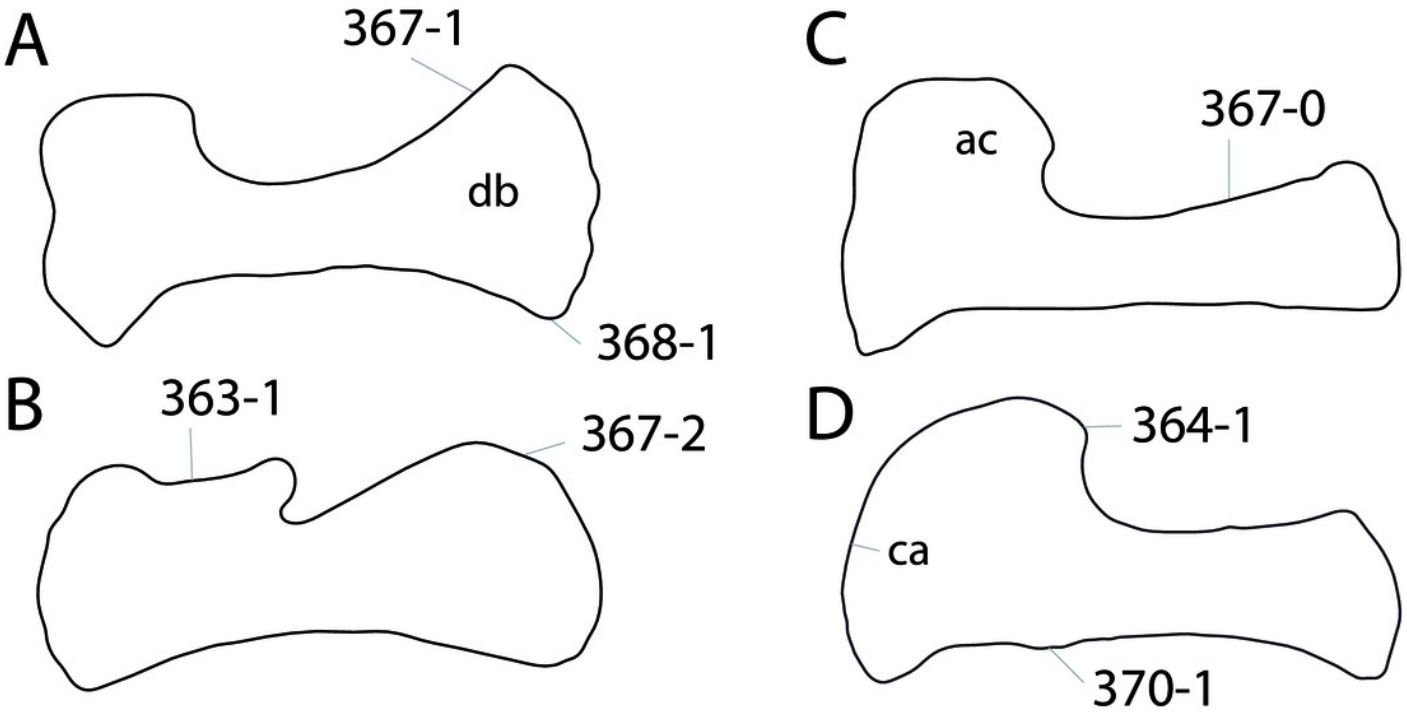


Figure 123

Apatosaurine scapulae

Figure 123: Right scapulae of *Elosaurus parvus* CM 566 (A) and *Brontosaurus excelsus* YPM 1980 (B) in lateral view. Note the excavated area between the acromial edge and the distal blade (A; C365-0) and the flat muscle scar at the base of the distal blade (B; C369-1). Abb.: acr, acromial ridge; db, distal blade. Scaled to same length.

PeerJ Reviewing Manuscript

PeerJ Reviewing Manuscript

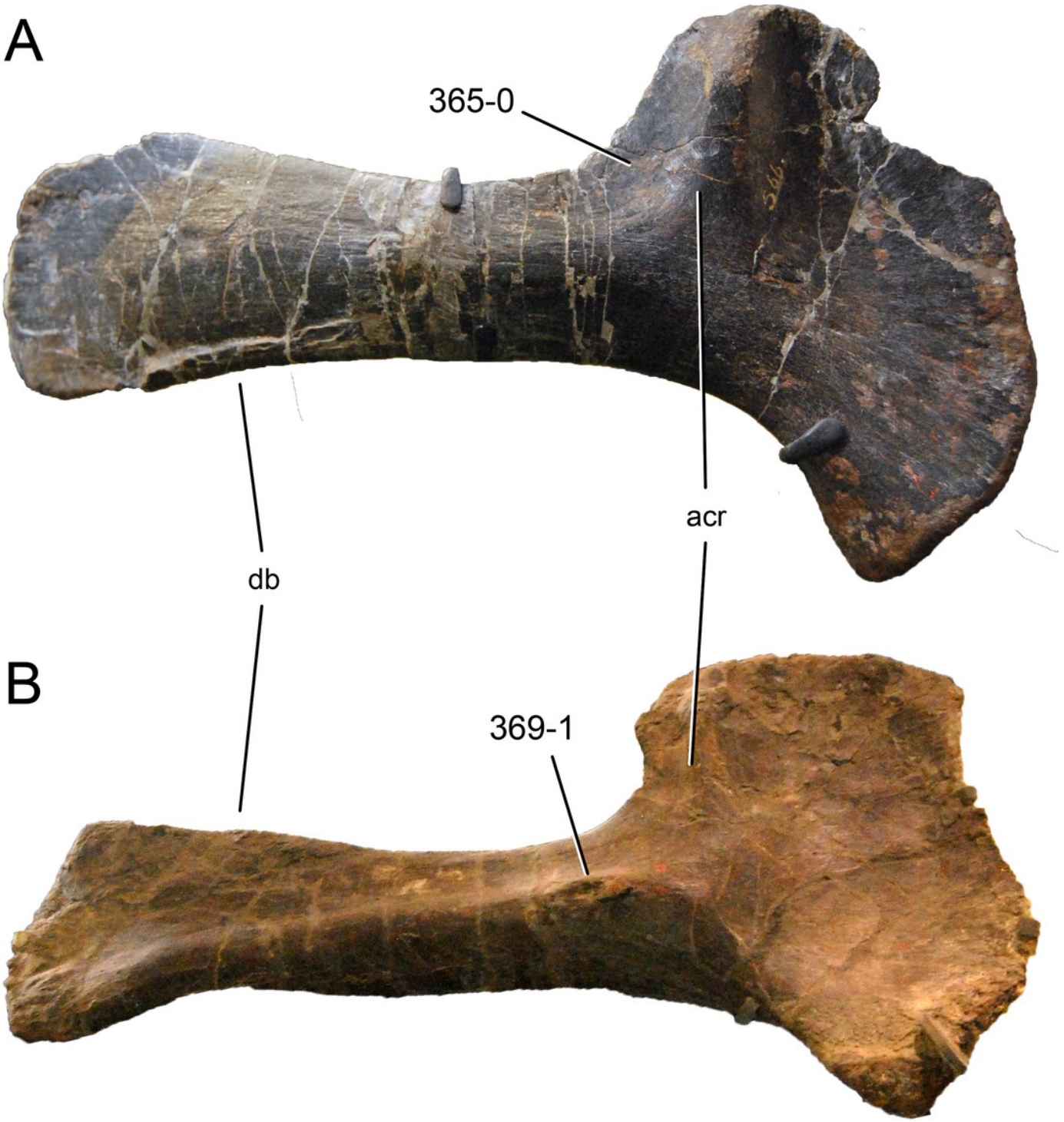
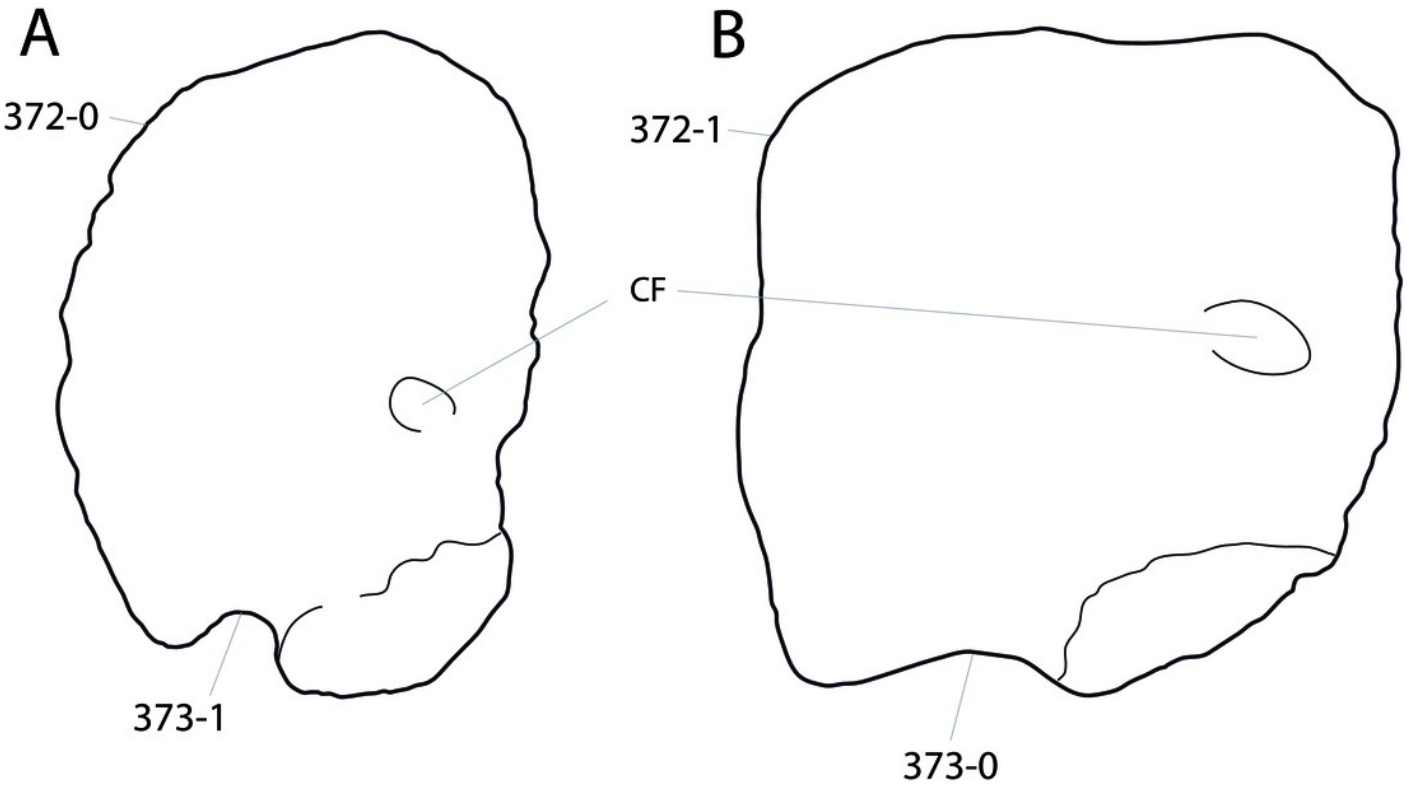


Figure 124

Neosauropod coracoids

Figure 124: Left coracoids of *Amphicoelias altus* AMNH 5764? (A) and *Apatosaurus ajax* YPM 1860 (B; traced from Bakker, 1998) in anterolateral view. Note the rounded (A; C372-0) instead of rectangular shape (B; C372-1), and the deep (A; C373-1) in contrast to shallow infraglenoid groove (B; C373-0). Abb.: CF, coracoid foramen. Scaled to the same height.



PeerJ Reviewing Manuscript

PeerJ Reviewing Manuscript

Figure 125

Neosauropod sternal plates

Figure 125: Right (A, B) and left (C) sternal plates of *Giraffatitan brancai* MB.R.2181 (A; modified from Janensch, 1961), *'Brontosaurus' amplus* YPM 1981 (B), and *Tornieria africana* MB.R.2726 (C) in ventral view. Note the different shapes (oval, B, C374-0; triangular, C, C374-1; crescentic, A, C374-2), the longitudinal ridge (A; C375-1), the anterior dorsoventral thickening (C; C376-1), and the straight posterior border (C; C377-1). Scaled to same length.

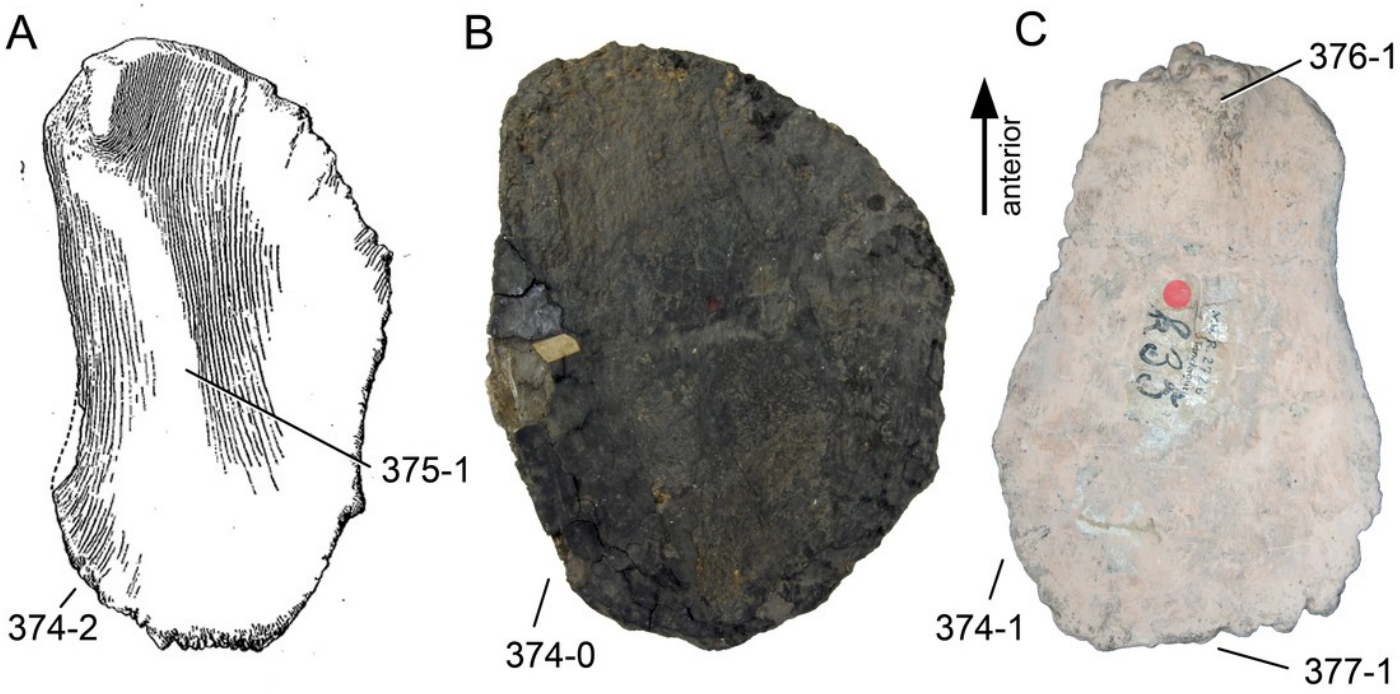
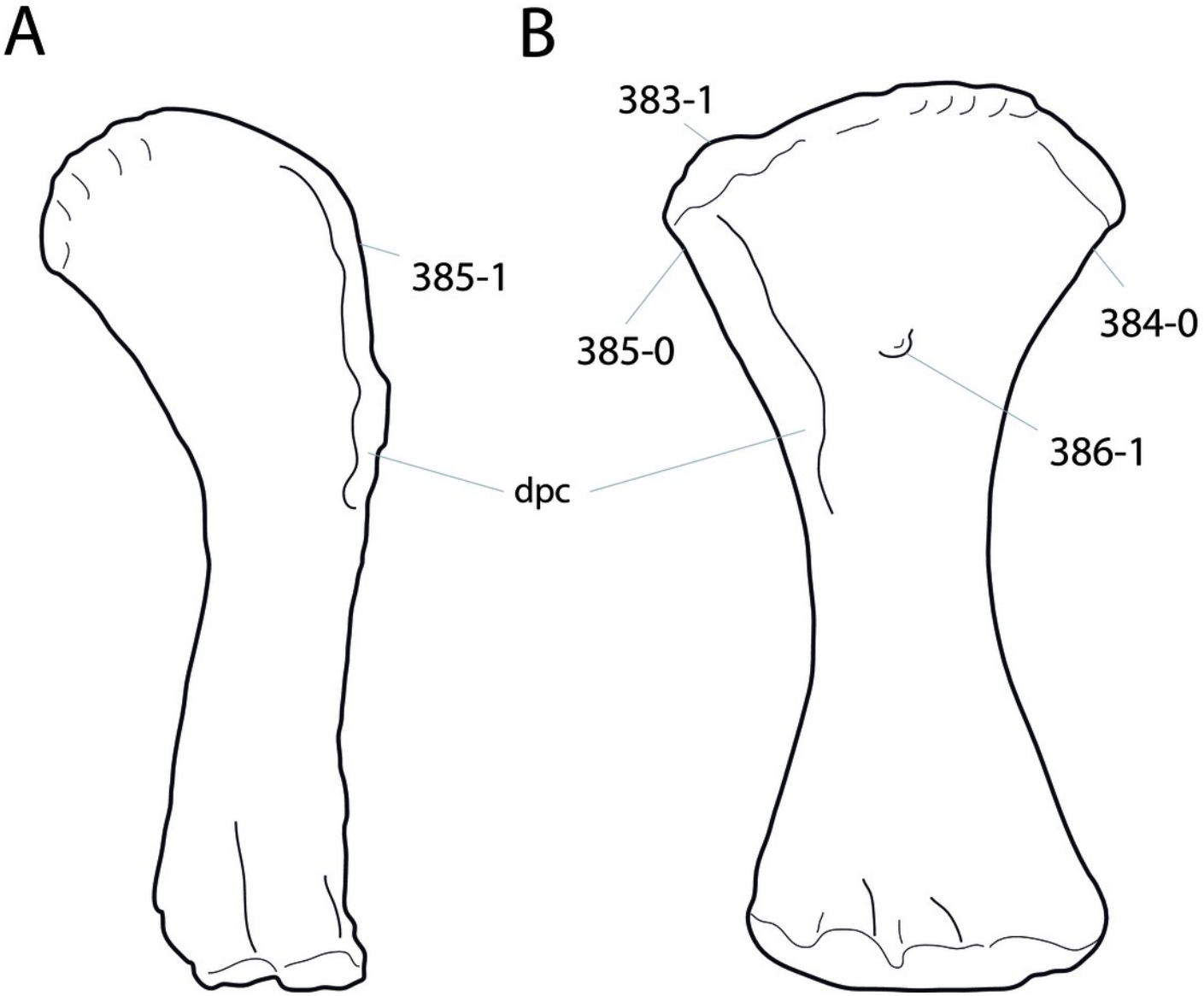


Figure 126

Eusauropod humeri

Figure 126: Humeri of *Turiasaurus riodevensis* CPT 1195-1210 (A; traced from Royo-Torres et al., 2006) and *Suuwassea emilieae* ANS 21122 (B; traced from Harris, 2007) in anterior view. Note the pronounced proximolateral corner (B; C383-1), the symmetrical proximal transverse expansion (B; C384-1), the unexpanded (A; C385-1) or expanded lateral edges (B; C385-0), and the tubercle marking the center of the proximal concavity (B; C386-1). Abb.: dpc, deltopectoral crest. Scaled to same length.



PeerJ Reviewing Manuscript

Figure 127

Distal half of radius of *Dyslocosaurus polyonychius* AC 663

Figure 127: Distal half of radius of *Dyslocosaurus polyonychius* AC 663 illustrating the very weak ridges for the articulation with the ulna (C392-0). Scale bar = 10 cm.

PeerJ Reviewing Manuscript

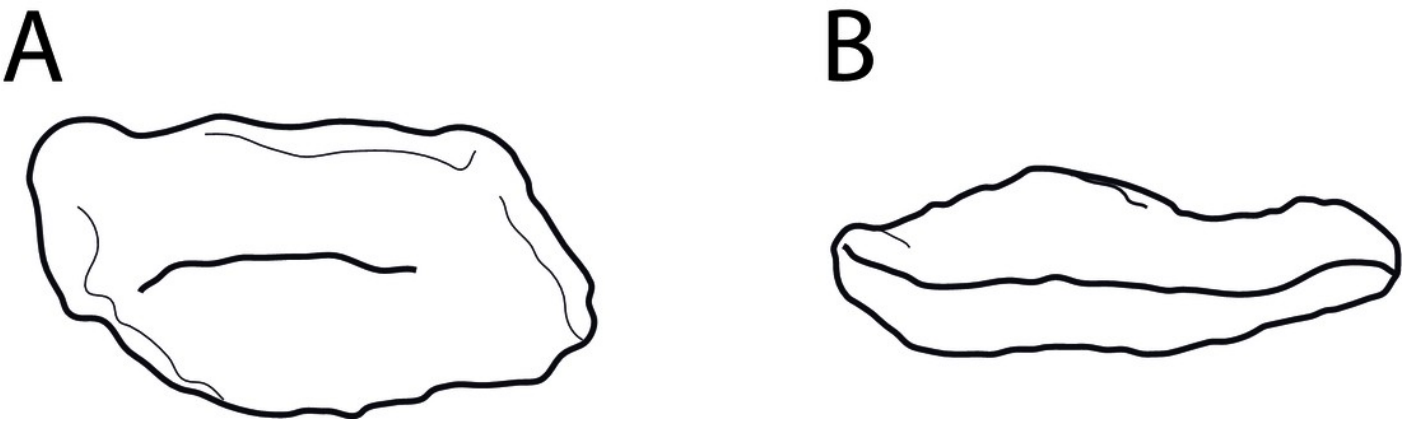
PeerJ Reviewing Manuscript



Figure 128

Diplodocid carpals

Figure 128: Carpal elements of *Galeamopus* [redacted] SMA 0011 (A) and '*Apatosaurus*' *parvus* UW 15556 (B; traced from Bonnan, 2003) in anterior view, illustrating the two different shapes described in C396: 0) block-like (A), and 1) disc-like (B). Scaled to the same transverse width.

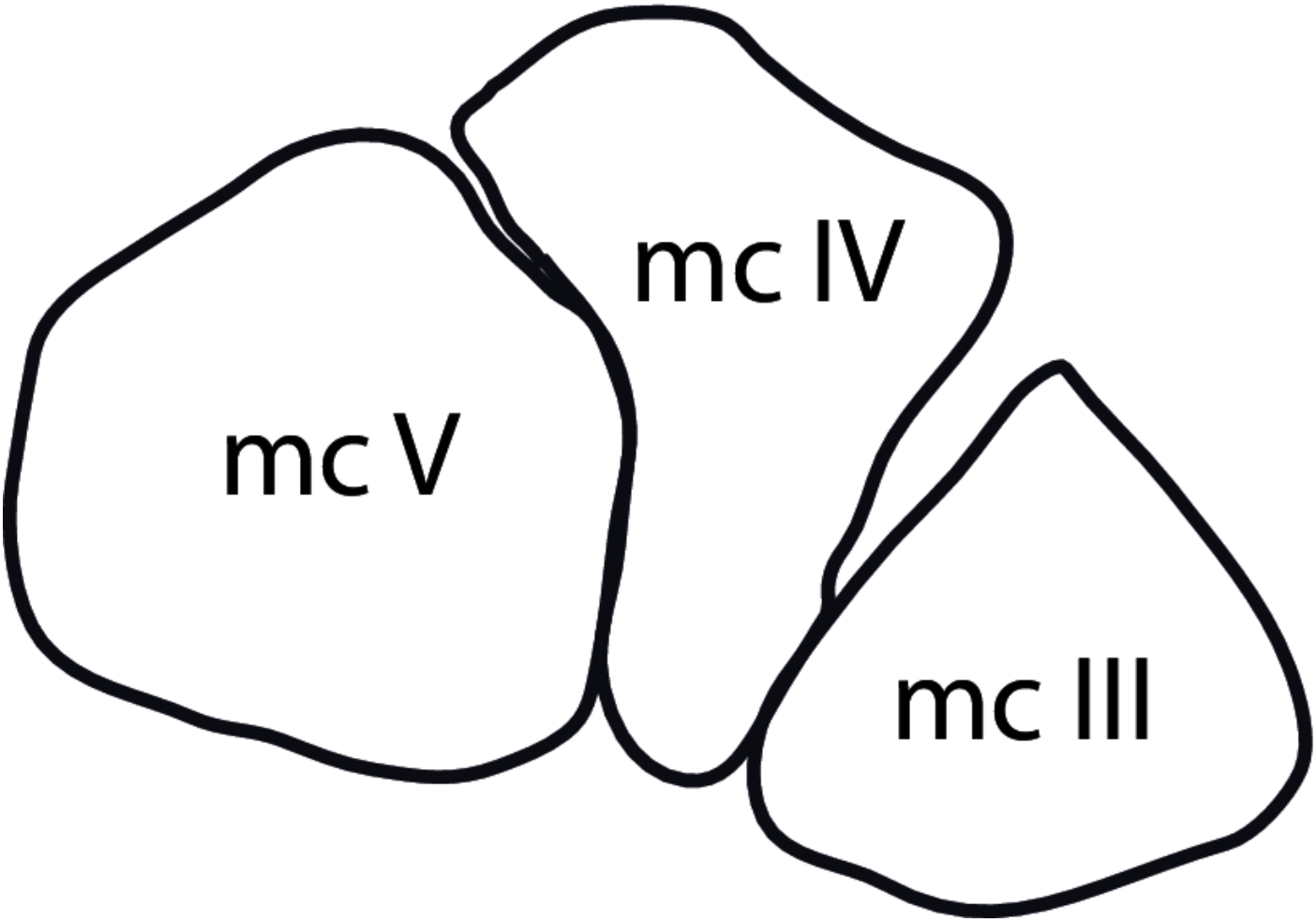


PeerJ Reviewing Manuscript

Figure 129

Metacarpals III-V of *Apatosaurus louisae* CM 3018

Figure 129: Articulated metacarpals III-V of *Apatosaurus louisae* CM 3018 in proximal view (traced from Gilmore, 1936), showing the greatly enlarged mc V, in comparison to mc III and IV (C403-1).

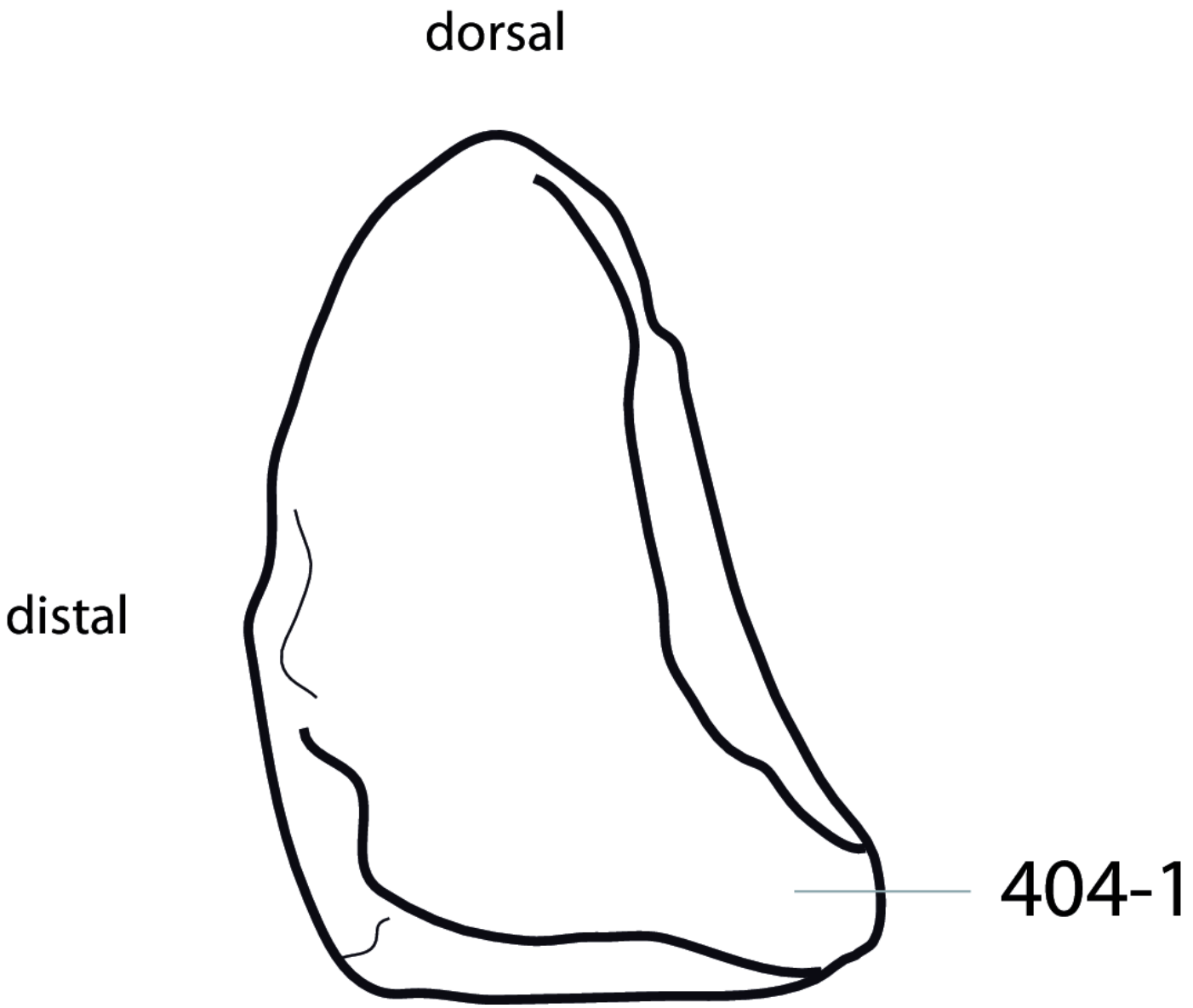


PeerJ Reviewing Manuscript

Figure 130

Manual phalanx phm I-1 of Apatosaurinae indet. NSMT-PV 20375

Figure 130: Manual phalanx phm I-1 of Apatosaurinae indet. NSMT-PV 20375 in medial view (traced from Upchurch et al., 2004b), showing the proximoventral lip-like projection (C404-1).



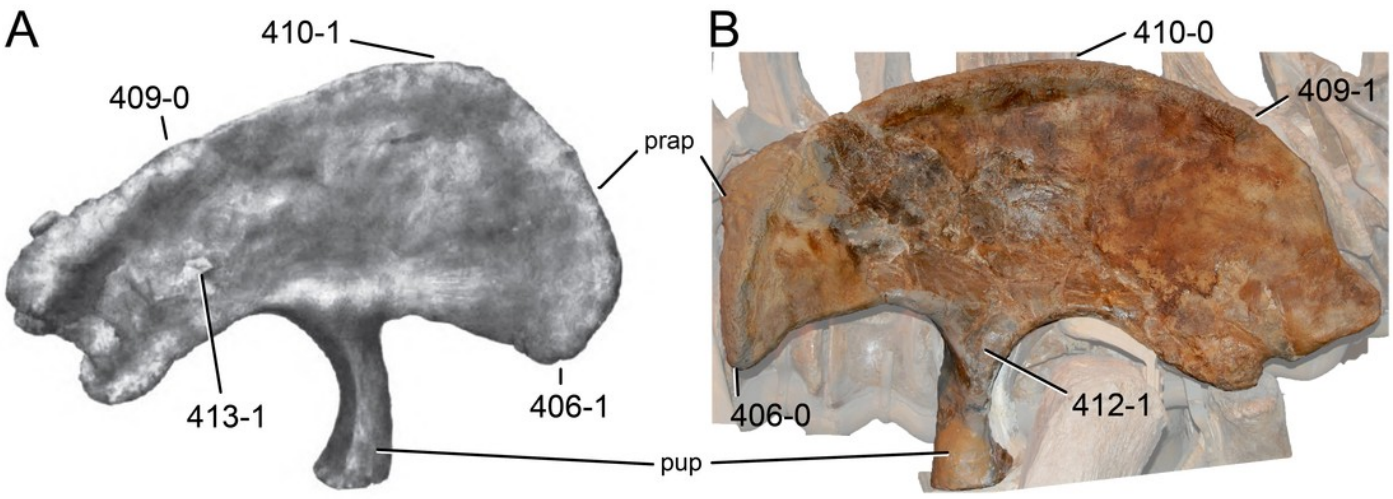
PeerJ Reviewing Manuscript

PeerJ Reviewing Manuscript

Figure 131

Neosauropod ilia

Figure 131: Right (A) and left (B) ilium of *Brachiosaurus altithorax* FMNH P25107 (A; modified from Riggs, 1904) and *Diplodocus hallorum* DMNS 1494 (B) in lateral view. Note the pointed (B; C406-0) or semicircular preacetabular process (A; C406-1), the straight (A; C409-0) or strongly convex dorsal edge (B; C409-1), the location of the highest point (anterior to pubic peduncle, A, C410-1; posterior to pubis peduncle, B, C410-1), the triangular fossa on the pubic peduncle base (B; C412-1), and the tubercle in the postacetabular region (A; C413-1). Abb.: prap, preacetabular process; pup, pubic peduncle. Scaled to same height.



PeerJ Reviewing Manuscript

Figure 132

Neosauropod pubes

Figure 132: Left (A, C) and right (B, reversed) pubis of *Camarasaurus supremus* AMNH 5761 (A; modified from Osborn and Mook, 1921), *Dicraeosaurus hansemanni* MB.R.4886 (B; modified from Janensch, 1961), and *Brontosaurus excelsus* YPM 1980 (C; modified from Ostrom and McIntosh, 1966) in lateral view. Note the different sizes of the ambiens process (C414, arrowheads: absent, A; hook-like, B; incipient, C). Abb.: ac, acetabular surface; ip, iliac peduncle; isa, ischial articular surface; of, obturator foramen. Scaled to same length.

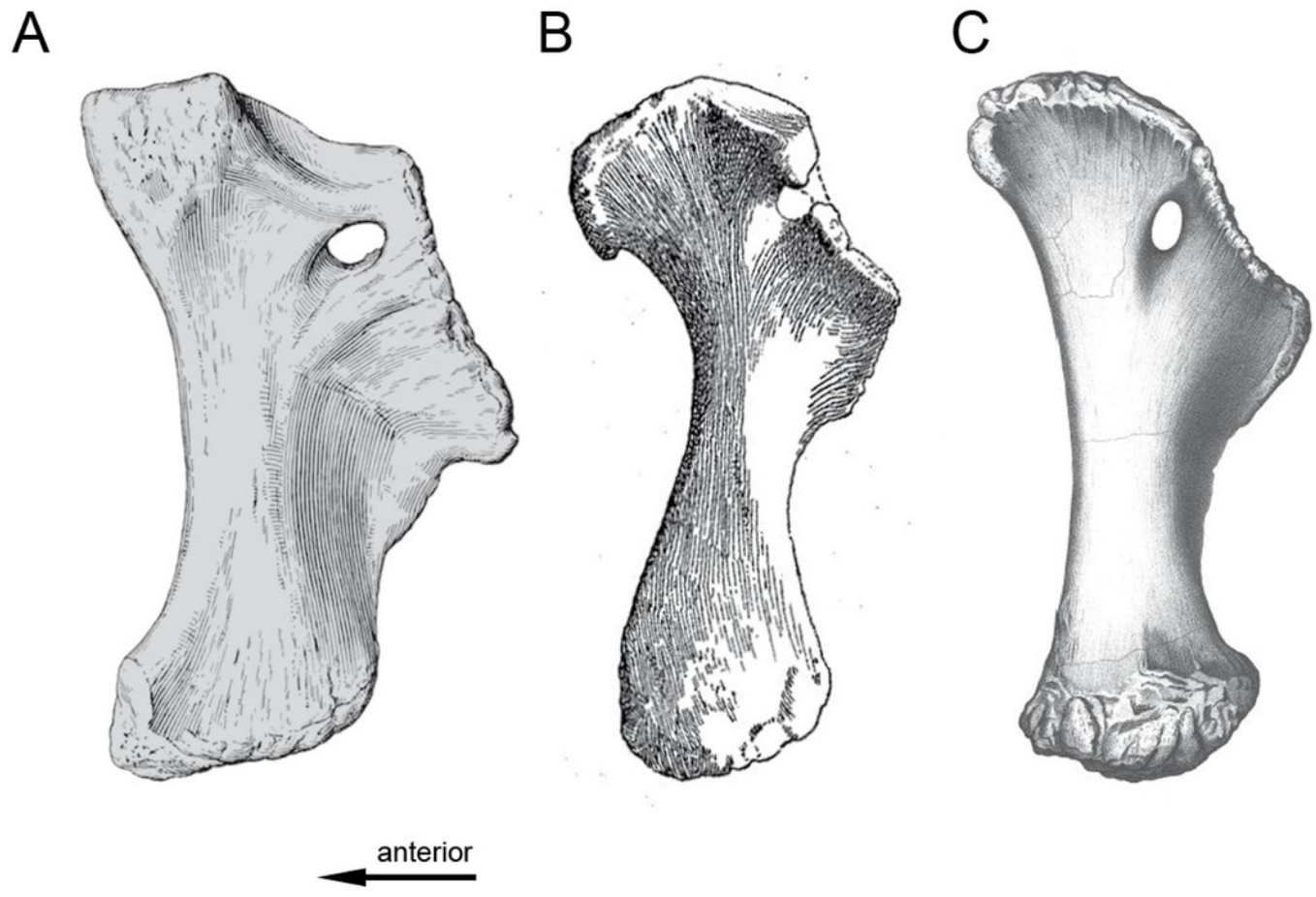


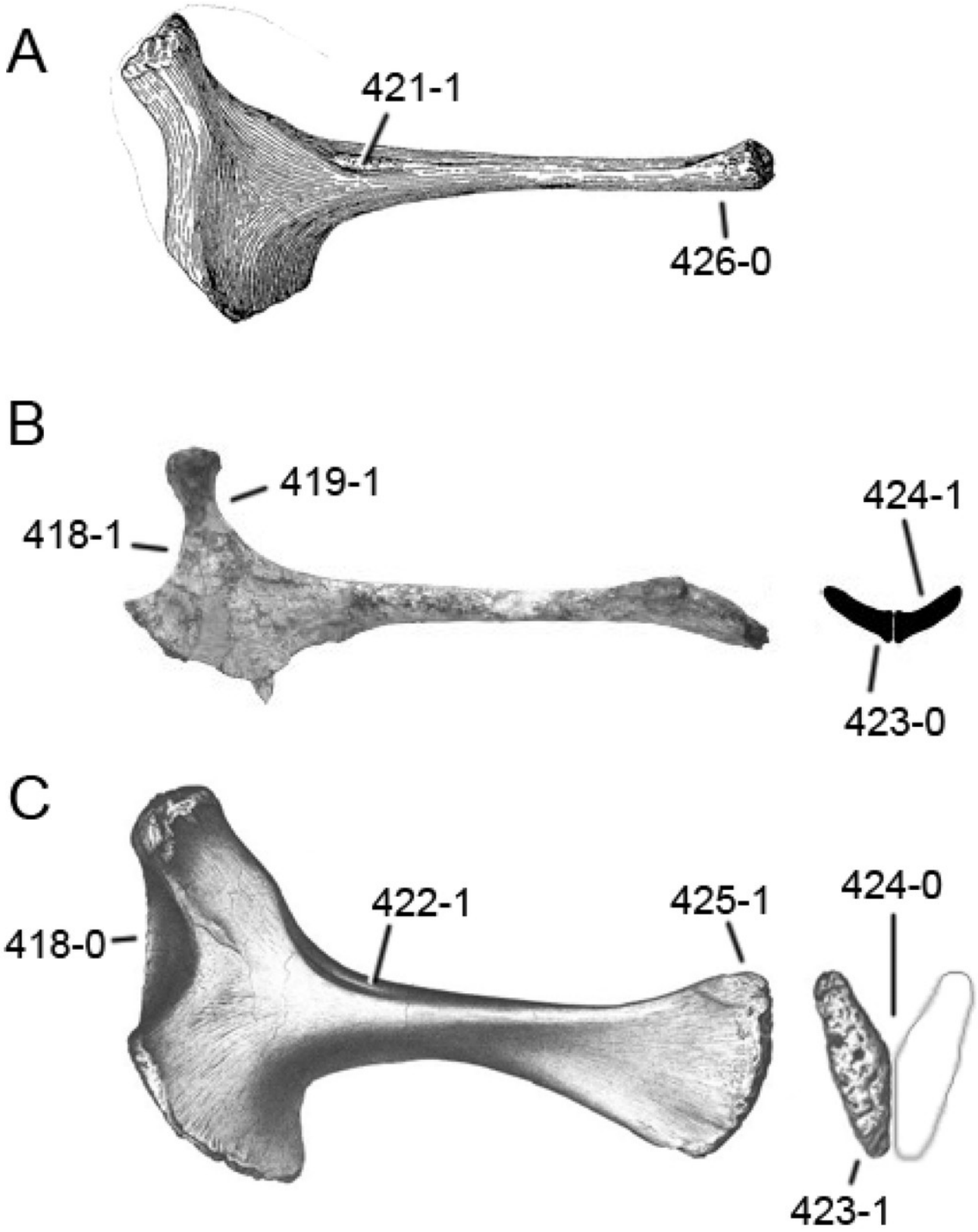
Figure 133

Diplodocoid ischia

Figure 133: Left ischium of *Haplocanthosaurus priscus* CM 572 (A; modified from Hatcher, 1903), *Demandasaurus darwini* MPS-RVII,18 (B; modified from Pereda Suberbiola et al., 2003), and *Brontosaurus excelsus* YPM 1980 (C; modified from Ostrom and McIntosh, 1966) in lateral (left) and distal (right) view. Note the flat (C; C418-0) in contrast to strongly concave acetabular margin (B; C418-1), the constricted neck of the iliac tubercle (B; C419-1), the elongate muscle scar on the proximal shaft (A; C421-1), the lateral fossa at the base of the blade (C; C422-1), the blade-like (B; C423-0) or medially expanded distal ends (C; C423-1), which form a more or less straight line (B; C424-1) or a V (C; C424-0), and can be straight (A; C426-0) or expanded dorsoventrally as well as transversely (C; C425-1). The light gray line in B indicates the distal view of the right ischium. Scaled to same length.

PeerJ Reviewing Manuscript

PeerJ Reviewing Manuscript



PeerJ Reviewing Manuscript

Figure 134

Neosauropod femora

Figure 134: Right femur of *Giraffatitan brancai* MB.R. St291 (A), *Dicraeosaurus hansemanni* MB.R.4886 (B; both modified from Janensch, 1961), and *Tornieria africana* SMNS 12140 (C; modified from Fraas, 1908) in anterior view. Note the lateral bulge (A; C428-1), the medial deflection of the femoral head (A; C429-1), the different positions of the highest point of the femoral head (C431), the stepped ventral margin of the head (B; C432-1), the nutrient foramen (B; C434-1), the fourth trochanter, which is visible in anterior view (A; C436-0), and the anteriorly extended distal articular surface of the condyle (C; C439-1). Scaled to same length.

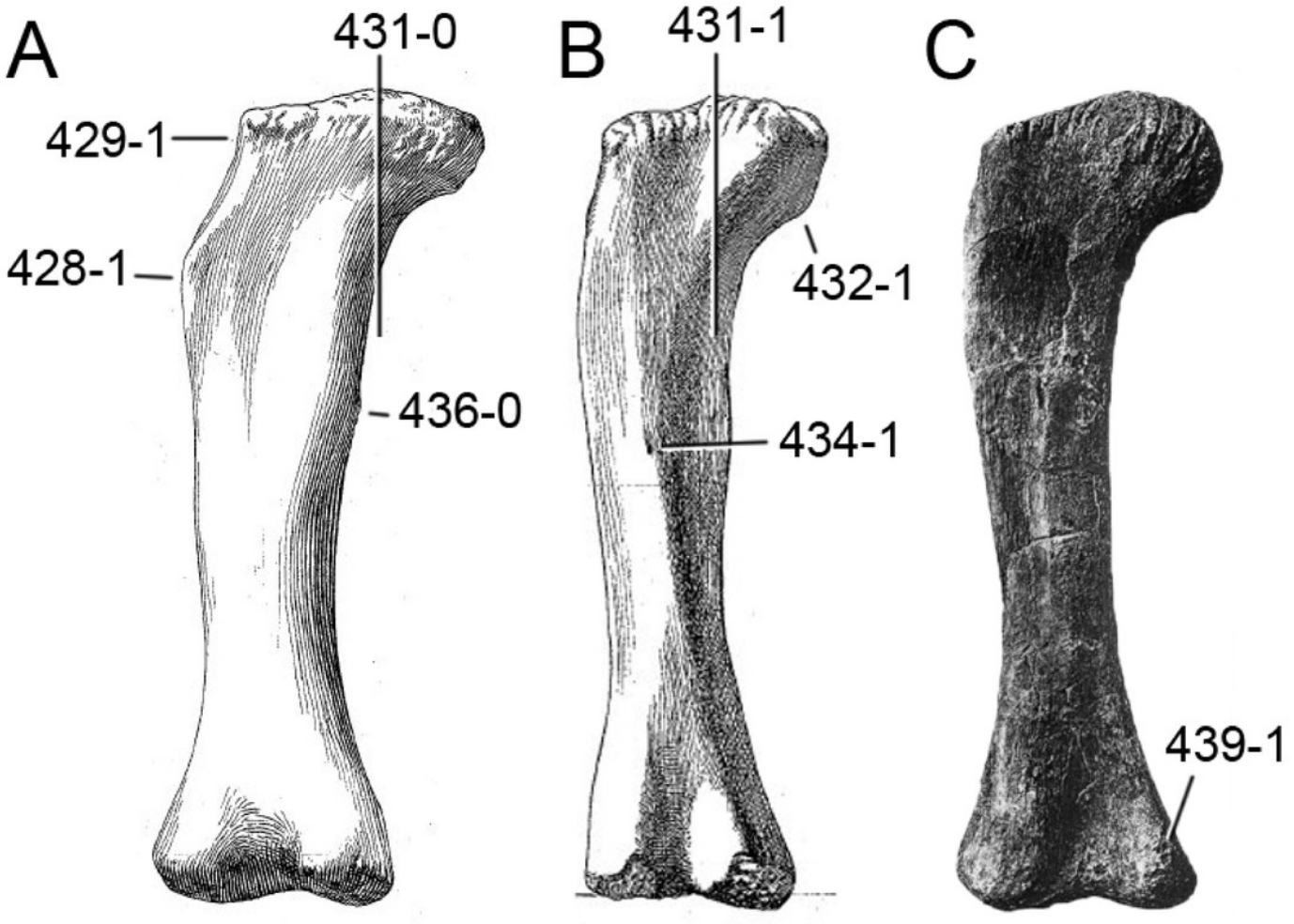
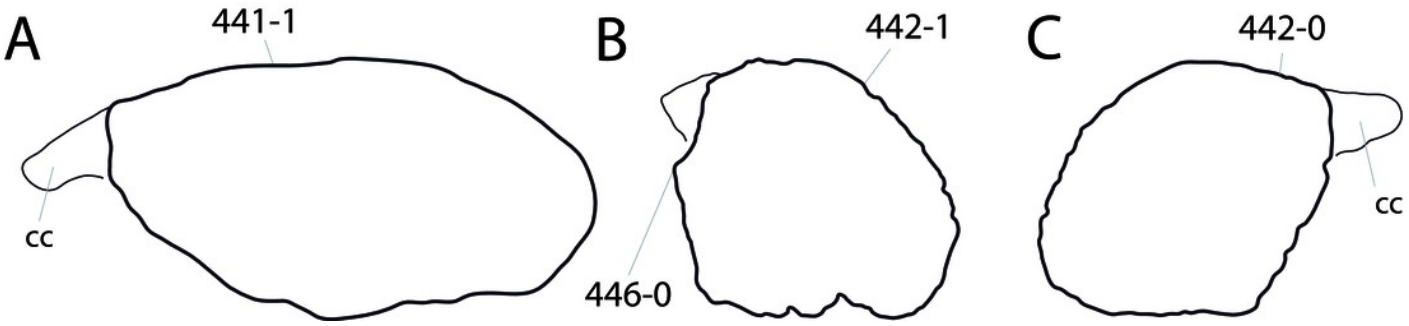


Figure 135

Eusauropod tibiae

Figure 135: Tibia of *Omeisaurus tianfuensis* ZDM T5701 (A; traced from He et al., 1988), *Dyslocosaurus polyonychius* AC 663 (B), and *Apatosaurus louisae* CM 3018 (C; traced from Gilmore, 1936) in proximal view. Note the different outlines (anteroposteriorly compressed, A, C441-1; subtriangular, B, C442-1; subrectangular, C, C442-0), and the projection posterior to the cnemial crest (B; C446-0). Abb.: cc, cnemial crest. Scaled to same anteroposterior length.



PeerJ Reviewing Manuscript

Figure 136

Distal end of tibia of *Dyslocosaurus polyonychius* AC 663

Figure 136: Distal end of tibia of *Dyslocosaurus polyonychius* AC 663 in medial view, illustrating the transverse ridge on the anteromedial surface, close to the distal end (C443-1). Scale bar = 10 cm.

PeerJ Reviewing Manuscript

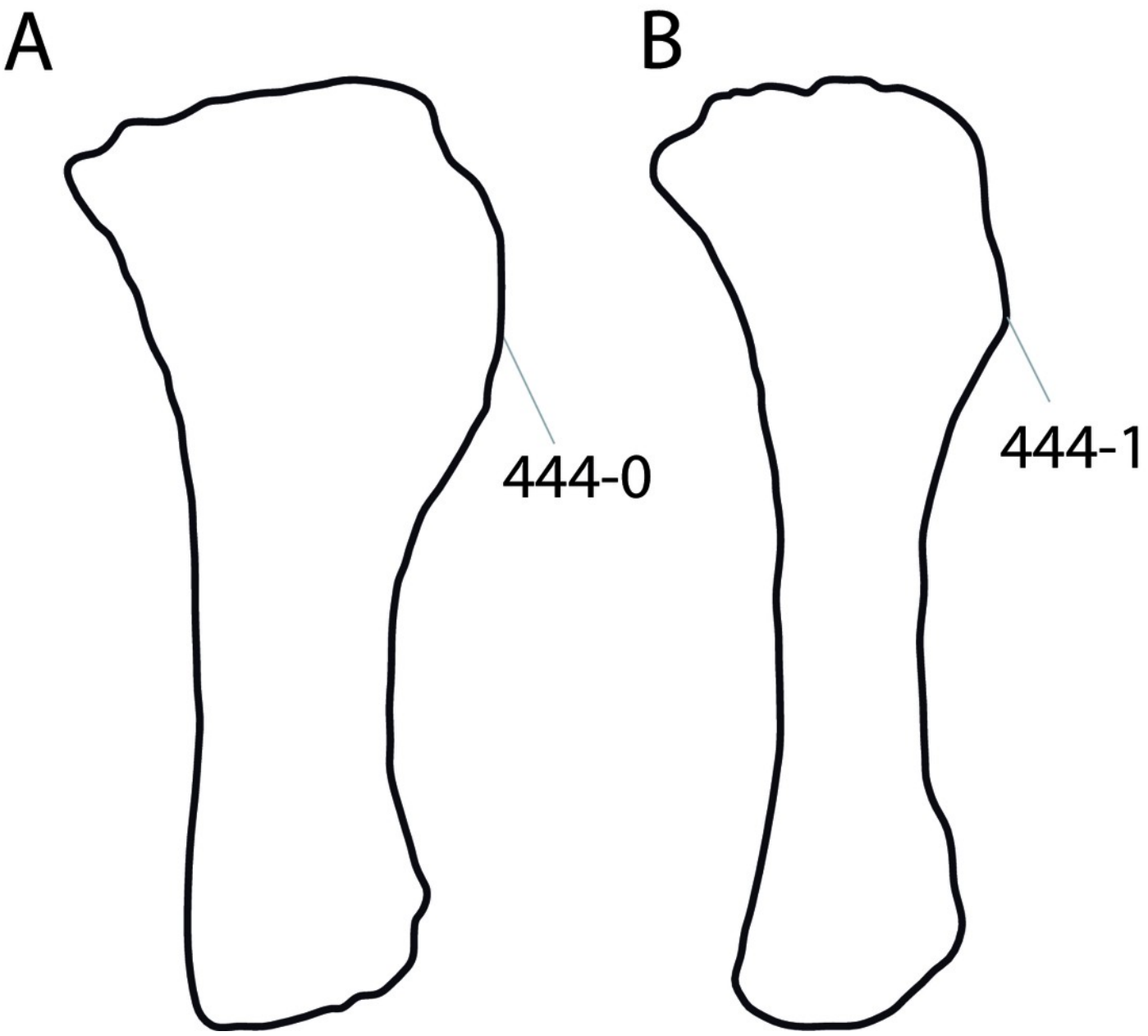
PeerJ Reviewing Manuscript



Figure 137

Diplodocoid tibiae

Figure 137: Tibia of *Zapalasaurus* sp. MOZ-Pv 1244 (A; traced from Salgado et al., 2012) and *Tornieria africana* MB.R.2572 (B; traced from Remes, 2006) in anterolateral view, illustrating the different shapes of the cnemial crest (widely rounded, A, C444-0; triangular, B, C444-1). Scaled to same length.



PeerJ Reviewing Manuscript

Figure 138

Proximal end of the tibia of *Suuwassea emilieae* ANS 21122

Figure 138: Proximal end of the tibia of *Suuwassea emilieae* ANS 21122 in posterolateral view, showing the distinct fibular trochanter on the posterior surface of the cnemial crest (C445-1). Scale bar = 10 cm.

PeerJ Reviewing Manuscript

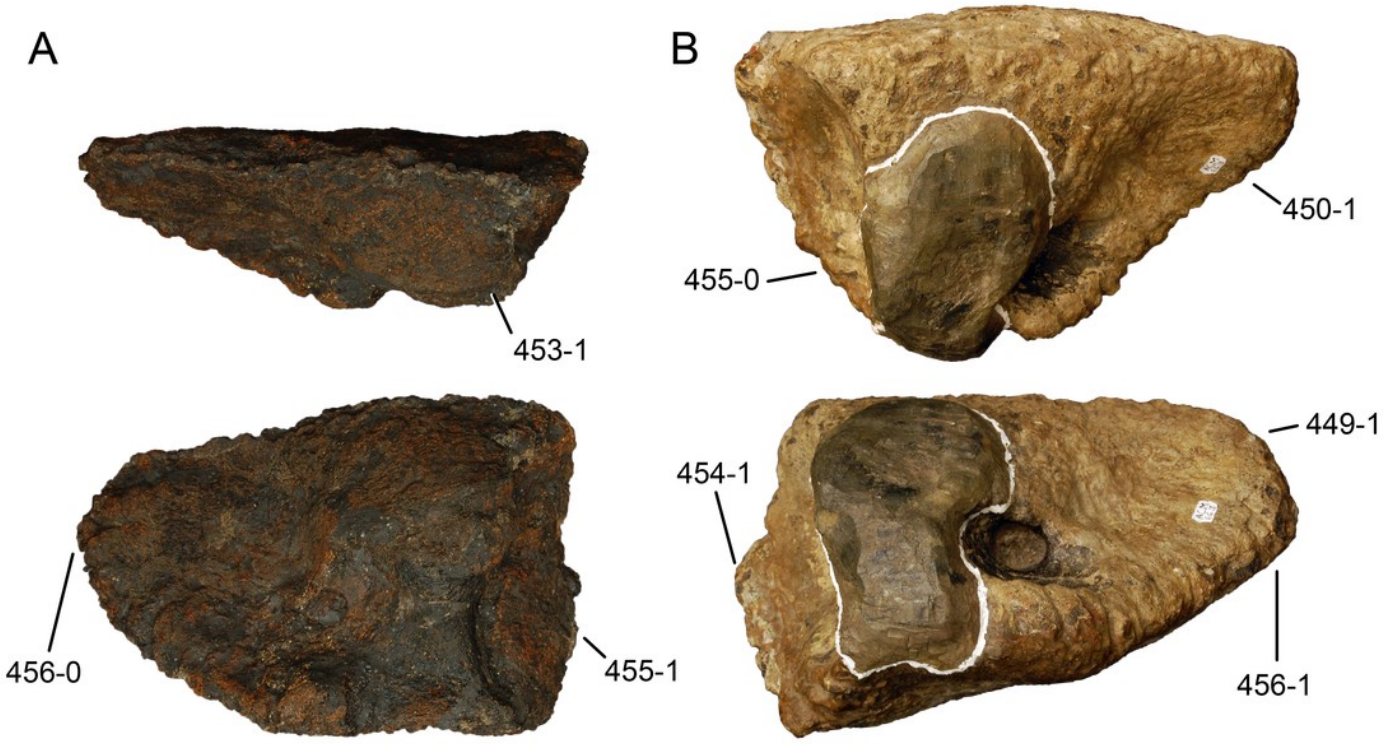
PeerJ Reviewing Manuscript



Figure 139

Flagellicaudatan astragali

Figure 139: Astragalus of SMA 0087 (A) and *Dyslocosaurus polyonychius* AC 663 (B) in dorsal (top) and posterior (bottom) view. Note the triangular shape in both views (B; C449-1, C450-1), the ascending process that reaches the posterior border (A; C453-1), the anterior border of the fibular facet, which is visible in posterior view (B; C454-1), the presence (B; C455-0) or absence (A; 455-1) of a sheet underlying the fibula, and the blunt (A; C456-0) in contrast to elongate medial end (B; C456-1). Scaled to the same proximodistal height.

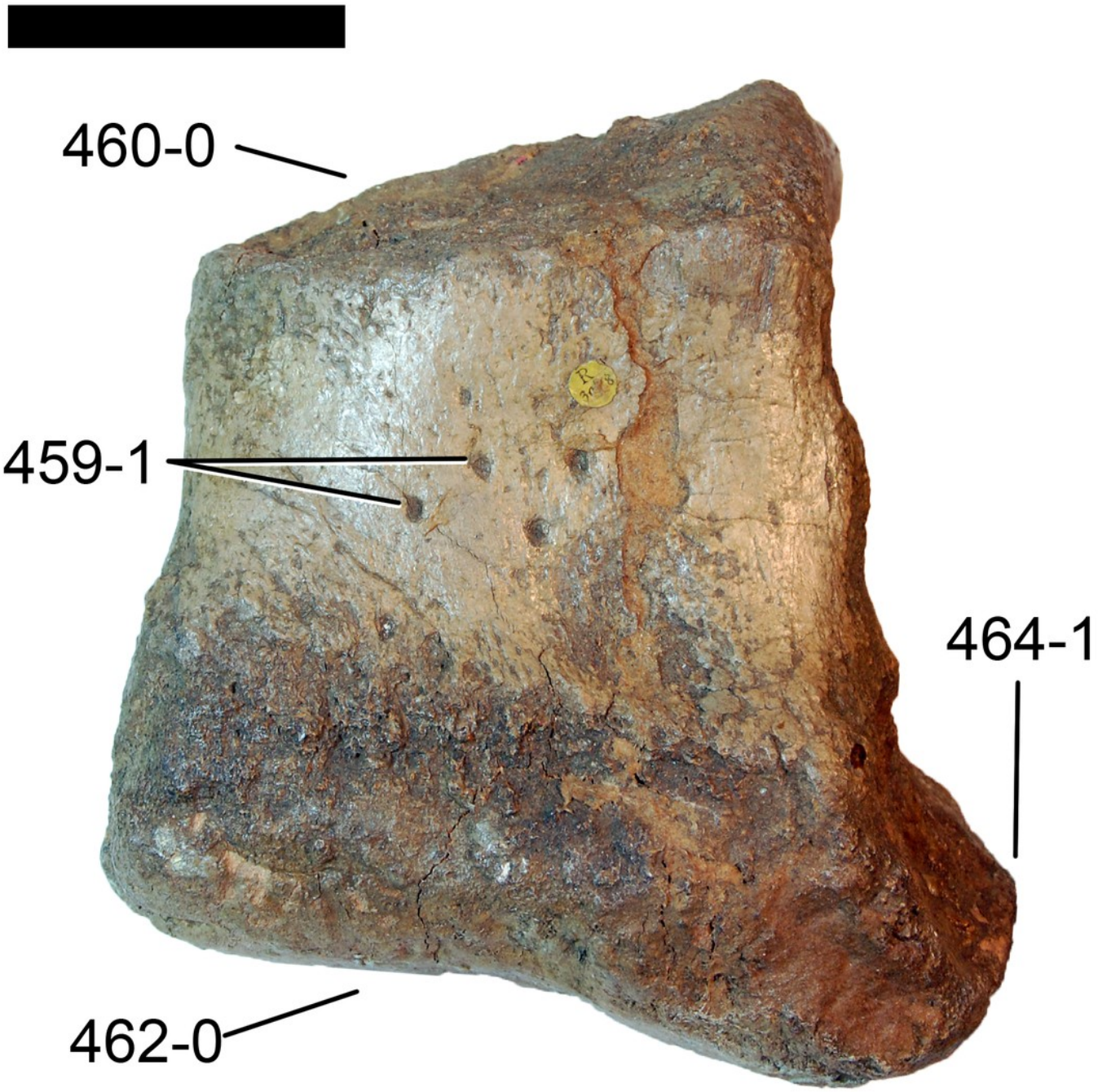


PeerJ Reviewing Manuscript

Figure 140

Metatarsal I of *Cetiosauriscus stewarti* NHMUK R3078

Figure 140: Metatarsal I of *Cetiosauriscus stewarti* NHMUK R3078 in dorsal/anterior view. Note the foramina (C459-1), the angled proximal (C460-0) and distal articular surfaces (C462-0), and the distinct posterolateral process on the distal articular surface (C464-1). Scale bar = 5 cm.



PeerJ Reviewing Manuscript

PeerJ Reviewing Manuscript

Figure 141

Flagellicaudatan metatarsals II

Figure 141: Right (A) and left (B) metatarsal II of SMA 0087 (A) and *Dyslocosaurus polyonychius* AC 663 in dorsal/anterior view. Note the dorsolateral rugosity (C465-1) with its different developments (reduced, laterally, A, C468-0; prominent, reaching center or shaft, B, C468-1), or the posterolateral process (absent, A, C469-0; present, B, C469-1). Scaled to same proximodistal length.

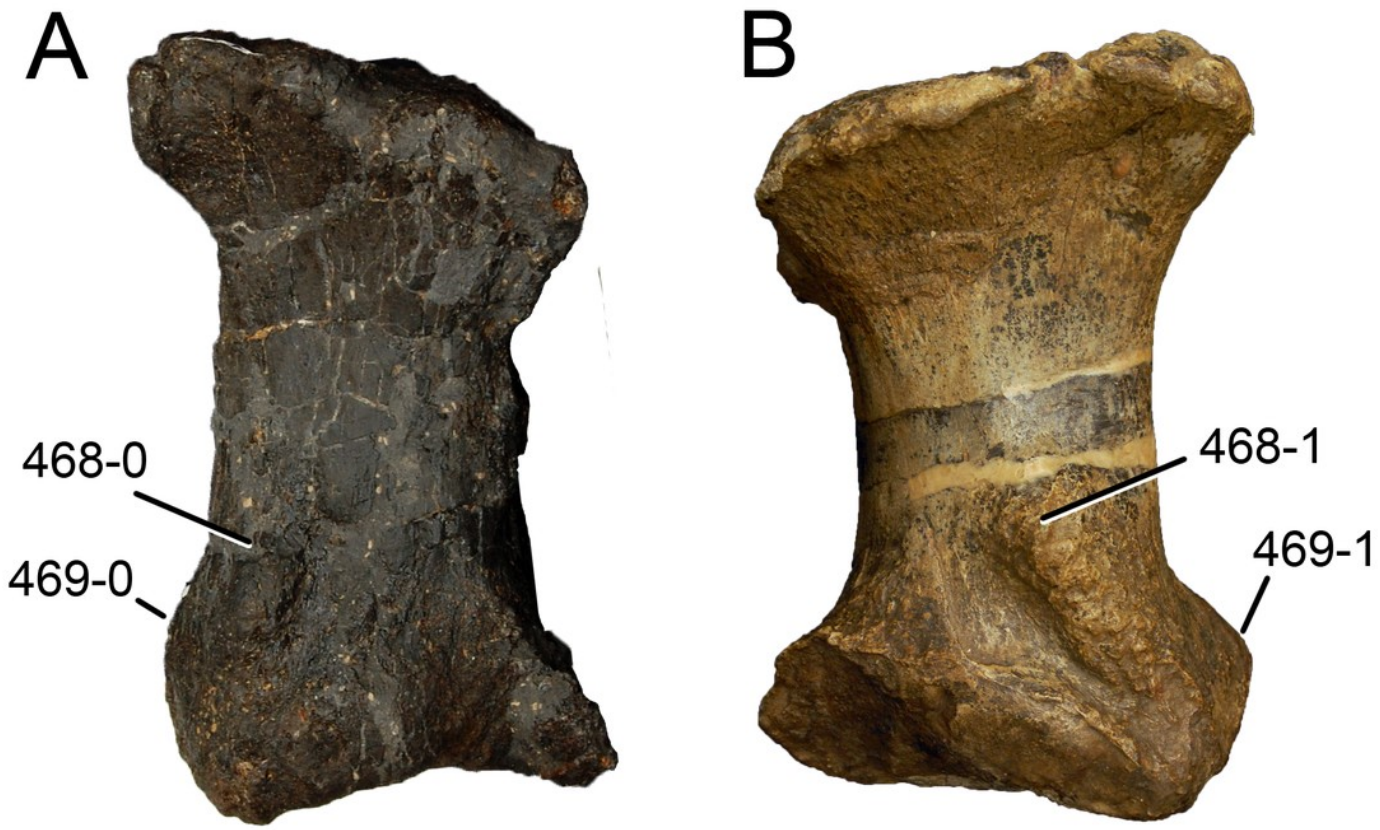
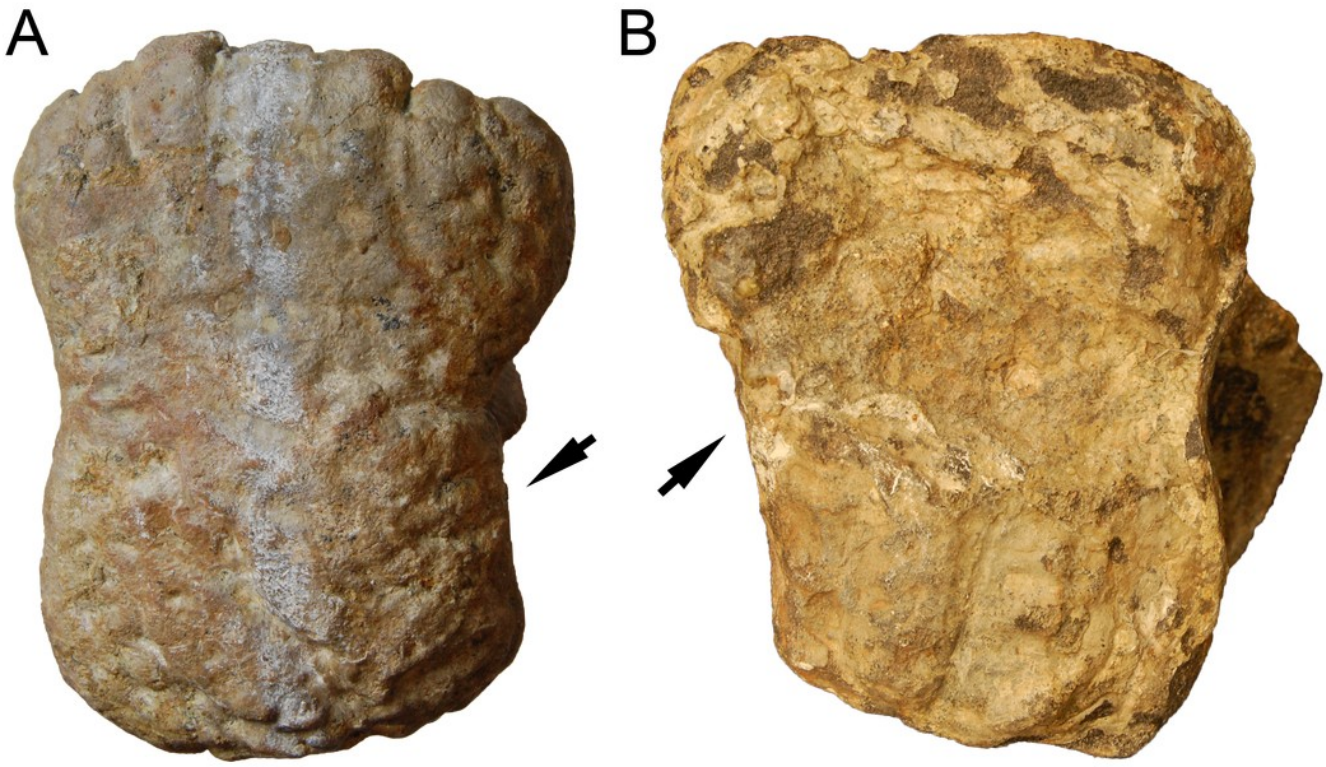


Figure 142

Dicraeosaurid metatarsals II

Figure 142: Right (A) and left (B) metatarsal II of *Suuwassea emilieae* ANS 21122 (A) and *Dyslocosaurus polyonychius* AC 663 (B) in proximal view, illustrating the concave (A) and straight (B) lateral margins (arrows; C467). Scaled to the same dorsoventral height.

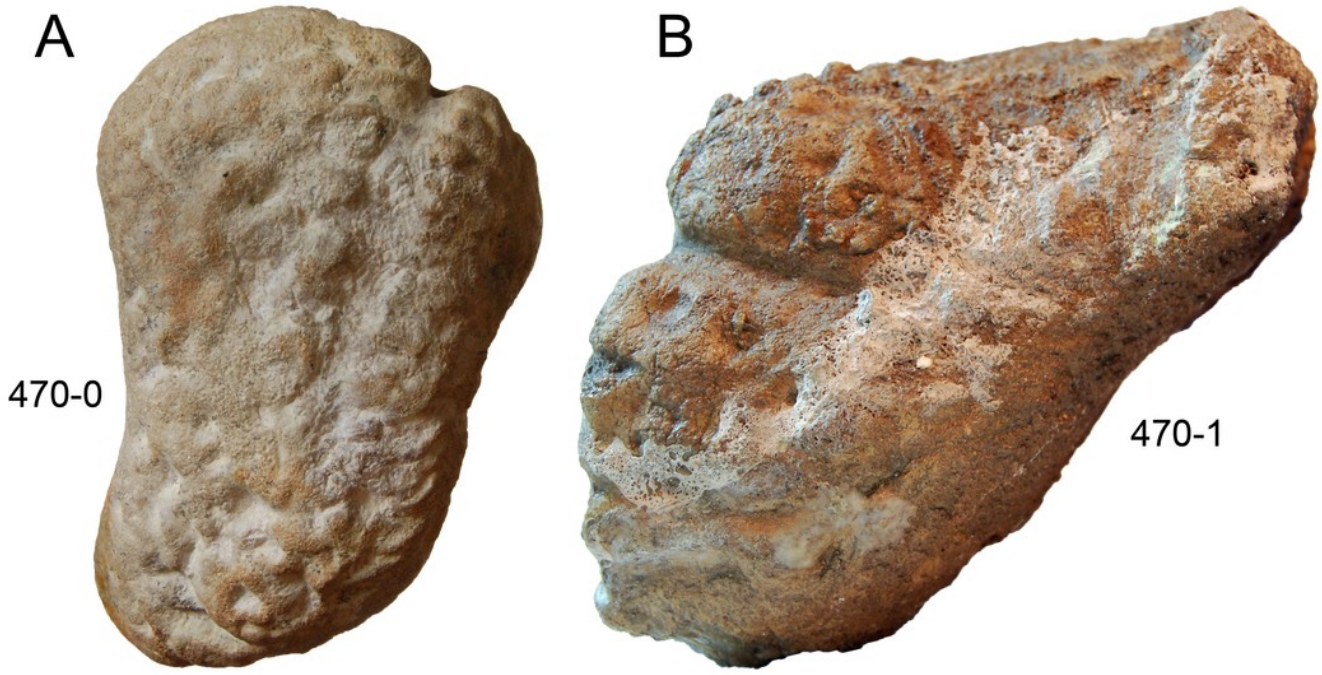


PeerJ Reviewing Manuscript

Figure 143

Eusauropod metatarsals IV

Figure 143: Right (A) and left (B) metatarsal IV of *Suuwassea emilieae* ANS 21122 (A) and *Cetiosauriscus stewarti* NHMUK R3078 (B) in proximal view, illustrating the curved (A; C470-0) and subtriangular outlines (B; C470-1). Scaled to the same dorsoventral height.



PeerJ Reviewing Manuscript

Figure 144

Diplodocid metatarsal V

Figure 144: Metatarsal V of *Barosaurus affinis* YPM 419 (A) and SMA 0087 (B) in proximal view, illustrating the rhomboid (A; C471-1) or triangular outline of the articular surface (B; C471-0). Scaled to the same transverse width.

PeerJ Reviewing Manuscript

PeerJ Reviewing Manuscript

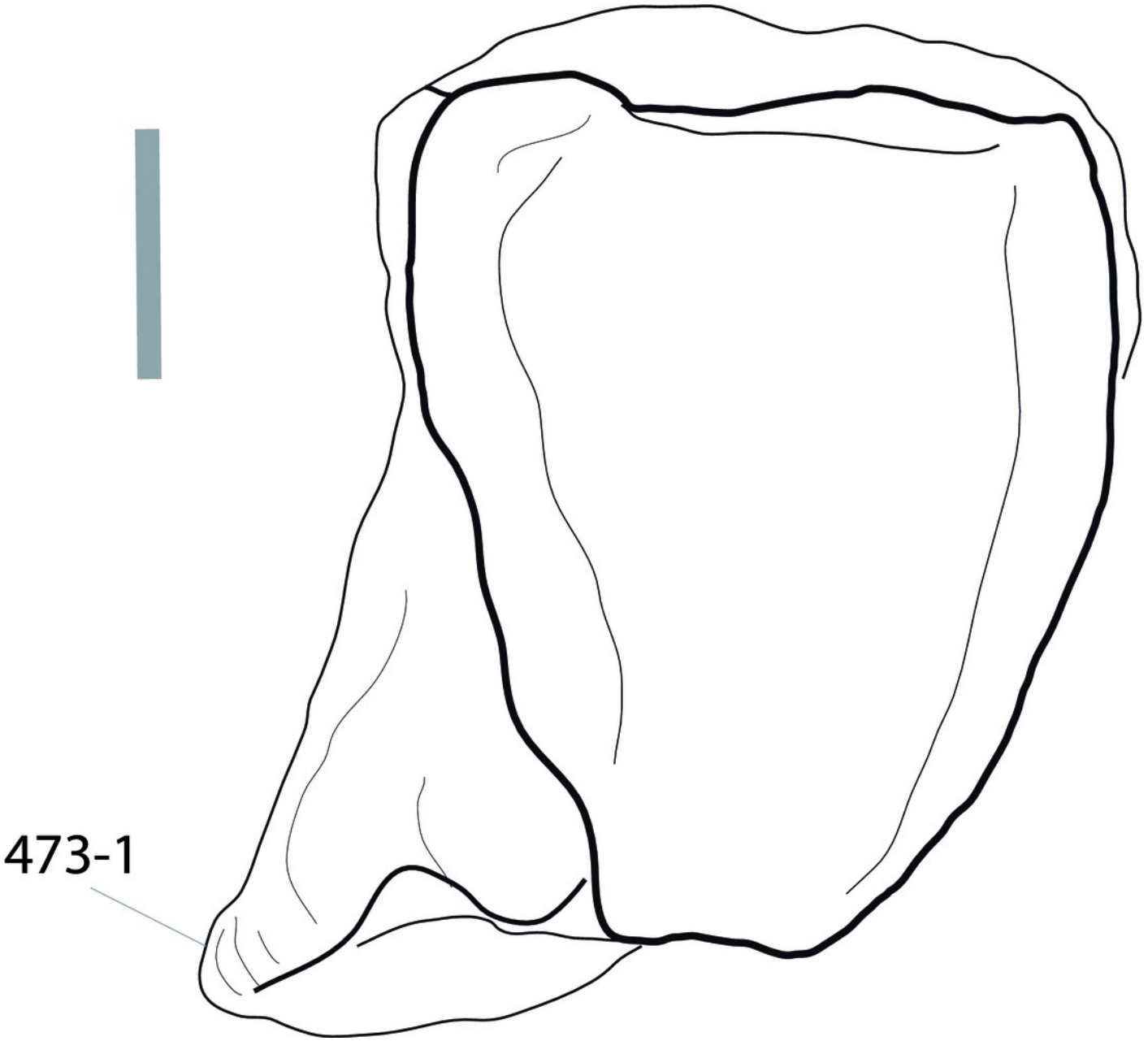




Figure 145

Pedal phalanx I-1 of *Apatosaurus* sp. NHMUK R3215

Figure 145: Pedal phalanx I-1 of *Apatosaurus* sp. NHMUK R3215 in medial view, illustrating the ventral shelf (C473-1). Scale bar = 2 cm.



PeerJ Reviewing Manuscript

Figure 146

Eusauropod pedal ungual I

Figure 146: Pedal ungual I of *Cetiosauriscus stewarti* NHMUK R3078 (A) and *Dyslocosaurus polyonychius* AC 663 (B) in lateral view, illustrating the two different courses of the canals (curved, A, C477-0; straight, B, C477-1). Dotted lines indicates the broken tip. Scaled to same proximal articular surface height.

PeerJ Reviewing Manuscript

PeerJ Reviewing Manuscript

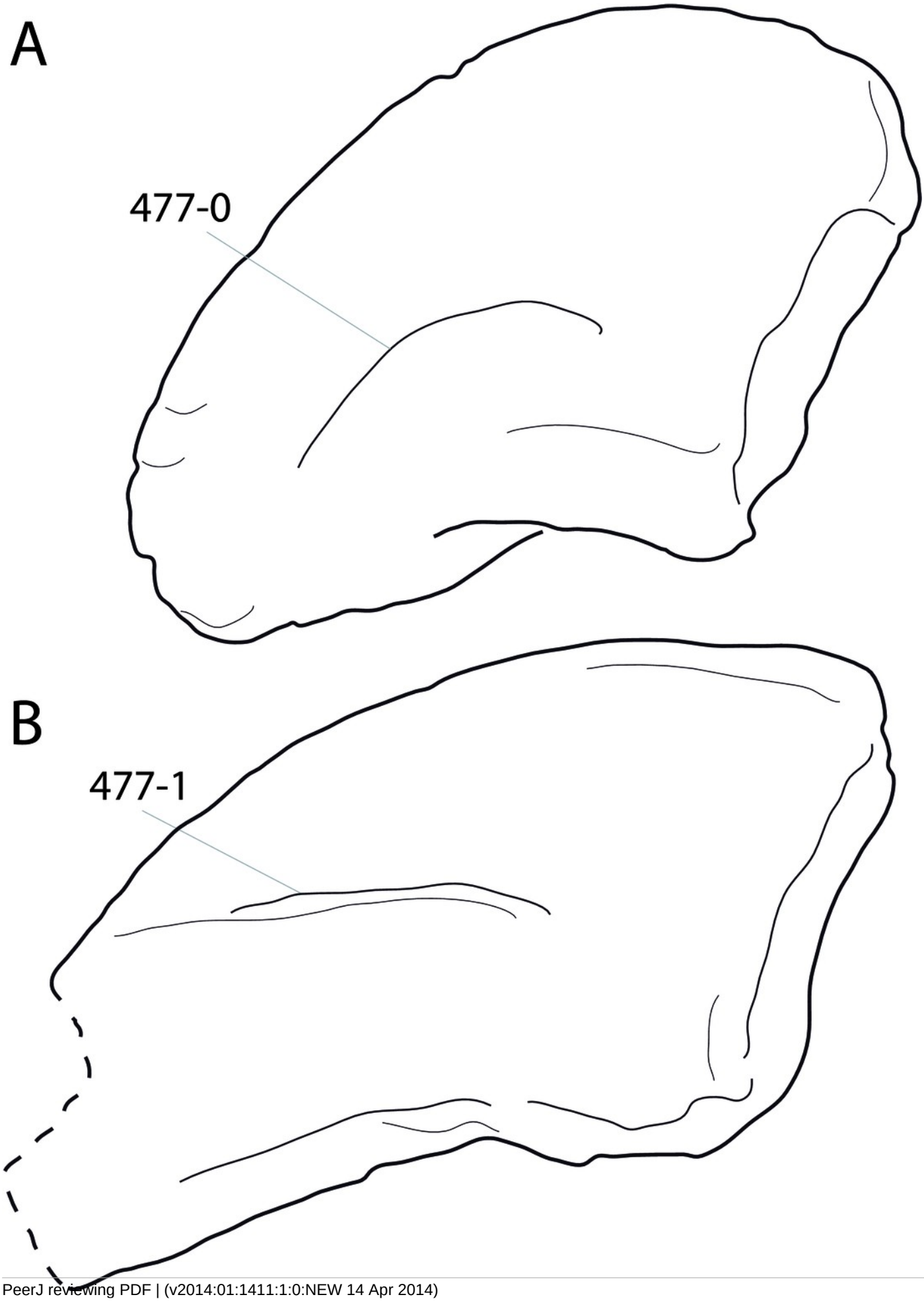


Figure 147

Strict consensus tree of the complete analysis with equal weighting

Figure 147: Strict consensus tree of the complete analysis with equal weighting. OTUs with species names and specimen numbers are type specimens. Tree length is 1897 steps. Note the brachiosaurid affinities of *Australodocus*.

PeerJ Reviewing Manuscript

PeerJ Reviewing Manuscript

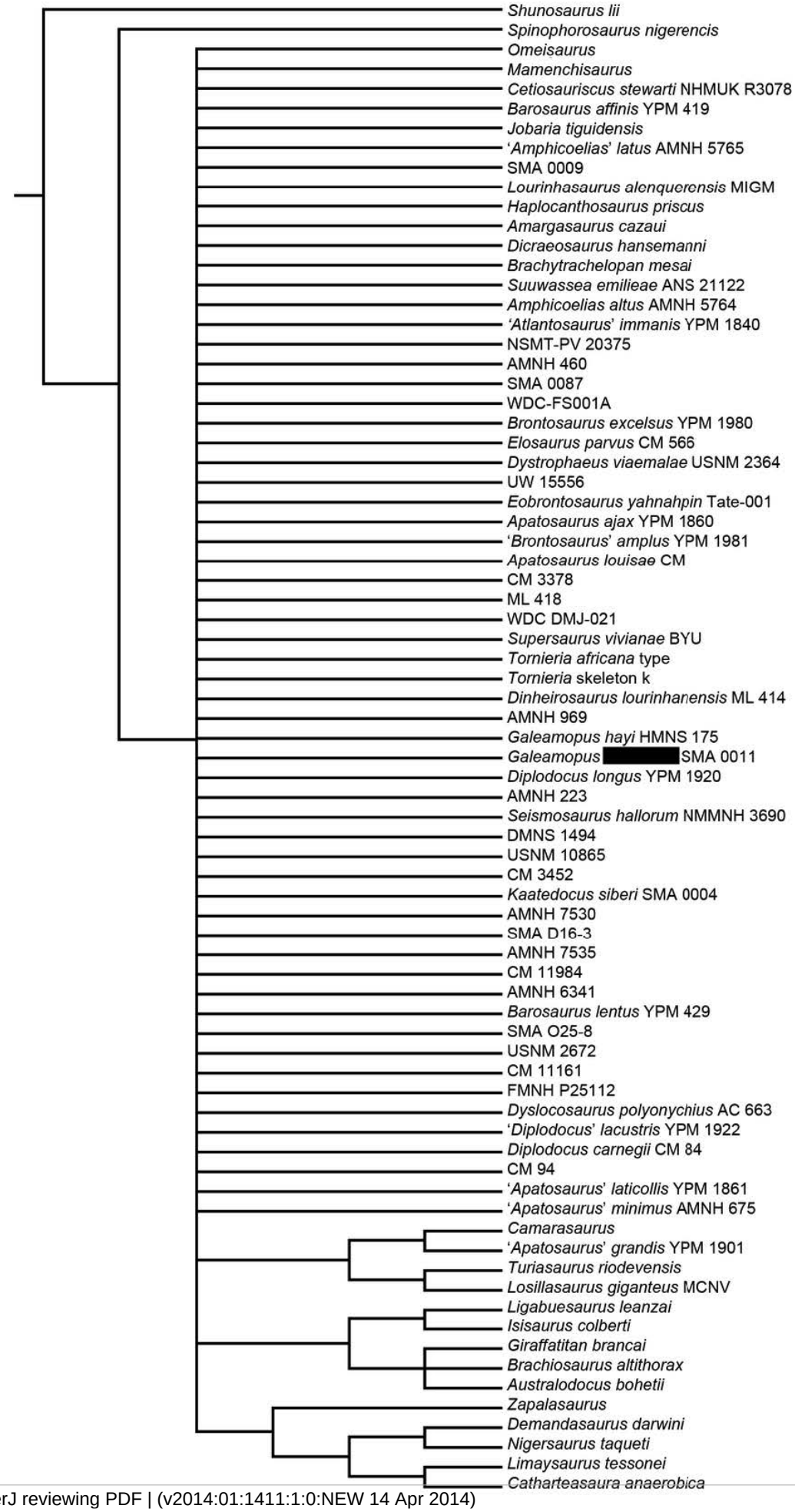


Figure 148

Pruned strict consensus tree obtained by equal weighting

Figure 148: Pruned strict consensus tree obtained by equal weighting, after the a posteriori deletion of '*Apatosaurus*' *minimus* AMNH 675, '*Barosaurus*' *affinis* YPM 419, '*Diplodocus*' *lacustris* YPM 1922, *Dystrophaeus viaemalae* USNM 2364, ML 418, and SMA O25-8. Note the dicraeosaurid affinities of *Dyslocosaurus* and *Suuwassea* (arrowheads).

PeerJ Reviewing Manuscript

PeerJ Reviewing Manuscript

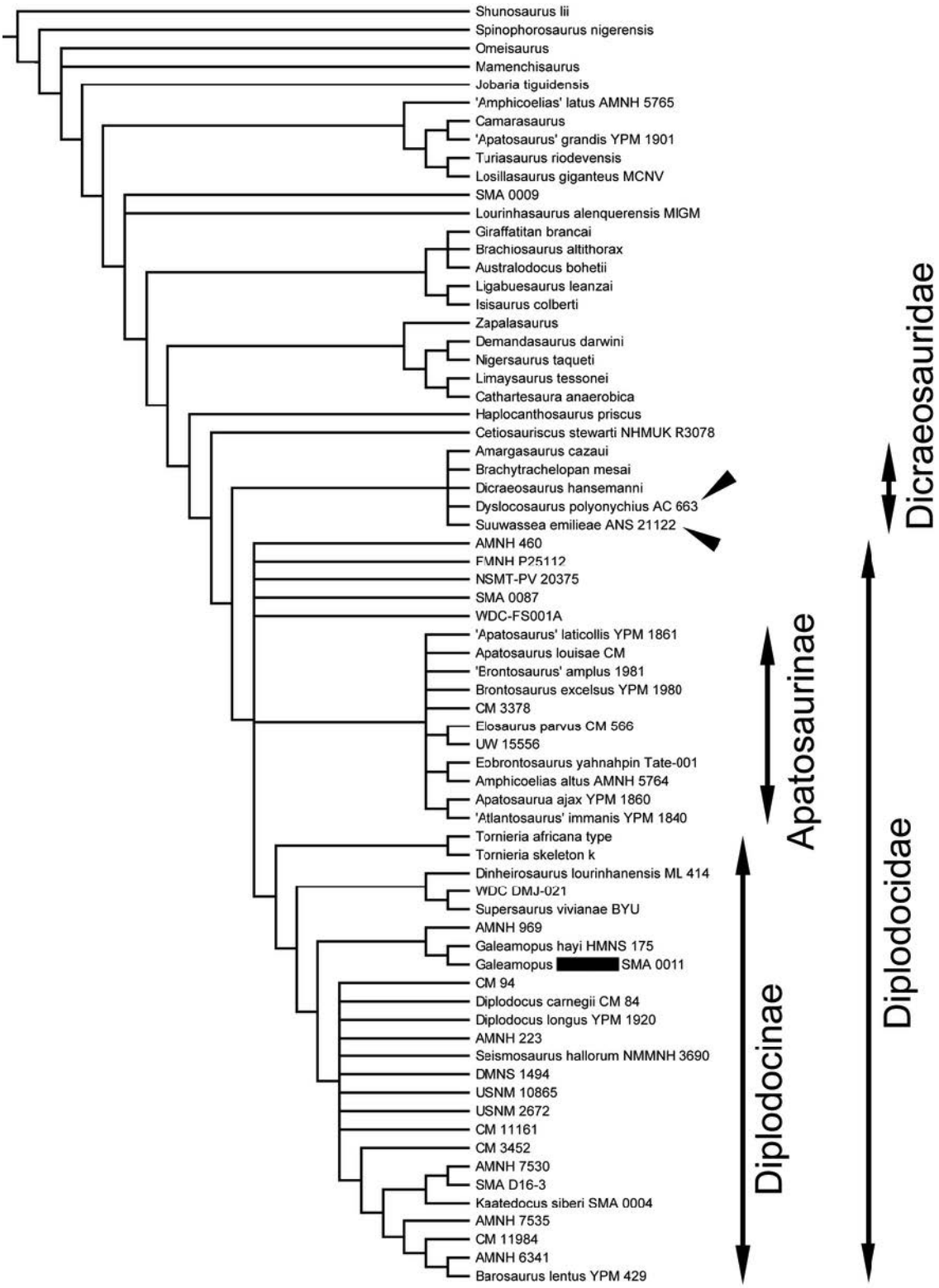


Figure 149

Reduced consensus tree obtained by equal weighting

Figure 149: Reduced consensus tree obtained by equal weighting, after the a posterior deletion of 25 OTUs.

PeerJ Reviewing Manuscript

PeerJ Reviewing Manuscript

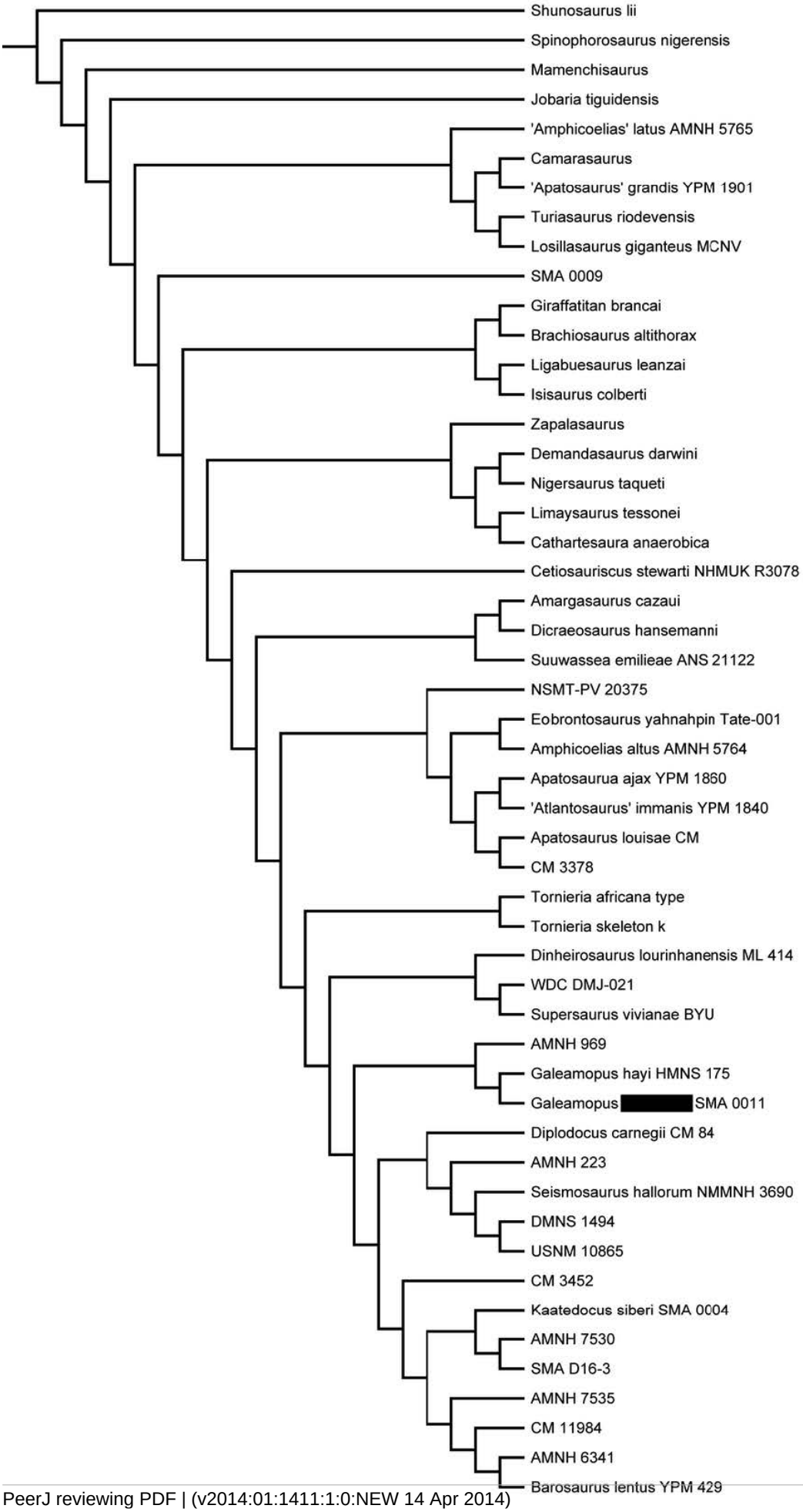


Figure 150

Strict consensus tree of the complete analysis with implied weighting

Figure 150: Strict consensus tree of the complete analysis with implied weighting. OTUs with species names and specimen numbers are type specimens. Tree length is 187.97214 steps. Note the basal position of *Barosaurus affinis*, *Cetiosauriscus stewarti*, and the somphospondylian affinities of '*Apatosaurus*' *minimus*.

PeerJ Reviewing Manuscript



PeerJ Reviewing Manuscript

Figure 151

Pruned strict consensus tree obtained by implied weighting

Figure 151: Pruned strict consensus tree obtained by implied weighting, after the a posteriori deletion of the skull-only specimens, YPM 1922, CM 11161, USNM 2672, and SMA O25-8. Note the position of *Amphicoelias altus* as most basal diplodocid, *Dystrophaeus viaemalae* within Apatosaurinae, and *Australodocus bohetii* as a diplodocine (arrowheads).

PeerJ Reviewing Manuscript

PeerJ Reviewing Manuscript

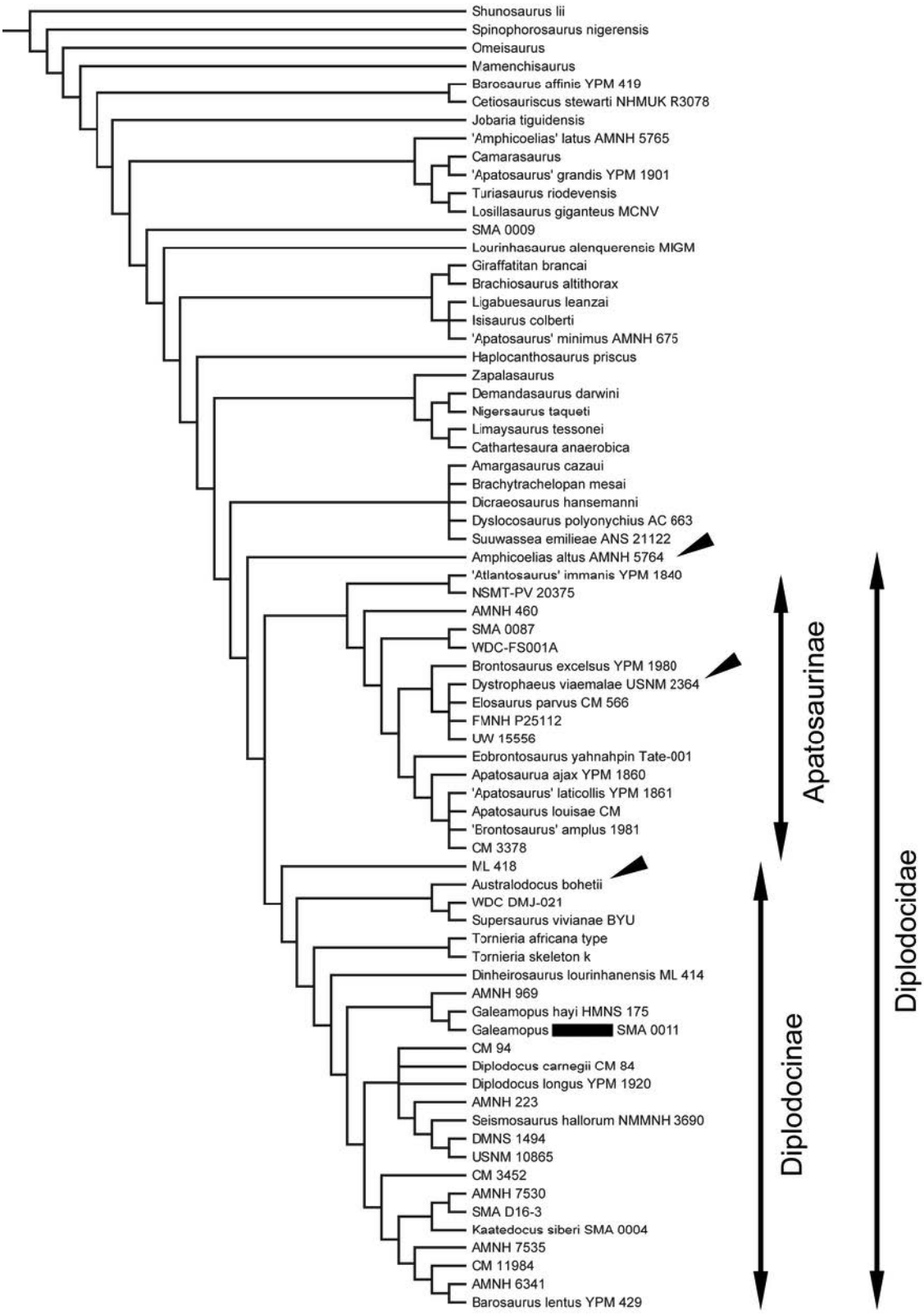
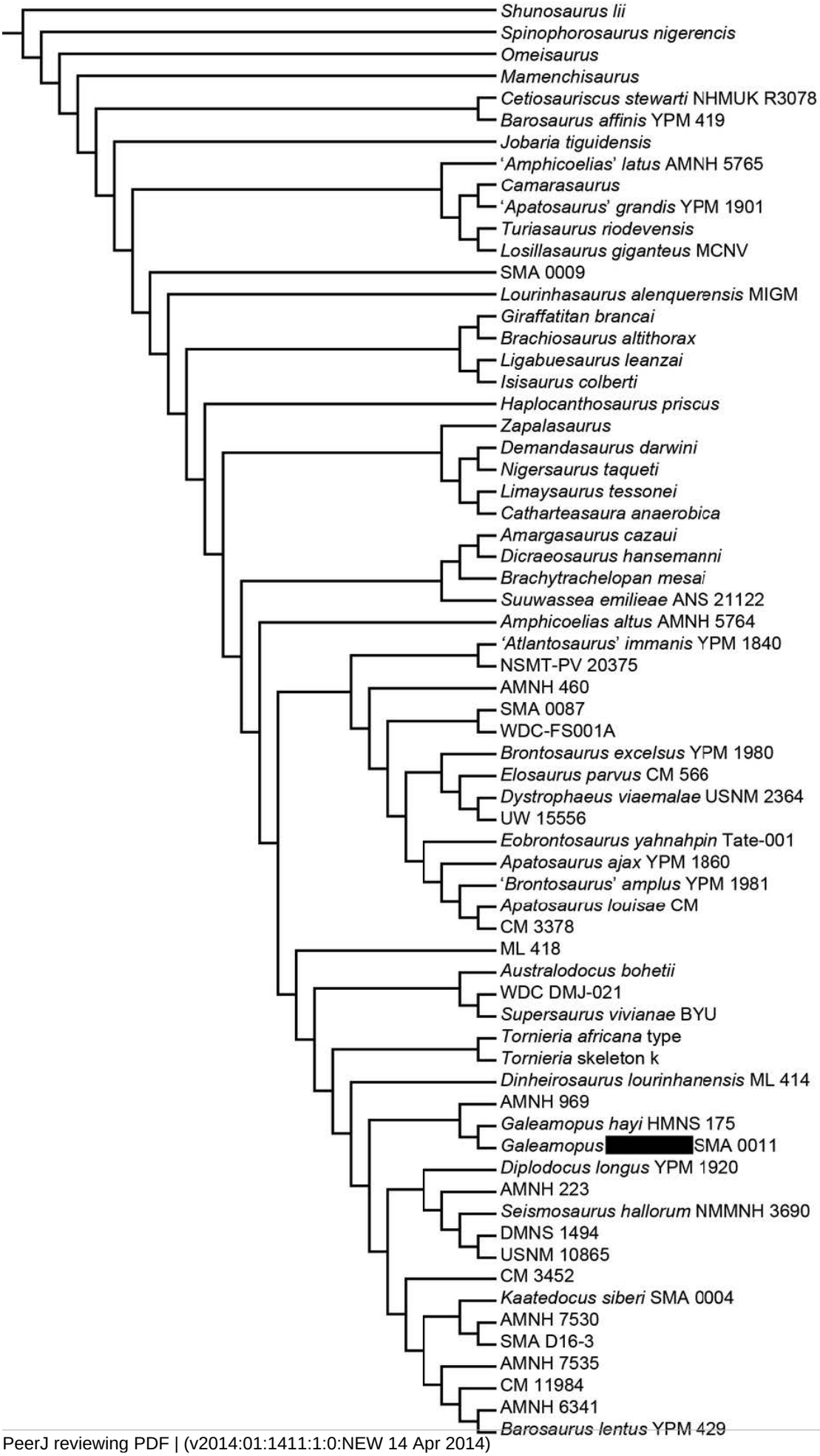


Figure 152

Reduced consensus tree obtained by implied weighting

Figure 152: Reduced consensus tree obtained by implied weighting, after the a posteriori deletion of 10 OTUs.

PeerJ Reviewing Manuscript



PeerJ Reviewing Manuscript

PeerJ Reviewing Manuscript

Figure 153

Strict consensus trees of previous phylogenetic analyses

Figure 153: Strict consensus trees of previous phylogenetic analyses with special focus on diplodocoid intrarelationships, with the number of taxa (T) and characters (C) indicated. In brackets the number of diplodocid taxa and newly proposed characters. Taxon names were changed according to more recent publications, and diplodocid OTU highlighted with the red box.

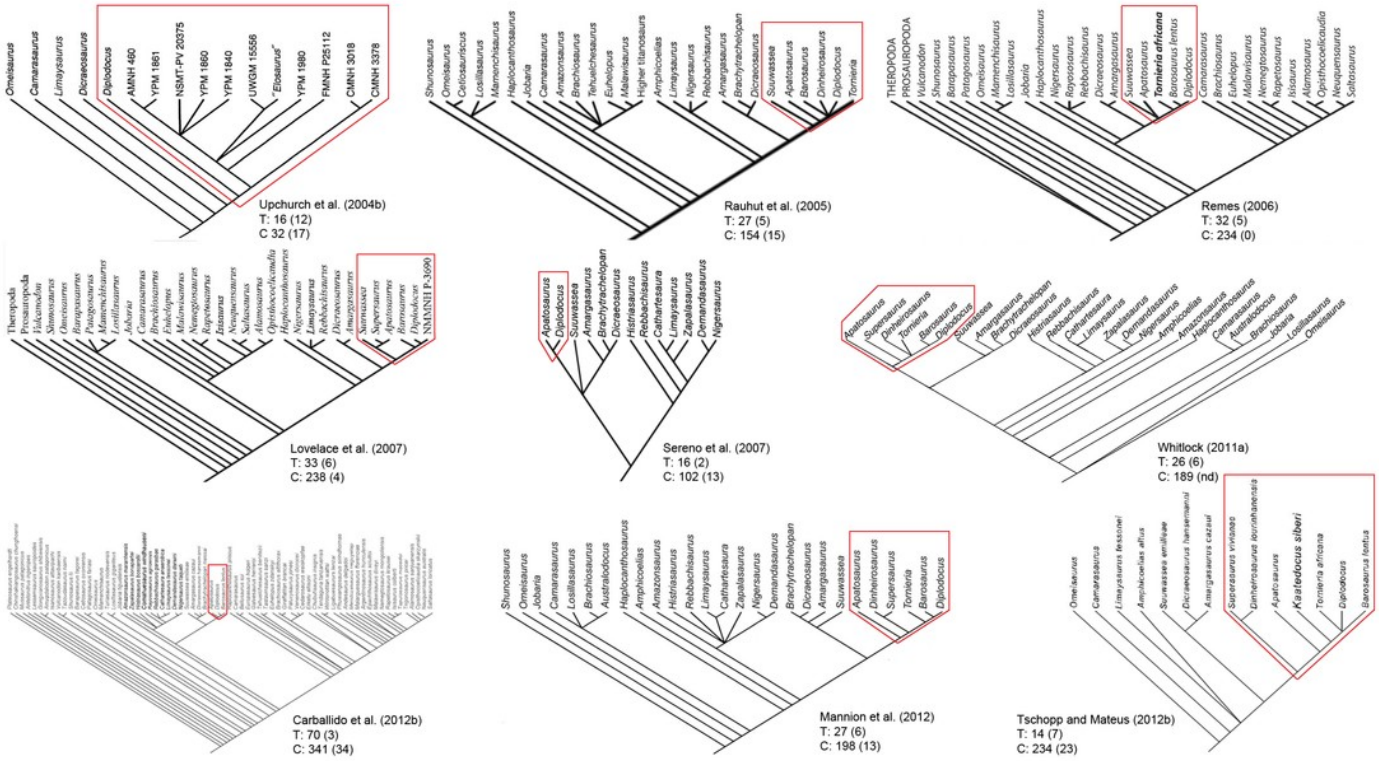


Figure 154

Combined cladogram of diplodocid species-level intrarelationships

Figure 154: Combined cladogram of diplodocid species-level intrarelationships, summarizing the results of this study. Stem-based higher-level taxa are marked by an arrowhead, node-based taxa by a dot.

PeerJ Reviewing Manuscript

PeerJ Reviewing Manuscript

